

**Some pages of this thesis may have been removed for copyright restrictions.**

If you have discovered material in Aston Research Explorer which is unlawful e.g. breaches copyright, (either yours or that of a third party) or any other law, including but not limited to those relating to patent, trademark, confidentiality, data protection, obscenity, defamation, libel, then please read our [Takedown policy](#) and contact the service immediately (openaccess@aston.ac.uk)

**TRANSITION METAL ION COORDINATION**  
**IN HYDROPHILIC POLYMER**  
**MEMBRANES.**

ANDREW LENNARD LEWIS

DOCTOR OF PHILOSOPHY

THE UNIVERSITY OF ASTON IN BIRMINGHAM

SEPTEMBER 1991

This copy of the thesis has been supplied on condition that anyone who consults it is understood to recognise that its copyright rests with its author and that no quotation from the thesis and no information derived from it may be published without the author's prior, written consent.

THE UNIVERSITY OF ASTON IN BIRMINGHAM

**TRANSITION METAL ION COORDINATION IN  
HYDROPHILIC POLYMER MEMBRANES.**

**ANDREW LENNARD LEWIS.**

Submitted for the Degree  
of Doctor of Philosophy.

September 1991.

**SUMMARY.**

This thesis is concerned with the investigation of transition metal (TM) ion complexation with hydrophilic membranes composed of copolymers of 4-vinyl pyridine & 4-methyl-4'-vinyl-2,2'-bipyridine with 2-hydroxyethyl methacrylate. The Cu(II), Co(II) & Fe(II) complexes with these coordinating membranes were characterised by a variety of techniques, in order to assess the effect of the polymer on the properties of the complex, and *vice versa*. A detailed programme of work was instigated into the kinetics of formation for the polymer-bound *tris*(bipyridyl) iron(II) complex; the rate and extent of complex formation was found to be anion-dependent. This is explained in terms of the influence of the anion on the transport properties and water content of the membrane, the controlling factor in the development of the *tris*-complex being the equilibrium concentration of Fe(II) in the gel matrix.

A series of transport studies were performed with a view to the potential application of complexing hydrogel membranes for aqueous TM ion separations. A number of salts were studied individually and shown to possess a range of permeabilities; the degree of interaction between particular metal-ion:ligand combinations is given by the lag-time observed before steady-state permeation is achieved. However, when two TM salts that individually display different transport properties were studied in combination, they showed similar lag-times & permeabilities, characteristic of the more strongly coordinating metal ion. This 'anti-selective' nature thus renders the membrane systems unsuitable for TM ion separations. Finally, attempts were made to synthesise and immobilise a series of N,O-donor macrocyclic ligands into hydrogel membranes. Although the functionalisation reactions failed, limited transport data was obtained from membranes in which the ligands were physically entrapped within the polymer matrix.

**Keywords:**        **Complexing membrane, hydrogel, iron(II)*tris*(bipyridine), anti-selective transport, macrocycles.**

*To June Rose Lewis,  
my Mother.*

## **ACKNOWLEDGEMENTS.**

Firstly, I would like to thank Dr. J.D.Miller, for his excellent supervision, undying enthusiasm and continual support throughout the course of this study. I would also like to extend thanks to the other academic staff of the University, especially Dr. A.W.P. Jarvie, for her advice on many-an organic synthesis.

Recognition must go to Andy Hall for a nice try at macrocycle functionalisation, to Adrian Trevett for his assistance with the tensometric work, to Dr. M. Perry for the NMR spectra, and to Mike, Denise, and the rest of the technical staff for their services. Thanks also to Dr. D. Walton of Lanchester Polytechnic for use of their cyclic voltammetry equipment.

My appreciation goes to the Science & Engineering Research Council for financial support over the duration of this work, and to those at ICI C & P Runcorn, for the use of their resources whilst 'writing-up' this thesis.

Thanks to all my colleagues in the department for their friendship, and cheers to all the "Little People" of Handsworth Wood for those times that made life worth living, and preserved our sanity over the past three years.

Finally, despite her total lack of patience, interest or pity, my greatest thanks go to Liz- for just being Liz.

## **CONTENTS.**

	<b><u>Page</u></b>
<b>SUMMARY.</b>	2
<b>DEDICATION.</b>	3
<b>ACKNOWLEDGEMENTS.</b>	4
<b>CONTENTS.</b>	5
<b>LIST OF TABLES.</b>	14
<b>LIST OF FIGURES.</b>	16
<b>LIST OF ABBREVIATIONS.</b>	25
 <b><u>CHAPTER ONE:</u></b>	
<b>INTRODUCTION. "STRATEGIES FOR THE DESIGN OF A HYDROPHILIC-COMPLEXING POLYMER SYSTEM.</b>	
 1.1 INTRODUCTION.	28
1.2 THE USE OF HYDROGEL POLYMERS.	31
1.2.1 The Hydrophilic Nature of the Polymer.	33
1.3 THE CHOICE OF LIGANDS.	35
1.3.1 The Case for a Pyridine Ligand.	36
1.3.2 The Case for a Bipyridine Ligand.	36
1.4 THE APPLICATION OF MEMBRANE PROCESSES.	39
1.4.1 Transition Metal-Ion Separations by Membranes.	42
1.5 SUMMARY OF OBJECTIVES.	44
 <b><u>CHAPTER TWO:</u></b>	
<b>MATERIALS AND METHODS.</b>	
 SECTION (A):	
THE SYNTHESIS AND PURIFICATION OF VINYLIC LIGANDS AND COMPLEXES.	47
2.1 INTRODUCTION.	47
2.2 4-VINYLPYRIDINE.	47

2.2.1	Nuclear Magnetic Resonance Spectra of 4-VPy.	48
2.3	4-METHYL 4'-VINYL-2,2'-BIPYRIDINE.	50
2.3.1	(i) Preparation of 4,4'-Dimethyl-2,2'-Bipyridine.	52
2.3.2	(ii) Preparation of 4-Methyl 4'-Methoxyethyl-2,2'-Bipyridine.	54
2.3.3	(iii) Preparation of 4-Methyl 4'-Vinyl-2,2'-Bipyridine.	55
2.3.4	Nuclear Magnetic Resonance Spectra for Bipyridyl Derivatives.	56
2.4	PREPARATION OF TRIS(4-METHYL 4'-VINYL-2,2'-BIPYRIDINE) IRON (II).	62
2.5	POLYMERISATION PROCESSES.	62
2.5.1	Reagents used in Polymer Preparations.	62
2.5.2	Preparation of Hydrogel Membranes.	64
2.5.2.1	Measurement of Equilibrium Water Contents.	65
2.5.3	Preparation of Linear Hydrophilic Polymers by Solution Polymerisation.	66
2.5.4	Suspension Polymerisation of HEMA Copolymers.	66
SECTION (B):	TECHNIQUES USED IN TRANSITION METAL- ION COORDINATION STUDIES.	68
2.6	INTRODUCTION.	68
2.7	ULTRAVIOLET AND VISIBLE ABSORPTION SPECTROSCOPY.	69
2.7.1	Spectrophotometer Instrumentation.	70
2.7.2	Application of UV/Visible Spectrophotometry to Membrane Studies.	73
2.7.3	Application to the Study of Ion-Binding Kinetics.	75
2.8	MEASUREMENT OF MECHANICAL PROPERTIES.	76
2.8.1	Instrumentation and Techniques.	77
2.9	COATED-WIRE ELECTRODE STUDIES.	79
2.9.1	Coated-Wire Electrode Construction and Use.	79
2.9.2	Cyclic Voltammetric Studies of Coated-Wire Electrodes.	80
2.9.2.1	Cyclic Voltammetry: Instrumentation and Operation.	81
2.9.2.2	Choice of Solvent and Support Electrolyte.	82

2.10	TRANSITION METAL ION PERMEATION STUDIES.	84
2.10.1	Permeability Cell Design.	84
2.10.2	The Spectrophotometric Study of TM Ion Transport.	87
2.10.3	The Conductimetric Study of TM Ion-Transport	88
2.10.3.1	Calibration of the Conductivity Cell.	90
2.10.4	Transport Studies on Mixed TM Solutions.	92
2.11	THE USE OF ATOMIC ABSORPTION SPECTROSCOPY.	92
2.11.1	Application of AAS to Membrane Studies.	94
2.12	THE USE OF TRANSITION METAL SALT SOLUTIONS.	94

### **CHAPTER THREE: THE INVESTIGATION OF TRANSITION METAL COMPLEXES IN LIGAND-MODIFIED HYDROGEL POLYMERS.**

3.1	INTRODUCTION.	97
3.2	POLYMERS IN PERSPECTIVE.	98
3.2.1	Ligand Distribution within the Copolymers.	98
3.2.2	Effect of Copolymer Composition on the EWC.	99
3.3	POLYMER INTERACTIONS WITH TRANSITION METAL IONS	100
3.4	THE STUDY OF POLYMER-BOUND COMPLEXES BY VISIBLE SPECTROSCOPY.	104
3.4.1	Cu(II) Coordination in Pyridyl- & Bipyridyl Copolymer Membranes.	105
3.4.1.1	Cu(II) Ligand Field Spectra.	105
3.4.1.2	Effect of Ligand Loading on Cu(II)-Coordination to Pyridyl-Copolymer Membranes.	107
3.4.1.3	Effect of Cu(II) Concentration on its Coordination to Pyridyl-Copolymer Membranes.	110
3.4.1.4	Effect of Dehydrating Cu(II)-Coordinated Pyridyl-Copolymer Membranes.	111
3.4.1.5	Cu(II) Coordination in Bipyridyl-Copolymer Membranes.	113

3.4.2	Co(II) Coordination in Pyridyl- & Bipyridyl-Copolymer Membranes.	116
3.4.2.1	Spectra of Co(II) Ions & Complexes.	116
3.4.2.2	Effect of Ligand Loading on Co(II) Coordination to Pyridyl-Copolymer Membranes.	117
3.4.2.3	Effect of Dehydrating Co(II)-Coordinated Pyridyl-Copolymer Membranes.	120
3.4.2.4	Co(II) Interaction with Bipyridyl-Copolymer Membranes.	122
3.4.3	Properties of the Co(I) <i>tris</i> (Bipyridyl-Polymer) Complex.	124
3.4.3.1	Visible Absorption Spectra of the Co(I) Complex.	126
3.4.3.2	Co(I) <i>tris</i> (Bipyridyl-Polymer) Complex Redox Processes.	126
3.4.3.3	Oxygen Scavenging Ability of Co(I)-Coordinated Bipyridyl-Copolymer Membranes.	131
3.4.4	Fe(II) Interactions with Bipyridyl-Copolymer Membranes.	133
3.4.4.1	Visible Absorption Spectra of the Fe(II) <i>tris</i> (Bipyridine) Complex.	133
3.4.4.2	Effect of Ligand Loading on Fe(II)-Coordination to Bipyridyl-Copolymer Membranes.	134
3.5	PRELIMINARY STUDIES ON COPOLYMER COATED-WIRE ELECTRODES.	136
3.5.1	Evaluation of Ligand-Based Copolymer Coatings for TM Ion-Sensitive Electrodes.	137
3.5.2	Studies on the Electroactive Nature of Complex-Bound CWE's using Cyclic Voltammetry.	140
3.5.2.1	Electrochemistry of the Uncomplexed Polymer Coatings.	140
3.5.2.2	Electrochemistry of the Complexed Polymer Coatings.	143
3.6	CROSS-LINKING OF HYDROGEL NETWORKS THROUGH METAL-LIGAND COORDINATION.	146
3.6.1	Effect of Membrane Composition on Mechanical Properties.	148

3.6.2	Effect of Coordination Cross-Linking on Mechanical Properties.	149
3.6.3	Analysis of the Elastomeric Properties of Coordination-Cross-Linked Hydrogel Membranes.	156
3.7	CONCLUDING REMARKS.	160

## **CHAPTER FOUR: THE KINETICS OF IRON (II) COORDINATION IN BIPYRIDYL-BASED COPOLYMER MEMBRANES.**

4.1	INTRODUCTION.	162
4.2	DETERMINATION OF THE MAXIMUM BINDING CAPACITY OF BIPYRIDYL-BASED MEMBRANES.	164
4.2.1	Determination of the Molar Absorption Coefficient for Polymer-Bound Fe(II) <i>tris</i> Vinyl Bipyridine.	165
4.3	DETERMINATION OF THE KINETIC FORM FOR THE REACTION OF FERROUS SALTS WITH BIPYRIDYL-BASED MEMBRANES.	168
4.3.1	The Influence of Ferrous Salt Concentration & Type on the Kinetic Profiles of the Fe(II)/Bipyridyl System.	171
4.3.2	Least-Squares Analysis Computer Treatment.	176
4.3.3	First Order Methods where $A_{\infty}$ is Uncertain.	178
4.3.3.1	The Guggenheim Method.	178
4.3.3.2	The Kezdy/Swinbourne Method.	180
4.3.4	Second Order Methods when $A_{\infty}$ is Uncertain.	180
4.4	FORMULATION OF A MECHANISM FOR THE COORDINATION OF IRON (II) WITH POLYMER-BOUND BIPYRIDINE.	187
4.4.1	Derivation of a Mechanism that Fits the Second Order Kinetic Form for the Coordination of Ferrous Chloride & Perchlorate.	189
4.4.2	Suggested Mechanism that Fits the First Order Kinetic Form for the Coordination of Ferrous Sulphate.	193
4.4.3	Variation in the Infinity Absorbance and Rate Constant for ferrous Chloride & Perchlorate Kinetics.	195
4.4.3.1	Confirmation of an $[\text{Fe}^{2+}]$ -Dependent Equilibrium.	195

4.4.3.2	Derivation of a Relationship to Describe Variations in $A_{\infty}$ for Ferrous Chloride & Perchlorate Salt Concentration.	199
4.4.3.3	A Modified Approach to Considering Infinity Absorbances.	202
4.4.4	Variations in Infinity Absorbance and Rate Constant for Ferrous Sulphate Kinetics.	208
4.5	PROPOSED MECHANISM FOR THE COORDINATION OF FERROUS SALTS TO BIPYRIDYL-BASED MEMBRANES.	210
4.6	CONCLUDING REMARKS.	213

**CHAPTER FIVE:      TRANSITION METAL-ION TRANSPORT  
ACROSS COMPLEXING HYDROGEL  
MEMBRANES.**

5.1	INTRODUCTION.	218
5.2	A BACKGROUND TO TRANSPORT PHENOMENA IN HYDROGEL MEMBRANES.	220
5.3	THE COLLECTION OF PERMEABILITY DATA.	221
5.3.1	Consistency Between Permeability Runs and Rigs.	222
5.4	PERMEATION OF TRANSITION METAL IONS THROUGH POLY(HEMA) MEMBRANES.	222
5.5	PERMEATION OF TRANSITION METAL IONS THROUGH LIGAND-MODIFIED HYDROGEL MEMBRANES.	228
5.5.1	Investigation of the Lag-Time Phenomenon	234
5.5.2	Effect of Salt Concentration on Membrane Transport Properties.	238
5.5.3	Effect of Ligand-Loading on Membrane Transport Properties.	241
5.6	SOME STUDIES OF COMPETITIVE TRANSPORT.	245
5.6.1	Transport through Precomplexed Membranes.	246
5.6.2	Transport of Binary Salt Solutions.	248
5.7	PROPOSAL OF A TRANSPORT MECHANISM.	252
5.8	CONCLUDING REMARKS.	255

**CHAPTER SIX:        PREPARATORY INVESTIGATIONS OF  
THE INCORPORATION OF MACRO-  
CYCLIC LIGANDS INTO HYDROPHILIC  
POLYMERS.**

6.1	INTRODUCTION.	258
6.2	SYNTHESIS OF THE MACROCYCLIC LIGANDS.	261
	SECTION (A):	
	Synthesis of the Oxygen, Nitrogen-Donor Macrocyclic Ligands.	264
6.2.1	Preparation of 1,4-Bis(2'-Formylphenyl)-1,4-Dioxabutane, ( <i>O-en</i> ).	264
6.2.2.1	Nuclear Magnetic Resonance Spectra of <i>O-en</i> .	264
6.2.2	Preparation of 1,5-Bis(2'-Formylphenyl)-1,5-Dioxapentane, ( <i>O-tn</i> ).	264
6.2.2.1	Nuclear Magnetic Resonance Spectra of <i>O-tn</i> .	267
6.2.3	Preparation of 5,6,7,8,9,10,16,17-Octahydrodibenzo[e,m] [1,4] Dioxo[8,11] Diazacyclotetradecine, ( <i>O-en-NH-tn</i> ).	267
6.2.4	Preparation of 3,4:9,10-Dibenzo-1,12-Diaza-5,8-Dioxo- Cyclopentadecane-1,11-Diene, ( <i>O-en-N-tn</i> ).	270
6.2.4.1	Nuclear Magnetic Resonance Spectra of ( <i>O-en-N-tn</i> ).	270
6.2.5	Preparation of 6,7,8,9,10,11,17,18-Octahydro-5H-Dibenzo [e,n][1,4] Dioxo[8,12] Diazacyclopentadecine, ( <i>O-en-NH-tn</i> ).	273
6.2.5.1	Nuclear Magnetic Resonance Spectra of ( <i>O-en-NH-tn</i> ).	273
6.2.6	Attempted Preparation of 5,6,7,8,9,10,17,18-Octahydro- 16H-Dibenzo[f,n][1,5] Dioxo[9,12] Diazacyclopentadecine, ( <i>O-tn-NH-en</i> ).	276
6.2.7	Preparation of 3,4:10,11-Dibenzo-1,12-Diaza-5,8-Dioxo- Cyclopentadecane-1,11-Diene, ( <i>O-tn-N-tn</i> ).	276
6.2.7.1	Nuclear Magnetic Resonance Spectra of ( <i>O-tnN-tn</i> ).	277

6.2.8	Preparation of 6,7,8,9,10,11,18,19-Octahydro-5H,17H-Dibenzo[f,o][1,5] Dioxo[9,13] Diazacyclohexadecine, ( <i>O</i> -tn- <i>NH</i> -tn).	277
6.2.8.1	Nuclear Magnetic Resonance Spectra of ( <i>O</i> -tn- <i>NH</i> -tn).	280
6.2.9	Attempted Preparation of 1,12,15-Triaza-3,4,9,10-Dibenzo 5,8-Dioxacycloheptadecane, ( <i>O</i> -en-3 <i>NH</i> -dien).	280
6.2.10	Attempted Preparation of 5,6:15,16-Dibenzo-1,4-Dioxo 8,13-Diazacyclohexadecine ( <i>O</i> -en- <i>NH</i> -bn) & 6,7:16,17-Dibenzo-1,5-Dioxo-9,14-Diazacycloheptadecine, ( <i>O</i> -tn- <i>NH</i> -bn).	283
SECTION (B):		
	Synthesis of the N <sub>4</sub> -Type Macrocyclic Ligands.	284
6.2.11	Preparation of (Diethylene Diamine) Copper (II) Perchlorate.	284
6.2.12	Preparation of (3,10-Dimethyl-3,10-Dinitro-1,4,8,11-Tetra-Azacyclodecane) Copper (II) Perchlorate, (Cu[Dinamac](ClO <sub>4</sub> ) <sub>2</sub> ).	286
6.2.13	Preparation of the Multidentate Ligand (1,9-Diamino-5-Methyl 5-Nitro-3,7-Diazonane) Copper (II) Perchlorate, (Cu[Nelin](ClO <sub>4</sub> ) <sub>2</sub> ).	286
6.2.14	Preparation of (10-Methyl-10-Nitro-1,4,8,12-Tetra Azacyclopentadecane) Copper (II) Nitrate, (Cu[Nemac](ClO <sub>4</sub> ) <sub>2</sub> ).	287
6.2.15	Reduction of the Nitro-Functions of Cu(Dinamac), Cu(Nemac) & Cu(Nelin).	287
6.3	ATTEMPTED FUNCTIONALISATION AND IMMOBILISATION OF <i>O</i> -en- <i>NH</i> -tn & <i>O</i> -tn- <i>NH</i> -tn MACROCYCLES.	288
SECTION (C):		
	Functionalisation of <i>O</i> -en- <i>NH</i> -tn.	289
6.3.1	Reaction with Allyl Chloride.	289
6.3.1.1	Nuclear Magnetic Resonance Study of Allyl Chloride Product.	289
6.3.2	Reaction with Acryloyl Chloride.	290

6.3.2.1	Nuclear Magnetic Resonance Study of Acryloyl Chloride Product.	293
SECTION (D):		
	Direct Immobilisation of <i>O</i> -en- <i>NH</i> -tn & <i>O</i> -tn- <i>NH</i> -tn.	293
6.3.3	Allyl Chloride Copolymer Membranes.	293
6.3.4	Chloro-Ethyl Vinyl Ether Copolymer Membranes.	296
6.3.5	2-(Chloro-Ethyl) Methacrylate Membranes.	296
6.3.6	Procedure for Immobilisation onto Membranes.	296
6.4	TRANSPORT OF IONS THROUGH MEMBRANES WITH ENTRAPPED MACROCYCLES.	297
6.4.1	Transport of Binary Salt Solutions Across Membranes with Entrapped Macrocyclic Ligands.	298
6.5	CONCLUDING REMARKS.	304

## **CHAPTER SEVEN: DISCUSSION AND CONCLUSIONS.**

7.1	SUMMARY OF THE THESIS.	306
7.2	SUGGESTIONS FOR FURTHER WORK.	310

## **REFERENCES.**

## **APPENDICES.**

APPENDIX ONE.	COMPUTER PROGRAM LISTINGS AND FLOW CHARTS.	331
APPENDIX TWO.	SELECTED ABSORBANCE & WAVELENGTH DATA FROM CHAPTER THREE.	385
APPENDIX THREE.	SPREAD-SHEET TABLES FOR THE CALCULATION OF STRESS-STRAIN DATA.	389

## LIST OF TABLES.

	<u>Page</u>
Table 1.1:	Selection of Commercially Available Ion-Exchange Resins. 37
Table 1.2:	Ion-Exchange Resins Based on the Pyridine Ligand. 37
Table 2.1	Reagents Used in Polymer Preparations. 63
Table 2.2:	Concentration Range for Standard Solutions Used in Calibration of Conductivity Cell. 90
Table 2.3:	AAS Data for the Elements Under Study. 93
Table 3.1:	Stability Constants for Cu(II) Complexes. 113
Table 3.2:	Effect of Crystal-Field Splitting on Visible Spectra of Co(II) Complexes. 118
Table 3.3:	Mechanical Property Data for Ligand-Modified Membranes: Complexed & Uncomplexed. 150
Table 4.1:	Spectral Details for Some Fe(Bipy) <sub>3</sub> <sup>2+</sup> Complex Derivatives. 167
Table 4.2:	Kinetic Data for (0.08M) FeSO <sub>4</sub> Binding. 179
Table 4.3:	Kinetic Data for (0.24M) FeCl <sub>2</sub> Binding. 182
Table 4.4:	Kinetic Data for (0.08M) Fe(ClO <sub>4</sub> ) <sub>2</sub> Binding. 183
Table 4.5:	Collection of Data & Constants from Kinetic Studies on the Ferrous Sulphate-Bipyridyl Membrane System. 184
Table 4.6	Collection of Data & Constants from Kinetic Studies on the Ferrous Chloride-Bipyridyl Membrane System. 185
Table 4.7:	Collection of Data & Constants from Kinetic Studies on the Ferrous Perchlorate-Bipyridyl Membrane System. 186
Table 4.8:	Data from [Fe <sup>2+</sup> ] 'Hopping' Experiments. 198
Table 4.9:	Collection of Equilibrium Constant Data. 208
Table 5.1:	Permeability Data for Selected Metal Salts through PolyHEMA Membranes. 224
Table 5.2:	Crystal, Stoke's & Hydrodynamic Radii for Some Ions. 228

Table 5.3:	Permeability of Selected Metal Salts through Vinylpyridine-Based Membranes.	230
Table 5.4:	Permeability of Selected Metal Salts through Vinylbipyridine-Based Membranes.	231
Table 5.5:	Permeation Data for Ligand-Based Membranes & Stability Constant Data for the Free Ligands.	236
Table 5.6:	Calculated Data for the Number of Water Molecules/Complex.	244
Table 5.7:	Transport Data for Metal Salts in Competition Studies: Precomplexed Systems.	248
Table 5.8:	Transport Data for Metal Salts in Competition Studies: Binary Salt Systems.	250
Table 5.9:	Single & Binary Salt Transport Data for Pyridyl-Based Copolymer Membranes.	250
Table 6.1:	Membranes Tested with Entrapped Macrocycles.	298
Table 6.2:	Competitive Transport Data for Macrocycle-Entrapped Membranes.	302
Table 6.3:	Stability Constants for Macrocyclic Ligands in Solution.	303

## LIST OF FIGURES.

	<u>Page</u>
Figure 1.1: Classes of Metal-Containing Polymers.	29
Figure 1.2(a): Structure of SPHERON OXINE 1000 HEMA-Based Chelating Resin.	32
Figure 1.2(b): Structure of SPHERON THIOL 1000 HEMA-Based Chelating Resin.	32
Figure 1.3(a): Structure of HEMA/DIOP:Rh(I) Copolymer for Catalytic Hydrogenations.	32
Figure 1.3(b): Structure of HEMA/Phoshinopyrrolidine:Rh(I) Copolymer for Catalytic Hydrogenations.	32
Figure 1.4: The Nature of Water in Hydrogel Polymers.	34
Figure 1.5: Structure of 4-Vinyl Pyridine.	36
Figure 1.6: Structure of 2,2'-Bipyridine.	38
Figure 1.7: Series of Vinyl-Substituted 2,2'-Bipyridines.	39
Figure 1.8: Membrane Filtration Spectrum.	40
Figure 1.9: The Principle of Donnan-Dialysis.	42
Figure 2.1(a): <sup>1</sup> H-Spectrum of 4-Vinylpyridine.	49
Figure 2.1(b): <sup>13</sup> C-(J-Mod) Spectrum of 4-Vinylpyridine.	49
Figure 2.2: Structure of 4-Vinylpyridine.	50
Figure 2.3: The Preparation of 4-Methyl 4'-Vinyl 2,2'-Bipyridine.	51
Figure 2.4(a): Scheme for Lithium Diisopropylamine Formation.	54
Figure 2.4(b): Scheme for Lithiation of Dimethyl Bipyridine.	54
Figure 2.4(c): Scheme for 4-Methyl 4'-Methoxyethyl Bipyridine Formation.	55
Figure 2.5: Scheme for 4-Methyl 4'-Vinyl Bipyridine Formation.	56
Figure 2.6: Numbering Scheme in Bipyridyl Derivatives.	57
Figure 2.7(a): <sup>1</sup> H-Spectrum of 4,4'-Dimethyl 2,2'-Bipyridine.	58
Figure 2.7(b): <sup>13</sup> C-(J-Mod) Spectrum of 4,4'-Dimethyl 2,2'-Bipyridine.	58
Figure 2.8(a): <sup>1</sup> H-Spectrum of 4-Methyl 4'Methoxyethyl 2,2'-Bipyridine.	59
Figure 2.8(b): <sup>13</sup> C-(J-Mod) Spectrum of 4-Methyl 4'Methoxyethyl-2,2'-Bipyridine.	59
Figure 2.9(a): <sup>1</sup> H-Spectrum of 4-Methyl 4'-Vinyl-2,2'-Bipyridine.	61

Figure 2.9(b):	$^{13}\text{C}$ -( <i>J</i> -Mod) Spectrum of 4-Methyl 4'-Vinyl-2,2'-Bipyridine.	61
Figure 2.10:	Representation of a Membrane Mould.	64
Figure 2.11:	Schematic Representation of the Pye-Unicam SP8-100 Spectrophotometer.	71
Figure 2.12:	Schematic for the SP8-100/BBC Micro Interface.	72
Figure 2.13(a):	SCANSPEC Absorption Spectrum of $\text{Co}(\text{SCN})_2$ .	74
Figure 2.13(b):	SCANSPEC Absorption Spectrum of $\text{NiCl}_2$ .	74
Figure 2.14:	Kinetics Trace of $\text{Fe}^{2+}$ Binding to a VBipy Membrane.	76
Figure 2.15:	Hypothetical Stress-Strain Curve.	77
Figure 2.16:	Electrochemical Cell for CWE.	80
Figure 2.17:	Three-Electrode Cell Cyclic Voltammetry Arrangement.	82
Figure 2.18:	Reaction at a Polymer Modified Electrode.	83
Figure 2.19(a):	Permeability Cell Design for Single TM Solution.	85
Figure 2.19(b):	Permeability Cell Design for Mixed TM Solution.	85
Figure 2.20:	Proposed Spectrophotometric Arrangement for the Study of TM Ion-Transport.	88
Figure 2.21:	Conductimetric Arrangement for the Study of TM Ion-Transport.	89
Figure 2.22(a):	CONDUCTIPILOT Permeability Run for $\text{NiNO}_3$ through a PolyHEMA Membrane.	91
Figure 2.22(b):	CONDUCTIPILOT Permeability Run for $\text{CuCl}_2$ through a VBipy/HEMA Membrane.	91
Figure 3.1(a):	HEMA:VBipy Ratios for Various Comonomer Mixes.	99
Figure 3.1(b):	HEMA:4VPy Ratios for Various Comonomer Mixes.	99
Figure 3.2:	Variation of EWC as a Function of Ligand Loading.	100
Figure 3.3:	Variation of TM Salt Partition into PolyHEMA Membranes.	101
Figure 3.4:	TM Content Associated with Ligand-Modified Membranes.	102
Figure 3.5(a):	Ratio of [TM]:[Ligand] in Pyridyl-Polymer Membranes.	103
Figure 3.5(b):	Ratio of [TM]:[Ligand] in Bipyridyl-Polymer Membranes.	104
Figure 3.6:	Correlation of Electronic Configuration and Spectroscopic Terms for Octahedral $\text{Cu}(\text{II})$ .	105
Figure 3.7:	Visible Absorption Spectra of $\text{Cu}(\text{II})$ Complexes with Pyridine.	107

Figure 3.8(a):	Effect of [Ligand] on Cu(II) Visible Absorption Spectra of Pyridyl-Copolymers.	108
Figure 3.8(b):	Effect of Leaching Cu(II) from Pyridyl Copolymers.	108
Figure 3.9:	Effect of [VPy]:[Cu(II)] Ratio on Pyridine-Based Membrane Coordination Chemistry: (A) High [Cu(II)] - (C) Low [Cu(II)].	109
Figure 3.10:	Effect of Cu(II) on the Visible Absorption Spectra of 8% VPy-Based Copolymer Membranes.	111
Figure 3.11(a):	Effect of Dehydrating CuCl <sub>2</sub> -Soaked Pyridyl Copolymer Membranes on Visible Absorption Spectra.	112
Figure 3.11(b):	Effect of Dehydration on Coordination Chemistry in Pyridyl Copolymer Membranes.	113
Figure 3.12:	Cu(II) <i>bis</i> (Bipyridyl Polymer) complex.	115
Figure 3.13(a):	Effect of [Ligand] on Cu(II) visible Absorption Spectra of Bipyridyl-Copolymers.	114
Figure 3.13(b):	Effect of Leaching Cu(II) from Bipyridyl-Copolymers.	114
Figure 3.14:	Correlation of Spectroscopic Terms and Absorption Bands for Co(II).	117
Figure 3.15(a):	Effect of [Ligand] on Co(II) Spectra of Pyridyl-Copolymer Membranes.	119
Figure 3.15(b):	Absorption Spectrum of Co(SCN) <sub>2</sub> in Pyridyl-Copolymers.	119
Figure 3.16:	Effect of Dehydration on the Coordination Chemistry of Co(II) in Pyridyl-Copolymer Membranes.	121
Figure 3.17:	Effect of Dehydration on the Visible Absorption Spectra of Co(II)-Coordinated Pyridyl-Copolymer Membranes.	121
Figure 3.18:	Visible Absorption Spectra of HEMA:VBipy-Copolymer Membranes Soaked in CoCl <sub>2</sub> .	123
Figure 3.19:	Octahedral Co(II) <i>tris</i> (Bipyridyl Copolymer) Complex.	124
Figure 3.20:	Visible Absorption Spectra of Co(II) <i>tris</i> (VBipy) in Membranes of Various Ligand Loadings.	126
Figure 3.21:	Visible Absorption Spectra Showing the Reoxidation of a Co(II) <i>tris</i> (VBipy) Membrane.	127
Figure 3.22:	First Order Plot for the Reoxidation of Co(II) <i>tris</i> (VBipy).	127
Figure 3.23:	Effect of Co(I)/Co(II) Redox Cycling on Absorbance Maxima @ 455nm.	129

Figure 3.24:	Proposed Mechanism for the Reduction of Co(II) to Co(I).	131
Figure 3.25:	Comparison of the Rate of Co(I) Reoxidation in Hydrated & Dehydrated Membranes.	132
Figure 3.26:	Electronic Configuration and Transitions for the Fe(II)- <i>tris</i> (Bipyridine) Complex.	133
Figure 3.27:	Effect of [Ligand] on Fe(II) Spectra of Bipyridyl Copolymer Membranes.	135
Figure 3.28:	Effect of Anion on Abs <sub>∞</sub> of Fe(II) <i>tris</i> -complex.	136
Figure 3.29:	Potentiometric Response of a PolyHEMA CWE in CuCl <sub>2</sub> .	138
Figure 3.30:	Potentiometric Response of a 2%Pyridyl-Based Hydrogel CWE in CuCl <sub>2</sub> .	139
Figure 3.31:	Cyclic Voltammogram of 0.1M KCl.	140
Figure 3.32:	Cyclic Voltammogram of a PolyHEMA Coating.	141
Figure 3.33:	Cyclic Voltammograms of (a) 2%VPy Copolymer: (b) 2%VBipy Copolymer: (c) Voltage Sweep of (a): (d) Voltage Sweep of (b).	142
Figure 3.34:	Cyclic Voltammograms of (a) 2%VBipy:[Fe(II)]: (b) 2%VBipy:[Cu(II)]: (c) 2%VBipy:[Co(II)].	144
Figure 3.35:	Cyclic Voltammograms of (a) 2%VBipy:[Fe(II)] Copolymer: (b) 2%VPy:[Cu(II)] Copolymer: (c) Voltage Sweep of (a): (d) Voltage Sweep of (b).	145
Figure 3.36:	(a) 3-Centred Cross-Link of the <i>tris</i> (VBipy) Fe(II) Complex: (b) 4-Centred Cross-Link of the <i>tetra</i> (VPy) Cu(II) Complex.	147
Figure 3.37:	Polymer-Immobilised <i>bis</i> & <i>tris</i> (Acac) Complexes.	148
Figure 3.38(a):	Load-Extension Curves for VBipy-Based Membranes.	151
Figure 3.38(b):	Load-Extension Curves for VPy-Based Membranes.	151
Figure 3.39(a):	Load-Extension Curves for VBipy:[Fe(II)]-Based Membranes.	152
Figure 3.39(b):	Load-Extension Curves for VPy:[Cu(II)]-Based Membranes.	152
Figure 3.40(a):	Effect of Cross-Linking on σ for VBipy:[Fe(II)] Copolymers.	154
Figure 3.40(a):	Effect of Cross-Linking on ε <sub>b</sub> for VBipy:[Fe(II)] Copolymers.	154
Figure 3.41(a):	Effect of Cross-Linking on σ for VPy:[Cu(II)] Copolymers.	155
Figure 3.41(b):	Effect of Cross-Linking on ε <sub>b</sub> for VPy:[Cu(II)] Copolymers.	155
Figure 3.42(a):	Stress-Strain Plots for VBipy Polymer.	158
Figure 3.42(b):	Stress-Strain Plots for VBipy:[Fe(II)] Polymer.	158

Figure 3.43(a):	Stress-Strain Plots for Vpy Polymer.	159
Figure 3.43(b):	Stress-Strain Plots for VPy:[Cu(II)] Polymer.	159
Figure 4.1:	Confirmation of Beer's Law for Polymer-Bound Iron(II) <i>tris</i> (Bipyridine) Complex.	166
Figure 4.2:	Confirmation of Beer's Law for the Iron(II) <i>tris</i> (Vinyl-Bipyridine) Complex.	166
Figure 4.3:	Low Concentration Binding Profile for 0.01M FeSO <sub>4</sub> .	171
Figure 4.4:	Kinetics for the Coordination of Ferrous Sulphate to Bipyridyl-Based Membranes.	173
Figure 4.5:	Kinetics for the Coordination of Ferrous Chloride to Bipyridyl-Based Membranes.	174
Figure 4.6:	Kinetics for the Coordination of Ferrous Perchlorate to Bipyridyl-Based Membranes.	175
Figure 4.7:	First Order Guggenheim Plot of (0.08M) FeSO <sub>4</sub> Binding Kinetics.	179
Figure 4.8:	Kezdy/Swinbourne First Order Plot of (0.08M) FeSO <sub>4</sub> Data.	181
Figure 4.9:	Kezdy/Swinbourne Method for Estimating A <sub>∞</sub> for (0.08M) FeSO <sub>4</sub> .	181
Figure 4.10:	Second Order Kezdy/Swinbourne Plot for (0.24M) FeCl <sub>2</sub> Binding Kinetics.	182
Figure 4.11:	Second Order Kezdy/Swinbourne Plot for (0.08M) Fe(ClO <sub>4</sub> ) <sub>2</sub> Binding Kinetics.	183
Figure 4.12:	Visible Spectra for the <i>mono</i> - & <i>tris</i> - Bipyridyl Complexes with Fe <sup>2+</sup> .	190
Figure 4.13:	Early Kinetic Stages for the Complexation of Fe <sup>2+</sup> to a Vinyl-Bipyridine Copolymer Membrane.	190
Figure 4.14:	Variation of K <sub>C</sub> with 1/[Fe(II)].	192
Figure 4.15:	Proposed Second Order Mechanism for k <sub>2</sub> Stage.	194
Figure 4.16:	Overall Scheme for Cl <sup>-</sup> & ClO <sub>4</sub> <sup>-</sup> Kinetics.	194
Figure 4.17:	Variation of A <sub>∞</sub> with [Fe <sup>2+</sup> ] for Ferrous Chloride.	196
Figure 4.18:	Variation of A <sub>∞</sub> with [Fe <sup>2+</sup> ] for Ferrous Perchlorate.	196
Figure 4.19:	Variation of Computed Rate Constant (K <sub>C</sub> ) with [Fe <sup>2+</sup> ].	197

Figure 4.20	Variation of Kezdy/Swinbourne Slopes for $\text{Cl}^-$ & $\text{ClO}_4^-$ with $[\text{Fe}^{2+}]$ .	197
Figure 4.21:	$[\text{Fe}^{2+}]$ 'Hopping' Experiment, Showing a Hysteresis-Type Effect.	200
Figure 4.22:	Baxendale's Data on the Influence of $[\text{Fe}^{2+}]$ on $[\text{Fe-tris(Bipy)}]$ Formation.	200
Figure 4.23:	Equilibrium Dependence of $A_\infty$ for $\text{FeCl}_2$ .	203
Figure 4.24:	Equilibrium Dependence of $A_\infty$ for $\text{Fe}(\text{ClO}_4)_2$ .	203
Figure 4.25:	$\text{FeCl}_2$ Absorbance Data to Fit Equation 4.39.	204
Figure 4.26:	$\text{Fe}(\text{ClO}_4)_2$ Absorbance Data Fit to Equation 4.39.	204
Figure 4.27:	Final Absorbance Relationship that Describes $\text{FeCl}_2$ Equilibrium.	207
Figure 4.28:	Final Absorbance Relationship that Describes $\text{Fe}(\text{ClO}_4)_2$ Equilibrium.	207
Figure 4.29:	Variation of $A_\infty$ with $[\text{Fe}^{2+}]$ for Ferrous Sulphate.	209
Figure 4.30:	Variation of Rate Constants with $[\text{Fe}^{2+}]$ for Ferrous Sulphate.	209
Figure 4.31:	Proposed Mechanism for the Coordination of Ferrous Salts to VinylBipyridine-Based Hydrogel Membranes.	211
Figure 4.32:	Spectrophotometer Cell Design (Oblique View).	215
Figure 4.33:	Spectrophotometer Cell Design (Top View).	215
Figure 5.1:	Permeation Mechanism for CCMC Dialysis in a Liquid Membrane.	218
Figure 5.2:	Permeability of Metal Chloride Salts through PolyHEMA.	225
Figure 5.3:	Permeability of Cobalt Salts through PolyHEMA.	226
Figure 5.4:	Relationship Between EWC, $P_c$ & Lag-Time for $\text{Co(II)}$ Salts.	227
Figure 5.5:	Permeability of Metal Chlorides through VinylPyridine Copolymer Membranes.	232
Figure 5.6:	Permeability of Metal Chlorides through Vinylbipyridine Copolymer Membranes.	233
Figure 5.7:	Relationship Between Lag-times through VinylPyridine Copolymer Membranes and $\log K_1$ Stability Constants for Free Complex.	237

Figure 5.8:	Relationship Between Lag-times through VinylBipyridine Copolymer Membranes and logK <sub>3</sub> Stability Constants for Free Complex.	237
Figure 5.9:	Relationship Between EWC & Lag-Time for Various Metal Chlorides.	238
Figure 5.10:	Effect of [Ligand] on CuCl <sub>2</sub> Transport through HEMA:VPy Copolymer Membranes.	239
Figure 5.11:	Plot of 1/Lag-Time Versus Concentration of CuCl <sub>2</sub> .	241
Figure 5.12:	The Effect of Ligand Concentration on Cu <sup>2+</sup> Transport Across Pyridyl-Copolymer Membranes.	240
Figure 5.13:	The Effect of Ligand Concentration on Cu <sup>2+</sup> Transport Across Bipyridyl-Copolymer Membranes.	240
Figure 5.14:	The Relationship Between EWC, %VPy & Lag-Time for CuCl <sub>2</sub> .	243
Figure 5.15:	Effect of VBipy Loading within Membranes on Lag-Time of CuCl <sub>2</sub> .	245
Figure 5.16:	Permeability of Cu(II) & Mn(II) through Precomplexed 2% Vinylpyridine-Based Copolymer Membranes.	247
Figure 5.17:	Permeability of Cu(II) & Mn(II) through Precomplexed 2% Vinylbipyridine-Based Copolymer Membranes.	247
Figure 5.18:	Permeability of Cu(II)/Mn(II) Binary Salt Solution through 2% Vinylpyridine-Based Copolymer Membranes.	249
Figure 5.19:	Permeability of Cu(II)/Mn(II) Binary Salt Solution through 2% Vinylbipyridine-Based Copolymer Membranes.	249
Figure 5.20:	Permeability of 0.25M CaCl <sub>2</sub> through HEMA-Only & 2% Vinylpyridine-Based Copolymer Membranes.	251
Figure 5.21:	Permeability of Ca(II)/Cu(II) Binary Salt Solution through 2% Vinylpyridine-Based Copolymer Membranes.	251
Figure 5.22:	Permeability Coefficient for TM Ions in Different Membrane Systems.	252
Figure 6.1:	(a) Haem <i>b</i> ; (b) Chlorophyll <i>a</i> ; (c) Vitamin B <sub>12</sub> .	258
Figure 6.2:	(a) Valinomycin-K <sup>+</sup> ; (b) Enterochelin-Fe <sup>3+</sup> .	259

Figure 6.3:	(a) O <sub>2</sub> N <sub>2</sub> -Macrocycles Appended to Polystyrene; (b) O <sub>2</sub> N <sub>3</sub> -Macrocycle Appended to Silica Gel.	260
Figure 6.4:	Selection of Macrocycles Chosen for Synthesis.	262
Figure 6.5:	Route to N,O-Donor Macrocycle Synthesis.	263
Figure 6.6:	<sup>1</sup> H-NMR Spectrum <i>O</i> -en.	265
Figure 6.7:	<sup>13</sup> C-( <i>J</i> -Mod) NMR Spectrum of <i>O</i> -en.	266
Figure 6.8:	<sup>1</sup> H-NMR Spectrum <i>O</i> -tn.	268
Figure 6.9:	<sup>13</sup> C-( <i>J</i> -Mod) NMR Spectrum of <i>O</i> -tn.	269
Figure 6.10:	<sup>1</sup> H-NMR Spectrum <i>O</i> -en- <i>N</i> -tn.	271
Figure 6.11:	<sup>13</sup> C-( <i>J</i> -Mod) NMR Spectrum of <i>O</i> -en- <i>N</i> -tn.	272
Figure 6.12:	<sup>1</sup> H-NMR Spectrum <i>O</i> -en- <i>NH</i> -tn.	274
Figure 6.13:	<sup>13</sup> C-( <i>J</i> -Mod) NMR Spectrum of <i>O</i> -en- <i>NH</i> -tn.	275
Figure 6.14:	<sup>1</sup> H-NMR Spectrum <i>O</i> -tn- <i>N</i> -tn.	278
Figure 6.15:	<sup>13</sup> C-( <i>J</i> -Mod) NMR Spectrum of <i>O</i> -tn- <i>N</i> -tn.	279
Figure 6.16:	<sup>1</sup> H-NMR Spectrum <i>O</i> -tn- <i>NH</i> -tn.	281
Figure 6.17:	<sup>13</sup> C-( <i>J</i> -Mod) NMR Spectrum of <i>O</i> -tn- <i>NH</i> -tn.	282
Figure 6.18:	Mechanism for Template Synthesis of Macrocycles.	285
Figure 6.19:	Route for Functionalisation of Macrocycle.	289
Figure 6.20:	<sup>1</sup> H-NMR Spectrum of Reaction Product Between <i>O</i> -en- <i>NH</i> -tn & Allyl Chloride.	291
Figure 6.21:	<sup>13</sup> C-( <i>J</i> -Mod) NMR Spectrum of Reaction Product Between <i>O</i> -en- <i>NH</i> -tn & Allyl Chloride.	292
Figure 6.22:	<sup>1</sup> H-NMR Spectrum of Reaction Product Between <i>O</i> -en- <i>NH</i> -tn & Acryloyl Chloride.	294
Figure 6.23:	<sup>13</sup> C-( <i>J</i> -Mod) NMR Spectrum of Reaction Product Between <i>O</i> -en- <i>NH</i> -tn & Acryloyl Chloride.	295
Figure 6.24:	Permeability of Cu(II)/Ni(II) Binary Salt Solutions through Membranes Containing Entrapped Macrocycles.	299
Figure 6.25:	Permeability of Cu(II)/Co(II) Binary Salt Solutions through Membranes Containing Entrapped Macrocycles.	300
Figure 6.26:	Permeability of Ni(II)/Co(II) Binary Salt Solutions through Membranes Containing Entrapped Macrocycles.	301
Figure 6.27:	Comparison of Permeabilities for TM Ion Combinations through Membranes Containing Entrapped Macrocycles.	302

Figure 6.28: Comparison of Lag-Times for TM Ion Combinations  
through Membranes Containing Entrapped Macrocycles.

303

## LIST OF ABBREVIATIONS.

<b>AAS</b>	Atomic Absorption Spectroscopy.
<b>Abs</b>	Absorbance.
<b>Abs<sub>∞</sub></b>	Absorbance at Time Infinity.
<b>A<sub>∞</sub><sup>obs</sup></b>	Observed Abs <sub>∞</sub> .
<b>A<sub>∞</sub><sup>c</sup></b>	Computer Calculated Abs <sub>∞</sub> .
<b>A<sub>∞</sub><sup>g</sup></b>	Guggenheim Calculated Abs <sub>∞</sub> .
<b>A<sub>∞</sub><sup>k/s</sup></b>	Kezdy/Swinbourne Calculated Abs <sub>∞</sub> .
<b>Abs<sub>t</sub></b>	Absorbance at Time t.
<b>AZBN</b>	Azo-Bis-Isobutyronitrile.
<b>Bipy, dipy</b>	2,2'-Bipyridine.
<b>CWE</b>	Coated Wire Electrode.
<b>CV</b>	Cyclic Voltammetry.
<b>Δ</b>	Crystal-Field Splitting.
<b>ε<sub>b</sub></b>	Elongation to Break.
<b>ε<sub>max</sub></b>	Extinction Coefficient at Maximum Absorbance.
<b>EWc</b>	Equilibrium Water Content.
<b>EGDM, EDMA</b>	Ethylene Glycol Dimethacrylate
<b>FT-IR</b>	Fourier Transform Infra-Red.
<b>HEMA</b>	2-Hydroxyethyl Methacrylate.
<b>ISE</b>	Ion-Selective Electrode.
<b>k<sub>c</sub></b>	Computer-Calculated Rate Constant.
<b>k<sub>g</sub></b>	Guggenheim-Calculated Rate Constant.
<b>k<sub>k/s</sub></b>	Kezdy/Swinbourne Calculated Rate Constant.
<b>NMR</b>	Nuclear Magnetic Resonance.
<b>O-en-NH-tn</b>	6,7,8,9,10,11,17,18-Octa-Hydro-5H-Dibenzo [e,n][1,4]Dioxa[8,12] Diazacyclopenta-Decine.

<b><i>O</i>-tn-<i>NH</i>-tn</b>	3,4:10,11-Dibenzo-1,12-Diaza-5,8-Dioxacyclo Pentadecane-1,11-Diene.
<b>P<sub>c</sub></b>	Permeability Coefficient.
<b>σ</b>	Tensile Strength.
<b>SCE</b>	Saturated Calomel Electrode.
<b>Sm</b>	Partition Coefficient.
<b>SSD</b>	Sum of Squared Differences.
<b>TM</b>	Transition Metal.
<b>t<sub>∞</sub></b>	Time Infinity.
<b>VBipy</b>	4-Methyl 4'-Vinyl 2,2'-Bipyridine.
<b>4VPy, VPy</b>	4-Vinyl Pyridine.

## **CHAPTER ONE**

### **INTRODUCTION.**

**"STRATEGIES FOR THE DESIGN OF A HYDROPHILIC  
COMPLEXING-POLYMER SYSTEM."**

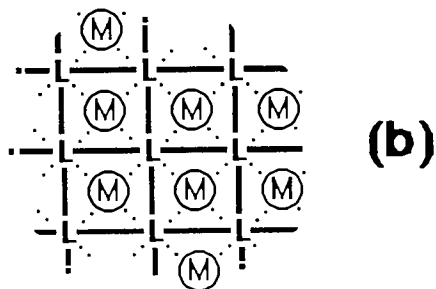
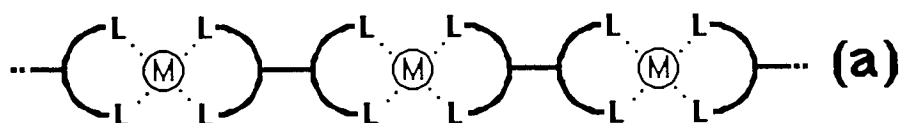
## **1.1 INTRODUCTION.**

Conventionally, polymer chemists have restricted themselves to the preparation of polymers containing the elements C, H, N, O, S, P, Cl and Br. Since the number of readily available metals is well over forty, it is not surprising that in the early 1960's research into metal-containing polymers was initiated. The synthesis of such materials represents an attempt to give an organic polymer inorganic functions. Indeed, virtually every known catalyst has been immobilised on some sort of polymeric support <sup>1-4</sup>, and often the catalytic activity has been enhanced. In the case of some metalloenzymes, the conformation of the macromolecular protein chain is known to control the reactivity of the metal complex active site. Therefore, polymer-metal interactions are of extreme importance in these systems.

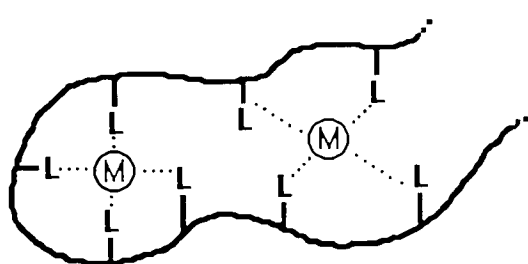
A combination of classification schemes of Tsuchida *et al.* <sup>5</sup> and Hodgkin <sup>6</sup> provides a convenient summary of polymer types (Figure 1.1). The complexation of metal ions with bifunctional ligands can lead to the formation of a polymer in which the metal is an integral part of the backbone chain (Figure 1.1(a)). The complexation step is analogous to a condensation polymerisation, which often lends to the name 'polycondensation coordination polymer' to the product. 'Network-coordinated polymers' (Figure 1.1(b)) result from reaction between functional groups on the ligand, made possible by a *template-effect* induced by metal ion coordination. The poly(metallo-phthalocyanine) chelated-type structure is a classic example of this sort of polymer.

The other broad class of chelating polymer is that in which the ligands are present as pendant groups along the length of the polymer chain (Figure 1.1(c-f), overleaf).

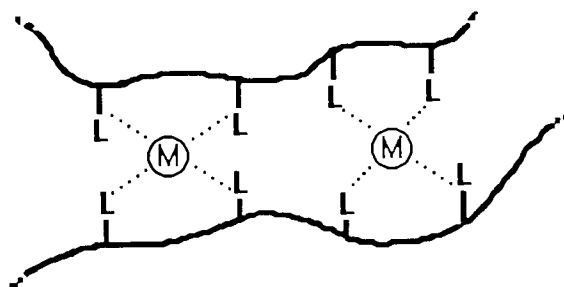
Figure 1.1 Classes of Metal-Containing Polymers.



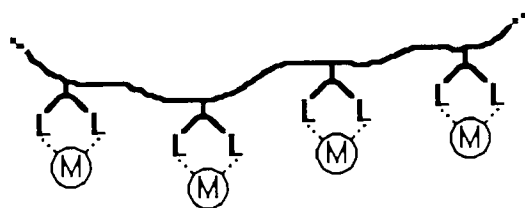
Chain-Linked by Metal Ion Complexation



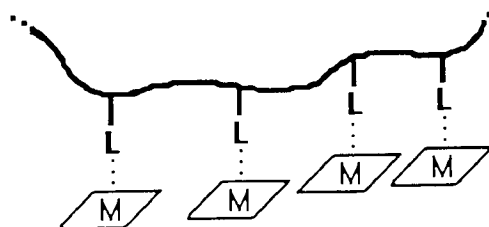
(c)



(d)



(e)



(f)

Chelate-Forming Type

Included within this class of polymer are the ion-exchange resins; they offer the advantage of being stable to removal of the coordinated metal ion from the polymer, leaving the macromolecular integrity intact and thus regenerating the polymeric ligand structure. Typically, complexation may involve metal ion interaction with a number of ligands, either from the same chain to produce an intermolecular bridge (Figure 1.1(c)), or from different chains to give intramolecular bridging structures (Figure 1.1(d)). Alternatively, the pendant ligand may be polydentate in nature and chelate to the metal to produce high stability complexes (Figure 1.1(e)). If the valency of the metal will permit further coordination, then complexation will produce bridged structures as shown previously in Figures 1.1(c) & (d). The polymers produced in this study fall into this pendant-type ligand category of chelating system. Finally, coordination of monodentate pendant ligands such as those in Figure 1.1 (c) & (d) with a metal ion or complex with only one labile position will yield a monodentate pendant complex (Figure 1.1(f)). The absence of bridging structures often means an enhanced solubility and the coordination structure within the polymer is very clear. Although the parent polymers in this case can be thought of as 'super-chelates', once the complex is coordinated the polymer is no longer strictly a chelate-forming type.

Chelating agents are used extensively in a range of applications including therapeutic agents in medicine <sup>7,8</sup>, in analytical chemistry <sup>9</sup> and for the separation of metal ions by ion-exchange materials <sup>10-12</sup>. This has prompted work on the design of ligands for the selective complexation of metal ions in solution <sup>13</sup>. Donor atom selection based on Pearson's hard and soft acid and base principle <sup>14</sup>, coupled with the pioneering work of Lehn and others <sup>15</sup> on molecular architecture, has brought the idea of a 'tailor-made' metal ion-specific ligand system within the reach of the coordination chemist. It was the intention of this project to combine these underlying concepts with 'in-house' polymer

technology to arrive at a deliberately designed hydrophilic complex-forming polymer for use in the aqueous environment.

It is possible to envisage two possible scenarios by careful choice of the ligands for copolymerisation into the proposed hydrophilic complexing systems:

- (a) A polymer that may interact selectively but reversibly with metal ions to produce a system for the separation of specific ions in solution;
- (b) A polymer that will bind 'irreversibly' to a metal to produce a new polymer in which the complexes will be present in what is still predominantly an aqueous environment.

The scope of this work covers both of these areas and this thesis presents results on the formation and characterisation of polymer-metal complexes on the one hand, and the evaluation of a polymeric membrane system for selective metal ion separation on the other.

## **1.2 THE USE OF HYDROGEL POLYMERS.**

In recent years, there has been an increasing application of hydrophilic porous polymers as polymeric matrices for ion-exchange materials, instead of the more traditional hydrophobic alternatives such as polystyrene. For instance, iminodiacetate, ethylenediamine, and mercapto groups amongst others, have been appended to glycidyl methacrylate/ethylene dimethacrylate copolymers (GMA-EDMA) to produce sorbents for metal ion separations<sup>16,17</sup>. Likewise, copolymers of hydroxyethyl methacrylate/ethylene dimethacrylate (SPHERON) have been used to obtain sorbents with salicylic acid<sup>18,19</sup>, thiol<sup>20</sup> and 8-hydroxyquinoline groupings<sup>21-24</sup> (Figure 1.2(a) & (b)). These materials are distinguished by their hydrophilicity, high degree of porosity and large internal surface area, which ensures a rapid attainment of equilibrium during sorption. With characteristics such as

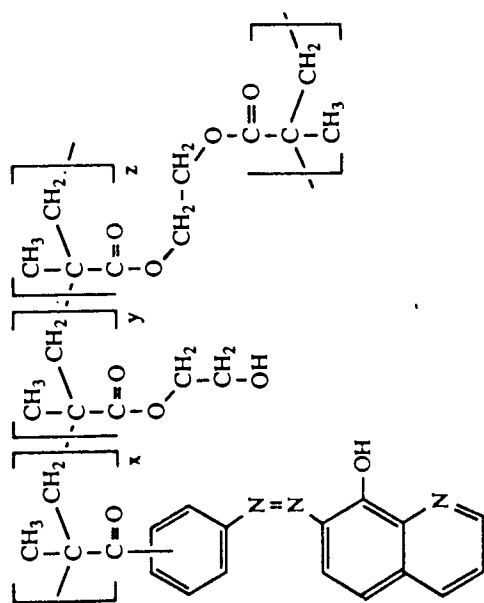


**Figure 1.2(a) Structure of SPHERON OXINE 1000 HEMA-Based Chelating Resin.**

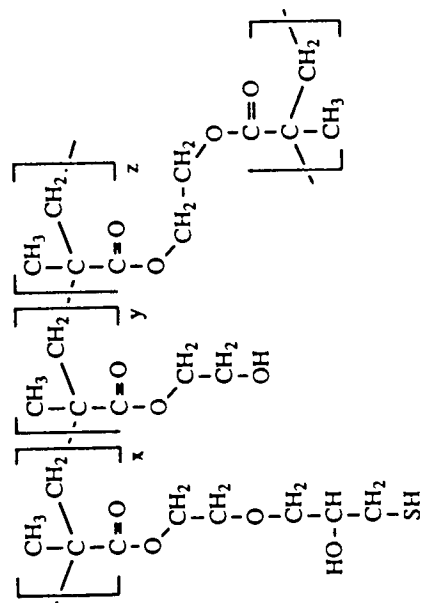


**Figure 1.2(b) Structure of SPHERON THIOL 1000 HEMA-Based Chelating Resin.**

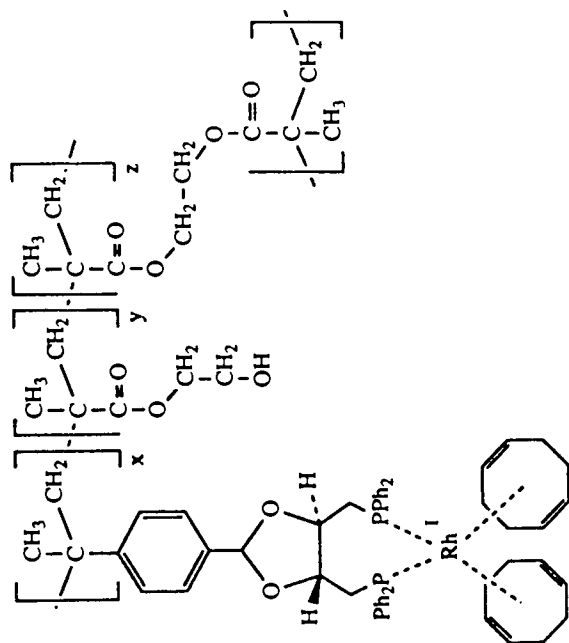


**Figure 1.3(a) Structure of HEMA/DIOP:Rh(I) Copolymer for Catalytic Hydrogenations.**

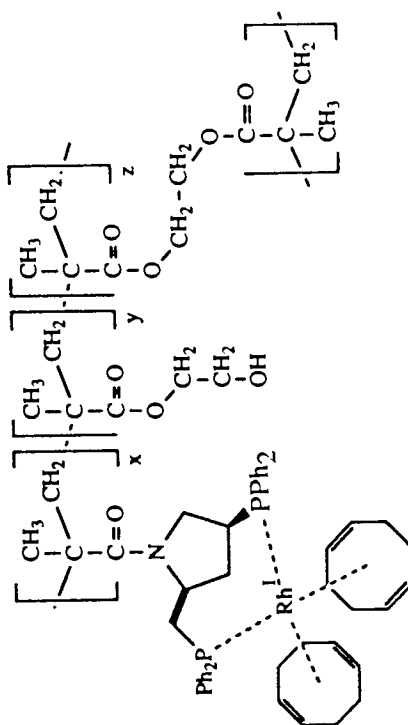


**Figure 1.3(b) Structure of HEMA/Phosphinopyrrolidine:Rh(I) Copolymer for Catalytic Hydrogenations.**

these, it is not surprising that a series of rhodium hydrogenation catalysts have been immobilised on such hydrophilic materials <sup>25,26</sup> in order to take advantage of their ability to swell in polar solvents (Figure 1.3(a) & (b)).

The Speciality Materials Group at Aston has carried out extensive research into such hydrogels, (the term used for the family of synthetic polymers in which the matrix swells but does not dissolve in water). The material used in this study was that used for SPHERON sorbents, poly(2-hydroxyethyl methacrylate) (PHEMA), because it had been previously well-characterised by the group <sup>27-29</sup> and was readily available. It was thought that the presence of interstitial water in the gel may provide a medium for the transport and coordination of metal ions to ligands immobilised within the matrix. The majority of work was performed on free-radically polymerised copolymers fabricated in the form of chelating membranes. These provided an ideal test-bed for the study of metal ion transport through, and coordination to, the ligand-modified systems. The membrane form also ensured reproducibility and allowed direct comparison with previous systems <sup>29</sup>.

### **1.2.1 The Hydrophilic Nature of the Polymer.**

The chemical components of the PHEMA confer the ability to interact with water by hydrogen-bonding through the hydroxyl and other polar functions on the chain. Evidence suggests <sup>30</sup> that the water imbibed by the polymer can be thought of as ranging between two extremes. Water that is intimately associated with the polymer is bound extremely tightly and is known as 'bound' or 'non-freezing' water. Further away from the backbone, and the structuring effects of the chemical groups, there is more mobile or 'freezing' water in the bulk interstitial spaces of the gel matrix (Figure 1.4). The equilibrium water content

(EWC) of the gel is the ratio of the weight of water in the gel, to the weight of gel at hydration (equation 2.1, Chapter Two). This is an extremely important property of the polymer, as it influences the physical characteristics of the gel, such as transport and mechanical properties amongst others.

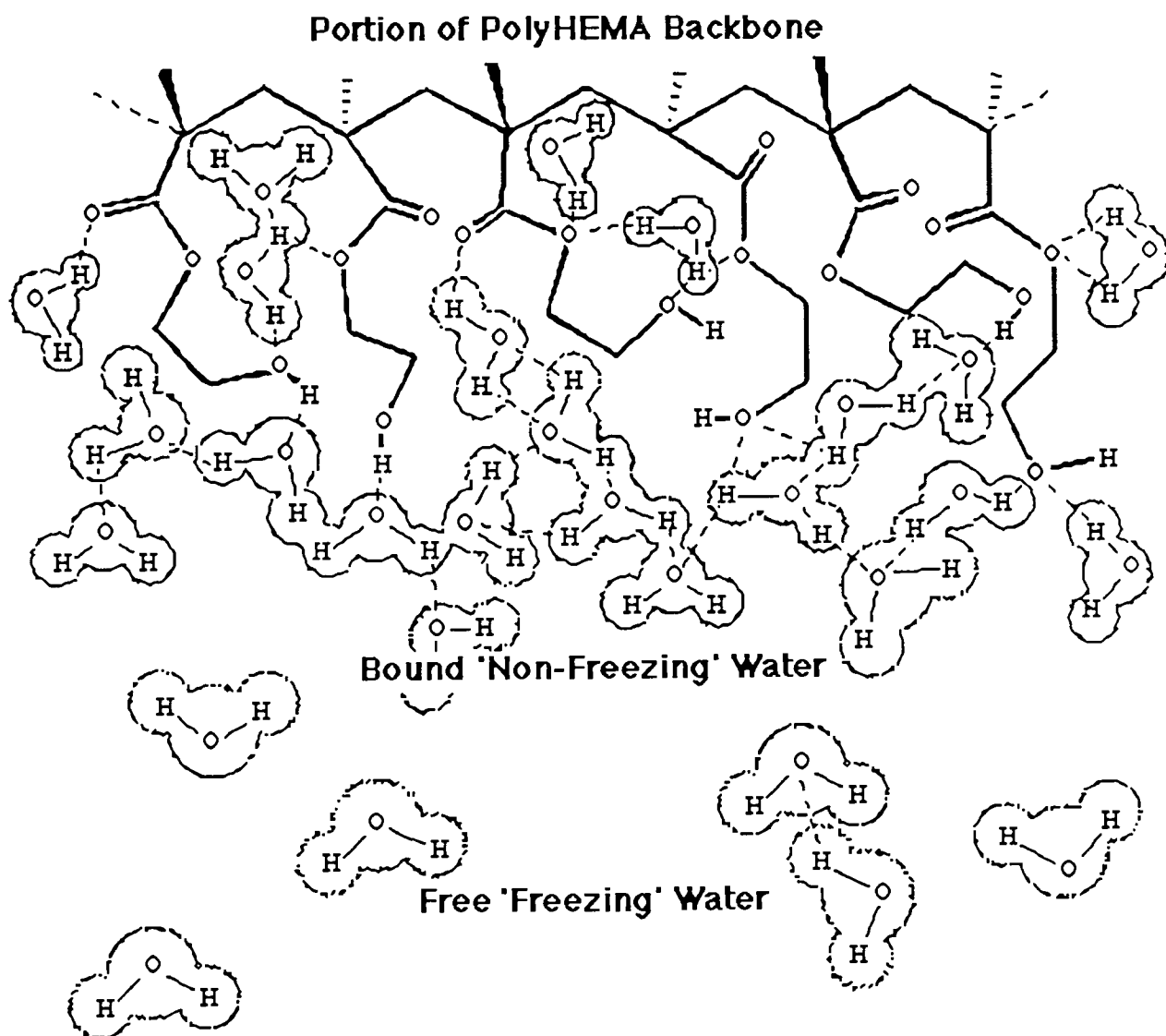


**Figure 1.4 The Nature of Water in Hydrogel Polymers.**

Hydrogel membranes made from PHEMA typically have 40% of the polymer's weight due to imbibed water. It is the bulk water that will provide the medium for transition metal ion diffusion into the chelating membrane systems, and subsequent coordination with the immobilised ligands will then occur in what is still, essentially, an aqueous environment. It

has been noted previously <sup>31,32</sup>, that the rate determining step of the sorption process on a chelating polymer system can thus either be diffusion, chemical reaction, or a combination of both depending on the properties of the polymer, metal ion, nature of the ligand and sorption conditions.

### **1.3 THE CHOICE OF LIGANDS.**

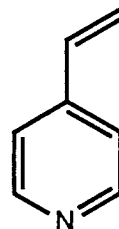
When considering the design of a chelating polymer, the choice of ligands will be determined by a number of factors, not least the proposed function of the system. Organo-metallic polymers used in industry as supported metal catalysts offer many advantages such as ease of separation and recovery. However, problems have arisen when the complexes have tended to be labile resulting in unacceptable degrees of metal leaching. On the other hand, if one considers the design of an ion-specific chelate resin, it is clear that if the ligand forms too strong a complex with the metal the resin cannot be regenerated and it will not fulfill the desired purpose.

It was the author's intention to investigate both the influence of immobilised ligands upon metal-ion transport across chelating hydrogel membranes, and the properties of any interesting polymer-bound complexes that might be formed. To this end, two ligands were sought to satisfy different functions. Both must be versatile enough to interact with a variety of metal ions, but one must yield labile complexes for ion-exchange purposes and the other must form more stable complexes. The final prerequisite in the choice of ligand is that it must possess a vinyl functional group (or a synthetic route to one), to allow copolymerisation with the HEMA comonomer.

### **1.3.1 The Case for a Pyridine Ligand.**

Table 1.1 lists a number of common ion-exchange resins and their chelating moiety. As can be seen, many of the commercial materials are based on iminodiacetate and analogous functionalities <sup>6,10-12</sup>. Recent advances have led to more ion-specific resins containing macrocyclic crown ether <sup>34,35</sup>, diazacrown ether <sup>36,37</sup> and cryptand-type <sup>38-40</sup> groups. However, none of these have an obvious route to vinyl functionalisation without a great deal of involved synthesis. Table 1.2 on the other hand displays a number of pyridine-based chelate resins which have been successfully used in ion-exchange <sup>41,42</sup>. Most however, are supported on hydrophobic matrices and suffer from low loading capacities due to inefficient swelling of the polymer.

**Figure 1.5**  
**Structure of**  
**4-Vinyl Pyridine**



4-Vinyl pyridine (4-VPy, Figure 1.5) is a widely used, easily available material that would be an ideal comonomer for the fabrication of chelating membranes. The synthesis and investigation of polymers based on 4-VPy is well documented in the literature <sup>43-48</sup>. Free-radical bulk polymerisation of the material has been known for some time, and so copolymerisation with HEMA should present few problems. For these reasons, 4-VPy was chosen as one of the ligands for use in this work.

### **1.3.2 The Case for a Bipyridine Ligand.**

2,2'-Bipyridine (Bipy, Figure 1.6 overleaf), its derivatives and structural relatives, are known to show remarkable versatility in complexing a large number of metal ions <sup>49-52</sup>.

Functional / Chelating Group	Commercial Name
	IMAC SYN 101 <sup>a</sup> Duolite ES 466 <sup>b</sup> Dowex A-1 <sup>c</sup> Chelex 100 <sup>d</sup> Dianion CR-20 <sup>e</sup> IRC-718 <sup>f</sup> Ligandex I <sup>g</sup>
	Ligandex E <sup>g</sup>
	Duolite ES 346 <sup>d</sup>
	IMAC TMR <sup>a</sup> Duolite ES 465 <sup>b</sup>
	Srafron NMRR <sup>a</sup> Ionac SR-3 <sup>f</sup>
	Duolite ES 467 <sup>b</sup>
	Kryptofix 221B <sup>j</sup>

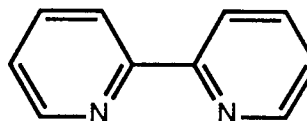
<sup>a</sup> Diamond Shamrock  
<sup>b</sup> Duolite Int. (Co. of Diamond Shamrock)  
<sup>c</sup> Dow Chemicals, USA  
<sup>d</sup> Bux Rad  
<sup>e</sup> Mitsubishi  
<sup>f</sup> Rohm & Haas  
<sup>g</sup> Reanal, Budapest  
<sup>h</sup> Ayalon, Haifa (Israel)  
<sup>i</sup> Ionac, Sybron Chem. Dev., USA  
<sup>j</sup> Parash Chem. Co., Utah USA

Chelating Group	Manufacturer	Commercial Name	Polymer Matrix
	Sumitomo, Japan	Sumichelate CR-2	Polyvinyl pyridine
	Dow Chemicals, USA	Dowex XF-4195 XF-4196	Polystyrene
	Dow Chemicals, USA	Dowex XFS-43084	Polystyrene
	Mintek, Randburg, Transvaal.	PI 1, 2, 3 & 4	Polystyrene
		Promising Resin <sup>41</sup> Under Development	

**Table 1.1 Selection of Commercially Available Ion-Exchange Resins.**

**Table 1.2 Ion-Exchange Resins Based on the Pyridine Ligand.**

**Figure 1.6**  
**Structure of**  
**2,2'-Bipyridine**



Bipy is a conjugated bidentate ligand which chelates to metal ions *via* the two basic nitrogen atoms in the heterocyclic rings, which function as effective  $\pi$ -acceptors in back-bonding. Amongst other properties, it is the excellent ion-binding capability, the ability to stabilise unusual oxidation states and the potential for complexes with a versatile photoactivity which makes this ligand a desirable choice for incorporation into polymers.

There has been a vast amount of work concerning the immobilisation of this ligand as a pendant group on a polystyrene matrix and subsequent reaction with metals such as tungsten <sup>53</sup> and palladium <sup>54-56</sup>, to produce a series of polymer-bound catalysts for hydrogenation reactions <sup>57-60</sup> (analogous to the polymer type described by Figure 1.1(e)). There have also been reports of the polymerisation of functionalised Bipy derivatives directly into the polymer backbone, such as Necker's diaminobipyridine-TDI polyureas <sup>61,62</sup> and Miller's dicarboxybipyridine-based polyesters <sup>63</sup>. These materials however, are few compared with the pendant type, as they are generally more difficult to work with and show no real advantages.

By far the most prevalent method in the literature for obtaining a Bipy-pendant polymer is the direct homo or copolymerisation of a vinyl functionalised Bipy derivative. Much of this work has arisen as a consequence of the extensive studies by Murray, Meyer, Calvert and others <sup>64-71</sup>, on the electropolymerisation of vinyl polypyridyl ligands and their complexes. Figure 1.7 shows a number of vinyl functionalised 2,2'-bipyridine derivatives

that have reported syntheses in the literature. 6-Vinyl-2,2'-bipyridine was first synthesised by Woltermann in 1976 <sup>72</sup> and since then routes to 4-methyl-4'-vinyl-2,2'-bipyridine by Ghosh & Spiro <sup>73</sup>, 6,6'-dimethyl-5-vinyl-2,2'-bipyridine by Newkome <sup>74</sup> and 6-methyl-4-vinyl, 3-methyl-6-vinyl & 4-methyl-4'-vinyl-2,2'-bipyridine by Kaschig & Lohmann <sup>75</sup> have been developed.

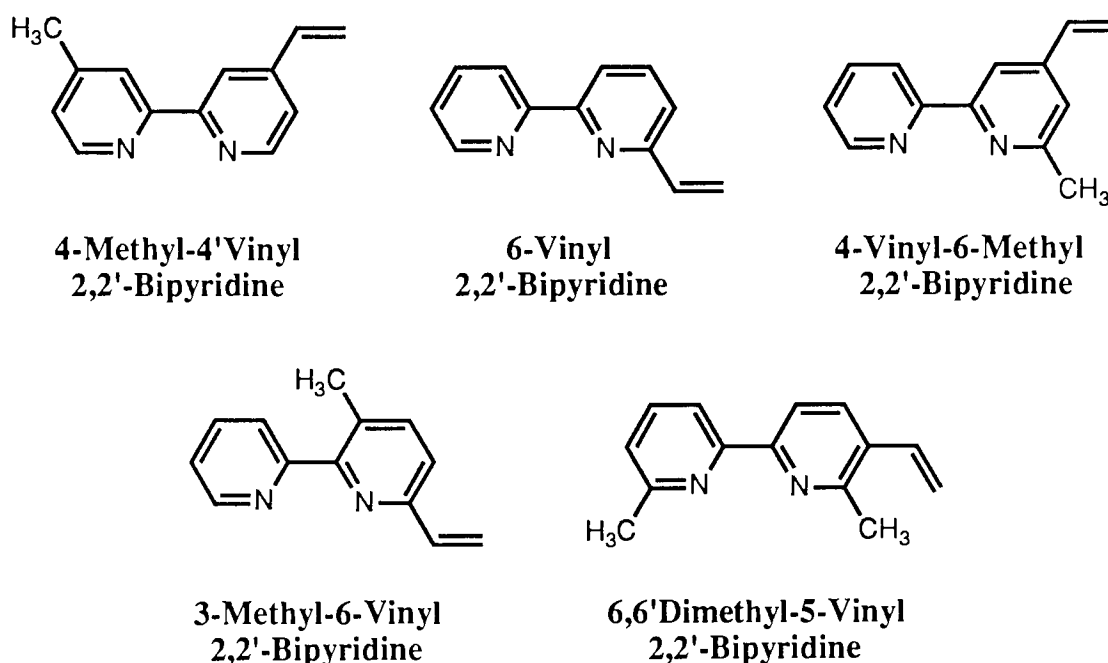


**Figure 1.7 Series of Vinyl-Substituted 2,2'-Bipyridines.**

The preparation of polymers from these materials, and their application to (i) metal ion-specific absorption in solution studies and, (ii) as supports for catalytic complexes, is well documented in the literature <sup>75-81</sup>. These materials have been previously copolymerised with the HEMA monomer <sup>75</sup>, but never in membrane form. There is therefore, a great deal of scope and potential for the use of these compounds in a chelating membrane environment.

#### **1.4 THE APPLICATION OF MEMBRANE PROCESSES.**

A membrane can be described as a barrier which displays some sort of selectivity towards

solutes, usually on the basis of size <sup>82</sup>. In general, membranes can be thought of as possessing pores of specific dimensions so that 'bulk flow' of solutes smaller than the size of the pore occurs, whereas species exceeding the pore-size are rejected. Figure 1.8 summarises the different types of membrane by classification according to the size of the species it will reject <sup>83</sup>:

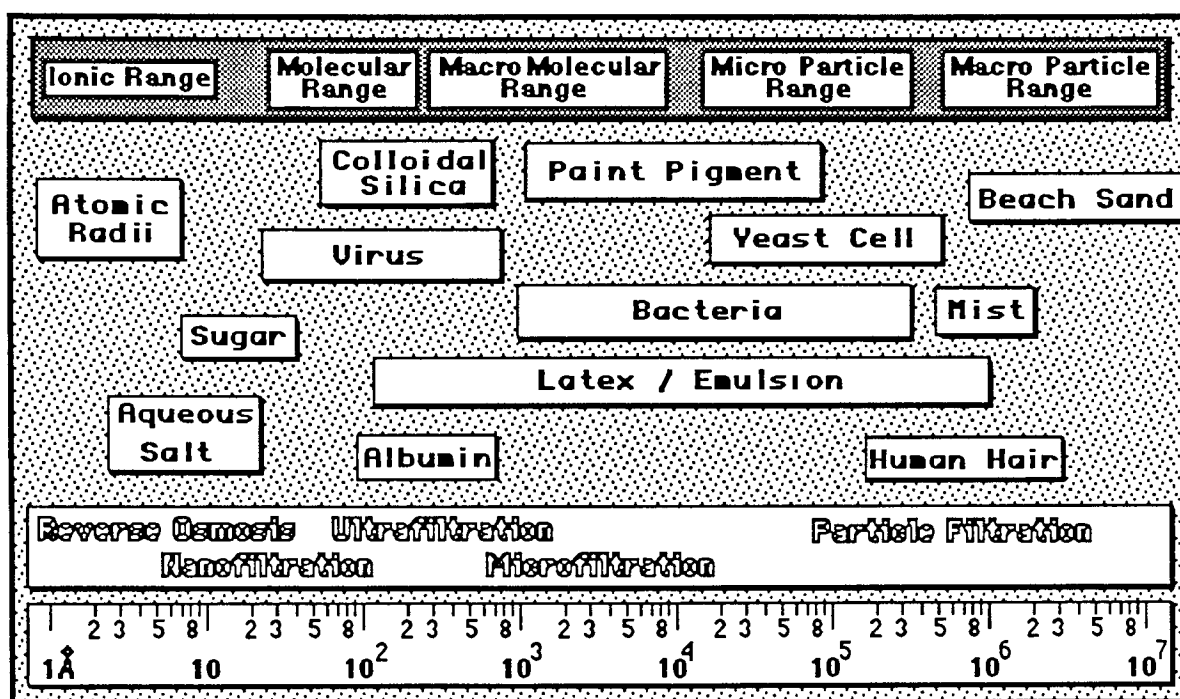


**Figure 1.8 Membrane Filtration Spectrum.**

Microfiltration (MF) membranes have pore sizes in the region 0.02-10  $\mu\text{m}$ , and are capable of removing suspended material such as bacteria, cells and some pigments. Similarly, ultrafiltration (UF) membranes have smaller pores 1-20 nm in size, and are characterised by a molecular-weight cut-off (MWCO), which is the highest  $M_w$  species that can be transported. Reverse osmosis (RO, or hyperfiltration) membranes have a different morphology to those previously mentioned. RO employs a semi-permeable membrane which allows transmission of solvent but not dissolved solutes. These membranes are not considered to possess a fixed pore system as such, but rather a

continuous thin active layer, through which the solvent can dissolve and diffuse through the matrix by a network of transient pores produced by the fluxionality of the polymer chains. Solutes are presumably less soluble in the polymer phase and are excluded from transport. For MF, UF and RO processes, it is necessary to have an applied pressure across the membrane, in order to drive the separation and attain respectable fluxes.

Hydrogel polymers do not have a fixed porous structure and membranes of these materials are classed as homogeneous in nature <sup>84</sup>. The high freezing water content of the gel serves to plasticise the highly mobile polymer chain segments, which leads to a series of randomly changing, water-filled spaces. Here then, lies the difference between the RO-type polymer film and the hydrogel; whereas solutes are unable to pass through the RO polymeric barrier, the hydrogel has a medium into which salts can dissolve and diffuse- a concept known as the solution-diffusion theory.

In this study, salts will diffuse across the membranes under the influence of a concentration gradient only, with no application of an external pressure. Fluxes through these materials will be low, as transport occurs purely as a result of mass transfer of a species from a high concentration to a lower one. This type of phenomenon is governed by Fick's First Law of Diffusion <sup>85</sup> (equation 1.1), which simply states that the diffusional flux is proportional to the concentration gradient:

$$J = -D \frac{dc}{dx} \quad (1.1)$$

$J$  = Flux-per-unit area       $D$  = Diffusivity       $dc/dx$  = Concentration Gradient

The mathematical theory that describes diffusion in gels is notoriously complex <sup>86</sup>, but on a more simplistic level, equation 1.1 is sufficient to derive the expressions necessary for the

calculation of the permeability coefficients for permeating transition metal-ion species in this study (Chapter Five, equations 5.1 & 5.2).

#### **1.4.1 Transition Metal-Ion Separations by Membranes.**

By far the most common membrane-based technique employed to separate and preconcentrate transition metal ions, is Donnan-dialysis <sup>83</sup> across an ion-exchange membrane <sup>87-90</sup>. The principles of Donnan-dialysis are demonstrated in Figure 1.9; two solutions of  $\text{CuSO}_4$  and  $\text{H}_2\text{SO}_4$  are separated by a cation exchange membrane:

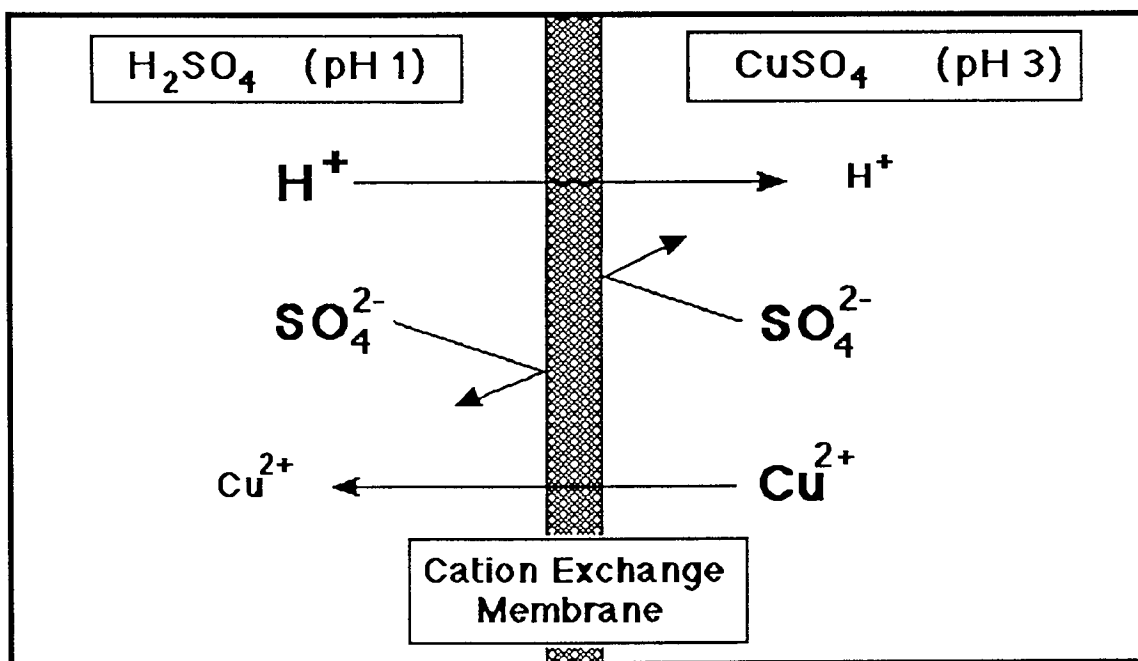


**Figure 1.9 The Principle of Donnan-Dialysis.**

The proton concentration in the  $\text{H}_2\text{SO}_4$  solution side is significantly greater than that in the  $\text{CuSO}_4$  solution, and so the proton gradient is the driving force for the flow of  $\text{H}^+$  across the membrane. Since the membrane is specific in its permeability to cations only, electrical neutrality is maintained by the counter-flow of  $\text{Cu}^{2+}$  ions in the opposite direction. As long as the concentration of  $\text{H}^+$  is maintained at a constant level in the  $\text{H}_2\text{SO}_4$  phase,

$\text{Cu}^{2+}$  ions will continue to be transported, even against their concentration gradient by the Donnan-effect, until the level of  $\text{Cu}^{2+}$  ions is equivalent to that of the  $\text{H}^+$  ions.

The problem with Donnan-dialysis through ion-exchange membranes is that the process is not selective enough to distinguish between different metal ions in solution. However, a number of groups have used liquid membranes as a vehicle for investigating more specific transport effects, utilising either linear chelating compounds <sup>91-93</sup>, or macrocyclic-type ligands <sup>94-96</sup> to achieve the desired selectivity (Chapter 5, section 5.1 & Chapter 6, section 6.1). There are, however, limitations to using liquid membrane arrangements. First being the lack of stability of the membrane (which is simply an immiscible organic phase sandwiched between two aqueous phases), and secondly there is a tendency for the metal-carrier complex to leach from the organic to the aqueous phase. This often necessitates the use of exotic synthetic methods in order to append some sort of lipophilic function to the carrier to increase its affinity for the organic phase.

There has been some work on the use of various polymeric membranes for metal-ion separations <sup>97-101</sup>, including studies by the Speciality Materials Group at Aston on hydrogels <sup>102,103</sup>. Recent investigations by the group have centred on the immobilisation of crown compounds into hydrogel membranes for controlling alkali and alkaline earth metal ion transport <sup>29,104</sup>, but generally, the examples of chelating polymer membranes in the literature are few and far between <sup>105,106</sup>. It is apparent that there is a niche available for a more thorough investigation into the design, synthesis and application of chelating membrane systems. It was with this thought in mind that much of the work in this thesis was undertaken.

## **1.5 SUMMARY OF OBJECTIVES.**

This chapter has dealt with some of the factors that have influenced the use of specific materials for the ultimate aim of producing a hydrophilic polymer system, capable of interacting with a variety of transition metal ions. The research project is based on a rather multi-disciplinary approach, and necessitates the communication of information from different areas of chemistry. It is hoped that the main introduction has given a brief flavour of the concepts involved, and each experimental chapter starts with a further introductory passage to complement this.

The initial part of this work uses a number of techniques, familiar to the inorganic, physical and polymer chemist alike, to determine how coordination of metal ions affects the physical properties of the polymer, and *vice versa*. The poly(2-hydroxyethyl methacrylate) hydrogel, which forms the basic hydrophilic matrix of the chelating membranes, is the polymer used in the manufacture of soft contact lenses. As such, membranes of these materials are optically clear in the visible region. It is well known that many transition metal complexes with pyridyl and bipyridyl ligands are coloured, and since the polymer itself will not interfere in this region, it is possible to use visible spectroscopy very effectively in the characterisation of these complexes.

This technique is taken one stage further by focussing on a spectroscopic study of the coordination-kinetics of the iron(II) salts with bipyridyl-based membranes, to obtain more subtle information concerning ligand-metal-polymer interactions. It is from observations of this system that important information is gained about the coordinating ability of these gel-type polymers, and the influential rôle of the anion in the transport of the metal salts

across the membranes.

By the application of membrane technology, the final part of this investigation assesses the ability of these chelating polymers for the potential to selectively discriminate between different transition metal ions in solution. Chapters Five and Six of this thesis discuss some of the results obtained by employing these techniques, and combined with the knowledge accumulated from the previous chapters, a mechanism for salt transport across ligand-modified membranes is proposed.

There are many angles from which to approach a project of this nature. This thesis is a novel account from the the inorganic/coordination chemists' stand-point.

## **CHAPTER TWO**

### **MATERIALS AND METHODS.**

## **SECTION (A): THE SYNTHESIS AND PURIFICATION OF VINYLIC LIGANDS & COMPLEXES.**

### **2.1 INTRODUCTION.**

The first half of this chapter is concerned with the synthesis and purification of the vinyl monomers based on the pyridine ligand, and complexes thereof. Spectroscopic evidence is used in the analysis of products where possible. Methods for the subsequent preparation and characterisation of various copolymer forms of these materials are described, with particular emphasis on membrane formulations. The remainder of the chapter is devoted to the techniques used in the study of transition metal ion binding within the membranes, and to the design and operation of the equipment used in ion-transport and coated wire electrode studies. The synthesis and preliminary investigations into the functionalisation, immobilisation and eventual entrapment of macrocyclic ligands into hydrogel membranes are discussed separately in Chapter Six.

### **2.2 4-VINYLPYRIDINE**, (CA No.[100-43-6])

The use of the monomer 4-vinylpyridine (4VPy) in the preparation of polymers with the ability to coordinate transition metal (TM) ions is well established, and as such can be purchased direct from a number of chemical companies. The 4VPy used in this study was obtained from the Aldrich Chemical Company; the monomer as supplied has a reddish-brown colouration caused by reaction with atmospheric oxygen, and must be purified by distillation under reduced pressure (62-64°C @ 15mm). The pure clear monomer is hygroscopic at ambient temperature and must be stored in a refrigerator under nitrogen until required, although it should be used within a few weeks of distillation as it

polymerises slowly on standing. Commercial supplies generally contain 100 ppm hydroquinone as a free radical inhibitor to prevent this polymerisation.

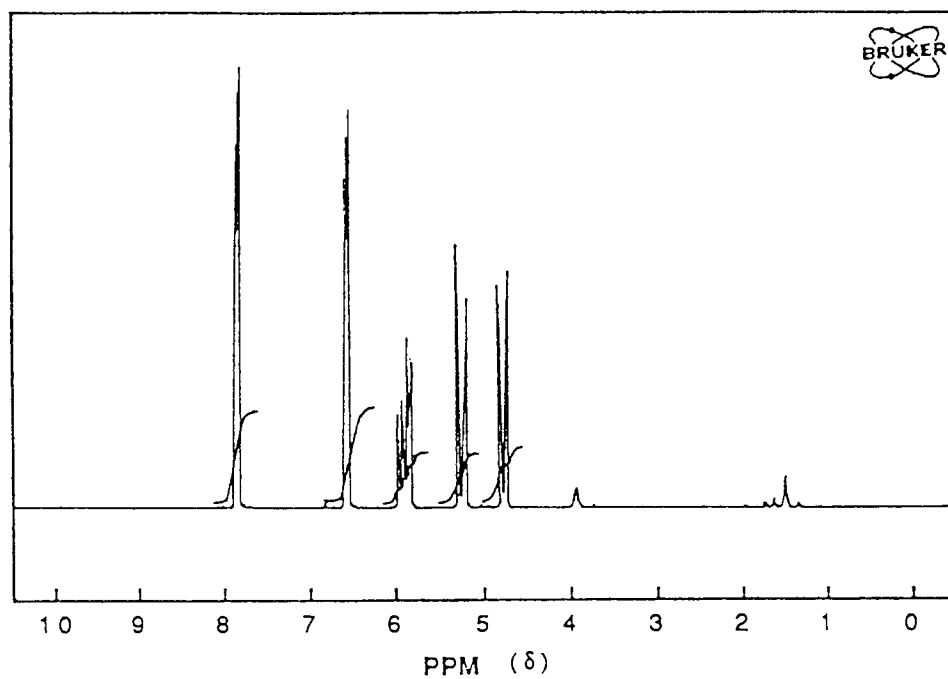
It should be noted that 4VPy has an unpleasant vapour rather like that of pyridine which can cause irritation to the eyes and respiratory tract. Skin contact results in more serious irritation and sometimes severe allergies develop in certain people, thus the wearing of protective gloves and the use of a fume cupboard when handling 4VPy is recommended.

### **2.2.1 Nuclear Magnetic Resonance Spectra of 4-VPy.**

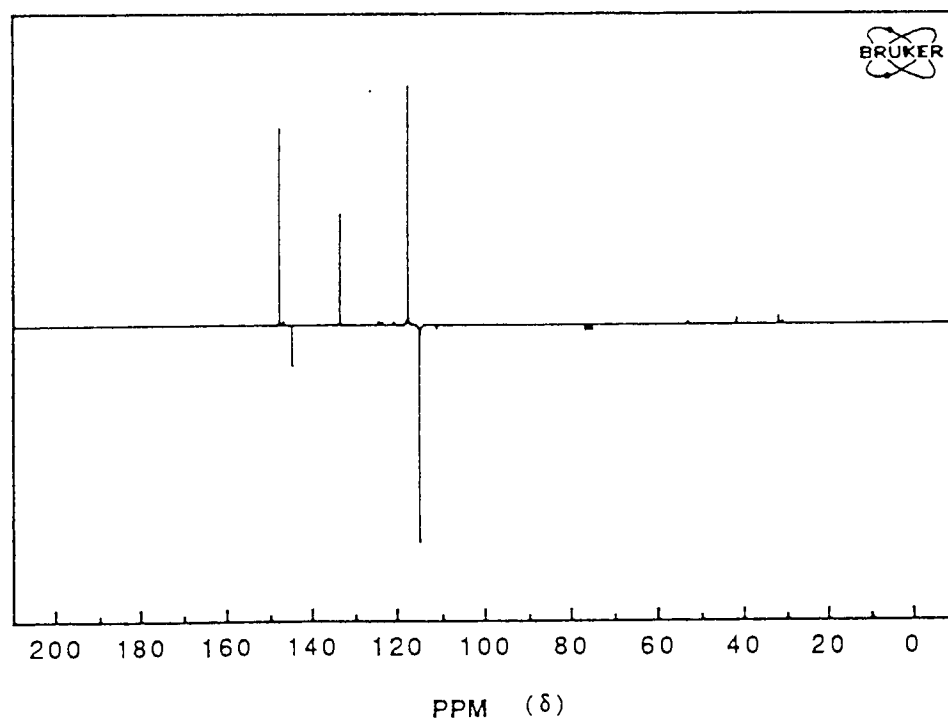
All spectra displayed in this chapter were taken on a Bruker AC-E 300MHz spectrometer. For  $^{13}\text{C}$  nmr, the large  $^{13}\text{C}$ - $^1\text{H}$  coupling constant (125-200Hz for directly bonded protons) results in multiplets which overlap to a considerable extent, making the spectrum difficult to analyse. Therefore, all  $^{13}\text{C}$  spectra are proton noise-decoupled so that each absorption appears as a sharp singlet; this increases sensitivity affording accurate chemical shift data but information available from spin-spin splitting patterns is lost. However, the Bruker spectrometer possesses software that can combine the proton noise-decoupling with another multi-pulse technique known as the *J*-modulated spin-echo sequence (*J*-mod). This allows identification of the different types of carbon atoms by using the proton-carbon couplings and the signal intensities they generate<sup>107</sup>. This can be seen clearly on the  $^{13}\text{C}$  spectra where peak inversion of methylene and quaternary carbons occurs i.e.  $\text{CH}_3$  &  $\text{CH}$  peaks point up (+);  $\text{CH}_2$  &  $\text{C}$  peaks point down (-).

Figure 2.1(a) shows the  $^1\text{H}$  nmr spectrum for 4VPy. The aromatic region of the spectrum (singlets with fine structure at 7.92 $\delta$  & 6.57 $\delta$ ), is much less complicated than that of pyridine itself owing to the replacement of the  $\gamma$  proton (which would ordinarily couple

**Figure 2.1(a)  $^1\text{H}$  Spectrum of 4-Vinylpyridine.**



**Figure 2.1(b)  $^{13}\text{C}$  (*J*-Mod) Spectrum of 4-Vinylpyridine.**



with the  $\alpha$  and  $\beta$  ring protons), by the vinyl group (Figure 2.2).

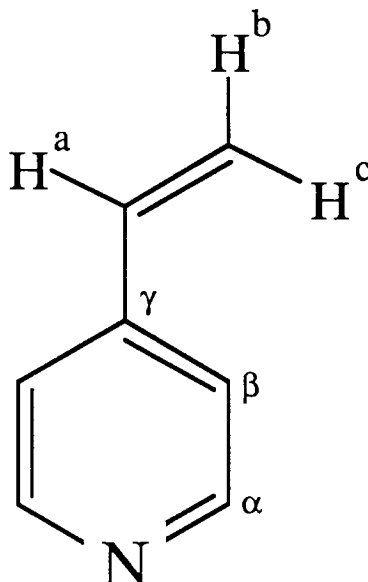


**Figure 2.2 Structure of 4-Vinylpyridine.**

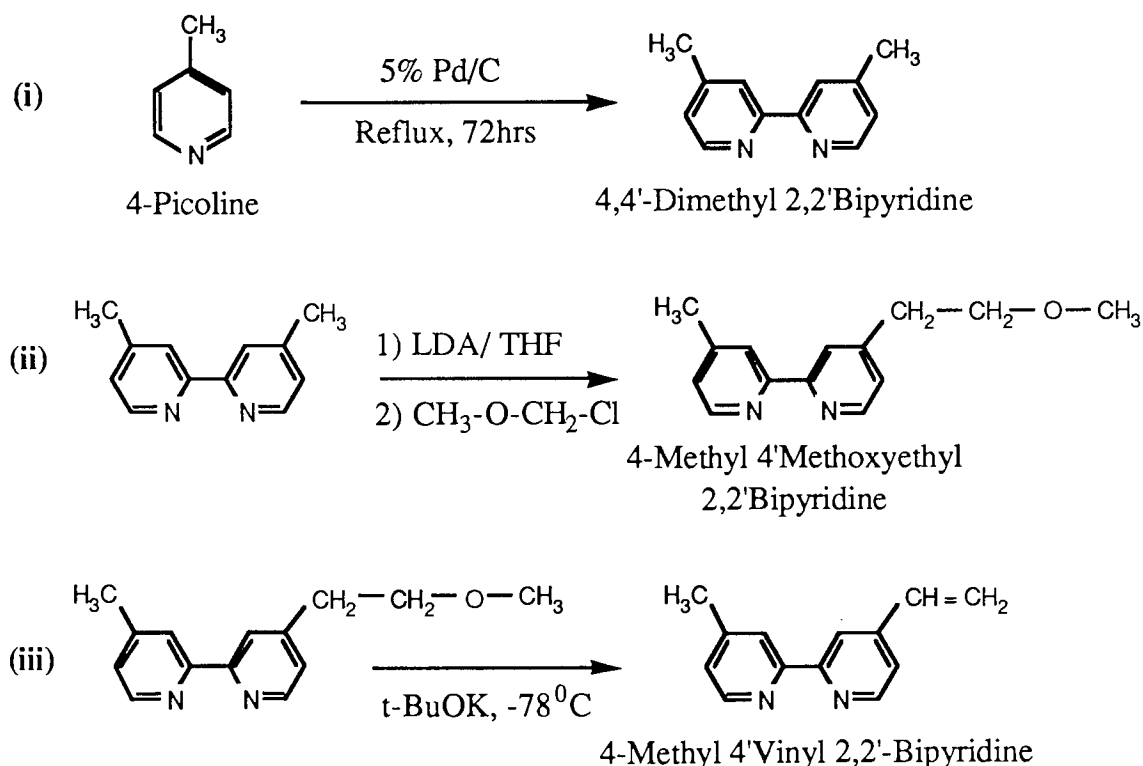
For the vinyl system,  $H_b$  and  $H_c$  are *trans* and *cis* respectively, which renders them inequivalent. Coupling of  $H_a$  to  $H_b$  and  $H_c$  gives rise to four equal peaks 5.91/5.95/5.97/6.01 $\delta$  for  $H_a$ , which in turn splits signals for  $H_b$  and  $H_c$  into doublets at 4.77/4.81 $\delta$  & 5.26/5.32 $\delta$

Figure 2.1(b) is the  $^{13}\text{C}$  spectrum for 4VPy. The vinylic methylene peak appears at 117.99 $\delta$  (-) and the methine at 120.18 $\delta$  (+). The  $\beta$  aryl carbons are at 134.1 $\delta$  (+), the  $\gamma\text{C}$  at 144.02 $\delta$  (-) and the  $\alpha\text{C}$ 's furthest downfield at 149.44 $\delta$  (+) as they are adjacent to the ring nitrogen.

### **2.3 4-METHYL 4'-VINYL 2,2'-BIPYRIDINE.**(CA No.[74173-48-1])

Ghosh & Spiro <sup>73</sup> were first to find a multi-gram synthetic route to 4-methyl 4'-vinyl 2,2'-bipyridine (VBipy, also known as 4-ethenyl 4'-methyl 2,2'-bipyridine in Chemical

Abstracts). Their method involved the use of lithium diisopropylamine (LDA) and gaseous formaldehyde to generate the 4-hydroxyethyl derivative, which was dehydrated with phosphorus pentoxide ( $P_2O_5$ ) to produce the vinyl group. Many workers <sup>108</sup> have found this preparation difficult to execute, therefore the VBipy used in this work was synthesised *via* an improved method of Abruna *et al.* <sup>109</sup> as represented by the scheme in Figure 2.3:



**Figure 2.3 The Preparation of 4-Methyl 4'Vinyl 2,2'Bipyridine.**

There have been various attempts in the literature to modify this method with an aim to improving the yields and purity <sup>110,111</sup> but this remains the simplest and most effective route to producing the vinyl derivative. Each stage in the experimental will now be described in more detail, followed by a summary of the  $^1\text{H}$  and  $^{13}\text{C}$  magnetic resonance spectra for the products of each of the stages

### **2.3.1 (i) Preparation of 4,4'-Dimethyl 2,2'-Bipyridine.**

The following syntheses involved the catalytic coupling of 4-picoline at the 2 position to give 4,4'-dimethyl 2,2'-bipyridine (DMBipy). After producing disappointing yields *via* these methods, it was decided a more cost-effective approach would be to purchase the DMBipy direct from the Aldrich Chem. Co. or TCI (Fluorochem) Ltd. (depending on availability), removing the necessity for stage (i).

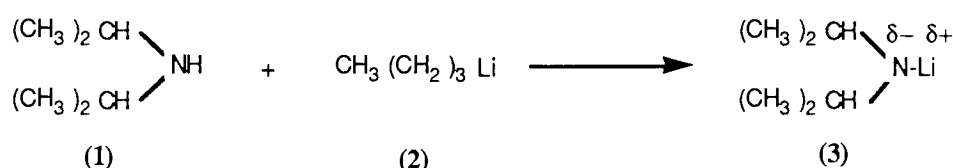
200ml of 4-picoline (Aldrich Chem. Co., b.p 145<sup>0</sup>C) was twice distilled over KOH and then refluxed with 8.93g of 5% Pd/C under nitrogen. After 70 hours, 75ml of benzene was added (to dissolve any solid product) and the refluxing continued for another 30 mins. The hot solution was filtered under pressure and white crystals precipitated out. The majority of the solvent was removed by vacuum distillation and the resulting solid recrystallised from ethyl acetate. Literature yields of product are in the range of 2g/g of catalyst. This method was repeated several times with sub-gram yields each time. Changes were implemented following a modified route of Sprintschnik *et al.* <sup>112</sup>, which recommended 10% Pd/C. This too proved non-productive and the only conclusion that could be drawn was that the catalyst was being inactivated, perhaps by some mechanism that resulted in poisoning of the catalyst surface. It was thought that the problem may be solved by the use of a more active catalyst such as Raney Nickel, the preparation and usage of which was potentially dangerous and thus approached with caution.

The preparation of W7-J Raney Nickel was based on the original procedure of Badger & Sasse <sup>113</sup>, with modifications by Sasse & Whittle <sup>114</sup> and it's final application to the production of DMBipy by the former authors <sup>115</sup>. 125g of nickel-aluminium alloy (50:50,

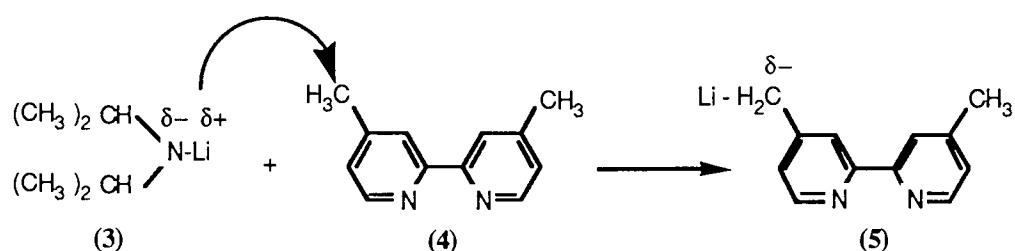
May & Baker Ltd.) was carefully added to a solution of NaOH (160g in 600ml water) in a 2l conical flask with stirring to control frothing, over a 10 minute period. The temperature quickly reached  $\sim 85^{\circ}\text{C}$ , and after complete addition the catalyst was digested at  $100^{\circ}\text{C}$  with gentle stirring for 6 hours. After being left at room temperature overnight, the catalyst was washed and transferred to a 3 neck round-bottomed flask with dropping funnel, for degassing. This catalyst can release hydrogen explosively at about  $80^{\circ}\text{C}/15\text{-}20\text{mm}$ , and so the flask was connected to a 5l Buchner flask which acts as a buffer, and in turn to an efficient water pump by thick-walled rubber tubing. The apparatus was evacuated at room temperature, and the flask containing the catalyst was warmed slowly to avoid vigorous boiling. The degassing process was left at  $100^{\circ}\text{C}/20\text{mm}$  for 2 hours and then 4-picoline (150ml) was added, *via* the dropping funnel, to the evacuated flask, with great care not to allow the access of air until the catalyst was thoroughly wetted. A condenser could then be fitted and the mixture refluxed for 50 hours. Hot 4-picoline (150ml) was added to dissolve any solid product, and the mixture was filtered to remove the catalyst. The catalyst is pyrophoric and must be kept wet by washing with hot 4-picoline while being filtered; it is then stored under water until required. [\* The literature recommends the use of hot benzene to dissolve solid material and keep the catalyst wet. However, it has been observed that the mixture of picoline and benzene forms an azeotropic mixture that is difficult to separate, and so the use of hot picoline itself meant that after vacuum distillation to obtain the product, the regenerated picoline could be directly reused in further syntheses]. The filtrate was mostly vacuum distilled to leave a solid that was recrystallised from ethyl acetate to yield white needles (15-25g, literature claims 56g), of m.p.  $170\text{-}172^{\circ}\text{C}$  (literature  $115\text{ m.p. } 171\text{-}172^{\circ}\text{C}$ ).

### 2.3.2 (ii) Preparation of 4-Methyl 4'Methoxyethyl 2,2'-Bipyridine.

The diisopropylamine for this experiment was purified by distillation over calcium hydride under nitrogen. The tetrahydrofuran (THF) solvent was distilled over Na/benzophenone, but the (chloromethyl) methyl ether and n-BuLi/hexane were used as received from the Aldrich Chemical Co.. Into a 1 l 3 neck round-bottomed flask, equipped with a 500ml dropping funnel and nitrogen inlet/outlet, was placed 11.4ml (81mmol) of diisopropylamine in 90ml of THF at 0°C and under a nitrogen atmosphere. 54.3ml (81.5mmol) of 1.5M n-BuLi in hexane was added to the flask, followed by the dropwise addition of 15g (81.5mmol) of DMBipy in 350ml of THF. {It should be noted that it was difficult to get all the DMBipy into solution and that vigorous stirring and elevated temperatures were necessary}. The n-Butyl lithium (1) and diisopropylamine (2) react to produce the strong base, lithium diisopropylamine (LDA) (3). [Scheme 2.4(a)]:

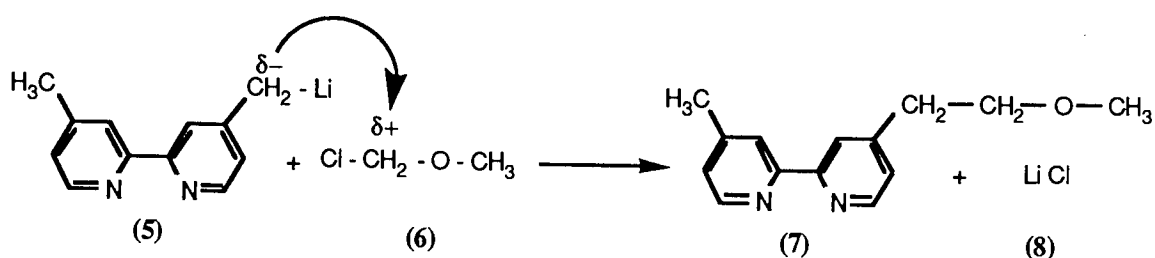


(3) reacts with a methyl group on the DMBipy (4) to give an intermediate, lithiated on one side chain (5). This is seen as a deep brown reaction mixture which is stirred at 0°C for 15 minutes. [Scheme 2.4(b)]:



6.9ml (90.9mmol) of (chloromethyl) methyl ether in 60ml of THF was again added dropwise, to produce a pale green/yellow mixture which was stirred at 0°C for 30 minutes.

This is the formation of the ether product (7) by the nucleophilic attack of the lithiated ( $\delta^-$ ) methyl side chain (5) on the chloride/oxygen carrying ( $\delta^+$ ) carbon in the (chloromethyl) methyl ether (6). [Scheme 2.4(c)]:

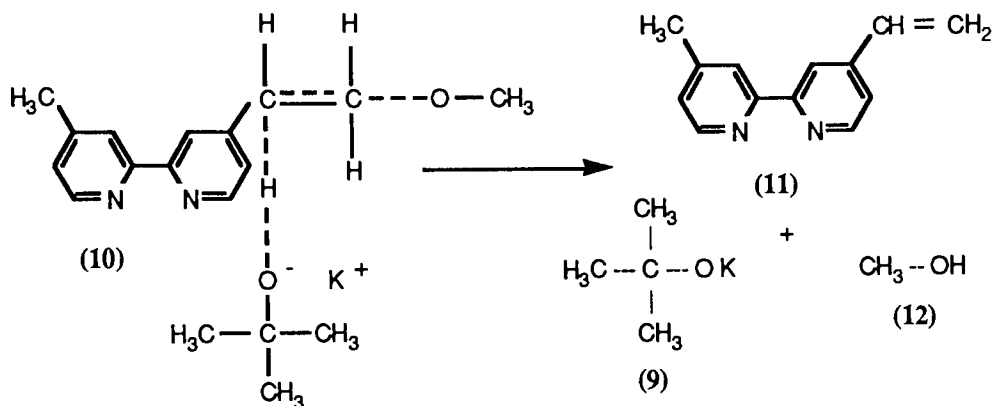


The solution was quenched with 90ml of water and partitioned between 50 ml of saturated  $\text{NaHCO}_3$  and 150ml of diethyl ether. Following two additional ether extraction steps, the combined ethereal layers were dried over sodium sulphate for a few days and then concentrated by rotary evaporation to yield a yellow oily product. This was left to stand for a week, and white crystals of unreacted DMBipy deposited out. The oil was ether eluted through a silica gel column to yield a pale yellow oil (16.3g, 88% yield, literature <sup>109</sup> 12.6g, 68%). Although the yield produced at first attempt was greater than that reported in the literature, it is thought that the product was still impure, as the pure oil is colourless, not yellow. Repeats of this experiment have produced more consistent yields in the range of 43-64%.

### **2.3.3 (iii) Preparation of 4-Methyl 4'-Vinyl 2,2'-Bipyridine.**

To a solution of 12.6g (52.2mmol) of 4-methyl 4'-methoxyethyl 2,2'-bipyridine (7) in 325 ml of THF at  $-78^\circ\text{C}$  under nitrogen, was added 12.4g (110.4mmol) of potassium tertiary butoxide (9) in 210ml of THF dropwise. (9) causes the elimination of methanol from (7), to give the vinyl derivative (11), [Scheme 2.5 (overleaf)]. The mixture was agitated by

nitrogen influx (stirring was not possible as the apparatus was immersed in a dewar containing acetone/dry ice to lower the temperature), for 1.5 hours at  $-78^{\circ}\text{C}$  and then for 15 mins at ambient temperature.



The reaction was quenched with 150 ml of water and extracted with 3 x 300ml aliquots of ether. The combined ethereal layers containing (11) were dried over sodium sulphate and stripped on a rotary evaporator to give a yellow solid. Polymeric residue was removed by ether elution through a 400 mesh 2inch silica column, to yield a yellow product which was recrystallised from ether/hexane to give crystals of the product (11) (7.75g, 48% overall yield from stage (ii)) of melting point  $88-90^{\circ}\text{C}$ .

Elemental Analysis:

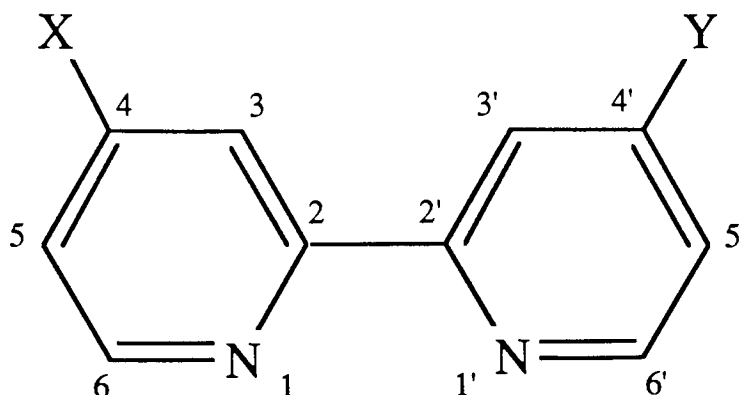
Anal. Calc. for  $\text{C}_{13}\text{H}_{12}\text{N}_2$ : C, 79.59; H, 6.12; N, 14.29.

Found: C, 79.14; H, 6.28; N, 14.77.

#### **2.3.4 Nuclear Magnetic Resonance Spectra for Bipyridyl Derivatives.**

The following NMR data will make reference to the numbering scheme in Figure 2.6 (overleaf), corresponding to hydrogen, carbon and substituent positions on the bipyridyl molecule. All spectra were recorded on a Bruker AC-E 300MHz spectrometer and all  $^{13}\text{C}$  subjected to noise-decoupling and  $J$ -modulated spin echo techniques.

**Figure 2.6 Numbering Scheme in Bipyridyl Derivatives.**



X = Y = H = 2,2'-Bipyridine

X = Y = CH<sub>3</sub> = 4,4'-Dimethyl 2,2'-Bipyridine

X = CH<sub>3</sub>, Y = CH<sub>2</sub>- CH<sub>2</sub>- O - CH<sub>3</sub> = 4-Methyl 4'-Methoxyethyl 2,2'-Bipyridine

X = CH<sub>3</sub>, Y = CH=CH<sub>2</sub> = 4 Methyl 4'-Vinyl 2,2'-Bipyridine

#### **4,4'-Dimethyl 2,2'-Bipyridine.**

Figure 2.7(a) shows the <sup>1</sup>H nmr spectrum for DMBipy in CDCl<sub>3</sub>. The sharp singlet at 2.36δ is from the methyl groups on positions 4 & 4'; the aromatic region consists of a doublet at 7.05/7.07δ from the protons on 5 & 5' coupling with those on 6 & 6' respectively and *vice versa* to produce a doublet at 8.46/8.48δ. The singlet at 8.16δ from the lone protons on 3 & 3'.

Figure 2.7(b) is the corresponding <sup>13</sup>C nmr spectrum in CDCl<sub>3</sub>. The peak at 21.12δ (+) is the CH<sub>3</sub> on 4 & 4'; the aromatic carbons appear in the order 121.95δ (+) C3,3'; 124.59δ (+) C5,5'; 148.06δ (-) C4,4'; 148.87δ (+) C6,6'; 156δ (-) C2,2'.

#### **4-Methyl 4'-Methoxyethyl 2,2'-Bipyridine.**

Figure 2.8(a) is the <sup>1</sup>H nmr spectrum of MEBipy in CDCl<sub>3</sub>. The CH<sub>3</sub> on 4 gives a singlet at 2.16δ. The methylene attached directly to 4' is split into a triplet 2.69/2.72/2.74δ by the

Figure 2.7(a)  $^1\text{H}$  Spectrum of 4,4'-Dimethyl 2,2'-Bipyridine.

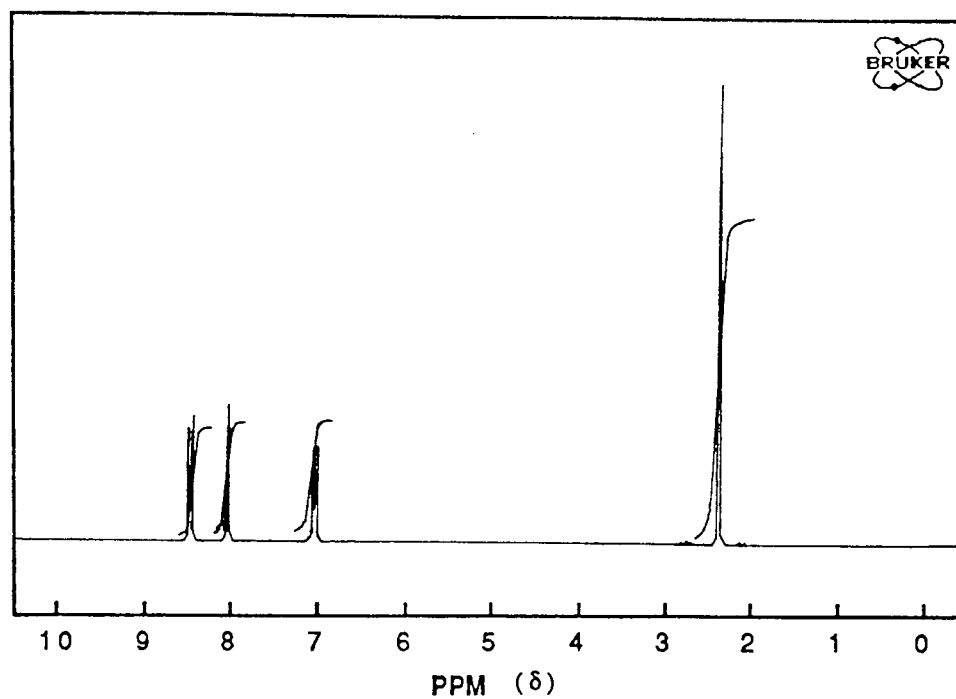
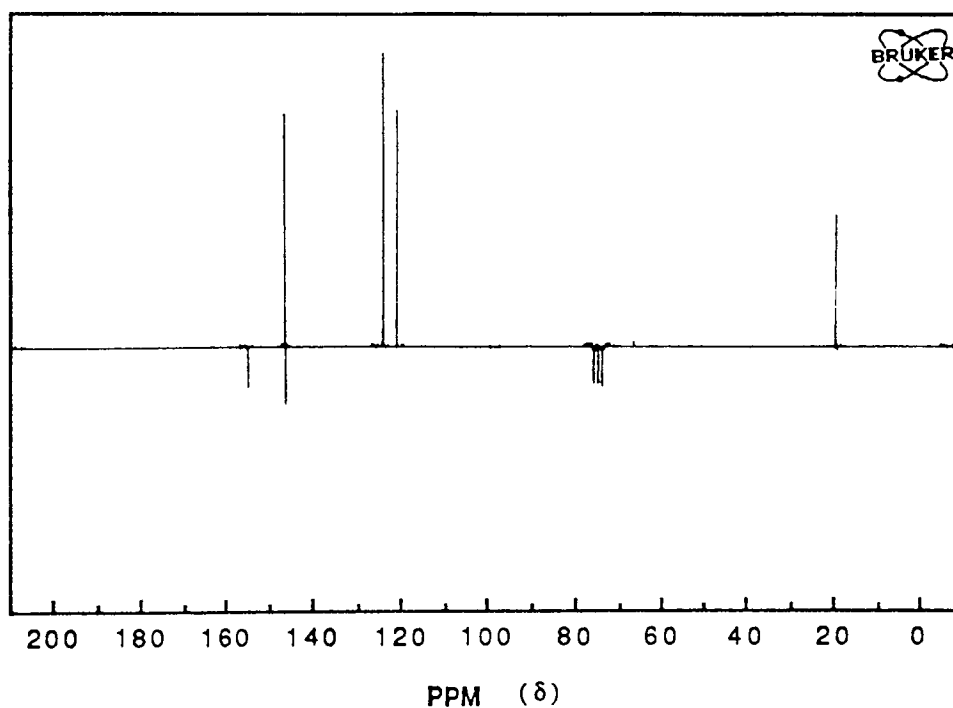
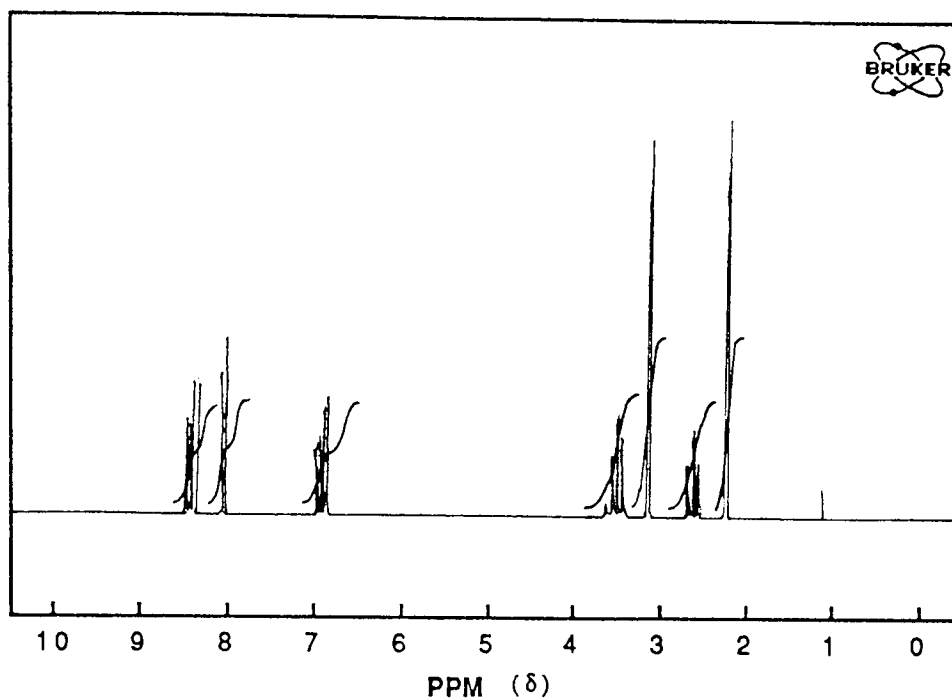


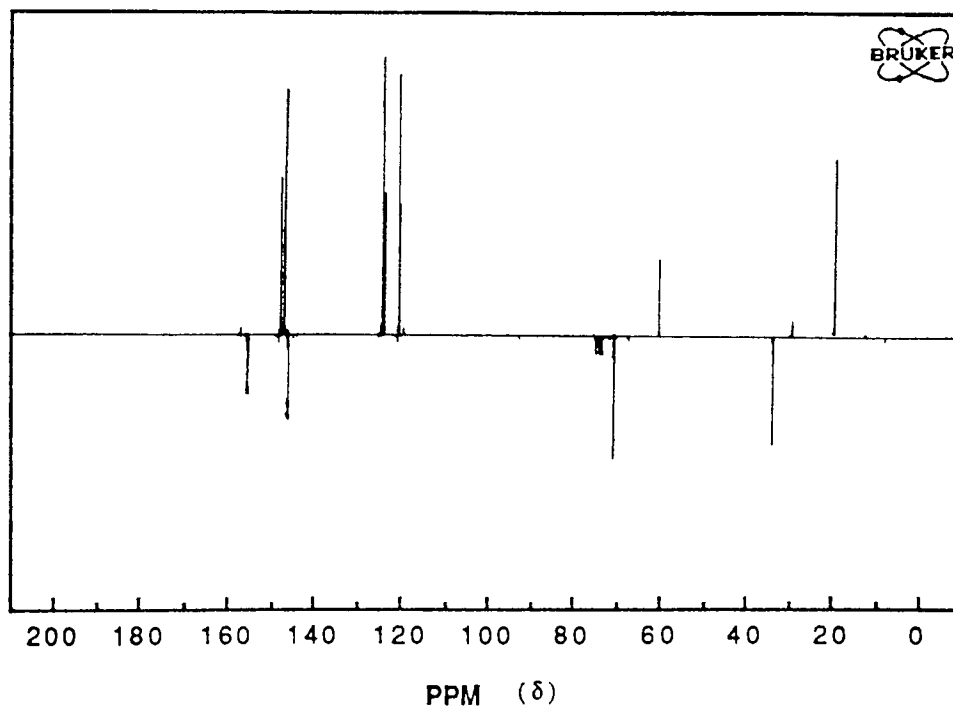
Figure 2.7(b)  $^{13}\text{C}$  (J-Mod) Spectrum of 4,4'-Dimethyl 2,2'-Bipyridine.



**Figure 2.8(a)  $^1\text{H}$  Spectrum of 4-Methyl 4'-Methoxyethyl 2,2'-Bipyridine.**



**Figure 2.8(b)  $^{13}\text{C}$  (*J*-Mod) Spectrum of 4-Methyl 4'-Methoxyethyl 2,2'-Bipyridine.**



neighboring CH<sub>2</sub>-O, which itself appears downfield and as a triplet 3.38/3.4/3.41 $\delta$  split by the methylene attached to 4'. The CH<sub>3</sub>-O is also pulled downfield by the oxygen and appears as a singlet at 3.11 $\delta$ . The aromatic region is relatively unchanged from that of DMBipy with a doublet 6.94/6.95 $\delta$  from protons on 5 & 5', singlet 8.05 $\delta$  from those on 3 & 3' and a doublet 8.33/8.34 $\delta$  from those on 6 & 6'.

Figure 2.8(b) shows the more complicated <sup>13</sup>C spectrum of MEBipy in CDCl<sub>3</sub>. Peaks at 28.93 $\delta$  (+) & 58.12 $\delta$  (+) are the methyl and methoxy carbons respectively. Those at 35.17 $\delta$  (-) & 71.65 $\delta$  (-) are the neighboring methylenes attached to the ring (at 4') and the oxygen of the methoxy group respectively. Aromatic carbons appear as for DMBipy- 121.15 $\delta$  (+) C3,3'; 123.86 $\delta$  (+) C5,5'; 148.52 $\delta$  (+) C6,6'; 147.58 $\delta$  (-) C4; 148.75 $\delta$  (-) C4'; 155.4 $\delta$  (-) C2,2', with some additional close side peaks indicating the possible presence of DMBipy impurity.

#### **4-Methyl 4'-Vinyl 2,2'-Bipyridine.**

Figure 2.9(a) is the <sup>1</sup>H nmr spectrum of VBipy in CDCl<sub>3</sub>. The methyl protons on 4 appear as a sharp singlet at 2.37 $\delta$ . The vinyl protons couple in a similar fashion as for 4VPy (section 2.2.1) to give a double quartet splitting pattern 5.45/5.48/6.01/6.07 $\delta$  & 6.66/6.69/6.72/6.75 $\delta$ . The vinyl group must interact through-space with the closest heterocyclic ring as the aromatic protons are rendered inequivalent- 5 & 5' doublets at 7.1/7.12 $\delta$  & 7.24/7.28 $\delta$ , 3 & 3' singlets at 8.21 & 8.38 $\delta$  and 6 & 6' doublets at 8.49/8.51 $\delta$  & 8.58/8.6 $\delta$ .

Figure 2.9(b) shows the <sup>13</sup>C nmr spectrum of VBipy in CDCl<sub>3</sub>. The peak at 29.38 $\delta$  (+) is the methyl group on C4. The vinyl CH & CH<sub>2</sub> appear at 118.44 $\delta$  (+) & 118.83 $\delta$  (-) respectively. The aromatic carbons appear in the order 120.56 $\delta$  (+) C3 & 122.01 $\delta$  (+) C3';

Figure 2.9(a)  $^1\text{H}$  Spectrum of 4-Methyl 4'-Vinyl 2,2'-Bipyridine.

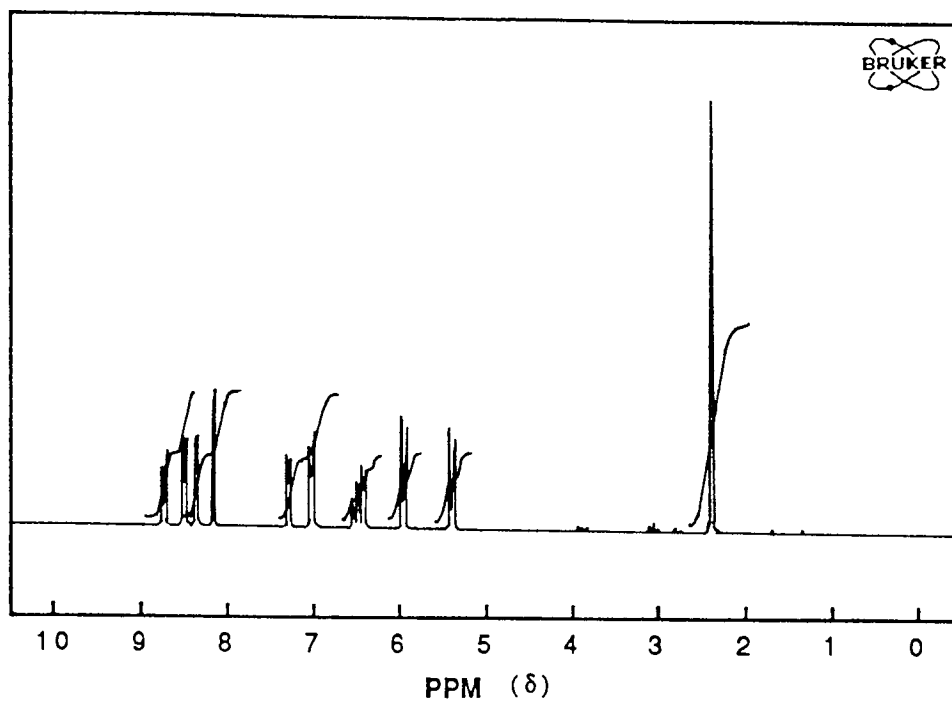
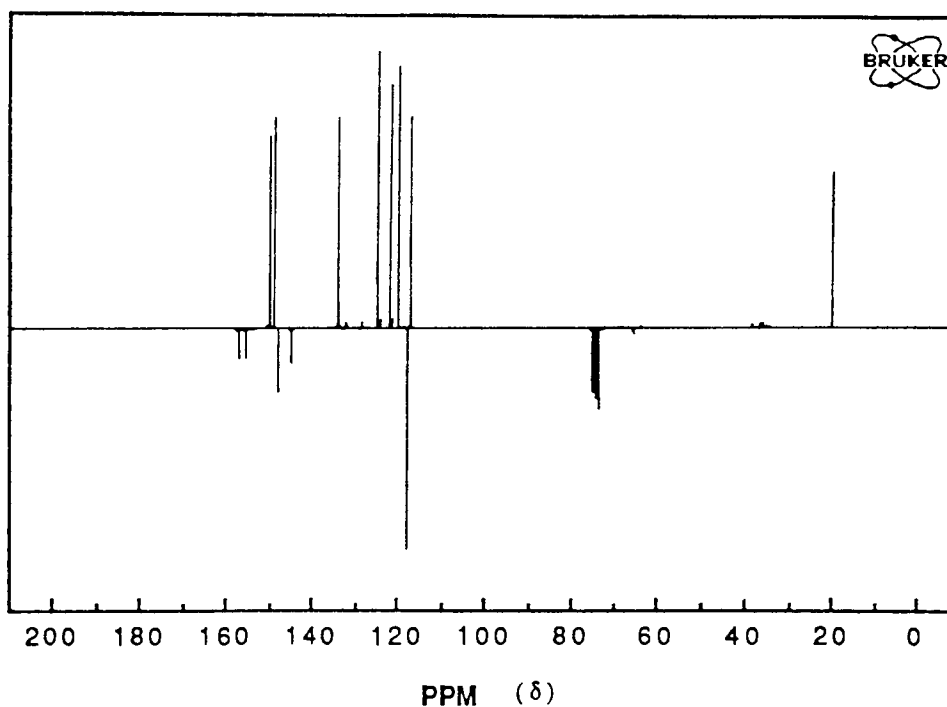


Figure 2.9(b)  $^{13}\text{C}$  (*J*-Mod) Spectrum of 4-Methyl 4'-Vinyl 2,2'-Bipyridine.



124.63 $\delta$  (+) C5 & 134.85 $\delta$  (+) C5'; 145.8 $\delta$  (-) C4 & 148.26 $\delta$  (-) C4'; 155.59 $\delta$  (-) C2 & 156.43 $\delta$  (-) C2'.

## **2.4 PREPARATION OF TRIS(4-METHYL 4'-VINYL 2,2'-BIPYRIDINE)**

### **IRON (II)** (CA No.[75675-26-2])

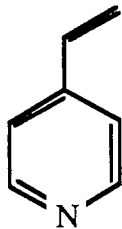
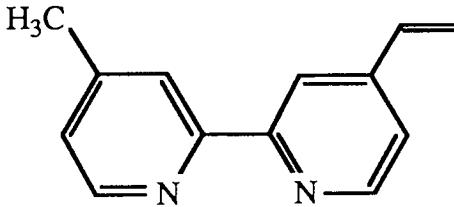
The preparation of the *tris* (4-methyl 4'-vinyl 2,2-bipyridine) Iron(II) complex (Fe<sup>2+</sup>(VBipy)<sub>3</sub>) was modified from that of the analogous tris(2,2'-bipyridine) complex by Smith and Cagle <sup>116</sup>. 0.47g of FeSO<sub>4</sub>.7H<sub>2</sub>O were dissolved in 40ml of distilled water. To the stirred solution, 0.98g of powdered VBipy was added producing an immediate deep red colouration. Stirring was continued until all the solid had disappeared and then 0.47g of NaClO<sub>4</sub>.H<sub>2</sub>O dissolved in 20ml of water was added to the Fe<sup>2+</sup>(VBipy)<sub>3</sub> solution. The resulting precipitate of [Fe(VBipy)<sub>3</sub>(ClO<sub>4</sub>)<sub>2</sub>] was filtered, thoroughly washed with distilled water and dried in vacuo overnight.

## **2.5 POLYMERISATION PROCESSES.**

### **2.5.1 Reagents used in Polymer Preparations.**

Table 2.1 lists all of the reagents used in the preparation of hydrophilic polymers. The hydrophilic monomer 2-hydroxyethyl methacrylate (HEMA), was obtained as the pure optical grade (for use in contact lens manufacture) and required no further purification. The ligand-based monomers were prepared as discussed previously. Both the cross-linking agent and the free-radical polymerisation initiator were used as supplied without further purification; all reagents were stored in a refrigerator until required.

**Table 2.1 Reagents Used in Polymer Preparations.**

<u>Reagent</u>	<u>Abbreviation</u>	<u>Structure</u>	<u>Supplier</u>
<hr/>			
Monomers:			
2-Hydroxyethyl Methacrylate	HEMA	$  \begin{array}{c}  \text{CH}_3 \\    \\  \text{H}_2\text{C} = \text{C} \\    \\  \text{C} = \text{O} \\    \\  \text{O} \\    \\  \text{CH}_2 - \text{CH}_2 - \text{OH}  \end{array}  $	Kelvin Lenses Ltd.
<hr/>			
4-Vinylpyridine	4VP		Aldrich
<hr/>			
4-Methyl 4'-Vinyl 2,2'-Bipyridine	VBipy		Synthesised
<hr/>			
Cross-Linking Agent:			
Ethylene Glycol Dimethacrylate	EGDM	$  \begin{array}{ccc}  \text{CH}_3 & & \text{CH}_3 \\    & &   \\  \text{H}_2\text{C} = \text{C} & & \text{C} = \text{CH}_2 \\    & &   \\  \text{C} = \text{O} & & \text{O} = \text{C} \\    & &   \\  \text{O} - \text{CH}_2 - \text{CH}_2 - \text{O}  \end{array}  $	B.D.H
<hr/>			
Initiator:			
Azo-Bis-Isobutyronitrile	AZBN	$  \begin{array}{ccc}  & \text{CH}_3 & \\  &   & \\  \text{H}_3\text{C} - \text{C} & - \text{N} = \text{N} - & \text{C} - \text{CH}_3 \\    & &   \\  \text{CN} & & \text{CN}  \end{array}  $	B.D.H

### 2.5.2 Preparation of Hydrogel Membranes.

Membranes were prepared by a method developed within the Speciality Materials Research Group at Aston<sup>27</sup>. Monomer reaction mixture (plus typically 0.5%/wt AZBN & 1%/wt EGDM, ~6g total) was degassed with nitrogen for 10 minutes and then injected by syringe into a membrane mould (Figure 2.10), consisting of two glass plates (10 x 15cm) with a poly(ethylene terephthalate) (melinex) sheet (10 x 12cm) fixed to the inner surface of each to aid in membrane removal.

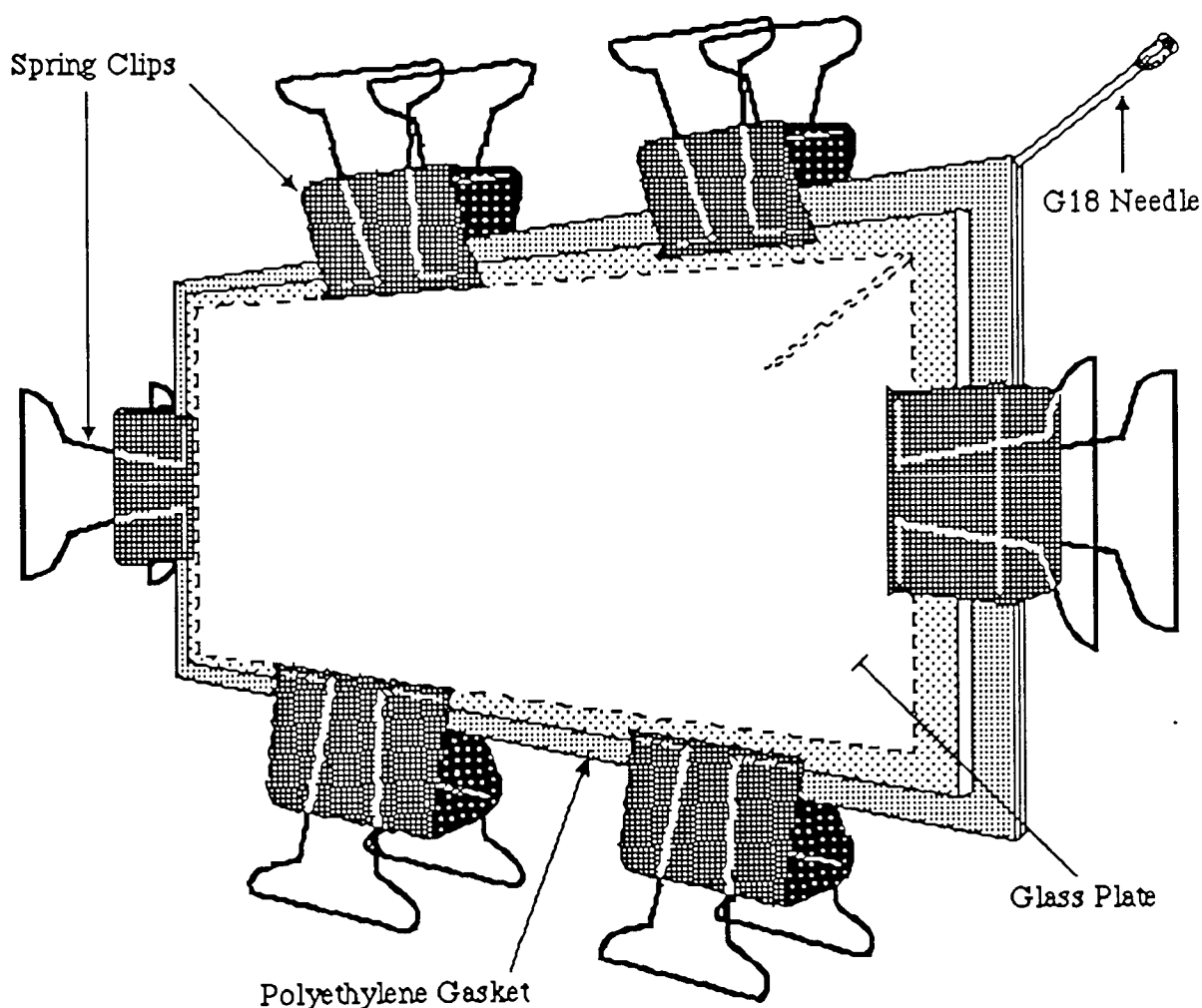


**Figure 2.10 Representation of a Membrane Mould.**

Sandwiched between the glass plates were two polyethylene gaskets (0.2mm thick) with a

rectangular hole (9 x 11cm) which forms the cavity of the mould. The complete arrangement was held together by bulldog clips and the reaction mixture transferred to the cavity *via* a G18 needle inserted between the plates. The mould was able to stand upright on two of the bulldog clips while the monomer mixture was injected. The mould did not totally fill when using a 6g sample, so that on removal of the needle, the plates squeezed together expelling excess liquid and filling the cavity to capacity. The mould was placed horizontally in an oven at 60<sup>0</sup>C to bulk polymerise for three days. This was followed by two hours post-curing at 90<sup>0</sup>C after which the mould was dismantled, the plates being separated while still hot by running a sharp knife along the edges. The melinex was carefully removed and the resulting membrane left to hydrate in distilled water for at least one week, preferably three, with frequent changes of water to allow leaching of unpolymerised material.

#### **2.5.2.1 Measurement of Equilibrium Water Contents.**

Four or five sample discs were cut from the appropriate hydrated membrane using a No.7 or No.10 cork borer. The excess surface water was carefully removed by blotting with filter paper and the samples weighed immediately to give the hydrated weight,  $W_{hyd}$ . The samples were dehydrated either in a vacuum oven overnight or in the microwave for 10-15 minutes (it was unclear as to whether the latter method removed all water in the gel, but results have been consistent to date). The dehydrated samples were again weighed immediately (as the gel can absorb water from the atmosphere), to give the dehydrated weight,  $W_{dehyd}$ . The EWC could then be calculated from equation 2.1:

$$EWC = \frac{W_{hyd} - W_{dehyd}}{W_{dehyd}} \times 100 \quad (2.1)$$

A statistical treatment of the error involved in the EWC determination by this technique using poly HEMA gives a standard deviation of  $\sigma_{n-1} = 0.4$ , an error of around 3% <sup>29</sup>.

### **2.5.3 Preparation of Linear Hydrophilic Polymers by Solution**

#### **Polymerisation.**

This technique was used to produce the polymer solutions required for dip-coating the platinum wire electrodes used in ion-sensor and cyclic voltammetry studies (section 2.9).

200ml of ethanol was placed into a 500ml three neck round-bottomed flask fitted with a dropping funnel, condenser and N<sub>2</sub> inlet. After 20 minutes degassing by bubbling through N<sub>2</sub>, a similarly degassed reaction mixture consisting of a total of about 15g of monomer in the appropriate ratio (i.e. 0.6g 4VP or VBipy & 14.4g HEMA for a 2% by wt.copolymer) together with initiator (0.5% by wt. AZBN), was added dropwise over 30 minutes. The system was immersed in a water bath at 60°C and left to polymerise under an N<sub>2</sub> atmosphere for 9 hours, after which the vessel was removed from the bath and left to cool overnight. Precipitated polymer was dissolved by reheating with stirring, and the viscous solution filtered under reduced pressure. The solutions were stored in stoppered glass bottles on the bench and always required reheating to solubilise precipitated polymer when dip-coating electrodes.

### **2.5.4 Suspension Polymerisation of HEMA Copolymers.**

This polymerisation technique was used in the production of HEMA:4VP copolymer beads, similar in form to those of an ion-exchange resin. The same procedure could be followed to produce HEMA:VBipy copolymer particles if desired. The basis of the

technique is to disperse the monomer mixture by mechanical agitation in a non-solvent continuous phase in the form of small globules <sup>117</sup>. Each droplet undergoes what is essentially an isolated bulk polymerisation, the continuous phase providing a medium for heat dissipation. Coalescence of the droplets is avoided by use of a stabiliser.

The organic phase consisted of 50ml of tetrachloroethane (TCE) solvent, 20g HEMA, 5g 4VP (~20% by wt copolymer beads), EGDM (1% by wt.) and AZBN (0.5% by wt.). The aqueous phase consisted of 120ml distilled water, 60g NaCl, 0.2% w/v xanthan gum (0.07g in 35ml) and 0.16%w/v hydroxypropyl methylcellulose (HPMC, 0.016g in 10ml). A 2l flat-bottomed polymerisation vessel was equipped with an overhead stirrer, condenser and N<sub>2</sub> inlet. The premixed aqueous phase was added to the flask and degassed with an N<sub>2</sub> purge for 1 hour. The monomers were dissolved in one half of the solvent and the initiator in the other, both were degassed then mixed and immediately added to the slowly stirring aqueous phase. The mixture was whisked at ~900 rpm for 15 minutes and the temperature raised to 70<sup>0</sup>C. After about 30 minutes the stirring rate was lowered to ~400 rpm for 3 hours, the inert atmosphere being maintained. After this time the stirring was stopped and the mixture allowed to cool for 12 hours. The resulting particles were washed thoroughly with water and ethanol to remove NaCl and TCE, shrunk with ether and dried in vacuo at 60<sup>0</sup>C overnight. Particle sizes were roughly separated by sieving into those <1000 $\mu$ m and those between 1000-2057 $\mu$ m (yield ~80%).

## **SECTION(B): TECHNIQUES USED IN TRANSITION METAL-ION**

### **COORDINATION STUDIES.**

#### **2.6 INTRODUCTION.**

The hydrogel matrix provides what is essentially an aqueous environment into which TM ions can permeate and coordinate with the ligand groups appended from the polymer backbone. However, many of the conventional physical and spectroscopic techniques used in the study of TM complex formation cannot be successfully employed in the case of such polymers (for example, FT-IR spectral detail is grossly obscured by large, broad water peaks around  $3400\text{-}3200\text{cm}^{-1}$  and  $1400\text{-}1200\text{cm}^{-1}$ ). Techniques utilised in this investigation can be summarised as follows:

- (i) Poly HEMA is used in the production of contact lenses and as such produces optically clear ligand-based copolymer membranes. Many of the TM complexes of these ligands are highly coloured and consequently, the rate and extent of metal coordination has been observed by monitoring the UV/Visible absorption spectra.
- (ii) Tensometric studies have been used in the investigation of potential cross-linking effects in the polymer membranes by metal ion complexation.
- (iii) Solutions of linear polymers have been used to dip-coat platinum wires for use in (a) ion-selective coated wire electrode sensors and (b) for investigations into the redox properties of polymer-immobilised complexes by cyclic voltammetry. Similarly, suspension polymerisation methods have been used to produce polymeric beads with a view towards ion-exchange capabilities.
- (iv) The possibility of selective TM ion transport and separation using ligand-modified membranes has been evaluated using various types of 'permeability apparatus' which

simply monitor the flow of ions from one side of the membrane to the other.

Permeation of a single TM ion species has been followed by the change in conductivity, but competition studies involving more than one type of metal were performed by taking regular samples and subjecting them to Atomic Absorption Spectroscopy (AAS).

- (v) Membrane samples have also been digested with acid to obtain the total metal content as found by AAS.

The type, design, set-up and operation of equipment used in points (i) - (iv) above will now be discussed in more detail.

## **2.7 ULTRAVIOLET AND VISIBLE ABSORPTION SPECTROSCOPY.**

The ions and complexes of both first and second row transition elements tend to absorb visible radiation in one, if not all of their oxidation states. The broad absorption bands are due to *d - d* electronic transitions and are strongly influenced by the chemical environment around the metal. In many TM complexes, one component acts as an electron donor and the other as an electron acceptor; absorption of radiation involves transfer of an electron from a donor orbital to one largely associated with the acceptor. As a result of this *charge-transfer absorption*, the excited state is a product of a type of internal redox process. Such charge-transfer complexes are particularly important because their molar absorptivities are very large ( $\epsilon_{\text{max}} > 10,000$ ) and thus provide a highly sensitive means for detecting and determining absorbing species.

Absorption measurements based upon UV/Visible radiation thus forms a useful, non-

destructive technique for the qualitative and quantitative determination of TM species within the hydrogel polymers. Spectrophotometers measure optical density ( $d$ ) as a function of wavelength, given by eqn. 2.2, where  $I_0$  is the intensity of light incident to the sample and  $I$  the intensity of the emergent light:

$$d = \log_{10} \frac{I_0}{I} \quad (2.2)$$

The molar absorption coefficient is given by eqn. 2.3, which can be rearranged to give Beer's law (eqn. 2.4), the most useful form of the equation:

$$\epsilon = \frac{d}{c \, l} \quad (2.3)$$

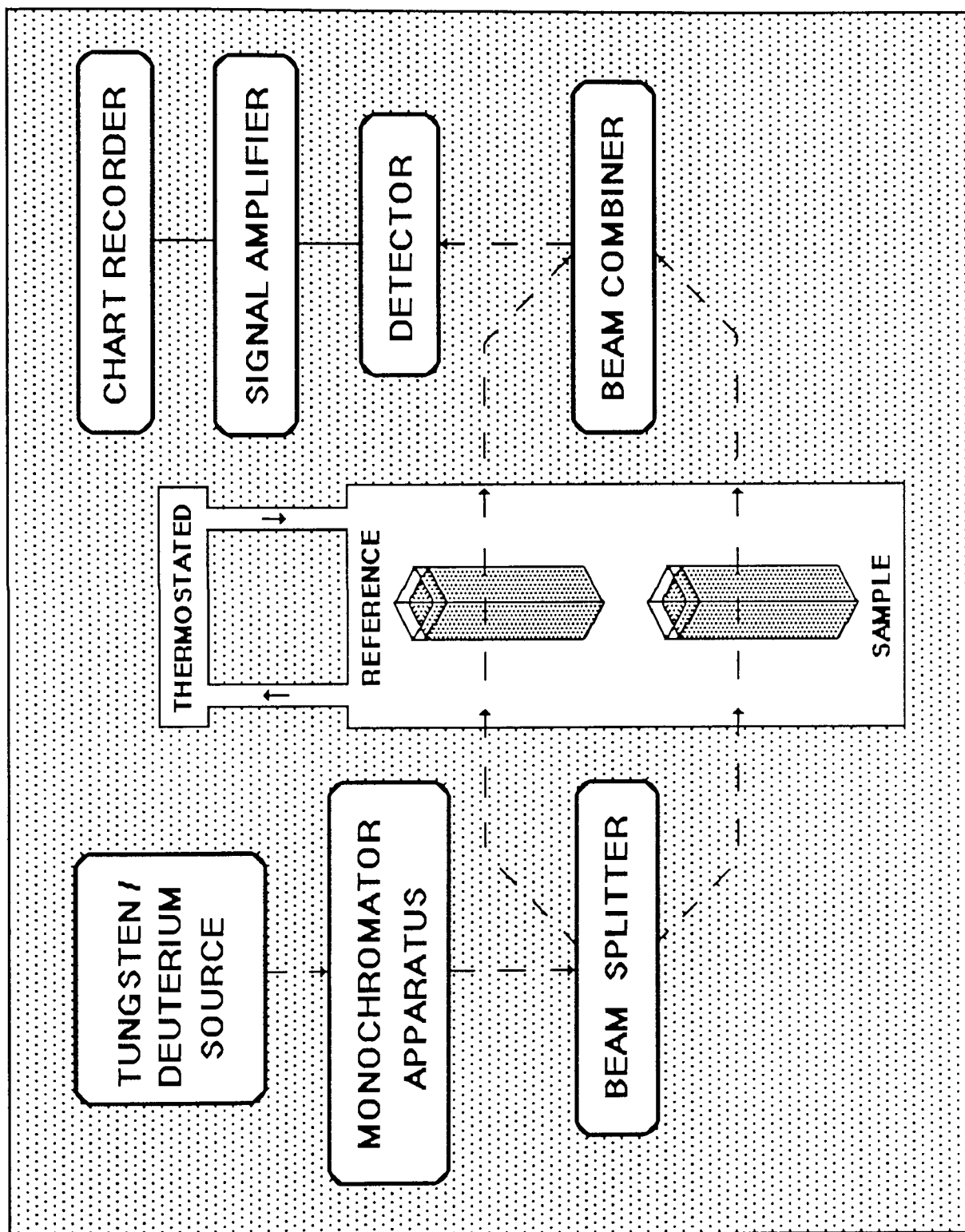
$$d = \epsilon \, c \, l \quad (2.4)$$

where  $c$  is the concentration of the absorbing species in gram-moles per litre and  $l$  is the path length in centimetres.

### **2.7.1 Spectrophotometer Instrumentation.**

The UV/Visible spectrophotometer used in this study was a Pye-Unicam SP8-100 double-beam instrument, possessing a wavelength range 190-890nm and variable band widths 0.2-1mm. Figure 2.11 outlines the basic features of such an instrument; more sophisticated machines are now fitted with micro-computers to allow the manipulation of spectra and storage on floppy disk. Owing to the nature of the work performed, it was decided to interface the SP8-100 to a BBC micro-computer to allow (i) the storage of spectra on disk and (ii), make possible the acquisition of data at regular time intervals over an extended period. The SP8-100 was modified by the addition of an analogue output (Figure 2.12). This was taken from across the signal input to the chart recorder, thus when the analogue output was being used the chart recorder was rendered inoperative, owing to excessive noise interference which caused the pen to vibrate violently.

**Figure 2.11 Schematic Representation of the Pye-Unicam  
SP8-100 Spectrophotometer.**



The BBC micro-computer is ideal for this type of project as it possesses an in-built 0-1.8V analogue input with analogue to digital converter (ADC). The SP8-100 was connected *via* a 15 pin connector, ground (GND) to analogue ground (AGND, pin 8) and live to channel 0 (CH0, pin 15):

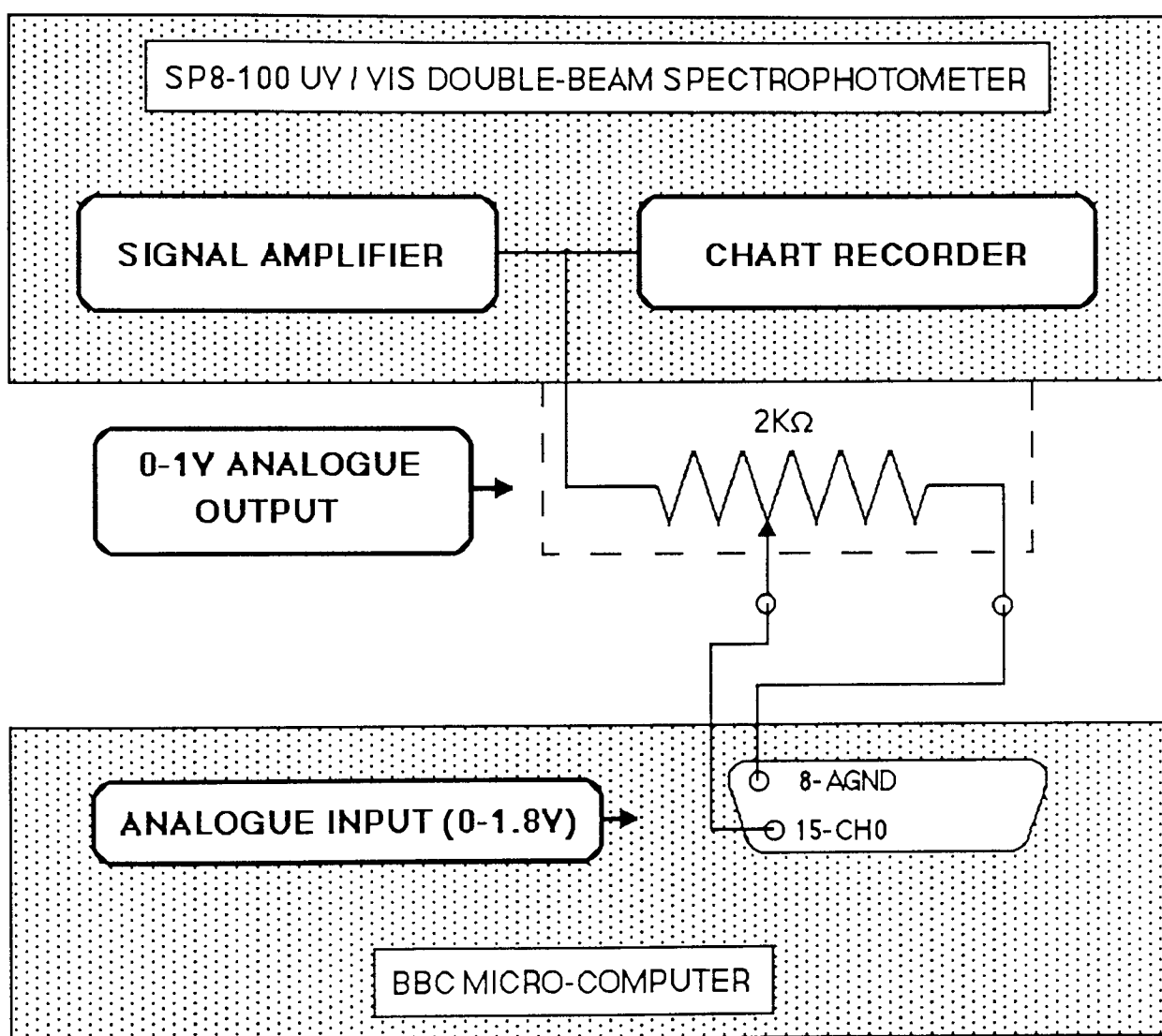


**Figure 2.12 Schematic for the SP8-100/BBC Micro Interface.**

The BBC has four input channels to which the spectrophotometer could be connected (pins 15, 7, 12 & 4: CH0, 1, 2 & 3 respectively), which are simply accessed in BASIC by the

command ADVAL x (x=1-4 corresponding to CH0-3).

Appendix One contains the program listings for the utilities used in conjunction with the SP8-100 spectrophotometer. As can be seen from the flow diagram, SCANSPEC is a simple program that records the absorbance measured on the SP8-100 during a wavelength scan (initially as a function of time but recalculated as wavelength by using the wavelength speed). The spectrum is thus saved as a data file on a 5<sup>1</sup>/<sub>4</sub> inch floppy and can be downloaded and replotted when required. Figures 2.13(a) & (b) are solution spectra of Co(SCN)<sub>2</sub> and NiCl<sub>2</sub> respectively, that have been saved and replotted in this way. The BBC micro used in this project has been fitted with a Watford motherboard that has allowed the addition of an Epson PRINTER ROM V1.0. Only with the use of this chip can graphic dumps of the quality of Figures 2.13(a) & (b) be produced.

### **2.7.2 Application of UV/Visible Spectrophotometry to Membrane Studies.**

Membranes produced by the copolymerisation of vinylic ligands with poly HEMA might be expected to coordinate TM ions when placed in a metal salt solution. The uncoordinated membrane is optically clear, and only begins to absorb when into the UV region of the spectrum (<300nm). A strip of membrane (1cm x 4cm) can thus be directly placed into the sample beam of the spectrophotometer (Figure 2.11) against either an air or blank membrane reference, and the visible absorption spectrum recorded. Membrane strips have been placed in cuvettes of path length 2mm in an effort to keep the hydrogel flat and upright. However, it has proved easier, and with greater reproducibility, to simply allow the hydrated membrane to adhere to the optical face of a cuvette, thus ensuring the beam enters the membrane square to it's surface. It is important that spectra are taken promptly as the membranes tend to dehydrate, warmed by the sample beam and general instrument environment, causing contraction away from the cuvette surface.

Figure 2.13(a) SCANSPEC Absorption Spectrum of  $\text{Co}(\text{SCN})_2$ .

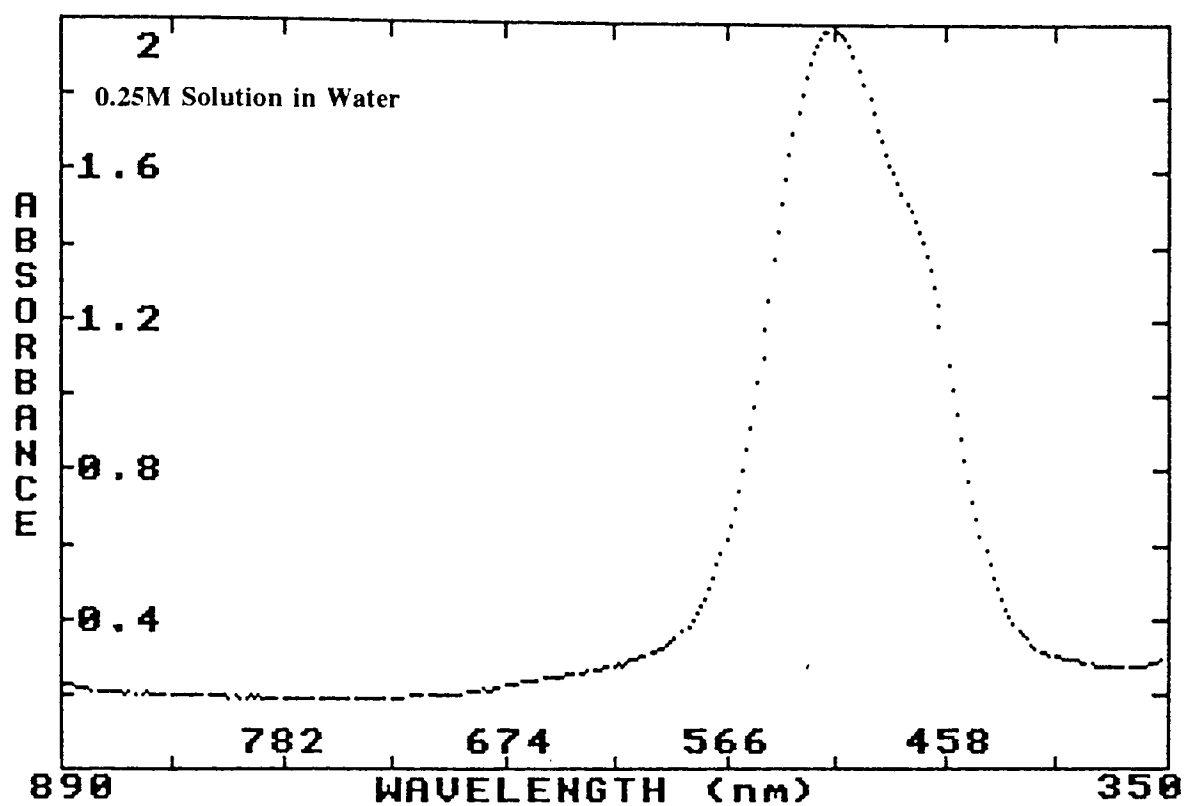
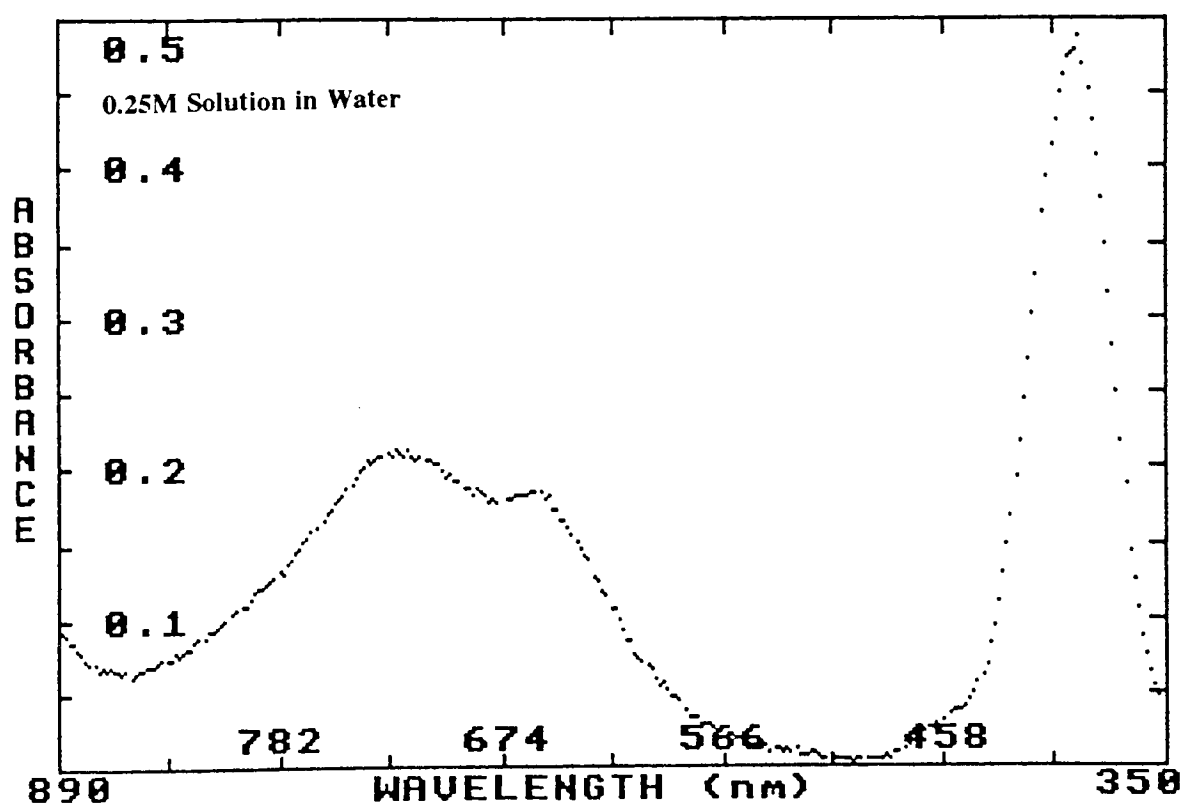


Figure 2.13(b) SCANSPEC Absorption Spectrum of  $\text{NiCl}_2$ .



### **2.7.3 Application to the Study of Ion-Binding Kinetics.**

If the formation of a complex results in a visible absorption, the concentration of the species giving rise to the absorption is proportional to the absorbance if Beer's Law is obeyed (eqn. 2.4). Therefore, providing a region of the spectrum is chosen where the absorption is due to a single species only, the complexation process can be followed spectrophotometrically by measurement of the absorbance at that fixed wavelength as a function of time.

The kinetics of ion-binding to ligands within the membranes has been studied using two techniques. The first was an *unattended* method which involved suspending a membrane strip inside a cuvette filled with the salt solution and observing the development of the complex colour with time. Obviously, this technique can only be applied to systems where the complex possesses a unique absorption, with no component due to the salt solution. One advantage of this method was that the micro-computer could be programmed to collect the data. Figure 2.14 is a kinetics trace following the coordination process of  $\text{Fe}^{2+}$  to a VBipy-based membrane, using the software utility SPECTROLOT (Appendix One) which was primarily developed to follow the transport of TM ions across such membranes (section 2.10.2). However, the membrane strips tended to move in the cuvette (even in a thermostated holder) and so the system was left unattended at one's peril.

The alternative, *attended* method, involved the periodic removal of membrane strips from thermostated sample bottles containing the salt solution, their absorbances subsequently recorded and the strips replaced in the salt solution. This procedure makes for the introduction of a larger error associated with the absorbance readings, just by the nature of

the process. It is also a very time-consuming operation that requires good timing and coordination to obtain the maximum amount of data over as little time as possible.

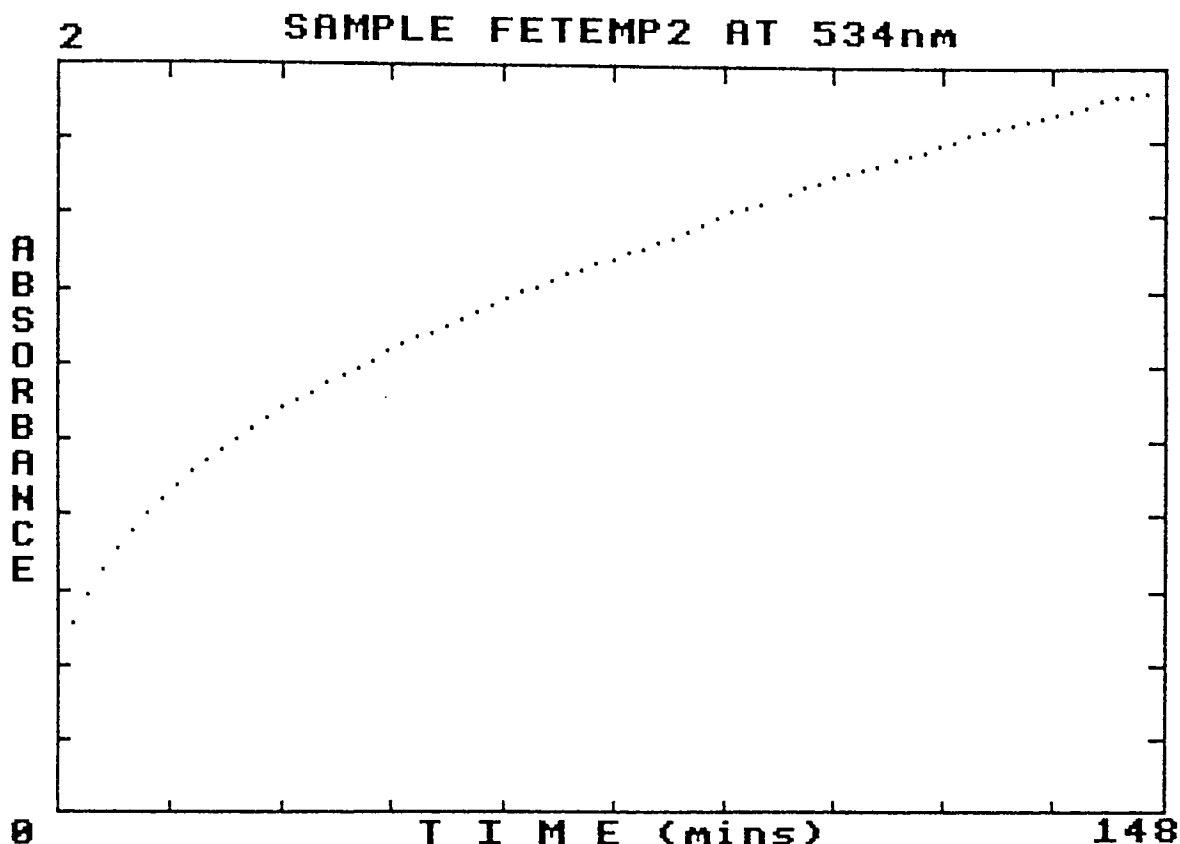


**Figure 2.14 Kinetics Trace of Fe<sup>2+</sup> Binding to a VBipy Membrane.**

## **2.8 MEASUREMENT OF MECHANICAL PROPERTIES.**

The mechanical properties of hydrogel-based polymers, including simple tension and to a lesser extent shear and uniform compression studies, is a well-characterised area of research at Aston <sup>28</sup>. The information derived from this type of investigation is of limited use as far as the objectives of this project is concerned. However, as shall be seen in Chapter Three, coordination of certain metal ions within the copolymer membranes can cause notable changes in the mechanical properties *via* a pronounced cross-linking effect. Data derived from stress-strain measurements are important from this viewpoint, providing information on the modulus, brittleness and the ultimate and yield strengths- all properties that change significantly with degree of cross-linking.

### **2.8.1 Instrumentation and Techniques.**

Tensile testing was performed on a 20KM Hounsfield Tensometer with 10N load cell, interfaced to an IBM 55SX computer with customised software to drive the equipment and allow data manipulation. By subjecting a 'dumbbell-shaped' membrane sample to a tensile force applied at a uniform rate, a curve resembling that in Figure 2.15 can be obtained.

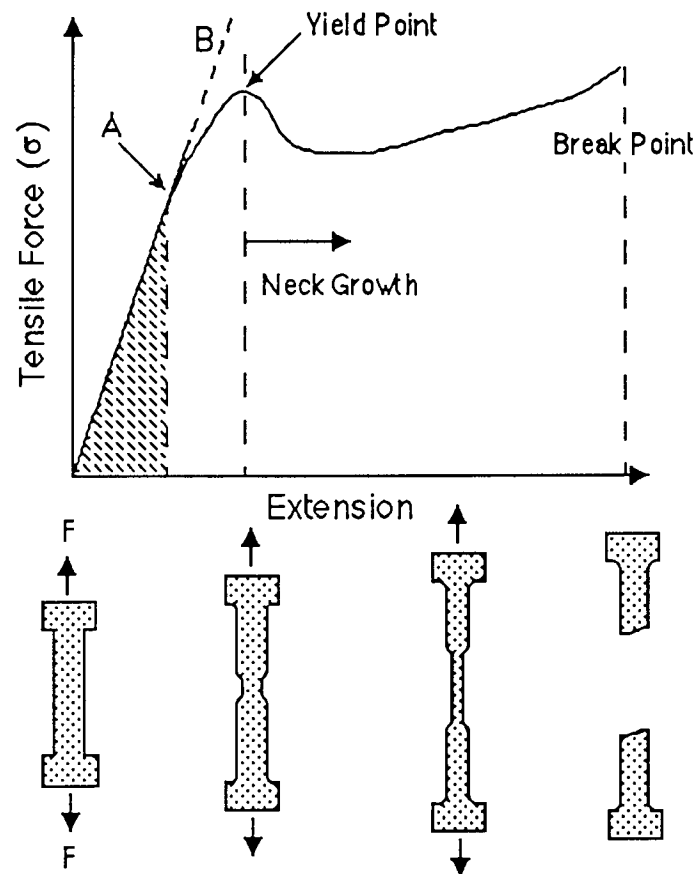


**Figure 2.15 Hypothetical Stress-Strain Curve.**

The tensile stress ( $\sigma$ ) is a measure of the force per unit area ( $F/A$ ) and the strain or elongation ( $\epsilon$ ) is defined as the extension per unit length; the two are related by a proportionality constant known as Young's modulus ( $E$ ) (eqn. 2.5):

$$\sigma = E \epsilon \quad (2.5)$$

The initial portion of the curve in Figure 2.15 is linear, the slope ( $B$ ) of which is used to

obtain E. The point A is the stress beyond which a brittle material will fracture, the hatched area under this curve being proportional to the energy required for brittle fracture. No fracture occurs in tougher material and the curve passes through a maximum known as the yield point. At this point 'necking' of the sample occurs until ultimate extension is reached at the break point. The area under the curve up to this point is the energy required for tough fracture to occur. The shape of such curves is dependent on many factors which must be kept constant and specified if meaningful comparisons of data are to be drawn. The parameters fixed for this study were chosen as the standard in previous investigations of this type <sup>28</sup> and include:

- (i) Temperature- Room temperature ( $\sim 21^{\circ}\text{C}$ ) is standard for these studies.
- (ii) Humidity- For hydrogel polymers it is important that they are maintained in a hydrated state for tensile readings to be consistent. Testing under water is impractical and so an alternative method of spraying the sample periodically with a fine mist of water seems to maintain the water content balance, providing 100% humidity.
- (iii) Strain rate- The speed at which the samples are pulled under tension effects the mechanical properties, faster speeds result in higher observed strengths but lower extensions. The strain rate used in this study was 200%/minute.
- (iv) Sample dimensions- The size of the sample was kept constant and the thickness of the membrane measured by micrometer to allow stress-strain calculations. The 'dumbbell' shape was adopted (the wider portions fitting within the jaws of the tensometer), as this shape produces a more uniform stress field. The gauge length (straight portion between the wider ends) was 8mm.

## **2.9 COATED-WIRE ELECTRODE STUDIES.**

Platinum wires possessing thin coatings of linear polymers prepared as in section 2.5.3, have been applied to the study of new sensing membrane formulations. It was thought that the presence of particular ligand groups would modify the electrode response to changes in activities of designated ions. The so called *coated-wire ion selective electrode* (CWISE) does not require an internal reference solution present in conventional ion selective electrodes (ISE's), and thus has the advantage of being inexpensive in addition to being easily and quickly constructed. The first half of this section is concerned with the construction of such electrodes and techniques to evaluate their behavior in solution.

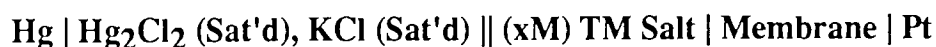
As previously discussed in Chapter One, the modification of electrodes by electroactive polymer films is a rapidly developing area of research <sup>118</sup> that is attracting the attention of scientists with interests as diverse as biochemical applications to device physics. While assessing the sensor potential of modified CWISE's, those coated with 4VP and VBipy copolymers were shown to complex with certain transition metal ions, thus immobilising a likely redox centre. Work in conjunction with the Electrochemistry group at Lanchester Polytechnic in Coventry, has involved subjecting such complex-bound electrodes to cyclic voltammetric methods. The remainder of this section describes the general procedure and instrumentation associated with this technique.

### **2.9.1 Coated Wire Electrode Construction and Use.**

The design and construction of coated wire electrodes has been described in detail elsewhere <sup>119,120</sup> and so this description will be limited to the essentials. The platinum wire used was obtained from Aldrich (Gold Label, 0.25mm dia.) and was cleaned before

coating by successive washing in detergent, distilled water and acetone, with a final rinse in chloroform and allowed to dry. The CWE tip consisted of a 2cm portion of Pt wire soldered onto a 110-in-line receptacle (R.S. Components Ltd.) to allow the tip to be detached from the connecting cable. The very tip of the wire was covered with an epoxy resin bead for insulation; this differs from the conventional construction which relies on a polymer bead deposited at the end of the wire, but is thought to produce a more stable response. The wire is then simply dipped in the polymer solution (section 2.5.3) five times quickly and the coating allowed to dry. This process is repeated until a film of about 1.5mm diameter covers the length of the wire. The tip is left to dry overnight and is then covered with Parafilm<sup>R</sup> up to 1cm from the beaded end of the wire, leaving a length of membrane exposed from insulation.

The CWE was attached to a PTI-6 digital pH/mV meter (R. W. Jennings Ltd.) by means of a coaxial cable to which a sliding terminal blade (250 blade, R.S. Components Ltd.) had been crimped and soldered to the inner copper strand. The CWE was tested as an ion-selective sensor on the electrochemical cell depicted below (**Figure 2.16**):



The test salt solution was magnetically stirred in a 100ml beaker into which the reference (saturated calomel electrode, SCE)/CWE electrode pair were placed, the resulting potential measured on the pH/mV meter.

### **2.9.2 Cyclic Voltammetric Studies of Coated-Wire Electrodes.**

Voltammetry is one of a group of electroanalytical methods that derive information about the analyte from the measurement of current as a function of the applied potential, obtained under conditions that encourage the polarisation of the indicator or working electrode <sup>121</sup>.

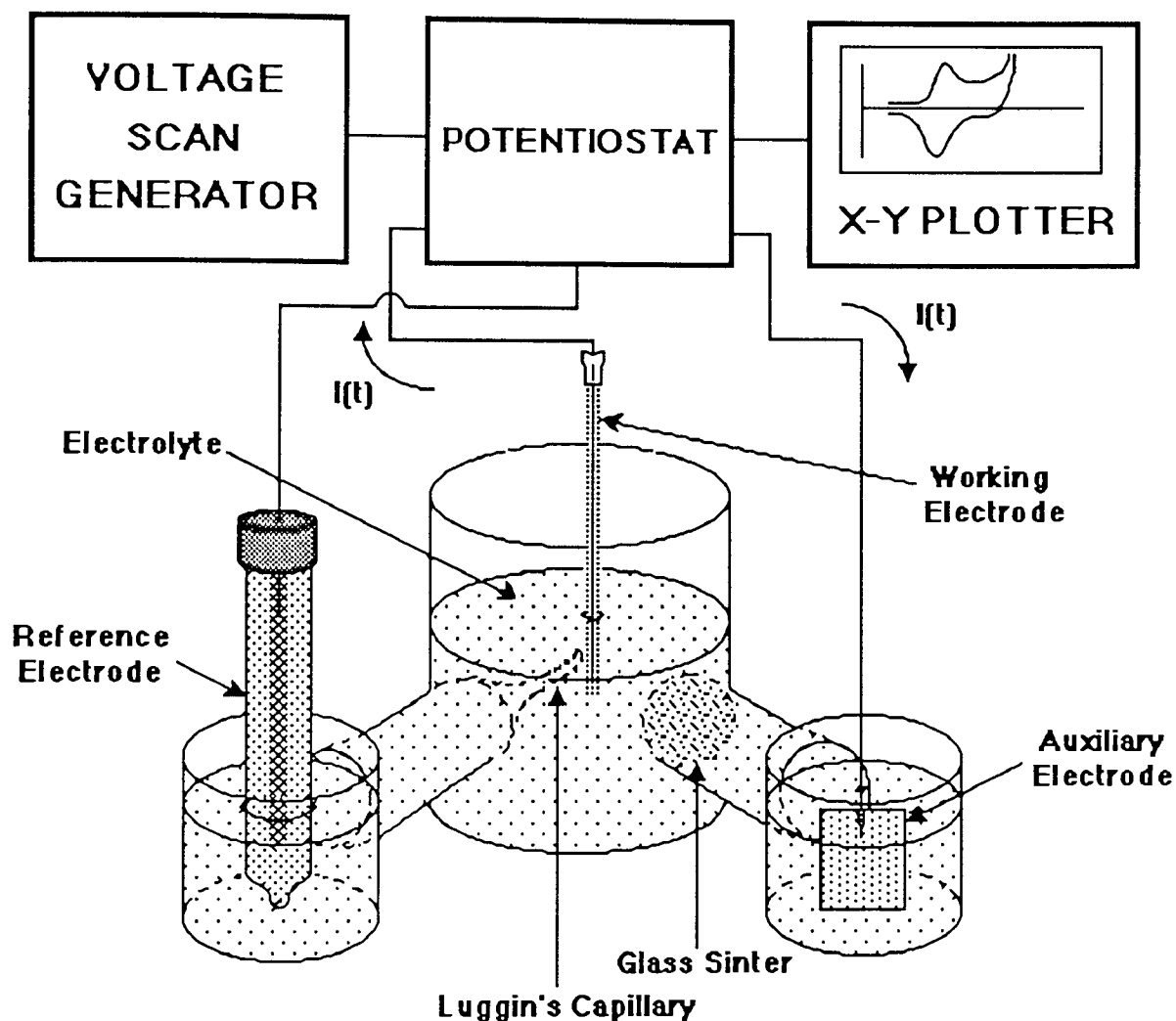
Cyclic voltammetry <sup>122</sup> (CV) is a modified polarographic technique in which the potential sweep follows a triangular form, increasing linearly to a peak and then decreasing to its start point at the same rate. The characteristic shape of a voltammetric wave produced in this way and its unequivocal position on the potential scale largely defines the electrochemical redox processes involved. CV has an additional attraction in that it can provide information on the kinetics of electron transfer reactions as well as the thermodynamics of redox systems.

In this study, it is the electroactive nature of the polymer film covering working electrode (WE) that is of interest. Coated-wire electrode construction was by much the same method as in section 2.9.1, except that the Pt wire was 6cm long and was not epoxy tipped. Once coated, the electrode was hydrated in distilled water for 24 hours before being transferred to the appropriate TM salt solution for complexation. The electrode was placed in a 0.1M KCl solution overnight before subjecting to CV to enable the supporting electrolyte to penetrate into the gel matrix.

#### **2.9.2.1 Cyclic Voltammetry: Instrumentation and Operation.**

Figure 2.17 outlines the basic three-electrode cell arrangement adopted for these investigations, which was connected to a Princeton Research Model 173 Potentiostat and conventional x-y plotter. Current flows through the auxiliary and working electrodes (AE & WE) but not through the high impedance reference electrode (RE, SCE). The RE is in close contact with the WE *via* a Luggin's capillary and provides a measure of the 'real' potential at the WE. The cell is filled with a suitable solvent containing an 'inert' support electrolyte which provides a conducting medium for the flow of current between

electrodes.



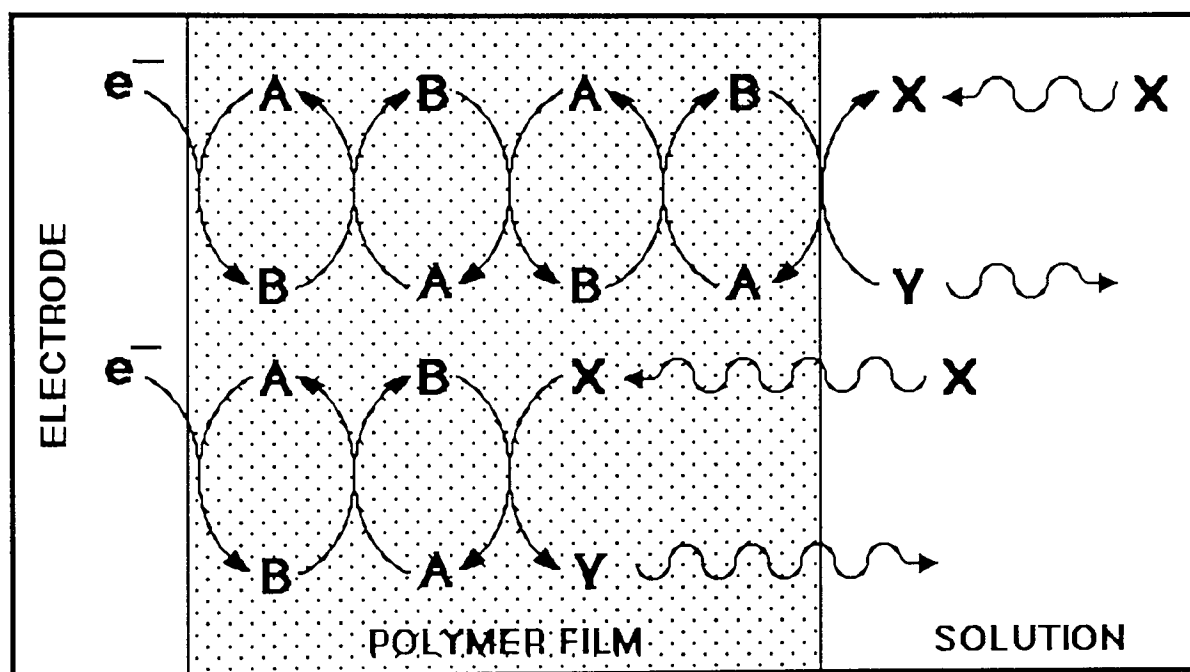
**2.17 Three Electrode Cell Cyclic Voltammetry Arrangement.**

#### **2.9.2.2 Choice of Solvent and Support Electrolyte.**

The supporting electrolyte used was 0.1M KCl but water is not the best of solvents for voltammetric studies as it has a rather narrow range of accessible potentials. The voltage "window" is support electrolyte dependent and has been quoted as ranging from around +1.4V to -1.3V<sup>123</sup>; it is limited on the negative side by the reduction of water to hydrogen and on the positive side by oxidation of the electrode material or by the formation of molecular or chemisorbed oxygen in water. This compares with the much wider window for other systems such as acetonitrile/tetraethylammonium perchlorate which has

limits around +2V to -3V. It was necessary to degas the solvent with an  $N_2$  purge to remove dissolved oxygen as it is readily reduced to produce two distinct waves, one corresponding to the reduction of  $O_2$  to peroxide and the second to the further reduction of peroxide to water.

Figure 2.18 represents a case where solution species (X) react with a mediator couple (A/B) at the surface of a film. The reactive redox state of the mediator (B) is eventually regenerated by reaction at the electrode:



**2.18 Reaction at a Polymer Modified Electrode.** (After Hillman <sup>124</sup>)

Water was the obvious choice of solvent for the study of hydrogel copolymer-coated electrodes because the gel contains imbibed water which provides a matrix for the permeation of electroactive solution species (X) to react with the reduced mediator sites (B) throughout the film. This provides a greater reaction flux or sensitivity than the with surface reaction only, the performance being limited by transport rates of X through the film.

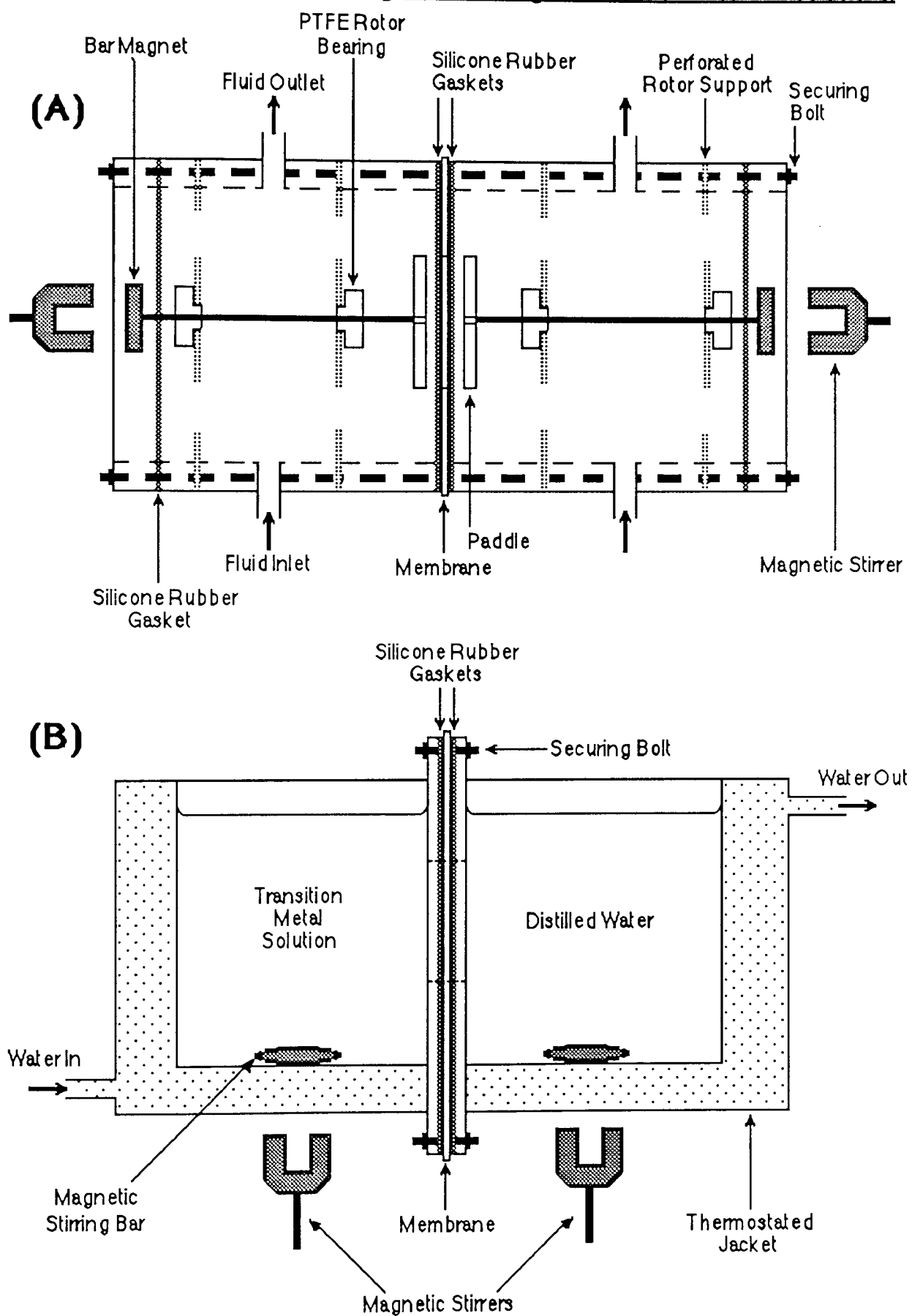
## **2.10 TRANSITION METAL ION PERMEATION STUDIES.**

Previous studies on the permeation of alkali and alkaline earth metal ions through poly HEMA membranes modified by crown ether ligands <sup>104</sup> suggested there may be potential for ion-selective transport, dependent on the extent of the interaction of the ion with the ionophore. Analogously, membranes modified with ligands specific for particular TM ions may infer the ability of selective transport and separation. Success in the study of membrane transport mainly revolves around the construction of a suitable permeation cell; it's design must take into account membrane parameters such as thickness, area and general integrity in addition to experimental variables such as temperature, concentrations, sampling ability and stirring rates. Considering the constraints imposed by the system, a wide variety of cell prototypes can be found in the literature <sup>125</sup>, generally categorised by mode of membrane placement i.e., horizontal or vertical. Two types of permeability cell were employed in this investigation, one used specifically for the study of a single metal species and the other for mixed metal solutions.

### **2.10.1 Permeability Cell Designs.**

Figure 2.19 outlines the main features of the two types of permeability cell employed during the course of this study. Both cells were constructed mainly of perspex to enable the condition of the rather fragile membranes to be observed. Cell (A) (Figure 2.19(A)) was based on the design of Misra *et al.* <sup>126</sup> used initially by Atherton <sup>127</sup> and subsequently by Hamilton <sup>102</sup> for ion-transport studies through hydrogel membranes. The cell (9 x 14cm) consisted of two chambers, one holding the TM salt solution, the other distilled water, separated by a sandwich of the test membrane between two silicone rubber gaskets (9cm diameter with 4cm diameter hole). The unit was clamped together by six

**Figure 2.19 Permeability Cell Designs for (A) Single TM & (B) Mixed TM Solutions.**



securing bolts to prevent leakage of the test solutions. Each chamber had a fluid inlet and outlet to allow circulation of the test solutions out of the cell *via* a flow-through conductivity cell, where the ion transport across the membrane could be monitored as a change in the conductivity of the low concentration side. Circulation of the fluid was achieved by a peristaltic pump with a flow rate around 30ml/min. The temperature of the system was regulated by immersing the cell in a vessel connected to a thermostatically controlled circulating water bath. Internal stirring paddles in both chambers could then be driven by magnetic coupling with external stirring motors, at a rate of about 150 rev/min (section 2.10.3).

Cell (B) (Figure 2.19(B)) possessed much the same features as (A), consisting of two chambers (8cm ht. x 7cm lg. x 5cm dp.) One side of each chamber was a backing plate (15cm x 14cm with a hole 4cm in diameter); the test membrane was placed between two silicone rubber sheets (of the same dimensions as the backing plates) and the 'membrane sandwich' completed by the bolting the plates 'back-to back' with the membrane moiety in the middle. The solution chambers were surrounded on four sides by a water jacket connected to a thermostatically controlled circulating water bath and the top of each chamber was left open to enable easy access for solution sampling. The vertical placement of the membrane certainly overcomes problems associated with hydrostatic pressure build-up and air bubble collection on the underside of horizontally placed membranes. However, stirring close to the membrane in this orientation is more difficult and is essential in the prevention of electrical double-layer build-up due to the migration of ions. It was decided that stirring from magnetic bars placed at the bottom of each chamber might be enough to prevent double-layer effects. Confidence in the design of this cell has increased since the

time of that decision, as permeability cells of a very similar design to that of (B) have been found in the literature, that of Uragami *et al.*<sup>99</sup> possessing an identical stirring mechanism. The use of cell (B) is described in sections 2.10.2 and 2.10.4.

### **2.10.2 The Spectrophotometric Study of TM ion Transport.**

The initial proposal was to study the permeation of TM ions across the polymer membrane by monitoring the development of the characteristic visible absorption spectra associated with many TM's (section 2.7) in the low concentration chamber of the permeability cell (B) discussed in section 2.10.1. The solution in the low concentration chamber was circulated *via* a peristaltic pump into a flow-through cuvette placed in the sample beam of the SP8-100 spectrophotometer (Figure 2.20). The spectrophotometer was set at the fixed  $\lambda_{\text{max}}$  for the particular TM involved (e.g. ~510nm for  $\text{Co}^{2+}(\text{aq})$ ) and the BBC micro computer left to collect the data for the increase in absorbance with time using the software utility SPECTROPLOT mentioned previously (section 2.7.3, Appendix One).

Unfortunately, this proposed method suffered from one serious flaw; the rate of transport of TM ions across such membranes is very slow and the  $\lambda_{\text{max}}$  is not sufficiently sensitive enough to allow TM transport to be studied by a spectrophotometric method. A possible solution to the problem may lie in the use of a colourimetric reagent in the low concentration side to form a complex of sufficiently large  $\lambda_{\text{max}}$  that it can be detected easily by the spectrophotometer. However, this may introduce the problem of 'back' permeation of the reagent across the membrane into the high concentration side. It was decided to look for an alternative method of monitoring TM ion transport.

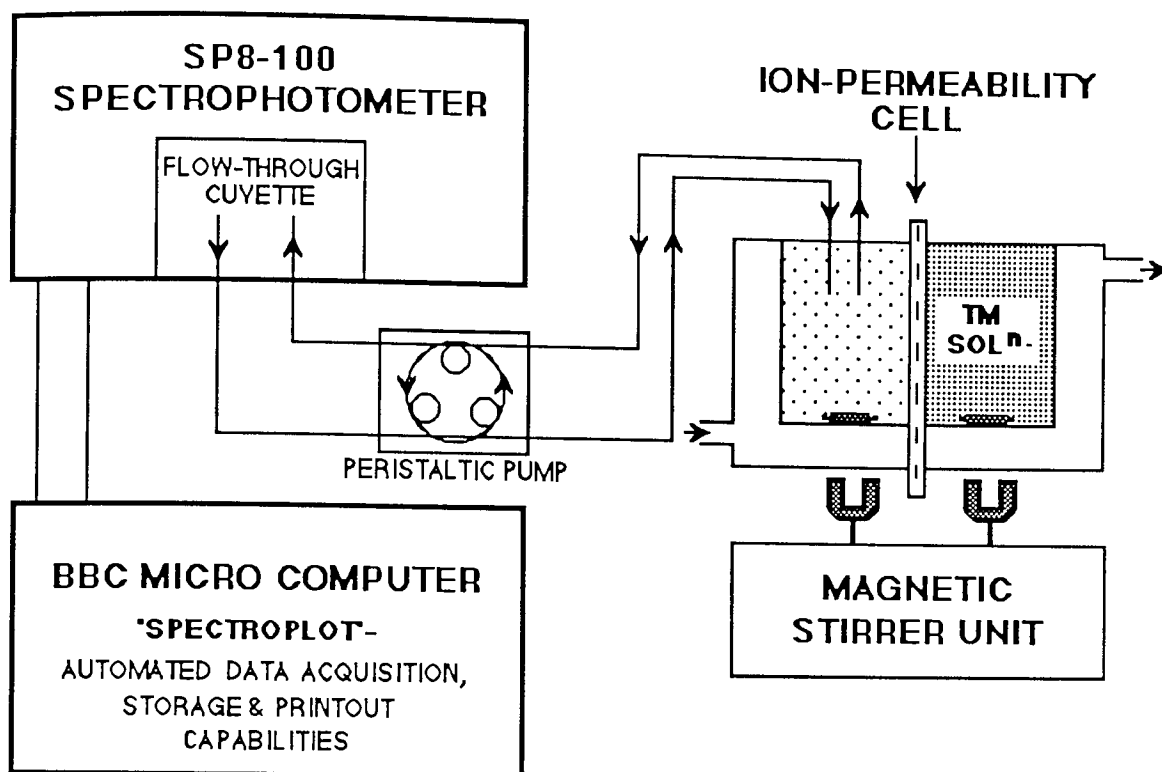
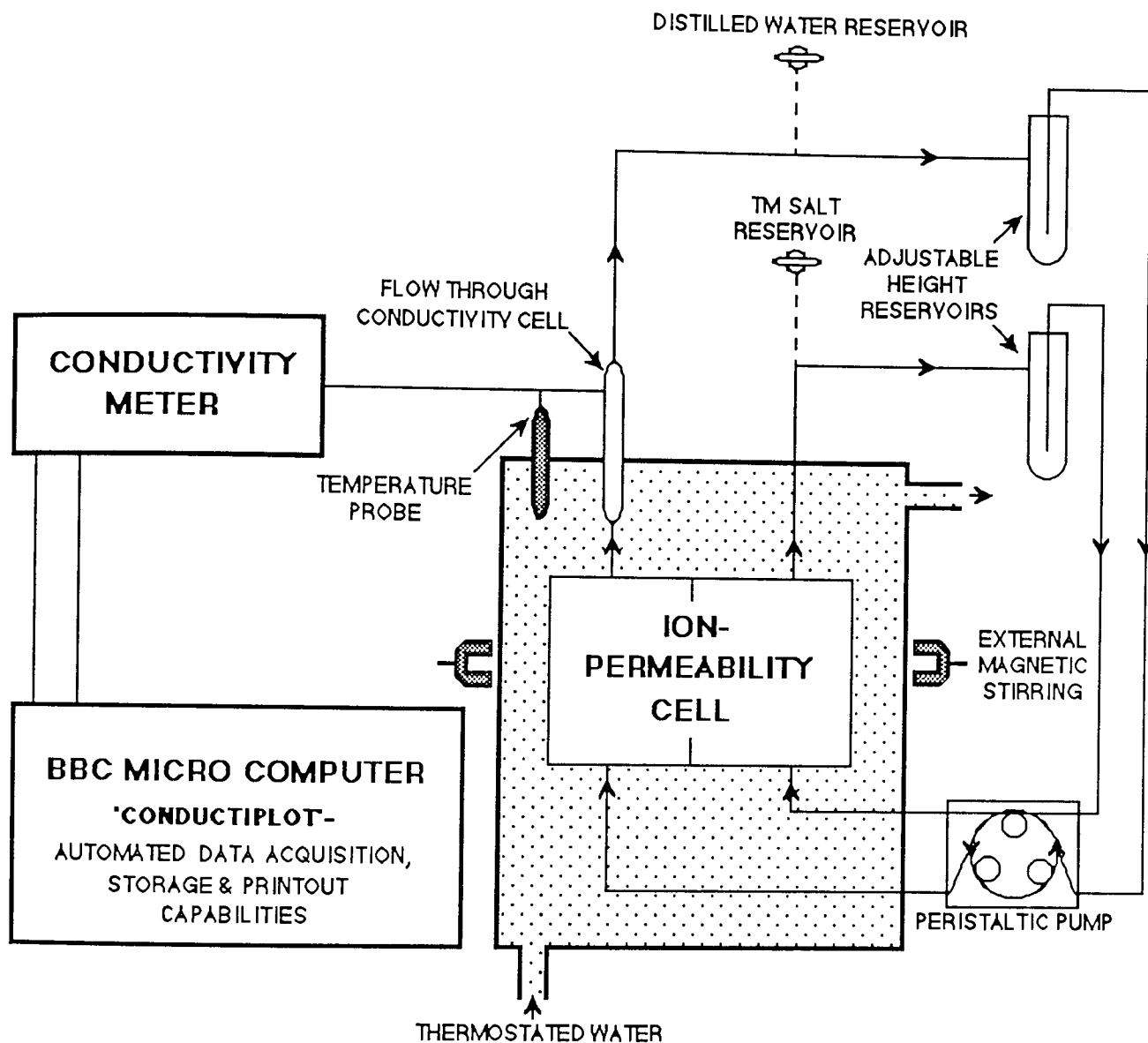


**Figure 2.20 Proposed Spectrophotometric Arrangement  
for the Study of TM Ion-Transport.**

### **2.10.3 The Conductometric Study of TM Ion-Transport.**

A membrane disc of minimum diameter 5cm was placed in permeability cell (A) as described in section 2.10.1 and the unit assembled. The rubber tubes were connected according to the diagrammatic solution flow 'circuit' shown in Figure 2.21. The flow through conductivity cell (cell constant  $k=1$ ) was connected to an AGB 1000 conductivity meter (Canterbury Sci. Inst. Ltd.), previously calibrated using a 1mM KCl solution according to the instructions provided. The cell was immersed in the water bath and both chambers of the cell were filled with the appropriate solutions from the respective reservoirs, care being taken to ensure the removal of any trapped air bubbles from the system.



### 2.21 Conductometric Arrangement for the Study of TM Ion-Transport.

Unequal hydrostatic pressures in one of the cell chambers would cause the membrane to bulge to one side, potentially causing damage to the hydrogel and affecting transport properties. The pressure differences could be compensated for by altering the height of one or other of the adjustable reservoirs, until the membrane was flat again. Once this had been achieved, the stirrers could be operated and the permeation process followed by the BBC

computer interfaced to the conductivity meter *via* the chart recorder output. A BASIC program called CONDUCTILOT (Appendix One) was implemented to automate the data acquisition process by storing the conductivity readings at specified time intervals. Figures 2.22(a) and (b) are example printouts of permeability runs monitored using this utility.

### **2.10.3.1 Calibration of the Conductivity Cell.**

In order to relate the change in observed conductivity with the concentration of TM salt passing across the membrane, it was necessary to calibrate the conductivity cell using solutions of known concentration. During the time period used for these studies (500 minutes max.) the change of concentration in the low concentration side of the permeability cell was always relatively small (0-20mM depending on the salt used). Although conductivity varies linearly with concentration over this range, three or more standard solutions in the appropriate range for the salt in question (Table 2.2) were used to construct a calibration graph, the gradient of which was necessary to convert  $\mu$ siemens into mM.

**Table 2.2 Concentration Range for Standard Solutions used in Calibration of Conductivity Cell.**

<u>TM SALT</u>	<u>CONC. RANGE (mM)</u>
Sulphate	0.05, 0.2, 0.4
Chloride	0.5, 1, 2
Nitrate	1.25, 2.5, 5
Thiocyanate	} 2.5, 5, 10, 20
Perchlorate	
Hexafluorophosphate	

By connecting a pipette filler to one of the glass side-arms on the flow-through cell, fluid could be drawn into the cell through the remaining side-arm. The conductivity of a

Figure 2.22(a) CONDUCTIPLLOT Permeability Run for  $\text{NiNO}_3$  through a PolyHEMA Membrane.

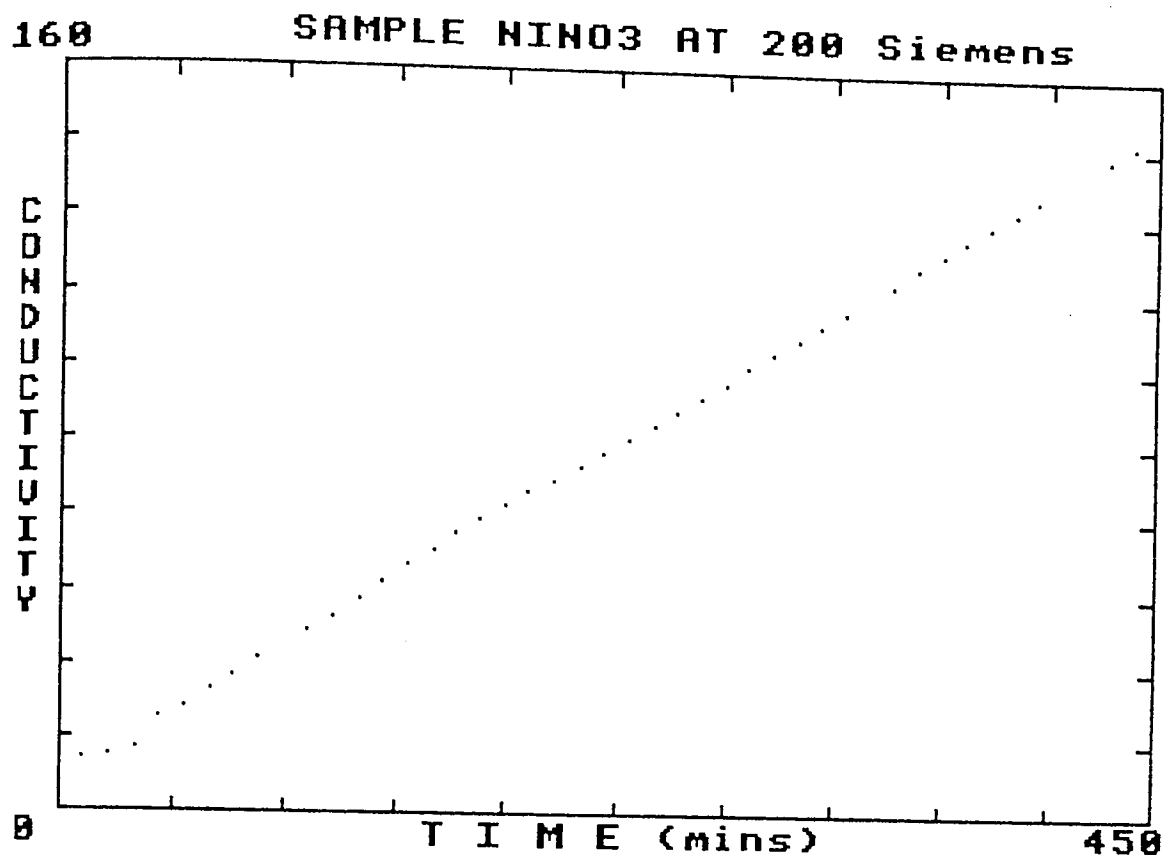
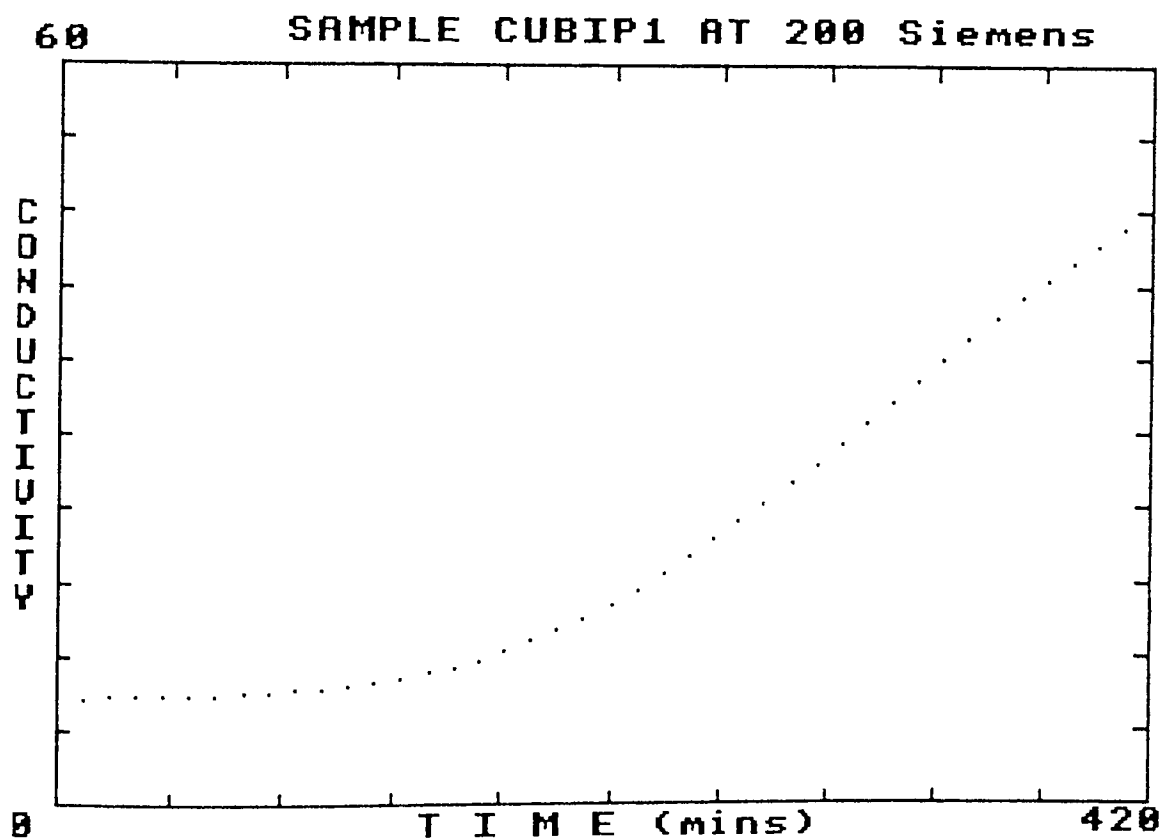


Figure 2.22(b) CONDUCTIPLLOT Permeability Run for  $\text{CuCl}_2$  through a VBipy/HEMA Copolymer Membrane.



solution was established by firstly flushing the cell with distilled water, followed by rinsing with the solution under study. Finally the cell was carefully filled with the solution, ensuring no air bubbles were present, and the ATC probe of the meter placed in a beaker of the same solution. The reading on the meter was noted and the process repeated to see if a consistent value could be obtained.

#### **2.10.4 Transport Studies on Mixed TM Solutions.**

The transport of two or more transition metal species simultaneously cannot be followed by conductometric methods alone, as it would be impossible to determine the individual contributions of each species represented to the total observed conductivity. Therefore, investigations into the transport of mixed TM solution required a permeability cell of type (B) (section 2.10.1) in which there was easy access to the solution chambers.

A disc of test membrane (5cm diameter) was placed between the two silicone gaskets and the cell unit assembled. The distilled water and test solution were poured into the respective chambers, the magnetic stirrers switched on and a stop clock started. At regular time intervals (15 minutes for the first 1.5 hours then every 50 minutes) 1ml aliquots were removed from both chambers of the cell. The sample from the low concentration side was diluted to 10ml and saved for later analysis by atomic absorption spectroscopy (section 2.11); that from the solution side was removed to maintain an equal hydrostatic pressure on the membrane and was thus discarded.

#### **2.11 THE USE OF ATOMIC ABSORPTION SPECTROSCOPY.**

The aspiration of a metallic salt solution into a flame (such as acetylene burning in air)

results in a vapour containing gaseous metal atoms, the majority of which remain in their ground state. These atoms are capable of absorbing radiant energy equivalent to their specific resonance wavelength (the wavelength of energy emitted if the atoms were excited from their ground state). The basis of atomic absorption spectroscopy (AAS) is to pass light of resonance wavelength through a flame containing such atoms, and to detect the corresponding absorption of energy which is proportional to the number of atoms present. The instruments used in this investigation were an Instrumentation Laboratory Ltd. Model 151 and Perkin Elmer Model 360 double-beam atomic absorption spectrophotometers. Table 2.3 outlines some AAS data for the elements studied:

**Table 2.3 AAS Data for the Elements under Study.**

<u>ELEMENT</u>	<u>MAIN RESONANCE W/L (<math>\lambda_{nm}</math>)</u>	<u>WORKING RANGE</u> <u>(<math>\mu g/cm</math>)</u>
Ca	422.7	1-4
Co	240.7	3-12
Cu	324.7	2-8
Fe	248.3	2.5-10
Mn	279.5	1-4
Ni	232.0	3-12
Zn	213.9	0.4-1.6

Calibration solutions of 1, 2 & 4ppm were made using B.D.H. AAS standards, to enable the conversion of the absorbances to metal concentrations. It was important that all samples were subjected to analysis within 48 hours, otherwise deterioration occurred owing to adsorption of the solute to the walls of the glass containers.

### **2.11.1 Application of AAS to Membrane Studies.**

Samples obtained from transport studies (section 2.10.4) could be directly subjected to AAS without further preparation.

In the determination of total metal content bound within ligand-modified membranes, it was necessary to firstly carry out a digestion of the organic material to leave just the metal oxide. This was accomplished by placing the sample in a digestion tube with a 10:3 mixture of conc. nitric acid:conc. sulphuric acid (B.D.H. Spectrosol for spectroscopic purposes). The tube was heated to dryness in a fume cupboard, care being taken to avoid loss of material from 'spitting'. This rather difficult and time-consuming process has been superseded in the literature by a microwave digestion technique that uses a sealed Teflon-based vessel to contain the digestion medium <sup>128,129</sup>. After cooling, the oxide coating was dissolved by several washings with small samples of 0.1M HCl and the solution made up in a known volume of the same. This could then be subjected to AAS as previously described.

### **2.12 USE OF TRANSITION METAL SALT SOLUTIONS.**

All of the salts used in this study were analytical reagents purchased from B.D.H or Aldrich. The cobalt hexafluorophosphate used in the permeability studies of Chapter Five, was not commercially available and was thus synthesised by the following procedure:

A slight stoichiometric excess of  $\text{KPF}_6$  (23.01g) was dissolved in 100ml of water @ 50°C and added to  $\text{Co}(\text{ClO}_4)_2$  solution (22.87g in 150ml) to give a 0.25M concentration w.r.t.  $\text{Co}(\text{II})$ . This was kept overnight @ 5°C when the insoluble  $\text{KClO}_4$  precipitated out and was filtered off. The amount of retained solid was in agreement with the theoretical yield

for 100% removal of all the perchlorate (~17.3g). A sample of the prospective  $\text{Co}(\text{PF}_6)_2$  was evaporated down and the solid subjected to infra-red analysis. This showed a symmetrical stretch  $\nu_1$  around  $740\text{ cm}^{-1}$  as expected for hexafluorophosphate, and no sign of the sharp  $\nu_1$  symmetrical stretch and  $\nu_4$  scissoring absorption seen at  $935\text{ cm}^{-1}$  and  $630\text{ cm}^{-1}$  respectively for perchlorate. This 0.25M solution was then used directly in EWC and permeability experiments.

### **CHAPTER THREE**

#### **THE INVESTIGATION OF TRANSITION METAL COMPLEXES IN LIGAND-MODIFIED HYDROGEL POLYMERS.**

### **3.1 INTRODUCTION.**

The first and most obvious question one would ask of potential chelating hydrophilic polymers is 'Are they capable of complexing with transition metal (TM) ions from solution?'. This chapter assesses the degree of interaction and selectivity of these materials with various TM ions and attempts to characterise the complexes formed using the techniques outlined Chapter Two.

Hydrogel materials do not lend themselves easily to the more straight-forward characterisation techniques by virtue of their inherent water-swollen and cross-linked nature. However, the following pages demonstrate very clearly that visible spectroscopy can be a simple and invaluable tool for the study of certain polymer-immobilised TM complexes. Often a change in the type or stereochemical arrangement of ligands, or a change in oxidation state of the metal, can result in a colour change of a complex. Observations of this type of occurrence with cupric, cobaltous or ferrous salts were of particular interest in this study.

Detailed within this chapter is a preliminary outline of the use of electrochemical methods for the study of complexes immobilised onto polymer-coated-wire electrodes. It is important to gain information concerning the extent to which the polymer influences the chelating ability of the ligands, as this will provide the foundations for the kinetic and transport studies discussed in Chapters Four and Five respectively.

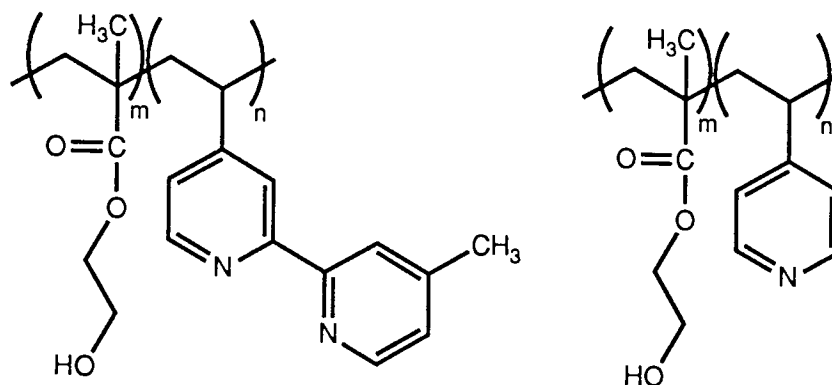
Finally, studies into the mechanical properties of the polymer are used to demonstrate the influence of metal-ion coordination on the effective cross-linking of the gel matrix, and how this relates overall to the physical properties of the polymer.

## **3.2 POLYMERS IN PERSPECTIVE.**

### **3.2.1 Ligand Distribution within the Copolymers.**

Before discussing in detail the coordination chemistry of pyridyl-based complexing copolymer membranes, it is advantageous to obtain an image of the arrangement of the ligands along the copolymer chains. It is possible to loosely predict the behaviour of two monomers which have never previously been combined by use of the  $Q-e$  scheme, a system that contrives to correlate copolymerisation tendencies by relating the reactivities or resonance effects ( $Q$ ) and the polar properties ( $e$ ) of monomers <sup>130</sup>. The reactivity ratios of the HEMA and 4VPy vinyl groups are very similar and would be expected to produce a copolymer with pendant pyridines arranged in a random fashion along the chains. An analogous situation applies to the VBipy ligand which is essentially 4VPy with a substituent group at position 2 and thus should possess a similar vinyl reactivity to 4VPy.

Chapter Two describes the synthesis of these polymers in terms of the respective weight percentage of comonomers in the polymerisation mixture. Assuming the reasonable scenario of random copolymer generation, it is possible to envisage the average copolymer sub-unit for the various monomer compositions employed during this study. Figure 3.1(a) displays the HEMA:VBipy ratio (m:n) in copolymers made from various weight percentages of VBipy in the reaction mixture. To enable direct comparison of the complexation processes in bipyridyl and pyridyl-based copolymers, it was necessary to adjust the weight percentage of 4VPy used in the pyridyl copolymer reaction mixtures, so as to produce polymers with equivalent numbers of coordinating nitrogens per unit mass to that of the bipyridyl polymers (Figure 3.1(b)).



<u>% Ligand by Weight.</u>	<u>~(m:n) Ratio.</u>	<u>% Ligand by Weight.</u>	<u>~(m:n) Ratio.</u>
0.05	3014:1	-	-
0.1	1505:1	-	-
0.25	601:1	-	-
0.5	300:1	0.54	150:1
1	149:1	1.07	75:1
2	74:1	2.14	37:1
4	36:1	4.29	18:1
8	17:1	8.57	9:1
-	-	17.14	4:1
-	-	20.0	3.2:1

**Figure 3.1(a) HEMA:VBipy Ratios  
for Various Comonomer Mixes.**

**Figure 3.1(b) HEMA:4VPy Ratios  
for Various Comonomer Mixes.**

### **3.2.2 Effect of Copolymer Composition on the EWC.**

It is the equilibrium water content (EWC) of the polymer that provides the medium for ion transport and coordination within the gel matrix. Therefore, it is important to establish whether the presence of the ligand moiety has any significant effect on the EWC. Using the technique outlined in Chapter Two (section 2.5.2.1), the EWC's of a range of VBipy:HEMA and 4VPy:HEMA copolymer membranes were determined. Figure 3.2 (overleaf) illustrates that the introduction of increasing proportions of the more hydrophobic ligand component does indeed lower the EWC of the membrane to some extent. However, 4VPy and VBipy are by no means as hydrophobic in nature as corresponding styrene and vinyl biphenyl analogues because the nitrogen atoms within the

heterocyclic rings of the ligands are able to hydrogen bond to water molecules <sup>130</sup>. As a consequence, the EWC was not appreciably altered over the loading range at which the majority of kinetic and transport studies were performed (i.e. 0.5-2%).

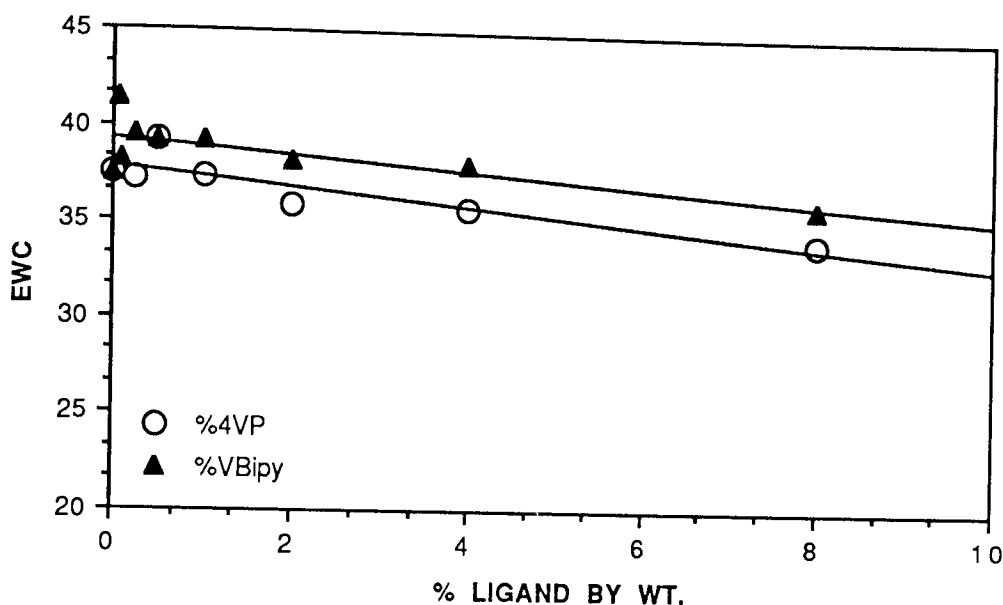


**Figure 3.2 Variation of EWC as a Function of Ligand Loading.**

It should be noted that all the membranes studied were cross-linked with 1% by weight of ethylene glycol dimethacrylate (EGDM) to strengthen the membrane and prevent it from tearing. Cross-linking has also been shown to reduce the EWC <sup>28,29</sup> but the 1% employed here has only a minor affect, reducing the EWC from ~37% to ~36%.

### **3.3 POLYMER INTERACTIONS WITH TRANSITION METAL IONS.**

In order to assess the degree of TM interaction within the polymers, samples were cut from pre-hydrated poly(HEMA), poly(HEMA:2% VPy) and poly(HEMA:2% VBipy) membranes using a No.10 cork borer. Pre-weighed specimens from each of the membranes were then placed in a range of 0.25M TM chloride solutions, one sample per salt, and left for a number of days. The metal content within the membrane was then

determined by removing the sample and carefully blotting any excess solution from the membrane surface with a filter paper. The sample was then subjected to acid digestion and the metal content found by AAS as described in Chapter Two (section 2.11.1).

If a membrane sample is placed in a salt solution, the solute will dissolve within the imbibed water of the gel matrix. The measure of the ability of the salt to partition between the membrane and equilibrating solutions is known as the partition coefficient, and it is important to have some idea of how this varies with the range of TM chlorides studied in an unmodified membrane before making any firm conclusions on the complexation effects of ligands within the polymers. It was for this reason that unmodified poly(HEMA) membranes were included in the metal-interaction studies described above. Figure 3.3 illustrates the variation in the partition of different TM chloride salts into a poly(HEMA) membrane, as represented by the number of moles of metal salt per mg wet weight of polymer.

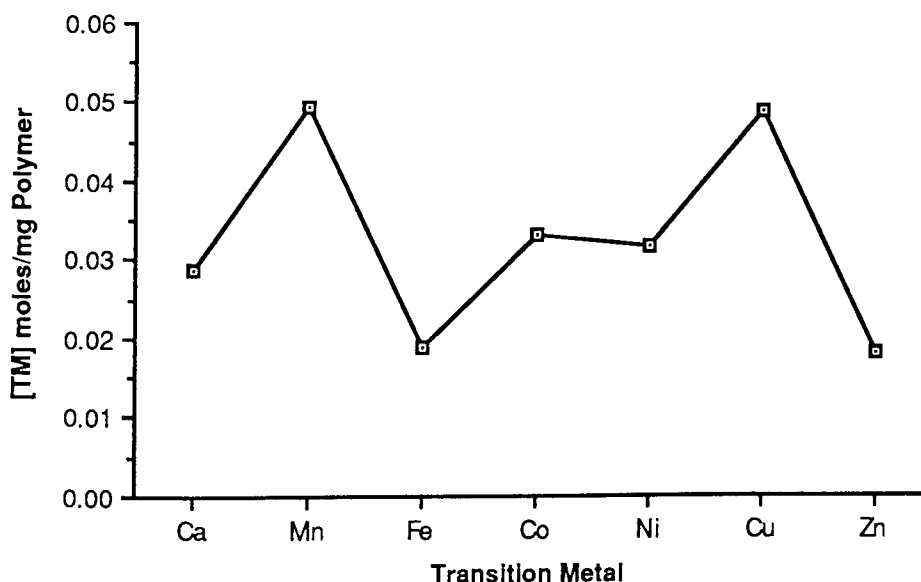


**Figure 3.3 Variation of TM Salt Partition into PolyHEMA Membranes.**

The observed differences between TM cations is probably a function of the influence of such ions and their large hydration spheres on the water content of the gel. In addition, some cations may have the ability to approach the polymer backbone more closely than others and so partition into both the aqueous and polymer phases is possible, a phenomenon certainly true for anions (Chapter Five).

The total metal ion content present within ligand-modified membranes consists of two components, (i) that partitioned into the bulk water of the gel matrix and (ii) that coordinated to the ligands, and/or the polymer. By subtracting the results shown in Figure 3.3, we can remove the effect of the first component to leave a true representation of the extent to which the ligands complex first-row TM ions (Figure 3.4).

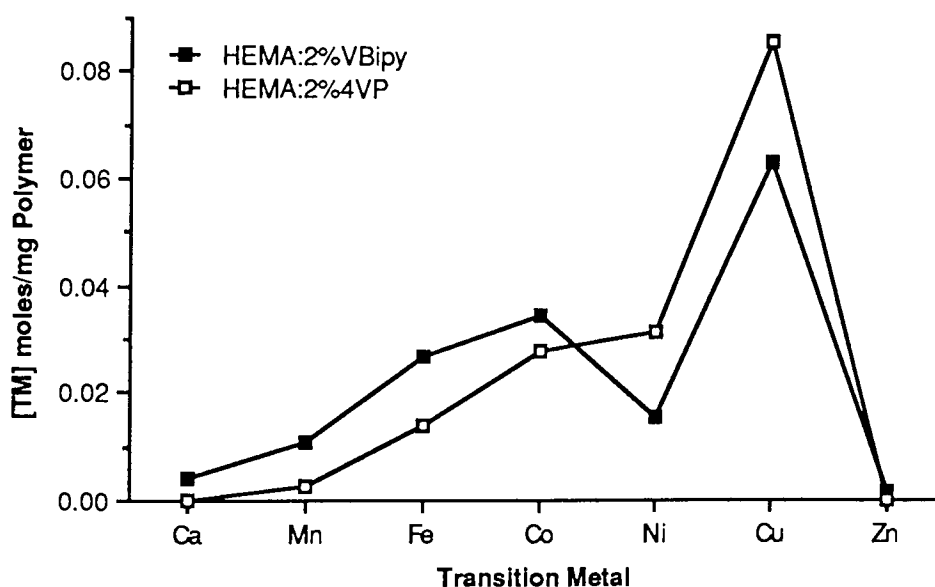
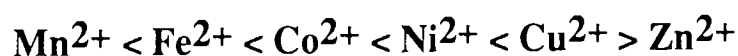


**Figure 3.4 TM Content Associated with Ligand-Modified Membranes.**

The *Irving-Williams series* shows that, for any given ligand, the stability constant for divalent ions of the first transition series generally follows the order:



The pyridine-based membrane seems to be interacting with metal ions in accord with this trend, the affinity of the polymer being greatest for  $\text{Cu}^{2+}$  as expected. The bipyridyl-based polymer appears to have anomalous interactions with  $\text{Fe}^{2+}$  and  $\text{Co}^{2+}$  but the processes occurring here become clear by combining knowledge of their conventional solution coordination chemistry with the data shown in Figures 3.5(a) & (b):

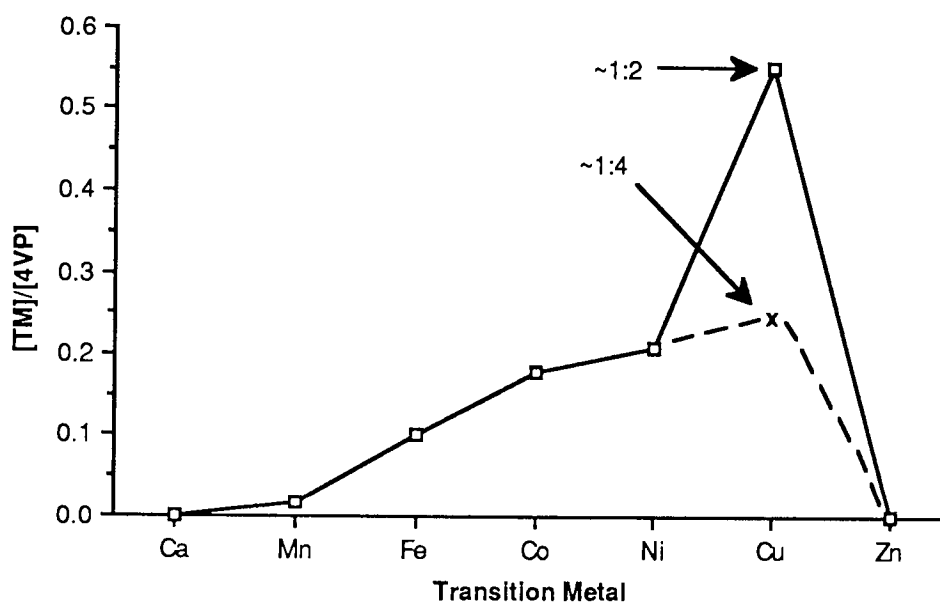


**Figure 3.5(a) Ratio of [TM]:[Ligand] in Pyridyl-Polymer Membranes.**

The solid lines in Figures 3.5(a) & (b- overleaf) represent the metal to ligand ratio achieved when a polymer membrane is left to stand in a 0.25M metal chloride solution. If however, the membrane is removed from the salt solution and allowed to leach in distilled water, the metal to ligand ratio changes, the most prominent cases being illustrated by the points (x). For the pyridyl polymer (Figure 3.5(a)), the initial  $\text{Cu}^{2+}$ :Pyridine ratio of between 1:1 and 1:2 is changed to 1:4 by placing the membrane in distilled water. As will be discussed in the following sections, it is thought that  $\text{Cu}^{2+}$  within the polymer matrix leaches out into the surrounding solution until the metal:ligand ratio approaches 1:4, indicative of the stable four coordinate  $\text{Cu(II)} (\text{pyridyl})_4$  complex.

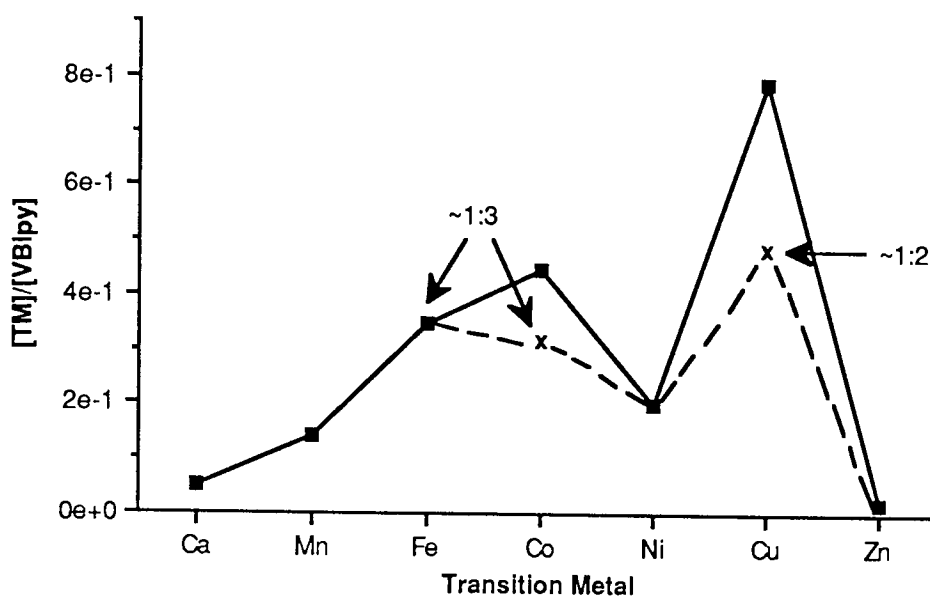


**Figure 3.5(b) Ratio of [TM]:[Ligand] in Bipyrindyl-Polymer Membranes.**

The same is also true for Cu(II) and the bipyrindyl polymer (Figure 3.5(b)), except that the ratio after leaching is 1:2, characteristic of the analogous Cu(II) bis (bipyrindyl) complex. A Metal:VBipy ratio of ~1:3 is attained for both Fe(II) and Co(II); this corresponds to the formation of the well-known Fe(II) tris (bipyrindyl) and the less renowned Co(II) tris (bipyrindyl) complexes. It is necessary to leach the Co<sup>2+</sup> from the membrane to obtain the 1:3 ratio, but the Fe<sup>2+</sup> tris complex is far more stable than the mono and bis complexes and requires no leaching of excess metal to encourage its formation.

### **3.4 THE STUDY OF POLYMER-BOUND COMPLEXES BY VISIBLE SPECTROSCOPY.**

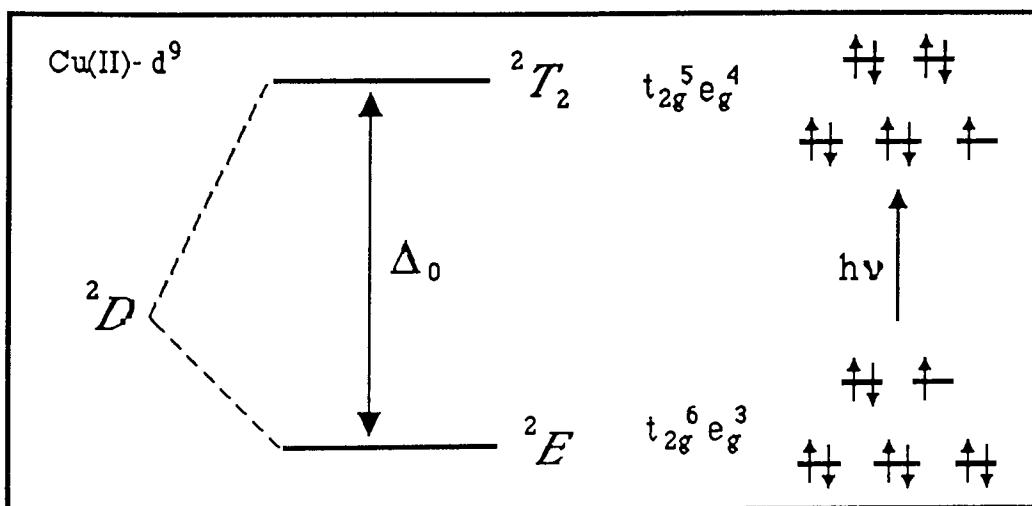
The following section is devoted to the study of the polymer-bound complexes suggested in the previous discussion. The main tool for this investigation was visible absorption spectroscopy, following the procedure explained in Chapter Two (section 2.7).

### 3.4.1 Cu(II) Coordination in Pyridyl and Bipyridyl Copolymer Membranes.

#### 3.4.1.1 Cu(II) Ligand Field Spectra,<sup>131,132</sup>

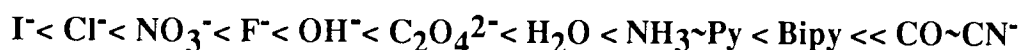
The vast majority of Cu (II) compounds are blue or green in colour because of a single absorption in the region  $11,000 - 16,000 \text{ cm}^{-1}$  (910-625 nm) region. The octahedral geometry is distorted for  $d^9$  systems by the *Jahn-Teller effect* and the resulting absorption spectrum is broad and unsymmetrical in appearance owing to a number of overlapping bands. In the case of the  $d^9$  system, it is possible to relate the electronic configuration to the spectroscopic observations by application of the Russell-Saunders coupling scheme, which allows derivation of spectroscopic terms by vectorial summation of the spin ( $m_s$ ) and orbital ( $l$ ) angular momenta of a multi-electron atom. The Cu(II) ground term  $^2D$  describes the total orbital ( $L$ ) and spin ( $S$ ) angular momenta, and therefore the lowest energy state, of the free ion. In the presence of a crystal field, this term would be expected to split into ground and excited configurations (Figure 3.6). The regular octahedral ground configuration  $t_{2g}^6 e_g^3$  is considered to possess a "positive hole" in either of the two  $e_g$  orbitals (producing a ground term  $E$ ), and when a  $t_{2g}$  electron is excited into the  $e_g$  set the "hole" is transferred into one of the three  $t_{2g}$  orbitals (producing an excited term  $T$ ).

Figure 3.6 Correlation of Electronic Configuration and Spectroscopic Terms for Octahedral Cu(II).



Thus, the spectra of Cu(II) ions can be explained in terms of a single electron transition giving rise to a configuration change from the ground state  $t_{2g}^6 e_g^3$  to the excited state  $t_{2g}^5 e_g^4$ , the two levels being separated by an energy of  $\Delta$  (the crystal-field splitting energy). Consequently, for Cu(II) complexes the wavelength of light responsible for the transition (i.e.  $\lambda_{\max}$  on the absorption spectrum) is approximately equal to  $\Delta$ , e.g.: for  $\text{Cu}(\text{H}_2\text{O})_6^{2+}$ ,  $\lambda_{\max} = 800 \text{ nm} = \Delta_o = 12,500 \text{ cm}^{-1}$ .

It has been shown that if ligands are arranged in ascending order of the  $\Delta$  produced by complexation to a given metal ion, with rare exception the order is the same independent of the metal. This order is known as the Fajans-Tsuchida *Spectrochemical Series*, part of which is illustrated below:



This series reflects the fact that ligands capable of accepting back-donation of charge through empty  $\pi$  orbitals that overlap with the  $t_{2g}$  orbitals of the metal, in effect increase the gap ( $\Delta$ ) between the  $e_g$  and  $t_{2g}$  levels by producing a set of  $t_{2g}$  molecular orbitals lower in energy than those produced by  $\sigma$  bonding only.

Figure 3.7 shows the experimentally obtained visible absorption spectra of Cu(II)(Pyridine)<sub>1-4</sub> complexes obtained here by adding a 0.25M CuCl<sub>2</sub> solution to pyridine in the Cu<sup>2+</sup>:Py ratios of 1:1, 1:2.5, 1:5 and 1:100 to obtain the 1:1, 1:2, 1:3 and 1:4 complexes respectively (these ratios are necessary to prevent precipitation of the Cu(Py)<sub>2</sub>Cl<sub>2</sub> species <sup>46</sup>). The pyridine ligand is higher than H<sub>2</sub>O in the spectrochemical series as it participates in back-bonding with the metal; therefore, for every pyridine complexed to the Cu(II) ion,  $\Delta$  will be increased and the position of the absorption  $\lambda_{\max}$

will be shifted to lower wavelength. By such spectroscopic observations it is possible to gain useful information about the coordination chemistry of Cu(II) within pyridyl and bipyridyl-based membranes.

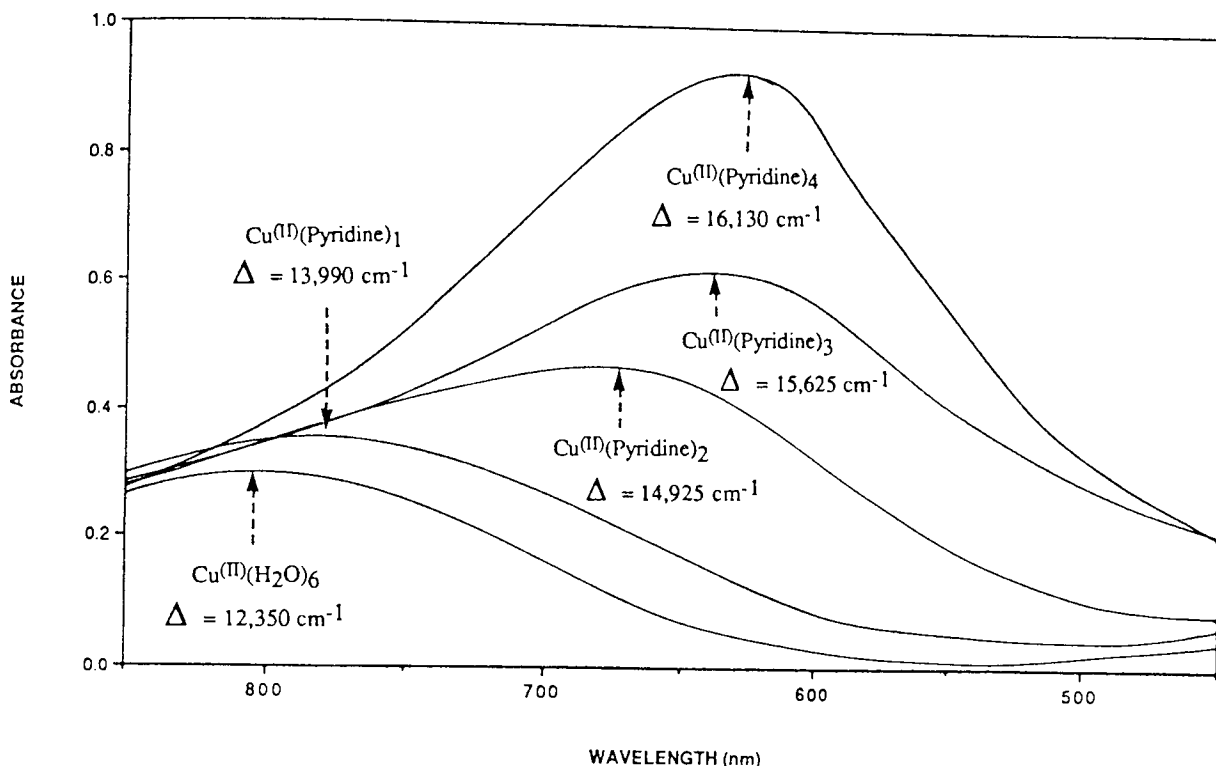
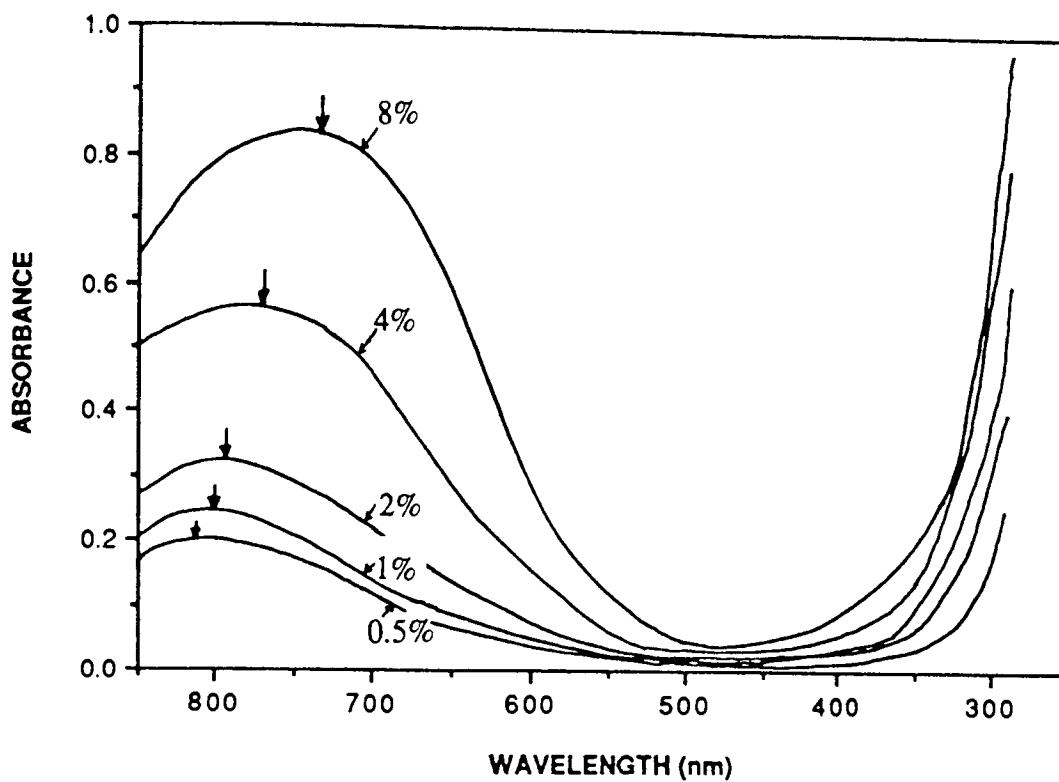


**Figure 3.7 Visible Absorption Spectra of Cu(II) Complexes with Pyridine.**

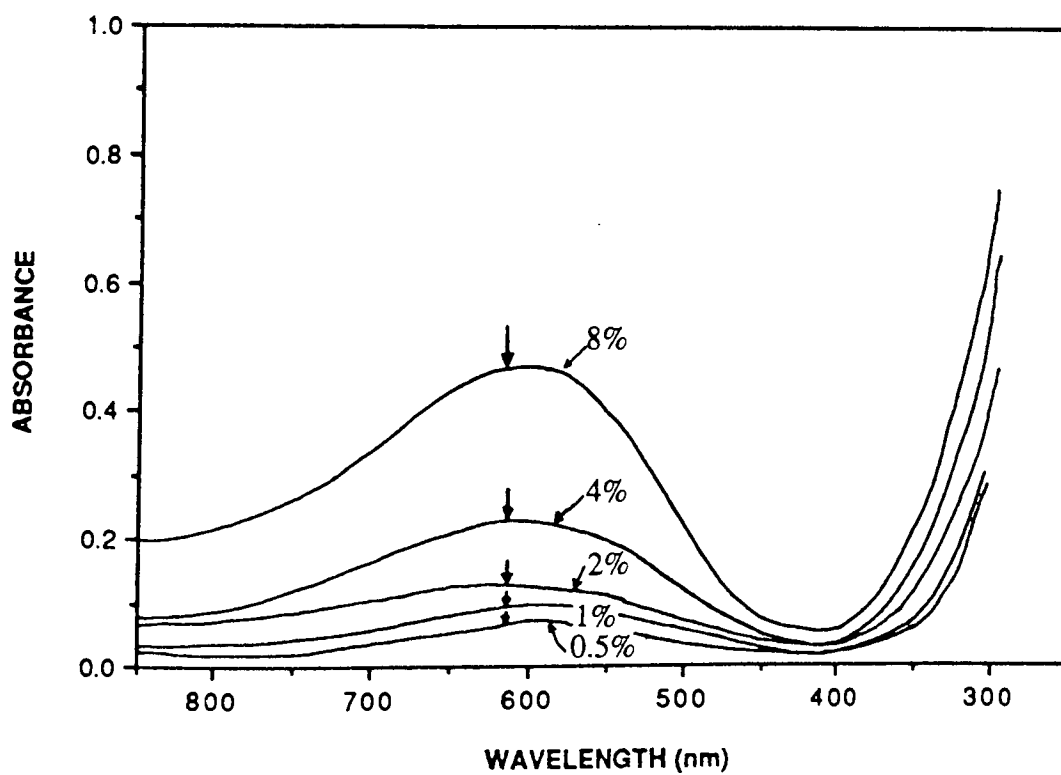
### **3.4.1.2 Effect of Ligand Loading on Cu(II) Coordination to Pyridyl-Copolymer Membranes.**

Figure 3.8(a) displays the Cu<sup>2+</sup> visible absorption spectra of HEMA:4VPy copolymer membranes of various ligand loadings placed in 0.25M CuCl<sub>2</sub> solutions for several hours. It is evident that there is an interaction between Cu<sup>2+</sup> ions and the pyridine groups within the membrane, as the intensity of the spectrum due to the  $^2E \rightarrow ^2T_2$  transition in the ion, is enhanced as the ligand content is increased. Obvious also, is the concomitant shift of the absorption  $\lambda_{max}$  to lower wavelength with increased ligand loading, a condition

**Figure 3.8 (a) Effect of [Ligand] on Cu(II) Visible Absorption Spectra of Pyridyl Copolymers.**



**Figure 3.8(b) Effect of Leaching Cu(II) from Pyridyl Copolymers.**



indicative of a greater number of pyridine groups coordinated per  $\text{Cu}^{2+}$  ion. It is likely that at low ligand concentrations, the  $\text{Cu}^{2+}$  that equilibrates within the gel matrix is in great excess and the pyridine coordination sites are 'saturated', probably as *mono-complexes* (Figure 3.9(A)). By increasing the ligand loading, the pyridine: $\text{Cu}^{2+}$  ratio is altered and more than one pyridine unit begins to coordinate per  $\text{Cu}^{2+}$  ion, effectively the onset of cross-linking within the polymer (Figure 3.9(B)).

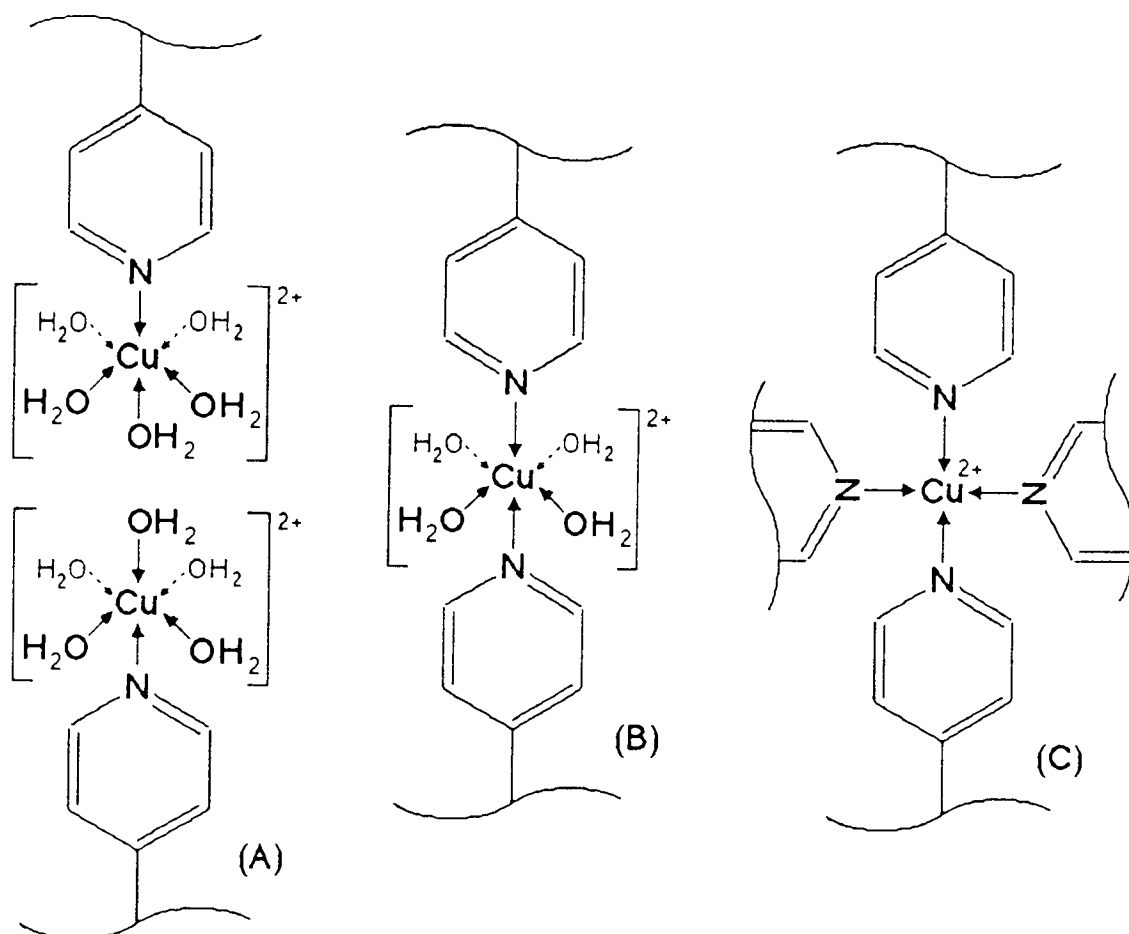


**Figure 3.9 Effect of  $[\text{VPy}]:[\text{Cu(II)}]$  Ratio on Pyridine-Based Membrane Coordination Chemistry: (A) High  $[\text{Cu(II)}]$  - (C) Low  $[\text{Cu(II)}]$ .**

The largest observed shift in  $\lambda_{\text{max}}$  in Figure 3.8(a) is from 800-740 nm for the 8% loaded copolymer, which by comparison with Figure 3.7, is equivalent to an average of 1.5 pyridines per  $\text{Cu}^{2+}$ . If however, the membranes are removed from the  $\text{CuCl}_2$  solutions

and placed in distilled water, the excess  $\text{Cu}^{2+}$  in the polymer matrix leaches out and the equilibrium is changed. Figure 3.8(b) shows that the  $\lambda_{\text{max}}$  for all ligand loadings is shifted down to below 630 nm after leaching. The pyridine: $\text{Cu}^{2+}$  ratio is effectively increased and eventually the 4-coordinate  $\text{Cu}(\text{II})(\text{Pyridyl})_4$  complex results (Figure 3.9(C)) as confirmed by comparison of the  $\lambda_{\text{max}}$  for  $\text{Cu}(\text{II})(\text{Pyridine})_4$  in Figure 3.7 with those in Figure 3.8(b).

#### **3.4.1.3 Effect of Cu(II) Concentration on its Coordination to Pyridyl-**

##### **Copolymer Membranes.**

Figure 3.10 (overleaf) is a three dimensional representation of the effect of  $\text{Cu}^{2+}$  concentration on the visible spectra of a HEMA:8%VPy copolymer membrane. Lines running parallel to the concentration axis are 'isometers' (lines of constant wavelength) and lines running parallel to the wavelength axis are the successive absorption spectra of membranes placed in different concentrations of  $\text{CuCl}_2$ .

It can be seen that the principles discussed in 3.4.1.2 are in operation here and that for high  $[\text{Cu}(\text{II})]$ , the  $\lambda_{\text{max}}$  is around 740 nm, comparable to slightly more than one pyridine unit per ion. By following the position of this maximum down the concentration scale (the broken line), it can be seen that at low  $[\text{Cu}(\text{II})]$  there is a relative shift of  $\lambda_{\text{max}}$  to 640 nm, as the ligand:metal ion ratio is much larger and the  $\text{Cu}(\text{II})(\text{Pyridine})_4$  complex exists. The point of interest that arises from this data, is the 'hump' in absorbance intensity observed in the middle of the concentration range. One explanation for the increase at 1.5 mmoles is based on the fact that the  $\lambda_{\text{max}}$  of the spectrum produced at this concentration is consistent with the formation of  $\text{Cu}(\text{II})$  bis (pyridine) complexes. The formation of the bis-

complex is the first step to cross-linking of the polymer which may, as a consequence, result in a contraction of the membrane (although, there is no independent evidence to suggest this). The spectrophotometer beam would be exposed to essentially a greater density of absorbing species in a contracted membrane and the specimen's absorbance would increase.

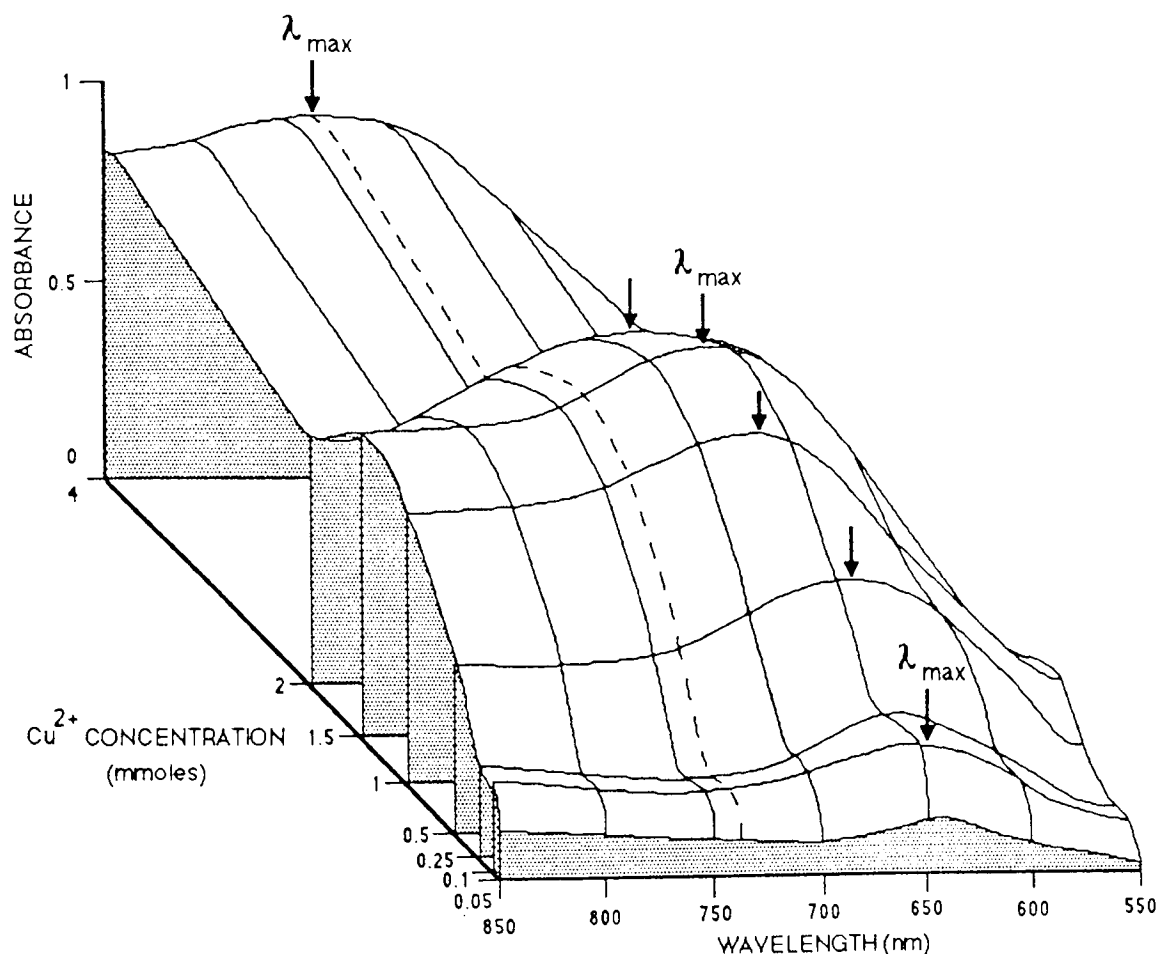


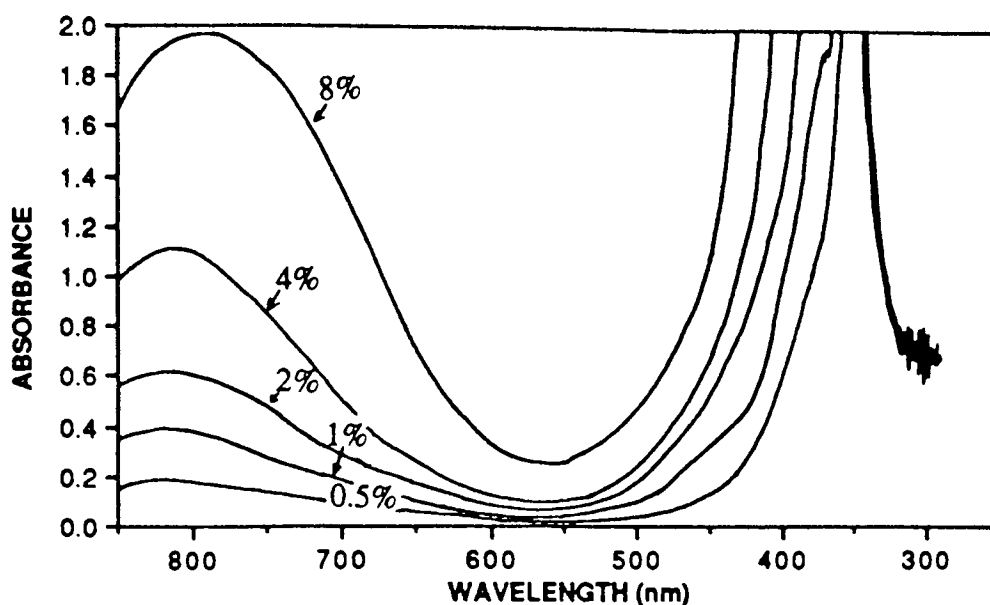
**Figure 3.10 Effect of [Cu(II)] on the Visible Absorption Spectra of 8% VPy-Based Copolymer Membranes.**

#### **3.4.1.4 Effect of Dehydrating Cu(II)-Coordinated Pyridyl Copolymer Membranes.**

If membranes of various ligand loadings are placed in 0.25M CuCl<sub>2</sub> overnight and then removed from the solution and dehydrated in an oven at 60°C for several hours, the colour of the membranes changes from blue to green. This is due to the combination of the

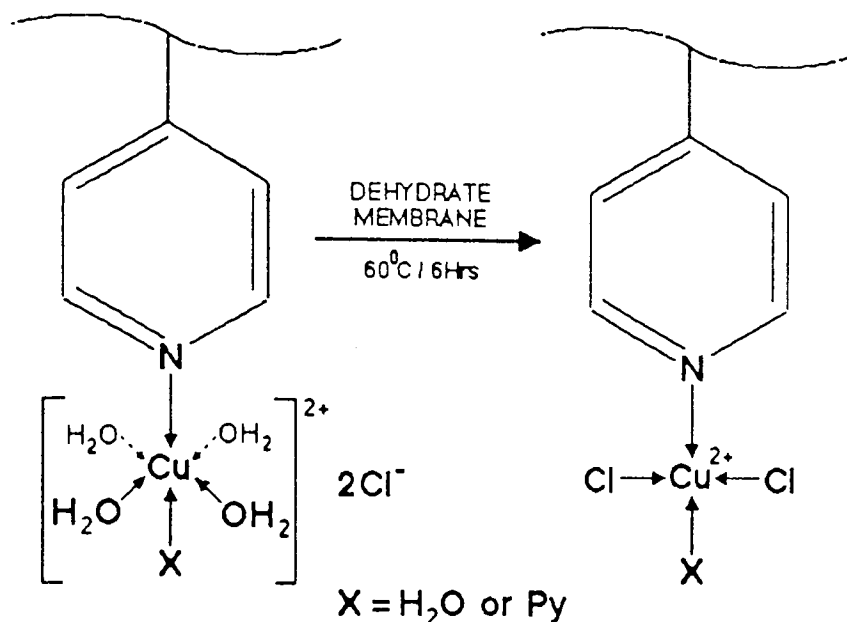
absorption in the red above 800 nm (producing the characteristic blue colour), with an additional new band in the violet around 350 nm (producing a yellow colour).

Figure 3.11(a) shows the visible absorption spectra for dehydrated HEMA:4VPy copolymer membranes of various ligand loadings, presoaked in copper chloride solution.



**Figure 3.11(a) Effect of Dehydrating CuCl<sub>2</sub>-Soaked Pyridyl Copolymer Membranes on Visible Absorption Spectra.**

Upon dehydration, any  $\text{Cu}(\text{H}_2\text{O})_6^{2+}$  present in the interstitial water will be converted to the  $\text{Cu}(\text{H}_2\text{O})_2\text{Cl}_2$  complex, which is characteristically green in colour. As for the  $\text{Cu}(\text{II})$  complexed to the polymer, this would probably be converted into the analogous  $\text{CuCl}_2(\text{VPy})\cdot\text{H}_2\text{O}$  complex (Figure 3.11(b), overleaf). The shift to lower wavelength of the 800 nm absorption observed for the 4% & 8% 4VPy loaded copolymer membranes may again indicate an increasing number of pyridine units coordinated per ion because of higher ligand:metal ratios. Thus, there may also be scope for the formation of the known  $\text{CuCl}_2(\text{VPy})_2$  complex within the membrane.



**Figure 3.11(b) Effect of Dehydration on Coordination Chemistry in Pyridyl Copolymer Membranes.**

If the membranes are leached in distilled water as described in section 3.4.1.2 to produce the tetra (pyridyl) complex, on subsequent dehydration the absorption spectrum remains unchanged from that of the tetra (pyridyl) complex (Figure 3.8(b)). This is because the stability of the  $\text{Cu}(\text{II})$  complex with pyridine is greater than that with chloride (Table 3.1, cf. Spectrochemical series, section 3.4.1.1).

**Table 3.1 Stability Constants for  $\text{Cu}(\text{II})$  Complexes.**

	$\log K_1$	$\log K_2$	$\log K_3$	$\log K_4$
$\text{Cu}(\text{II})/\text{Pyridine}$	2.52	1.86	1.31	0.85
$\text{Cu}(\text{II})/\text{Chloride}$	$\sim 0$	-0.4 to -1	-1.2 to -1.7	-2 to -2.5

#### **3.4.1.5 $\text{Cu}(\text{II})$ Coordination in Bipyridyl-Copolymer Membranes.**

The interaction of  $\text{Cu}^{2+}$  ions with bipyridyl copolymer membranes is generally analogous to that with pyridyl copolymers membranes. Figure 3.13(a) & (b) illustrate the same

**Figure 3.13 (a) Effect of [Ligand] on Cu(II) Visible Absorption Spectra of Bipyridyl Copolymers.**

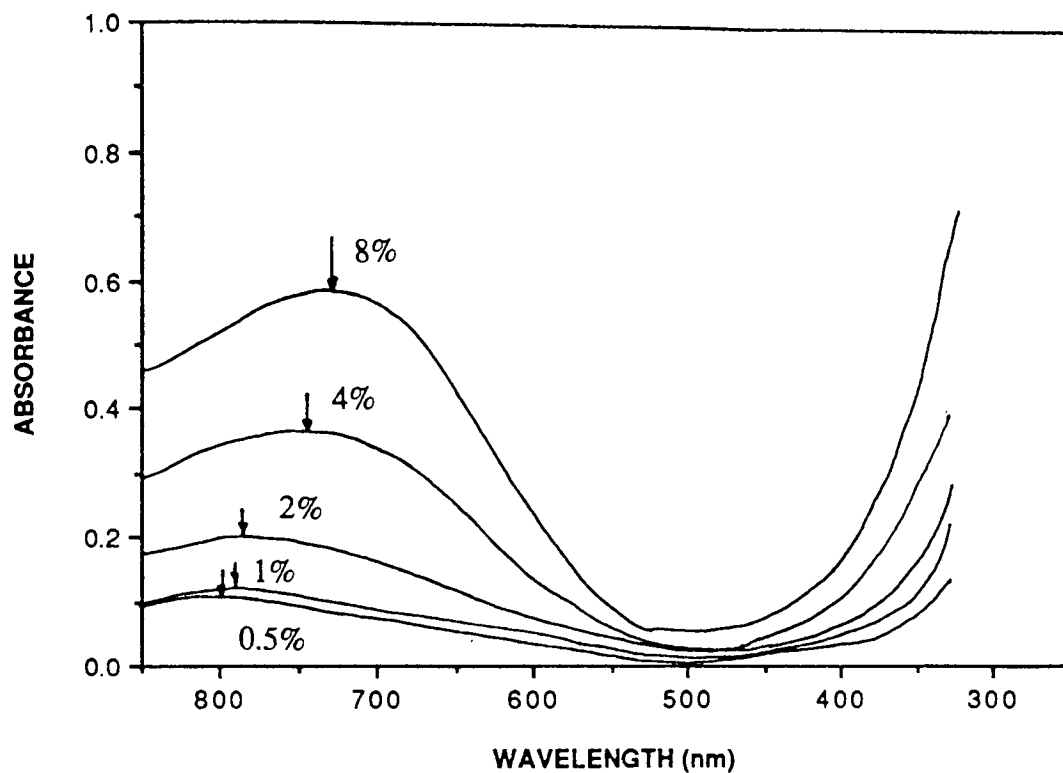
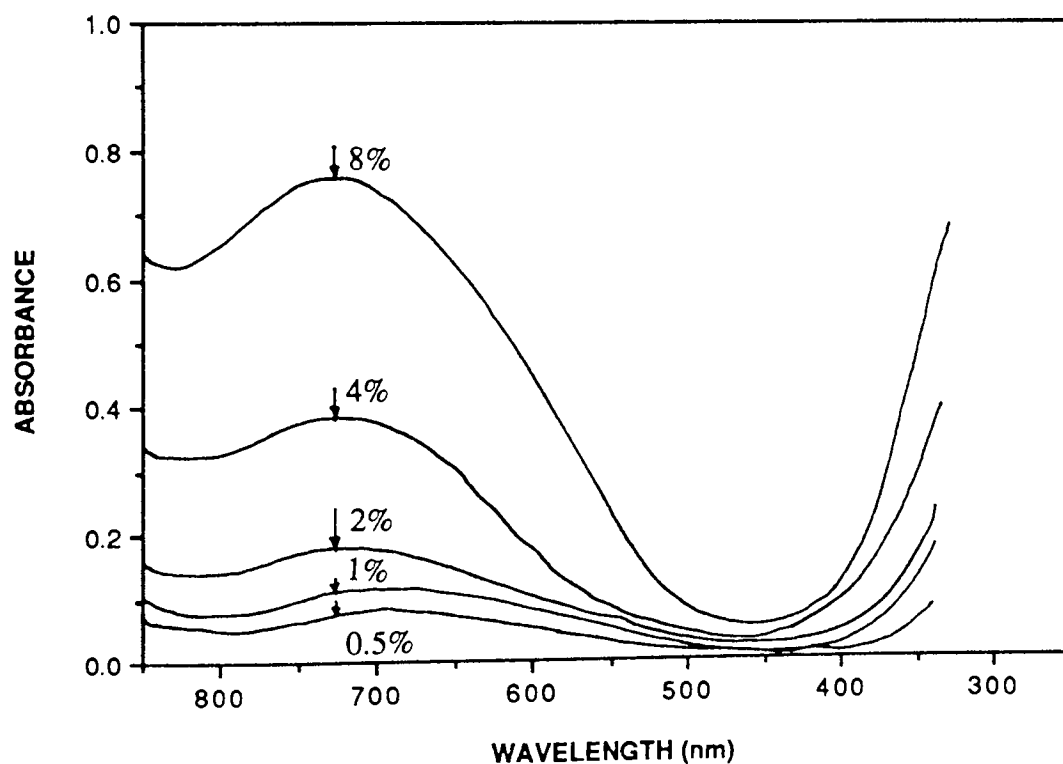


**Figure 3.13(b) Effect of Leaching Cu(II) from Bipyridyl Copolymers.**



effects of ligand loading and membrane leaching seen in section 3.4.1.2. Complexes of chelating ligands such as bipyridyl are in general more thermodynamically stable than those with an equivalent number of monodentate ligands- in this case pyridine. If the donor groups of the mono & bi-dentate ligands are isoenergetic, the so-called *chelate effect* is mainly driven by the change in entropy when a chelating ligand displaces two monodentate ligands.

It is clear from Figures 3.13(a) & (b), that  $\lambda_{\text{max}}$  after leaching is around 700nm compared with 620nm for the pyridyl system. The bipyridine ligand generally forms complexes that possess larger crystal field splitting than those for pyridine, hence their relative positions in the Spectrochemical Series (section 3.4.1.1). Therefore, if the bipyridyl system is moving towards a  $\text{Cu(II)}\text{N}_4$ - arrangement, one would expect to observe a  $\lambda_{\text{max}}$  at a wavelength lower than that for pyridine. This is not the case, which suggests that the resulting  $\text{Cu(II)}$  *bis*(Bipyridyl-polymer) complex (Figure 3.12) may be difficult to form, or a complex with a different coordination number might exist i.e.  $\text{Cu(II)}\text{N}_4(\text{H}_2\text{O} \text{ or } \text{Cl}^-)_x$ .

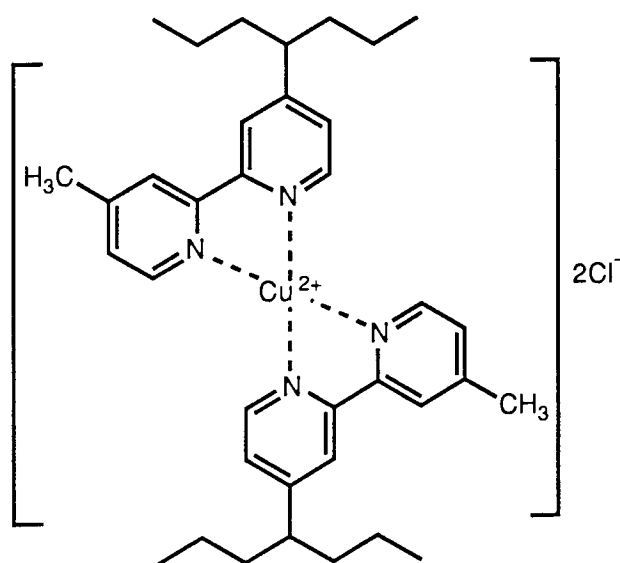
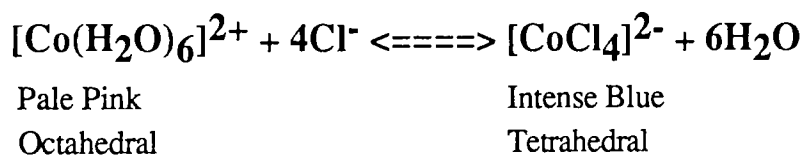


**Figure 3.12 Cu(II) *bis*(Bipyridyl Polymer) Complex.**

### 3.4.2 Co(II) Coordination in Pyridyl- and Bipyridyl-Copolymer Membranes.

#### 3.4.2.1 Spectra of Co(II) Ions and Complexes.<sup>133,134</sup>

The  $d^7$  configuration of cobalt-(II) complexes is favourable for the adoption of either tetrahedral or octahedral geometries, when considering overall stabilities and the crystal-field splitting energies (CFSEs),  $\Delta_o$  and  $\Delta_t$ . Thus, complexes can be categorised on the basis of stereochemistry into those which are octahedral high-spin  $t_{2g}^5 e_g^2$  or low-spin  $t_{2g}^6 e_g^1$ , and those which are tetrahedral high-spin  $e^4 t_2^3$ . The most common type is the high-spin octahedral, as ligands producing very high values of  $\Delta_o$  (such as  $CN^-$ ) are required to cause spin-pairing. However, an aqueous solution containing  $Co(H_2O)_6^{2+}$  would also contain in equilibrium, small amounts of  $Co(H_2O)_4^{2+}$ ; this is more clearly demonstrated in the classic case of the chloride, where the distinction between the two geometries is exemplified by the colour change:

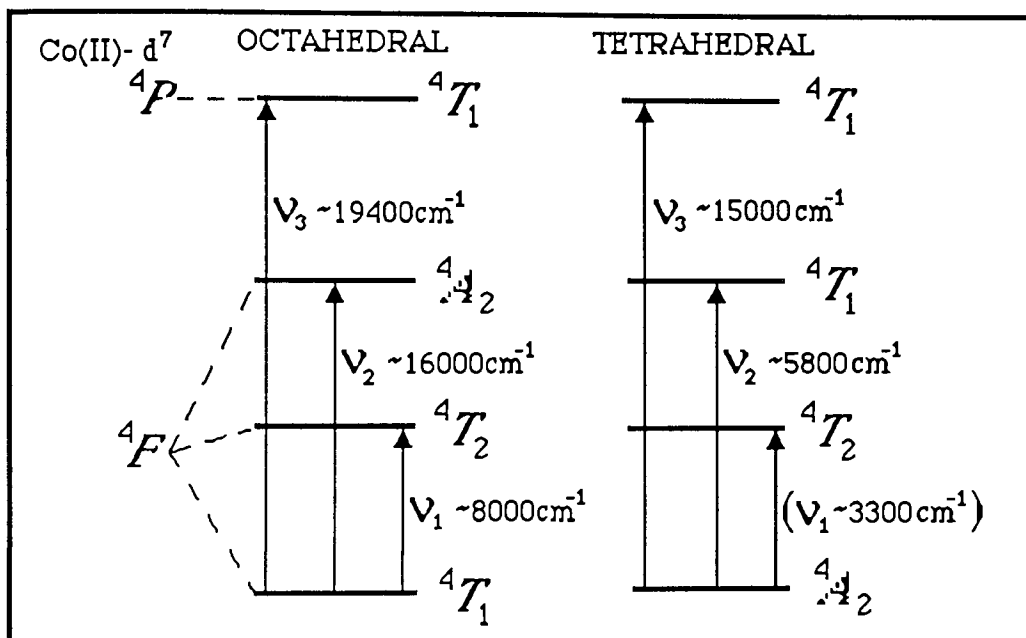


The  $d^7$  system gives rise to two free-ion terms,  $^4F$  and  $^4P$ , which are split in the presence of a crystal field in a manner dependent on the stereochemistry, as illustrated by Figure 3.14. The lowest energy band ( $\nu_1$ ) at  $8000\text{ cm}^{-1}$  ( $1250\text{ nm}$ ) is assigned to the  $^4T_{1g} \rightarrow ^4T_{2g}$  transition and is outside the scope of the instrumentation used in this study. The bands at  $16,000\text{ cm}^{-1}$  and  $19,400\text{ cm}^{-1}$  ( $\nu_2$ ) & ( $\nu_3$ ) at  $\sim 625\text{ nm}$  &  $515\text{ nm}$ ) are thought to be due to the  $^4T_{1g} \rightarrow ^4A_{2g}$  and  $^4T_{1g} \rightarrow ^4T_{1g} (P)$  transitions respectively, spin-orbit coupling effects adding an extra shoulder around  $21,600\text{ cm}^{-1}$  ( $460\text{ nm}$ ).

For tetrahedral  $Co(II)$ , the transition  $^4A_2 \rightarrow ^4T_2$  is expected around  $3300\text{ cm}^{-1}$  ( $\nu_1$ ), well

into the infra-red. The transition  ${}^4A_2 \rightarrow {}^4T_1(F)$  is also outside the instrumentation range at  $5800\text{ cm}^{-1}$  but the  ${}^4A_2 \rightarrow {}^4T_1(P)$  transition appears as an intense visible band at  $15,000\text{ cm}^{-1}$  ( $\sim 670\text{ nm}$ ).

**Figure 3.14 Correlation of Spectroscopic Terms and Absorption Bands for Co(II).**



There are a limited number of instances in which the pink and blue colours of the octahedral and tetrahedral are reversed, for example, the case of blue octahedral  $\text{CoCl}_2$ . In general however, the position of the main  $\nu_3$  band is influenced by the geometry and type of ligand around the metal. Thus, the absorption spectra of the pyridyl and bipyridyl membranes may provide information on both the stereo- and coordination-chemistry of these immobilised ligands with  $\text{Co(II)}$  ions.

#### 3.4.2.2 Effect of Ligand Loading on Co(II) Coordination to Pyridyl-Copolymer

##### Membranes.

A number of membranes of various ligand loadings were placed in  $0.25\text{M CoCl}_2$

solutions and left for a number of days to equilibrate. Figure 3.15(a) illustrates the effect of increasing the proportion of vinyl pyridine in the copolymer on the visible absorption spectra of these membranes. The most obvious observation is that the absorption band around 500 nm (characteristic of octahedral geometry as discussed in the previous section) becomes more intense with increasing ligand content, indicating that there must be an interaction between the  $\text{Co(II)}$  ions and the pyridine groups. Although it is not possible to directly compare the position of the  $\nu_3$  band to the absolute value of  $\Delta_o$ , it is reasonable to assume that ligands that are placed higher in the Spectrochemical Series will give a larger  $\Delta_o$  value and so produce a shift in the  $\lambda_{\text{max}}$  of the main  $\nu_3$  band (Table 3.2). Careful examination of the  $\lambda_{\text{max}}$  for the spectra in Figure 3.15(a) shows that there is an increase in  $\Delta$  from 19,530 to 20,000  $\text{cm}^{-1}$  when moving from 0.5 to 8% by weight ligand loading in the membrane. Since pyridine is higher in the spectrochemical series than water, it is supposed that the shift is due to the systematic displacement of water by pyridine as a coordinating group around the  $\text{Co(II)}$  ion.

<u>Complex</u>	<u><math>\nu_3</math> (main band)/<math>\text{cm}^{-1}</math></u>	<u><math>\Delta</math> <math>\text{cm}^{-1}</math></u>
$[\text{Co}(\text{Bipy})_3]^{2+}$	22,000	12,670
$[\text{Co}(\text{NH}_3)_6]^{2+}$	21,100	10,200
$[\text{Co}(\text{H}_2\text{O})_6]^{2+}$	19,400	9200
$\text{CoCl}_2$	17,250	6900

**Table 3.2 Effect of Crystal-Field Splitting on Visible Spectra of  $\text{Co(II)}$  Complexes.** (After Carlin <sup>133</sup>)

If copolymer membranes of various ligand contents are placed in 0.25M  $\text{Co(NCS)}_2$  solutions, a different set of spectra result (Figure 3.15(b)). The visible spectrum of  $\text{Co(NCS)}_2$  in solution is characteristic of the  $\text{Co(H}_2\text{O)}_6^{2+}$  complex, with a  $\lambda_{\text{max}}$  at 515 nm (19,400  $\text{cm}^{-1}$ ). However, if allowed to permeate into the membrane, the polymer

**Figure 3.15(a) Effect of [Ligand] on Co(II) Spectra of Pyridyl Copolymer Membranes**

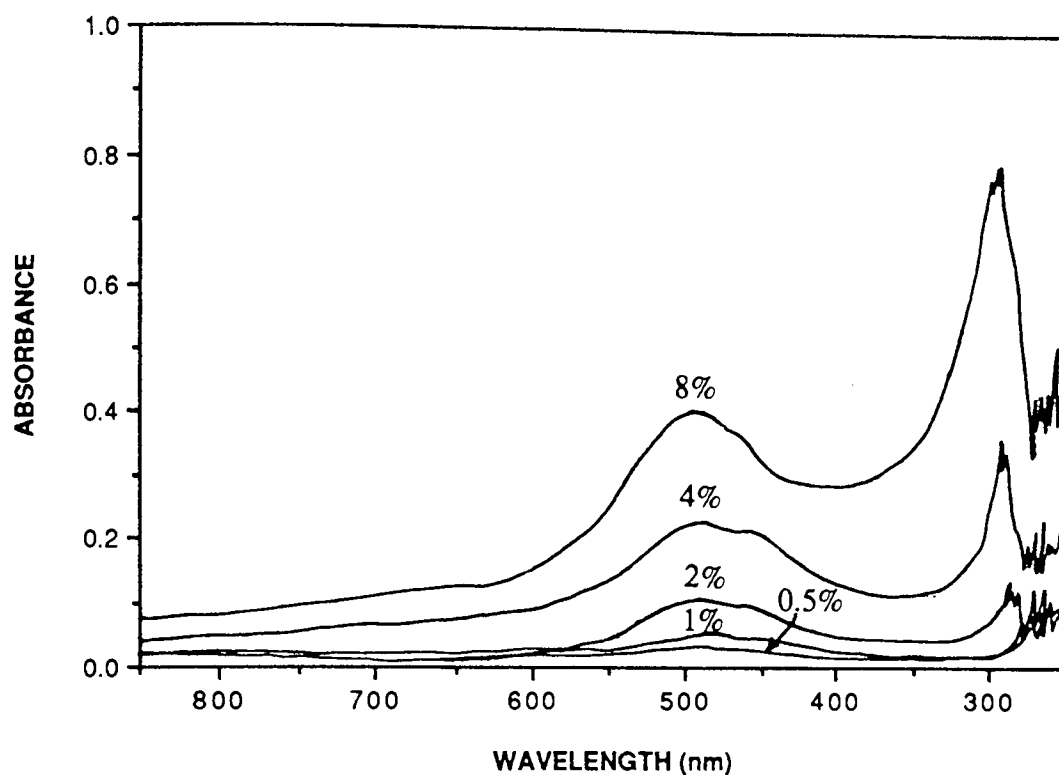
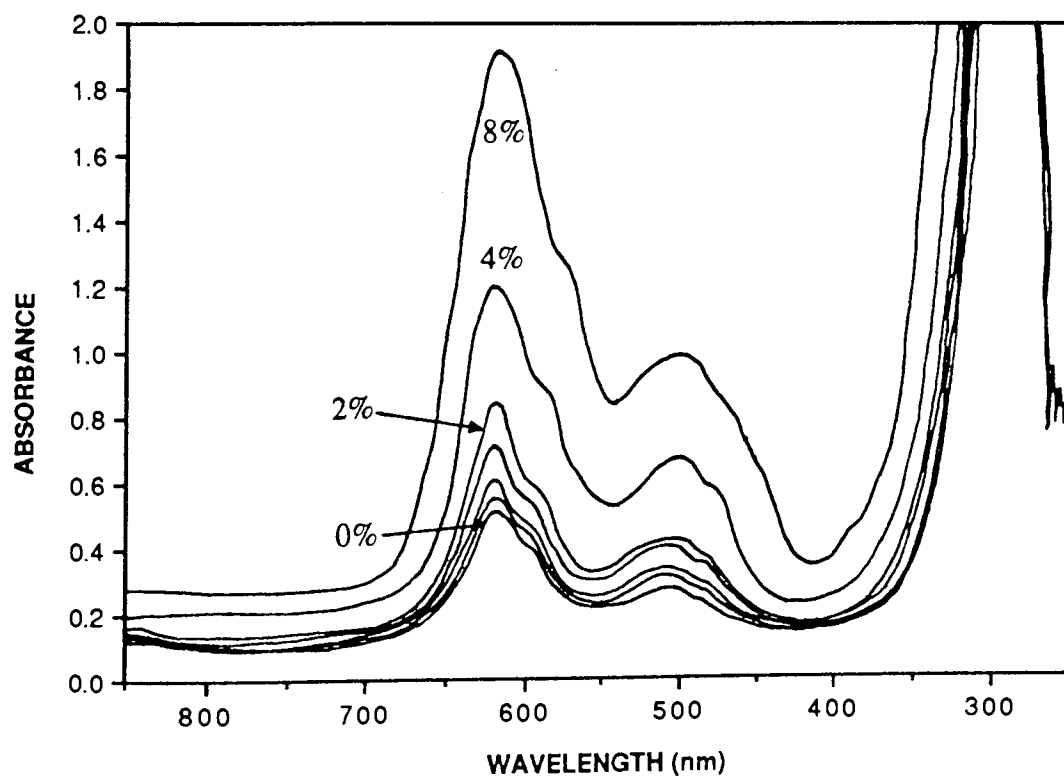
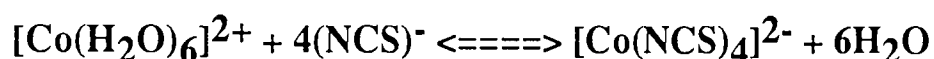


**Figure 3.15(b) Absorption Spectrum of Co(SCN)<sub>2</sub> in Pyridyl Copolymers.**



matrix enforces a modified environment, significantly different to that in solution and the octahedral-tetrahedral equilibrium is disturbed. Figure 3.15(b) clearly shows bands at 510 nm ( $19,610\text{ cm}^{-1}$ ) assigned to octahedral Co (II) and at 620 nm ( $16,130\text{ cm}^{-1}$ ) due to tetrahedral Co (II). It is the polymer environment and not the presence of ligand groups that induces this equilibrium phenomenon, as the effect is observed in purely poly HEMA membranes. The process is thought to be a result of the formation of the tetrahedral (tetrathiocyanate) complex which has a  $\lambda_{\text{max}}$  at 615 nm ( $16,250\text{ cm}^{-1}$ )<sup>133</sup>, close to that observed at 620 nm:



It is again obvious that the ligand groups present must be interacting with the complexes, as the intensity of the spectrum increases with ligand loading. It is known that a complete series of complexes of the form  $[\text{Co Py}_2 \text{X}_2]$  (X=halide, NCS) exist<sup>134,135</sup>, and it is feasible that the  $[\text{Co}(\text{NCS})_4]^{2-}$  ion may interact further with pyridine moieties to produce complexes such as  $[\text{Co}(\text{NCS})_2 \text{Py}_2]$ .

### **3.4.2.3 Effect of Dehydrating Co(II)-Coordinated Pyridyl-Copolymer**

#### **Membranes.**

If membranes of various ligand loadings are placed in 0.25M  $\text{CoCl}_2$  overnight and then removed from the solution and dehydrated in an oven at  $60^\circ\text{C}$  for several hours, the colour of the membranes changes from pink to an intense blue. This is consistent with the change in stereochemistry from octahedral to tetrahedral expected as a result of removing water from the polymer matrix and subsequently from the coordination sphere of the complex (Figure 3.16). Figure 3.17 is a three-dimensional representation of the visible absorption spectra of dehydrated Co(II)-coordinated pyridyl membranes.

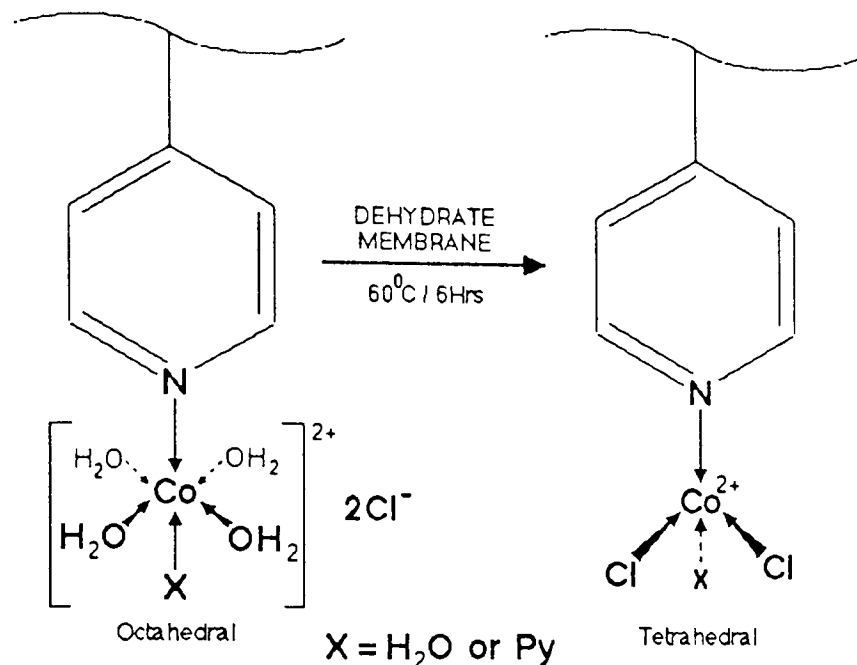


**Figure 3.16 Effect of Dehydration on the Coordination Chemistry of Co(II) in Pyridyl Copolymer Membranes.**

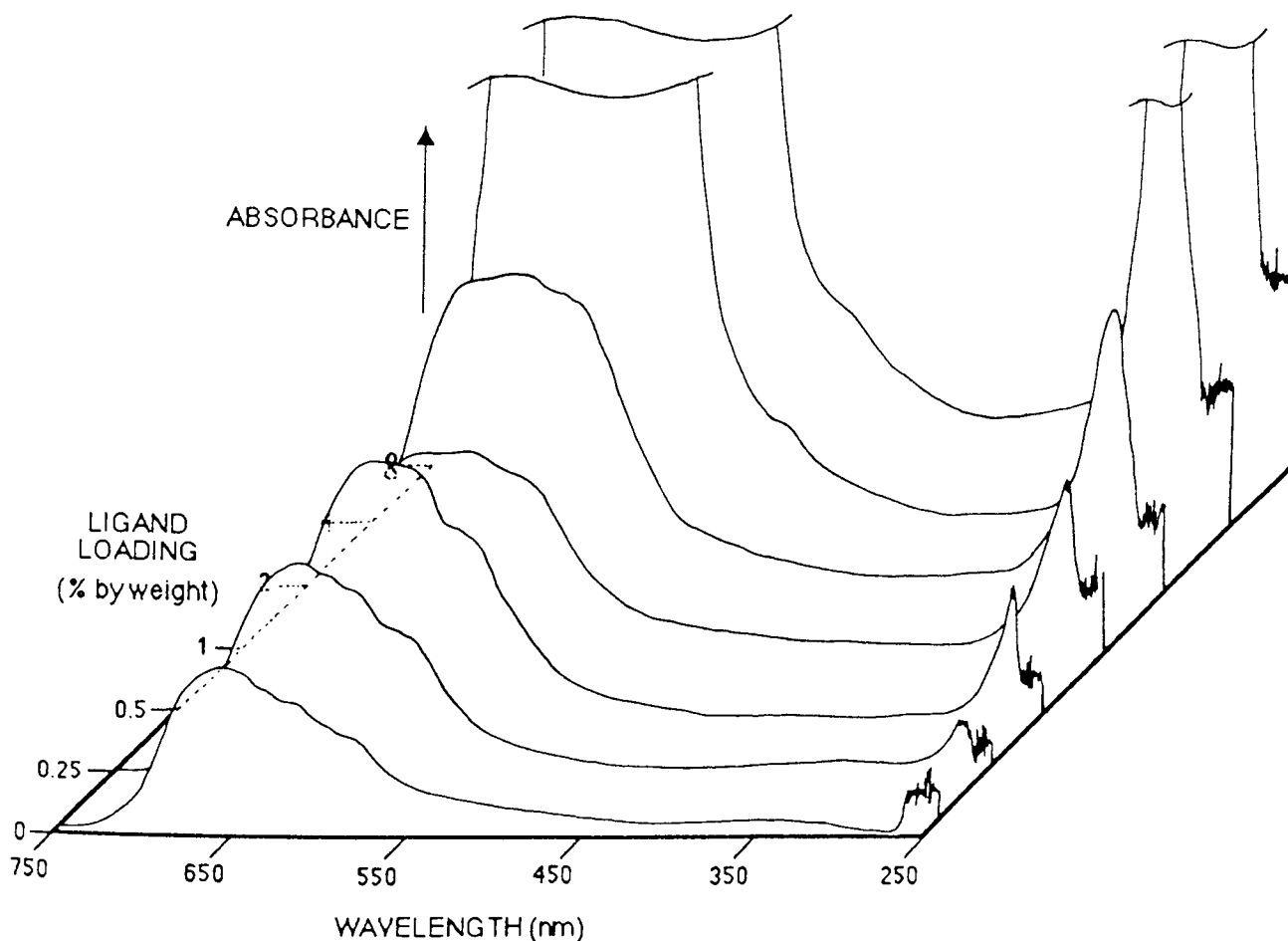


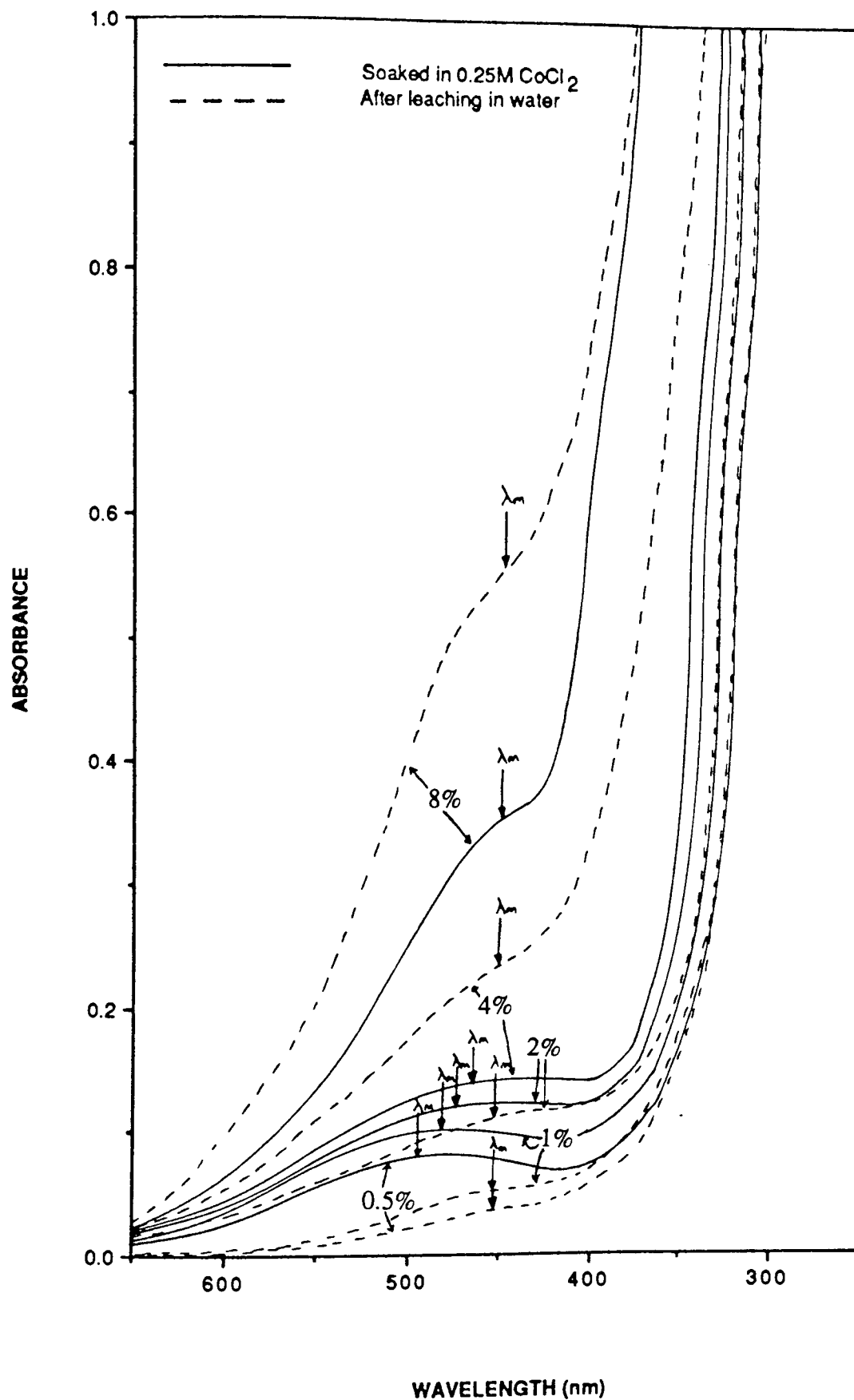
**Figure 3.17 Effect of Dehydration on the Visible Absorption Spectra of Co(II)-Coordinated Pyridyl-Based Membranes.**

The main  $\nu_3$  bands around  $16,000\text{ cm}^{-1}$  are indicative of tetrahedral  $\text{Co(II)}$  stereochemistry. The complicated 'fine structured' nature of the  $\nu_3$  band has been attributed to spin-orbit coupling effects and transitions to doublet states <sup>132</sup>. However, as one proceeds from low to high ligand loadings, the shape of this band begins to change, becoming more 'plateau-like'. In addition to this, there is an unexplained drop in the expected intensity between the 0.5 and 1% loading. Unfortunately, the 4 and 8% loadings produce spectra that are too intense for the instrumentation to reveal the fine structure; however, a small shoulder appears around 520 nm that might be assigned to low levels of octahedral  $\text{Co(II)}$ . There is insufficient information from these spectra to determine exactly the coordination processes occurring within the membranes upon dehydration. It is apparent though, that there is a definite interaction between the metal and ligand groups because of the effects observed in the electronic spectra. It would not be unreasonable to assume that as the concentration of ligand groups increases, the likelihood of forming such species as the metastable tetrahedral  $[\text{Co Cl}_2 \text{ Py}_2]$  becomes greater.

#### **3.4.2.4 Co(II) Interactions with Bipyridyl-Copolymer Membranes.**

If VBipy copolymer membranes of various ligand loadings are placed in 0.25M  $\text{CoCl}_2$  solutions and left to equilibrate for a few days, the visible absorption spectra depicted by the solid lines in Figure 3.18 result. In compliance with previous observations, as the ligand loading increases the position of the  $\lambda_{\text{max}}$  is altered, in this case from 515 nm ( $[\text{Co(H}_2\text{O)}_6]^{2+}$ ) to 455 nm ( $[\text{Co(VBipy)}_3]^{2+}$  - see Table 3.1 section 3.4.2.2). This is because the increase in ligand:metal ratio within the matrix results in the coordination of more bipyridine units per  $\text{Co(II)}$ ; since bipyridine is higher in the Spectrochemical Series than  $\text{H}_2\text{O}$ ,  $\Delta$  is larger and the position of the  $\nu_3$  absorption moves to higher energy.

**Figure 3.18 Visible Absorption Spectra of HEMA:VBipy Copolymer Membranes Soaked in  $\text{CoCl}_2$ .**



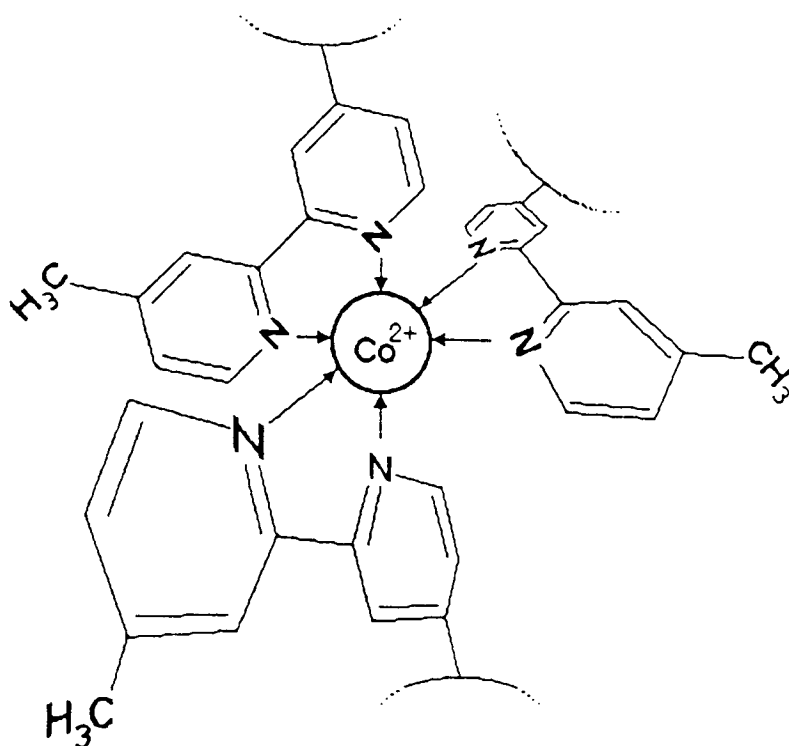


**Figure 3.19 Octahedral Cobalt (II) *tris*(Bipyridyl Copolymer) Complex.**

As expected, if the membranes are leached in distilled water, the ligand:metal ratio is increased by removal of excess  $\text{Co(II)}$  and the  $[\text{Co(VBipy)}_3]^{2+}$  complex can be achieved for all ligand loadings as shown by the broken lines in Figure 3.18.

The Cobalt (II) *tris* (4-methyl 4'-vinyl 2,2'-bipyridine) complex can be synthesised directly by a procedure analogous to that of Smith and Cagle <sup>116</sup> for the  $\text{Fe(II)}$  complex (Chapter 2, section 2.4), except that KI is used to precipitate the complex as the iodide. This can then be used to produce membranes with known loadings of the complex, a potentially useful procedure when considering the chemistry of this compound as described in following section.

### **3.4.3 Properties of the *tris*(Bipyridyl-Polymer) Co(II) Complex.**

It is known that for cobalt oxidation states lower than +2, the back-bonding ability of  $\pi$ -

acceptor ligands such as bipyridine is necessary for complex stabilisation, otherwise too great a negative charge density would reside on the metal atom. In 1957 both Vlcek <sup>136</sup> and Waide *et al.* <sup>137</sup> reported independently the discovery of a new univalent cobalt compound formed by the polarographic reduction of  $[\text{Co}(\text{Bipy})_3]^{2+/3+}$  at a dropping mercury electrode (DME). Chemical reduction of  $[\text{Co}(\text{Bipy})_3]^{2+}$  by  $\text{Na}(\text{Hg})$  and  $\text{Zn}(\text{Hg})$  <sup>138-140</sup> and  $\text{NaBH}_4$  <sup>136,139</sup> procedures has enabled direct synthesis of the  $\text{Co}(\text{I})$  derivative, and more recently Anson *et al.* <sup>141</sup> have utilised cyclic voltammetry in the study of the electrochemistry of this complex. It was decided that attempts would be made to see if the polymer-bound  $\text{Co}(\text{II})$  tris(bipyridyl) complex could be chemically reduced to produce this low-valence stabilisation observed in the free complex. Visible spectroscopy should allow easy monitoring of the conversion of the  $\text{Co}(\text{II})$  to the  $\text{Co}(\text{I})$  complex and *vice versa*, as the former absorbs weakly around 455 nm (the 550-700 nm region being clear), whereas the latter is reported to have an intense absorption around 600 nm <sup>139,142</sup> responsible for the characteristic dark blue colouration of the complex.

Membranes containing the polymer-bound  $\text{Co}(\text{II})$  tris(bipyridyl) complex were made by either the direct copolymerisation method or soak/leach procedure, as outlined in section 3.4.2.4. A small quantity of sodium borohydride ( $\text{NaBH}_4$ ) *ca.* 0.2g was placed in each of six sample bottles containing 20ml of distilled water, resulting in the immediate evolution of hydrogen. Six (4 x 1cm) samples of membrane containing original ligand loadings ranging from 0.25 to 8% by weight were placed in the appropriate bottles and left for a number of hours to enable diffusion of the reducing agent into the polymer matrix and ensure complete reduction of the complex. If bubbles ceased to form in the bottles, more borohydride was added, until the membrane produced a constant absorbance reading at 600 nm.

#### 3.4.3.1 Visible Absorption Spectra of the Co(I) Complex.

Figure 3.20 shows the visible absorption spectra obtained from the six membranes; the 0.25 and 0.5% loadings produced weak, unclear spectra and the 8% spectrum was too intense and outside the capabilities of the instrumentation. The 1, 2 and 4% membranes did show, however, a strong band at 600 nm and the hint of a shoulder around 430 nm blending into an intense, off-scale band below 350 nm. These bands are thought to be the result of 'metal to ligand' charge-transfer - the transfer of electrons from metal *d* orbitals to empty antibonding  $\pi$  orbitals of the ligand.

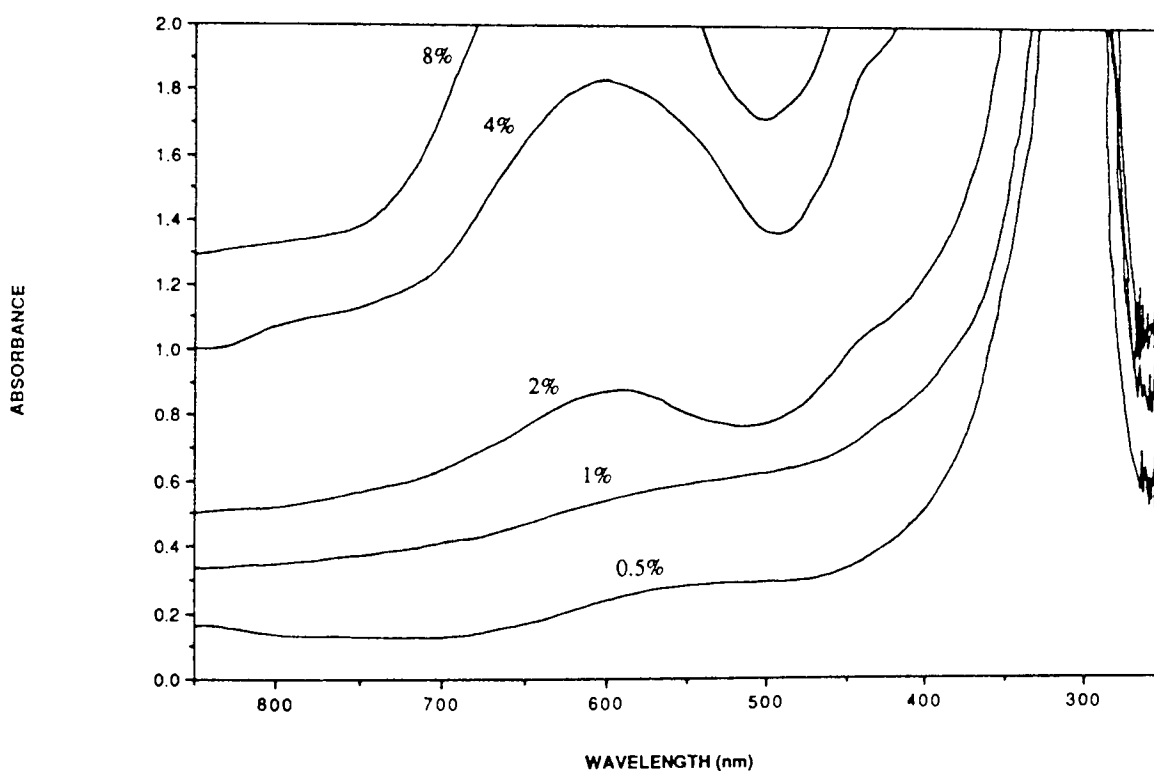


**Figure 3.20 Visible Absorption Spectra of Co(I)tris(VBipy) in Membranes of Various Ligand Loadings.**

#### 3.4.3.2 Co(I) tris(Bipyridyl-Polymer) Complex Redox Processes.

It has been long known that the Co(I) complex with bipyridine (it may be *bis* or *tris* as we will see later) is unstable in air, as it is sensitive to reoxidation by atmospheric oxygen<sup>136</sup>. A membrane containing the Co(II) *tris*(bipyridyl) complex, derived from an original

**Figure 3.21 Visible Absorption Spectra Showing the Reoxidation of Co(I)tris(VBipy) Membrane.**

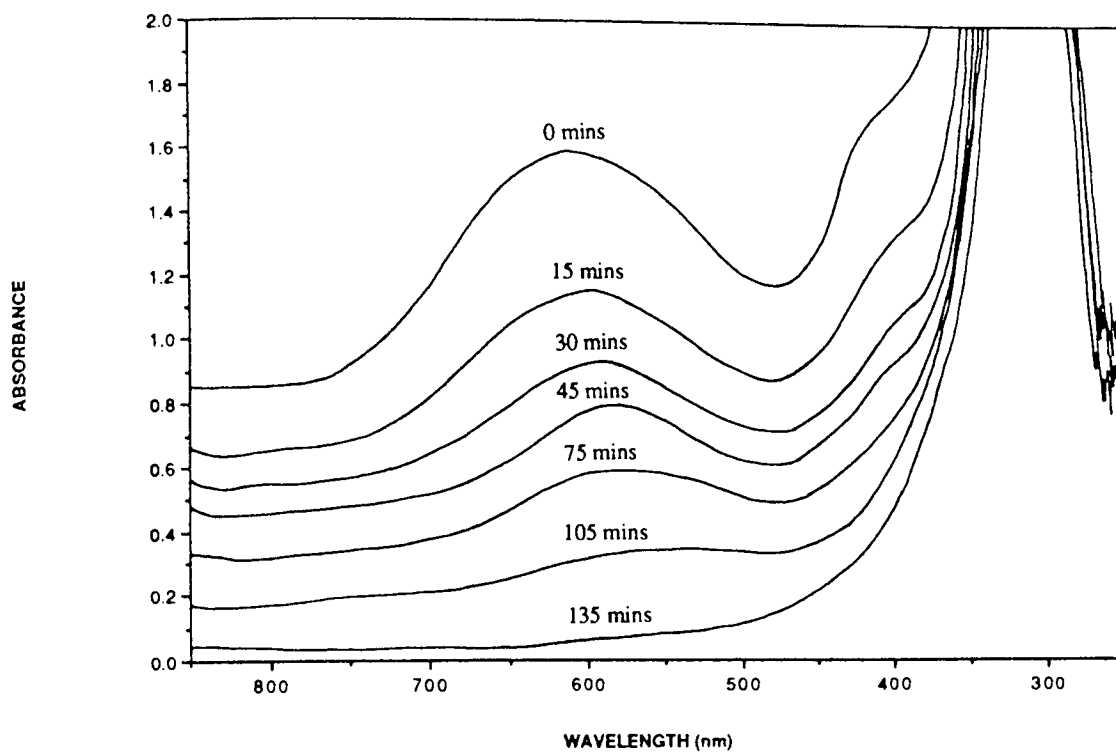
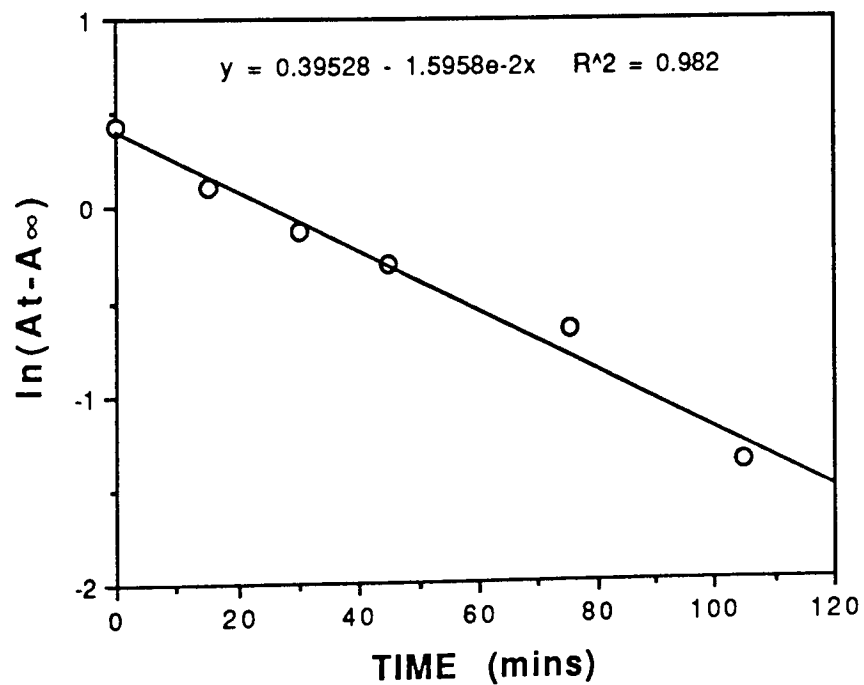


**Figure 3.22 First Order Plot for the Reoxidation of Co(I)tris(VBipy).**



2% loaded membrane, was reduced as previously described and then left in 100 ml of distilled water contained in a vessel open to the atmosphere. The absorption spectrum of the membrane was taken at regular intervals over a 2.5 hour period, resulting in Figure 3.21. This shows that over this time period, the Co(I) complex is totally reoxidised to the Co(II) complex, presumably by the oxygen dissolved in the distilled water which has a lower reduction potential than water itself.

The linear plot obtained for the loss in absorbance at 600nm ( $\log(A - A_{\infty})$ ) with time, indicates that reoxidation process is probably first-order in nature (Figure 3.22). The rate constant,  $k$ , for the reaction where  $-d/dt [\text{Co(I)}] = k[\text{Co(I)}]$  is  $2.5 \times 10^{-4} \text{ s}^{-1}$  and is probably the rate of oxygen permeation through the gel matrix. Time constraints limited the amount of work on this system, but it would be interesting to know how the rate varied with parameters such as the rate of stirring/agitation of the solution, partial pressure of oxygen over the solution, thickness of the membrane, and temperature.

One interesting question that relates to this study is, "Is there any loss of the complex from the system over a number of redox cycles?". This can be checked by continually reducing the complex, allowing it to reoxidise and then checking the absorbance  $\lambda_{\text{max}}$  at 455 nm, the intensity of which is a measure of the amount of the Co(II) *tris*(bipyridyl) complex present. Figure 3.23 (overleaf) illustrates the redox cycling data in terms of the % decrease of the absorbance at 455 nm. From this it is clear that over the initial cycle stages there is indeed a loss of complex from the system. However, as the number of cycles increases, the % loss of the complex decreases, depicted by a 'levelling-out' of the curves in Figure 3.23. Also, it is evident that membranes that contain a lower proportion of original ligand

loading experience a larger % dissociation of the complex.

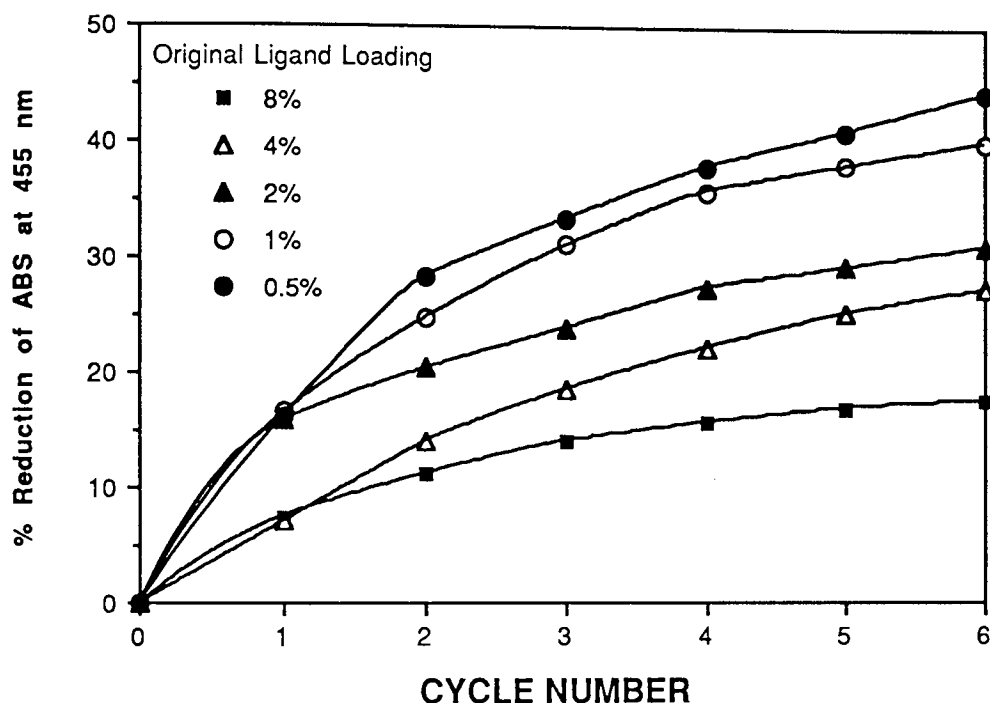


**Figure 3.23 Effect of Co(I)/Co(II) Redox Cycling on Absorbance Maximum @ 455nm.**

One explanation for these observations hinges on the idea that reduction of the complex to Co(I) may involve the dissociation of one of the bipyridyl groups from the complex. The *tris* complex may experience steric constraints imposed by the polymer, and on reduction to Co(I) and subsequent dissociation of one of the ligands, much of the 'strain' on the geometry is released. Also, dissociation of a bipy would be a necessary intermediate step in the formation of a 5-coordinate Co(I) species, the favoured geometry for this oxidation state\*.

\*[The formation of a 5 coordinate complex is not so surprising when one considers the requirements of the 18-electron or "effective atomic number" (EAN) rule. In basic terms, filling the bonding molecular orbitals of a complex can be considered as filling the outer 9 orbitals of the metal ion with its own d electrons, plus a  $\sigma$  electron pair from each ligand (18 electrons in total). The  $d^8$  configuration of  $Co^+$  provides 4 valence electron pairs and thus requires 5 adduct bond pairs for stability.]

On reoxidation to  $\text{Co(II)}$ , reformation of the *tris* complex may not be sterically permissible and a loss of complex results. Once all the 'strained' complexes are released by redox cycling, little or no further total dissociation occurs, as the polymer also acts to hold ligand groups in close proximity for recombination into the *tris* form. Lower ligand loadings result in an increased distance between ligands along the polymer chain, and therefore, less likelihood of re-forming the third  $\text{Co(II)}$ -bipy bond. This would account for the greater percentage losses of complex from these membranes.

For this explanation to be acceptable, it must be shown that dissociation of a bipyridine upon reduction is a plausible concept. Firstly, it should be noted that the existence of the stable  $\text{Co(I)}$  *bis*(bipyridine) complex has been known for as long as the *tris* complex<sup>136,138</sup>, and that it possesses a visible absorption spectrum virtually identical to that of the *tris* form<sup>142</sup> which renders the two complexes indistinguishable by visible spectroscopy. However, Sutin *et al.*<sup>143,144</sup> have used  $\text{Co(I)}$  *tris*(bipyridine) as a catalyst in the photoreduction of water and suggest that it may form an unstable hydride which would mediate the formation of hydrogen. This may provide a clue as to the mechanism involved in the use of borohydride as a chemical reducing agent for this reaction.

Consider now the proposed mechanism (Figure 3.24 overleaf) for the redox processes occurring within the membrane. Equation (1) is a dissociation step in which a ligand is lost to give the *bis*  $\text{Co(II)}$  complex; this step is almost inevitable, as both reductions with  $\text{BH}_4^-$  and oxidations with  $\text{O}_2$  are inner-sphere processes. This can consequently form an unstable hydride (2), probably initially with  $\text{BH}_4^-$  *via* hydride-bridges to the metal. The evolution of hydrogen (which also occurs during this process as a result of the reaction of

BH<sub>4</sub><sup>-</sup> with water), produces the stable Co<sup>(I)</sup> *bis* (bipyridyl) complex (3), which is free to reform the *tris* complex when it encounters a free ligand (4). It should be noted that although this mechanism fits the available evidence, much of it is conjectural in nature and there may be other plausible alternatives.

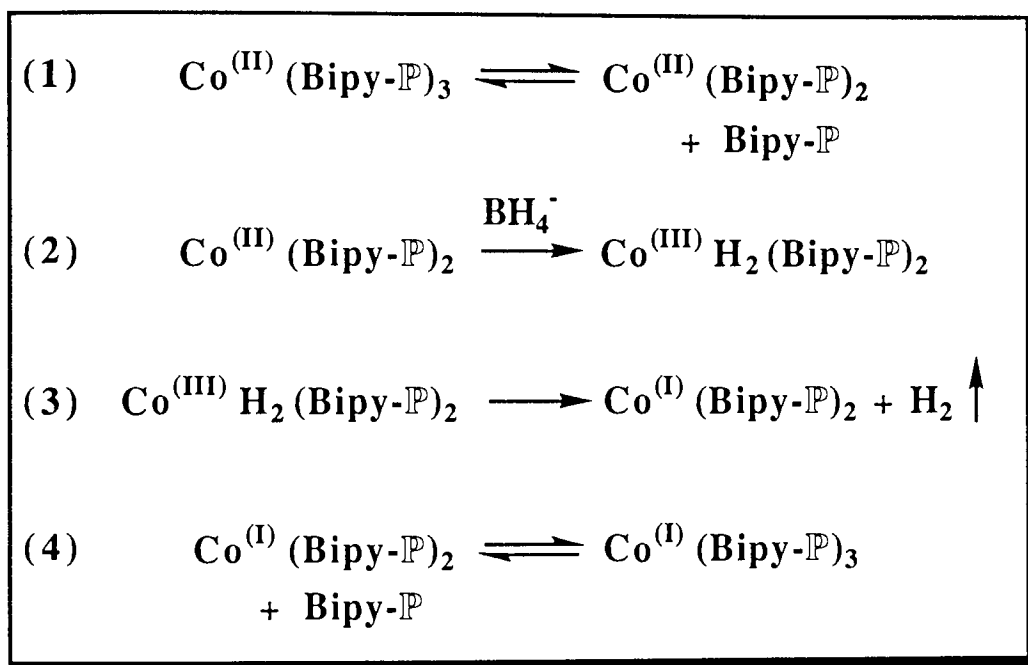
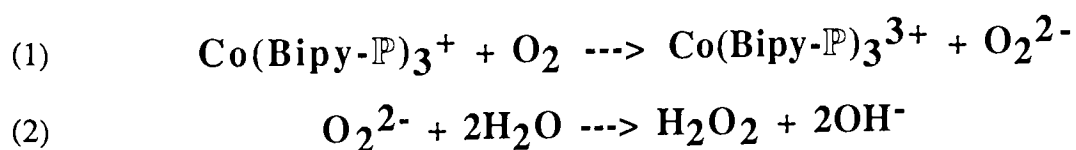


**Figure 3.24 Proposed Mechanism for the Reduction of Co(II) to Co(I).**

### **3.4.3.3 Oxygen Scavenging Ability of Co(I) Coordinated Bipyridyl-Copolymer**

#### **Membranes.**

The Co<sup>(I)</sup> *tris* (bipyridyl) complex is a powerful reducing agent with reported standard reduction potentials ( $E^0$ ) ranging from 1.0 to 1.37 V (vs. SCE) <sup>141</sup>. This is sufficiently high to reduce dioxygen to peroxide. The overall effect is to remove dissolved oxygen from solution, a potentially useful action:



This property has already been implemented by Homer *et al.* for the removal of oxygen

from samples used in NMR studies of spin-lattice relaxation times <sup>145</sup>. With such an array of possibilities open for the use of this complex, it may be advantageous if a method were available for the stabilisation of the polymer-bound derivative. Figure 3.25 overleaf demonstrates that just such a method is possible.

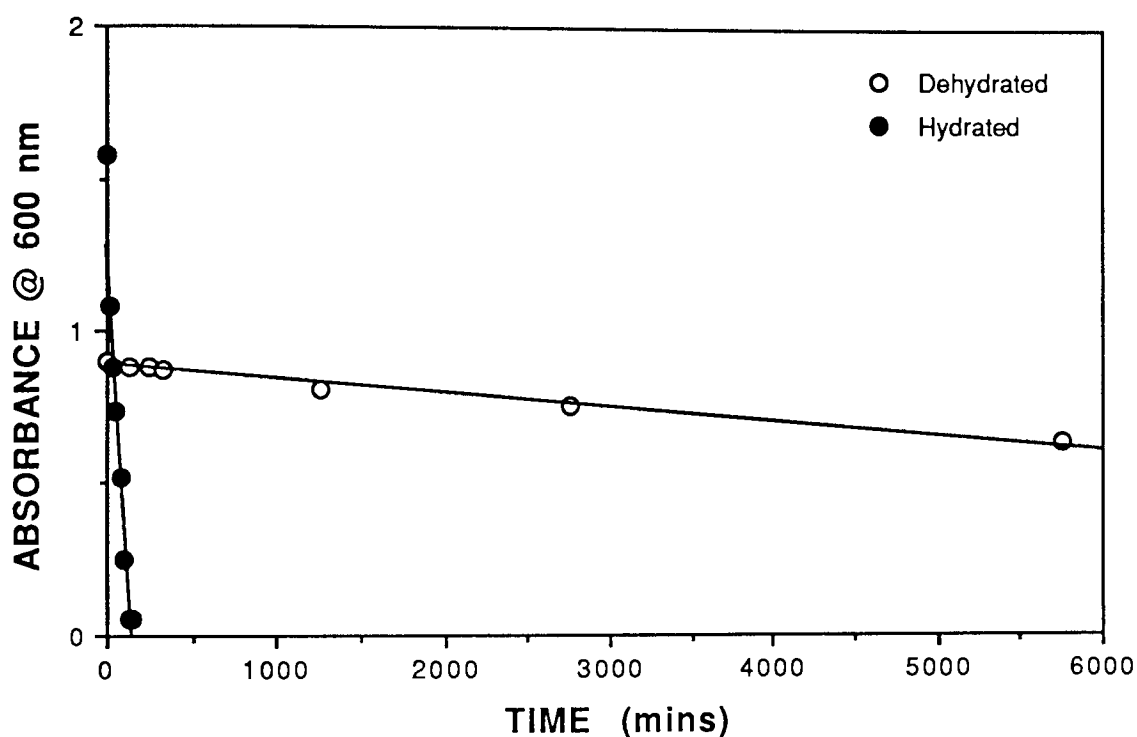


**Figure 3.25 Comparison of the Rate of Co(I) Reoxidation in Hydrated & Dehydrated Membranes.**

As seen previously, reoxidation of the complex whilst the membrane is in a hydrated state takes 2-3 hours. If however, the membrane is dehydrated in an oven at 60<sup>0</sup> C immediately after reduction of the complex is complete, the characteristic colour of the Co(I) complex is stabilised for days rather than hours. Oxygen is permeable in hydrated PolyHEMA as it is able to dissolve in the water content of the gel; this is the basis of the use of these polymers in extended-wear contact lenses. It has also been shown that dehydration of these polymers renders them impermeable to oxygen because the gas transport medium has been removed <sup>146</sup>. In fact, the slow decay of the blue colour is probably due to the slow absorption of atmospheric water by the membrane, which provides a medium for the

dissolution and transport of oxygen into the polymer. In addition, if complex reorganisation is necessary for the oxidation step, severe immobilisation of the polymer chains by removal of the plasticising effect of the water will prevent the process occurring. Therefore, by keeping the polymer in a dehydrated state and closed to the atmosphere, the Co(I) complex could potentially be stored for long time periods until required.

### **3.4.4 Fe(II) Interactions with Bipyridyl-Copolymer Membranes.**

#### **3.4.4.1 Visible Absorption Spectra of the Fe(II) tris(Bipyridine) Complex.**

Iron (II) forms complexes with a variety of different ligands, commonly forming octahedral high-spin compounds that have a free-ion  $^5D$  ground term, thus exhibiting a single band in the absorption spectrum corresponding to the  $^5T_{2g} (t_{2g}^4 e_g^2) \rightarrow ^5E_g (t_{2g}^3 e_g^3)$  transition <sup>147</sup>. When coordinating to ligands, such as bipyridine, which are high in the Spectrochemical Series, the crystal field splitting energy ( $\Delta$ ) is increased. On complexation of the third bipyridine  $\Delta$  becomes large enough to overcome the inter-electronic repulsion experienced by spin-pairing electrons in the  $t_{2g}$  orbitals <sup>50</sup>. The result is a  $d^6$  low spin configuration that exhibits charge-transfer transitions <sup>52</sup>:

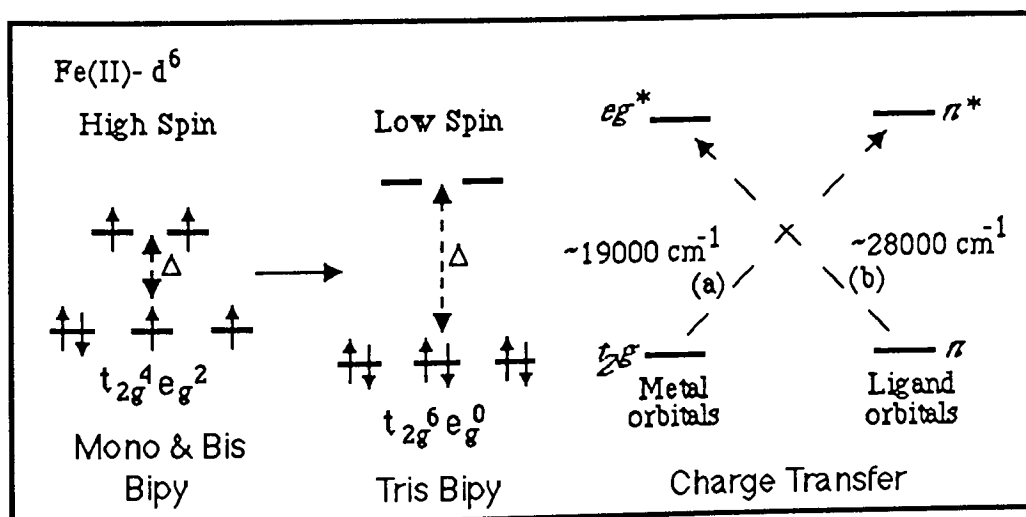


**Figure 3.26 Electronic Configuration and Transitions for the Fe(II) tris(Bipyridine) Complex.**

As far as this study is concerned, it is the Laporte allowed  $t_{2g} \rightarrow \pi^*$  transition around  $19,000\text{ cm}^{-1}$  (a) that is most important, but the  $\pi \rightarrow eg^*$  transition around  $28,000\text{ cm}^{-1}$  (b) should also be detectable. The intense red colour produced by the metal-to-ligand charge transfer (MTLCT) has made the  $\text{Fe(II)} \text{ tris}(\text{bipyridine})$  complex one of the most widely studied <sup>49,51</sup>, with international recognition as a prime colorimetric reagent for the determination of iron.

#### **3.4.4.2 Effect of Ligand Loading on Fe(II) Coordination to Bipyridyl-**

##### **Copolymer Membranes.**

Bipyridyl copolymer membrane samples (4 x 1cm) of ligand loadings 0.05, 0.1, 0.25, 0.5, 1 & 2% by weight, were placed in 0.01M  $\text{FeSO}_4 \cdot 7\text{H}_2\text{O}$  solutions and left to equilibrate for 48 hours; this will be referred to as time infinity, or  $t_\infty$ . Several observations could be made as a result of this action, the most obvious being that the membrane formed a red colouration, characteristic of  $\text{Fe(II)} \text{ tris}(\text{bipyridyl})$  complexation. Figure 3.27 shows the visible absorption spectra of membranes with various ligand loadings, placed in 0.01M  $\text{FeSO}_4$  for a time period,  $t_\infty$ , and resulting in an infinity absorbance maximum at 534nm, the  $\text{Abs}_\infty$ . It is interesting to note that even membranes with ligand loadings as low as 0.05% produced the red colouration. The 0.05% loading corresponds to approximately one ligand per 3000 units along the polymer chain and thus the formation of a *tris* complex requires a great deal of backbone segmental rotation and chain mobility. This is another example of the remarkable flexibility of the hydrogel polymer chains.

If 3 membranes each of 0.5% VBipy loading are placed in solutions of  $\text{FeSO}_4$ ,  $\text{FeCl}_2$  and  $\text{Fe}(\text{ClO}_4)_2$  and the visible spectra are recorded at  $t_\infty$ , Figure 3.28 is the result. The

**Figure 3.27 Effect of [Ligand] on Fe(II) Spectra of Bipyridyl Copolymer Membranes.**

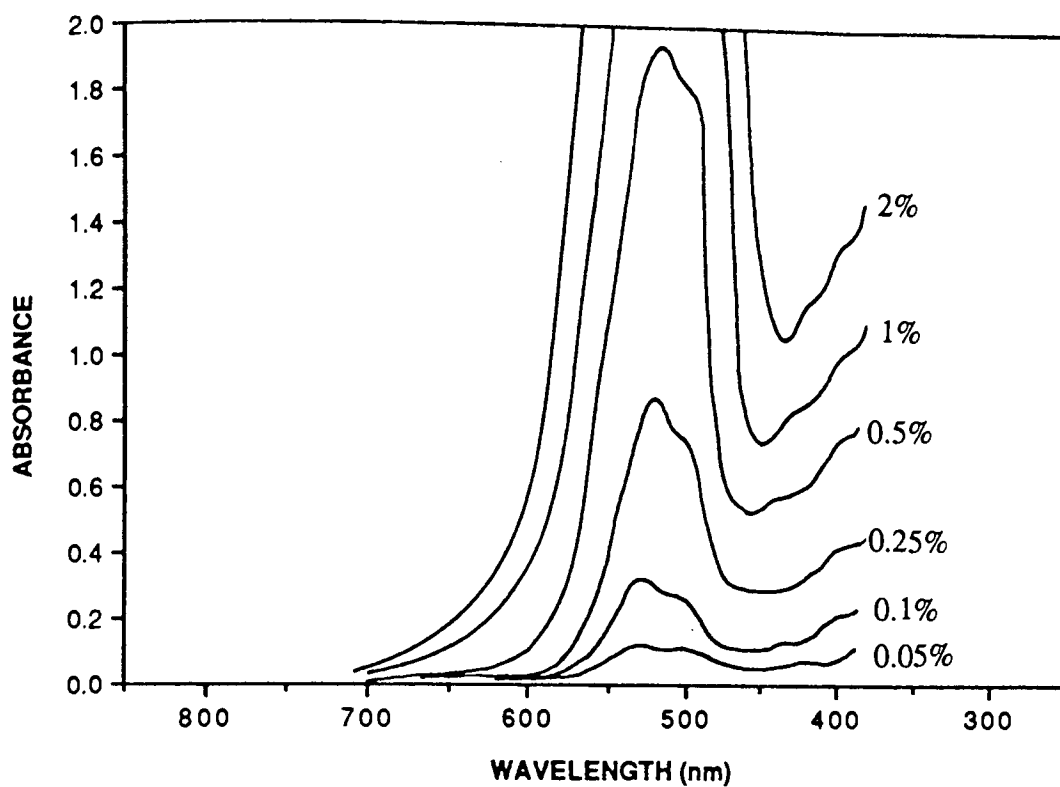
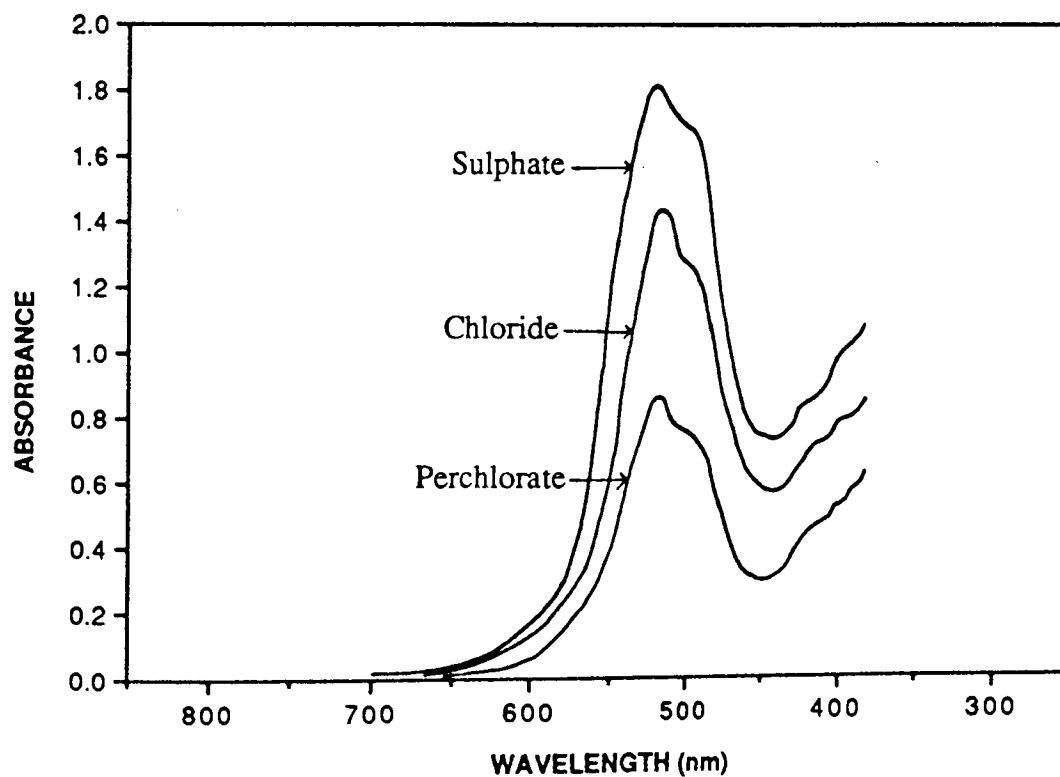


**Figure 3.28 Effect of Anion on  $ABS_{500}$  of Fe(II) tris Complex.**



differences in the observed  $\text{Abs}_\infty$  for the three types of anion were not immediately explicable with the available information. The results from studies of aqueous solutions of the monomeric ligands show that the absorbance is independent of the counterion. Here, that is not the case. Preliminary studies on the *rate* of *tris* complex formation by methods described in Chapter 2 (section 2.7.3) revealed an anion dependence, and to obtain a clear understanding of the events occurring within the polymer, it would be necessary to undertake a full kinetic study. This is the reasoning which lead to the series of experiments that constitute Chapter Four.

### **3.5 PRELIMINARY STUDIES ON COPOLYMER COATED-WIRE**

#### **ELECTRODES.**

The discovery in the early 1900's that certain glasses respond to hydrogen ion activity lead to the development of the the pH electrode, the first and best known ion-selective electrode. Advances in polymer technology have meant that membrane materials can be custom-engineered to produce the desired interaction with particular ions. Recently, considerable attention has been focussed on the use of ISE's as electrochemical sensors <sup>148-152</sup>. The selectivity of such 'chemical sensors' can be improved by the inclusion of a specific chelating agent dissolved within the polymer. It seemed a logical progression therefore, to assess the feasibility of using ligand-based copolymer coatings (Chapter Two, section 2.9) for TM ion sensor potential, as a slight digression from the main theme of this project.

One group of workers has recently concentrated on the preparation of electrodes modified with a polypyrrole film possessing appended aza-macrocycles <sup>153</sup> (see Chapter six). One of the suggested uses of these potential ion-selective electrodes is the measurement of

small levels of a transition metal ion species following its selective complexation by the ligand- an application that was indeed being investigated in this study for the pyridyl-based hydrogel electrodes.

Transition metal interaction with such coated electrodes results in a type of system where the presence of the immobilised metal centre can radically alter the electroactive nature of the coating and thus the electrode response. Certainly, the complexed aza-macrocycles mentioned earlier exhibit some electrocatalytic properties, which was an additional reason that influenced the fabrication of electrodes modified with these materials. This study was therefore extended to the investigation of electrodes modified by pyridyl-based hydrogel coatings by conventional triangular potential waveform cyclic voltammetry, a technique that can often provide information on the coverage of the electrode surface and kinetics of the electrode reaction (Chapter Two, section 2.9.2).

Unfortunately, time restrictions during the course of this project have limited the extent of progress with this work. The results of this preliminary investigation are not comprehensive, but are indicative of their potential application within the area.

### **3.5.1 Evaluation of Ligand-Based Copolymer Coatings for TM Ion-Sensitive**

#### **Electrodes.**

Figure 2.16 (Chapter Two) outlines the electrochemical cell used in the characterisation of the ligand-modified CWISE's. Initially, the test membrane under study was a simple polyHEMA coating which was calibrated by measuring the potential when the arrangement was placed in a TM solution. A series of  $\text{CuCl}_2$  solutions in the range  $10^{-1}\text{M}$

to  $10^{-6}\text{M}$  were made and the CWISE/SCE pair placed in the solution of lowest concentration. This solution was stirred gently by a magnetic stirrer until a stable potential was reached, the magnitude of which was noted and the process repeated by transferring the electrodes to the next solution. A calibration graph can be constructed by plotting the EMF (mV) vs.  $-\log \text{ TM ion activity}$  (as calculated from an extended form of the Debye-Huckel equation <sup>152</sup>):

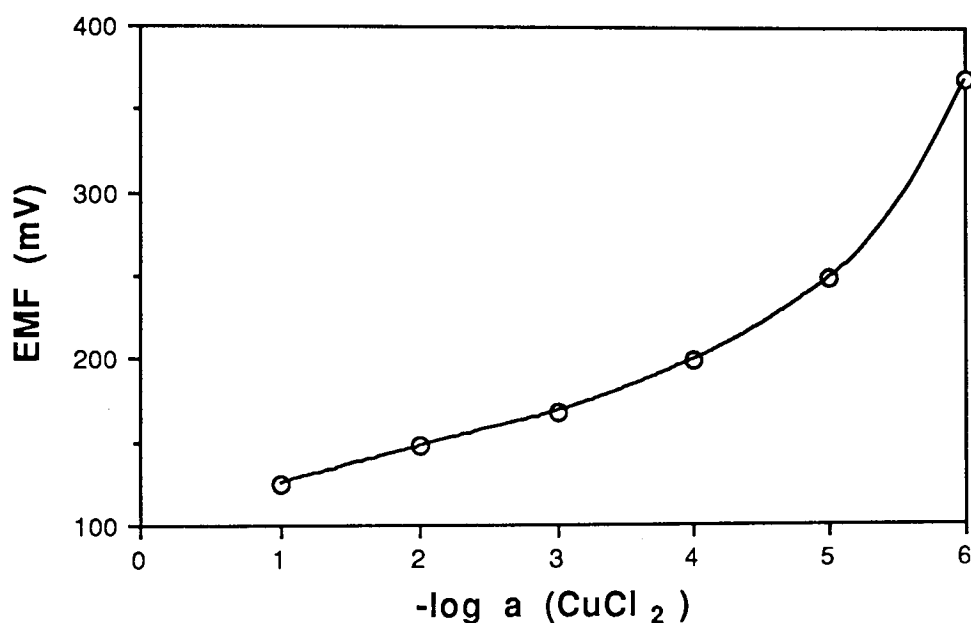


**Figure 3.29 Potentiometric Response of a Poly(HEMA)  
CWE in  $\text{CuCl}_2$ .**

Typically, electrodes produce a linear variation of EMF with activity known as a Nernstian type response. However, the electrodes made for this study produced an inconsistent non-Nernstian response, probably as a result of uneven and variable thickness of the membrane coating (Figure 3.29). If this technique is to be developed further, it will be necessary to devise a method of coating the platinum wire to obtain a uniform layer of reproducible thickness.

A series of CWE's with HEMA:2%Vpy and HEMA:2%VBipy copolymer coatings were

made but in the light of the previous results with unmodified electrodes, detailed studies were not undertaken. However, a pyridyl copolymer-coated electrode was placed in a  $\text{CuCl}_2$  solution and the potential monitored with time (Figure 3.30). Point A represents the placement of the CWE/SCE pair in the  $\text{Cu}(\text{II})$  solution. The potential drops but quickly stabilises for a period of time; this is thought to be the stage over which metal ions complex to the ligand groups, a process that prevents the ions reaching the electrode surface. The time lag is thus probably proportional to the concentration of ligand groups (% weight copolymer, membrane thickness) and concentration of  $\text{Cu}^{2+}$  ions.

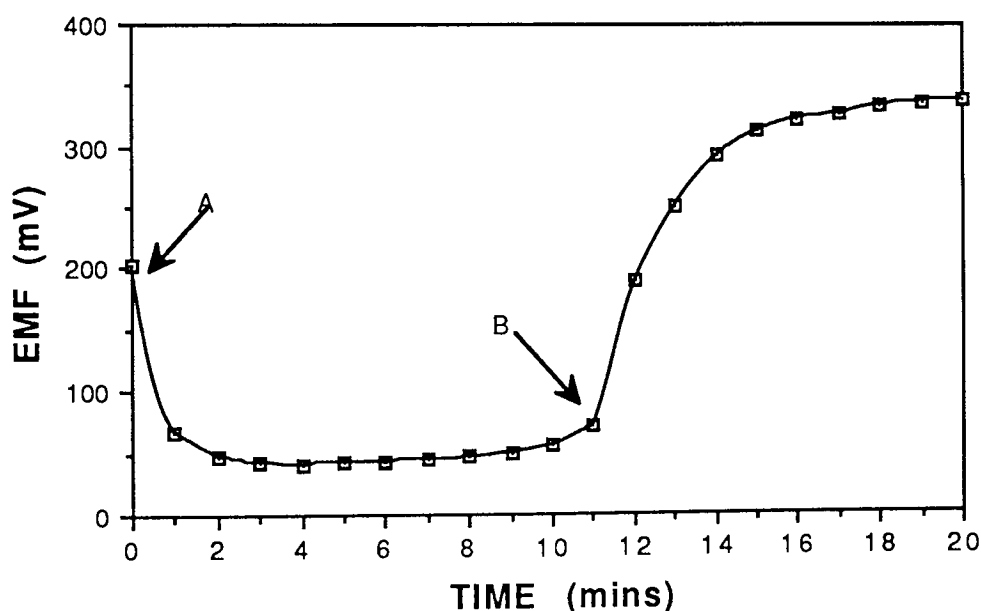


**Figure 3.30 Potentiometric Response of a 2% Pyridyl-Based Hydrogel CWE in  $\text{CuCl}_2$ .**

At Point B the potential increases rapidly and eventually reaches a constant level; this represents the stage at which the majority of the ligand groups have coordinated a metal ion, and the remaining ions are free to flow to the electrode surface causing an increase in the EMF. This information certainly correlates with the evidence obtained from the TM

permeability studies described in Chapter Five, where a similar lag-time is observed before TM ion transport begins.

### 3.5.2 Studies on the Electroactive Nature of Complex-bound CWE's using Cyclic Voltammetry.

The ligand-modified electrodes previously described were left in various TM salt solutions to enable the formation of the stable complexes described in section 3.4. These were then subjected to cyclic voltammetric techniques as described in Chapter Two, section 2.9.2, along with the uncomplexed precursor, and unmodified hydrogel coatings. Owing to limited time on the equipment, only a short study was possible on these samples. It is difficult to analyse these 'sparse data' in a quantitative manner, and consequently, this section is devoted to the brief description of the voltammograms produced.

#### 3.5.2.1 Electrochemistry of the Uncomplexed Polymer Coatings.

The support electrolyte window can clearly be seen in the voltammogram of Figure 3.31:

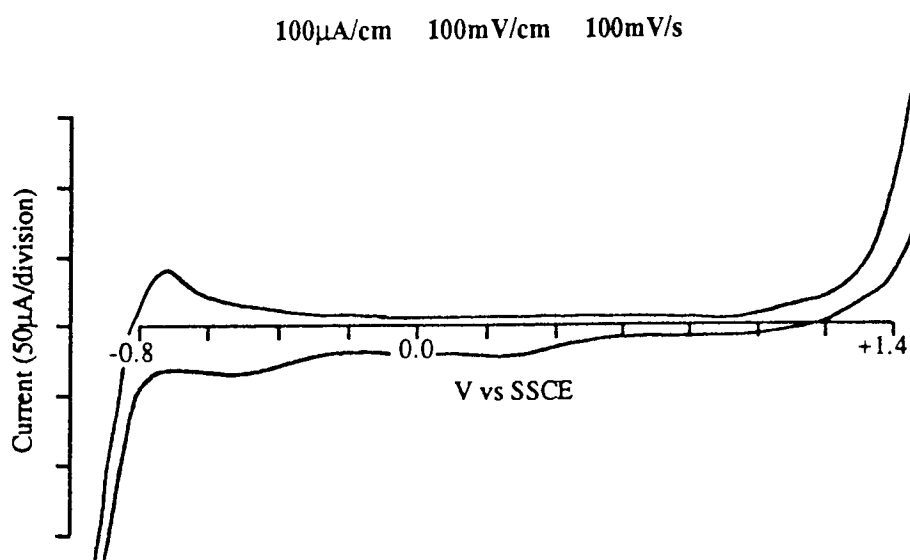
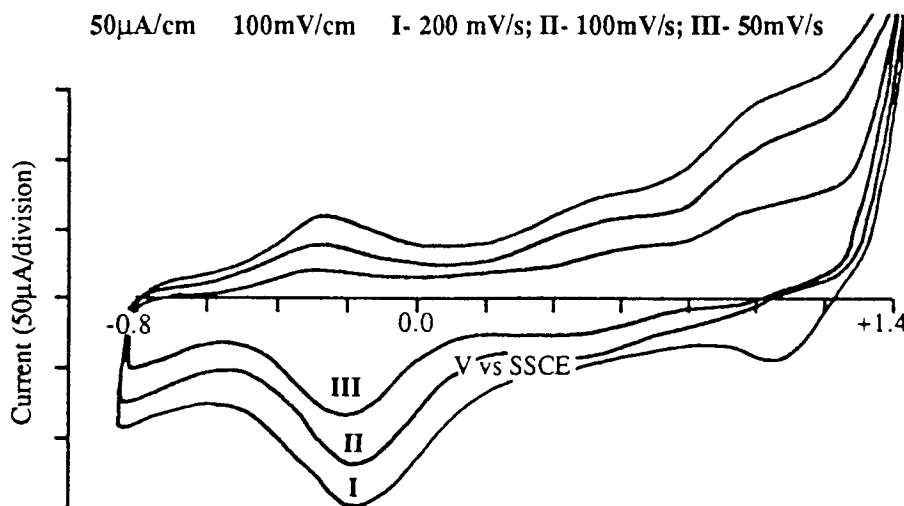


Figure 3.31 Cyclic Voltammogram of 0.1M KCl

The anodic wave at -0.8V corresponds, in simple terms, to the reduction of water to

hydrogen, and the cathodic wave to its oxidation to oxygen. It was necessary to see if the polyHEMA hydrogel itself was electroactive, so that the electrochemical effects due to the polymer could be distinguished from those of the immobilised complexes. At first glance, PolyHEMA appears to possess a reversible wave around -0.2V; however, we will see that this is indeed a characteristic of the gel, but it is not a reversible wave, the anodic peak observed at -0.2V being due to the reduction of some oxidation product produced  $> +0.7V$ . Considering the chemical constituents of polyHEMA, it is probable that the observed electrochemistry is that due to the hydroxyl groupings; other than this, no other firm conclusions can be drawn without further work.



**Figure 3.32 Cyclic Voltammogram of a PolyHEMA Coating.**

Figures 3.33(a) & (b) overleaf are the cyclic voltammograms of the 2% uncomplexed copolymers of VPy & VBipy with polyHEMA respectively. These voltammograms are similar to that of Figure 3.32, except that the three anodic waves and the cathodic wave at  $\sim -0.3V$  are more pronounced. Also it is clear that the exact position of these peaks varies somewhat. The presence of the lone pair of electrons on nitrogen groups of the pyridine and bipyridine rings may be expected to complicate the electrochemistry somewhat in these

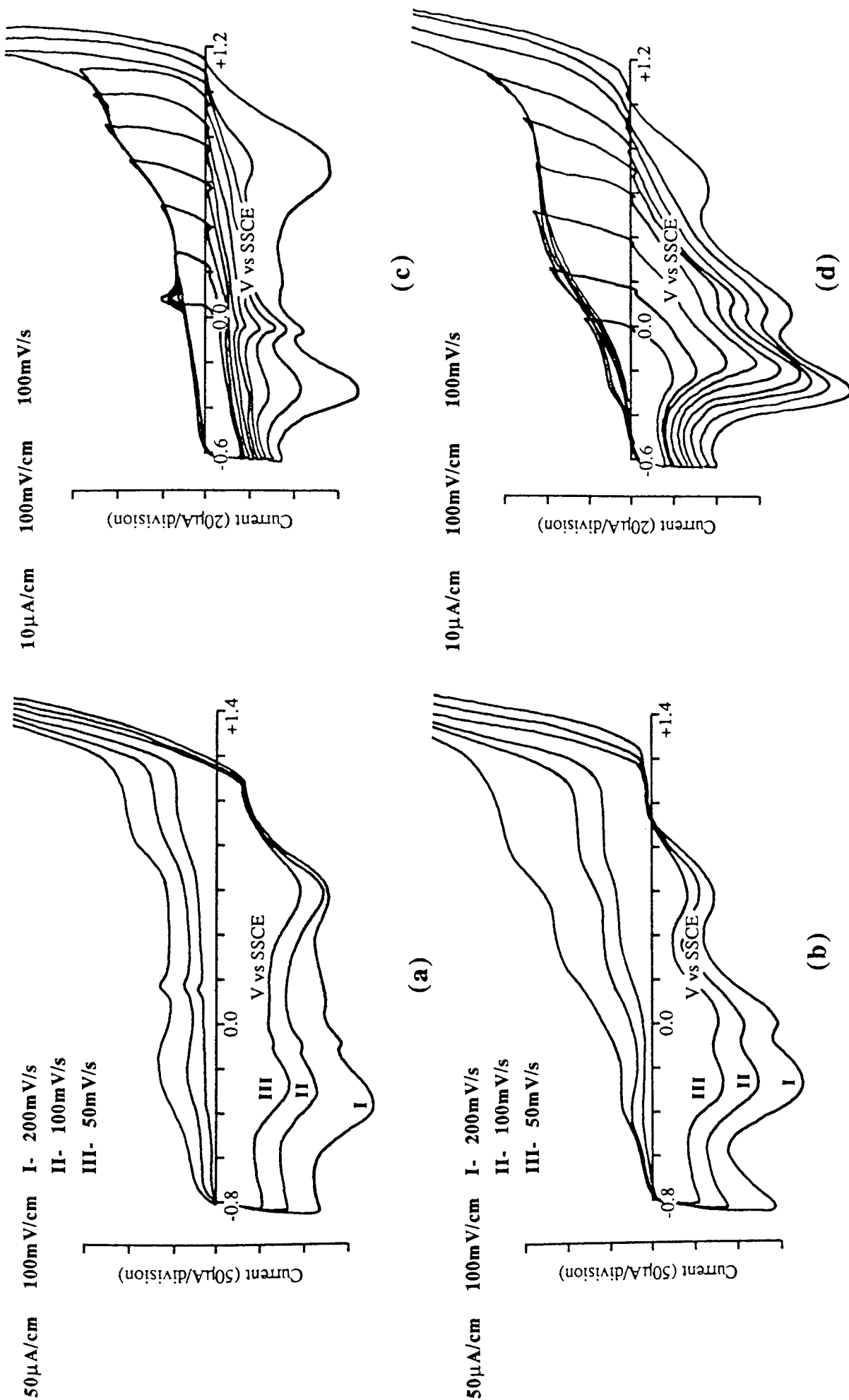


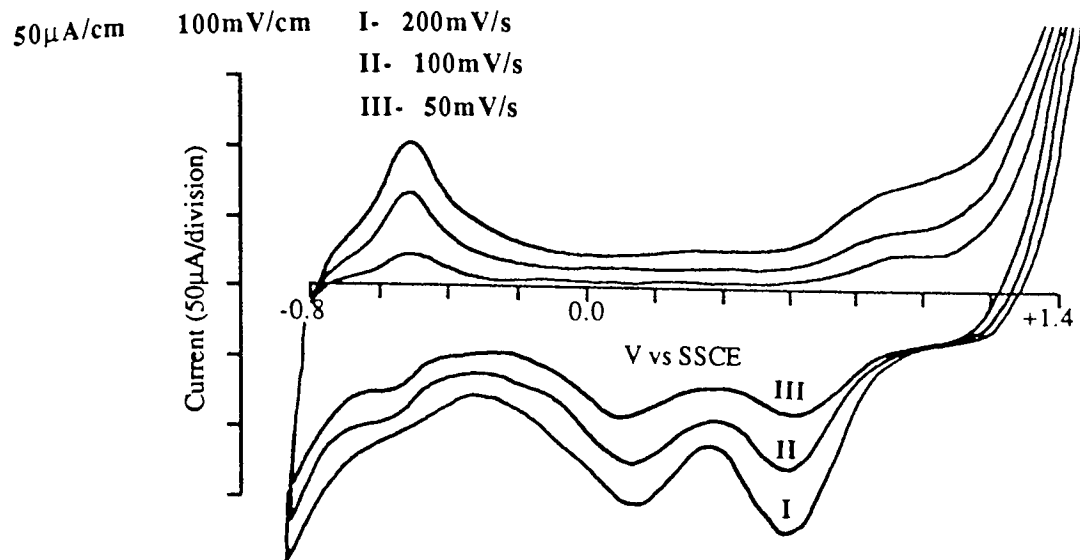
**Figure 3.33 Cyclic Voltammograms of (a) 2% VPy Copolymer; (b) 2% VBipy Copolymer; (c) Voltage Sweep of (a); (d) Voltage Sweep of (b).**

copolymers; indeed, the pH-dependent reduction of the pyridinium ion has been thoroughly investigated previously <sup>154</sup>. Figures 3.33(c) & (d) represent a sequence of 'voltage-sweeps', in which the electrode is started at -0.6V and cycled to increasingly positive potentials at regular intervals. This process helps to establish which oxidative and reductive peaks are coupled. A number of features are immediately obvious from these spectra: the cathodic wave at  $\sim -0.3\text{V}$  is missing- and therefore is the result of the oxidation of a product formed in the reductive cycle below  $-0.8\text{V}$ , i.e. may be associated with the reduction product from the aqueous support solvent. The reductive wave at  $\sim +0.6\text{V}$  only appears if the voltage sweep is taken to  $+1.3\text{V}$ , and so is associated with an oxidative product formed above this potential. It is of similar size to the reductive wave at  $\sim +0.2\text{V}$  (which is coupled with the broad cathodic shoulder that begins at  $+0.6\text{V}$ ) which perhaps could suggest that each of these peaks represents a one electron reduction step, in the overall two electron reduction of an oxidation product formed  $> +1.3\text{V}$ .

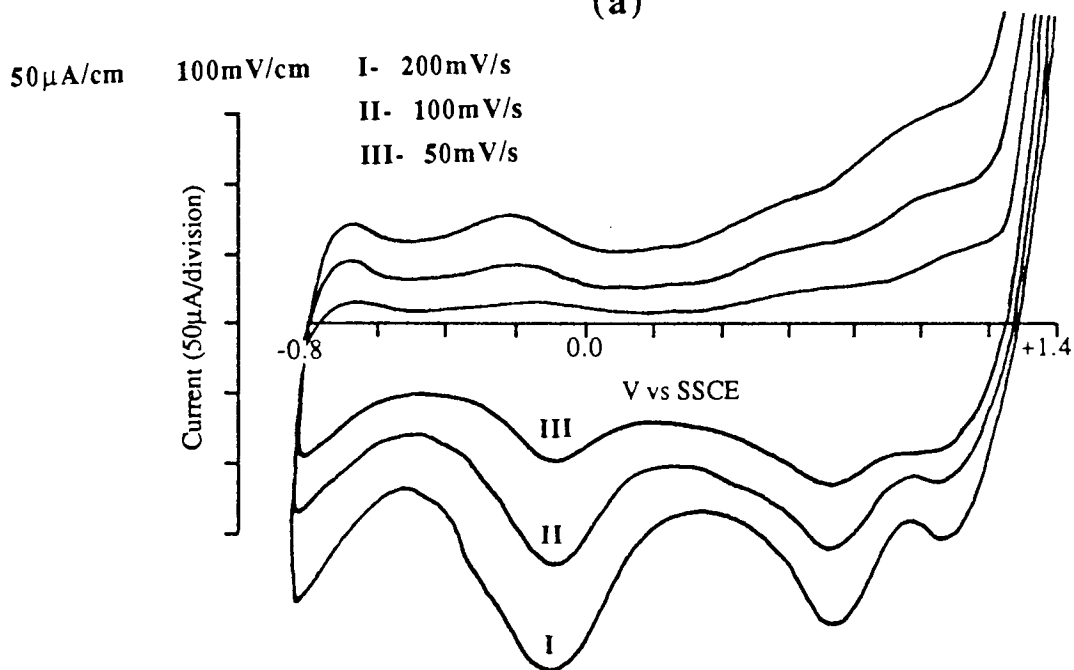
#### **3.5.2.2 Electrochemistry of Complexed Polymer Coatings.**

The introduction of transition metals as immobilised complexes on the electrode coatings further confuses the electrochemistry of these materials. Figures 3.34(a)-(c) show cyclic voltammograms for a 2% VBipy polymer film complexed with  $\text{Fe(II)}$ ,  $\text{Cu(II)}$  &  $\text{Co(II)}$  respectively. The colour of the electrode films was indicative of the formation of the *tris* complex for  $\text{Fe(II)}$  &  $\text{Co(II)}$  and the *bis* complex for  $\text{Cu(II)}$ , as described in the early sections of this chapter. Again, similar patterns for the cathodic and anodic waves are seen, with variations in number, intensity and position of the peaks.

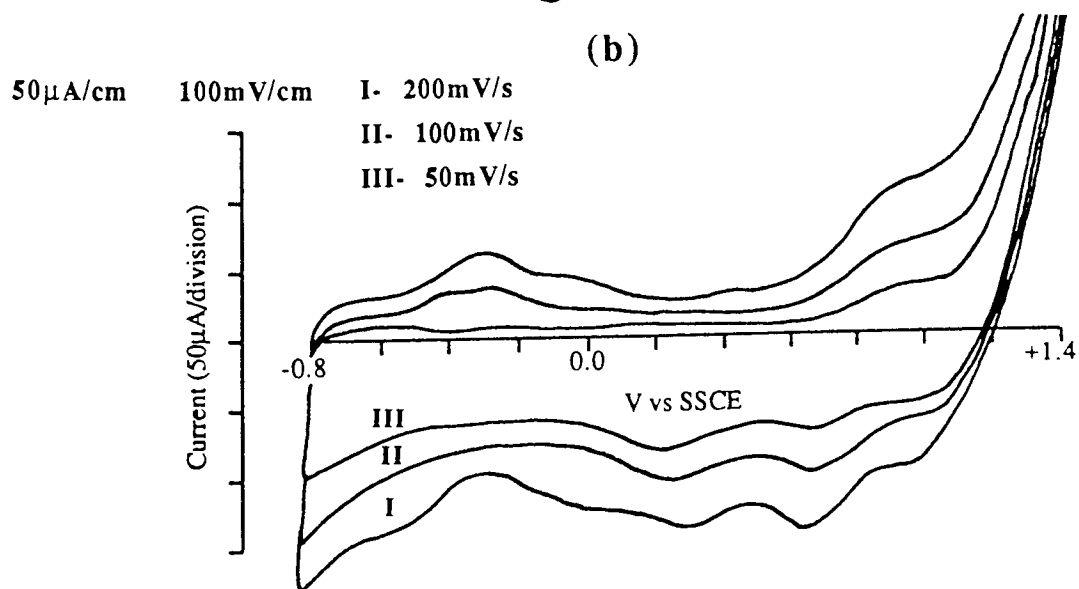
Figures 3.35(a) & (b) are cyclic voltammograms of 2% VPy-coated electrodes complexed



(a)

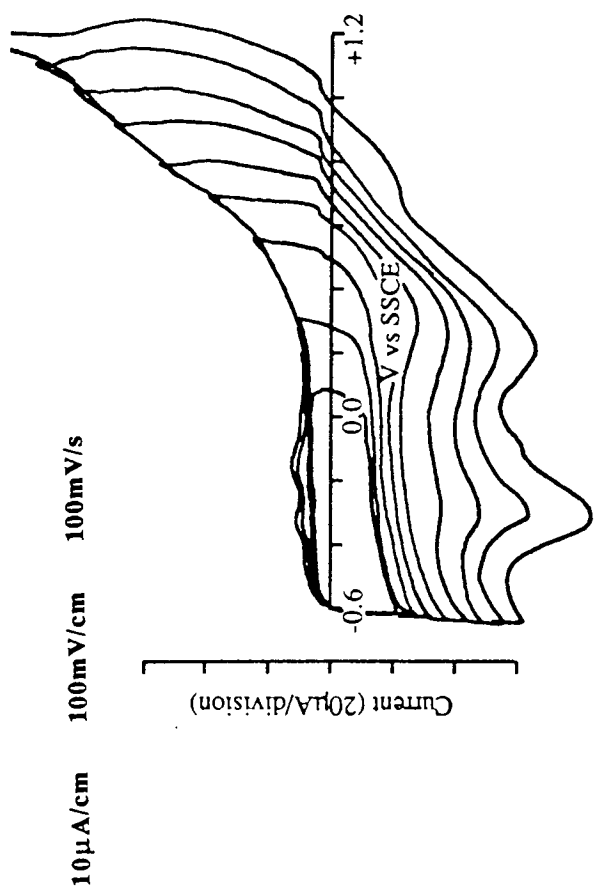


(b)

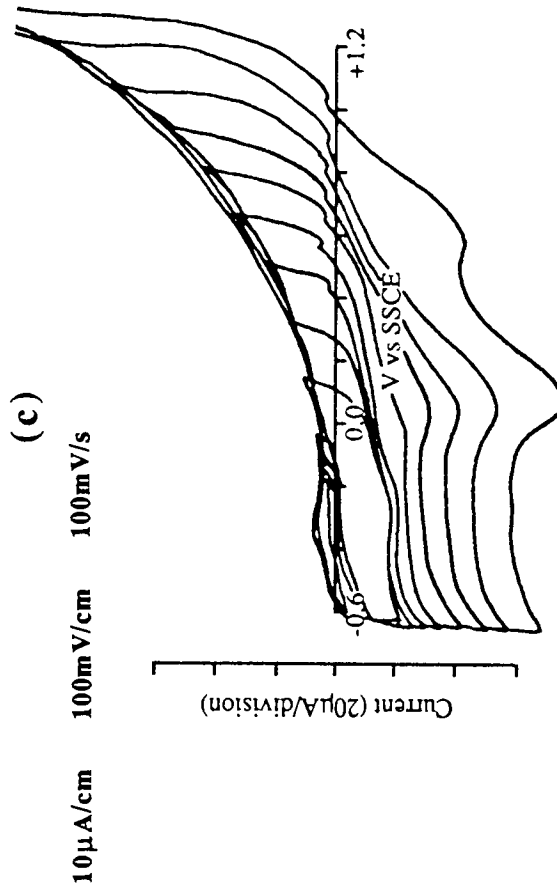


(c)

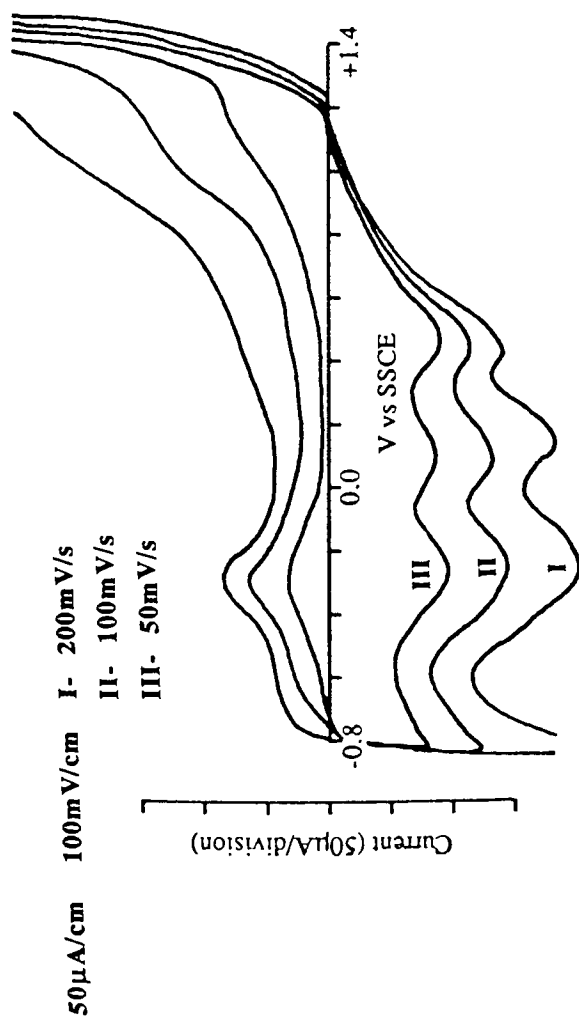
**Figure 3.34** Cyclic Voltammograms of (a) 2% VBipy:[Fe(II)]; (b) 2% VBipy:[Cu(II)]; 2% VBipy:[Co(II)].



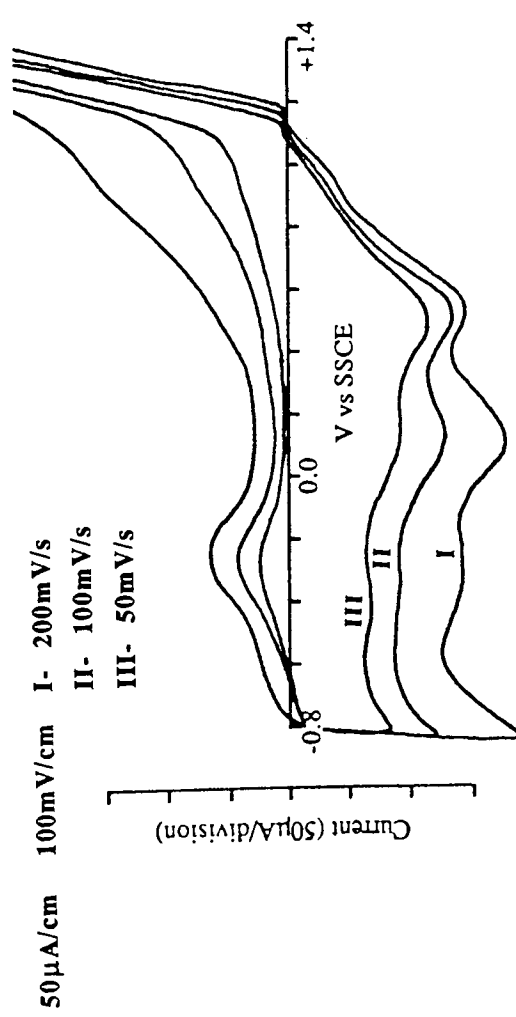
(c)



(d)



(a)



(b)

**Figure 3.35 Cyclic Voltammograms of (a) 2% VPy:[Fe(II)] Copolymer; (b) 2% VPy:[Cu(II)] Copolymer; (c) Voltage Sweep of (a); (d) Voltage Sweep of (b).**

with  $\text{Fe}(\text{II})$  (which was probably oxidised atmospherically to  $\text{Fe}(\text{III})$ , as suggested by its brown colouration), and  $\text{Cu}(\text{II})$ . Figures 3.36(c) & (d) are the voltage-sweep spectra of these electrodes. A small reversible wave is seen at +0.05V/-0.05V for the iron-containing polymer. It was first thought that this may well be due to the  $\text{Fe}(\text{II})/\text{Fe}(\text{III})$  couple, but this normally appears at +0.771V; allowing for the potential of the saturated calomel electrode at 25°C as 0.244V, there is no way that this wave can be attributed to the  $\text{Fe}(\text{II})/\text{Fe}(\text{III})$  couple. The  $\text{Cu}(\text{II})$ -complexed VPy film, again, shows more intense peaks than the other complexes. In this case there seems to be a definite double-set of oxidation waves at +0.2 & +0.6V of equal height. These peaks are coupled with the anodic waves at -0.3 & +0.1V respectively.

Other than this very routine descriptive analysis, little more can be said on the electrochemistry of these materials except that there does seem scope for a more in depth and organised study. The aqueous support electrolyte does limit the range of potential that can be utilised and reduces the chance of observing redox processes occurring at the metal centres. Alternative electrolytes could be sought, but removal of the aqueous electrolyte would alter the characteristics of the gel, and it is information on the local environment of the complex within the swollen polymer matrix that is of primary interest.

### **3.6 CROSS-LINKING OF HYDROGEL NETWORKS THROUGH METAL-LIGAND COORDINATION.**

We have already noted earlier in this chapter, the ability of ligand-modified hydrogel polymers to coordinate certain transition metal ions. Visible spectroscopy has been used to demonstrate that the pyridyl-copolymer can form the *tetra*(pyridyl)  $\text{Cu}(\text{II})$  complex,

while, the bipyridyl-copolymer forms the *tris*(bipyridyl) complex with Fe(II) salts. As a result of coordinating more than one ligand per metal, complex formation essentially acts as a novel method of cross-linking the gel matrix (Figures 3.36(a) & (b)). The understanding of structure-property relationships for polymeric materials is essential to their efficient utilisation. The chemical interlinking of the polymer chains is of extreme importance in determining the overall three-dimensional characteristics of the material, and it is therefore necessary to gain a full appreciation of its effects <sup>155</sup>.

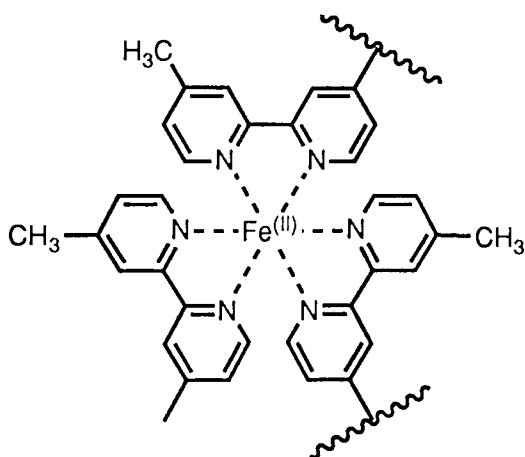


**Figure 3.36(a) 3-Centred Cross-Link of the *tris*(VBipy) Fe(II) Complex.**

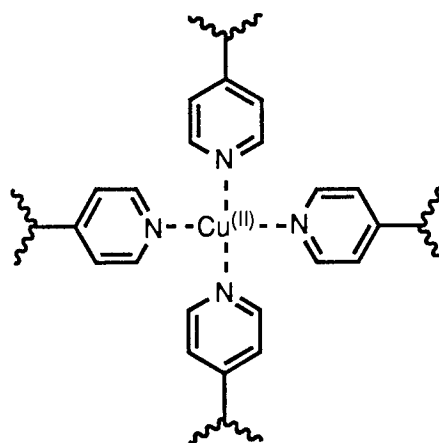


**Figure 3.36(b) 4-Centred Cross-Link of the *tetra*(VPy) Cu(II) Complex.**

Unfortunately, the very nature of the cross-linking process renders the polymer totally insoluble, and therefore inappropriate for the usual structural characterisation techniques.

Kopeikin <sup>156</sup> has reported the synthesis of a number of chelating polymers containing the acetylacetone (acac) group, and Eichinger *et al.* <sup>157</sup> have developed a number of spectroscopic means for studying the Cu(II), Fe(III) and Cr(II) *bis* and *tris* complexes of these polymers (Figure 3.37, overleaf).

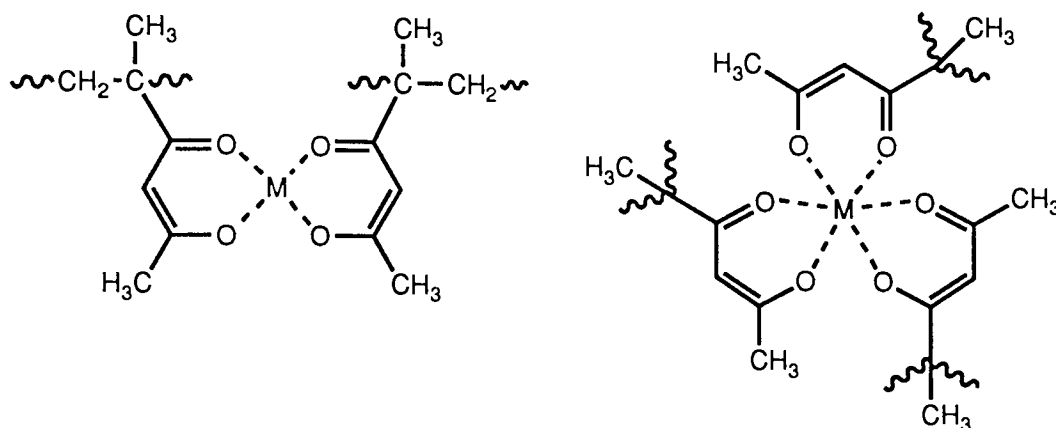


**Figure 3.37 Polymer-Immobilised *bis* & *tris* (Acac) Complexes.** <sup>156</sup>

They have extended their work to include a novel approach to the investigation of the effects of "coordination cross-linking", by a study of the mechanical properties of the polymers <sup>158</sup>. To date, this is one of the few reported studies of its kind in the literature.

The application of hydrogel polymers to the contact lens field has resulted in the extensive use of mechanical characterisation techniques for studying the physical properties of the cross-linked gels <sup>28</sup>. It has therefore been possible to adopt this approach in conjunction with the chelating membranes used in this project. The remainder of this chapter is devoted to the employment of the tensometric methods outlined in Chapter Two, section 2.8, in the investigation of the effects of cross-linking by complexation, on the physical traits of the ligand-based membrane systems.

### **3.6.1 Effect of Membrane Composition on Mechanical Properties.**

PolyHEMA membranes cross-linked with 1% EGDM have relatively poor mechanical properties, and are essentially soft materials capable of moderate elongation before failure. Typically, the tensile strength is reported to be in the region of 0.5MPa, with an elongation

to break ( $\epsilon_b$ ) around 200%. Copolymerisation with hydrophobic monomers such as styrene and methyl methacrylate, results in an increased tensile strength ( $\sigma$ ) with a concomitant reduction in the  $\epsilon_b$ , as the polymer undergoes a transition from a flexible to more rigid behaviour. This occurs because the bulk 'freezing' water content, and thus its plasticising effect on the polymer chains, is reduced in these copolymers.

Copolymerisation with the vinyl ligands has a different effect. It was shown earlier in this section that as the ligand content of the polymer increases, the E.W.C. of the membrane does show a small decrease, consistent with the addition of more hydrophobic constituents. However, increasing the amount of VBipy from 1-8% (Figure 3.38(a)) has the effect of increasing  $\sigma$  from 0.67-0.93MPa, and  $\epsilon_b$  from 130-170% (Table 3.3); similarly for increases in VPy from 2-16% (Figure 3.38(b)), we see an increase in  $\sigma$  from 0.68-2.24MPa, and  $\epsilon_b$  from 110-323%. The explanation for this effect is thought to lie in the hydrogen-bonding ability of the nitrogen functions in the heterocyclic rings. Weak hydrogen-bonding interactions between polymer chains forms temporary cross-links which aid in increasing the elongation and contribute to an improved strength. The effect is much more pronounced for the VPy ligand as it is only half the molecular weight of VBipy, and so there are twice as many distinct hydrogen-bonding sites per unit length of copolymer chain.

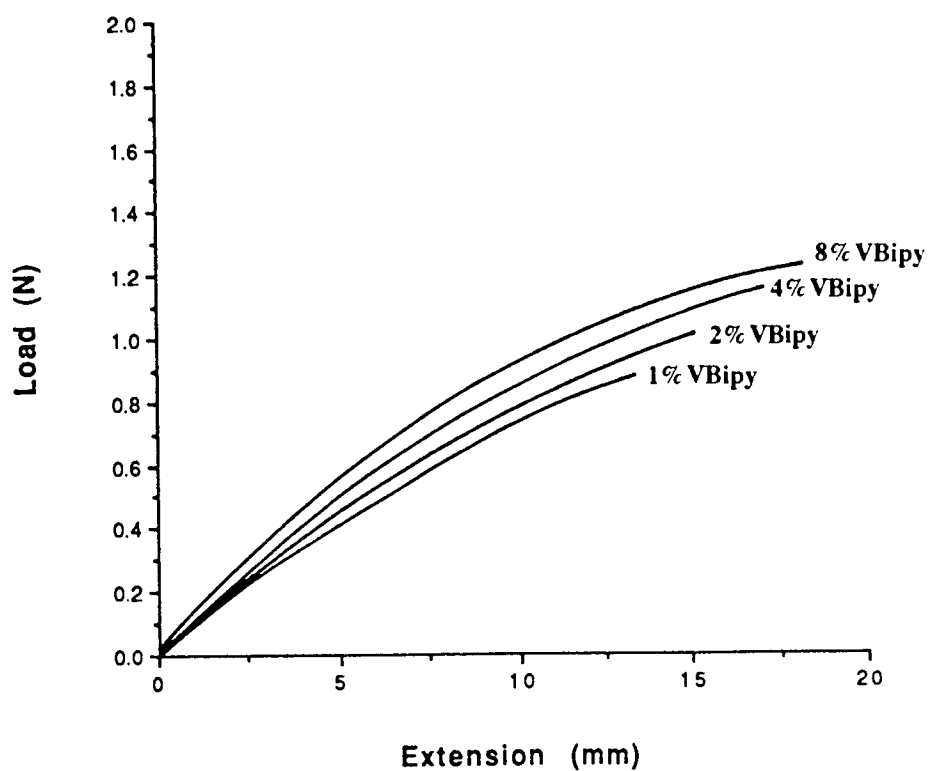
### **3.6.2 Effect of Coordination Cross-Linking on Mechanical Properties.**

Cross-linking the polymers by coordination with metal ions has a dramatic effect on the mechanical properties of the membranes. Figures 3.39(a) are the load-extension curves for VBipy membranes cross-linked with Fe(II) ions. Figure 3.40(a) shows that increasing the

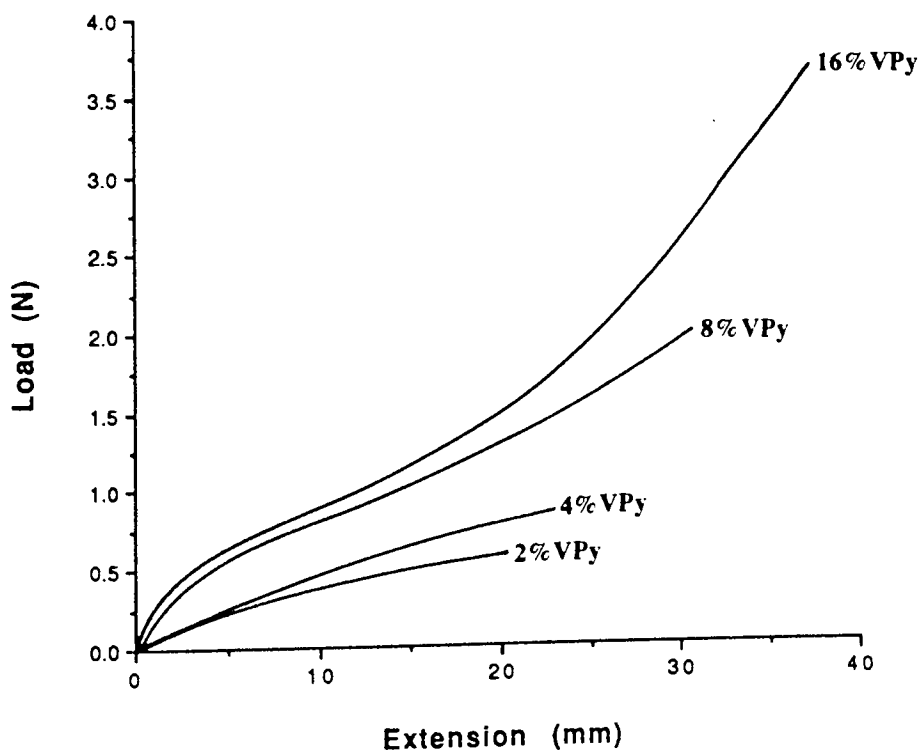
<u>Membrane Polymer Type</u>	<u>Modulus (E<sub>25</sub>, %)</u>	<u>Modulus (E<sub>50</sub>, %)</u>	<u>Tensile Strength (<math>\sigma</math>, MPa)</u>	<u>Elongation to Break (<math>\epsilon_b</math>, %)</u>
PHEMA	-	0.5 $\pm$ 0.06	0.52 $\pm$ 0.02	125 $\pm$ 24
1% VBipy	0.71 $\pm$ 0.02	0.63 $\pm$ 0.01	0.67 $\pm$ 0.11	130 $\pm$ 22
2% VBipy	0.7 $\pm$ 0.02	0.65 $\pm$ 0.04	0.75 $\pm$ 0.12	143 $\pm$ 21
4% VBipy	0.67 $\pm$ 0.12	0.66 $\pm$ 0.06	0.85 $\pm$ 0.11	155 $\pm$ 22
8% VBipy	-	0.68 $\pm$ 0.04	0.93 $\pm$ 0.13	170 $\pm$ 23
1% VBipy:[Fe <sup>2+</sup> ]	0.92 $\pm$ 0.04	0.83 $\pm$ 0.03	0.64 $\pm$ 0.04	85 $\pm$ 4
2% VBipy:[Fe <sup>2+</sup> ]	1.42 $\pm$ 0.1	1.25 $\pm$ 0.06	1.04 $\pm$ 0.2	85 $\pm$ 7
4% VBipy:[Fe <sup>2+</sup> ]	1.63 $\pm$ 0.09	1.69 $\pm$ 0.09	1.52 $\pm$ 0.39	83 $\pm$ 15
8% VBipy:[Fe <sup>2+</sup> ]	-	4.24 $\pm$ 0.23	2.88 $\pm$ 0.57	64 $\pm$ 8
2% VPy	-	0.32 $\pm$ 0.07	0.68 $\pm$ 0.13	110 $\pm$ 17
4% VPy	-	0.63 $\pm$ 0.02	0.68 $\pm$ 0.06	133 $\pm$ 13
8% VPy	0.47 $\pm$ 0.06	0.5 $\pm$ 0.02	0.99 $\pm$ 0.09	241 $\pm$ 18
16% VPy	0.33 $\pm$ 0.13	0.44 $\pm$ 0.04	2.24 $\pm$ 0.33	323 $\pm$ 27
2% VPy:[Cu <sup>2+</sup> ]	-	0.28 $\pm$ 0.02	0.52 $\pm$ 0.04	135 $\pm$ 18
4% VPy:[Cu <sup>2+</sup> ]	-	0.6 $\pm$ 0.02	0.69 $\pm$ 0.06	142 $\pm$ 9
8% VPy:[Cu <sup>2+</sup> ]	3.98 $\pm$ 0.24	2.7 $\pm$ 0.12	3.62 $\pm$ 0.54	264 $\pm$ 36
16% VPy:[Cu <sup>2+</sup> ]	4.25 $\pm$ 0.2	4.08 $\pm$ 0.11	4.58 $\pm$ 0.25	110 $\pm$ 22

**Table 3.3 Mechanical Property Data for Ligand-Modified Membranes:  
Complexed & Uncomplexed.**

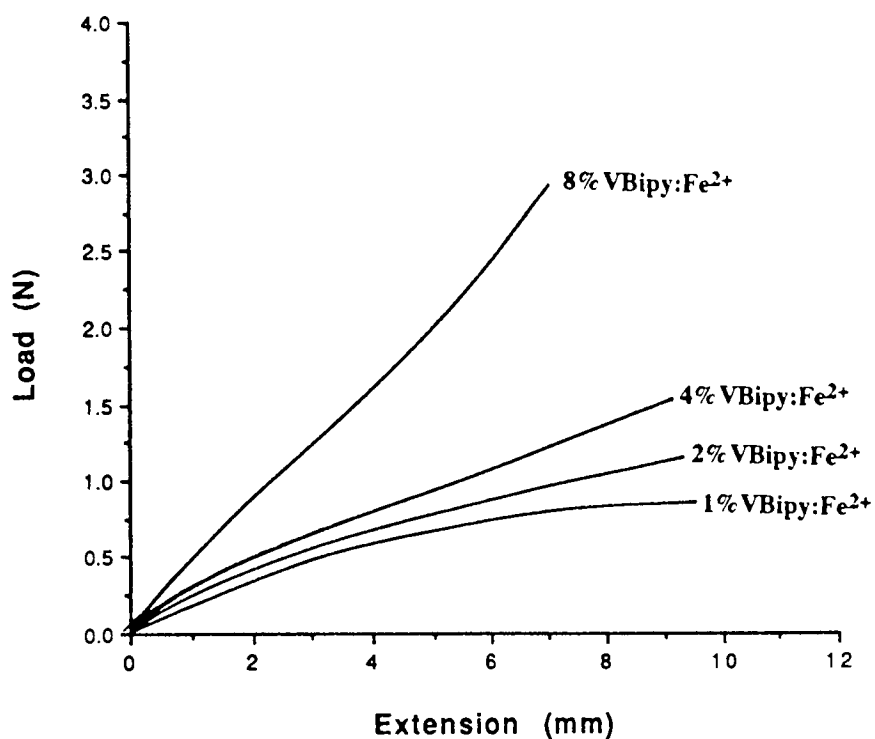
**Figure 3.38(a) Load-Extension Curves for VBipy-Based Membranes.**



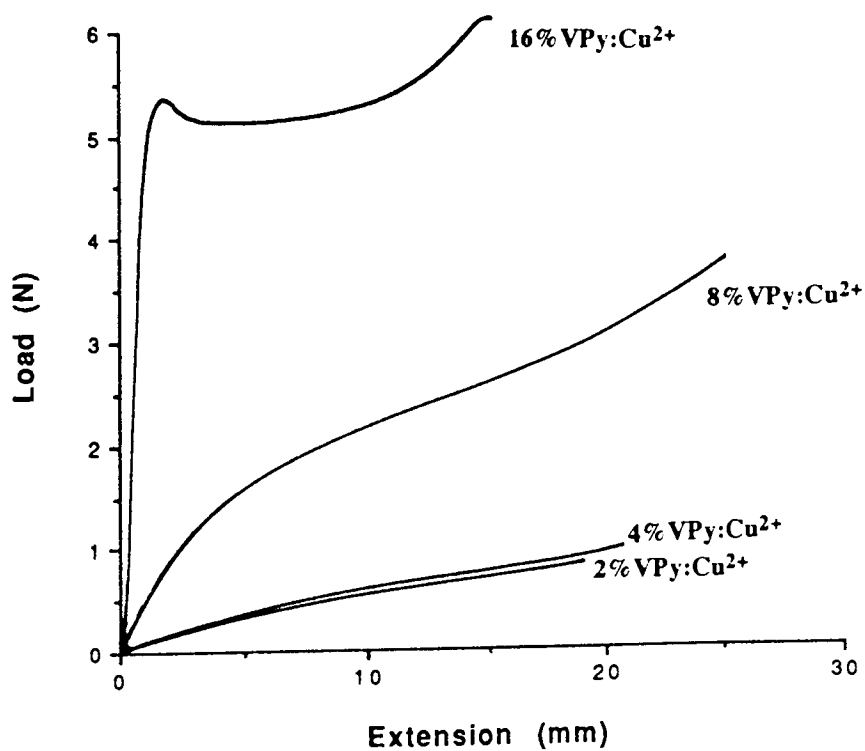
**Figure 3.38(b) Load-Extension Curves for VPy-Based Membranes.**



**Figure 3.39(a) Load-Extension Curves for VBipy:[Fe(II)]-Based Membranes.**



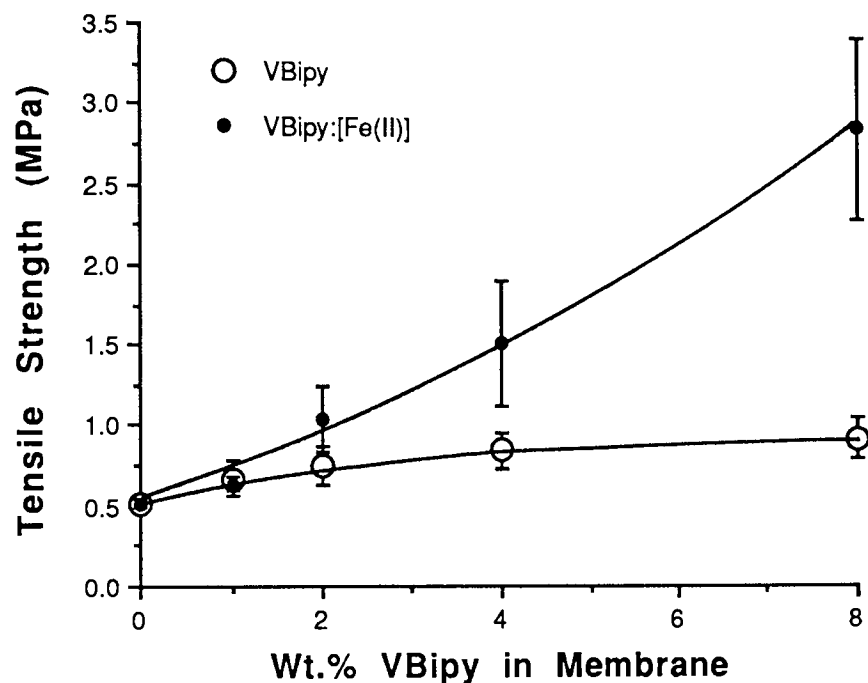
**Figure 3.39(b) Load-Extension Curves for VPy:[Cu(II)]-Based Membranes.**



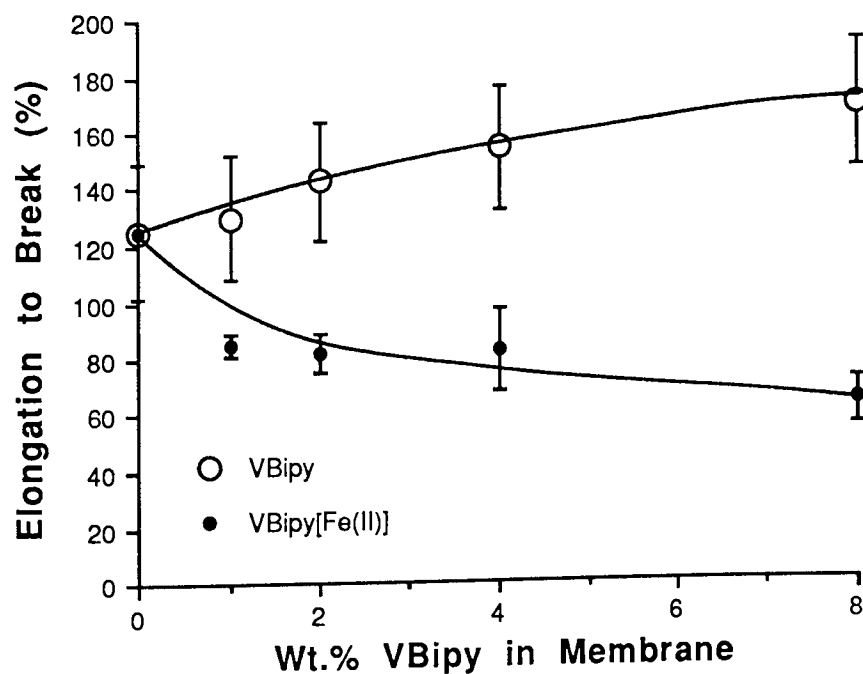
VBipy content, and hence the degree of cross-linking after complexation, vastly improves  $\sigma$ . The effect on  $\epsilon_b$  is severe, the material becoming extremely brittle as represented in Figure 3.40(b). The mechanical properties observed here are characteristic of highly crystalline, or more appropriately in this case, very highly cross-linked networks. As will be seen in Chapter Four, the polymer chains in these systems are extremely mobile and coordination of Fe(II) to over 80% of available ligand groups is not unusual.

Figure 3.39(b) shows the load-extension curves for VPy membranes coordinated to Cu(II) ions. As with VBipy, increasing the amount of VPy leads to an increase in  $\sigma$  after coordination to Cu(II) because of the increased cross-link density (Figure 3.41(a)). The effect on the  $\epsilon_b$  is not so straight-forward; moving from 2-8% VPy, the  $\epsilon_b$  increases from 135-264%, but drops again to 110% at 16% VPy (Figure 3.41(b)). The material behaves as an elastomer up to 8% VPy, but at 16% VPy the structure becomes too highly cross-linked, the load-extension curve being representative of a semi-crystalline material, possessing a yield point and showing evidence of strain-induced crystallisation just before  $\epsilon_b$ . The formation of the Cu(II) *tetra*(pyridyl) complex might essentially anchor the polymer chains at four points, as opposed to the three-centre cross-link of the VBipy system, if one ligand from four independent chains were to participate in the complex. Such high degrees of complexation in the VPy polymer should produce mechanical properties analogous to, if not more extreme than, the highly cross-linked VBipy materials. This is not the case, and although visible spectroscopy implies that a proportion of the ligands are involved in four-coordinate complexes, the mechanical studies suggest that the majority of these complexes probably consist of two or more ligands immobilised to the same chain. Hence, the cross-links are more likely to be two-centred in nature.

**Figure 3.40(a) Effect of Cross-Linking on  $\sigma$  for VBipy:[Fe(II)] Polymers.**



**Figure 3.40(b) Effect of Cross-Linking on  $\epsilon_b$  for VBipy:[Fe(II)] Polymers.**



**Figure 3.41(a) Effect of Cross-Linking on  $\sigma$  for VPy:[Cu(II)] Polymers.**

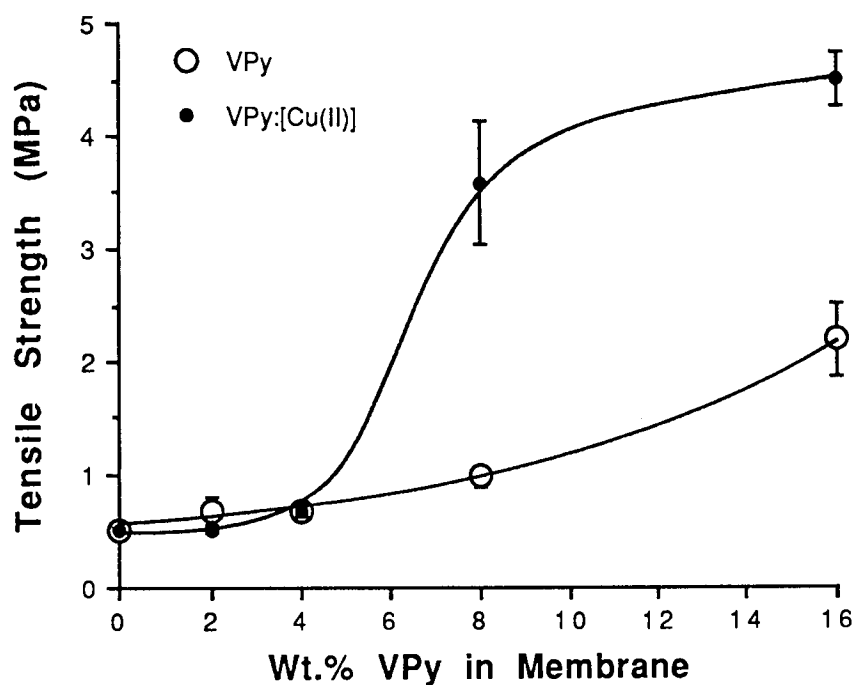
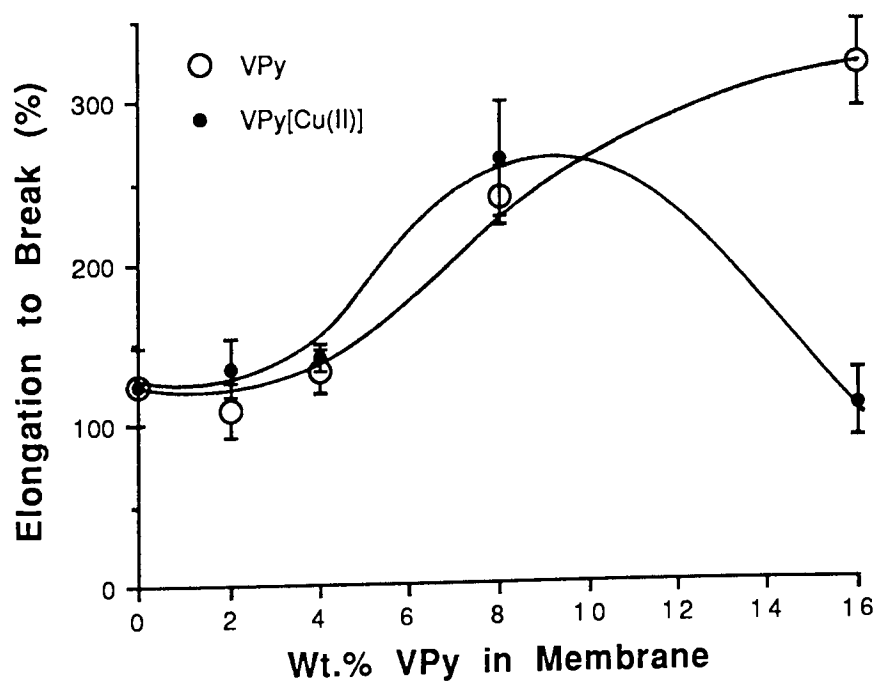


**Figure 3.41(b) Effect of Cross-Linking on  $\epsilon_b$  for VPy:[Cu(II)] Polymers.**



### 3.6.3 Analysis of the Elastomeric Properties of Coordination Cross-Linked Hydrogel Membranes.

Useful structural information concerning the degree of cross-linking can be obtained from elastomeric materials by re-expressing the information in a load-extension graph in terms of the reduced stress, or modulus ( $[f^*]$ ), defined by <sup>159</sup>:

$$[f^*] = \frac{\frac{f}{A} \cdot \sqrt[3]{v_2}}{(\alpha - \alpha^{-2})}$$

where  $f$ =force,  $A$ = cross-sectional area (unswollen),  $v_2$ = volume fraction of polymer  
 $\alpha$ = extension

The volume fraction of polymer in the swollen mass can be calculated by equations 3.2 & 3.3, where  $d_s$  is the density of the solvent and  $d_r$  the density of the polymer <sup>160</sup>:

$$v_2 = \frac{1}{1+Q} \quad (3.2)$$

$$Q = \frac{\text{wt solvent in gel}}{\text{wt of gel}} \cdot \frac{d_r}{d_s} \quad (3.3)$$

Typical stress-strain plots of  $[f^*]$  against  $\alpha^{-1}$  for elastomers, produce a straight line that tends to upturn sharply at high extensions (where the equation 3.1 is no longer valid). Least-squares analysis of the straight line portion allows the calculation of two constants,  $2C_1$  &  $2C_2$ , by the Mooney-Rivlin relationship <sup>159</sup>:

$$[f^*] = 2C_1 + 2C_2 \alpha^{-1} \quad (3.4)$$

The values of  $2C_1$  thus obtained can be used to calculate the structure factor ( $A_\phi$ ), defined

by equation 3.5:

$$A_{\phi} = \frac{2C_1M_c}{\rho RT(v_2)^{2/3}} \quad (3.5)$$

where  $M_c$  = molecular weight between cross-links,  $\rho$  = density of the network

The significance of the structure factor is that for tetra-functional cross-linked networks (such as the VPy case?),  $A_4$  has a theoretical value of 0.5, and for tri-functional networks (the VBipy system),  $A_3 = 0.33$ . If values of  $A_3$  &  $A_4$  could be obtained for the hydrogel systems, it would be possible to assess the degree of cross-linking by how closely these values adhered to the theoretical ones.

Appendix Three contains the data used to calculate  $[f^*]$  &  $\alpha^{-1}$  in an effort to reproduce the stress-strain plots previously mentioned. Figures 3.42(a) & (b) and 3.43(a) & (b) show the stress-strain plots for uncomplexed and complexed membranes of VBipy & VPy respectively. Disappointingly, only the curves shown for 1%VBipy & 16%VPy vaguely resemble those shown in the literature for other elastomers<sup>155,158-162</sup>. There are obvious trends such as slope of the curves, extension limits ( $\epsilon_b$ ) and the shear magnitude differences in the value of  $[f^*]$ . However, this does not provide any additional information to that already discussed in the previous section, and if the value of the structure factor is unobtainable, there seems little point in attempting to analyse this data any further.

It might prove fruitful to undertake a more comprehensive study into the effects of coordination cross-linking, using a wider spread of ligand loadings and different metal ions for cross-linking, to obtain a deeper appreciation of how the complexation process alters the physical form of the hydrogel. The use of competing ligand exchange reactions, or acid

**Figure 3.42(a) Stress-Strain Plots for VBipy Polymer.**

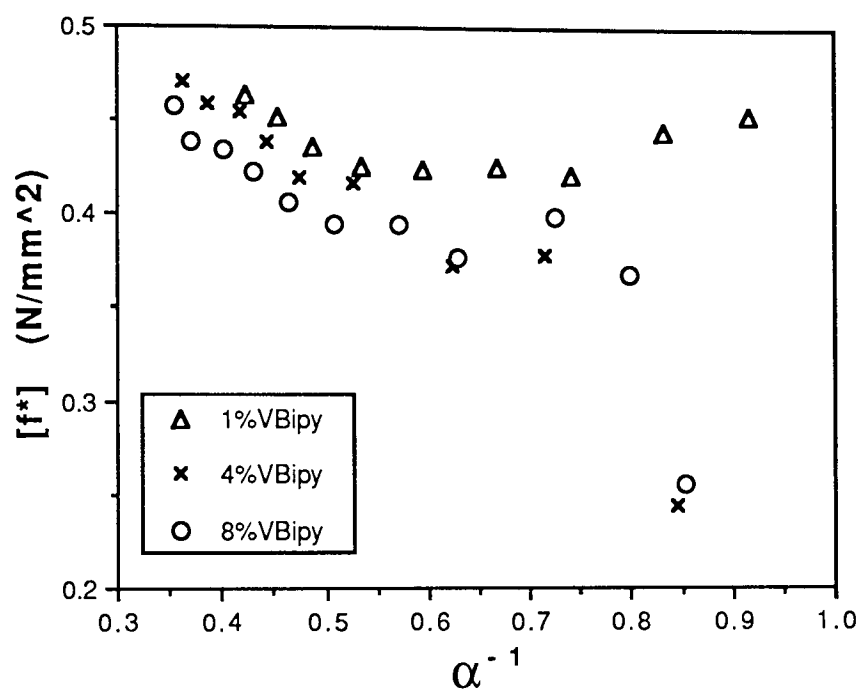


**Figure 3.42(b) Stress-Strain Plots for VBipy:[Fe(II)] Polymer.**

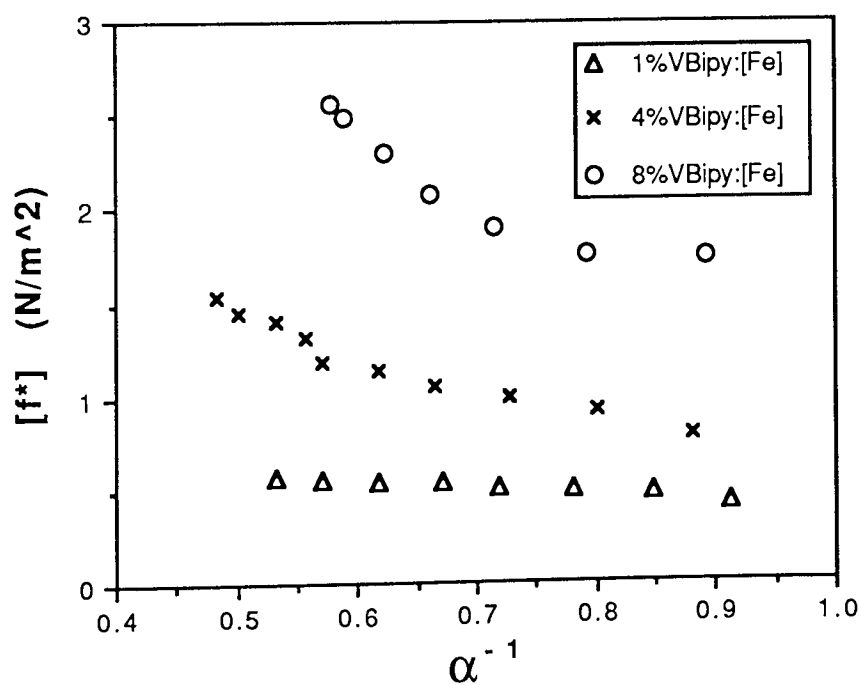


**Figure 3.43(a) Stress-Strain Plots for VPy Polymer.**

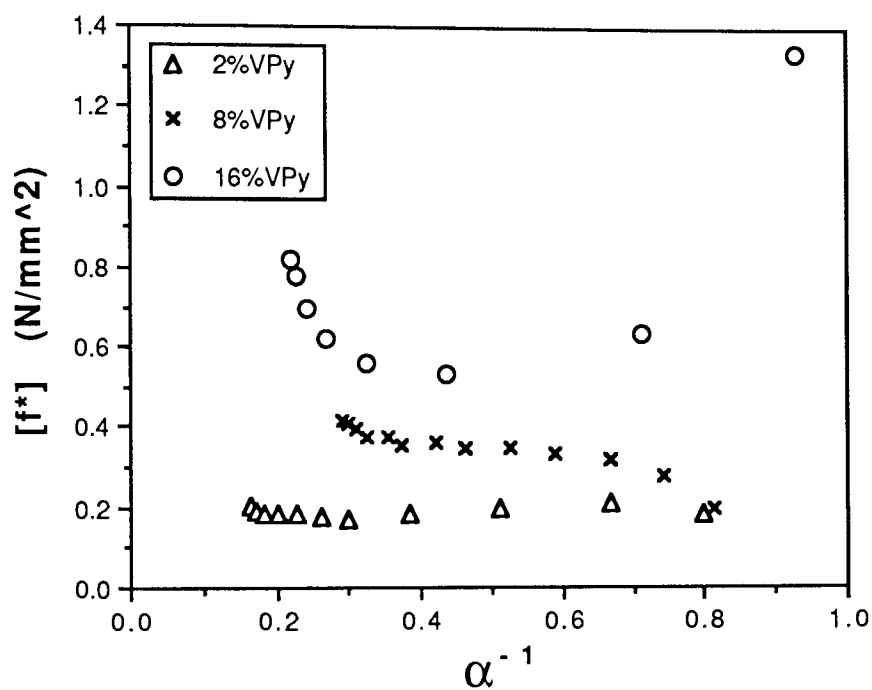
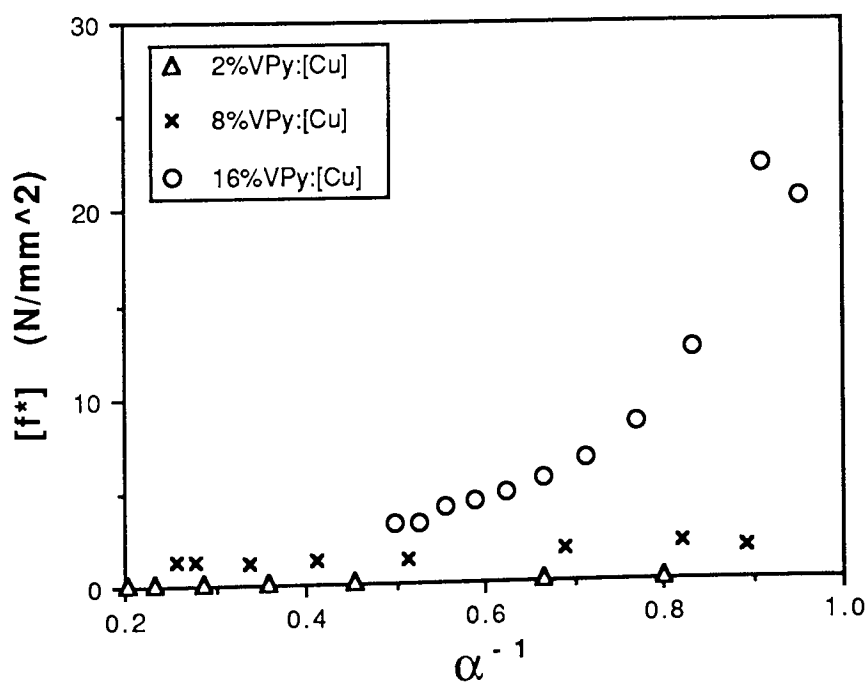


**Figure 3.43(b) Stress-Strain Plots for VPy:[Cu(II)] Polymer.**



leaching techniques, should make the cross-linking process highly reversible- a potentially useful property only barely mentioned in the literature 163-165.

### **3.7 CONCLUDING REMARKS.**

To summarise, those aspects of this research project concerned with the characterisation of a range of metal-ion complexes with bipyridyl- & pyridyl-based coordinating membranes, and indeed the properties of the polymers themselves, have been collected together in this chapter. Many of the standard characterisation techniques available to the coordination chemist could not be applied to these systems; however, by approaching the problem from a different angle, a great deal of interesting information was obtained using more unconventional techniques. This knowledge provides the foundations on which the remainder of the thesis is based.

## **CHAPTER FOUR**

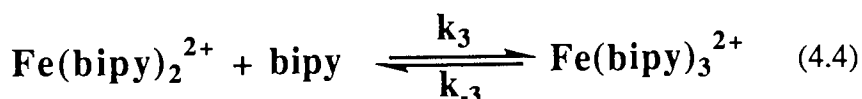
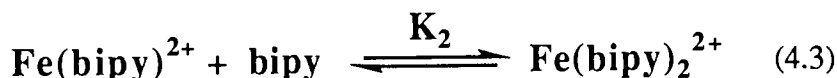
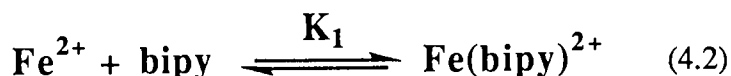
### **THE KINETICS OF IRON (II) COORDINATION IN BIPYRIDYL-BASED MEMBRANES.**

## 4.1 INTRODUCTION.

The ferrous-bipyridine system was first observed and isolated as early as 1888 by Blau 166, and has since been comprehensively studied by a variety of analytical and spectroscopic techniques. In solution, formation of the  $\text{Fe(II)}$  *tris*(bipyridyl) complex (Chapter 3, section 3.4.4) is rapid above pH 5, which makes measurement of the kinetic aspects of the system difficult. However, in solution of pH 3 or less the rate is retarded by protonation of the bipyridyl nitrogens, and data for the rate of complex formation can be obtained and shown to fit fourth order kinetics <sup>49</sup>:

$$\frac{d[\text{Fe(bipy)}_3^{2+}]}{dt} = k[\text{Fe}^{2+}][\text{bipy}]^3 \quad (4.1)$$

This suggests a step-wise formation:



Steps 4.2 & 4.3 are rapidly established equilibria and 4.4 is the rate determining step (which would normally be very fast in solution). The stability constants for the complex formation of the *mono*, *bis* and *tris* species (steps 4.2 - 4.4) are shown below <sup>52</sup>:

$\log K_1$	$\log K_2$	$\log K_3(k_3)$	$(\log \beta_3)$
4.3	3.7	9.5	17.5

The stability constant for the formation of the *mono*-complex is greater than that for the *bis*-complex; the spin change which accompanies coordination of the third bipyridine means that  $K_3$  is largest of all. The consequence of this is that, in solution, the concentration of  $\text{Fe(II)}(\text{Bipy})_2^{2+}$  is almost always very small compared to the *mono* and *tris*-forms.

It has been mentioned previously (Chapter 3, section 3.4.4.2) that *tris*-complex formation can be observed within bipyridyl-based copolymer membranes. Because in this case metal coordination involves molecular movement of the polymer chains in order to induce the correct ligand stereochemistry, the development of the characteristic red colour of the *tris* complex is slow enough to follow by visible spectroscopy. Also, in order to bind to ligand sites within the membrane, the ferrous ions must be transported into the matrix of the polymer. The balance of electrical neutrality must be maintained and thus an  $\text{Fe}(\text{II})$  ion is transported in association with its counterion; in light of evidence presented in Chapter 5 concerning the anion-dependent nature of ion permeability across hydrogel membranes of this sort, it is hardly surprising that in the studies described below, differences were observed between the kinetics of complex formation for various ferrous salts.

One feature of this study should be emphasised at this stage. In solution studies, research is normally carried out with the total concentration of ligand in excess or great excess of the total amount of metal ions. Here the relationship is reversed; within a membrane under study, the total  $[\text{Fe}(\text{II})]$  is normally far in excess of the total  $[\text{Bipy}]$ . This means that, unless the stability constants are many orders of magnitude less here than in solution, when once a membrane is fully penetrated by the reagent solution, essentially all the bipyridyl groups will be coordinated, initially as  $\text{Fe}(\text{Bipy})_1^{2+}$ . We will show later in this chapter that this is indeed the case.

This chapter attempts to investigate the process of *tris*-complex formation with the constraints of ligand immobilisation within a polymeric environment by analogy with the known ideas of complexation in free solution. Various mathematical treatments are

applied to the kinetic data for complex formation and to the study of equilibrium "infinity absorbances", and are coupled with spectroscopic evidence to produce a viable mechanism that explains the observed phenomena. As with any kinetic study in a heterogeneous system, techniques are particularly error-prone and the resulting data relatively imprecise. However, as will be demonstrated, data are reliable enough to produce a reasonable picture of the sequence of events occurring within the membrane.

#### **4.2 DETERMINATION OF THE MAXIMUM BINDING CAPACITY OF BIPYRIDYL-BASED MEMBRANES.**

Before any kinetic studies on  $\text{Fe}(\text{II})$  coordination could be undertaken, it was necessary to gain an appreciation of the maximum expected absorbance value for a particular % weight of ligand, that would result if all immobilised bipy groups were to partake in a *tris* complex. The procedure for the synthesis of the  $\text{Fe}(\text{II})$  *tris*(Vinylbipyridine) complex monomer is outlined in Chapter 2, section 2.4.; this compound was copolymerised in specific ratios with HEMA to produce membranes that possess equivalent % weights of *ligand* to those uncomplexed membranes used for the kinetic studies. Analysis of the water used to hydrate these complex-bound membranes revealed no leaching of *tris* complex from the membrane; hence all must be immobilised within the hydrogel. Measurement of the absorbance maximum at 534nm of membranes containing various % weight of complex, allows the construction of the graph depicted in Figure 4.1. This provides a value for the maximum absorbance possible (i.e. 100% utilisation of all bipy units upon metal coordination) for bipy-based membranes with ligand loadings of 0 to 0.5 wt.%. Concentrations of ligand higher than 0.5 wt.% would result in absorbances greater than ~2.5 which is outside the practical limitations of the visible spectrophotometric technique.

#### 4.2.1 Determination of the Molar Absorption Coefficient for Polymer-Bound tris (Vinyl Bipyridine) Iron(II).

The linear nature of Figure 4.1 shows that, as with the case of free *tris* complex in solution, the immobilised complex conforms closely to Beer's Law. It is possible to use this graph to determine the molar absorption coefficient, or extinction coefficient ( $\epsilon$ ), for the polymer-bound complex. Recalling equation 2.3 from Chapter 2, section 2.7:

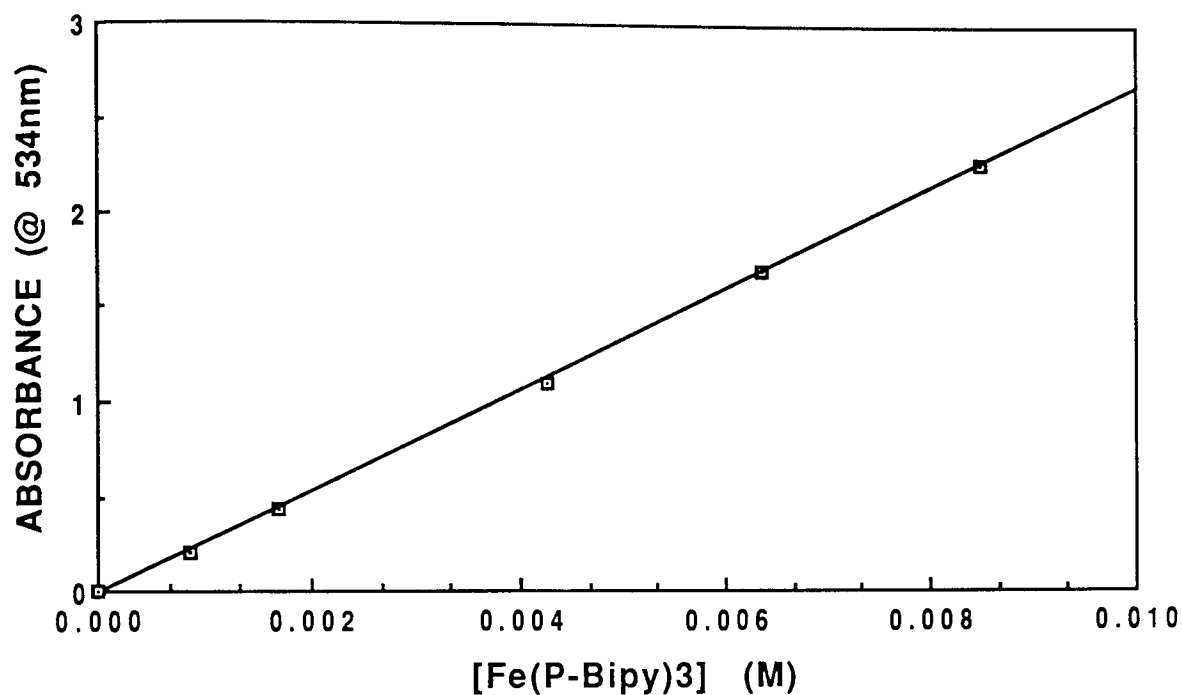
$$\epsilon = \frac{A}{c l} \quad (2.3)$$

The slope of the graph in Figure 4.1 gives the value of  $dA/dc$ , therefore:

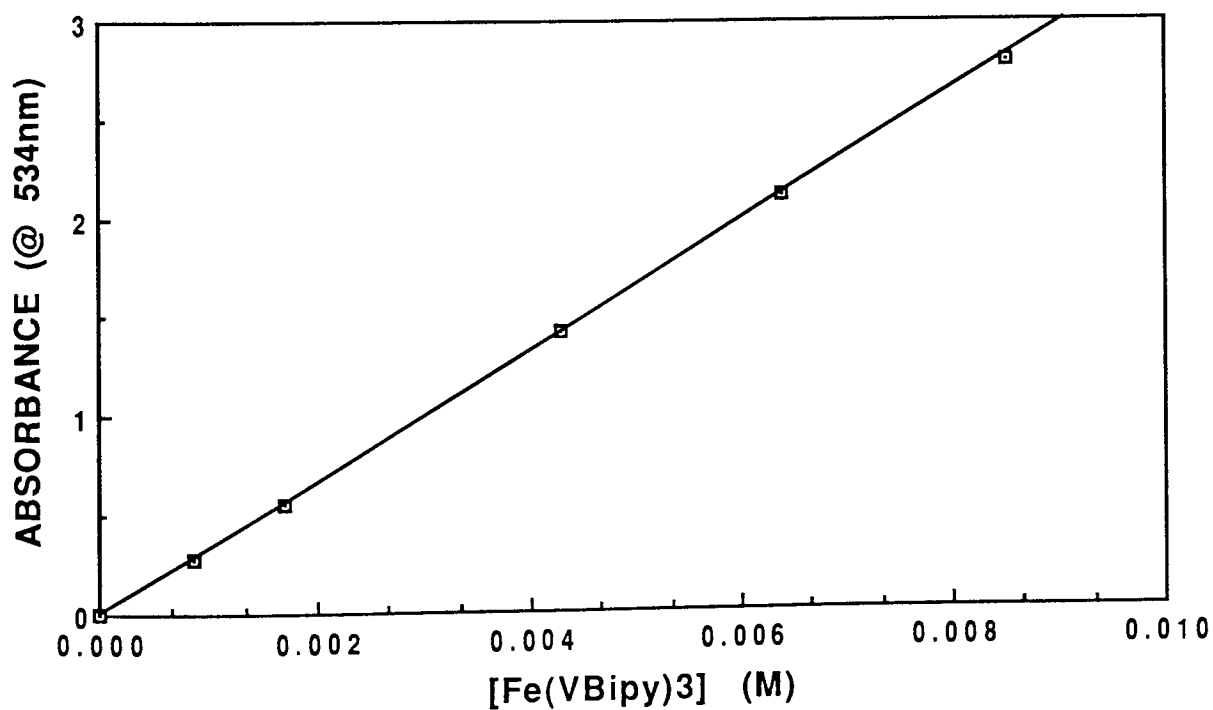
$$\epsilon = \frac{dA}{dc} (\text{slope}) \frac{1}{0.04 \text{ (l)}} \quad (4.6)$$

This produces a value of  $\epsilon = 6700 \text{ M}^{-1}\text{cm}^{-1}$  for the polymer-bound complex (where the unit  $\text{M}^{-1}$  refers to 'Per mole of tris-complex'). Figure 4.2 is a similar plot of absorbance versus  $[\text{Fe}(\text{VBipy})_3^{2+}]$  for the free vinyl complex monomer. By an analogous application of equation 4.6, a value for  $\epsilon$  of  $\sim 8240 \text{ M}^{-1} \text{ cm}^{-1}$  can be calculated. Comparison of the extinction coefficient for both the bound and unbound tris complex with that for complexes of bipyridyl and some of its substituted derivatives (Table 4.1) highlights some interesting points. In this table,  $\lambda_{\text{max}}$  refers to the maximum *visible* absorption; those in the UV are even more intense. It is immediately obvious that substitution in the 3,3' positions of the compound inhibits coplanarity of the pyridyl rings in the *cis* geometry (both nitrogens on the same side of the molecule), thus disrupting the chelating ability of the ligand. Since the intense absorption at visible  $\lambda_{\text{max}}$  for these compounds is due to metal-to-ligand charge transfer, any factor that reduces the efficiency of this process will exhibit a diminished

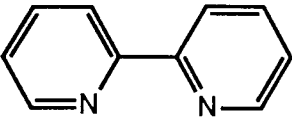
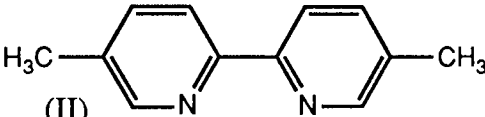
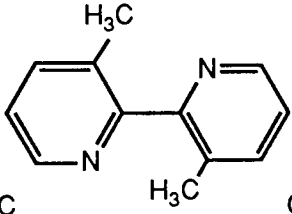
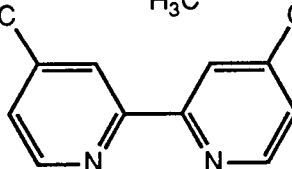
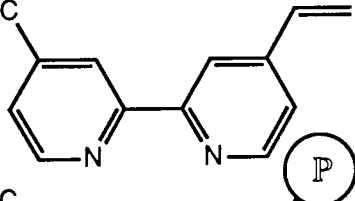
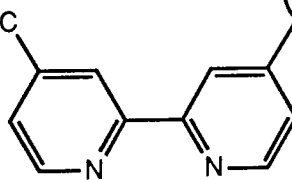
**Figure 4.1** Confirmation of Beer's Law for Polymer-Bound Iron (II) tris(Bipyridine) Complex.



**Figure 4.2** Confirmation of Beer's Law for the Iron (II) tris(Vinylbipyridine) Complex.



observed  $\epsilon$  (as does compound (III), Table 4.1):

COMPOUND	$\lambda_{\max}$ (nm)	$\epsilon$ ( $M^{-1}cm^{-1}$ )
(I) 	522* 522 <sup>+</sup>	8650*
(II) 	510*	8300*
(III) 	526*	1770*
(IV) 	529* 527 <sup>+</sup>	8470*
(V) 	535 <sup>+</sup>	8240 <sup>+</sup>
(VI) 	534 <sup>+</sup>	6700 <sup>+</sup>

**Table 4.1 Spectral Details for some  $Fe(Bipy)_3^{2+}$  Complex Derivatives.**

(+ = Determined here; \* = Ref. 52 & 167)

It is apparent that the presence of the vinyl group at position 4 of compound (V) has no significant effect on  $\epsilon$ , its value is extremely similar to those for bipyridine and the methyl

derivatives. However, the polymer-bound complex (compound (VI)) does seem to exhibit a reduced  $\epsilon$ . This may be explicable on the grounds that there is likely to be a 'molecular strain' induced within the polymeric structure, each complex acting essentially as a three-centred cross-linking point. The effect of immobilisation, although not as dramatic as substitution at the 3,3' position, will be to lengthen the inter-ligand distances and therefore the metal-ligands bonds, or to distort the preferred complex geometry, resulting in weaker orbital interaction and an observed  $\epsilon$  approximately 25% lower than that of the free complexes.

#### **4.3 DETERMINATION OF THE KINETIC FORM FOR THE REACTION OF FERROUS SALTS WITH BIPYRIDYL-BASED MEMBRANES.**

The goal of this particular kinetic study is to establish a possible reaction mechanism for the coordination of ferrous ions to membrane-bound bipyridine, to see how this differs from the reaction in solution and perhaps gain an insight into the nature of the polymeric system. The data may provide information that will distinguish between a single pathway and a sequence of reactions. They may show whether equilibria precede the rate determining step (r.d.s), or if one or more intermediate states are involved in the process. However, before it is possible to undertake such a study, there are a number of practical considerations that must be addressed. These are now discussed.

- (1) The first question one must ask when contemplating kinetics of this nature is, "Is the analytical technique employed sensitive enough to follow the reaction?" Spectrophotometry is a proven method for such purposes, and is suitable as long as the reaction proceeds at a rate that is easily measurable by the instrument. The extremely high extinction coefficient for the product *tris* complex ensures that the technique should be

more than adequate for use in a kinetic study, i.e. a 0.04cm thick membrane with 0.5% ligand loading will produce a maximum absorbance of about 2.3 if fully complexed

(2) The time scale over which the reaction occurs is of paramount importance when designing a kinetic experiment. Addition of  $\text{Fe}^{2+}$  to free bipy in solution results in the "instantaneous" formation of the tris complex; this however, is not the case for the immobilised ligand. It was observed that it could take a matter of *days* rather than seconds for the red colouration in the membrane to reach a maximum level. In view of this fact, the spectrophotometer was modified as described in Chapter 2, section 2.7.1 to enable the monitoring of the absorbance over extended time periods by computer. The program SPECTROLOT (Appendix One) was used initially in conjunction with an *unattended* technique that involved suspending the membrane in a cuvette containing the ferrous salt solution. This method was superseded however, by a rather less sophisticated and more tedious *attended* technique that was necessary to overcome practical difficulties encountered in the former approach, such as the problem of keeping a flexible membrane vertical and away from the walls of the cuvette (Chapter 2, section 2.7.3).

(3) The concentration ranges involved were determined by trial and error. The concentration of immobilised ligand was restricted to 0.5 wt.% maximum; exceeding this level resulted in membranes with final absorbances too intense for the instrumentation to measure ( $>2.5$ ). In an effort to reduce the number of changing variables, all the kinetic studies were performed on membranes with a 0.5 wt.% loading. On the other hand, there were no such restrictions on the concentration of ferrous salt, and its effects were investigated over a 48-fold concentration range (0.01M to 0.48M).

(4) Variations in temperature and pressure can provide useful information on the energetics of the system, particularly in the determination of activation parameters. In this study however, all experiments were performed at atmospheric pressure and under isothermal conditions, i.e. the reaction vessel was thermostated at 25°C. Some experiments were carried out at elevated temperature but seemed to promote the atmospheric oxidation of Fe(II) to Fe(III) with unacceptable consequences, as described in part (5). Ionic strength ( $\mu$ ) is another variable that is often important in kinetics, but there could be no investigations of this type with this system because introduction of additional salts will affect the equilibrium water content of the hydrogel membrane and consequently alter its permeability characteristics. That is, the added electrolyte will not be 'inert'.

(5) The *attended* method eventually adopted employed sample bottles with sealable tops to exclude atmospheric oxygen. However, it is extremely difficult to exclude air from an experiment and despite this precaution, there always appeared to be some formation of ferric ion, due to dissolved oxygen in solution and air entering the container each time the cap was removed. In extreme cases (particularly at elevated temperatures and especially with ferrous sulphate) oxidation resulted in a 'rust-like' precipitate; probably hydrated Fe(OH)<sub>3</sub>, which can form within the membrane and interfere with the observed absorbances. Perchlorate and chloride ferrous salts appeared less prone to this problem but the final  $A_{inf}$  values for various ferrous sulphate concentrations could be unreliable because of this interference. Therefore, it was necessary to apply the data to a number of mathematical treatments that allow analysis of the kinetics without relying on the observed value of  $Abs_{\infty}$ .

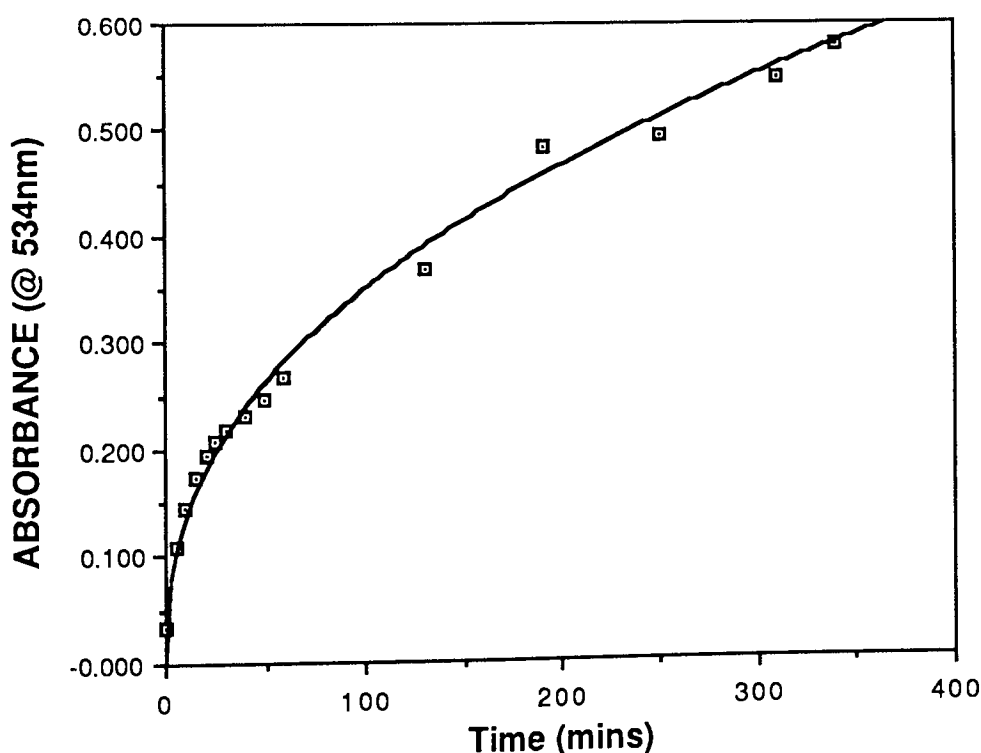
By overcoming these practical limitations and adhering to the described experimental

protocol, sufficient kinetic data can be collected to obtain an overall order of reaction, an estimate of the rate constants involved, and other information useful in the formulation of a mechanism to describe the complexation process.

#### 4.3.1 The Influence of Ferrous Salt Concentration & Type on the Kinetic Profiles of the Fe<sup>(II)</sup>/Bipyridyl System.

Initial studies on the coordination kinetics involved the *unattended* method. A membrane strip was positioned in a cuvette containing 4ml of 0.01M FeSO<sub>4</sub> solution, placed inside the visible spectrometer, and the absorbance monitored with time by micro-computer. The ratio of *tris*(bipy):Fe<sup>(II)</sup> in this case is in the order of 1:50 overall.

Figure 4.3 Low Concentration Binding Profile for 0.01M FeSO<sub>4</sub>.



This was first thought to be a sufficient excess to enable rapid saturation of available binding sites, but in view of the evidence from Chapter 5 which highlights the slow

transport of sulphate ions across these hydrogel-type membranes, it is not surprising that the observed kinetics are slow. In addition, a distinct dual mechanism is suggested from the shape of the binding curve (Figure 4.3, previous page). The initial 30 - 50 minutes approximate to first order kinetics and is thought to be a diffusion-controlled process relating to the transport and primary binding to sites of 'easy access' within the membrane matrix. This is followed by a second stage over many hours, where an approximately zeroth order contribution can be detected in addition to the tail-end of the first order reaction. This slowly levels out until  $A_{\infty}$  is attained. We felt that this phenomenon is probably due to a chain rearrangement process necessary to position the polymer chains in the correct stereochemistry for tris-complex formation.

The later method uses increased volumes of solution and enables much higher concentrations of ferrous salt to be used (0.01 to 0.48M), corresponding to greater *tris*(bipy):Fe(II) ratio's (1:250 to 1:11,300). At these higher concentrations the two stages are no longer obvious and the kinetics of the reaction up to 90% completion appear to be described by a single term. However, the first ten minutes of any run were considered to be a diffusion-controlled "settling-in" period, and were consequently discounted from the calculations. Figures 4.4 to 4.6 show typical reaction profiles for the development of the red colour for experiments over a concentration range for ferrous sulphate, chloride and perchlorate respectively. It is apparent that both the concentration of Fe(II) and the type of anion used influence the binding kinetics and the extent of coordination within the membrane.

In view of the experimental inaccuracies of the technique, it was thought that the use of

**Figure 4.4** Kinetics for the Coordination of Ferrous Sulphate to Bipyriddy-Based Membranes.

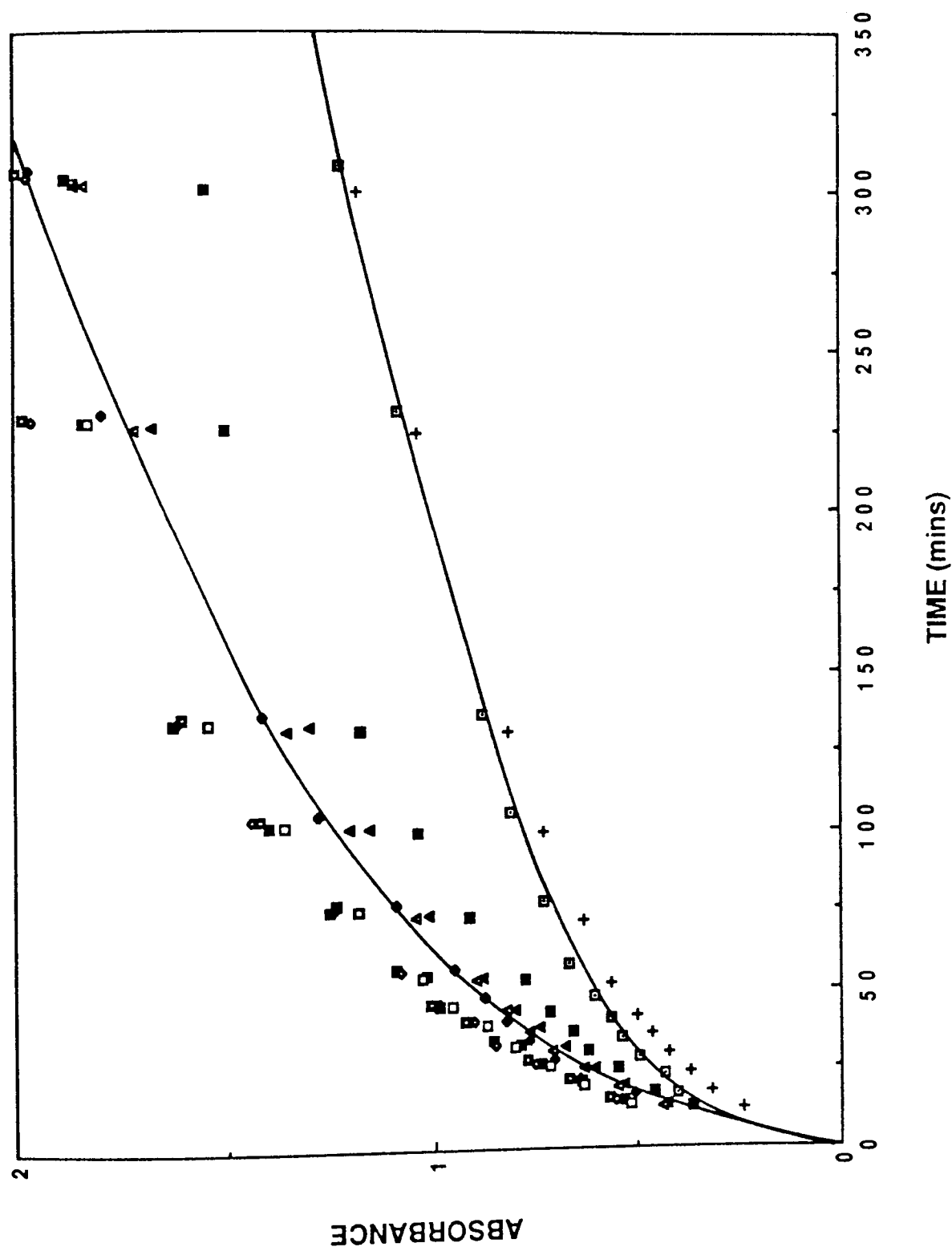


**Figure 4.5** Kinetics of the Coordination of Ferrous Chloride  
to Bipyridyl-Based Membranes.

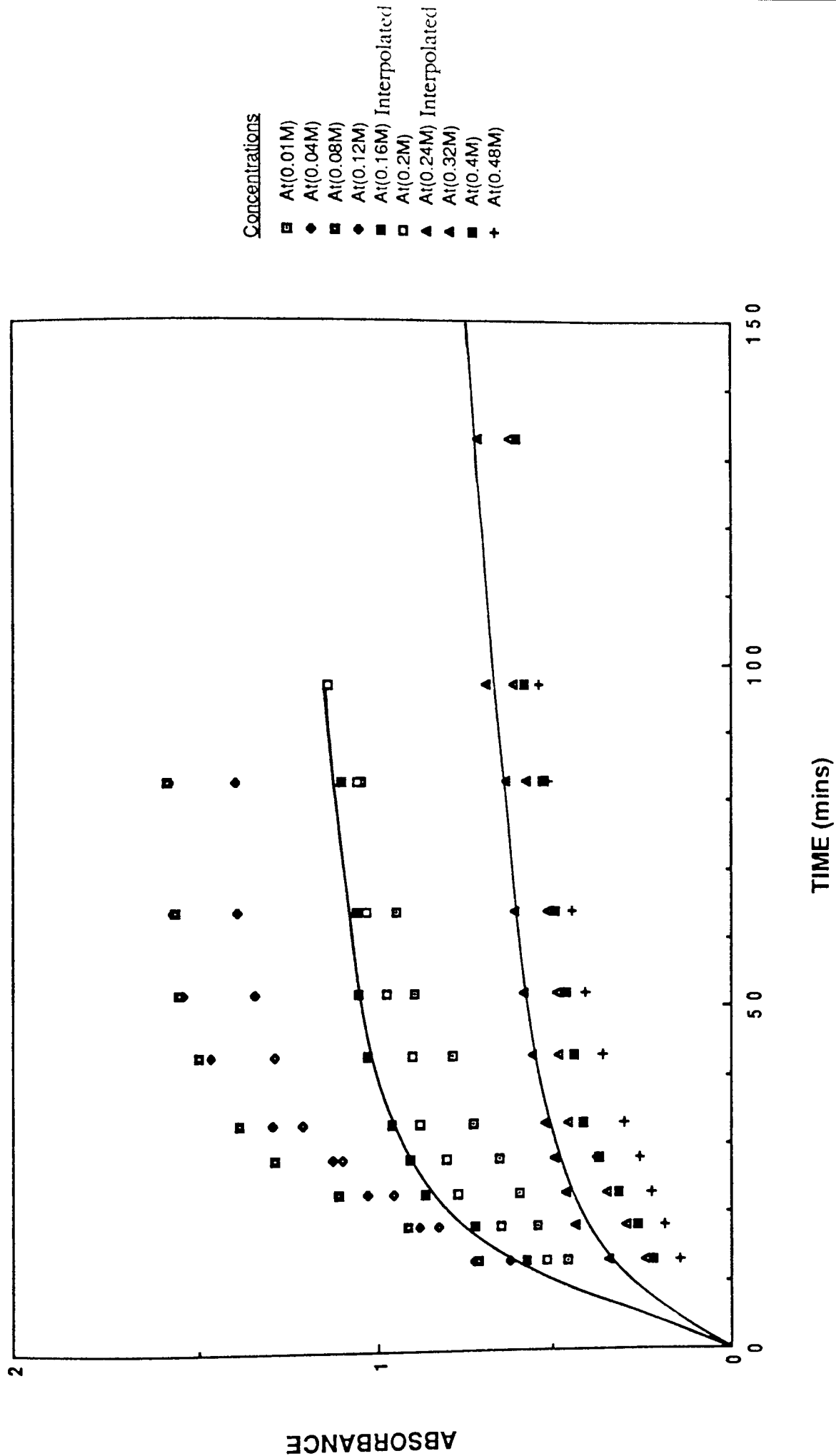
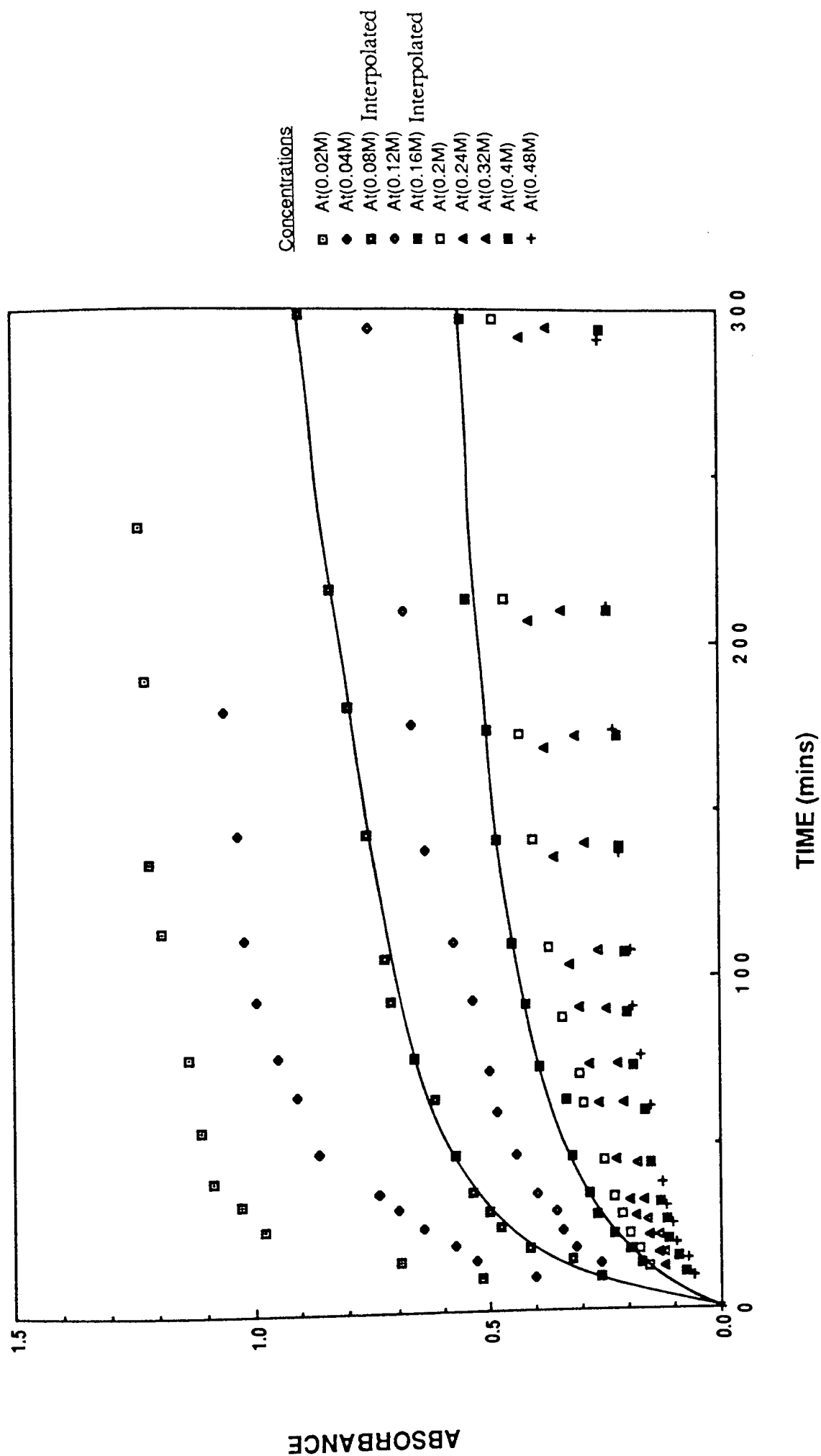


**Figure 4.6** Kinetics of the Coordination of Ferrous Perchlorate  
to Bipyridyl-Based Membranes.



several different mathematical treatments to obtain values for the rate constants, infinity absorbances and overall order of reaction for the various salts, would be more convincing when using these data to predict a mechanism. The following section describes with examples the methods used to treat the data depicted in Figures 4.4 to 4.6.

#### **4.3.2 Least-Squares Analysis Computer Treatment.**

The first step in the elucidation of the overall order of reaction for ferrous salt binding kinetics was to determine the order of reaction. This was done by entering all data both through a first and second order least-squares analysis computer program, and judging the quality of the fits thus obtained. Appendix One lists both programs (1st Order Test & 2nd Order Test) which were written and run on an Apple IIe computer. The programs are basically very similar and follow the format of the flow chart in Appendix One. A value of 90% was chosen for the maximum % reaction to be studied to rule out the major inaccuracies due to infinity point readings. The program allows the introduction of a value for the experimental  $A_{\infty}$ , and the computer finds the best fit, i.e. the lowest sum of squared differences (SSD), by altering the  $A_{\infty}$  within a specified band (usually  $\pm 10\%$ ). Once the data is entered into the main arrays of the program, maximum and minimum values for the rate constant are entered (initially trail and error), followed by a number which tells the program how many values of  $k$  to try within the specified range. It is quicker to use an interactive program and essentially to ask the computer to find the lowest SSD within a range of  $k$  &  $A_{\infty}$  values, rather than to tackle the much more difficult task of writing a routine that will seek out the minimum unsupervised. The Method of Least Squares defines the "best fit", any approach which finds that is acceptable.

The data is fitted to 1st or 2nd order by the least-squares analysis, depending on which program is being run. For the 1st Order Test program, the data is applied to the standard first order relation (4.7):

$$\frac{(A_{\infty} - A_t)}{(A_{\infty} - A_0)} = \exp (-kt) \quad (4.7)$$

where a plot of  $\ln(A_{\infty} - A_t)$  vs. time is a straight line with a gradient of  $-k$ . The 2nd Order Test program fits data according to the second order expression (4.8):

$$\frac{1}{(A_{\infty} - A_t)} = \frac{1}{(A_{\infty} - A_0)} + kt \quad (4.8)$$

where a plot of  $1/(A_{\infty} - A_t)$  vs. time is linear with a slope of  $k$ . In essence, the program actually takes each pair of trial values of  $k$  &  $A_{\infty}$  values and computes a *calculated absorbance*  $A_t$  using the appropriate relationship (4.7 or 4.8); it then determines and stores the sum of  $[(A_t)_{\text{calc}} - (A_t)_{\text{obs}}]^2$  and retains the values of  $k$  and  $A_{\infty}$  for which this is smallest. Unlike the majority of programs that perform this type of calculation, it is the SSD of the  $(A_t)_{\text{obs}}$  and not the logarithm which is computed. That is what the Method of Least Squares requires. The user is offered the option of improving the fit by entering new values for  $k$ , or if satisfied, of obtaining a printout. In this way, the SSD can be lowered to the minimum which should represent the best fit for the data. Tables 4.5, 4.6 & 4.7 display the appropriate SSD,  $k$  &  $A_{\infty}$  data for 1st and 2nd order fits to the  $\text{FeSO}_4$ ,  $\text{FeCl}_2$  &  $\text{Fe}(\text{ClO}_4)_2$  kinetics. The computer least-squares approach has provided the first stage in distinguishing the order of reaction for these reactions. The general trend implied from the data is that the  $\text{FeSO}_4$  approximates more closely to first order than second: that  $\text{FeCl}_2$  is definitely second order, except at low  $[\text{Fe}^{2+}]$  where the decision is unclear: and that

$\text{Fe}(\text{ClO}_4)_2$  is predominantly second order except perhaps at the very lowest concentrations. These conclusions can now be utilised in the treatment of the data by classical kinetic methods which do not rely as heavily upon the value  $A_\infty$ .

#### **4.3.3 First Order Methods where $A_\infty$ is Uncertain.**

It has been shown that the observed  $A_\infty$  values can sometimes be unreliable due to interference from oxidation products such as  $\text{Fe}(\text{OH})_3$ , especially in the case of ferrous sulphate solutions. The proper use of commonly applied kinetic expressions requires an accurate value of  $A_\infty$ , because the term  $(A_\infty - A_t)$  is linearly related to the concentration of the absorbing species. Any small error in  $A_\infty$  will result in systematic deviations in kinetic plots due to the repeated misuse of an incorrect datum. In the literature there are descriptions of other methods for tackling the problem of an unknown or uncertain infinity reading. These date from a time when computing facilities were much poorer and where there was no possibility of interaction by the user. The following methods are alternatives to those devised by us at Aston, and were used as such.

##### **4.3.3.1 The Guggenheim Method.**

Consider first order data at a time  $t$ , and then at a time  $\tau$ , two to three half times later. The absorbance at each time is given by equations 4.9 & 4.10:

$$A_t = (A_\infty - A_0) \exp(-kt) + A_\infty \quad (4.9)$$

$$A_{t+\tau} = (A_\infty - A_0) \exp(-k(t+\tau)) \exp(-kt) + A_\infty \quad (4.10)$$

In the Guggenheim Method<sup>168,169</sup> the two equations are subtracted to give:

$$(A_t - A_{t+\tau}) = (A_\infty - A_0) (1 - \exp(-k\tau)) \exp(-kt) \quad (4.11)$$

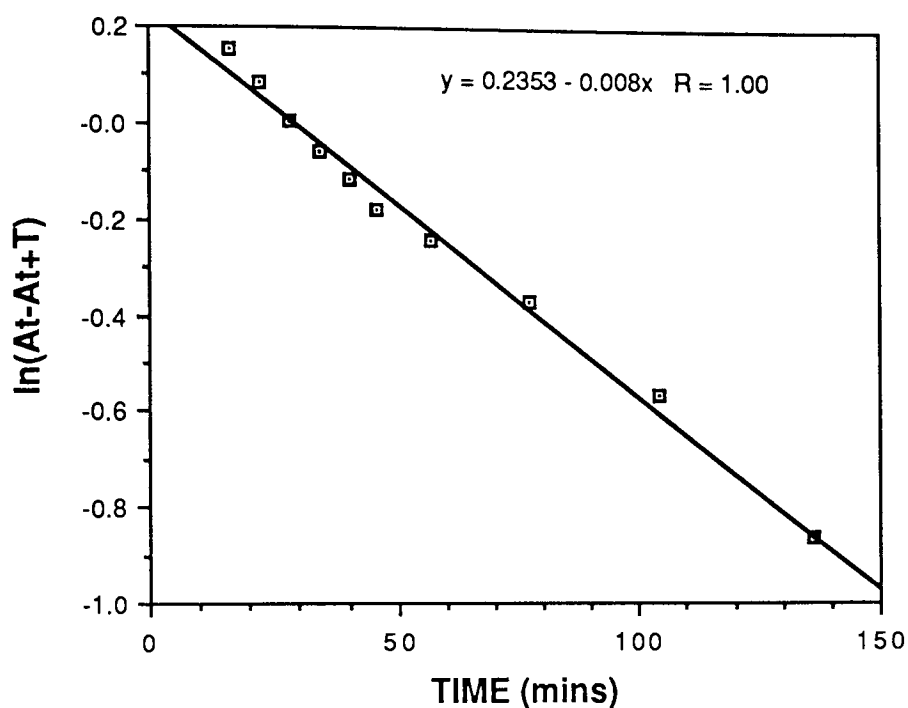


**Figure 4.7 First Order Guggenheim Plot of (0.08M) FeSO<sub>4</sub> Binding Kinetics.**

TIME (mins)	KEZDY/SWINBOURNE METHOD		GUGGENHEIM METHOD
	$A_t$	$A_{t+\tau}$	$\ln(A_t - A_{t+\tau})$
16	0.571	1.74	0.156
22	0.669	1.76	0.087
28	0.774	1.78	0.006
34	0.858	1.78	-0.06
40	0.929	1.8	-0.115
46	1.013	1.85	-0.18
57	1.095	1.88	-0.242
77	1.239	1.93	-0.37
104	1.421	1.99	-0.564
136	1.609	2.03	-0.865
$\tau = 150$ mins	$R=1.00$	$k_g=8 \times 10^{-3}$	$k_{k/s}=8.04 \times 10^{-3}$

**Table 4.2 Kinetic Data for (0.08M) FeSO<sub>4</sub> Binding.**

A plot of  $\ln(A_t - A_{t+\tau})$  vs. time is linear with a slope of  $-k$ . Table 4.2 is an example set of  $\text{FeSO}_4$  binding data, and Figure 4.7 the corresponding Guggenheim plot. As can be seen, the data fit a first order relationship very well.

#### 4.3.3.2 The Kezdy/Swinbourne Method.

The Kezdy/Swinbourne Method <sup>170,171</sup> divides the two spaced times as previously described in the Guggenheim Method:

$$\frac{A_\infty - A_t}{A_\infty - A_{t+\tau}} = \exp(k\tau) \quad (4.12)$$

Solving for  $A_t$  gives equation 4.13:

$$A_t = A_\infty(\exp(k\tau)-1) + A_{t+\tau} \exp(k\tau) \quad (4.13)$$

A plot of  $A_t$  vs.  $A_{t+\tau}$  is a straight line with a slope  $\exp(k\tau)$  i.e:  $k = \ln \text{slope} / \tau$ . The data in Table 4.2 is replotted as a Kezdy/Swinbourne plot in Figure 4.9. Again, the data fit the first order expression very well. A value of  $A_\infty$  can be obtained graphically when  $A_t = A_{t+\tau} = A_\infty$ . Thus, the intersection of the extrapolated slope with a  $45^\circ$  line gives the value of  $A_\infty$ . Table 4.5 displays the combined kinetic data for  $\text{FeSO}_4$  from the treatments described. The reaction is best described as first order, deviating only at very high  $\text{Fe(II)}$  concentrations. This information will be coupled with analysis of the  $A_\infty$  and  $k$  values in a proposal for a mechanism of reaction in section 4.4.

#### 4.3.4 Second Order Methods when $A_\infty$ is Uncertain.

An analogous method to the Guggenheim & Kezdy/Swinbourne procedure <sup>172</sup> was used in the analysis of  $\text{FeCl}_2$  &  $\text{Fe(ClO}_4)_2$  data. [This will be referred to as the K/S method

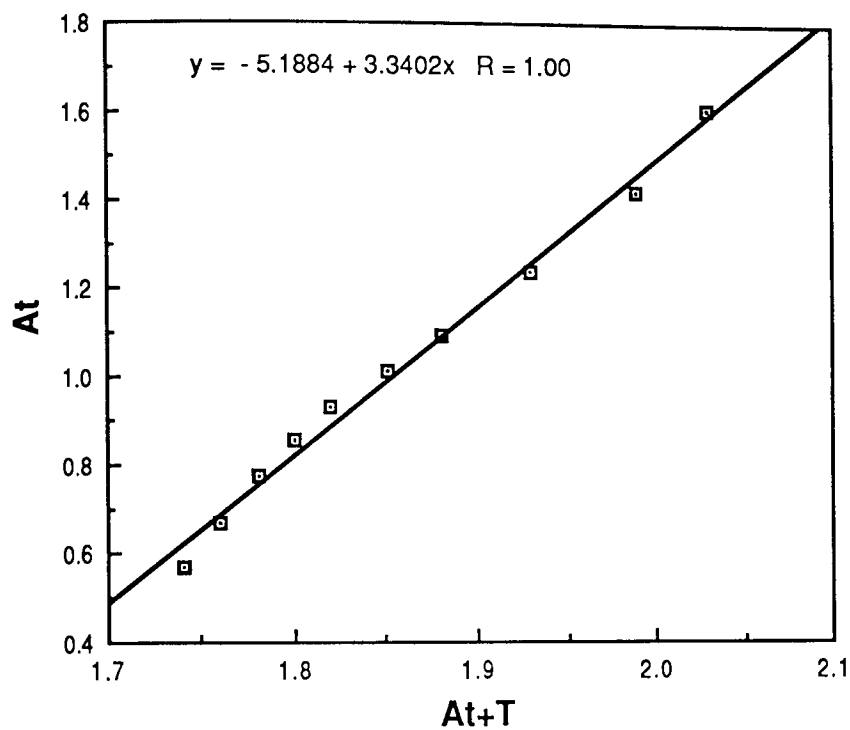


**Figure 4.8 Kezdy/Swinbourn First Order Plot of (0.08M)  $\text{FeSO}_4$  Data.**

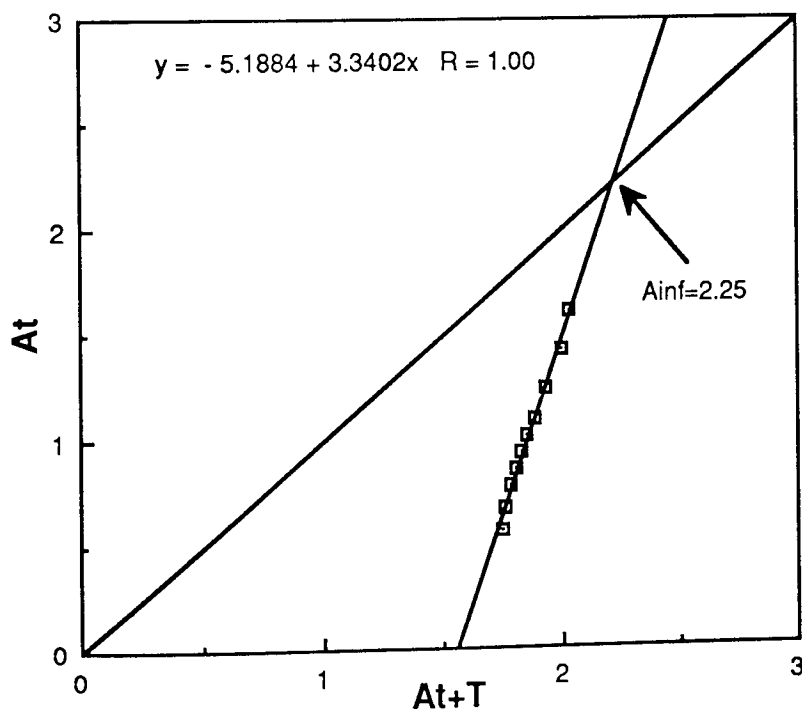


**Figure 4.9 Kezdy/Swinbourn Method for Estimating  $A_\infty$  for (0.08M)  $\text{FeSO}_4$ .**

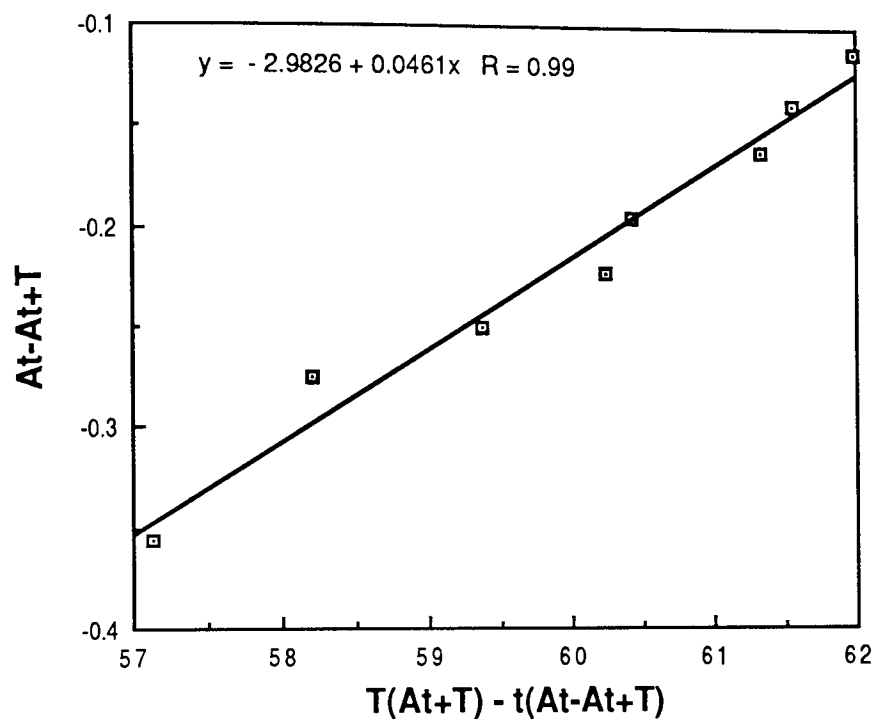


**Figure 4.10 Second Order Kezdy/Swinbourne Plot for (0.24M)  $\text{FeCl}_2$  Binding Kinetics.**

TIME (mins)	ABSORBANCE	KEZDY/ SWINBOURNE METHOD	
	$A_t$	$(A_t - A_{t+\tau})$	$\tau(A_{t+\tau}) - t(A_t - A_{t+\tau})$
13	0.344	-0.356	57.128
18	0.435	-0.275	58.2
23	0.465	-0.25	59.375
28	0.497	-0.223	60.244
33	0.525	-0.195	60.435
43	0.563	-0.162	61.341
52	0.587	-0.138	61.551
64	0.617	-0.113	61.982
<hr/>			
$\tau = 75 \text{ mins}$	$R=0.99$	$\text{Slope}_{k/s} = 0.0461$	$A_{\infty} k/s = 1.694$

**Table 4.3 Kinetic Data for (0.24M)  $\text{FeCl}_2$  Binding.**

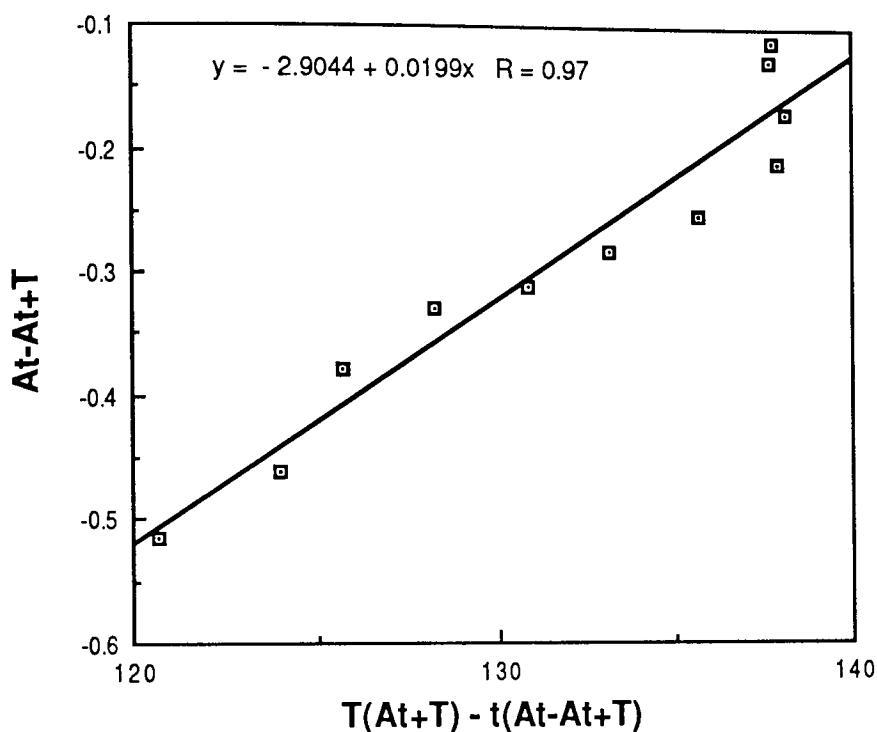


**Figure 4.11 Second Order Kezdy/Swinbourne Plot for (0.08M)  $\text{Fe}(\text{ClO}_4)_2$  Binding Kinetics.**

TIME (mins)	ABSORBANCE	KEZDY/ SWINBOURNE METHOD	
	$A_t$	$(A_t - A_{t+\tau})$	$\tau(A_{t+\tau}) - t(A_t - A_{t+\tau})$
10	0.256	-0.514	120.64
15	0.318	-0.462	123.93
19	0.412	-0.378	125.652
25	0.472	-0.328	128.2
30	0.499	-0.311	130.83
36	0.538	-0.282	133.152
47	0.572	-0.253	135.641
64	0.621	-0.209	137.876
76	0.665	-0.170	138.17
93	0.714	-0.126	137.718
106	0.729	-0.111	137.766
<hr/>			
$\tau = 150 \text{ mins}$	$R=0.96$	$\text{Slope}_{k/s}=0.0199$	$A_\infty k/s=0.946$

**Table 4.4 Kinetic Data for (0.08M)  $\text{Fe}(\text{ClO}_4)_2$  Binding.**

CONC. (M)	$R_g^{1st}$	$R_{k/s}^{1st}$	$SSD^{1st}$	$SSD^{2nd}$	$k_g$ ( $\text{min}^{-1}$ )	$k_{k/s}$ ( $\text{min}^{-1}$ )	$k_c$ ( $\text{min}^{-1}$ )	$A_{\infty}^{obs}$	$A_{\infty}^{k/s}$	$A_{\infty}^c$
0.01	0.97	0.99	9.9e <sup>3</sup>	2.96e <sup>3</sup>	5.2e <sup>-3</sup>	4.94e <sup>-3</sup>	4.13e <sup>-3</sup>	1.763	1.49	1.637
0.04	0.98	1.00	1.02e <sup>6</sup>	3.12e <sup>5</sup>	5.5e <sup>-3</sup>	5.46e <sup>-3</sup>	4.79e <sup>-3</sup>	1.999	2.35	1.846
0.08	1.00	1.00	1.65e <sup>7</sup>	2.2e <sup>6</sup>	8.0e <sup>-3</sup>	8.04e <sup>-3</sup>	4.51e <sup>-3</sup>	1.869	2.25	2.40
0.12	1.00	0.99	1.15e <sup>7</sup>	2.2e <sup>6</sup>	8.9e <sup>-3</sup>	8.98e <sup>-3</sup>	6.70e <sup>-3</sup>	1.808	2.20	2.266
0.16	0.99	0.99	6.06e <sup>4</sup>	3.55e <sup>4</sup>	1.18e <sup>-2</sup>	1.22e <sup>-2</sup>	9.19e <sup>-3</sup>	2.095	1.90	2.217
0.2	1.00	0.99	9.9e <sup>6</sup>	1.9e <sup>6</sup>	9.4e <sup>-3</sup>	9.88e <sup>-3</sup>	7.72e <sup>-3</sup>	1.724	2.05	2.00
0.24	0.98	0.99	5.02e <sup>3</sup>	1.17e <sup>5</sup>	5.7e <sup>-3</sup>	5.12e <sup>-3</sup>	5.62e <sup>-3</sup>	2.15	2.15	2.132
0.32	0.99	0.99	2.89e <sup>3</sup>	5.25e <sup>4</sup>	6.5e <sup>-3</sup>	6.3e <sup>-3</sup>	6.03e <sup>-3</sup>	2.049	2.10	2.235
0.4	0.99	1.00	1.64e <sup>4</sup>	4.45e <sup>3</sup>	7.5e <sup>-3</sup>	7.72e <sup>-3</sup>	8.18e <sup>-3</sup>	1.886	1.75	2.172
0.48	0.94	0.97	1.32e <sup>4</sup>	2.77e <sup>3</sup>	5.1e <sup>-3</sup>	5.12e <sup>-3</sup>	8.96e <sup>-3</sup>	1.90	1.49	1.70

$R_g^{1st}, R_{k/s}^{1st}$  = Regression parameters for best-fit lines on Guggenheim & Kezdy/Swinbourne plots respectively.  
 $SSD^{1st}, SSD^{2nd}$  = Computer sum of squared differences for first and second order fits of the data.  
 $k_g, k_{k/s}, k_c$  = Guggenheim, Kezdy/Swinbourne and Aston computer calculated first order rate constants respectively.  
 $A_{\infty}^{obs}, A_{\infty}^{k/s}, A_{\infty}^c$  = Observed, Kezdy/Swinbourne and computer calculated final 'infinity' absorbances respectively.

**Table 4.5 Collection of Data & Constants from Kinetic Studies on the Ferrous Sulphate/Bipyridyl Membrane System.**

CONC. (M)	$R_{k/s}^{1st}$	$R_{k/s}^{2nd}$	$SSD^{1st}$	$SSD^{2nd}$	$M_{k/s}^{1st}$	$M_{k/s}^{2nd}$	$k_c^{2nd}$ ( $M^{-1}min^{-1}$ )	$A_{\infty}^{obs}$	$A_{\infty}^{k/s}$ (1st)	$A_{\infty}^{k/s}$ (2nd)	$A_{\infty}^c$
0.01	0.98	0.64	$5.21e^4$	$9.67e^3$	0.0320	0.0415	253.9	1.627	1.125	1.334	1.231
0.04	0.95	0.82	$1.99e^5$	$2.56e^5$	0.0540	0.0664	297.9	1.751	1.65	1.648	1.846
0.08	0.97	0.88	$1.39e^5$	$1.51e^5$	0.0503	0.1070	480.7	1.906	1.70	1.694	1.783
0.12	1.00	0.55	$8.8e^5$	$7.8e^4$	0.0395	0.0911	487.4	1.666	1.43	1.469	1.581
0.16	0.98	0.92	$2.77e^4$	$2.49e^4$	0.0304	0.0791	751.5	1.371	1.22	1.312	1.225
0.2	0.98	0.77	$4.51e^4$	$9.15e^3$	0.0291	0.0658	517.9	1.387	1.20	1.301	1.322
0.24	-	0.99	$9.25e^3$	$4.43e^3$	-	0.0461	209.9	1.167	-	0.863	0.932
0.32	-	0.96	$7.89e^3$	$4.79e^3$	-	0.0293	176.0	1.094	-	0.837	0.885
0.4	-	0.96	$6.76e^3$	$2.74e^3$	-	0.0400	162.5	0.983	-	0.761	0.868
0.48	-	0.95	$1.63e^4$	$4.07e^3$	-	0.0230	142.2	0.917	-	0.551	0.852

$R_{k/s}^{1st}, R_{k/s}^{2nd}$  = Regression parameters for best-fit lines on Kezdy/Swinbourne first & second order plots respectively.

$SSD^{1st}, SSD^{2nd}$  = Computer sum of squared differences for first and second order fits of the data.

$M_{k/s}^{1st}, M_{k/s}^{2nd}$  = Gradient of first and second order Kezdy/Swinbourne plots respectively.

$k_c$  = Computer calculated second order rate constant.

$A_{\infty}^{obs}, A_{\infty}^{k/s}, A_{\infty}^c$  = Observed, Kezdy/Swinbourne (1st & 2nd order) and computer calculated 'infinity' absorbances respectively.

**Table 4.6 Collection of Data & Constants from Kinetic Studies on the Ferrous Chloride/Bipyridyl Membrane System.**

CONC. (M)	$R_{k/s}^{1st}$	$R_{k/s}^{2nd}$	$SSD^{1st}$	$SSD^{2nd}$	$M_{k/s}^{1st}$	$M_{k/s}^{2nd}$	$k_c^{2nd}$ ( $M^{-1}min^{-1}$ )	$A_{\infty}^{obs}$	$A_{\infty}^{k/s}$ (1st)	$A_{\infty}^{k/s}$ (2nd)	$A_{\infty}^c$
0.02	0.81	0.77	1.58e5	6.57e <sup>3</sup>	0.0189	0.0667	778.6	1.376	1.30	1.356	1.273
0.04	0.98	0.60	1.67e5	6.59e <sup>4</sup>	0.0194	0.0489	267.4	1.225	1.10	1.158	1.198
0.08	-	0.97	5.19e <sup>4</sup>	1.72e <sup>3</sup>	-	0.0199	182.8	1.057	-	0.973	0.996
0.12	-	0.96	2.09e <sup>4</sup>	1.14e <sup>3</sup>	-	0.0092	135.4	0.955	-	0.946	0.820
0.16	-	0.93	9.79e <sup>3</sup>	2.11e <sup>3</sup>	-	0.0120	220.0	0.682	-	0.708	0.635
0.2	-	0.91	2.79e <sup>3</sup>	3.71e <sup>2</sup>	-	0.0068	270.8	0.625	-	0.702	0.522
0.24	-	0.92	6.09e <sup>3</sup>	2.56e <sup>2</sup>	-	0.0120	257.3	0.531	-	0.544	0.486
0.32	-	0.95	1.74e <sup>3</sup>	2.19e <sup>2</sup>	-	0.0102	311.4	0.529	-	0.465	0.433
0.4	-	0.95	3.85e <sup>3</sup>	3.04e <sup>2</sup>	-	0.0139	501.0	0.302	-	0.305	0.288
0.48	-	0.87	3.56e <sup>3</sup>	1.6e <sup>2</sup>	-	0.0145	276.8	0.329	-	0.294	0.328

$R_{k/s}^{1st}, R_{k/s}^{2nd}$  = Regression parameters for best-fit lines on Kezdy/Swinbourne first & second order plots respectively.  
 $SSD^{1st}, SSD^{2nd}$  = Computer sum of squared differences for first and second order fits of the data.  
 $M_{k/s}^{1st}, M_{k/s}^{2nd}$  = Gradient of first and second order Kezdy/Swinbourne plots respectively.  
 $k_c$  = Computer calculated second order rate constant.  
 $A_{\infty}^{obs}, A_{\infty}^{k/s}, A_{\infty}^c$  = Observed, Kezdy/Swinbourne (1st & 2nd order) and computer calculated 'infinity' absorbances respectively.

**Table 4.7 Collection of Data & Constants from Kinetic Studies on the  
Ferrous Perchlorate/Bipyridyl Membrane System.**

for simplicity]. The basic second order equation can be reorganised from it's more familiar presentation to give:

$$A_t = A_0 - k[\text{Reactants}]_0 t(A_\infty - A_t) \quad (4.14)$$

A similar expression is written for A at a time  $\tau$  later, and the equations subtracted to give:

$$(A_t - A_{t+\tau}) = k[R]_0 (\tau A_{t+\tau} - t(A_t - A_{t+\tau})) - k[R]_0 \tau A_\infty \quad (4.15)$$

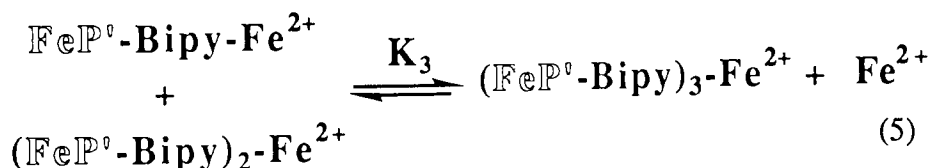
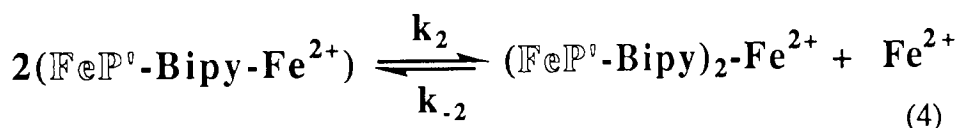
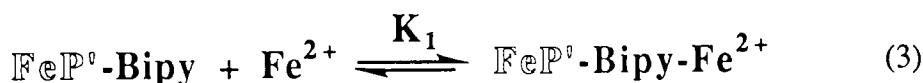
A plot of  $A_t - A_{t+\tau}$  vs.  $\tau A_{t+\tau} - t(A_t - A_{t+\tau})$  should be linear with a slope equal to  $k[R]_0$ . Tables 4.3 & 4.4, and Figures 4.10 & 4.11 illustrate the use of this method for  $\text{FeCl}_2$  &  $\text{Fe}(\text{ClO}_4)_2$  data. As can be seen from the reasonable fit of the data, a second order process is implied; the intercept of the line gives the value of  $A_\infty$ . Tables 4.6 & 4.7 summarise the second order parameters derived from these plots. Both chloride and perchlorate fit the second order expression at high iron concentrations, but deviate at low concentrations. The formulation of a mechanism based on these results is discussed in section 4.4.

#### **4.4 FORMULATION OF A MECHANISM FOR THE COORDINATION OF IRON (II) WITH POLYMER-BOUND BIPYRIDINE.**

The kinetics and  $A_\infty$  data highlighted in bold typeface in Tables 4.5 - 4.7 will now be interpreted in terms of the opening-up of the membrane by the salt, and the coordination of  $\text{Fe}^{2+}$  to the bipyridyl units, with differing steps being rate determining depending on the concentration and the anion. It is important to remember that the hydrogel polymer backbone is very flexible and that the ratio of HEMA:Bipy units is about 300:1; subsequently, the ligand groups can be treated as independent and unconnected.

A reader who is unfamiliar with this work may find the complexity of the system difficult to follow. Therefore, it may be worth-while studying the mechanism finally deduced, before becoming embroiled in the detailed arguments leading to it. Below is a summary of Figure 4.31, the final mechanism proposed in section 4.5 of this chapter:

**Summary of Proposed Mechanism (See Figure 4.31).**

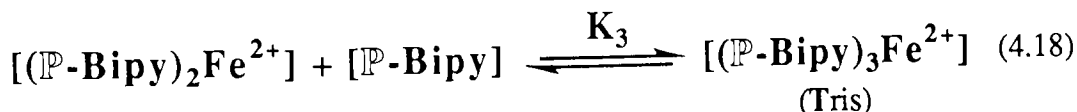
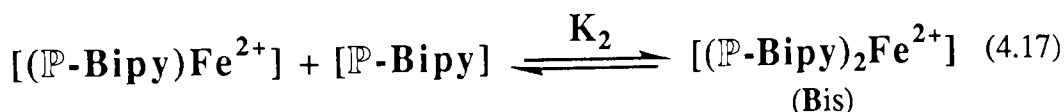
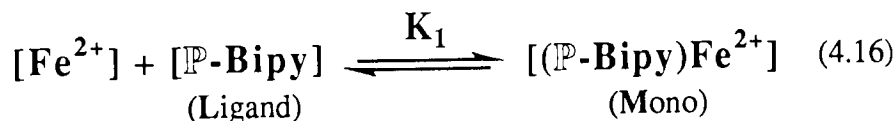


It will be shown that there is an anion-dependent equilibrium of ferrous salt ( $K_0$ ), present at *non-ligand* 'sites' within the membrane (represented by  $\text{FeP}$  - stage (1)), which is followed by a reorganisation within the polymer (2) that is necessary for the coordination of  $\text{Fe}^{2+}$  to bipyridyl ligands. The first order kinetics observed for ferrous sulphate suggest that stage (2) is probably the rate-determining step in this instance. The second order kinetics of  $\text{Cl}^-$  &  $\text{ClO}_4^-$  indicate that stage (4) is rate-limiting for these salts, with the final

equilibrium concentration of *tris*-complex (5) being dependent on  $[\text{Fe}^{2+}]$ . The reader may find it helpful to bear these details in mind when proceeding into the discussion of the following sections.

#### **4.4.1 Derivation of a Mechanism that Fits the Second Order Kinetic Form** **for the Coordination of Ferrous Chloride & Perchlorate.**

To recap, the kinetic profile for ferrous chloride and perchlorate coordination to bipyridyl membranes is best described as second order, except perhaps at very low  $[\text{Fe}^{2+}]$ , which is more likely first order. In this section, a mechanism is proposed which takes account of the observed kinetic trends. Consider the following sequence:



It is reasonable to assume that the chelating hydrogel shows similar  $K_1:K_2:K_3$  ratios to those for free bipyridine in solution (section 4.1). Spectroscopic evidence certainly suggests that the main complex present is the tris-form. However, because for these studies  $[\text{Fe}^{2+}] \gg [\text{Bipy}]$ , it is possible to detect spectrophotometrically<sup>173</sup> the presence of the mono-species at the very highest  $[\text{Fe}^{2+}]$  and early on in a run (Figures 4.12 & 4.13).

Therefore, we can deduce that:

$$[\text{L}] \ll [\text{M}] \gg [\text{B}] \ll [\text{T}] \quad (4.19)$$

Figure 4.12: Visible Spectra for the *Mono* & *Tris* Bipyridyl Complexes with  $\text{Fe}^{2+}$ .

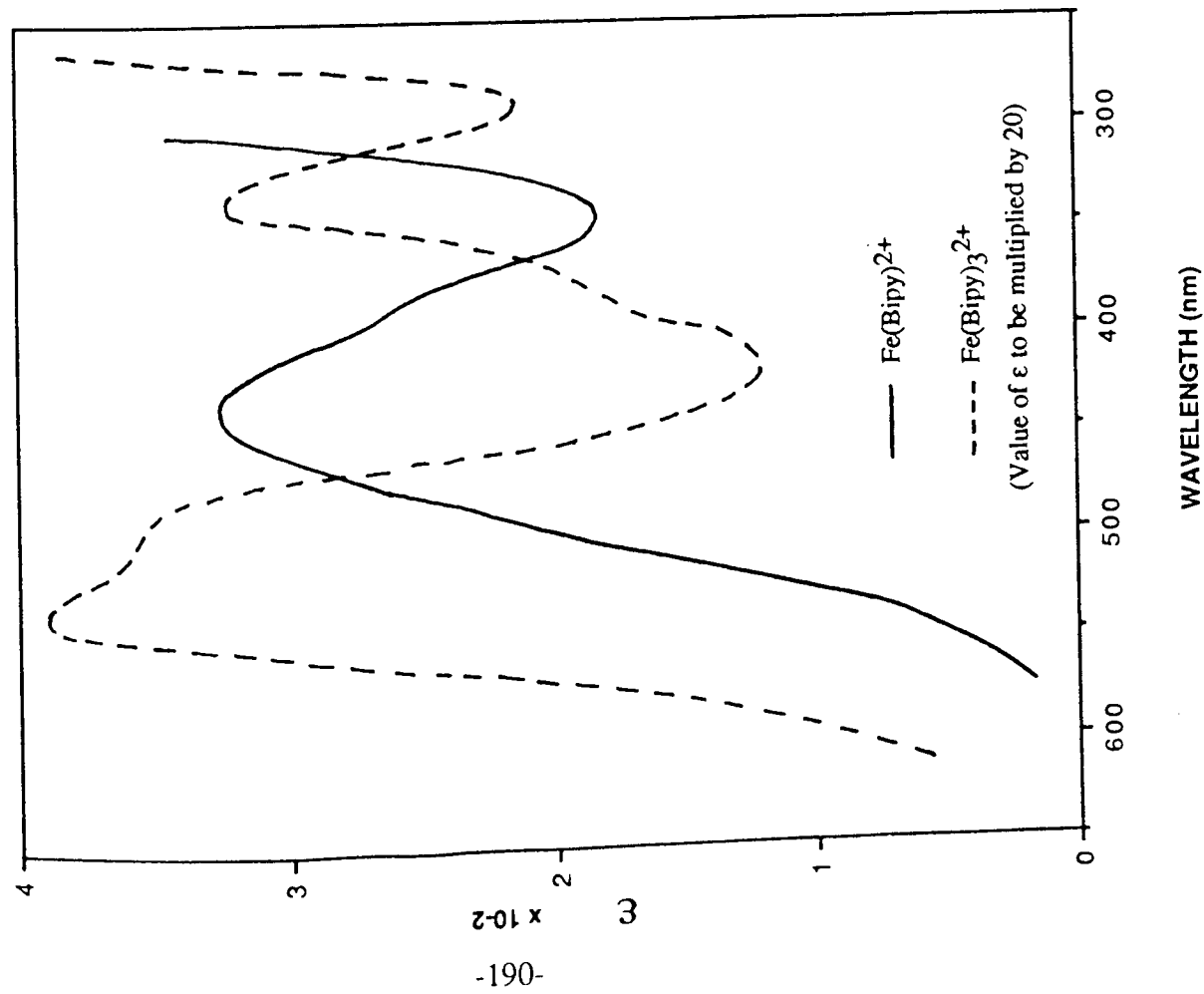
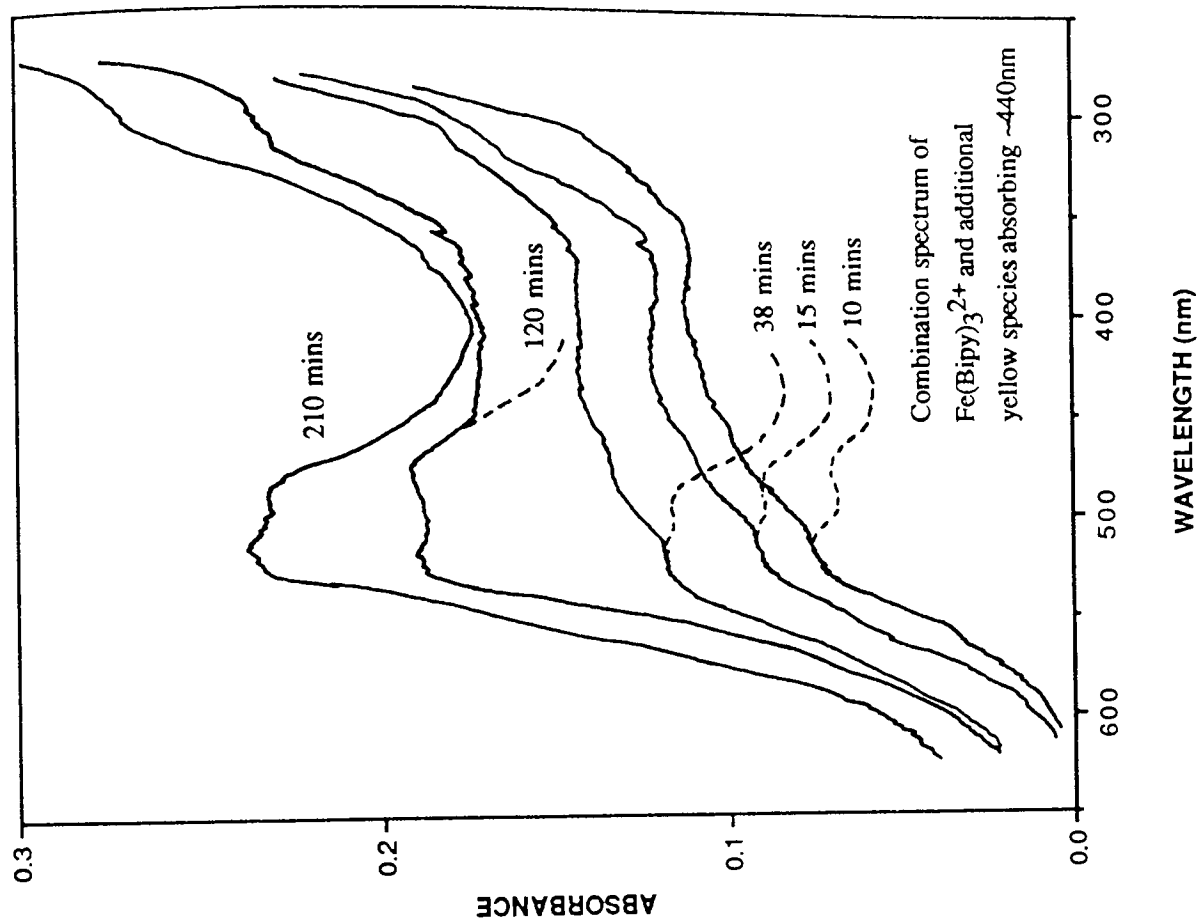


Figure 4.13: Early Kinetic Stages for the Complexation of  $\text{Fe}^{2+}$  to a VinylBipyridine Copolymer Membrane.



Equations can now be derived for each of these quantities in terms of others and the respective rate constants:

$$[\text{Bipy}]_{\text{total}} = [\text{L}] + [\text{M}] + m[\text{B}] + n[\text{T}] \quad (4.20)$$

(where m & n are constants relating to the number of blocked sites upon coordination:  
simply T if conversion is ~ complete.)

$$[\text{M}] = [\text{Bipy}]_t - n[\text{T}] \quad (4.21)$$

and if complete conversion:  $[\text{Bipy}] = n[\text{T}]_{\infty} \quad (4.22)$

Therefore,

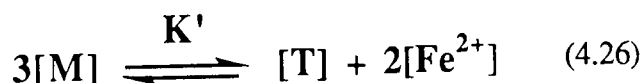
$$[\text{M}] = n\{[\text{T}]_{\infty} - [\text{T}]\} \quad \propto (A_{\infty} - A_t) \quad (4.23)$$

$$[\text{L}] = [\text{M}] / K_1 [\text{Fe}^{2+}] \quad \propto (A_{\infty} - A_t)/[\text{Fe}^{2+}] \quad (4.24)$$

$$[\text{B}] = K_2 [\text{M}] [\text{L}]$$

thus,  $[\text{B}] = K_2 [\text{M}]^2 / K_1 [\text{Fe}^{2+}] \quad \propto (A_{\infty} - A_t)^2/[\text{Fe}^{2+}] \quad (4.25)$

and for later use in the discussion of  $A_{\infty}$  values:



$$K' = \frac{[\text{T}][\text{Fe}^{2+}]^2}{[\text{M}]^3} \quad \propto \frac{A_{\infty} [\text{Fe}^{2+}]^2}{(c - A_{\infty})^3} \quad (4.27)$$

(where c is a constant which = the value of  $A_{\infty}$  obtained if all Bipyridyls are converted to the *tris* complex.)

Now recall that the experimental findings suggest that the kinetic term which describes the  $\text{Cl}^-$  and  $\text{ClO}_4^-$  reactions is second order; if re-written in formulae, this could be due to one of the following:

$$(i) \quad d/dt [T] = k [M]^2 \quad \text{i.e. } k [\text{Fe}(\text{Bipy})]^2 \quad (4.28)$$

$$\text{or } (ii) \quad d/dt [T] = k [M] [L] \quad \text{i.e. } k [\text{Fe}(\text{Bipy})] [\text{Bipy}] \quad (4.29)$$

$$\text{or } (iii) \quad d/dt [T] = k [B] \quad \text{i.e. } k [\text{Fe}(\text{Bipy})_2] \quad (4.30)$$

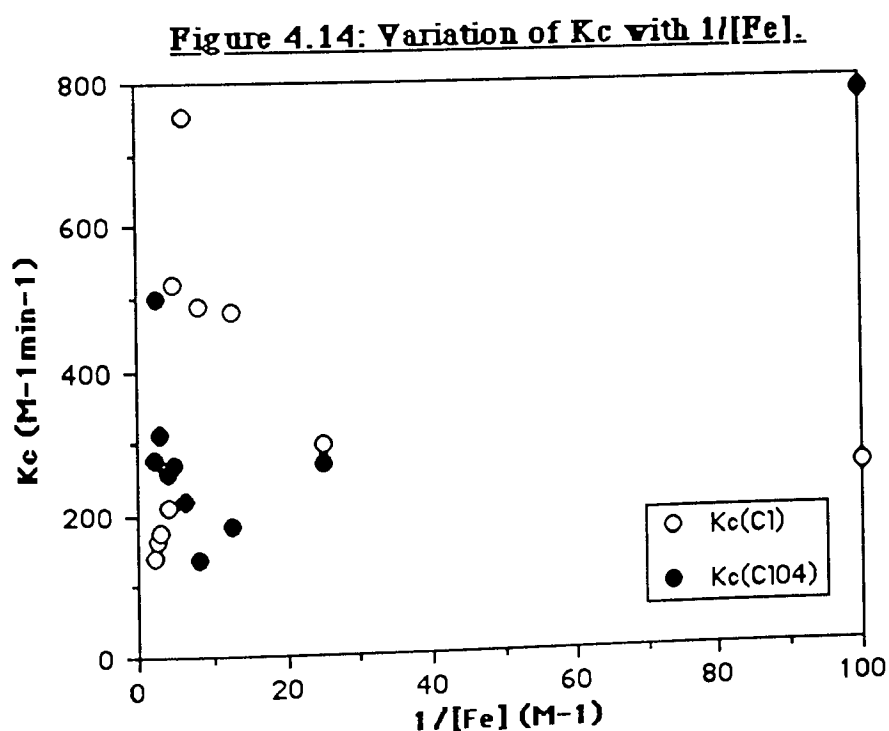
All of these formulae indeed represent second order processes, but re-writing them in terms of equations 4.21 - 4.25 they become:

$$(i) \quad = kn^2 ([T]_{\infty} - [T])^2 \quad (4.31)$$

$$\text{or } (ii) \quad = kn^2 ([T]_{\infty} - [T])^2 / K_1 [\text{Fe}^{2+}] \quad (4.32)$$

$$\text{or } (iii) \quad = K_2 kn^2 ([T]_{\infty} - [T])^2 / K_1 [\text{Fe}^{2+}] \quad (4.33)$$

The value of the computed rate constant  $k_c$  shows little variation with  $[\text{Fe}^{2+}]$  considering its 48-fold change in concentration ( $142$  to  $752 \text{ M}^{-1}\text{min}^{-1}$  for chloride and  $135$  to  $779 \text{ M}^{-1}\text{min}^{-1}$  for perchlorate, Tables 4.6 & 4.7), certainly too little to interpret very closely. However, what is certain from Figure 4.14 is that  $k_c$  is in no way related to  $1/[\text{Fe}^{2+}]$ .



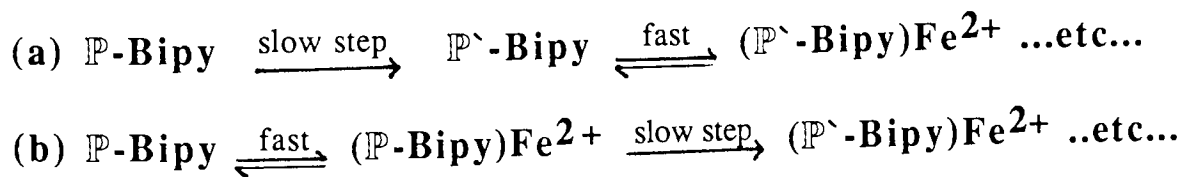
It is now possible to distinguish between a mechanism described by 4.31 and those by 4.32 & 4.33 because 4.31 does not show an inverse dependence on  $[\text{Fe}^{2+}]$  (c.f. Figure

4.14). The mechanism therefore presumably involves the combination of two mono-species {P-Bipy-Fe<sup>2+</sup>}, with the release of an Fe<sup>2+</sup>, in the rate determining step (Figure 4.15). At low Fe<sup>2+</sup> the indications are that this mechanism breaks down and a first order step becomes the rate determining one (compare first and second order fits for Cl<sup>-</sup> & ClO<sub>4</sub><sup>-</sup> at 0.01-0.04M [Fe<sup>2+</sup>]). It may be that either K<sub>1</sub> becomes the slow step (although unlikely), or that some sort of chain reorganisation may occur between the steps governed by K<sub>1</sub> & k<sub>2</sub>, and that is the slow step (Figure 4.16 overleaf).

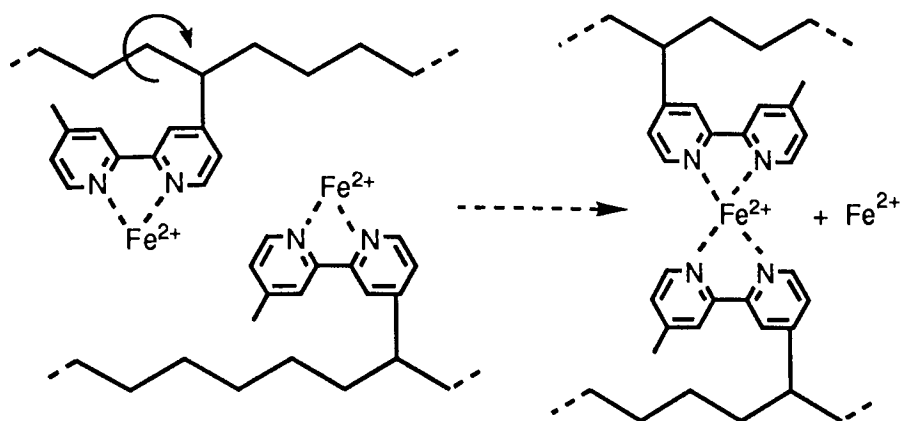
#### 4.4.2 Suggested Mechanism that Fits the First Order Kinetic Form

##### for the Coordination of Ferrous Sulphate.

It has previously been observed in the last section, that at low [Fe<sup>2+</sup>] the kinetics for ferrous chloride and perchlorate coordination is best described by a first order term. This is also the case over the entire concentration range studied for ferrous sulphate (Table 4.5). This phenomenon can be explained by one of two processes:



where P<sup>'</sup> signifies some sort of reorganisation occurring within the polymer in order to allow coordination of further bipyridine groups. It is difficult to visualise the need for a chain rearrangement *before* any Fe<sup>2+</sup> has coordinated (case (a)) on the grounds that the ligand groups are essentially unconnected (~300 units apart) and that the polyHEMA backbone is very flexible. A far more likely situation involves the formation of a mono-complex very rapidly, followed by a slow molecular rearrangement of what is now a rather 'bulky' substituent, necessary to position the groups correctly for further coordination (case (b) & the low [Fe<sup>2+</sup>] scheme in Figure 4.16).



(Counterions Omitted)

**Figure 4.15 Proposed Second Order Mechanism for  $k_2$  Stage.**

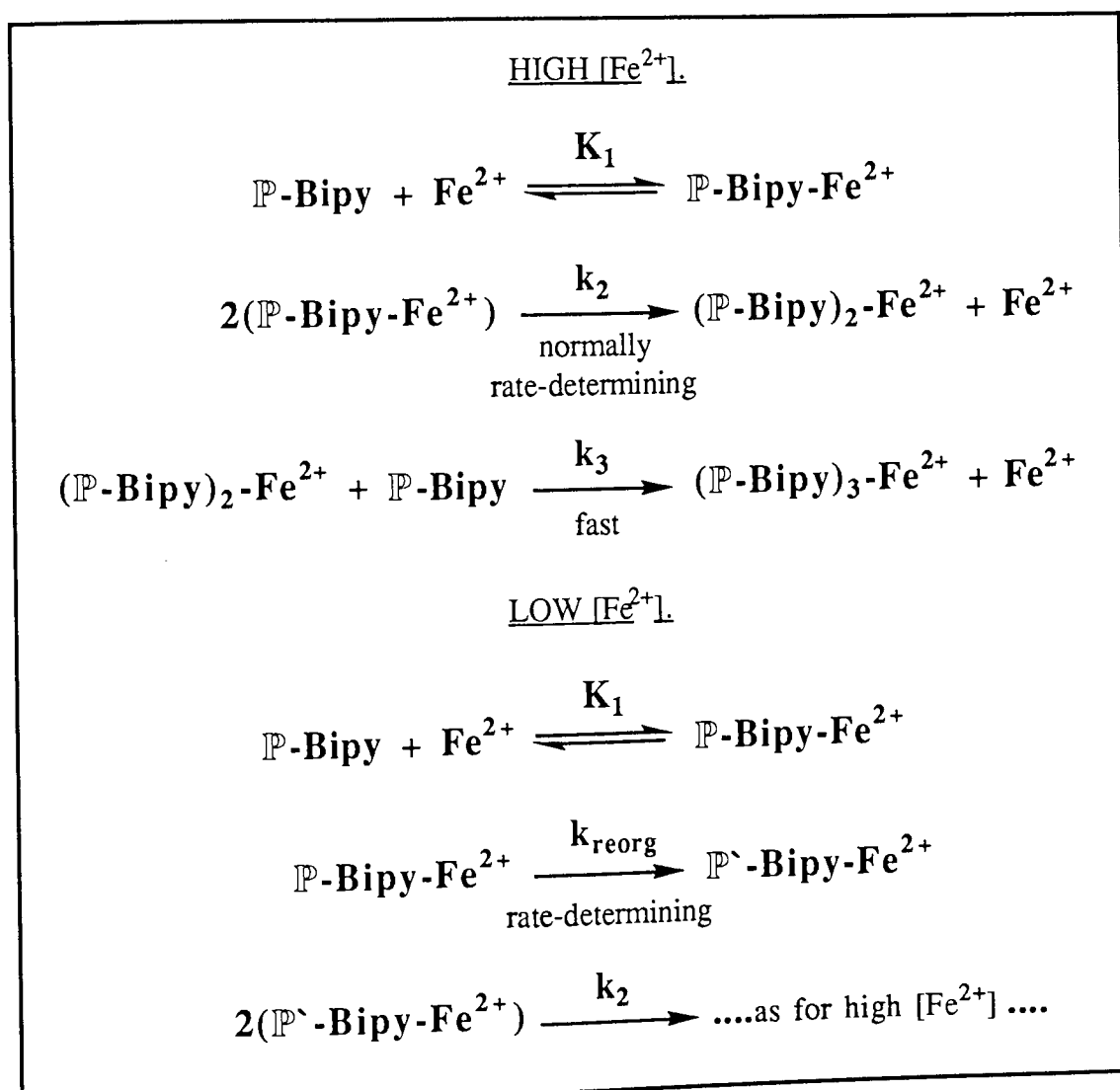


**Figure 4.16 Overall Scheme for  $\text{Cl}^-$  &  $\text{ClO}_4^-$  Kinetics.**

To summarise, the difference observed between the first order kinetics of ferrous sulphate and the second order kinetics of ferrous chloride and perchlorate, is that the reorganisational step is slow and rate-determining for the  $\text{SO}_4^{2-}$  (and for  $\text{Cl}^-$  &  $\text{ClO}_4^-$  at low  $[\text{Fe}^{2+}]$ ), but relatively fast for higher concentrations of  $\text{Cl}^-$  &  $\text{ClO}_4^-$ . By combining the observations made from the kinetic studies with those made in Chapter Five on the influence of anions on the properties of the hydrogel, a postulate is proposed in the conclusion which encompasses the experimental evidence.

#### **4.4.3 Variations in the Observed Infinity Absorbance and Rate Constants for Ferrous Chloride and Perchlorate Kinetics.**

Figures 4.17 & 4.18 show the variation of the observed  $A_\infty$  listed in Tables 4.6 & 4.7 with  $[\text{Fe}^{2+}]$  for ferrous chloride and perchlorate respectively. These graphs highlight an unexpected variation of  $A_\infty$  with  $[\text{Fe}^{2+}]$ ; if this effect is indeed real, it can be explained in terms of an equilibrium process (section 4.4.4). Similarly, Figure 4.19 lists the computer-calculated rate constants ( $k_c$ ) for the complexation process. The results are too scattered to draw any firm conclusions, except that if the slopes of the Kezdy/Swinbourne plots are used instead (described in section 4.3.4 and listed in Tables 4.6 & 4.7), the graph shapes produced seem to 'echo' those for the respective  $A_\infty$  plots. Owing to the inconsistency of the data, detailed arguments based on variations of the rate constants will not be used in the formulation of an overall mechanism for the coordination process. However, let us examine in more detail the variation in  $A_\infty$ .

##### **4.4.3.1: Confirmation of an $[\text{Fe}^{2+}]$ -Dependent Equilibrium.**

The equilibrium effect suggested from Figures 4.17 & 4.18 was confirmed by a series of

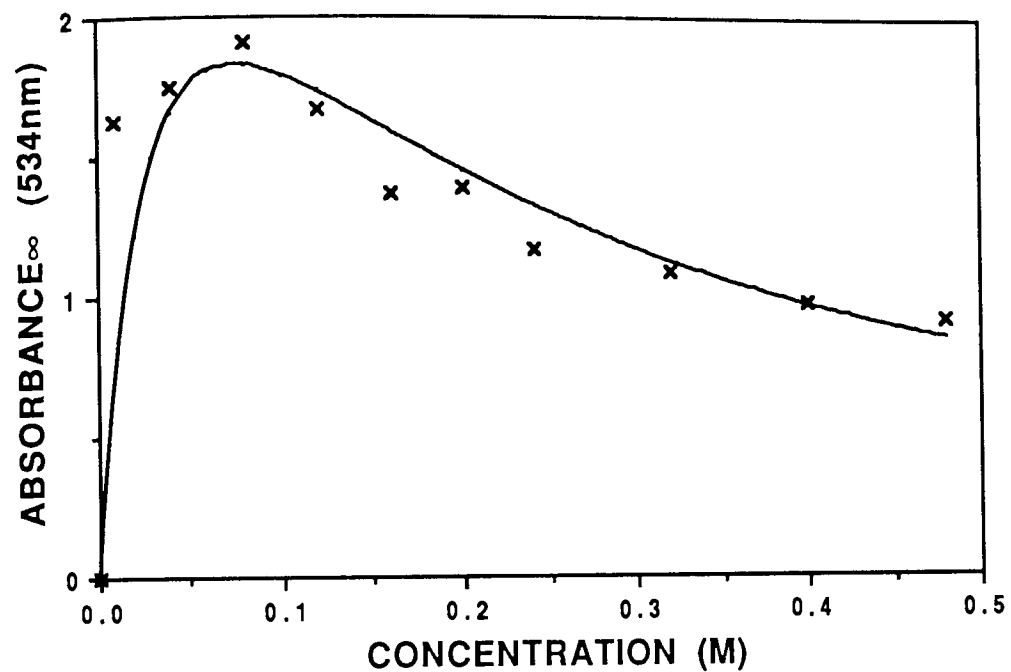


Figure 4.17 Variation of  $A_{\infty}$  with  $[\text{Fe}^{2+}]$  for Ferrous Chloride.

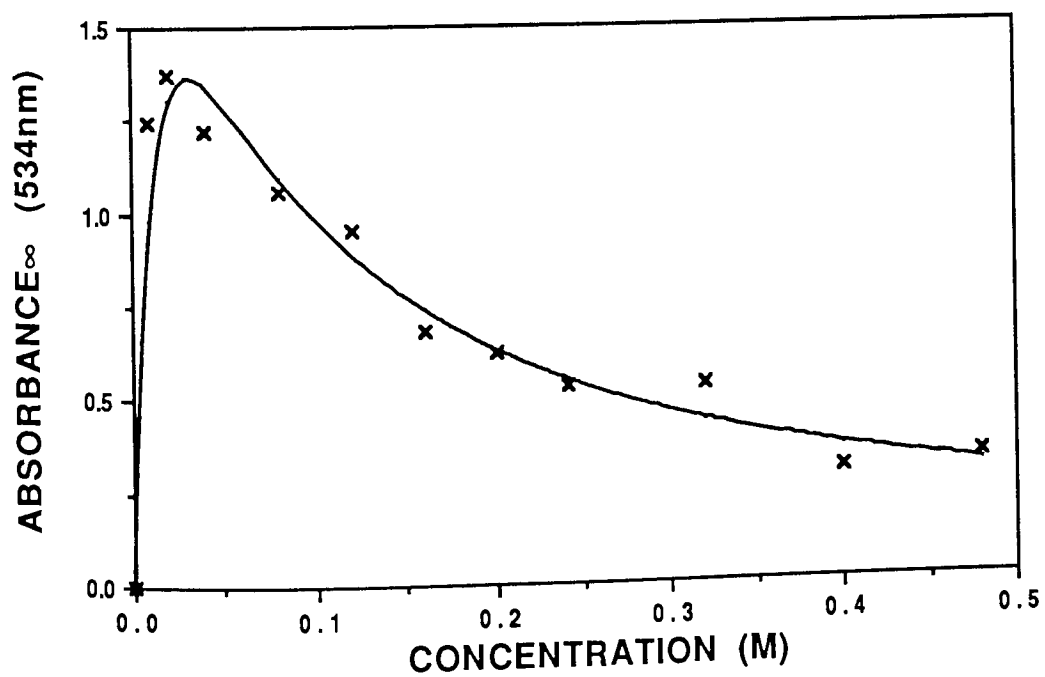
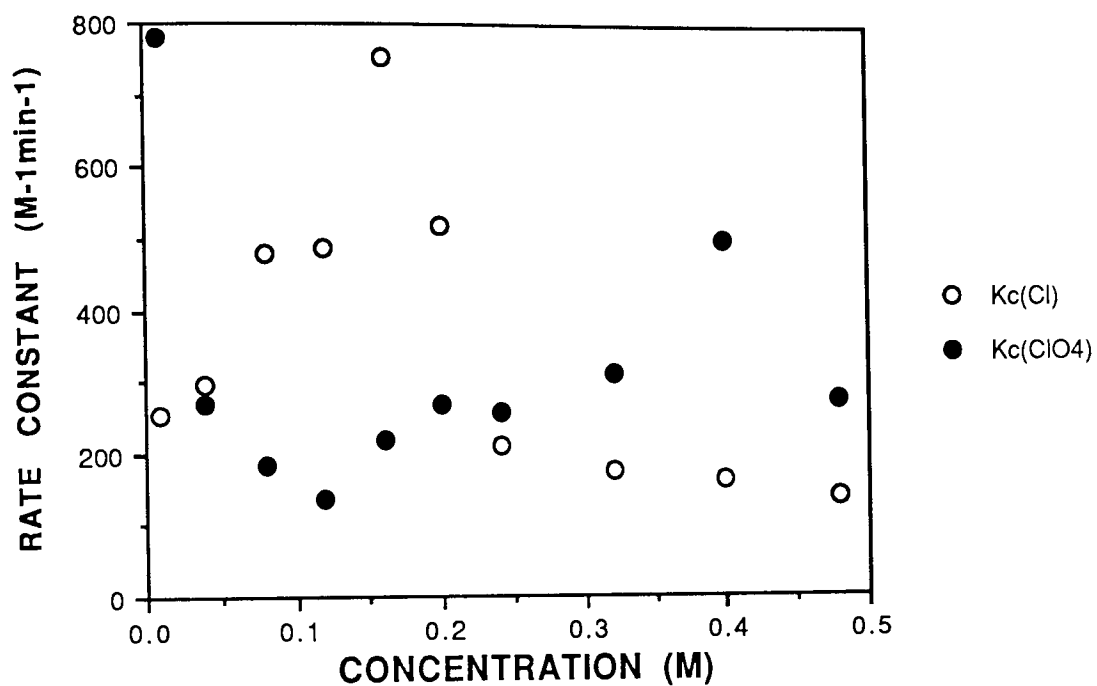
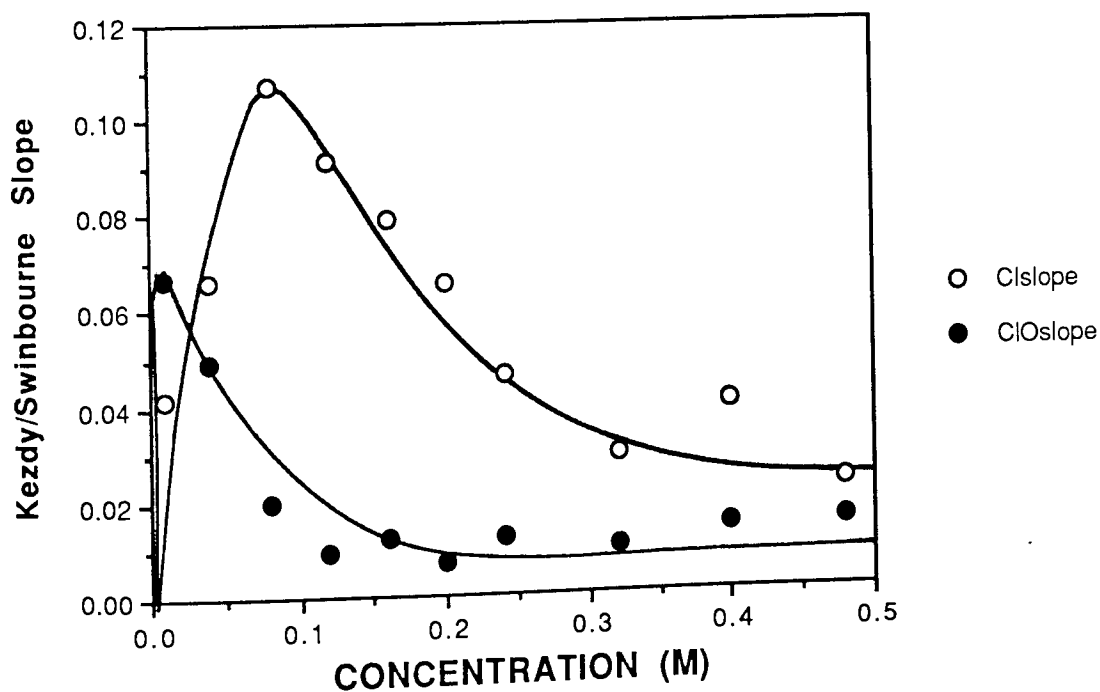


Figure 4.18 Variation of  $A_{\infty}$  with  $[\text{Fe}^{2+}]$  for Ferrous Perchlorate.



**Figure 4.19** Variation of Computed Rate Constant ( $K_c$ ) with  $[Fe^{2+}]$ .



**Figure 4.20** Variation of Kezdy/Swinbourne Slopes for  $Cl^-$  &  $ClO_4^-$  with  $[Fe^{2+}]$ .

[Fe<sup>2+</sup>] 'hopping' experiments in which a membrane sample was placed in a high [Fe<sup>2+</sup>] solution, left to equilibrate for a day before the absorbance was read, and the specimen was then consequently placed in another [Fe<sup>2+</sup>] solution of lower concentration than the previous, and the process repeated. In other experiments the specimen was first placed in a low [Fe<sup>2+</sup>] solution and subsequently moved step-wise into higher [Fe<sup>2+</sup>] solutions; the results are outlined in Table 4.8 (overleaf) and depicted graphically in Figure 4.21. This plot shows the comparison between the experimentally observed A<sub>∞</sub> for Fe(ClO<sub>4</sub>)<sub>2</sub> and points obtained by 'hopping' the same sample from a solution of high concentration to that of a lower concentration (open circles), and *vice versa* (black circles), both in day intervals (data in Table 4.8:).

<u>Conc. (M).</u>	<u>Absorbance (@ 534nm)</u>	<u>Conc. (M).</u>	<u>Absorbance (@ 534nm)</u>
0.4	0.309	0.01	1.588
0.2	0.378	0.05	1.503
0.1	0.453	0.1	1.374
0.05	0.539	0.2	1.257
0.01	0.605	0.4	1.067
Starting at High [Fe <sup>2+</sup> ]		Starting at low [Fe <sup>2+</sup> ]	

**Table 4.8: Data from [Fe<sup>2+</sup>] Hopping Experiments.**

It is clear that there is an equilibrium set up in which the presence of increasing [Fe<sup>2+</sup>] causes the dissociation of *tris*-complex. The data produced from the 'hopping' experiments does not however, move up and down the A<sub>∞</sub> curve observed for ferrous perchlorate; there is in fact an *Hysteresis Effect* in which the starting point in each case lies close to the line, but subsequently moving down the line in the direction of the arrows highlights an increasing deviation from the A<sub>∞</sub> curve. The Hysteresis Effect is probably due to the fact that the equilibrium is a very slow process and one day is not long enough

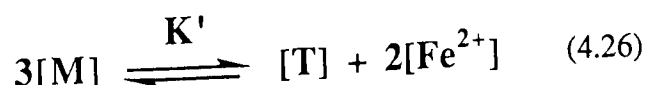
for full equilibrium to be reached. If the same experiment were to be repeated with one *week* intervals then perhaps a more accurate representation of the  $A_{\infty}$  curve would probably result. This could not be carried out during the course of this study, as the idea came at the very end of the research period.

Baxendale and George <sup>174</sup> observed similar equilibrium reactions for 2,2'-bipyridyl and ferrous ions in solution, using spectrophotometric evidence such as that shown in Figures 4.12 & 4.13, section 4.4.1. Their data can be represented as in Figure 4.22 which shows a basically similar shaped curve to those observed in this study. However, Baxendale's data shows that 100% conversion to *tris*-complex occurs at the expected 1:3 ratio of  $[\text{Fe}^{2+}]:[\text{Bipy}]$ , and that below this ratio conversion obviously falls off and is dependent solely on the amount of  $\text{Fe}^{2+}$  present. It is difficult to predict the ratio of  $\text{Fe}^{2+}:\text{Bipy}$  in the polymeric system but the deviation at low  $[\text{Fe}^{2+}]$  has maxima at different positions for chloride and perchlorate and the absorbance does not 'fall-off' as steeply as one might expect if the deviation is due to simply being below the 1:3 ratio. Any mechanism that describes the equilibrium kinetics may have to take this low concentration deviation into consideration.

#### 4.4.3.2 Derivation of a Relationship to Describe Variations in $A_{\infty}$ for Ferrous

##### Chloride and Perchlorate Salt Coordination.

Recalling the equations 4.26 & 4.27 from section 4.4.1, it was shown that the equilibrium for *tris*-formation:



can be described by the equation:

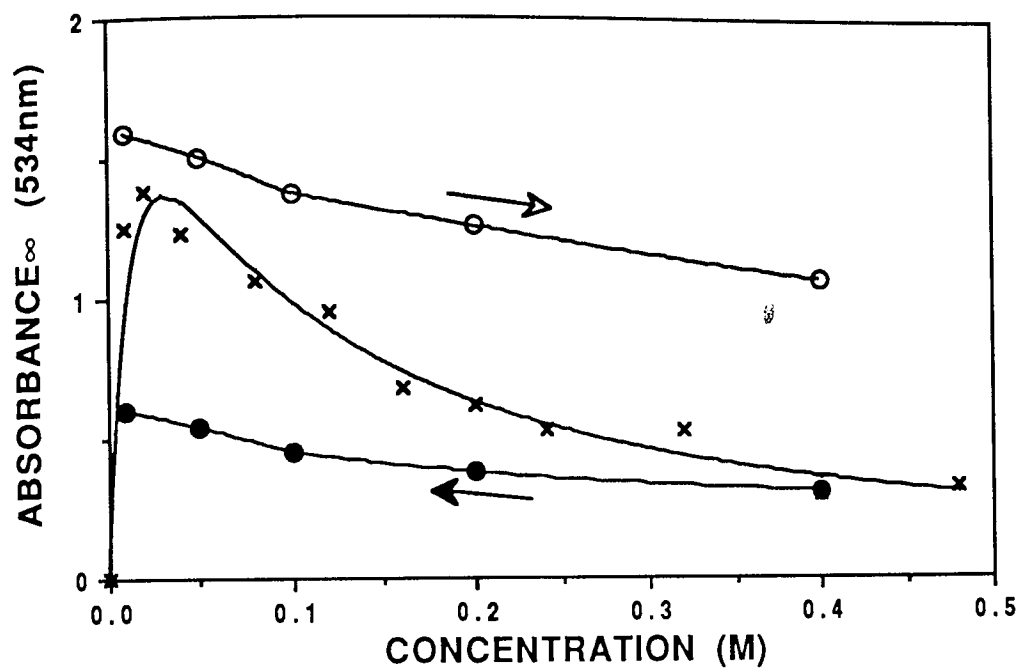


Figure 4.21:  $[\text{Fe}^{2+}]$  'Hopping' Experiment, Showing a Hysteresis-Type Effect.

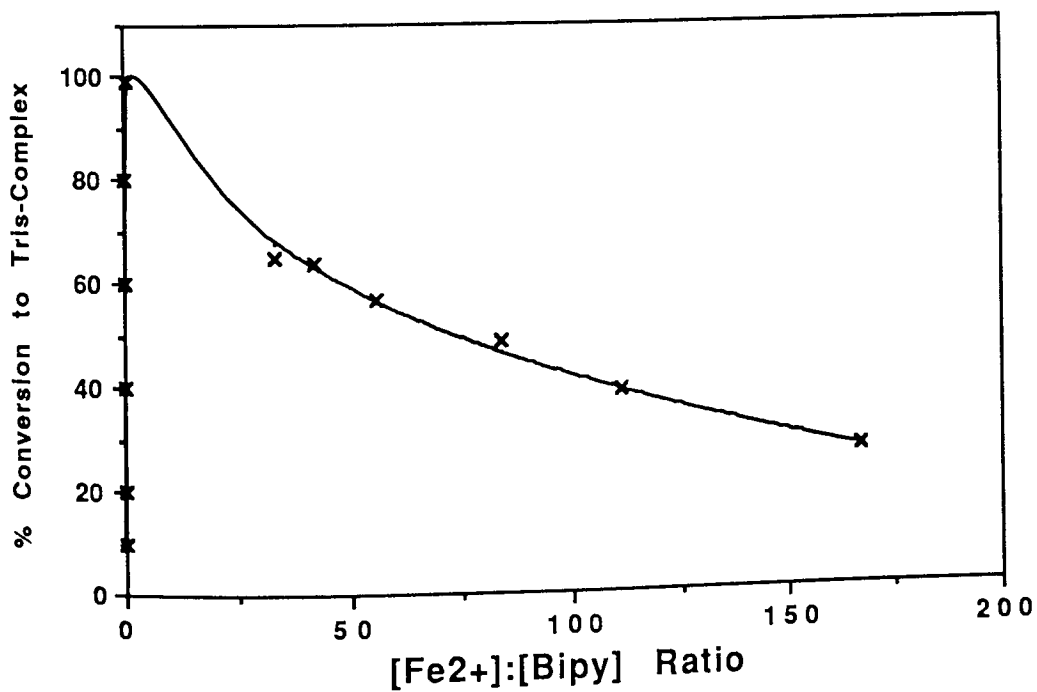


Figure 4.22: Baxendale's Data on the Influence of  $[\text{Fe}^{2+}]$  on  $[\text{Fe-tris(Bipy)}]$  Formation.

$$K' = [T] [Fe^{2+}]^2 / [M]^3 \quad (4.27)$$

K' can be represented in terms of K<sub>1</sub>, K<sub>2</sub> & K<sub>3</sub> by substitution of the terms derived from equations 4.16 to 4.18 into 4.27:

$$K' = K_2 K_3 / (K_1)^2 \text{ or } \beta_3 / (K_1)^3 \quad (4.34)$$

Using literature values for K<sub>1</sub>, K<sub>2</sub> & K<sub>3</sub><sup>52</sup>, it is possible to obtain a value of K' for equilibria involving bipyridyl itself in aqueous solution:

$\underline{K}_1(M^{-1})$	$\underline{K}_2(M^{-1})$	$\underline{K}_3(M^{-1})$	$\underline{K}'$
$2 \times 10^4$	$5 \times 10^3$	$3.2 \times 10^9$	$4 \times 10^4$

This value is compared with those values of K' derived for the polymeric system (Table 4.9, section 4.4.3.3) by the following procedure:

First assume all ligand groups can become coordinated. Then taking equation 4.27:

$$K' = [T] [Fe^{2+}]^2 / 3^3(X-[T])^3 \quad (4.35)$$

{where X= the value of [T] if all the Bipys are converted to T}

Expanding in terms of absorbances gives:

$$K' = A_{\infty} [Fe^{2+}]^2 \epsilon^2 / 27(Y - A_{\infty})^3 \quad (4.36)$$

{where Y= the value of A<sub>∞</sub> if all Bipys are tris-complexed}

If 4.36 is correct, then a straight line will result for:

$$(Y - A_{\infty}) = \sqrt[3]{\frac{A_{\infty} [Fe^{2+}]^2 \epsilon^2}{27K'}} \quad \text{or} \quad (4.37)$$

$$A_{\infty} = Y - \sqrt[3]{\frac{A_{\infty} [Fe^{2+}]^2 \epsilon^2}{27K'}} \quad (4.38)$$

Figures 4.23 & 4.24 are plots of  $A_{\infty}$  versus  $\sqrt[3]{(A_{\infty} [\text{Fe}^{2+}]^2)}$  for  $\text{Cl}^-$  &  $\text{ClO}_4^-$  respectively according to equation 4.38. A number of constants can be obtained from these plots. Firstly, the intercept gives us the value of Y; studies on maximum binding capacity in section 4.2 show that the maximum absorbance value if all ligands coordinate is about 2.25, i.e. if  $[\text{Fe}(\text{bipy})_3] = [\text{bipy}]_{\text{total}}/3$ . The value of Y for  $\text{Cl}^-$  &  $\text{ClO}_4^-$  is 1.99 and 1.54 respectively. Examination of the  $A_{\infty}$  graphs 4.17 & 4.18 shows that these are indeed reasonable estimates of the maximum absorbances produced for these salts. The gradients of the graphs are equal to  $\sqrt[3]{(\epsilon^2 / 27K')}$  from which it is possible to calculate  $K'$  for  $\text{Cl}^-$  &  $\text{ClO}_4^-$  as  $3.1 \times 10^5$  &  $6.34 \times 10^4$  units respectively. (Table 4.9). Regression analysis shows that a straight line is a reasonable fit to the data considering the experimental scatter involved ( $R = 0.78$  &  $0.93$  for  $\text{Cl}^-$  &  $\text{ClO}_4^-$  respectively). However, it is also possible to represent the data in terms of the  $[\text{Fe}^{2+}]$  that would give rise to a particular absorbance, using a rearranged form of equation 4.38:

$$[\text{Fe}^{2+}] = \sqrt{\frac{(Y - A_{\infty})^3 27K'}{A_{\infty}^2 \epsilon^2}} \quad (4.39)$$

Figures 4.25 & 4.26 show that the equation fits the experimental data to a curve that continually increases in absorbance as the  $[\text{Fe}^{2+}]$  decreases, i.e. does not go through a maximum as suggested by Figures 4.17 & 4.18. The fit is again reasonable but these plots highlight a deviation at low  $[\text{Fe}^{2+}]$  for both salts. An additional factor must be in operation in order to produce a low concentration deviation, and this must be defined in the kinetics in order to gain a full appreciation of the mechanism of reaction.

#### 4.4.3.3 A Modified Approach to Considering Infinity Absorbances.

When considering the penetration of the ferrous salt within the membrane, it is useful to

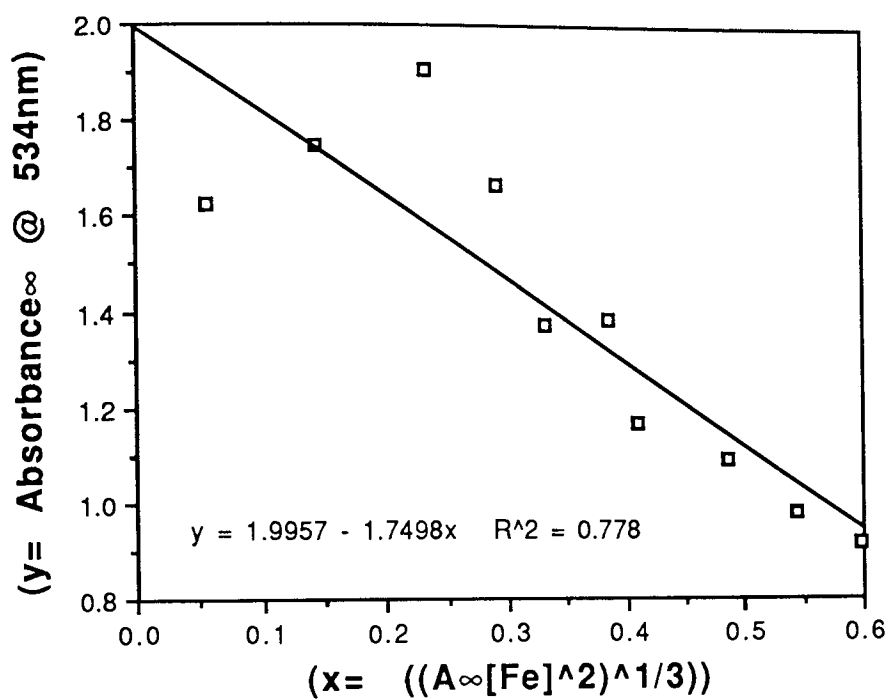


**Figure 4.23: Equilibrium Dependence of  $A_\infty$  for  $\text{FeCl}_2$ .**

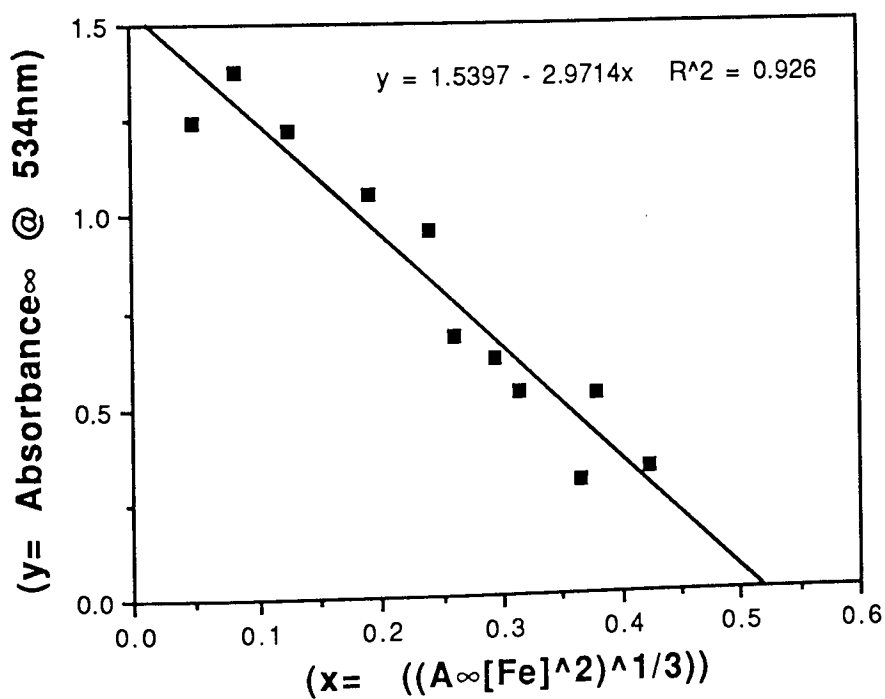


**Figure 4.24: Equilibrium Dependence of  $A_\infty$  for  $\text{Fe}(\text{ClO}_4)_2$ .**

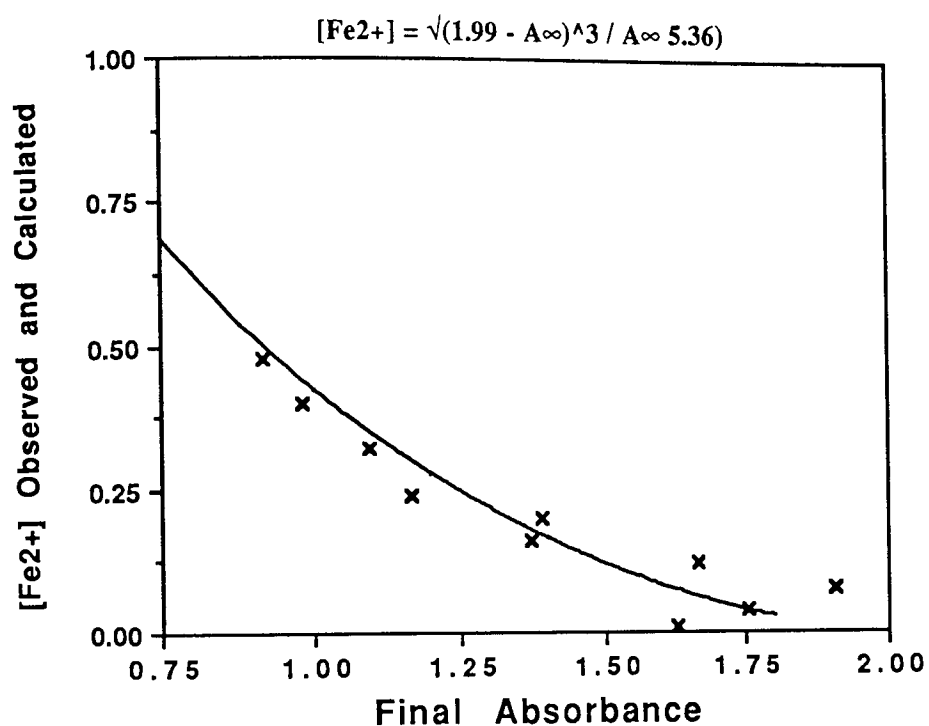


Figure 4.25:  $\text{FeCl}_2$  Absorbance Data Fit to Equation 4.39.

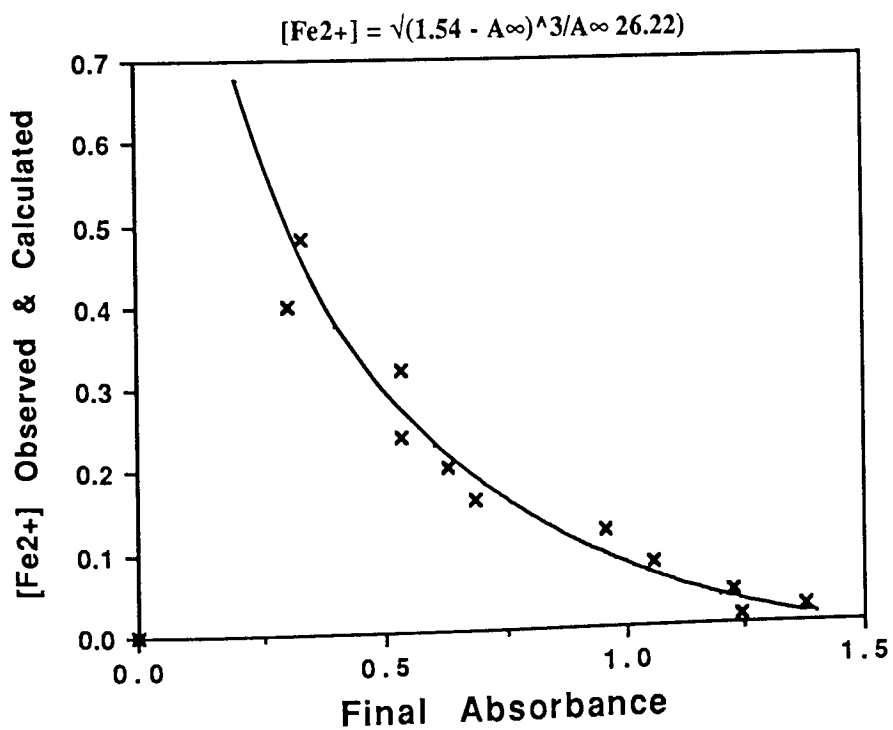


Figure 4.26:  $\text{Fe}(\text{ClO}_4)_2$  Absorbance Data Fit to Equation 4.39.

remember that the ions will significantly influence the structuring of the water present in the interstitial spaces of the hydrogel. Structure-breaking ions such as perchlorate, and to a lesser extent chloride (cf. Chapter Five) will increase the water content of the membrane and effectively plasticise the polymer chains producing an enhanced mobility. It is also conceivable that the oxygen atoms of the HEMA molecules in the polymer could interact with ferrous ions (which have an affinity for oxygen donor ligands) as well as the bipyridyl ligands. Therefore, if transport of  $\text{FeX}_2$  in fact results in an opening of the membrane, certain ligand groups may be made more accessible by the presence of the salt. Consider an equilibrium that utilises S, a 'coordination' site within the membrane from which a bipyridyl is accessible for complexation with iron as  $\text{Fe}(\text{S})$  but not for S only:



Then the fraction of Bipy that is accessible for complexation is given by:

$$f = \frac{[\text{FeS}]}{[\text{S}] + [\text{FeS}]} \quad (4.41)$$

but,

$$K_0[\text{S}] [\text{Fe}^{2+}] = [\text{FeS}] \quad (4.42)$$

therefore:

$$f = \frac{K_0[\text{S}] [\text{Fe}^{2+}]}{[\text{S}] + K_0[\text{S}] [\text{Fe}^{2+}]} = \frac{K_0 [\text{Fe}^{2+}]}{1 + K_0 [\text{Fe}^{2+}]} \quad (4.43)$$

Reconsidering equation 4.38 of section 4.3.3, the total  $[\text{FeBipy}]$  (written as  $[\text{M}]$ ) given by  $(Y - A_\infty)$ , should be replaced by the *accessible* Bipy. That is, each term should be multiplied by  $f$ , the fraction of accessible Bipy in equation 4.43. Equation 4.38 then

becomes equation 4.44:

$$K' = \frac{A_{\infty} \epsilon^2 [Fe^{2+}]^2}{27(Y - A_{\infty})^3} \cdot \left( \frac{1 + K_0 [Fe^{2+}]}{K_0 [Fe^{2+}]} \right)^3 \quad (4.44)$$

which rearranges to give:

$$\left( \frac{27K'K_0^3}{\epsilon^2} \right) = \left( \frac{1 + K_0 [Fe^{2+}]}{Y - A_{\infty}} \right)^3 \cdot \frac{A_{\infty}}{[Fe^{2+}]} \quad (4.45)$$

that is,

$$(Y - A_{\infty}) \cdot \sqrt[3]{\frac{[Fe^{2+}]}{A_{\infty}}} = \sqrt[3]{\frac{\epsilon^2}{27K'K_0^3}} \cdot (1 + K_0 [Fe^{2+}]) \quad (4.46)$$

Using this modified form of the equation, a straight line would be the expected result for a plot of the left-hand side versus  $[Fe^{2+}]$ . Earlier in section 4.2, the maximum theoretical binding capacity of a 0.5% membrane was calculated as giving an absorbance of around 2.25; this figure must now be used as the value for  $Y$ - the absorbance if all Bipys were to be complexed. Figures 4.27 & 4.28 are the graphs for the kinetic equilibrium dependence of ferrous chloride and perchlorate respectively. Taking into consideration the inherent experimental errors previously discussed, one could not hope to see a much better fit for the experimental data, with regression parameters of 0.98 for each plot. These plots enable the calculation of  $K_0$  by expanding equation 4.46 into it's full form:

$$(Y - A_{\infty}) \cdot \sqrt[3]{\frac{[Fe^{2+}]}{A_{\infty}}} = \sqrt[3]{\frac{\epsilon^2}{27K'K_0^3}} + \sqrt[3]{\frac{\epsilon^2}{27K'K_0^3}} K_0 \cdot [Fe^{2+}] \quad (4.47)$$

( y                    =                    c                    +                    mx )

$K_0$  is then simply the value of the gradient (m) divided by the intercept (c). Once  $K_0$  has been calculated,  $K'$  is found by simply rearranging the term for the intercept in equation

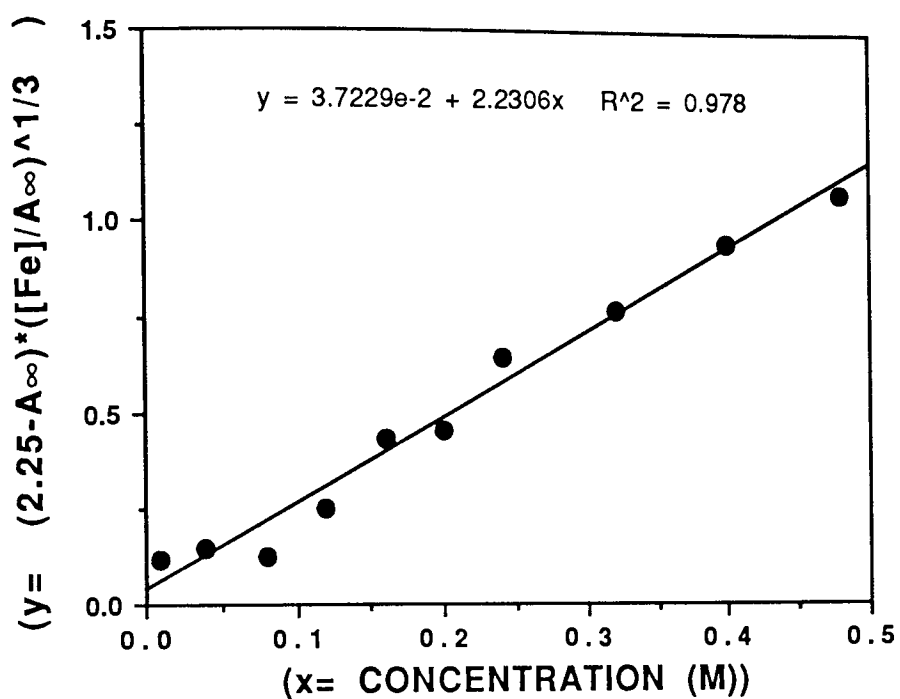


**Figure 4.27: Final Absorbance Relationship that Describes the  $FeCl_2$  Equilibrium.**

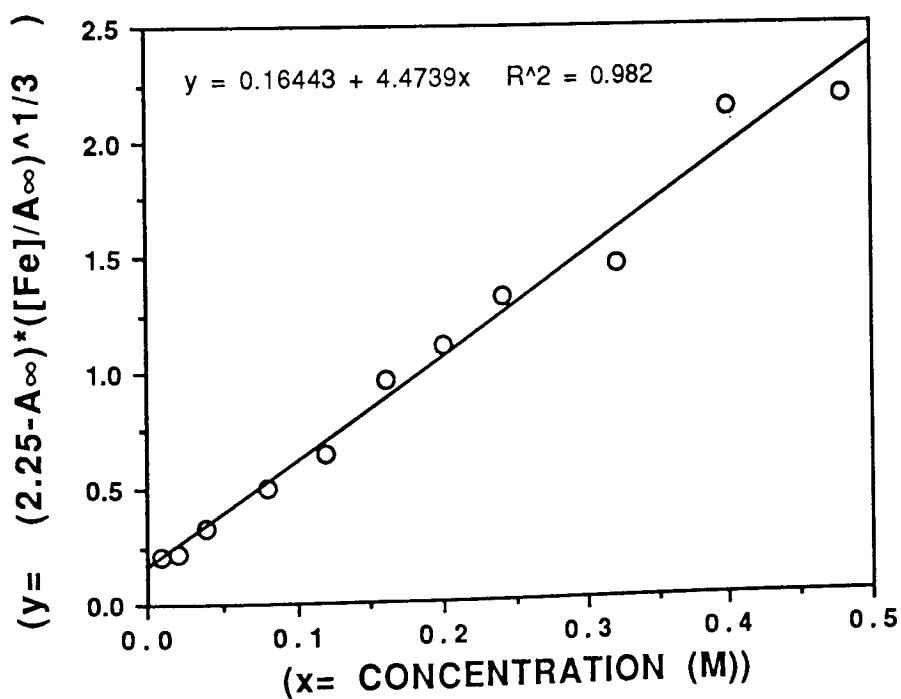


**Figure 4.28: Final Absorbance Relationship that Describes the  $Fe(ClO_4)_2$  Equilibrium.**

4.47:

$$K' = \left( \frac{\epsilon^2}{c^3 27 K_0^3} \right) \quad (4.48)$$

Values for the equilibrium constants are displayed in Table 4.9 below, along with constants calculated previously from literature data and from the unmodified equation of section 4.3.3:

<u>Ferrous Salt</u>	<u>Equilibrium Constant</u>	<u>Technique</u>	<u>Value</u>
SO <sub>4</sub> <sup>2-</sup>	K'	Solution <sup>52</sup>	4 x 10 <sup>4</sup>
Cl <sup>-</sup>	K'	Eqn. 4.38	3.1 x 10 <sup>5</sup>
ClO <sub>4</sub> <sup>-</sup>	K'	Eqn. 4.38	6.3 x 10 <sup>4</sup>
Cl <sup>-</sup>	K'	Eqn. 4.47	1.5 x 10 <sup>5</sup>
ClO <sub>4</sub> <sup>-</sup>	K'	Eqn. 4.47	1.9 x 10 <sup>4</sup>
Cl <sup>-</sup>	K <sub>0</sub>	Eqn. 4.47	60 M <sup>-1</sup>
ClO <sub>4</sub> <sup>-</sup>	K <sub>0</sub>	Eqn. 4.47	27 M <sup>-1</sup>

**Table 4.9 Collection of Equilibrium Constant Data.**

#### **4.4.4: Variations in Infinity Absorbance and Rate Constants for Ferrous Sulphate**

##### **Kinetics.**

Contrary to the observations made with ferrous chloride and perchlorate, ferrous sulphate shows very little variation in the observed infinity absorbance with change in [Fe<sup>2+</sup>] (Figure 4.29). In addition to this, even though there is a 48-fold concentration range, the rate constants as calculated by the computer, Guggenheim and Kezdy/Swinbourne methods all show scatter around an essentially constant value (Figure 4.30). The mechanism that describes the different sequence of events occurring for sulphate must also take into account the fact that A<sub>∞</sub> is constant for all concentrations studied.

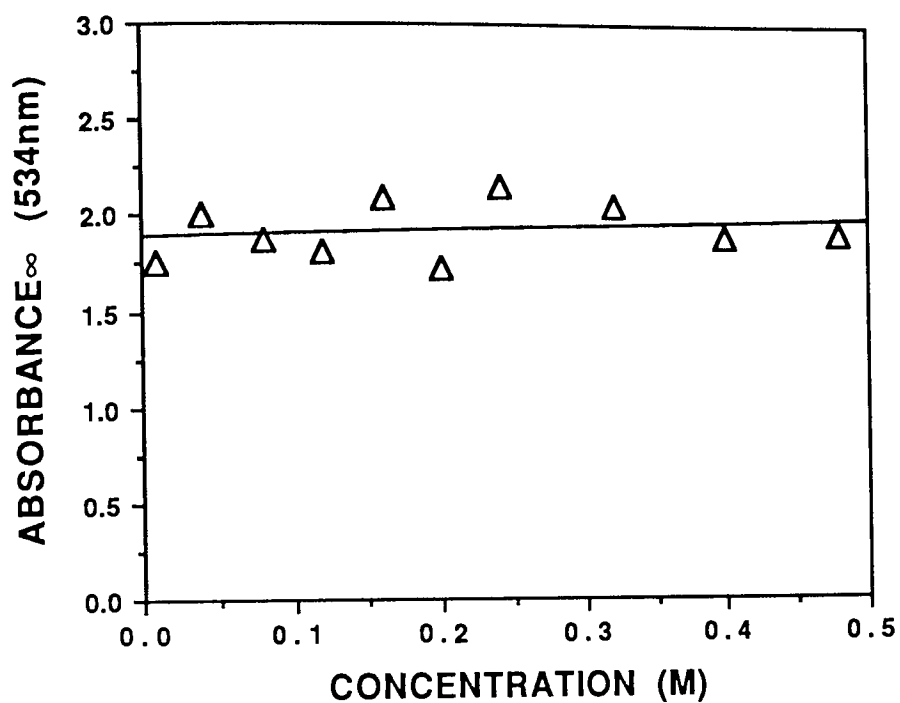


Figure 4.29: Variation of  $A_{\infty}$  with  $[\text{Fe}^{2+}]$  for Ferrous Sulphate.

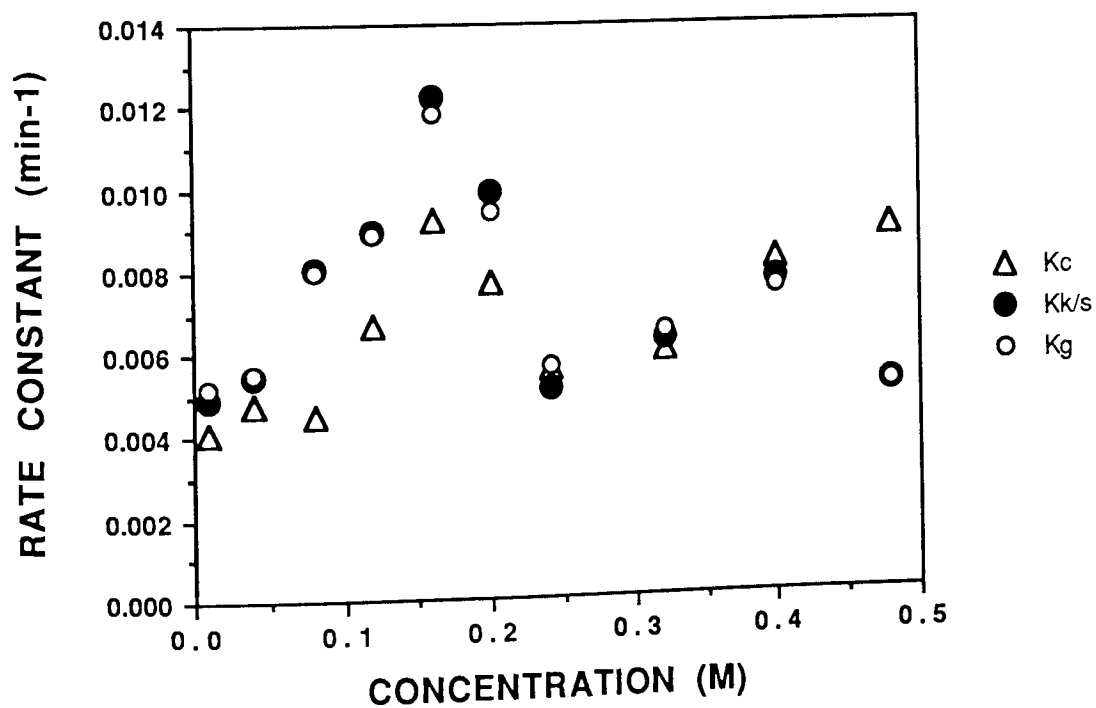
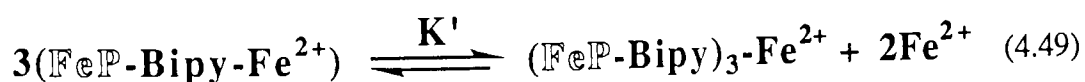


Figure 4.30: Variation of Rate Constants with  $[\text{Fe}^{2+}]$  for Ferrous Sulphate.

#### 4.5 PROPOSED MECHANISM FOR THE COORDINATION OF FERROUS SALTS TO BIPYRIDYL-BASED MEMBRANES.

It is now necessary to combine all previous ideas and observations to produce the best overall explanation for the observed data. The mechanistic scheme proposed in Figure 4.31 is one possible solution that describes the observations made. Starting with step (i), it was demonstrated in section 4.4.3.3 that the variation in  $A_{\infty}$  with  $[\text{Fe}^{2+}]$  for  $\text{Cl}^-$  &  $\text{ClO}_4^-$  could only be described satisfactorily if one assumed that it was necessary for  $\text{Fe}^{2+}$  to be *coordinated* to (or at least present at) some site within the membrane, in order to make previously inaccessible ligand groups available for coordination. This state is represented in the mechanistic scheme as  $\text{FeP-Bipy}$ ; this step is common for all salts and in fact, the equilibrium constant for step (i) ( $K_0$ ) has been calculated for  $\text{Cl}^-$  &  $\text{ClO}_4^-$  (Table 4.9) but not for  $\text{SO}_4^{2-}$ . From the second order kinetics displayed by  $\text{Cl}^-$  &  $\text{ClO}_4^-$ , it is possible to deduce that the rate-determining step for those anions must be stage (iv) with  $k_{-2}$  being too small to affect the kinetic observations. The  $A_{\infty}$  varies with  $[\text{Fe}^{2+}]$  because of the equilibrium outlined in equation 4.49:



$K'$  can indeed be calculated (Table 4.9) and is shown to be of the same order of magnitude as that for the equivalent process in solution (calculated from known values for  $K_1$ ,  $K_2$  &  $K_3$ ). It is obvious from 4.49 that the higher the concentration of  $\text{Fe}^{2+}$  present within the membrane, the further the equilibrium will be pushed to the left in favour of the *mono*-species and hence causing a reduction in the absorbance due to the *tris* complex.

The second order kinetics are consistent with  $\{[\text{Ligand}] \ll [\text{Mono}] \gg [\text{Bis}] \ll [\text{Tris}]\}$  so that

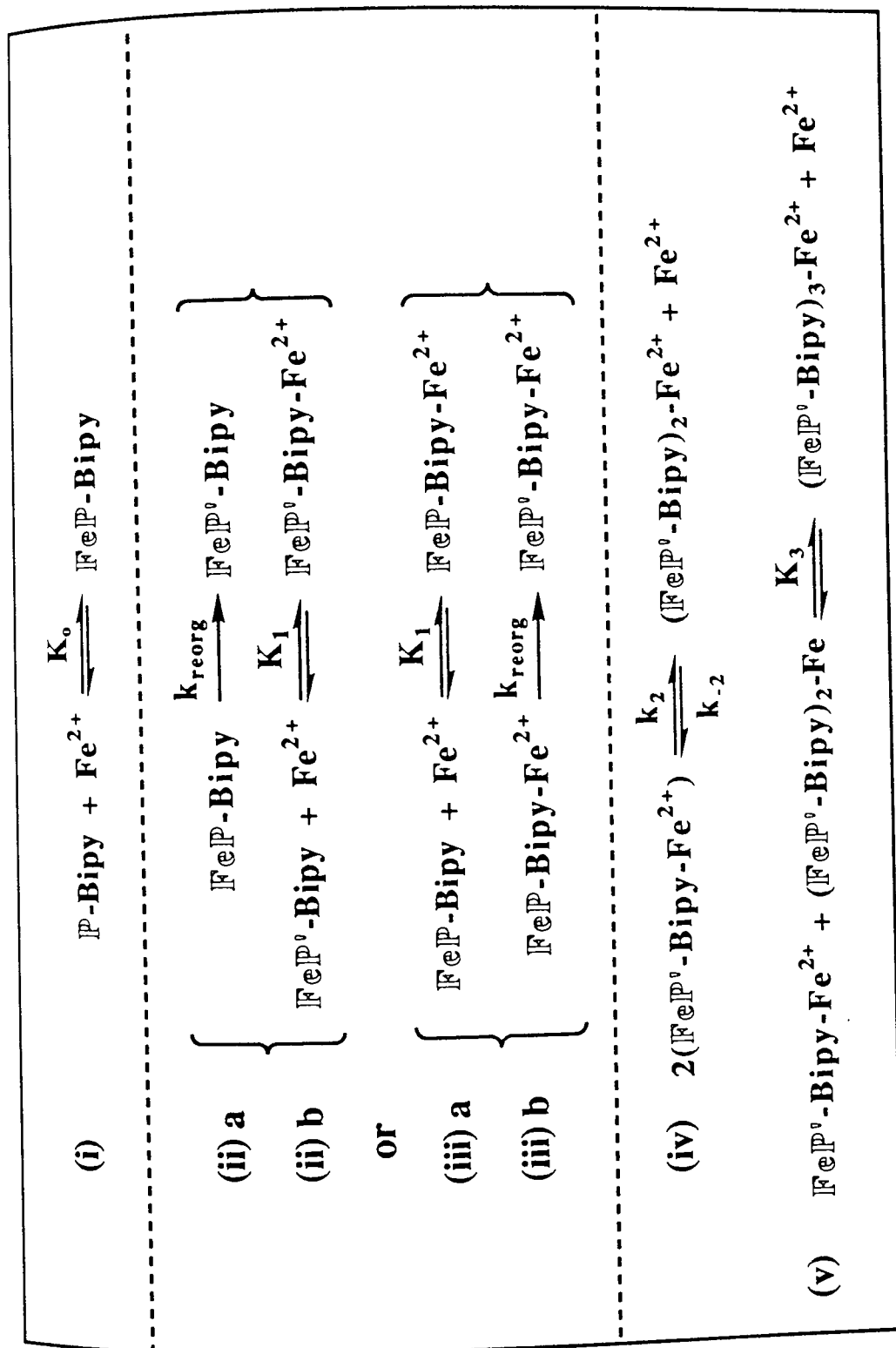


Figure 4.31: Proposed Mechanism for the Coordination of Ferrous Salts to VinylBipyridine-Based Hydrogel Membranes.

$(A_{\infty} - A)$  is proportional to  $[\text{P-Bipy-Fe}]$ . If this order still holds for the first order process, then the kinetics may go *via* route (iii), the rate determining step for  $\text{SO}_4^{2-}$  being step (iii)b in which a reorganisation occurs after coordination of the first  $\text{Fe}^{2+}$  to Bipy, as argued in section 4.4.2. The alternative route (ii) is ruled out as it requires step (ii)a to be rate determining which necessitates the reorganisation to occur after  $\text{Fe}^{2+}$  has diffused into the membrane and interacted with the polymer, but *before* the formation of the *mono*-species. This now changes the concentration ratios to {Ligand » Mono » Bis « Tris} because the concentration of *mono*-species is disappearing faster than that of the ligand. Hence,  $(A_{\infty} - A)$  is proportional to  $[\text{FeP-Bipy}]$  and,

$$d[\text{Tris}]/dt = k_{\text{reorg}} [\text{FeP-Bipy}] \quad (4.50)$$

or,

$$d[\text{Tris}]/dt = \left( \frac{k_{\text{reorg}} K_o [\text{Fe}^{2+}]}{1 + K_o [\text{Fe}^{2+}]} \right) ([\text{Bipy}] - 3[\text{Tris}]) \quad (4.51)$$

A number of observations can be made as a consequence of the relationship in equation 4.51; the observed rate constant ( $k_{\text{obs}}$ ) would be proportional to  $K_o[\text{Fe}^{2+}]/1+K_o[\text{Fe}^{2+}]$  (f) and may be independent of  $[\text{Fe}^{2+}]$  if  $K_o[\text{Fe}^{2+}] \gg 1$ . It has been shown that  $A_{\infty}$  is effectively constant for  $\text{SO}_4^{2-}$  which also requires  $f$  to be constant. Since in the range studied,  $\text{Fe}^{2+}$  concentrations as low as 0.01M are used,  $K_o \gg \sim 500$  (approx) in order to produce a constant value for  $f$ ; any lower than this and  $f$  begins to become a significant fraction.

If  $K_o(\text{SO}_4^{2-}) > K_o(\text{Cl}^- \text{ \& } \text{ClO}_4^-)$  ( $>500$  compared to 27 & 60 respectively), then  $K'(\text{SO}_4^{2-}) > K'(\text{Cl}^- \text{ \& } \text{ClO}_4^-)$  in order for the  $A_{\infty}$  to be constant for  $\text{SO}_4^{2-}$ . This anion

dependence is reasonable on the grounds that the anions which encourage higher water contents will most probably swell the membrane with a greater concentration of  $[\text{Fe}^{2+}]$  compared to the deswelling effect of sulphate. The greater amounts of  $[\text{Fe}^{2+}]$  associated with  $\text{Cl}^-$  &  $\text{ClO}_4^-$  will undoubtedly push the  $K'$  equilibrium to the left, resulting in the characteristic  $[\text{Fe}^{2+}]$ -dependent  $A_\infty$  plots. As for the value of  $K_0(\text{SO}_4^{2-})$ , it is difficult to state unequivocally why this salt interacts or *coordinates* with the polymer in such a way as to make more of the ligand groups accessible for complexation. I feel that the answer lies in the influence of the water content and the plasticising effect of the salt on the polymer chains. The presence of high concentrations of sulphate in the polymer interstices will reduce the mobility of the chains, making it harder for the necessary rearrangement to occur. Hence, the reorganisation step after sulphate has entered the membrane is more likely to be the rate determining one (step (ii)a), the preferred kinetic mechanism being that from step (i) through stages (ii)a & (ii)b and finally steps (iv) & (v).

#### **4.6 CONCLUDING REMARKS.**

Considering observations made in this study and previously elsewhere on the dominating influence of anions on the physical properties of hydrogel-type polymers, it is not surprising that the kinetics for ferrous ion coordination in bipyridyl-based membranes of such polymers is also anion-dependent. The actual processes at work within the membrane have probably been over-simplified by this gross kinetic overview. With a heterogeneous, and possibly non-uniform system such as that under study here, more than one mechanistic pathway may be significant. Various mathematical treatments only show real advantages when the original data are good; the intrinsic nature of the experimental procedure for this study produced scattered data and made interpretation of the

observations difficult. The initial proposal of an *unattended* technique, although impractical at the time, would almost certainly be the way forward for further study of this system. This would require the design and manufacture of a spectrophotometric cell capable of a number of basic operations:

- (i) The cell would need to fit in place of the multicell carriage exchange on the SP8 100, and be partitioned into 4 individual compartments to allow the spectrophotometer to be programmed to read each cell in turn at designated intervals. This would generate much more data in one time period and relieve the tedium associated with the *attended* technique by automation.
- (ii) Each cell compartment would possess some sort of frame assembly for clamping the membrane in an upright and stable position, allowing access of the salt solution to both sides of the membrane.
- (iii) Finally, it must be ensured that the solutions are protected from degradation by atmospheric oxygen by an air-tight sealing mechanism. The cells would also have to be thermostated in some way to prevent heating effects from the spectrophotometer (which would also accelerate oxidation of the ferrous solution).

Figures 4.32 & 4.33 detail one such potential cell design, based very much on the ideas used for the design of the permeability cells used in Chapter Five. The cell halves could be made from Perspex as it is the visible region that is of interest, which would make fabrication much simpler. Dimensions would be such that as the carriage mechanism shuffled from one position to another, the windows marked at 1,2 3 & 4 would align with the spectrophotometer beam. In this way, four membranes could be tested at a time. Individual membrane pieces could be used, held in position by gaskets around each

**Figure 4.32: Spectrophotometer Cell Design (Oblique View)**

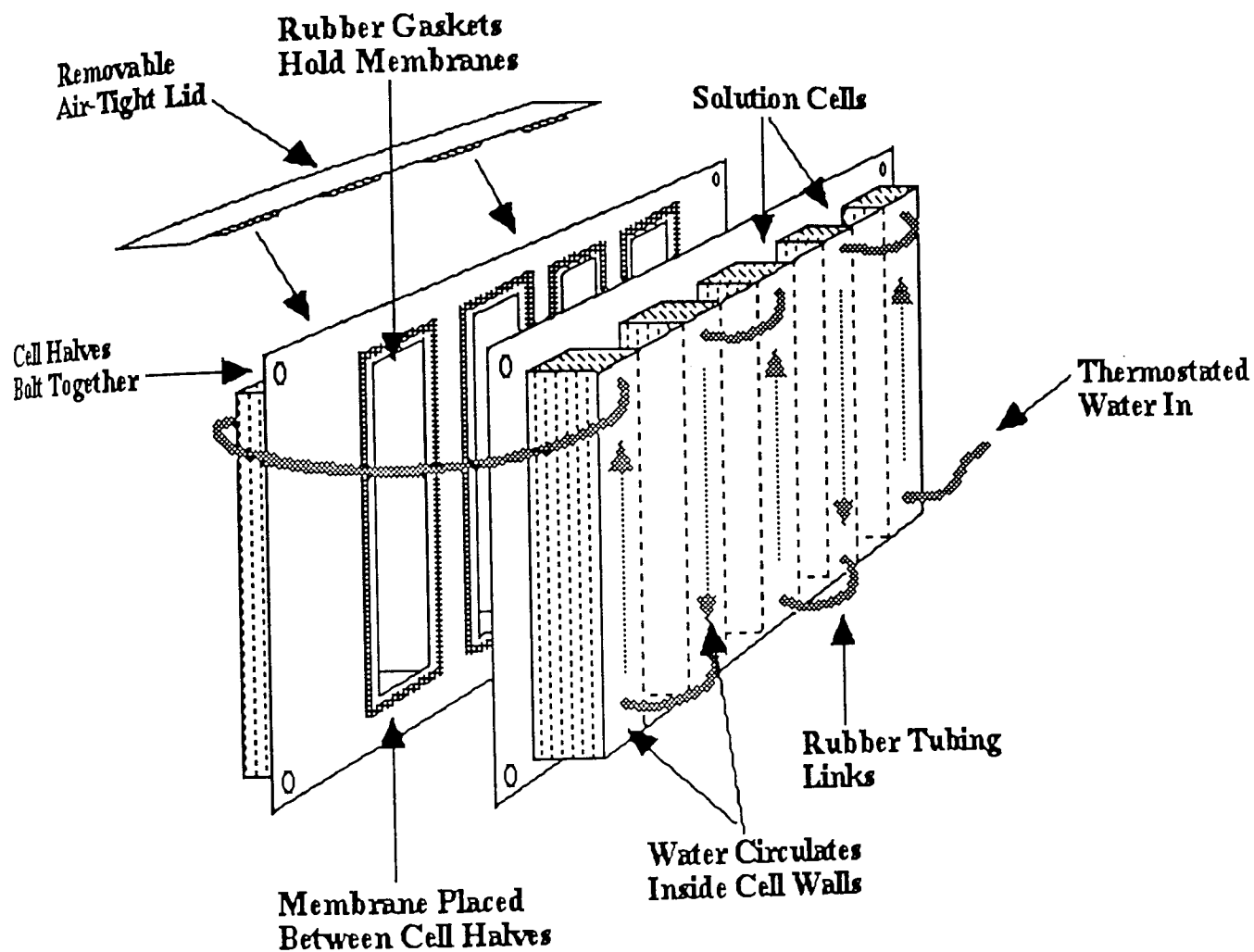
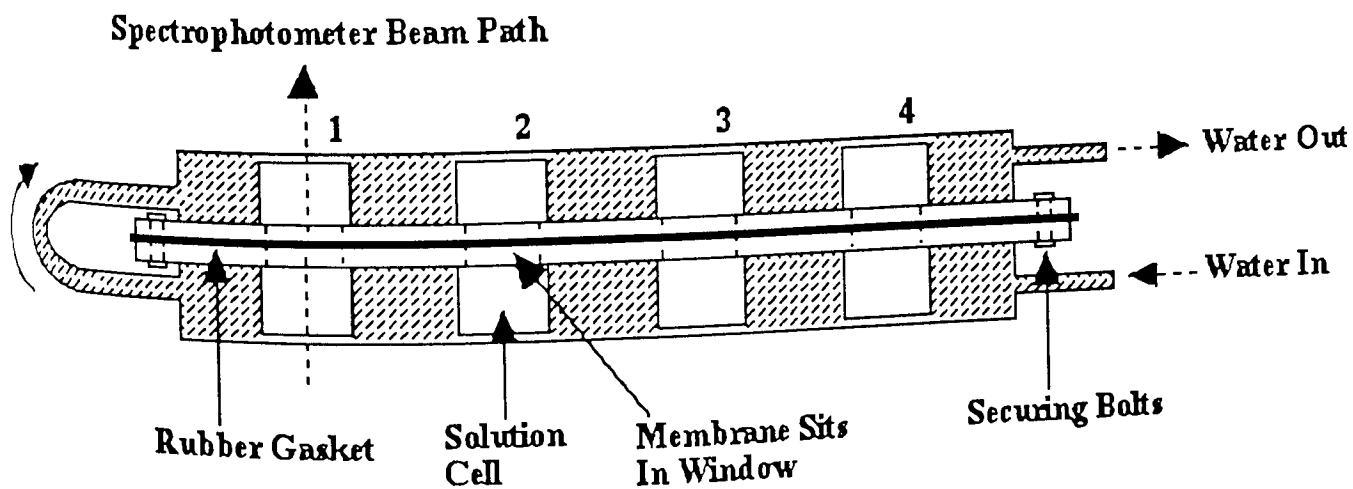


**Figure 4.33: Spectrophotometer Cell Design (Top View)**



window (Figure 4.32) or one large membrane could be fitted between the cell halves, held in place by two equivalent sized gaskets (as in the permeability cells- Figure 4.33). This, or any similar, design is likely to be dominated by problems of water-tightness.

It may prove interesting to extend the range of ferrous salts studied in order to predict more precisely the kinetic behavior of the complexation reaction. Furthermore, it would be possible to produce an analogous 1,10-phenanthroline-based membrane since there is a literature method for producing a vinyl phenanthroline <sup>175</sup>. The comparison of the kinetics of this polymer-bound species and ferrous salts with those for bipyridine would be interesting, as phenanthroline has an even greater affinity for  $\text{Fe}^{2+}$  and it is a rigidly planar ligand, whereas free bipyridyl adopts the *trans* configuration and must undergo ring-ring rotation before coordination.

Chapter Five of this study now progresses into the investigation of transition metal salt permeability through ligand-bound hydrogel membranes, with a view to using the various degrees of metal ion interaction with the ligands as a means of separating them in solution.

## **CHAPTER FIVE**

### **TRANSITION METAL ION TRANSPORT ACROSS COMPLEXING HYDROGEL MEMBRANES.**

## 5.1 INTRODUCTION.

In recent years, growing interest in membrane processes has lead to the use of such techniques as electrodialysis, Donnan dialysis and charge-coupled mobile carrier (CCMC) dialysis as a means to preconcentrate and/or separate metal ions in solution. Much of the initial work in this area has involved Donnan dialysis through liquid membrane systems. An ionic gradient across an ion-exchange membrane phase establishes a potential that drives the appropriately charged analyte from lower (sample) to higher (receiver) ionic strength ( $\mu$ ) solutions <sup>87,88</sup>. Only modest separation factors from this method has led to the incorporation of mobile carriers into the membrane phase, to aid the selective removal of ions from the sample <sup>91-93,96</sup> (Figure 5.1):

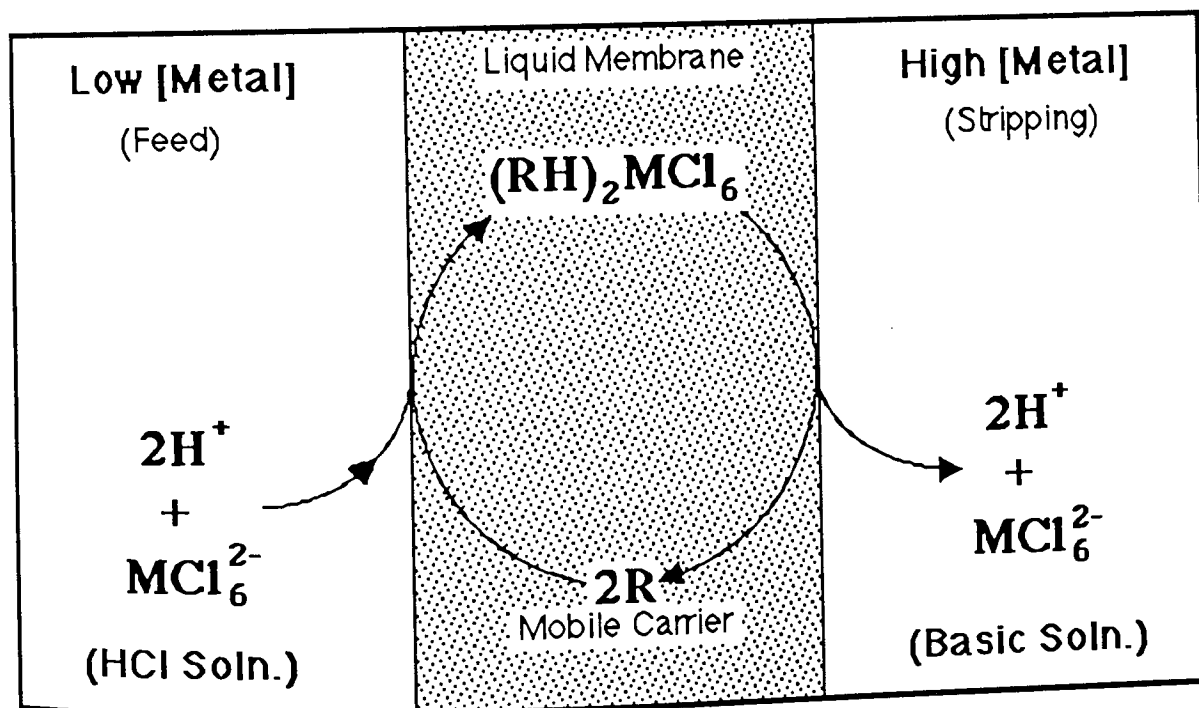


**Figure 5.1 Permeation Mechanism for CCMC Dialysis  
in a Liquid Membrane.**

A system such as that outlined in Figure 5.1 has been used to separate Pt ions as  $[\text{PtCl}_6]^{2-}$  (a species that is particularly slow in its substitution reactions), using trioctyl amine (TOA) as the carrier in a xylene membrane. The driving force in such instances

is often the pH gradient or the presence of a chelating agent such as EDTA in the stripping solution.

Severe instability of liquid membrane systems prevents large scale application of the technology and limits analytical usage. There has been some movement toward the development of polymeric membranes as substitutes for the liquid phase. Ideal conditions for Donnan-type processes require high ion-exchange capacity membranes which permit site-to-site diffusion, with cross-linking below 15% and a polymer backbone flexibility to allow a continuous polyelectrolyte network throughout the bulk of the structure <sup>89</sup>. Anion exchange membranes of 4VPy with low density polyethylene have proved useful membranes of this nature; quaternisation of the pyridine nitrogens and subsequent modification with thoron chelating agent (Arsenazo III) results in a chelating membrane <sup>105</sup>.

Hydrogel polymers are a potential starting point for chelating membranes of this sort because their physical properties are ideal and can be controlled by altering the degree of hydrophilicity and cross-link density. Osmotic forces swell the hydrogel in aqueous media causing a concomitant increase in permeant concentration, which in turn increases the mobility of polymer chain segments owing to enhanced permeant-polymer interactions <sup>176,177</sup>. The previous chapters have examined specific metal ion interactions with pyridyl- and bipyridyl-based complexing hydrogel membranes. Extending on these findings, this chapter is concerned with the application of coordinating membranes to the selective transportation and separation of transition metal ions in aqueous solution.

## 5.2 A BACKGROUND TO TRANSPORT PHENOMENA IN HYDROGEL MEMBRANES.

In order to interpret correctly the transport phenomena observed with chelating membranes, it was necessary to undertake a permeability study for transition metal ions using polyHEMA-only membranes to establish a 'base-line' that would make it possible to distinguish between effects due to ligands and those due to the hydrogel. Previous work by Hamilton <sup>29</sup> has used detailed studies of EWC, partition coefficient ( $S_m$ ), water-structuring and hydrodynamic radii to develop a model that describes the transport behavior of hydrogel membranes toward alkali and alkaline earth metal ions. He showed that the observed permeability order for cations and anions through polyHEMA membranes cannot be explained simply on the grounds of hydrodynamic size. In brief outline, anions have a dominant influence over these simple cations when considering permeability behavior. The best description of this phenomenon compares the observed permeability order of the salts with the Hofmeister (or lyotropic) series, which is an arrangement of ions according to the influence they exert on reactions in colloidal solution and on their powers of coagulation. The two are very similar, following the order:



Working on the basis that the ionic structures of the various anions influence the surrounding water to different degrees, it is thought that small ions and multivalent ions cause electrostriction of water molecules beyond the primary hydration shell of the ion, inducing long-range ordering and effectively increasing the viscosity of the water. Thus, ions such as  $\text{SO}_4^{2-}$  are classed as 'structure-makers' and consequently permeate more slowly. Large monovalent ions such as  $\text{ClO}_4^-$  are 'structure-breakers' because they

generate weaker electrostatic fields, leaving much of the bulk water unperturbed and 'fluid', allowing faster permeation rates. These types of argument can be used to explain the high permeation rates not obviously explicable on the basis of size.

The model briefly detailed in this section provides sufficient background concerning transport properties through polyHEMA membranes. It is not my intention in this chapter to extend the work on transport phenomena in polyHEMA membranes to include transition metal salts, but rather to build a foundation on which to discuss the influence of ligands on TM transport in these systems.

### **5.3 THE COLLECTION OF PERMEABILITY DATA.**

The two types of permeability apparatus used to study single and mixed metal ion solutions are detailed in Chapter 2, sections 2.10.1 and 2.10.3. Both techniques provide two important pieces of information:

- (i) The 'lag-time' or induction period is a measure of how long it takes for the permeant to be transported through the membrane and appear on the low concentration side. This parameter is especially relevant in the study of the chelating systems, as it is an indication of the extent of interaction of the permeating ions with the ligands.
- (ii) The permeability coefficient ( $P_c$ ) is a quantity that allows comparison of the *rate* at which different permeants traverse a membrane. It can be obtained from the gradient of the  $[M^{2+}]_{\text{low side}}$  versus time plot, by implementation of equations 5.1 & 5.2 (overleaf) which have been derived previously from Fick's first law of diffusion in solution (equation 1.1) 29,85,86.

$$P_c = F \times \frac{L}{A C_L} \quad (5.1)$$

$$F = G \times V \quad (5.2)$$

$P_c$  = Permeability Coefficient

$F$  = Flow rate

$L$  = Membrane thickness

$A$  = cross-sectional area

$C_L$  = Conc. of low side

$G$  = Gradient of conc. vs time  
plot

$V$  = Volume of low conc. cell  
half

### **5.3.1 Consistency Between Permeability Runs and Rigs.**

The conductivity-based rig (Chapter 2, section 2.10.3) has been well characterised<sup>29</sup> and shown to produce reproducible results within  $\pm 2.5\%$  between runs, as long as both the high and low sides of the cell are stirred. Equally important in this particular study is the ability to compare runs performed on the conductivity rig with those obtained by the atomic absorption method. Permeation of 0.25M  $\text{CaCl}_2$  through polyHEMA as determined by the conductivity technique yielded a permeability coefficient ( $P_c$ ) of  $2.83 \times 10^{-6} \text{ cm}^2\text{min}^{-1}$ . This is in excellent agreement with the  $P_c$  value of  $2.75 \times 10^{-6} \text{ cm}^2\text{min}^{-1}$  produced by the AAS approach. Thus, the two rigs have a reproducibility of  $\pm 2.5\%$  and a consistency between rigs around  $\pm 3\%$ .

## **5.4 PERMEATION OF TRANSITION METAL IONS THROUGH POLYHEMA MEMBRANES.**

In order to observe the effects of the transition metal cation on permeation behavior, a selection of 'AnalR' (B.D.H.) chloride salts were used at 0.25M concentration. The original list included  $\text{FeCl}_2$ , but this salt proved to be unsuitable; it was used in a permeability run but was found to be prone to oxidation to  $\text{Fe}^{3+}$  producing a 'rust-like' precipitate in the equipment (cf. Chapter 4) and raising the pH slightly (which would itself have a significant effect on transport as the membranes are pH sensitive).

Therefore, for simplicity the range of metal chlorides was restricted to  $\text{Ca}^{2+}$ ,  $\text{Mn}^{2+}$ ,  $\text{Co}^{2+}$ ,  $\text{Ni}^{2+}$  and  $\text{Cu}^{2+}$ , and Figure 5.2 shows the permeation data used to calculate the  $P_c$  for each salt.

A range of cobalt salts were available in order to investigate the effect of the anion on transport behavior. The hexafluorophosphate salt was not commercially available and was therefore synthesised by the procedure outlined in section 2.12, Chapter Two. Figure 5.3 shows the permeation data used to calculate the  $P_c$  for the  $\text{SO}_4^{2-}$ ,  $\text{Cl}^-$ ,  $\text{NO}_3^-$ ,  $\text{SCN}^-$ ,  $\text{ClO}_4^-$  and  $\text{PF}_6^-$  salts of cobalt. Table 5.1 contains all of the collected permeation data for various transition metal salts through polyHEMA membranes. Considering the previous findings discussed earlier in section 5.2, there are no great inconsistencies that would suggest the proposed theory did not hold in this case. Figure 5.2 and data for other transition metal salt series from Table 5.1 clearly show that  $P_c$  for the various metal ions varies according to the order:

$$\text{Ca}^{2+} > \text{Cu}^{2+} > \text{Ni}^{2+} > \text{Mn}^{2+} \geq \text{Co}^{2+}$$

This is also the order in which the TM salts influence the equilibrium water content of the membrane. The variation in degree of hydration relies upon the extent of interaction between the permeant ions and water; this will subsequently be related to the extent to which the salt partitions into the membrane phase i.e. the partition coefficient ( $S_m$ ). The various ions swell or de-swell the hydrogel as indicated by the variations in membrane thickness listed in Table 5.1. The effect is demonstrated more dramatically by comparing changes in anion. Equation 5.3 shows there is a relationship between the partition and permeability coefficients,  $S_m$  and  $P_c$ , involving the *diffusivity* of the permeant ( $D$ ):

$$P_c = S_m.D \quad (5.3)$$

<u>T.M. Salt</u>	<u>Concentration</u> (M)	<u>E.W.C.</u> (with TM present)	<u>Thickness</u> (cm)	<u>Gradient</u> (mM min <sup>-1</sup> )	<u>Time Lag</u> (mins)	<u>Permeability Coeff.</u> (cm <sup>2</sup> min <sup>-1</sup> )
CuSO <sub>4</sub>	0.25	32.6	0.037	2.76e-8	>50	6.42e-8
CuCl <sub>2</sub>	0.25	34.1	0.041	9.29e-7	32	2.4e-6
Cu(NO <sub>3</sub> ) <sub>2</sub>	0.25	38.0	0.0395	2.3e-6	25	5.71e-6
Cu(ClO <sub>4</sub> ) <sub>2</sub>	0.25	45.2	0.042	3.44e-5	~5	9.08e-5
CoSO <sub>4</sub>	0.25	29.5	0.038	1.64e-8	~60	3.92e-8
CoCl <sub>2</sub>	0.25	30.7	0.04	5.57e-7	23	1.38e-6
Co(NO <sub>3</sub> ) <sub>2</sub>	0.25	36.9	0.04	1.5e-6	30	3.76e-6
Co(SCN) <sub>2</sub>	0.25	41.1	0.0425	5.5e-6	15	1.49e-5
Co(ClO <sub>4</sub> ) <sub>2</sub>	0.25	43.4	0.043	6.2e-6	10	1.64e-5
Co(PF <sub>6</sub> ) <sub>2</sub>	0.25	46.1	0.045	8.2e-6	<5	2.32e-5
NiSO <sub>4</sub>	0.25	32.3	0.038	2.29e-8	>50	5.47e-8
NiCl <sub>2</sub>	0.25	33.7	0.039	7.89e-7	37	1.93e-6
Ni(NO <sub>3</sub> ) <sub>2</sub>	0.25	38.0	0.041	1.9e-6	28	4.9e-6
Ni(ClO <sub>4</sub> ) <sub>2</sub>	0.25	44.2	0.042	7.1e-6	7	1.87e-5
Ni(PF <sub>6</sub> ) <sub>2</sub>	0.25	49.6	0.0485	1.51e-5	4	4.29e-5
MnCl <sub>2</sub>	0.25	33.4	0.039	6.1e-7	23	1.5e-6
CaCl <sub>2</sub>	0.25	35.8	0.041	1.17e-6	5	2.83e-6

**Table 5.1 Permeability Data for Selected Metal Salts Through PolyHEMA Membranes.**

Figure 5.2: Permeability of Metal Chloride Salts through PolyHEMA.

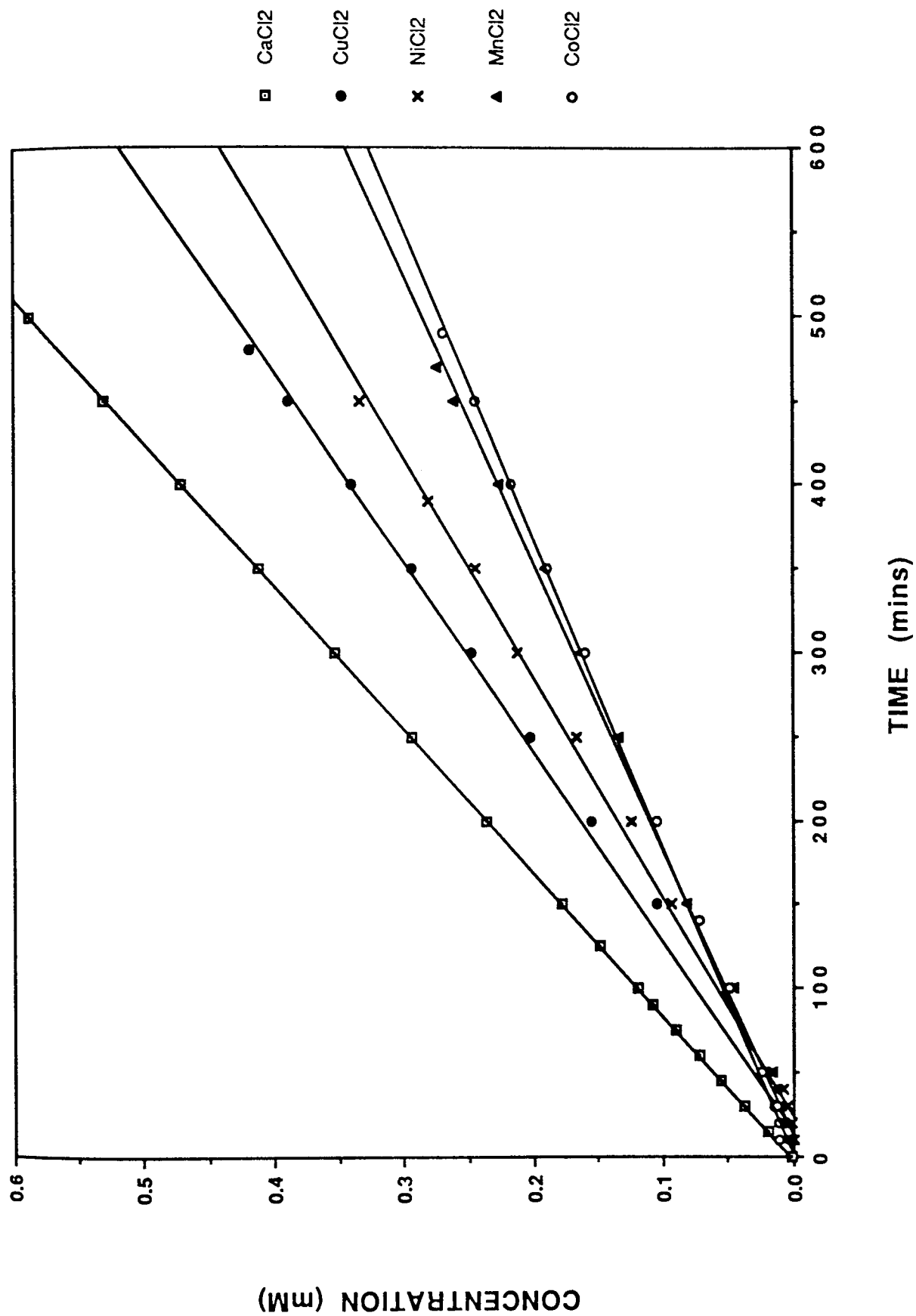
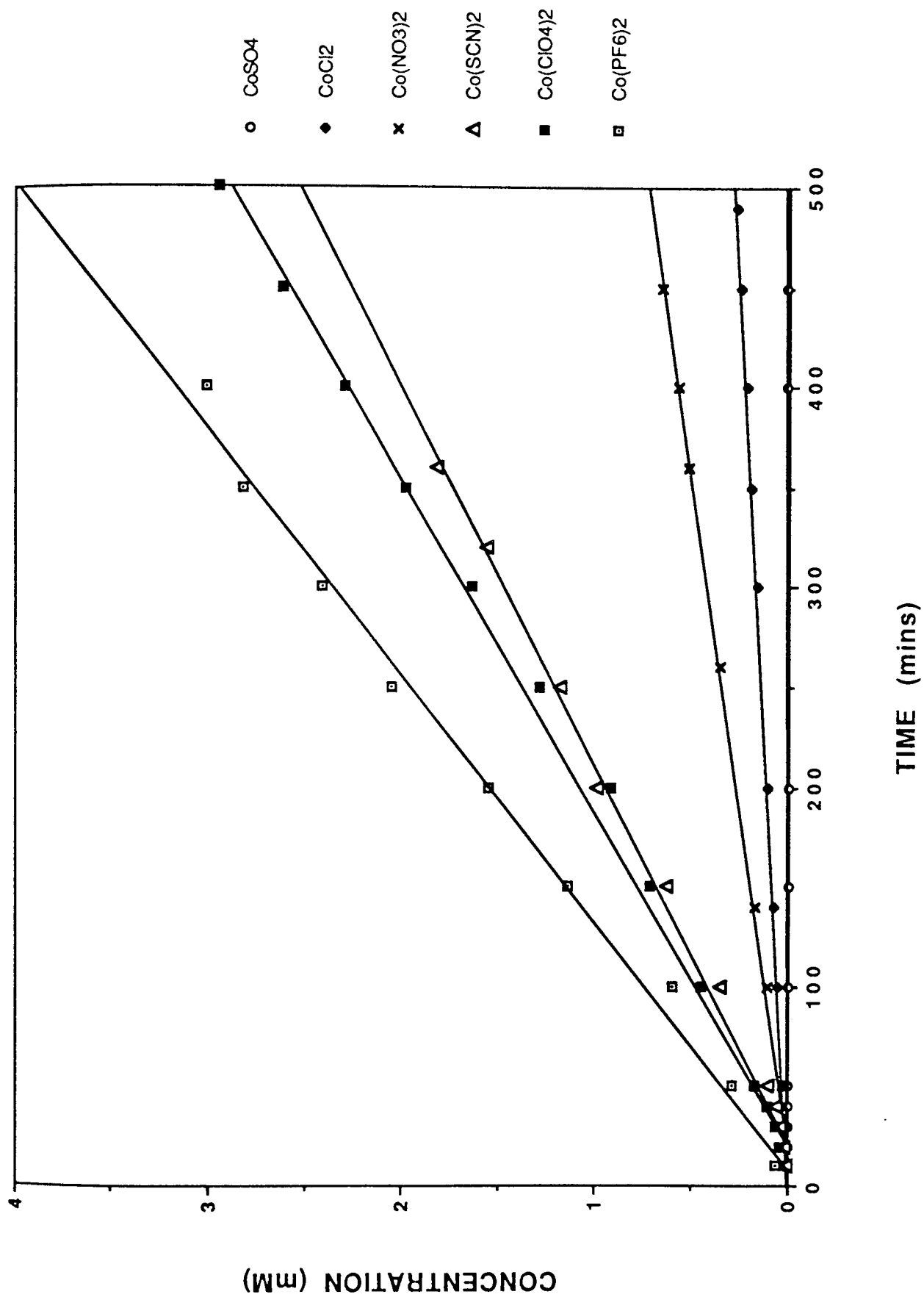
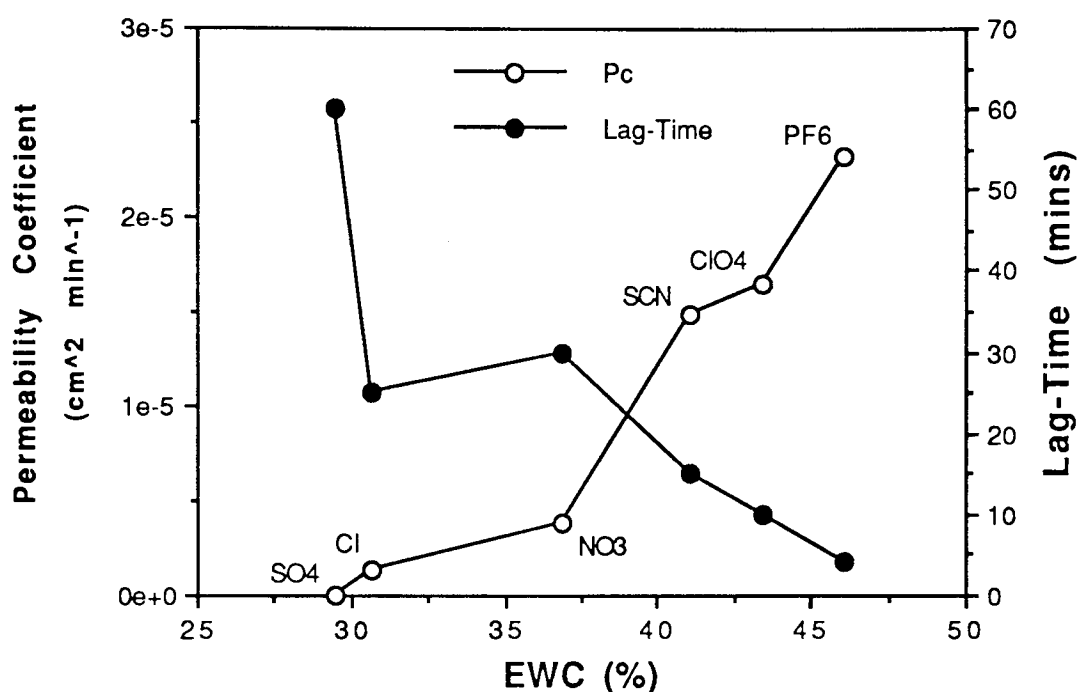


Figure 5.3: Permeability of Cobalt Salts through PolyHEMA



Thus, there is indeed a correlation between the EWC imposed by the salt and its permeability through the polymer. The Lag-Time is the time it takes for a permeant to appear on the low concentration side of the membrane. This too can be thought of as a function of EWC and permeability coefficient (Figure 5.4):



**Figure 5.4 Relationship Between EWC,  $P_c$  & Lag-Time for Co(II) Salts.**

However, equation 5.3 shows us that there are in fact two components to the permeability process: the solubilisation of the salt into the polymer phase is a thermodynamically-controlled stage (expressed in terms of  $S_m$ ), followed by a kinetically-controlled transport step (represented by  $D$ ). Previous work <sup>29</sup> has shown that if the effect of salt dissolution is taken into account, diffusion across the membrane can demonstrate *size* effects when the hydrated size of the cation is larger than that of the counter anion. Table 5.2 below lists the Crystal, Stoke's and Hydrodynamic Radii of some ions. This clearly shows that all of the cations under study here have larger Hydrodynamic and Stoke's radii than the common

anions used. However, what should be remembered when attempting to interpret the permeability data obtained from ligand-modified membranes, is that normally transition metal salt solutions are used at 0.25M concentrations *with respect to the metal*. This means that, with the exception of sulphate, the counter-anions are present at 0.5M concentrations. At these levels the anions will have significant influence on the transport processes.



Aston University

Content has been removed for copyright reasons

**Table 5.2 Crystal, Stoke's & Hydrodynamic Radii for Some Ions.**<sup>(178)</sup>

## **5.5 PERMEATION OF TRANSITION METAL IONS THROUGH LIGAND-MODIFIED HYDROGEL MEMBRANES.**

A series of experiments was performed to investigate the influence of immobilised ligand groups within the hydrogel membrane on the permeability of a series of transition metal chloride salts. All permeability runs were carried out as before, at 25°C and using 0.25M salt concentration in the high side. The membranes chosen for the initial study were 2% by weight copolymers of HEMA:Vinylpyridine and HEMA:Vinylbipyridine; this particular weight percentage was thought to be low enough not to alter the properties of the hydrogel but high enough to allow the detection of a significant effect on the permeability

characteristics.

Tables 5.3 & 5.4 list the transport data for the metal salts through the pyridine and bipyridine-based membranes respectively. Some features are clear. The permeability coefficient varies with metal ion type and is proportional to the concentration of the metal, but independent of % ligand loading in the membrane. The most striking difference between these data and those for polyHEMA-only membranes is the presence of a significant induction period or 'lag-time' associated with the ligand-based systems (Figures 5.5 & 5.6). A small lag-time of between 5 and 30 minutes is seen in the transport data for chloride salts through polyHEMA-only membranes (Table 5.1), and is probably a consequence of the differing rates at which the metal ions permeate. However, the time-lag now observed for the coordinating membranes must be at least a two component parameter. It is affected both by the rate at which the salt permeates, and also by the extent of interaction between the metal ions and the ligand groups within the membrane. The permeability coefficients for each salt were calculated by a least-squares analysis of the data *after the point of inflection* i.e. after the induction period is over. Here we define the lag-time as the intercept of the straight line fit with the concentration equals zero axis

A number of experiments were performed, firstly involving different salt and ligand concentrations, and then competitive transport studies using precomplexed and binary salt solutions, in order to gain a fuller appreciation of the processes occurring within the membrane. The following sections summarise the effect of these parameter changes on the lag-times and permeability coefficients for particular ligand-salt combinations. These observations provide the basis on which the proposed mechanisms are discussed.

<u>% Ligand</u> (by wt.)	<u>T.M. Salt</u>	<u>Concentration</u> (M)	<u>E.W.C.</u> (with TM present)	<u>Thickness</u> (cm)	<u>Gradient</u> (mM min <sup>-1</sup> )	<u>Time Lag</u> (mins)	<u>Permeability Coeff.</u> (cm <sup>2</sup> min <sup>-1</sup> )
2% VPy	CuCl <sub>2</sub>	0.25	38.0	0.041	1.88e <sup>-6</sup>	252	4.85e <sup>-6</sup>
2% VPy	CoCl <sub>2</sub>	0.25	36.9	0.04	6.67e <sup>-7</sup>	176	1.68e <sup>-6</sup>
2% VPy	NiCl <sub>2</sub>	0.25	37.4	0.039	1.33e <sup>-6</sup>	216	3.26e <sup>-6</sup>
2% Vpy	MnCl <sub>2</sub>	0.25	33.9	0.039	7.81e <sup>-7</sup>	48	1.91e <sup>-6</sup>
2% Vpy	CaCl <sub>2</sub>	0.25	35.7	0.041	8.57e <sup>-7</sup>	50	3.04e <sup>-6</sup>
0.5% Vpy	CuCl <sub>2</sub>	0.25	36.0	0.041	1.73e <sup>-6</sup>	102	4.46e <sup>-6</sup>
1% Vpy	CuCl <sub>2</sub>	0.25	36.1	0.04	1.76e <sup>-6</sup>	158	4.43e <sup>-6</sup>
2% VPy	CuCl <sub>2</sub>	0.25	38.0	0.041	1.88e <sup>-6</sup>	252	4.85e <sup>-6</sup>
4% Vpy	CuCl <sub>2</sub>	0.25	39.9	0.041	1.54e <sup>-6</sup>	354	3.97e <sup>-6</sup>
0.5% Vpy	CuCl <sub>2</sub>	0.05	-	0.0395	1.11e <sup>-7</sup>	250	1.38e <sup>-6</sup>
0.5% Vpy	CuCl <sub>2</sub>	0.1	-	0.04	3.13e <sup>-7</sup>	190	1.97e <sup>-6</sup>
0.5% Vpy	CuCl <sub>2</sub>	0.175	-	0.04	8.93e <sup>-7</sup>	120	3.21e <sup>-6</sup>
0.5% Vpy	CuCl <sub>2</sub>	0.25	36.0	0.041	1.73e <sup>-6</sup>	102	4.46e <sup>-6</sup>

**Table 5.3: Permeability of Selected Metal Salts through VinylPyridine-Based Membranes.**

<u>% Ligand</u> (by wt.)	<u>T.M. Salt</u>	<u>Concentration</u> (M)	<u>E.W.C.</u> (with TM present)	<u>Thickness</u> (cm)	<u>Gradient</u> (mM min <sup>-1</sup> )	<u>Time Lag</u> (mins)	<u>Permeability Coeff.</u> (cm <sup>2</sup> min <sup>-1</sup> )
2% VBipy	CuCl <sub>2</sub>	0.25	34.2	0.041	1.04e <sup>-6</sup>	220	2.68e <sup>-6</sup>
2% VBipy	CoCl <sub>2</sub>	0.25	34.6	0.0395	3.47e <sup>-7</sup>	257	8.62e <sup>-7</sup>
2% VBipy	NiCl <sub>2</sub>	0.25	33.8	0.04	4.69e <sup>-7</sup>	275	1.18e <sup>-6</sup>
2% VBipy	MnCl <sub>2</sub>	0.25	32.4	0.039	6.94e <sup>-7</sup>	246	1.7e <sup>-6</sup>
0.5% VBipy	CuCl <sub>2</sub>	0.25	34.4	0.04	1.2e <sup>-6</sup>	78	3.02e <sup>-6</sup>
1% VBipy	CuCl <sub>2</sub>	0.25	34.4	0.04	1.04e <sup>-6</sup>	125	2.62e <sup>-6</sup>
2% VBipy	CuCl <sub>2</sub>	0.25	34.2	0.041	1.04e <sup>-6</sup>	220	2.68e <sup>-6</sup>
4% VBipy	CuCl <sub>2</sub>	0.25	35.9	0.041	-	-	-

**Table 5.4: Permeability of Selected Metal Salts through VinylBipyridine-Based Membranes.**

Figure 5.4: Permeability of Metal Chlorides through

VinylBipyridine Copolymer Membranes.

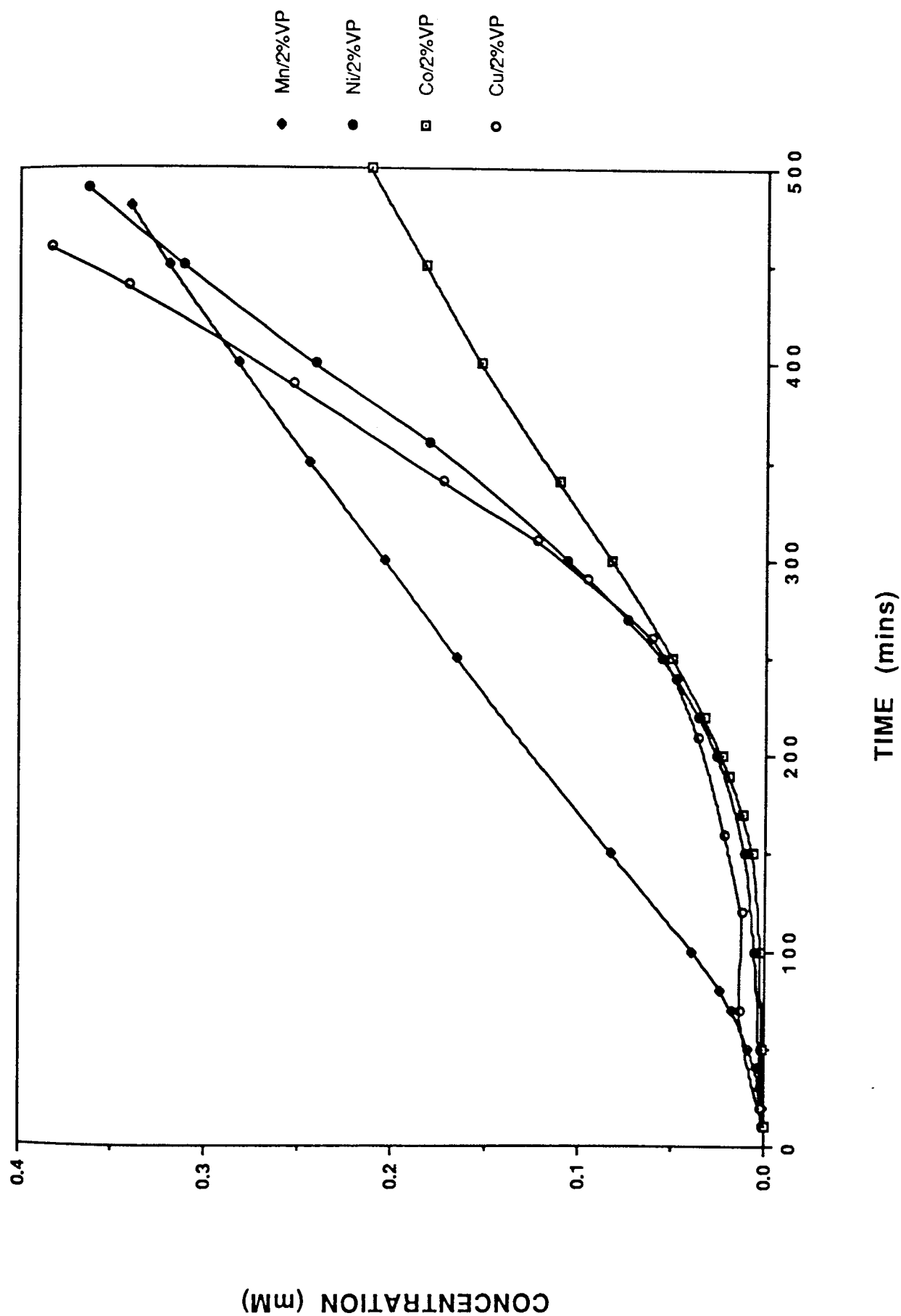
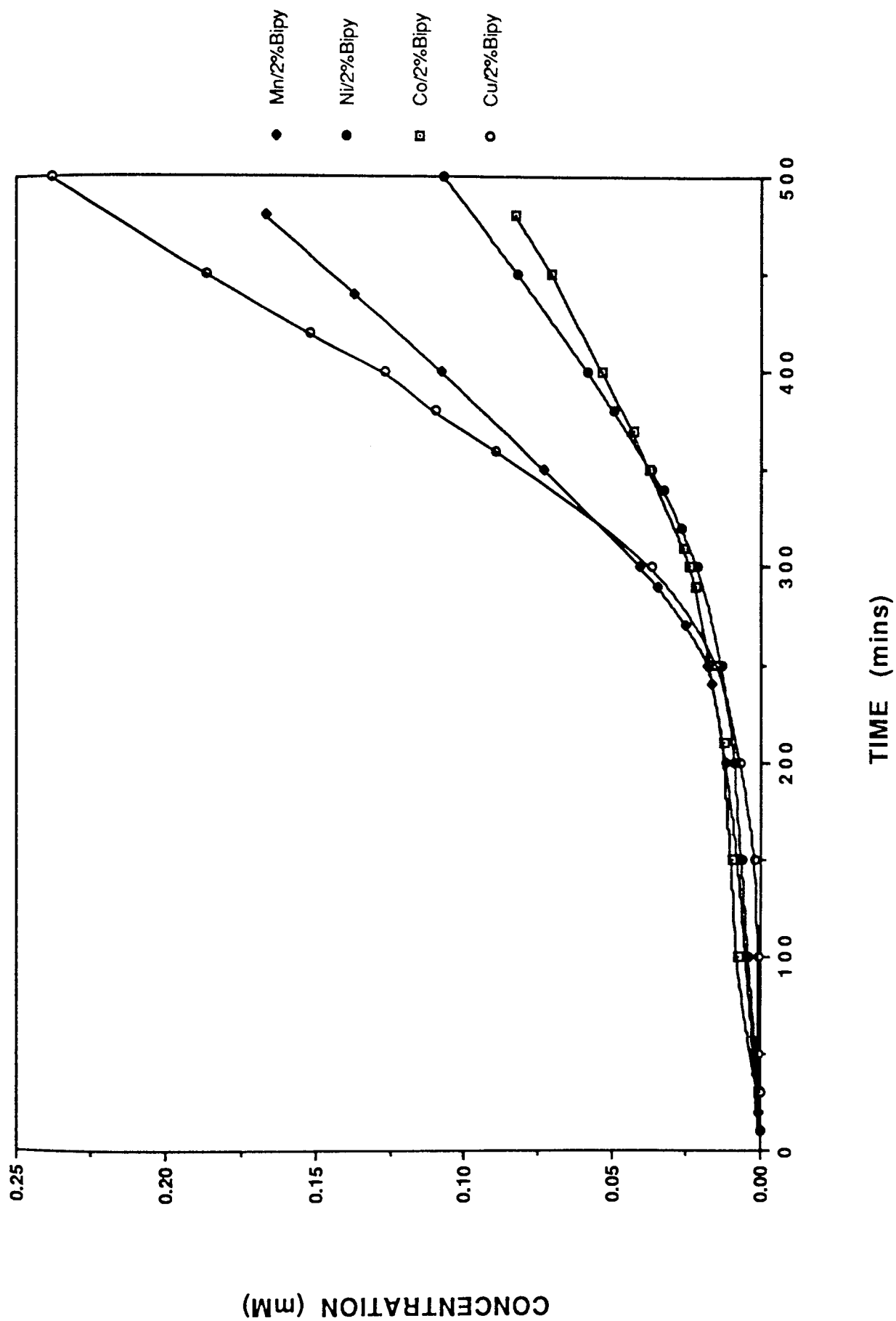


Figure 5.5: Permeability of Metal Chlorides through

VinylBipyridine Copolymer Membranes.



### 5.5.1 Investigation of the Lag-Time Phenomenon.

It has been demonstrated previously by spectroscopic methods that if a coordinating membrane is swollen with a high concentration of a transition metal salt solution, a large proportion of the ligands are present as *mono*-type complexes, i.e. the membrane is 'saturated'. If we assume that the immobilised ligands interact with metal ions to produce complexes of similar stability to their 'free' analogues and that comparative time scales are such that local equilibria apply, by a simple calculation it can be shown that for the reaction:



95% completion occurs when:

$$K_1 = \frac{[ML]}{[M][L]} = \frac{95}{(5) 0.25} \quad (5.4)$$

Therefore, the saturation condition is essentially satisfied for any metal-ion-ligand pairing which has a stability constant in excess of approximately  $80 \text{ M}^{-1}$ . If we assume similar values for the stability constants of free ligands in aqueous solution and those for the systems synthesised here, we can estimate the levels of saturation achieved with different metal ions.  $K_1 \geq 80 \text{ M}^{-1}$  is satisfied for any of the bipyridyl combinations, but is true only for  $\text{Cu(II)}$  &  $\text{Ni(II)}$  in the pyridyl system (complexation by  $\text{Co(II)}$  &  $\text{Mn(II)}$  would be only 80% & 25% complete respectively).

It is reasonable to expect that the use of a massive excess of permeating salt solution (0.25M) will result mainly in 1:1 interactions between ligands and metal ions. If this is so, then one might seek a relationship between the lag-time observed by the permeating species

and the stability constant for the addition of the first ligand to that ion, i.e.  $\log(K_1)$  (see equation (5.5), Table 5.5). Figure 5.7 depicts such a plot for the pyridyl-system. The observed correlation between the  $\log(K_1)$  and lag-time values shown by each of the metal ions supports this idea of *mono*-complex formation; with the lag-time being controlled by equilibrium parameters, rather than by the rate of dissociation of the complex.

A similar comparison plot of  $\log(K_1)$  and lag-times for the bipyridyl-system does not show such good correlation (Table 5.5). The best comparison in this instance is that between  $\log(K_3)$  and the observed lag-time (Figure 5.8). However, it is unlikely given the massive excess of metal ions present in the system, that the lag-time for the bipyridyl membranes is a consequence of the formation of *tris*-type cross-linking complexes. As we have seen in Chapter Four, only in the case of  $\text{Fe}(\text{II})$  is the value of  $\log(K_3)$  large enough to enforce *tris*-complex formation in the presence of such a large metal:ligand ratio.

For pyridine complexes with a range of metal ions, the variations in  $K_1$  are mirrored by the variations in  $K_2$ ,  $K_3$  etc., where these have been evaluated. Therefore, for the pyridyl-membranes, the pattern seen for the variation of  $K_1$  with metal (II) ion does not conclusively prove that the lag-time is determined by the formation of the *mono*-complex. For the bipyridyl-membranes a correlation of lag-time with a set of  $K$  values is less clear cut. It is probably true to say that for polymer-supported ligands in general, there will be new steric factors which will affect the magnitude of the stability constants, and it is therefore wrong to assume that complex formation will necessarily resemble that for the same species in free solution. Thus, because of steric features,  $K_1$  for the polymer might closely parallel  $K_i$  for the free ligands in solution, where  $i > 1$ .

T.M. Salt. (0.25M)	Membrane Type	P <sub>c</sub> (cm <sup>2</sup> min <sup>-1</sup> )	Lag-Time. (mins)	Stability Constants.							
				(logK <sub>1</sub> )	(logK <sub>2</sub> )	(logK <sub>3</sub> )	(logK <sub>4</sub> )	(logβ <sub>2</sub> )	(logβ <sub>3</sub> )	(logβ <sub>4</sub> )	(Ref.)
CuCl <sub>2</sub>	VPy	4.85e-6	252	2.52	1.86	1.31	0.85	4.38	5.69	6.54	(179)
NiCl <sub>2</sub>	VPy	3.26e-6	216	1.78	1.05	0.31	-	2.83	3.14	-	(179)
CoCl <sub>2</sub>	VPy	1.68e-6	176	1.14	0.40	-	-	1.54	-	-	(179)
MnCl <sub>2</sub>	VPy	1.91e-6	48	0.14	-	-	-	-	-	-	(179)
CuCl <sub>2</sub>	VBipy	2.68e-6	220	8.1	5.5	3.4	-	13.6	17.0	-	(52)
NiCl <sub>2</sub>	VBipy	1.18e-6	275	7.1	6.8	6.2	-	13.9	20.2	-	(52)
CoCl <sub>2</sub>	VBipy	8.62e-7	257	5.7	5.6	4.8	-	11.2	15.9	-	(52)
MnCl <sub>2</sub>	VBipy	1.7e-6	246	2.6	2.0	1.0	-	4.6	5.6	-	(52)

**Table 5.5 Permeation Data for Ligand-Based Membranes & Stability Constant Data for the Free Ligands.**

The stability constants quoted are those for the step-wise addition of *free* ligand to metal ion (in solution) as given by the expressions:

$$\left\{ \begin{array}{l} K_1 = \frac{[M^{2+}(L)]}{[M^{2+}][L]}, K_2 = \frac{[M^{2+}(L)_2]}{[M^{2+}(L)][L]}, K_3 = \frac{[M^{2+}(L)_3]}{[M^{2+}(L)_2][L]} \dots etc. \end{array} \right\} \quad (5.5)$$

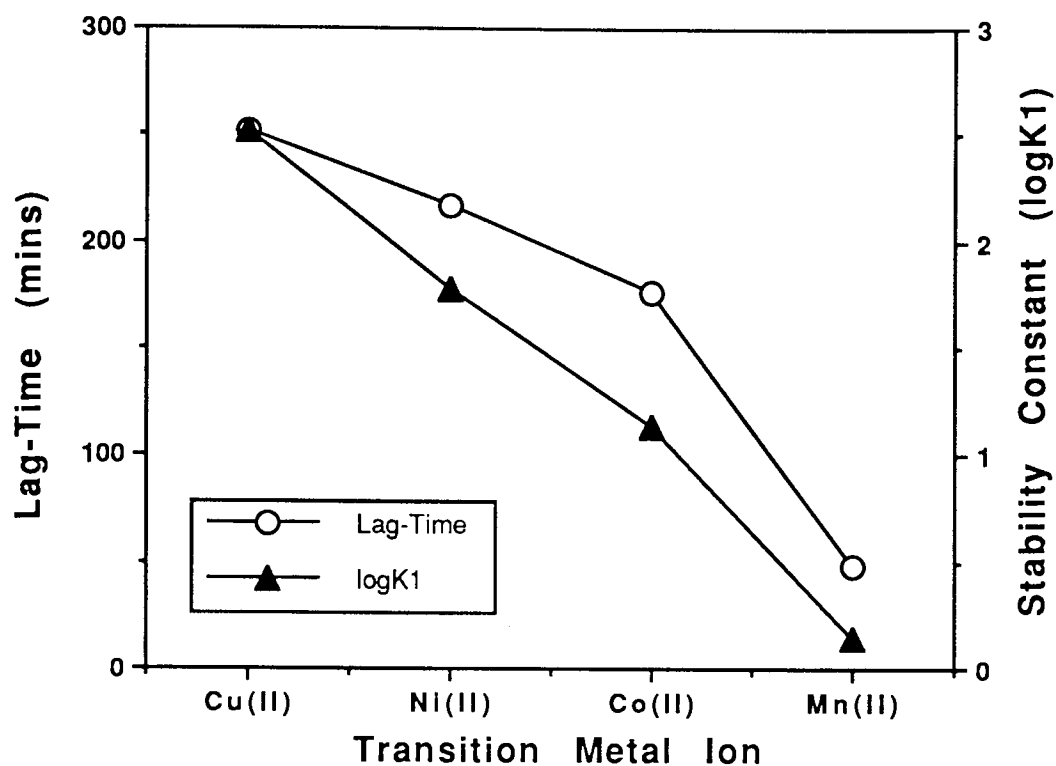


**Figure 5.7 Relationship Between Lag-Times through Vinyl-Pyridine Copolymer Membranes and  $\log K_1$  Stability Constant for Free Complex.**

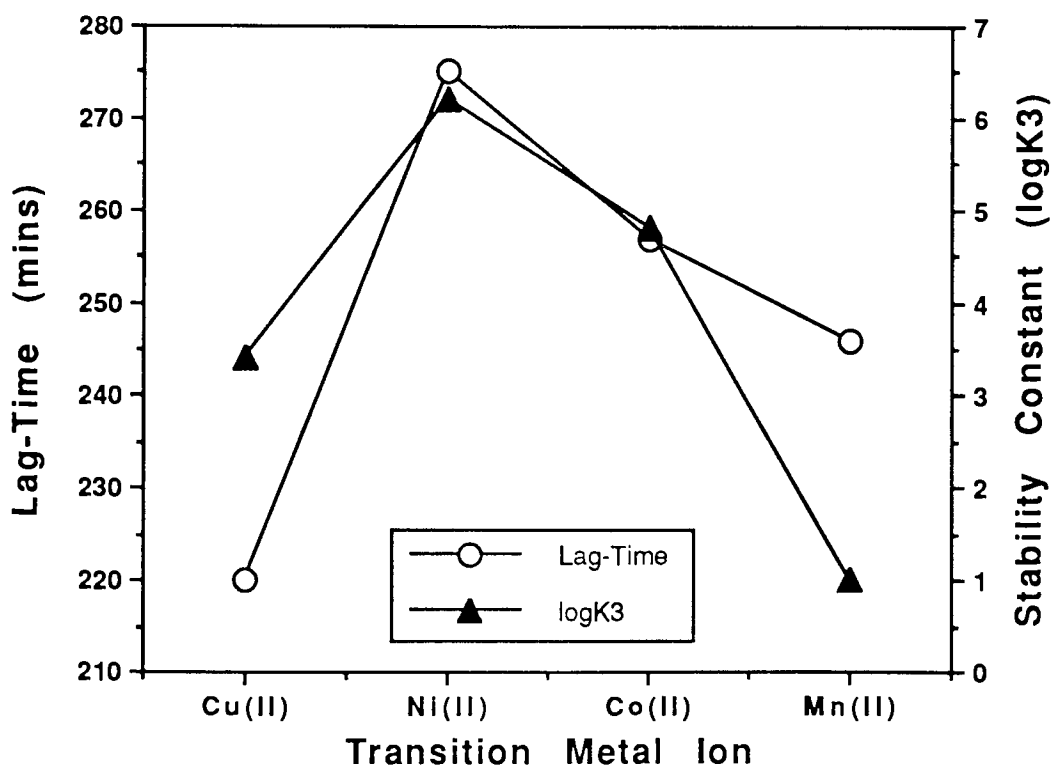


**Figure 5.8 Relationship Between Lag-Times through Vinyl-Bipyridine Copolymer Membranes and  $\log K_3$  Stability Constant for Free Complex.**

The basic idea of relating the extent of metal-ligand interaction to the time it takes for that metal species to permeate across a membrane containing those ligands, provides a useful entry to the interpretation of transport data. However, closer examination of the data in Tables 5.3 & 5.4 reveals an additional trend in lag-times for the various metal ions. Figure 5.9 depicts the relationship between the equilibrium water content (EWC) imposed by the salt on a 2% pyridyl-based membrane, and the lag-times observed for each particular species:

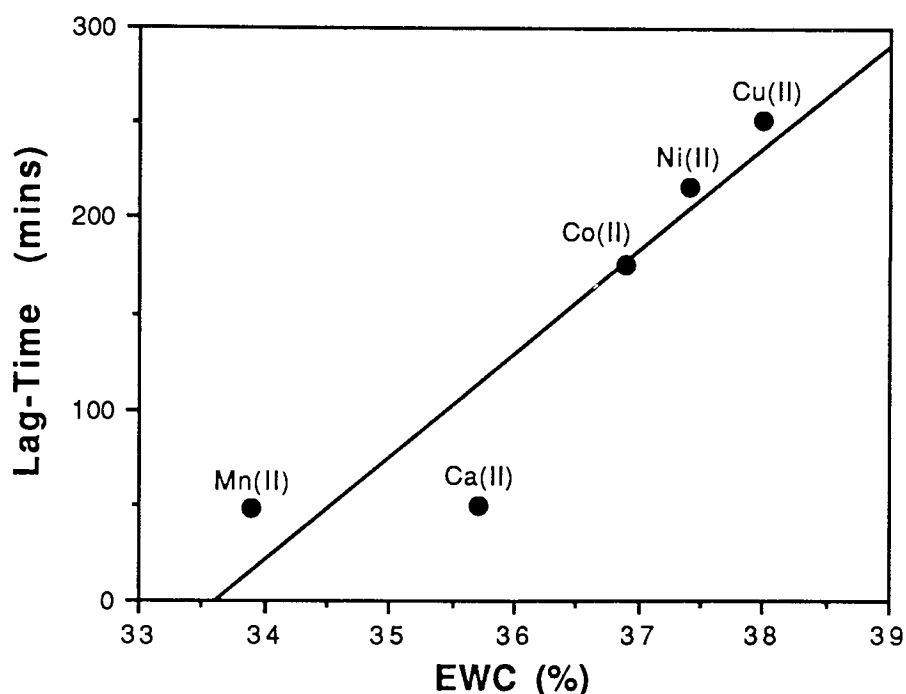


**Figure 5.9 Relationship Between EWC & Lag-Time for Various Metal Chlorides.**

Another relationship, between EWC after metal ion saturation and the % VPy within the membrane, is discussed in more detail in section 5.5.3. There are no such comparable effects for the bipyridyl-based systems, and this might point towards the two ligands having different modes of interaction within the polymeric environment. This possibility is reviewed more thoroughly later on in this chapter.

### 5.5.2 Effect of Salt Concentration on Membrane Transport Properties.

In order to guarantee the observation of any effects of changing salt concentration, it was thought best to use a 0.5% Vinylpyridine-based copolymer membrane and  $\text{CuCl}_2$  (the fastest permeating salt) for this experiment. Figure 5.10 shows the resulting transport data:

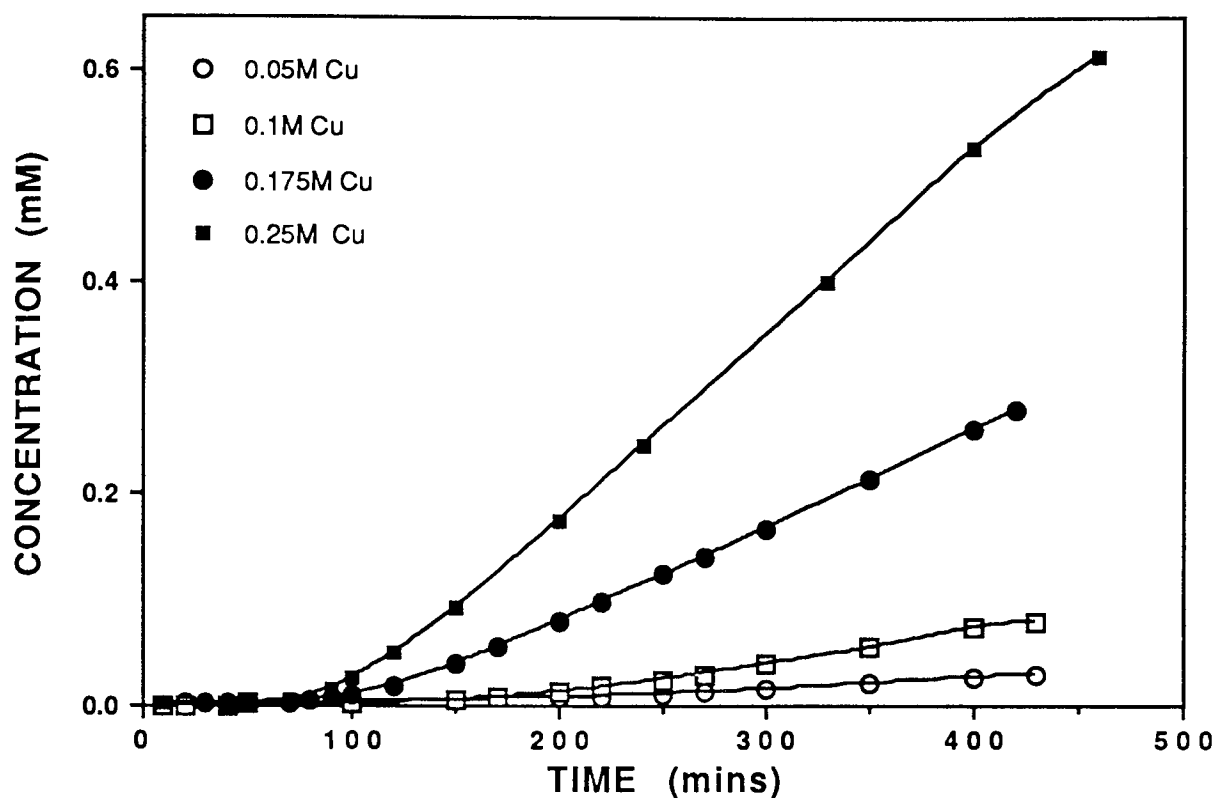


**Figure 5.10 Effect of [Ligand] on  $\text{CuCl}_2$  Transport through HEMA:VPy Copolymer Membranes.**

Table 5.3 contains the lag-time and permeability coefficient data for this series of experiments. Since the definition of  $P_c$  includes a term for concentration of permeating species (equation 5.1), it is no surprise to see the value for  $P_c$  dropping with decreasing concentration of salt. Similarly, as concentration of metal ions decreases, not only will the flux of ions into the membrane be reduced, but also it will take longer to saturate the ligand groups. Therefore, the observed lag-time period increases as a function of decreasing the salt concentration.

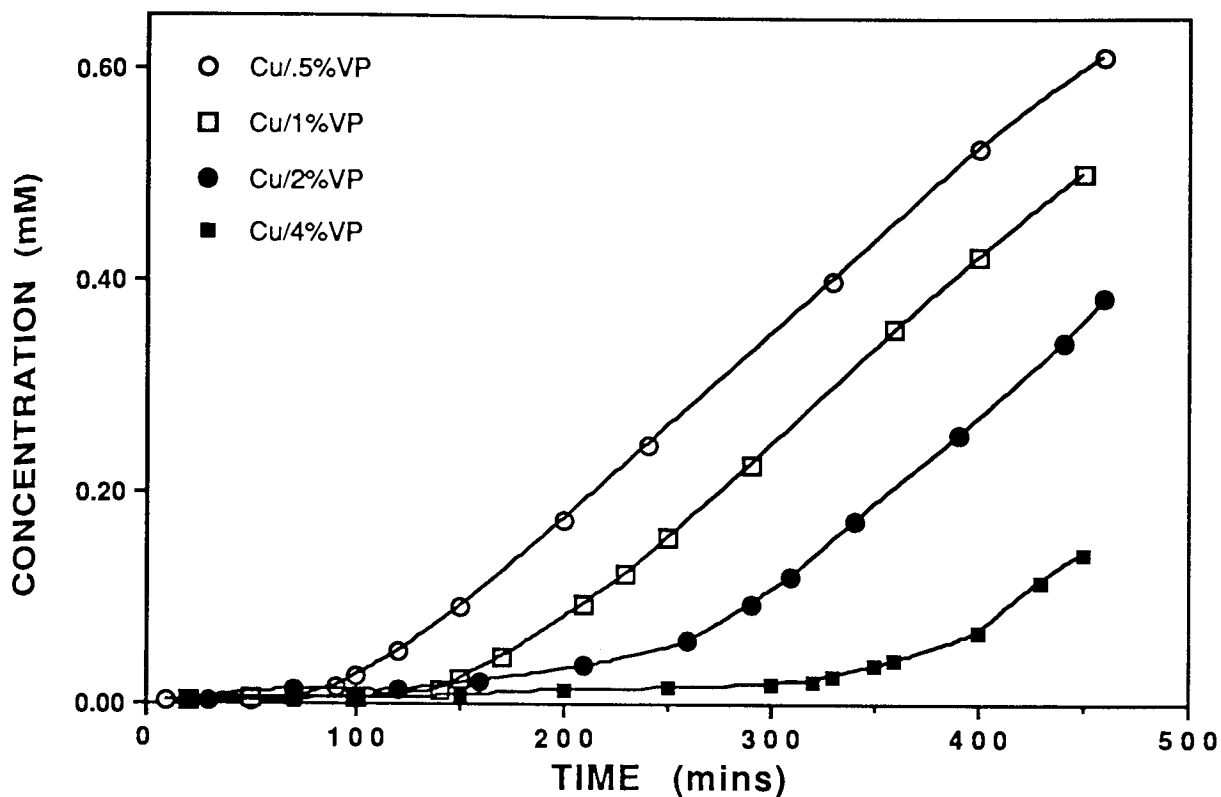


**Figure 5.12** The Effect of Ligand Concentration on  $\text{Cu}^{2+}$  Transport Across Pyridyl-Copolymer Membranes.

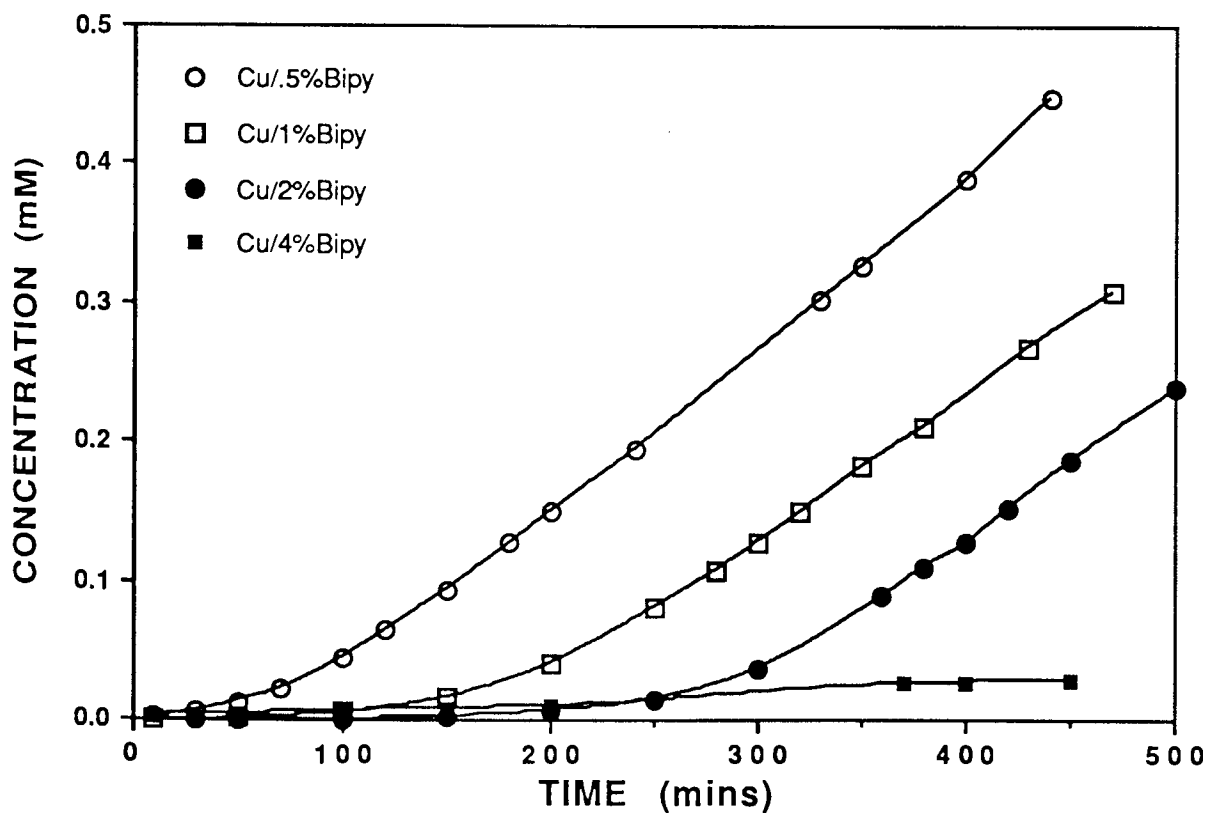


**Figure 5.13** The Effect of Ligand Concentration on  $\text{Cu}^{2+}$  Transport Across Bipyridyl-Copolymer Membranes.

If saturation of a membrane with metal ions is discussed as though it were simply a pseudo-first order reaction an insight into the process is easily gained. The rate at which saturation occurs would be proportional to the concentration of metal. Then, just as the half life would be proportional to the reciprocal of the metal concentration, so here the lag-time would show the same dependence. A plot of  $1/\text{lag-time}$  versus metal ion concentration should therefore be linear as it is in Figure 5.11. The pseudo-first order model is obviously appropriate here.

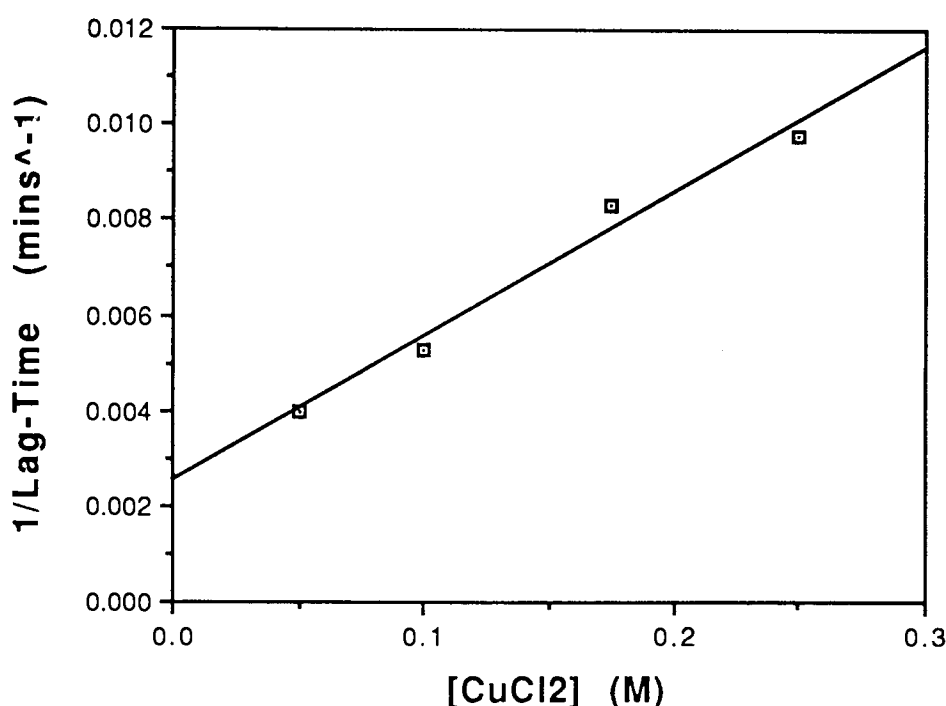


**Figure 5.11 Plot of  $1/\text{Lag-Time}$  Versus Concentration of  $\text{CuCl}_2$ .**

### **5.5.3 Effect of Ligand-Loading on Membrane Transport Properties.**

A series of transport studies were performed on 0.25M  $\text{CuCl}_2$  using 0.5, 1, 2 & 4 % (by wt.) ligand-loaded membranes (Tables 5.3 & 5.4). Figures 5.12 & 5.13 are the primary transport data for pyridyl & bipyridyl copolymer membranes respectively. As one might expect, a consequence of increasing the ligand concentration present within the membrane is an increased lag-time, as there are more coordination sites to be filled. Intriguingly, the final

steady-state permeability of the metal salt is *unaffected* by changing the ligand concentrations in range 0 to 4% (although, there is uncertainty about the 4% bipyridyl copolymer, for which the transport data fell outside the time constraints of this study).

This observation goes some way in helping to define the precise transport mechanism involved. If an active transport mode is considered in which metal ions effectively 'hopped' from one coordination site to another, in addition to bulk diffusion through the interstitial areas, one would expect to see a change in the final value of  $P_c$  if the number of those sites were to be increased. Such is not the case in this instance. The proposal of an alternative theory is not a simple task because of the complex nature of the hydrogel membrane. These systems are not considered to possess fixed pores as such, but rather have a dynamic structure in which the pore network is fluxional. The coordination of a large hydrated metal ion to an immobilised ligand may alter the characteristics of the transient 'pore' in which it is sited, either causing a constriction or an opening up that pore. Either way, the evidence suggests that the addition of the metal to the membrane somehow *conditions* the system towards further transport.

It was suggested in section 5.5.1 that there was a relationship between EWC after 'saturation' with metal ions, the observed lag-time for that metal, and the %VPy in a pyridyl-membrane. Figure 5.14 (overleaf) shows a plot which compares these parameters. The number of complexes within the membrane at saturation is determined by the initial ligand content of the polymer. Each complex possesses its own shell of water molecules, and so as the number of complexes within the membrane increases, so does the water content within the gel matrix. Assuming from previous evidence a 1:1 Cu(II):Pyridine ratio at

saturation, it is possible to calculate the number of moles of water associated with each hydrated complex in the membrane. If a saturated membrane has E% EWC, then:

$$E = \frac{w}{(100 + w + c)} \quad (5.6)$$

(where w= weight of water, c= weight of CuCl<sub>2</sub>)

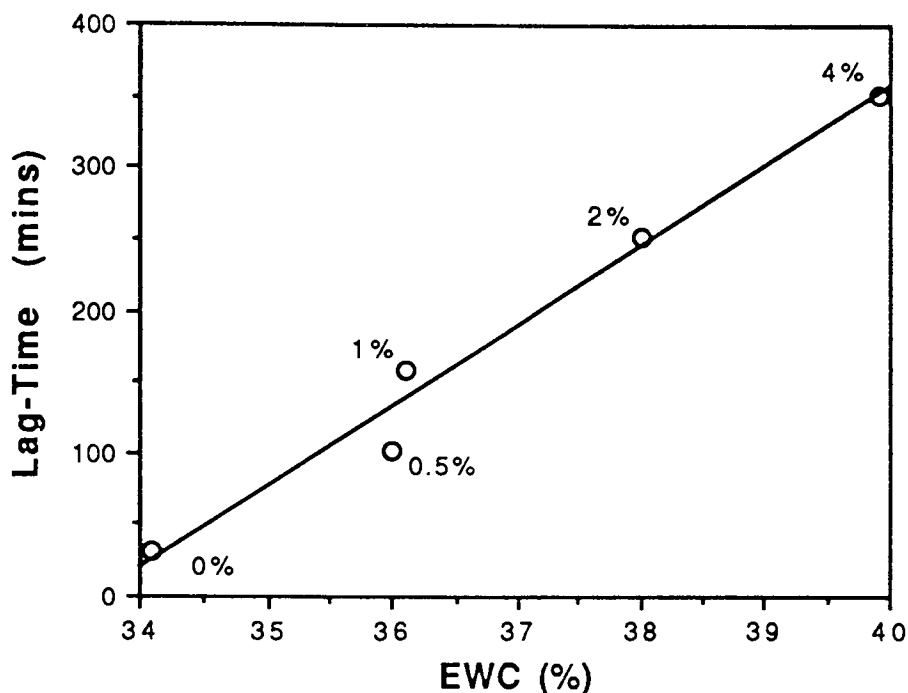


**Figure 5.14 Relationship Between EWC, %VPy & Lag-Time for CuCl<sub>2</sub>.**

Assuming 1:1 Cu(II):VPy and rearranging for w gives,

$$w = \frac{(100 + 1.28x) E}{(1 - E)} \quad (5.7)$$

(where x= %VPy)

From equation 5.7 it is possible to calculate the weight of water responsible for a particular change in EWC, and therefore the number of water molecules associated per pyridine complex (Table 5.6, overleaf). The results from Table 5.6 suggest that passing CuCl<sub>2</sub> through a pyridyl-based membrane leads to the conversion of [P---Py] to [P---Py-(CuCl<sub>2</sub>).~30H<sub>2</sub>O] (where P denotes 'polymer-bound'). This sort of figure is in agreement

with literature values <sup>180</sup> which quote the number of water molecules associated with  $\text{Cu}^{2+}$  and  $2 \times \text{Cl}^-$  as 34 & 10 respectively.

<u>%Vpy</u>	<u>EWc</u>	<u>No. mol H<sub>2</sub>O</u>	<u>H<sub>2</sub>O : VPy</u>
0	34.1	2.9	-
0.5	36.0	3.1	52
1	36.1	3.2	29
2	38.0	3.5	31
4	39.9	3.9	26

**Table 5.6 Calculated Data for the Number of Water Molecules/Complex.**

Allowing for blockage of one hemisphere of the  $\text{Cu}^{2+}$  ion by the pyridine itself, an estimate of approximately 30 water molecules per complex is not unreasonable. The molar volume of water is  $18 \text{ cm}^3$  (but will be slightly less when associated with  $\text{M}^{2+}$  because of electrostriction), which means that every mole of VPy that coordinates with the metal will produce a molar volume increase within the polymer of around  $400\text{-}500 \text{ cm}^3$ . This effect will require a considerable reorganisation of polymer chains within the swollen membrane, which in turn necessitates a greater lag-time (c.f. Figure 5.14).

Although the bipyridine membranes show essentially no change in EWC with % ligand loading, Figure 5.15 demonstrates that the lag-time is still extended in alliance with increasing the VBipy concentration. The lag-time in this case can be construed as a consequence of the rather better bipyridine ligand interacting with, and essentially 'stripping-out,' the cupric ions until all coordinating sites are occupied by a metal ion. The next section describes how the apparently different modes of interaction of the two ligands under study may also account for the different effects each of these compounds has on the permeability

coefficients of the permeating species.

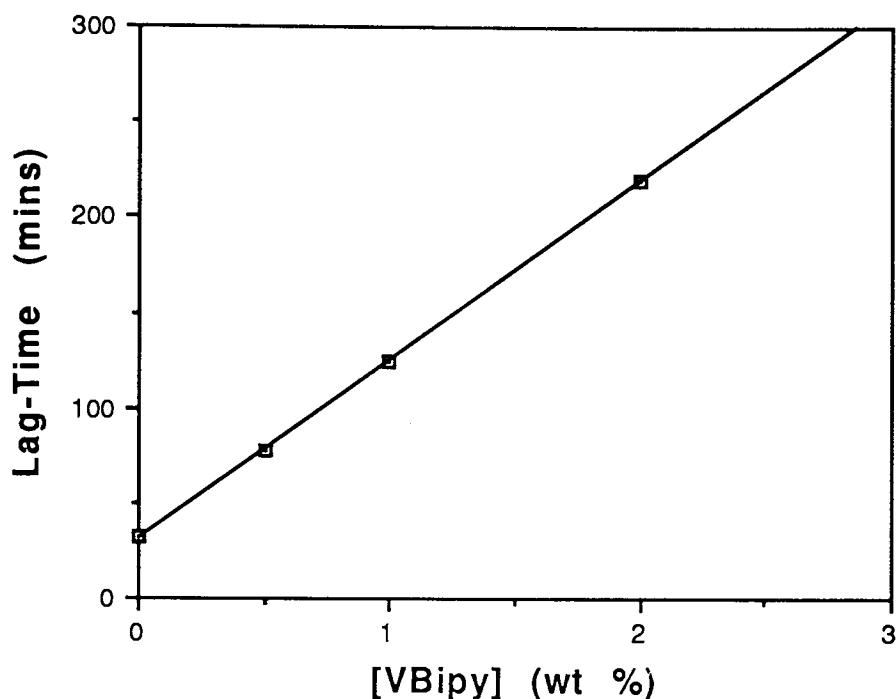


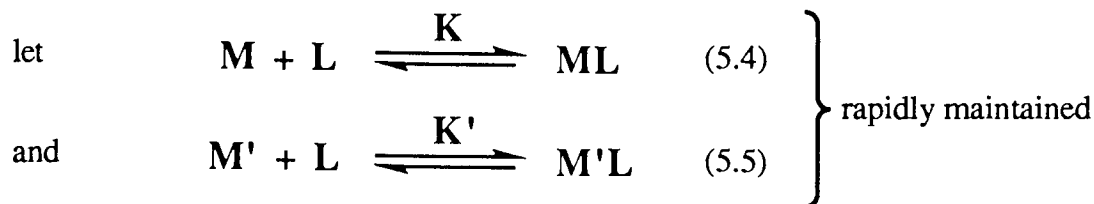
**Figure 5.15 Effect of VBipy Loading within Membrane on Lag-Time of  $\text{CuCl}_2$ .**

### **5.6 SOME STUDIES OF COMPETITIVE TRANSPORT.**

Competitive studies were approached from two discrete directions: firstly, ligands were coordinated with a particular ion by soaking the membrane 0.25M solution overnight. The precomplexed membrane was then subjected to a transport study using a different permeating ion. The second approach involved the assessment of direct competitive transport between two different permeating species in a binary salt solution. In both sets of experiments  $\text{Cu}(\text{II})$  and  $\text{Mn}(\text{II})$  were used as competitors, as it was thought that the most pronounced effects would be demonstrated using one strongly coordinating and one weakly coordinating transition metal ion species.

Consider the coordination of two different metal ions, M & M', to a particular ligand

system:



$$\text{this has} \quad \text{K}'' = \text{K}/\text{K}' \quad (5.7)$$

$$\text{and therefore,} \quad \frac{[\text{ML}]}{[\text{M}'\text{L}]} = \frac{\text{K} [\text{M}]}{\text{K}' [\text{M}']} \quad (5.8)$$

These statements must be true no matter what transport model is developed. They are used in the following discussions.

### **5.6.1 Transport through Precomplexed Membranes.**

In the case where we have pre-saturation by M' followed by permeation of M,  $[\text{M}] \gg [\text{M}']$  and while M' is swept out of the membrane  $[\text{M}]$  is maintained. Therefore,  $[\text{ML}]$  must be very much greater than  $[\text{M}'\text{L}]$  in this particular instance, unless  $\text{K}/\text{K}'$  is massive (which is not so in this case, Table 5.5). Figures 5.16 & 5.17 show both the permeation profiles for  $[\text{M}]$  and the leaching profiles for  $[\text{M}']$  in the pyridyl and bipyridyl systems respectively. Where the key reads  $\text{Cu} > [\text{PyMn}]$  the data correspond to the permeation of  $\text{Cu}(\text{II})$  through a  $\text{Py}:[\text{Mn}]$  precomplexed membrane; alternatively,  $[\text{PyCu}] > \text{Mn}$  corresponds to the displacement and leaching of  $\text{Mn}(\text{II})$  from the membrane by permeating  $\text{Cu}(\text{II})$ . Comparison of the transport data for precomplexed membranes (Table 5.7) with that for uncoordinated membranes in Tables 5.3 & 5.4, indicates that the membrane transport properties are not significantly altered by the precomplexation of the membrane by another ion.

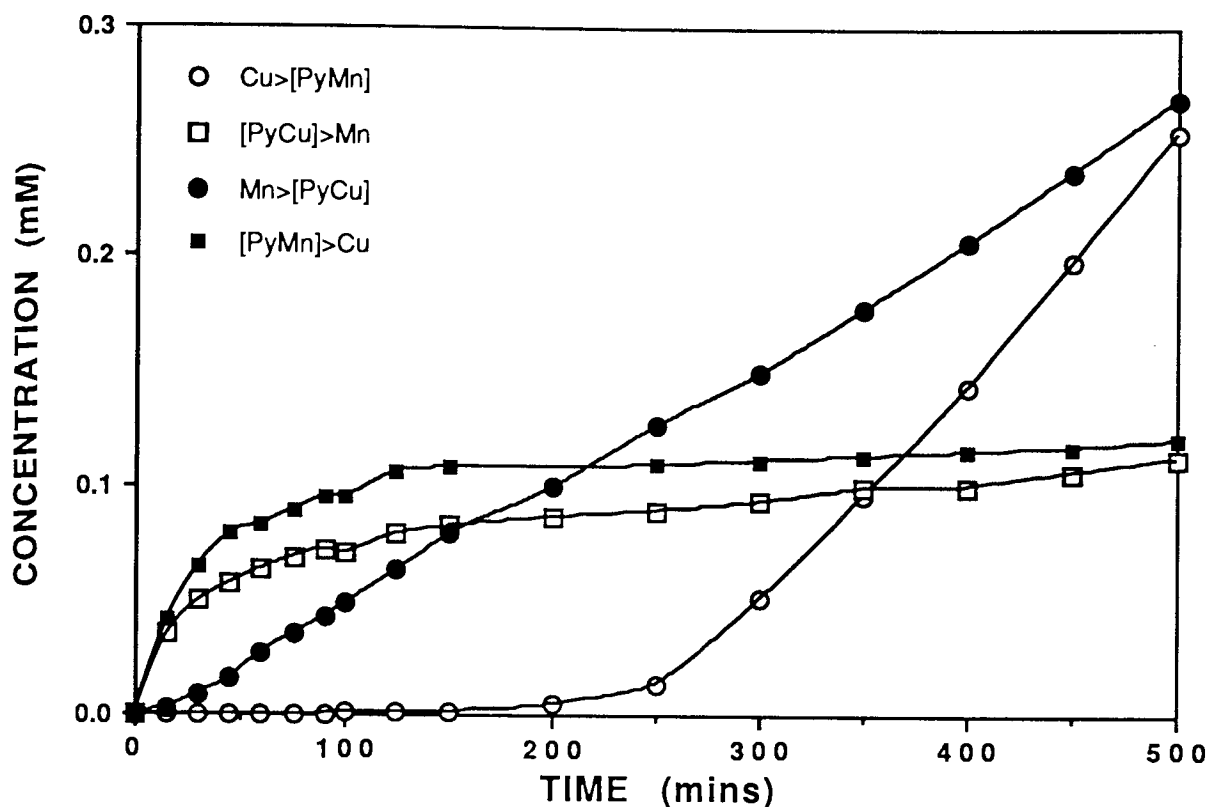


**Figure 5.16 Permeability of Cu(II) & Mn(II) through Precomplexed 2% Vinylpyridine-Based Copolymer Membranes.**

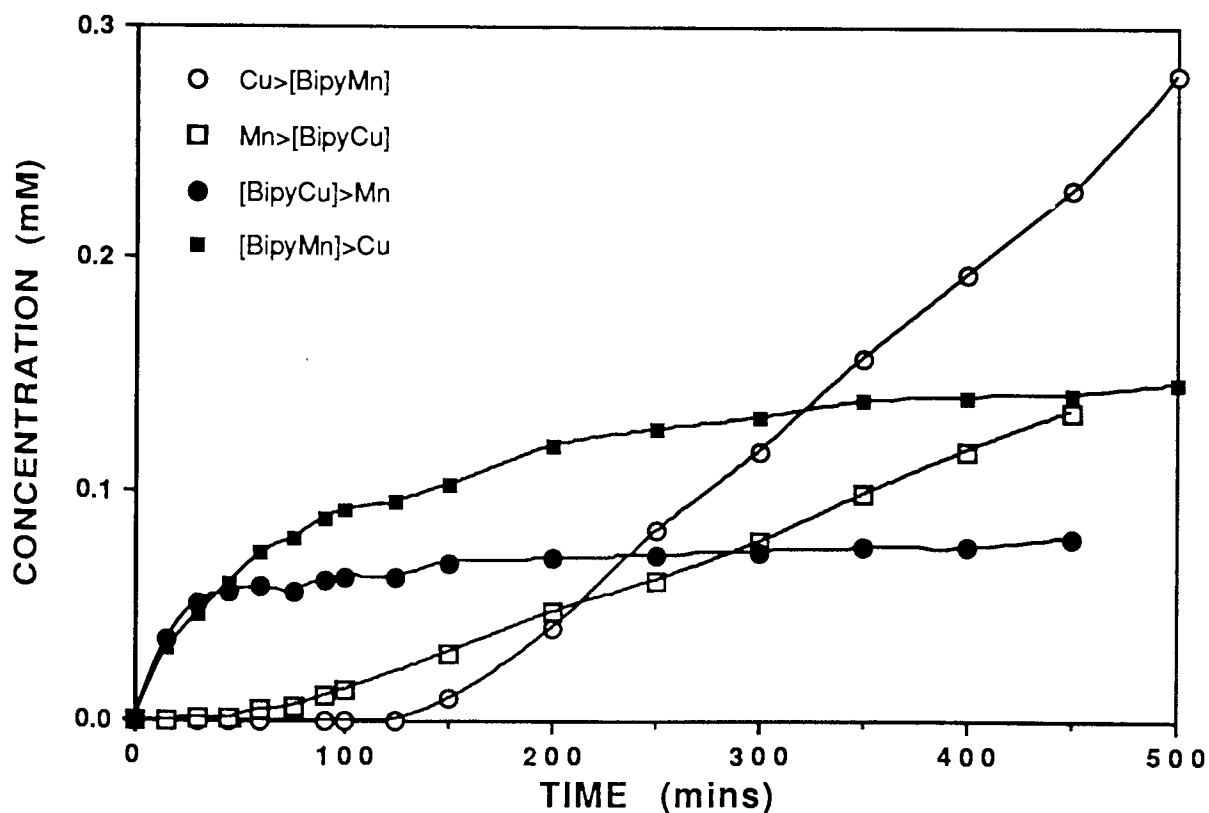


**Figure 5.17 Permeability of Cu(II) & Mn(II) through Precomplexed 2% Vinylbipyridine-Based Copolymer Membranes.**

<u>Membrane Environment.</u>	<u>Metal Ion System.</u> (0.25M each)	<u>Lag-Time.</u> (mins)	<u>Perm. Coeff.</u> (cm <sup>2</sup> min <sup>-1</sup> )
2% VPy:[Cu(II)]	MnCl <sub>2</sub>	~15	1.9e <sup>-6</sup>
2% VPy:[Mn(II)]	CuCl <sub>2</sub>	237	3.2e <sup>-6</sup>
2% VBipy:[Cu(II)]	MnCl <sub>2</sub>	~100	1.2e <sup>-6</sup>
2% VBipy:[Mn(II)]	CuCl <sub>2</sub>	145	2.8e <sup>-6</sup>

**Table 5.7 Transport Data for Metal Salts in Competition Studies:  
Precomplexed Systems.**

### **5.6.2 Transport of Binary Salt Solutions.**

Using the scheme of equations 5.8 - 5.12, consider the competitive transport of two different metal ions where  $[M]/[M'] = 1$ , and therefore  $[ML]/[M'L] = K/K'$ . If  $K > K'$ , then the ligand groups within the membrane will be almost entirely occupied by the more strongly coordinating metal ion, M. In the case of the competitive transport of Cu(II) & Mn(II)  $K/K' = 240$  for pyridine and  $= 3.16 \times 10^5$  for bipyridyl (based on free ligand values of K), and so the membrane will almost entirely saturate with Cu(II) in both cases.

Figures 5.18 & 5.19 are the primary transport curves for the competitive transport of a binary salt solution through pyridyl and bipyridyl copolymer membranes respectively (full data in Table 5.8). It is quite obvious that, when in competition, both metal ion species have very similar lag-time and steady-state permeability values. Comparison of the transport data for the salts in competition (Table 5.8) with that for the individual studies (Tables 5.3 & 5.4) indicates that for a binary system, the induction period exhibited by both metal salts is similar to, and characteristic of, that of the more strongly coordinating species, as is the final

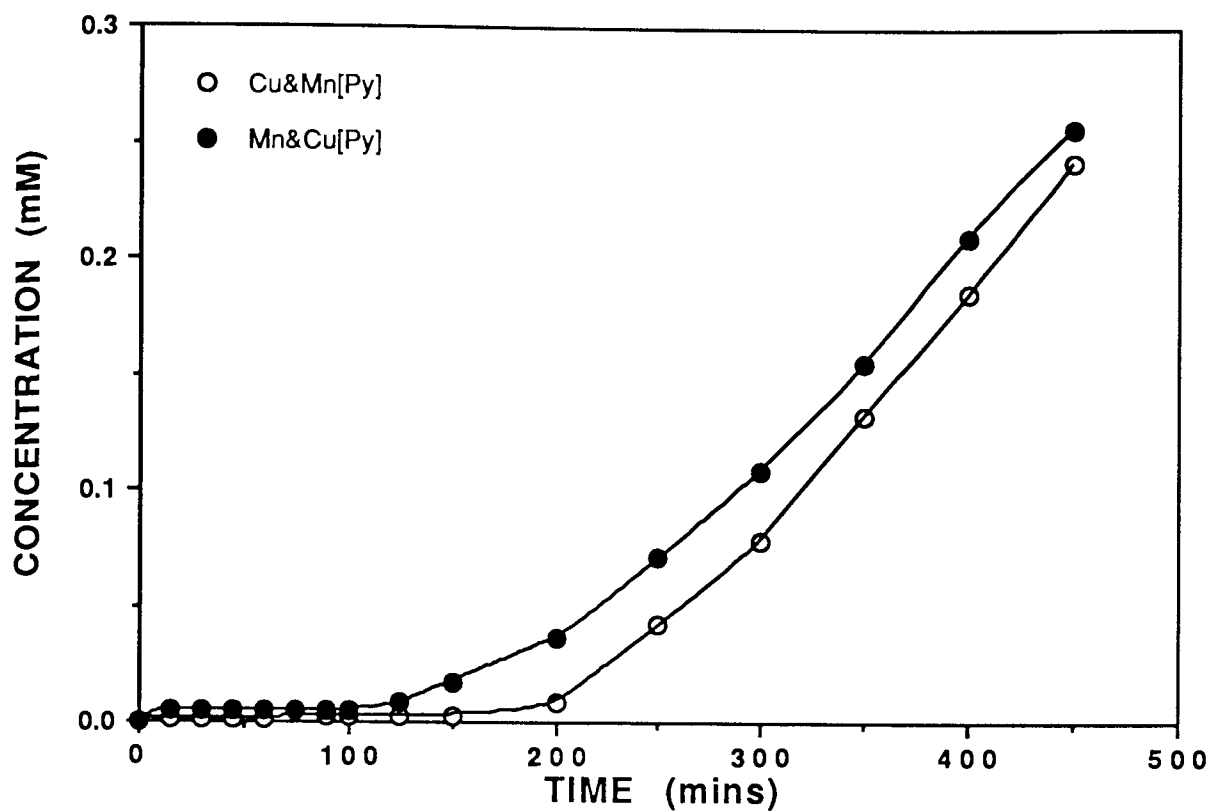


**Figure 5.18** Permeability of Cu(II)/Mn(II) Binary Salt Solution through 2% Pyridyl-Based Copolymer Membranes.

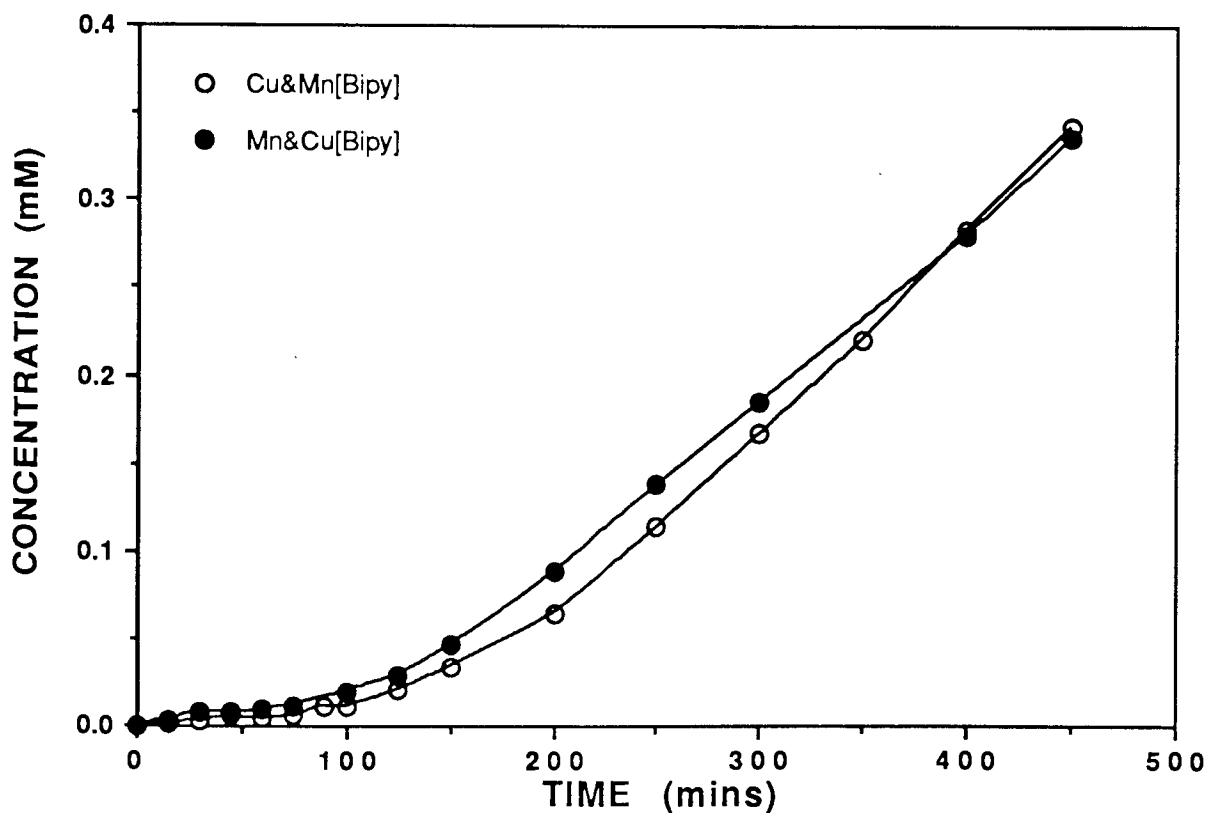


**Figure 5.19** Permeability of Cu(II)/Mn(II) Binary Salt Solution through 2% Bipyridyl-Based Copolymer Membranes.

steady-state permeability (Table 5.9).

<u>Membrane Environment.</u>	<u>Binary System.</u> (0.25M each)	<u>Ion Monitored</u>	<u>Lag-Time.</u> (mins)	<u>Perm. Coeff.</u> (cm <sup>2</sup> min <sup>-1</sup> )
2% VPy	Cu/MnCl <sub>2</sub>	Cu	180	3.5e <sup>-6</sup>
2% VPy	Cu/MnCl <sub>2</sub>	Mn	135	3.9e <sup>-6</sup>
2% VBipy	Cu/MnCl <sub>2</sub>	Cu	~130	4.0e <sup>-6</sup>
2% VBipy	Cu/MnCl <sub>2</sub>	Mn	~120	3.5e <sup>-6</sup>
2% VPy	CaCl <sub>2</sub>	Ca	~40	2.8e <sup>-6</sup>
2% VPy	Ca/CuCl <sub>2</sub>	Ca	~200	7.7e <sup>-6</sup>
2% VPy	Ca/CuCl <sub>2</sub>	Cu	180	5.3e <sup>-6</sup>

**Table 5.8 Transport Data for Metal Salts in Competition Studies:  
Binary Salt Systems.**

This rather unexpected result was confirmed by repeating the experiment with a Cu(II)/Ca(II) binary salt solution, again through a pyridyl-based membrane.

<u>Experiment Type.</u>	<u>Metal Ion.</u> (0.25M)	<u>Lag-Time.</u> (mins)	<u>P<sub>c</sub></u> (cm <sup>2</sup> min <sup>-1</sup> x 10 <sup>-6</sup> )
Single Salt	Cu	252	4.9
Single Salt	Mn	48	1.9
Binary Salt	Cu (& Mn)	180	3.5
Binary Salt	Mn (& Cu)	135	3.9
Single Salt	Ca	~40	3.0
Binary Salt	Cu (& Ca)	180	5.3
Binary Salt	Ca (& Cu)	~200	7.7

**Table 5.9 Single & Binary Salt Transport Data for Pyridyl-  
Based Copolymer Membranes.**

Figure 5.20 demonstrates the small lag-time shown by Ca(II)-only passage through a

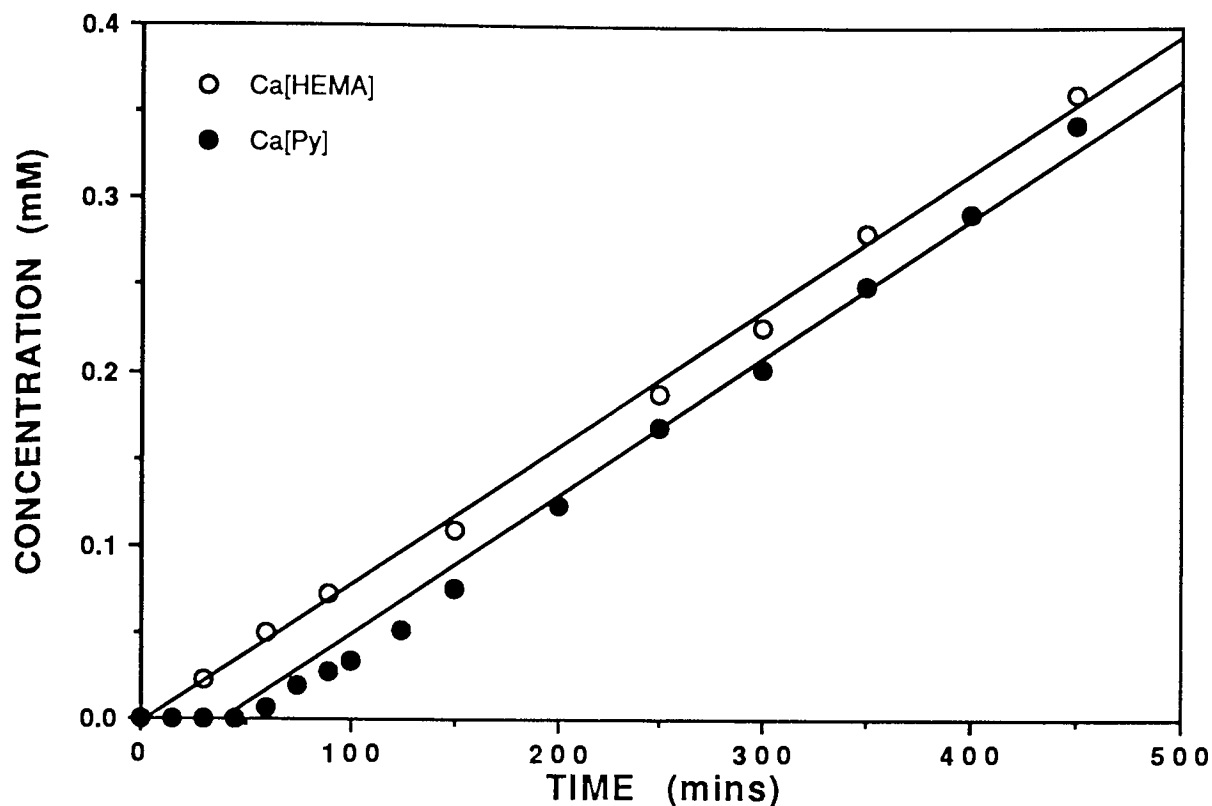


**Figure 5.20 Permeability of 0.25M  $\text{CaCl}_2$  through HEMA-only and 2% Pyridyl-Based Membranes.**

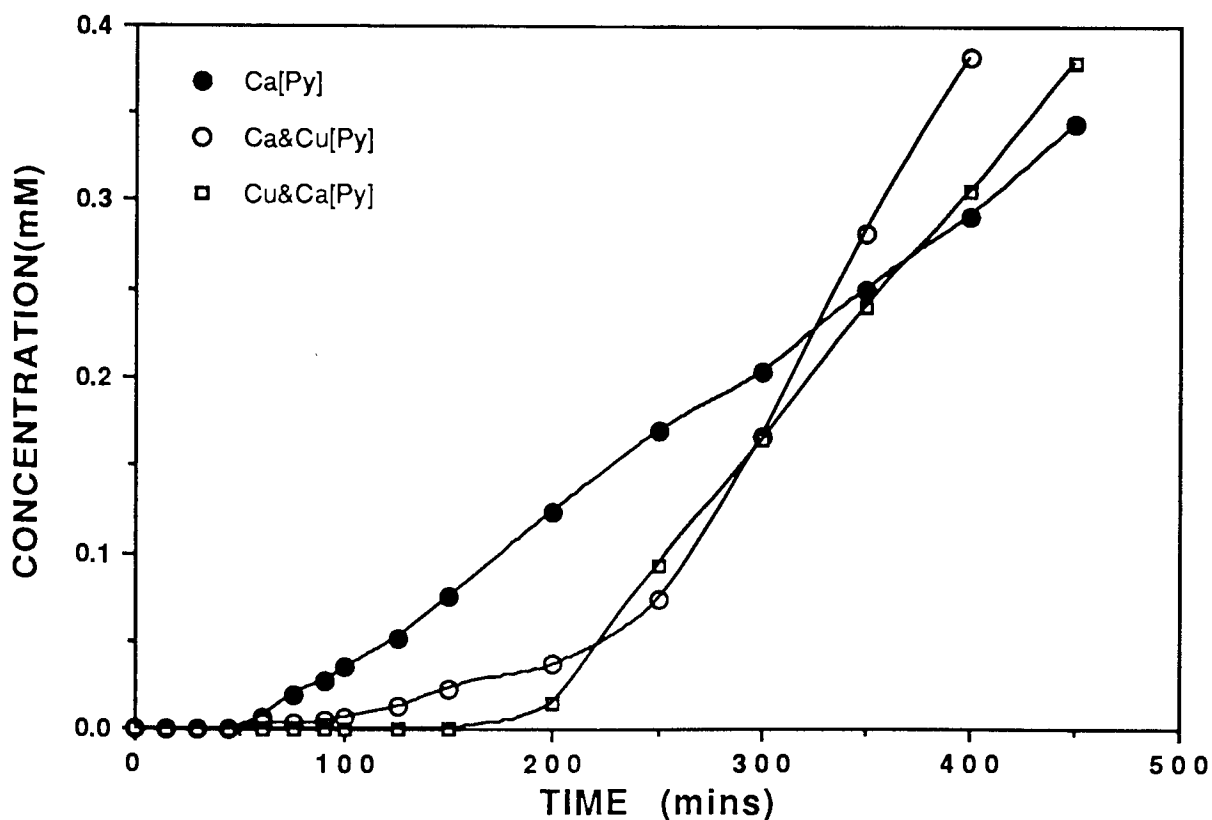


**Figure 5.21 Permeability of Ca(II)/Cu(II) Binary Salt Solution through 2% Pyridyl-Based Copolymer Membranes.**

VPy:HEMA membrane, and the unaffected rate of permeability. However, the Cu(II)/Ca(II) system (Figure 5.21) showed once again the dominating influence of a strongly coordinating metal ion on the transport properties of the membrane (Table 5.9). These membranes appear to be non- or even *anti*-selective in nature.

### 5.7 PROPOSAL OF A TRANSPORT MECHANISM.

We have already seen how the presence of ligand groups within the membrane alters the transport profile for transition metal salts. The most dominant feature is the characteristic lag-time interval before steady-state transport is achieved, which has been attributed mostly to the differing degrees of interaction between particular metal-ligand pairings. However, the presence of ligands within the membrane can also affect the final rate of permeation of a species.

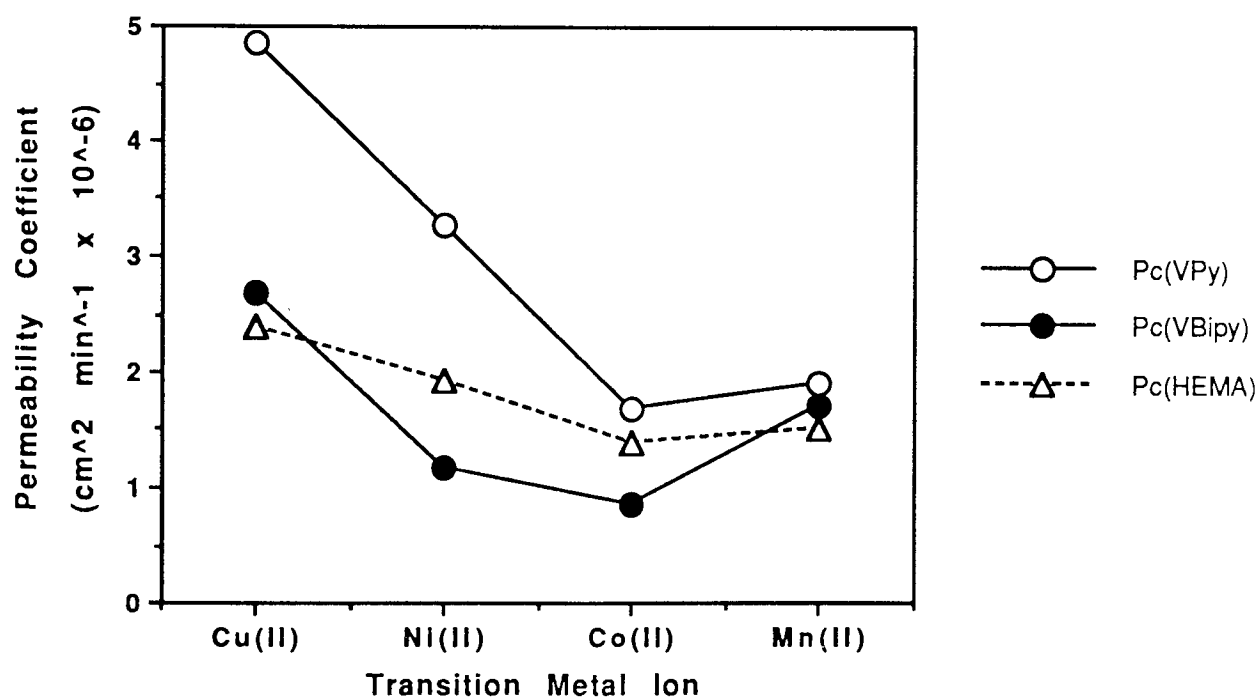


**Figure 5.22 Permeability Coefficient for T.M. Ions in Different Membrane Systems.**

Figure 5.22 shows that the pyridyl ligand somehow 'opens' the membrane towards transport of Cu(II) & Ni(II) (Co(II) & Mn(II) remaining essentially unaltered), whereas the bipyridyl ligand seems to introduce some 'constriction' which impedes Co(II) & Ni(II) transport (Cu(II) & Mn(II) remaining unchanged). The aim of this final section is to attempt to pull together these observations and present a single coherent explanation to describe the transport phenomena of the coordinating membrane systems.

A simple way of explaining these observations is to assume that the coordination of a large hydrated metal ion to a ligand site enforces some reorganisation in the polymer chain, such that the available space within the fluxional pore system is altered in some manner (be it a constriction or an expansion in size). This sort of effect has been demonstrated earlier in this chapter by comparing the water content of the membranes with various VPy loadings after saturation with a particular metal ion. Predictions were made as to the number of water molecules associated with each complex within the membrane, and it was suggested that the presence of such large, hydrated complexes pendant to the polymer chains would require considerable chain movement to accomodate these substituents. Consider that these complexes define the path for further transport, with an effective cylindrical radius  $r_c$ . As we have seen many times previously, transport in these systems is anion dominated and will occur as ion-pairs. Therefore, a hydrated metal ion and its counter-ion of effective radius  $r_{ip}$  will pass with a rate dependent on both  $r_c$  &  $r_{ip}$ , perhaps proportional to  $(r_c - r_{ip})^2$  is a reasonable guess. Therefore, different metal ions (in single salt studies) will indeed show characteristic values of  $P_c$ , which will be dependent on  $(r_c - r_{ip})^2$ . Additionally, for competition studies using binary salt solutions the more strongly coordinating metal ion (M) will still define  $r_c$ , and therefore its value of  $P_c$  is essentially unchanged, whereas the value of  $P_c$  for the other metal ion (M') will become proportional to  $(r_c - r_{ip'})^2$ , as opposed to  $(r_c - r_{ip})^2$ . As  $r_{ip} \approx r_{ip'}$ , the two transition metal ion species

will have very similar rates of permeation, close to that of M on its own. This is essentially what has been observed for the binary salt competition studies.

One final question that remains unanswered is "Are the ligands involved in the active transport of metal ions across the membrane?". The lag-time phenomenon provides an unsophisticated indicator of the extent of metal-ligand interaction within the membrane;  $\text{Cu(II)}$  interacts very strongly with both types of ligand, whereas  $\text{Mn(II)}$  shows a much lesser affect. However, binary salt competition reveals that both salts are transported to the same extent- a sign that the actual ligand sites are not directly involved with ion transport (although complexation to these sites is crucial in modifying the overall transport properties of the membrane). Additionally, it was shown in section 5.5.3 that the concentration of the ligand groups had little effect on the final steady-state permeability of a species. These observations may be explained by use of the analogy that the metal ions pass through the modified 'constrictions' in a similar manner to a football crowd passing through a series of consecutive turnstiles; the number of turnstiles is largely irrelevant, it is simply the presence of the initial constriction-to-flow that is important. With the range of ligand concentrations used in this study, it is probable that a permeating species must encounter at least one 'constriction site' on its passage across the membrane; the number of additional sites encountered after the first is unimportant, as it is  $r_c$  at this point which determines the rate of permeation. Therefore, changing the concentration of ligand groups or the membrane thickness should alter the lag-time- the time needed to fill all coordination sites, but should not alter the value of  $P_c$ - a measure of the time it takes to pass through one defining constriction.

## **5.8 CONCLUDING REMARKS.**

This chapter has described the nature of transition metal ion transport through hydrogel membranes, and has extended these studies to include the effects of the immobilised ligands vinylpyridine & vinylbipyridine on the transport properties of the membrane. In order to further elucidate the transport mechanism and to substantiate further the interpretation of these observations, it would be useful to under-take a study using differential scanning calorimetry (D.S.C.) in order to distinguish between bulk and 'bound' water. This technique should be capable of measuring the amount of water in the membrane associated with the ions and complexes because the melting endotherms of bulk interstitial water, and the 'non-freezing' water held in close proximity to ions by electrostatic forces, are different.

One firm conclusion that can be drawn from this study is that, in their present form, this type of chelating hydrogel membrane is a totally unsuitable means of separating transition metal ions from solution. The selective nature of the ligands that prompted the urge to immobilise them into hydrophilic membranes, is not reflected in the overall properties of these systems. The failure of these membranes to demonstrate any selectivity lies in the nature of the hydrogel polymer itself, as the gel matrix does not provide a selective enough barrier against the passage of various solutes in the first instance. A more ideal situation would involve the membrane providing a more-or-less impermeable barrier, transport being solely dependent on the active uptake of metal ions by the immobilised ligand groups at the membrane surface; this would then rely totally on the selectivity of the ligand. Chapter Six describes the attempts to immobilise a range of macrocyclic ligands within the framework of a hydrophilic membrane. It was thought that these compounds may provide the opportunity to 'tune' the ion-selectivity by controlling the cavity size of the macrocycle.

The anti-selective nature of these systems may find an alternative application in a rôle where it would be desirable to pass a particular metal ion species that individually would normally demonstrate poor transport across a membrane. By using a strongly coordinating transition metal ion in combination with the poorly transported species, the dominant ion would define the transport parameters of the membrane and reasonable permeation of both ion types could be expected

The PHEMA polymer has been utilised successfully in the past in the form of SPHERON chelating resins <sup>18-24</sup>. During this course of study, the application of HEMA:VPy copolymer chelating beads was briefly investigated (but will not be reported here, as it is outside the scope of this thesis). These materials showed reasonable ion-binding capacity and were easily regenerated by use of acid leaching techniques (as the polymer swells enormously in acid). The most encouraging observation during this study was the selective nature of the beads towards Cu(II) ions from binary salt studies. Perhaps this is a pointer for the direction in which these water-swellaable coordinating polymers should be developed.

## **CHAPTER SIX**

### **PREPARATORY INVESTIGATIONS OF THE INCORPORATION OF MACROCYCLIC LIGANDS INTO HYDROPHILIC POLYMERS.**

## 6.1 INTRODUCTION.

The following account represents a programme of work which was run in parallel with that previously discussed. The purpose of these studies was to investigate methods for the functionalisation, and subsequent immobilisation, of macrocyclic ligands into the hydrophilic polymer systems already described. Much of this work was inspired by papers presented in meetings of the U.K. Macrocycle Group at Warwick and Birmingham Universities during the 1987-89 period. Escalating interest in macrocyclic chemistry in a variety of areas within chemistry and biochemistry has been demonstrated by recent recognition of the U.K. Group by Royal Society of Chemistry sponsorship.

Naturally occurring macrocyclic complexes have an important rôle to play in a multitude of biological systems. The macrocyclic ligand provides the necessary stabilisation to enable the metal to undergo vital redox changes. Figure 6.1 shows three of the more prevalent macrocyclic systems<sup>181</sup>; in each of these cases, the metal is held firmly within the ligand structure to prevent leaching of the metal ion from the system on change of oxidation state.

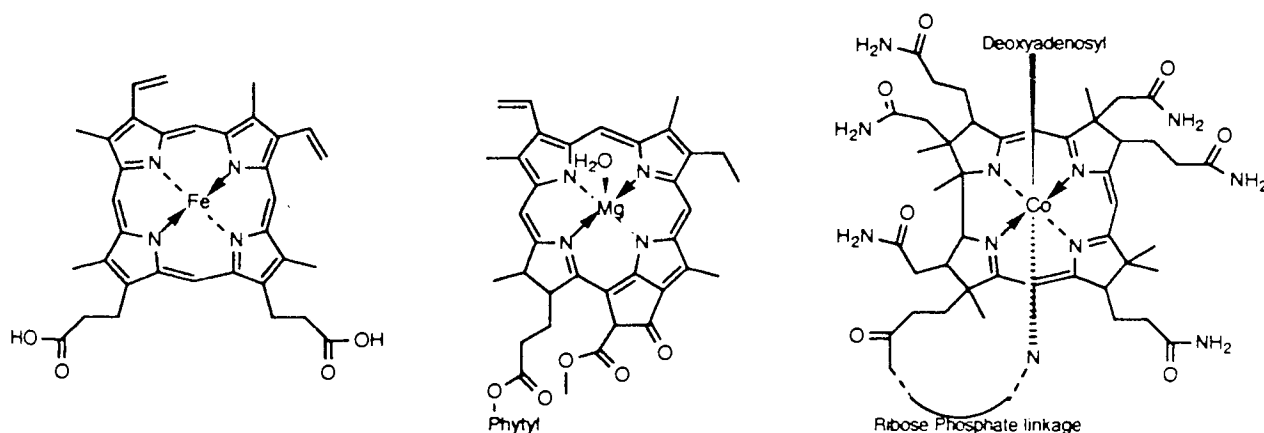


**Figure 6.1(a): Haem *b***

**(b) Chlorophyll *a***

**(c) Vitamin B<sub>12</sub>**

However, there are many compounds which exist in nature which will selectively bind and transport metal ions. The macrocyclic antibiotic ionophores such as valinomycin (Figure

6.2(a)) and the monactin group aid selective transport of alkali metal cations across biological membranes <sup>182</sup>. It was not until the discovery of the crown ether family of ionophores by Pedersen <sup>183</sup> in 1967, that serious synthetic alternatives were available for metal-selective transport studies. Crown compounds containing all-oxygen donor atoms are excellent for alkali and alkaline earth metals, but in general show little or no transport of first row transition metals <sup>94</sup> (although, the bacterial siderophore, *enterochelin* (Figure 6.2(b)), has one of the largest stability constants of any known complex <sup>184</sup>). Therefore, it is necessary to introduce nitrogen donor atoms into the macrocyclic structure in order to efficiently coordinate these ions.

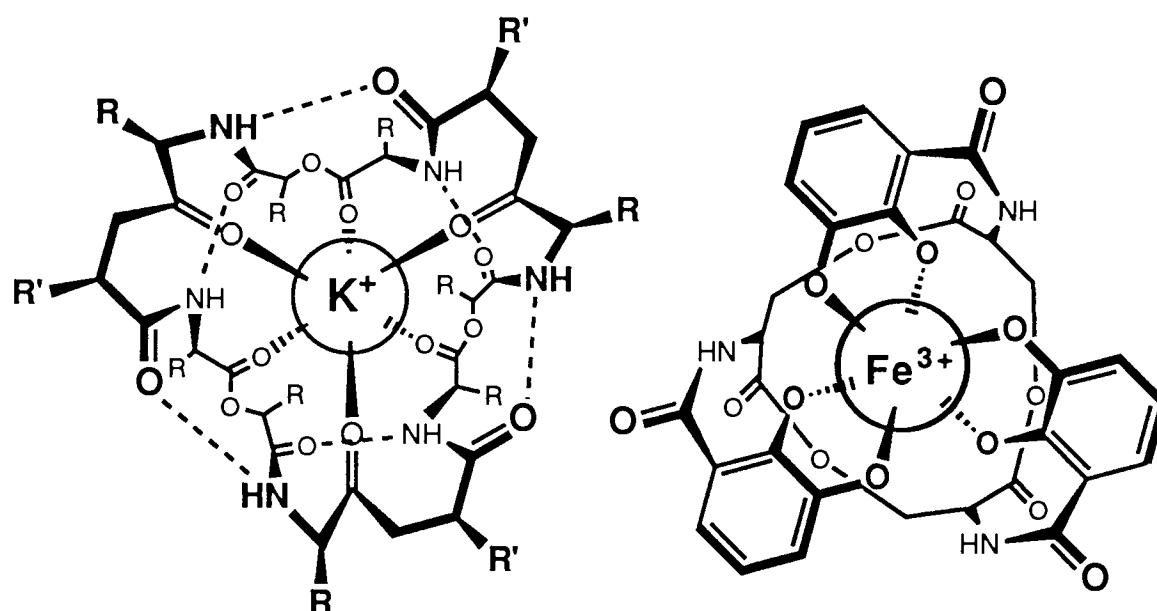


**Figure 6.2(a) Valinomycin-K<sup>+</sup>**

**(b) Enterochelin-Fe<sup>3+</sup>**

Moore and co-workers have recently been working on the electropolymerisation of cyclam-appended polymer films for the preparation of ion-selective electrodes <sup>153</sup>. These systems are still undergoing extensive study, but it is thought that the selective chelation of transition metal ions by the macrocyclic ligand will enable the amperometric estimation of the species in solution.

Lindoy *et al.* have developed a family of oxygen-nitrogen mixed donor macrocycles <sup>185-191</sup> which have enabled them to discuss at great length the effect of changing parameters such as donor atom type, backbone structure and macrocyclic cavity size, on the ability of a macrocyclic ligand to recognise a particular metal ion <sup>192</sup>. They have studied macrocycle-facilitated metal-ion transport through liquid membranes but found it necessary to append long-chain aliphatic groups to the ligand to prevent leaching of the complex from the organic phase <sup>193</sup>. The problems associated with liquid membrane instability led these workers to immobilise a series of ligands to a polystyrene matrix <sup>194</sup> (Figure 6.3(a)), with only mixed success due to the hydrophobic nature of the polymer, which resulted in poor swelling of the matrix in aqueous media. In an analogous investigation, macrocycles were immobilised on a more hydrophilic silica gel matrix <sup>195</sup> (Figure 6.3(b)).

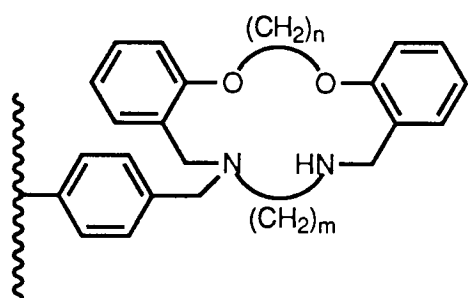
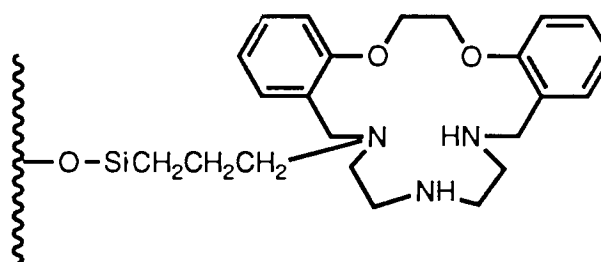


**Figure 6.3(a) O<sub>2</sub>N<sub>2</sub> Macrocycle Appended to Polystyrene.**



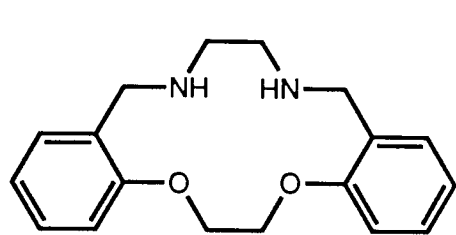
**(b) O<sub>2</sub>N<sub>3</sub> Macrocycle Appended to Silica gel.**

The binding capacity of the gel was much more satisfactory and the polymer was shown to undergo no degradation over a number of loading/leaching cycles. However, the system was still far from ideal; the polymer support was still not hydrophilic enough to utilise the full capability of the resin and the degree of macrocycle immobilisation was uncontrolled and reproducibility was poor. It is at this point that one can visualise the rôle of the hydrogel polymer in providing the ideal hydrophilic support for metal-ion recognition in the aqueous environment.

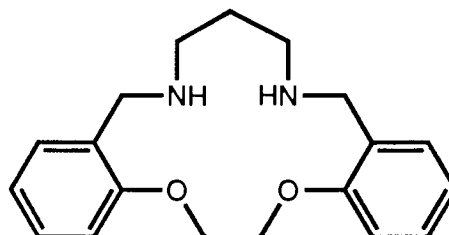
The first step in this programme of study was to synthesise a number of Lindoy-type O,N-donor macrocycles with varying ring sizes to immobilise onto the polymer. This proved to be a far from trivial exercise. The rather time-consuming experimental preparations were multi-step, with the final product yield often being very low. This was overcome by a sizeable scale-up procedure but more often than not, the resulting products were unmanageable 'gums' rather than the crystalline materials reported. Obviously Lindoy's team have gained considerable experience over a number of years in handling these compounds and much of the necessary expertise has not been translated into print. This chapter reports the problems encountered in the synthesis and subsequent functionalisation and immobilisation of a series of macrocyclic ligands. It is by no means a complete account but more of a preparatory foundation on which to build. It demonstrates that there is more to research than just a good idea.

## **6.2 SYNTHESIS OF THE MACROCYCLIC LIGANDS.**

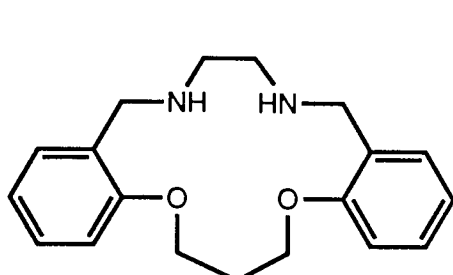
Figure 6.4 overleaf shows the structure and abbreviated names for the selection of macrocycles that were chosen for this study. As shall be seen as this section develops, only *O-en-NH-tn* & *O-tn-NH-tn* could be synthesised in appreciable quantities. Synthesis of the N,O-mixed donor macrocycles was basically similar for all seven compounds (Figure 6.5): firstly a Williamson-type condensation between two molecules of the alkoxide of salicylaldehyde and a dibromo compound, followed by condensation of the dialdehyde moieties with a diamine to produce the Schiff-base cyclisation. Finally, the diimine is reduced by sodium borohydride to give the desired macrocyclic product. The synthesis of the N,O-macrocycles will now be considered in further detail. The three N<sub>4</sub>-type macrocycles listed in Figure 6.4 are discussed later in section 6.2.11.



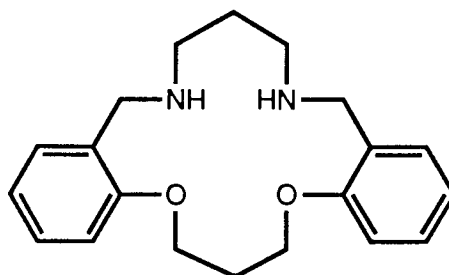
*O-en-NH-en*



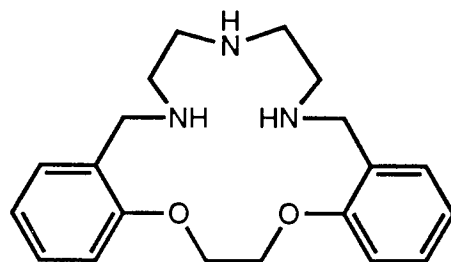
*O-en-NH-tn*



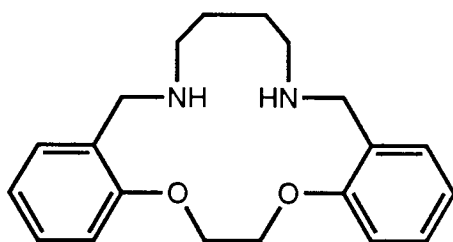
*O-tn-NH-en*



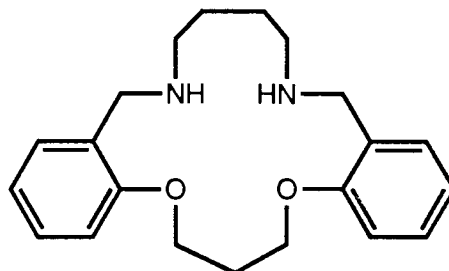
*O-tn-NH-tn*



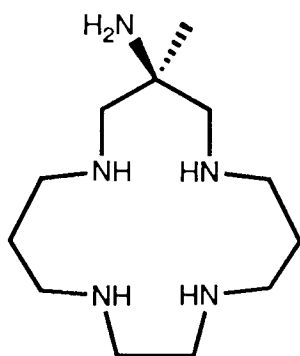
*O-en-3NH-dien*



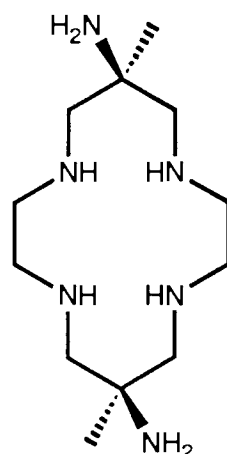
*O-en-NH-bn*



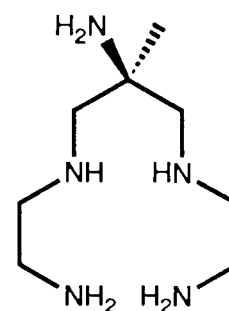
*O-tn-NH-bn*



**AmmachH**



**DiammachH<sub>2</sub>**



**AmlinH**

**Figure 6.4 Selection of Macrocycles Chosen for Synthesis.**

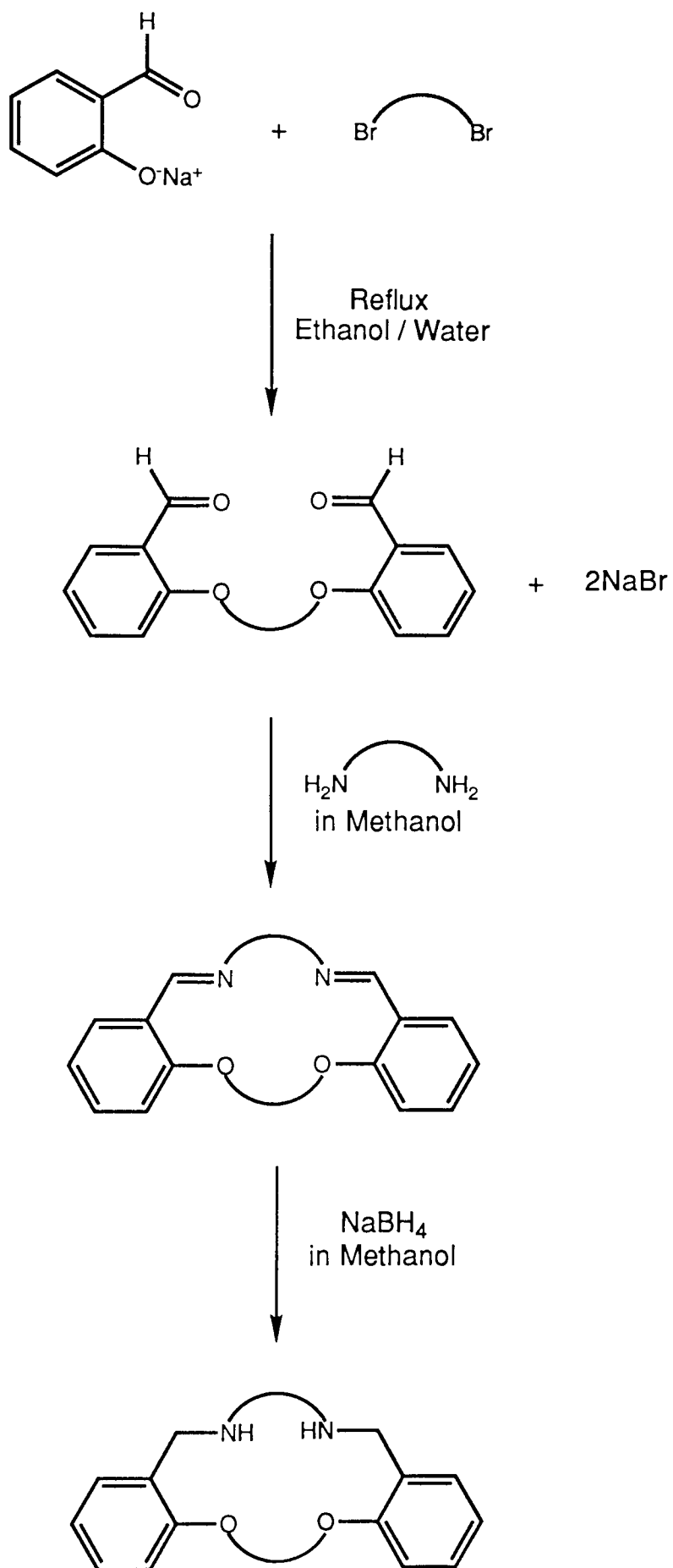


**Figure 6.5 Route to N,O-Donor Macrocycle Synthesis**

## **SECTION (A): Synthesis of the Oxygen, Nitrogen-Donor Macrocyclic Ligands.**

### **6.2.1 Preparation of 1,4-Bis(2'-Formylphenyl)-1,4-Dioxabutane, (*O-en*).**

To 24.4g (0.2 mol) of salicylaldehyde (Aldrich) in 20ml of absolute ethanol was added 8g (0.2 mol) of sodium hydroxide in 400ml of water. The mixture was warmed and 18.4g (0.1 mol) of 1,2-dibromoethane (Aldrich) was added along with a further 300ml of ethanol. The solution refluxed under nitrogen for 60 hours, after which it was left to stand @ 0°C. Off-white crystals were collected, washed with water and recrystallised from ether-chloroform. Yield 15.5g (57%), melting point 128-129°C (literature 40%, m.p. 129°C 187).

#### **6.2.1.1 Nuclear Magnetic Resonance Spectra of *O-en*.**

Figure 6.6 is the  $^1\text{H}$  nmr spectrum for *O-en* in  $\text{CDCl}_3$ . The sharp singlet at 4.5 $\delta$  is due to the O-CH<sub>2</sub> bridging methylene groups (integral of 4). The singlet at 10.4 $\delta$  is a result of the aldehydic protons (integral of 2). The aromatic protons give rise to a triplet centralised around 7.05 $\delta$ , a triplet with fine structure around 7.55 $\delta$  and a split doublet at 7.8/7.82 $\delta$  (total integral of 8).

The  $^{13}\text{C}$  nmr spectrum in  $\text{CDCl}_3$  (Figure 6.7) shows the bridging methylene (66.9 $\delta$  (-)), the quaternary ring carbons attached to the oxygen (160.8 $\delta$  (-)) and the aldehyde (125.1 $\delta$  (-)), the four ring CH's (112.6 $\delta$ , 121.4 $\delta$ , 129.5 $\delta$ , 135.9 $\delta$  (+)), and the aldehydic carbon (189.2 $\delta$  (+)). The nmr spectra are in excellent agreement with the proposed structure and indicate high purity.

### **6.2.2 Preparation of 1,5-Bis(2'-Formylphenyl)-1,5-Dioxapentane, (*O-tn*).**

By an exactly analogous procedure to that described in 6.2.1, 20.2g (0.1 mol) of dibromo-

**Figure 6.6**  $^1\text{H}$  NMR Spectrum of *O*-en.

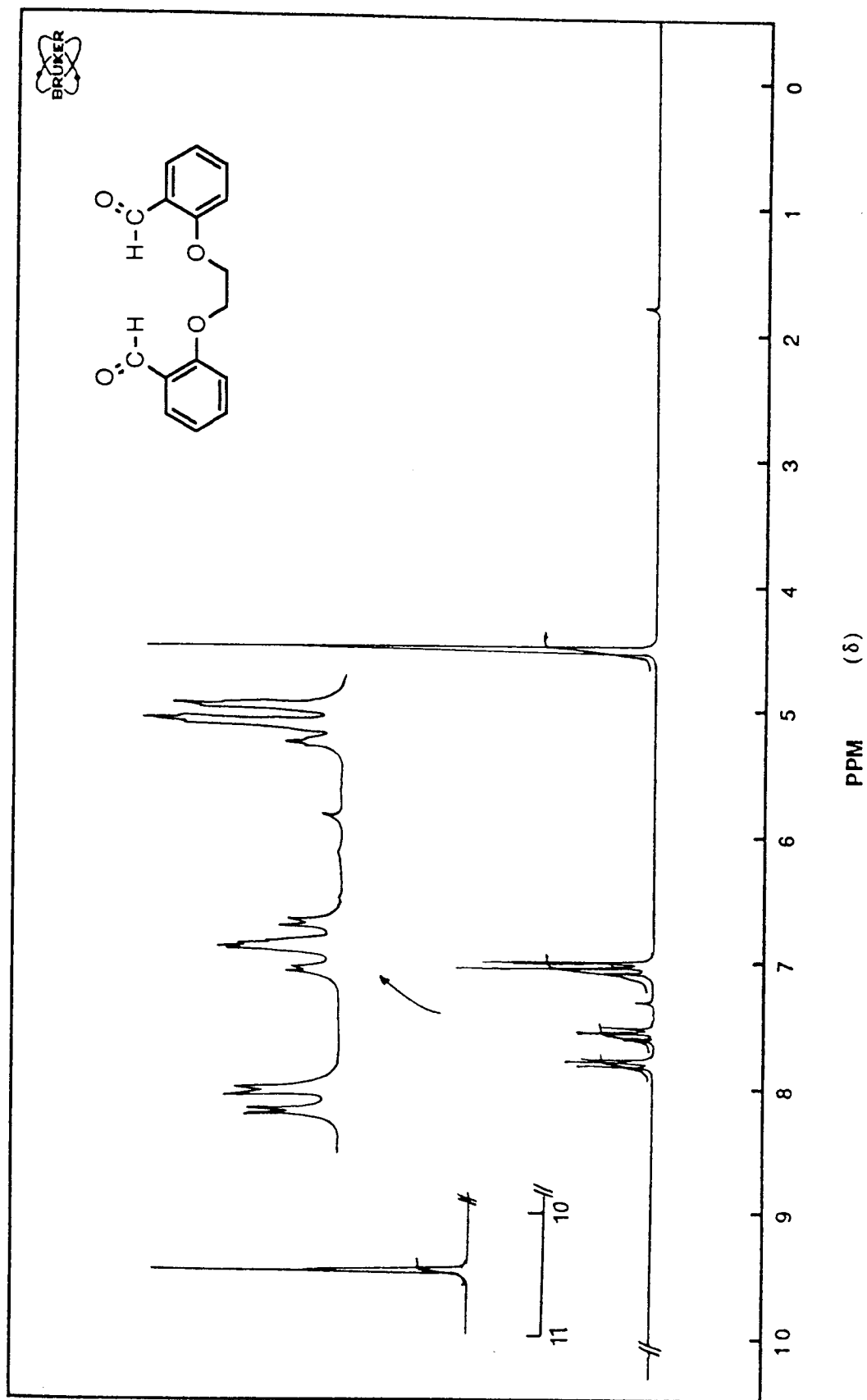
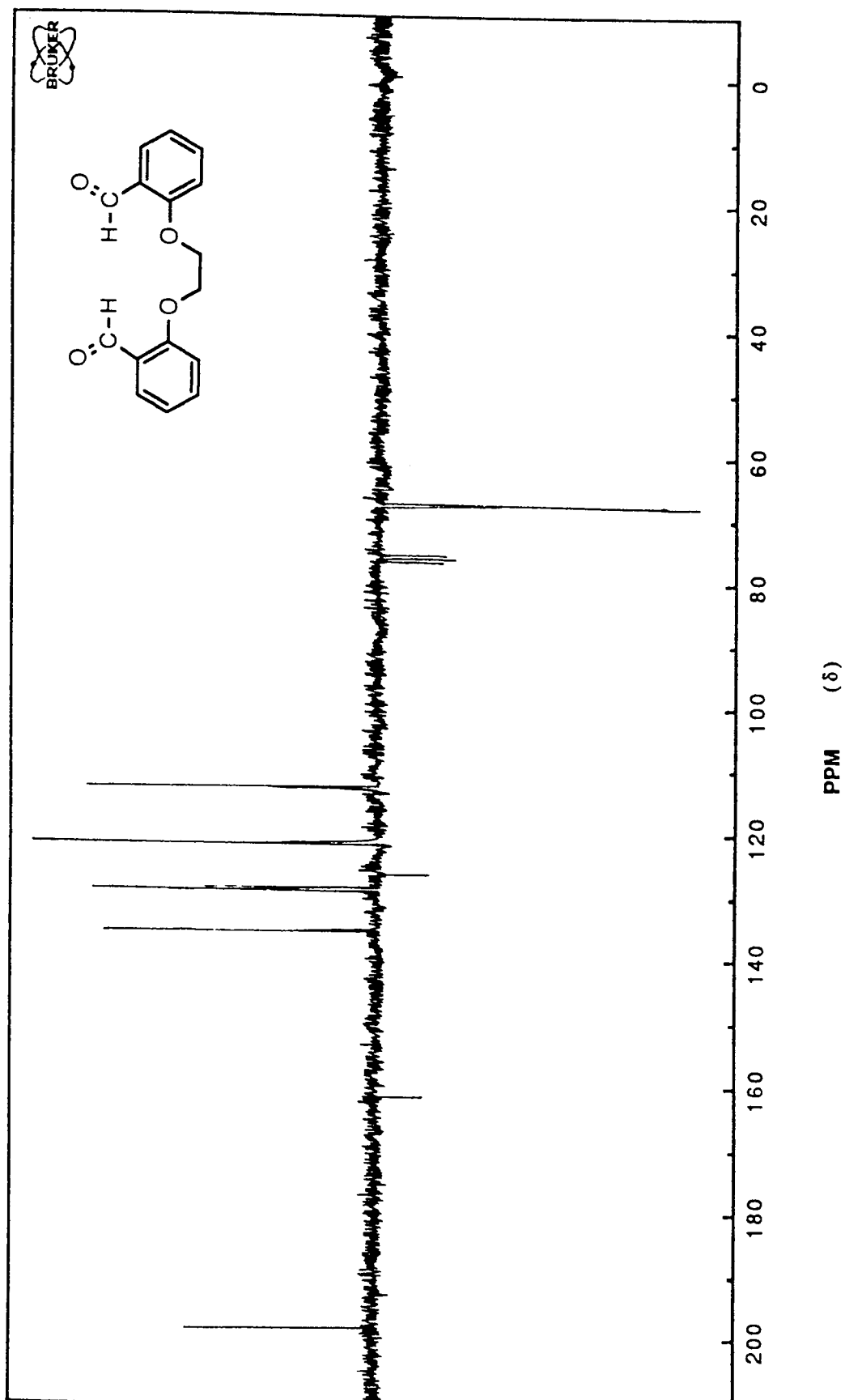


**Figure 6.7**  $^{13}\text{C}$  (*J*-Mod) NMR Spectrum of *O*-en.



propane (Aldrich) yielded 16.8g of white crystals (59%), m.p.98-99°C (literature 63%, m.p. 99°C 187).

#### **6.2.2.1 Nuclear Magnetic Resonance Spectra of *O*-tn.**

The  $^1\text{H}$  nmr spectrum of *O*-tn shown in Figure 6.8 is similar to that for *O*-en previously discussed. The aromatic protons again take the form of triplet, triplet, doublet around 6.99 $\delta$ , 7.49 $\delta$  & 7.76 $\delta$  respectively, with a fine splitting pattern observable. The aldehydic proton is still present at 10.45 $\delta$  but the bridging methylenes are split by the introduction of an extra  $-\text{CH}_2$ . The two  $\text{CH}_2\text{-O}$  groups now give rise to a triplet at 4.28 $\delta$  (integral of 4) and the additional central methylene is a quintet at 2.38 $\delta$  (integral of 2).

The  $^{13}\text{C}$  spectrum in  $\text{CDCl}_3$  (Figure 6.9) is straight forward with aldehydic carbon at +189.2 $\delta$ , the four ring CH's (112.3 $\delta$ , 120.8 $\delta$ , 128.4 $\delta$  & 135.9 $\delta$  (+)) and quaternary ring carbons (125.8 $\delta$  & 160.9 $\delta$  (-)) as with *O*-en, and the methylene bridge carbons at 64.5 $\delta$  (-) & 29.8 $\delta$  (-). Again, the purity of the compound is of a high standard.

*O*-en & *O*-tn are the basic starting materials for the synthesis of the seven O,N-macrocycles in Figure 6.4. The procedure for the preparation of these compounds will now be outlined, with reference to the problems associated with these materials.

#### **6.2.3 Preparation of 5,6,7,8,9,10,16,17-Octahydrodibenzo[e,m][1,4]Dioxo[8,11]**

##### **Diazacyclotetradecine, (*O*-en-NH-en).**

Ethane-1,2-diamine (Aldrich) (0.6g, 0.01 mol) in 30ml dry methanol was slowly added to a warm solution of 2.7g (0.01 mol) *O*-en in 150ml dry methanol. Once all amine had been added, 0.5g of borax and 1.0g of sodium borohydride were added to effect a one-step

**Figure 6.8**  $^1\text{H}$  NMR Spectrum of *O*-tn.

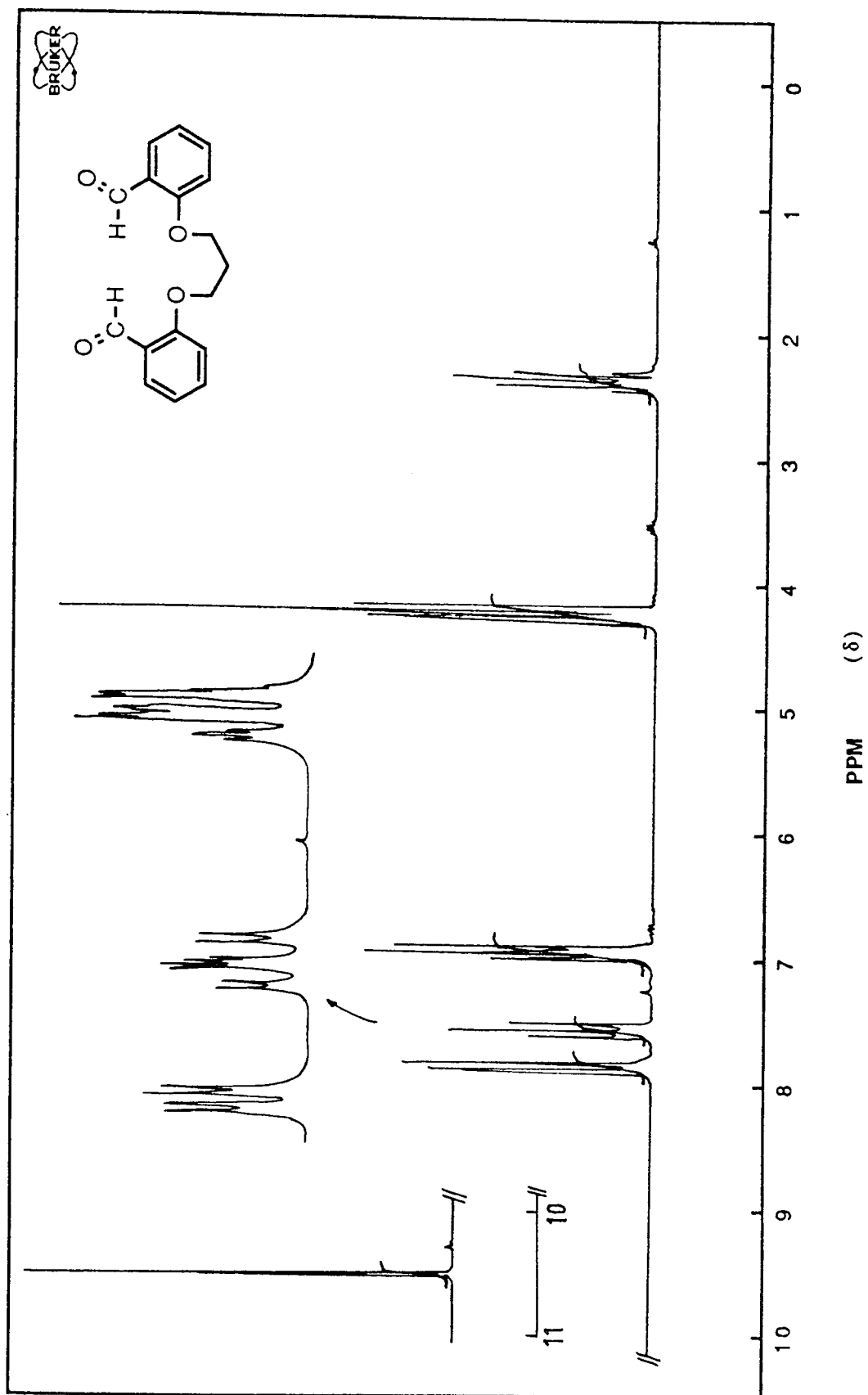
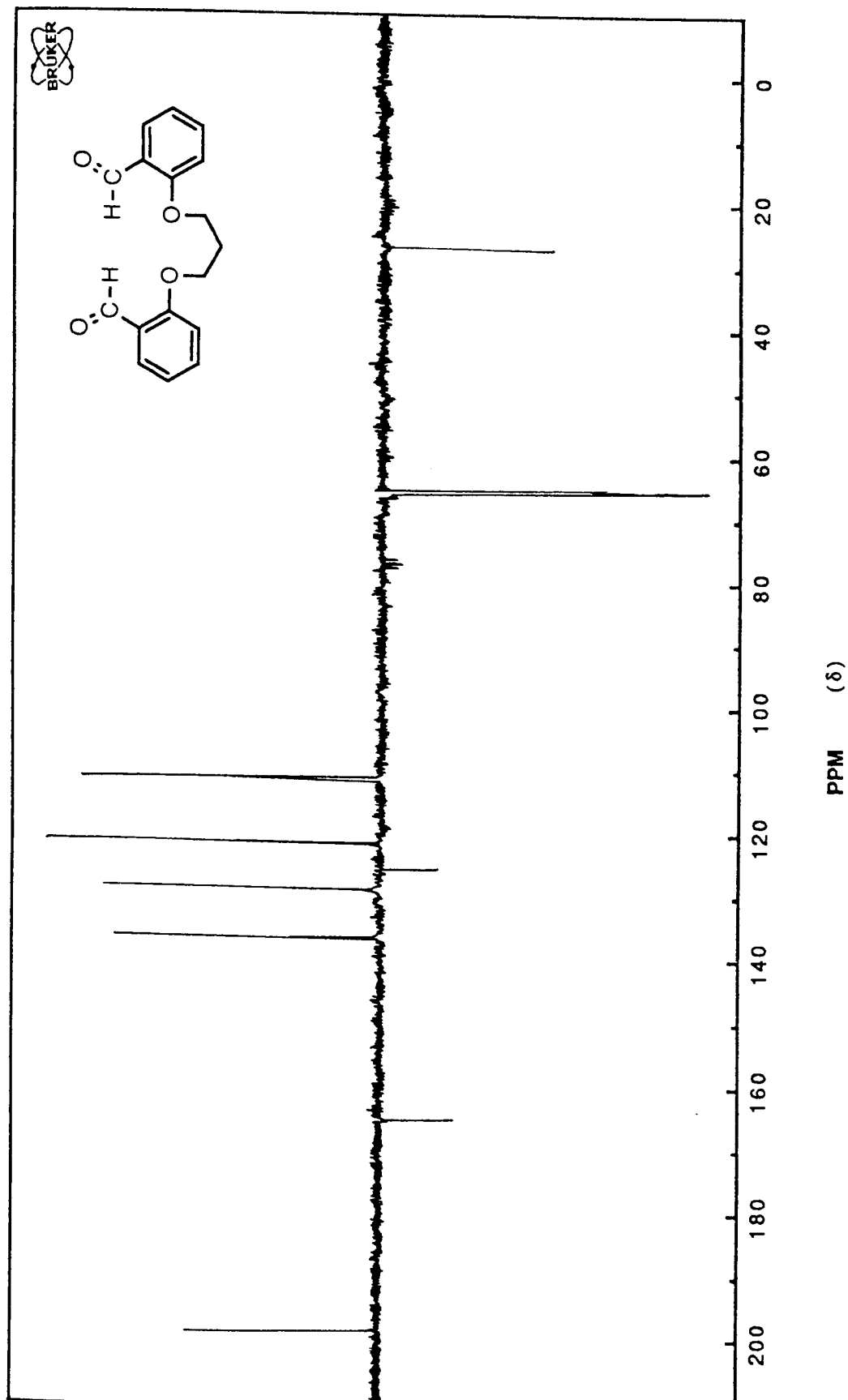


**Figure 6.9**  $^{13}\text{C}$  (*J*-Mod) NMR Spectrum of *O*-tn.



cyclisation and reduction. The solution was concentrated to 75ml and 200ml of water added. The product was extracted into chloroform, dried over Na<sub>2</sub>SO<sub>4</sub> and evaporated to dryness to yield extremely low yields of a yellow oil. This failed to crystallise from ether or ethyl acetate as reported <sup>186</sup>, and so the preparation was abandoned at this point.

#### **6.2.4 Preparation of 3,4:9,10-Dibenzo-1,12-Diaza-5,8-Dioxacyclopentadecane-1,11-Diene. (*O-en-N-tn*).**

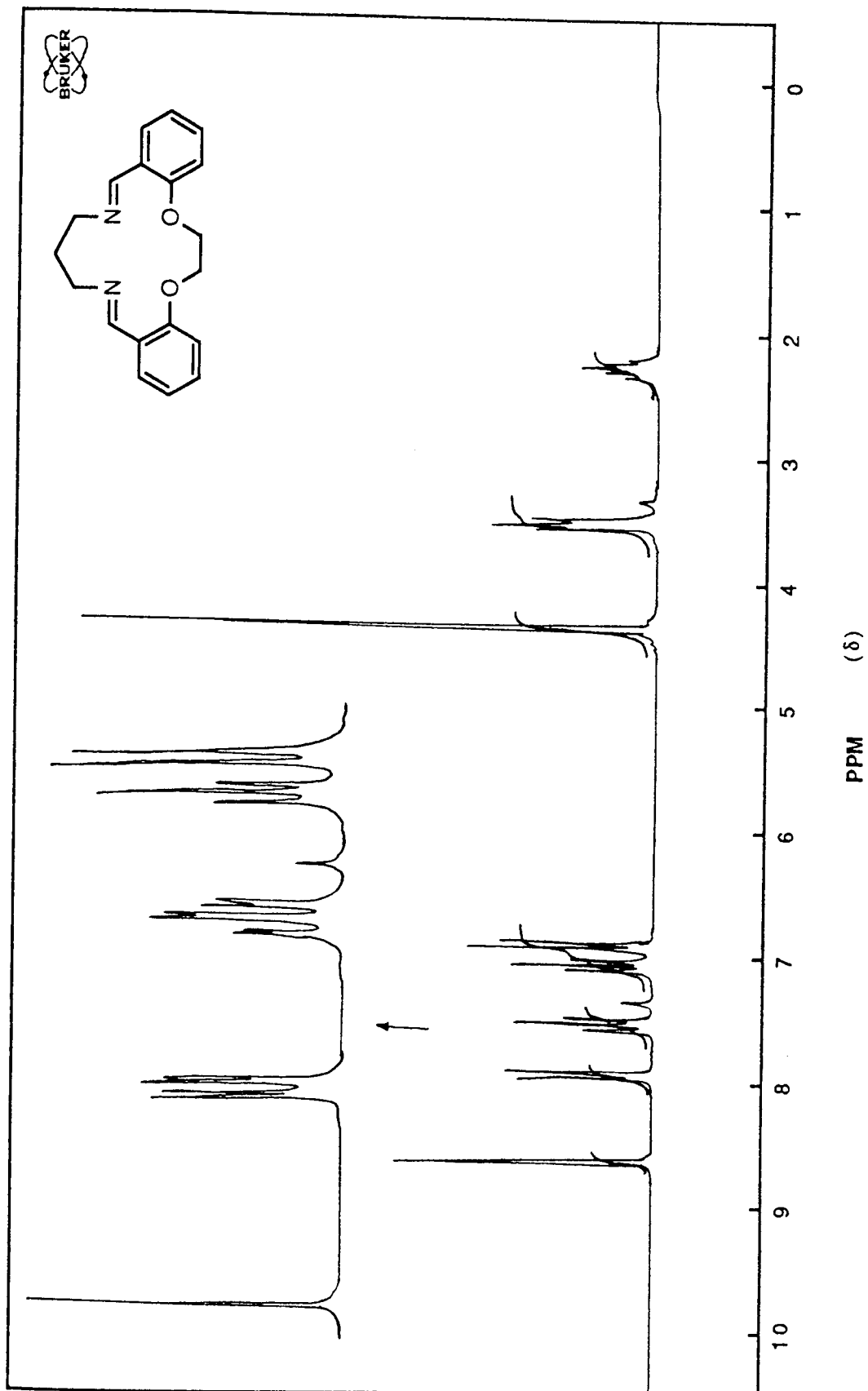
1,3-Diaminopropane (Aldrich) (0.74g, 0.01mol) in 30ml absolute methanol, was added to a solution of 2.7g (0.01 mol) *O-en* in 150ml absolute methanol. The solution was refluxed for 1 hour after which 200ml of distilled water was added and the resulting white suspension left to stand at 0°C overnight. White needle-like crystals were collected, washed with water and recrystallised from ether to yield 2.8g (91%) of crystals m.p. 163-165°C (literature <sup>187</sup> 97%, m.p. 164°C).

##### **6.2.4.1 Nuclear Magnetic Resonance Spectra of *O-en-N-tn*.**

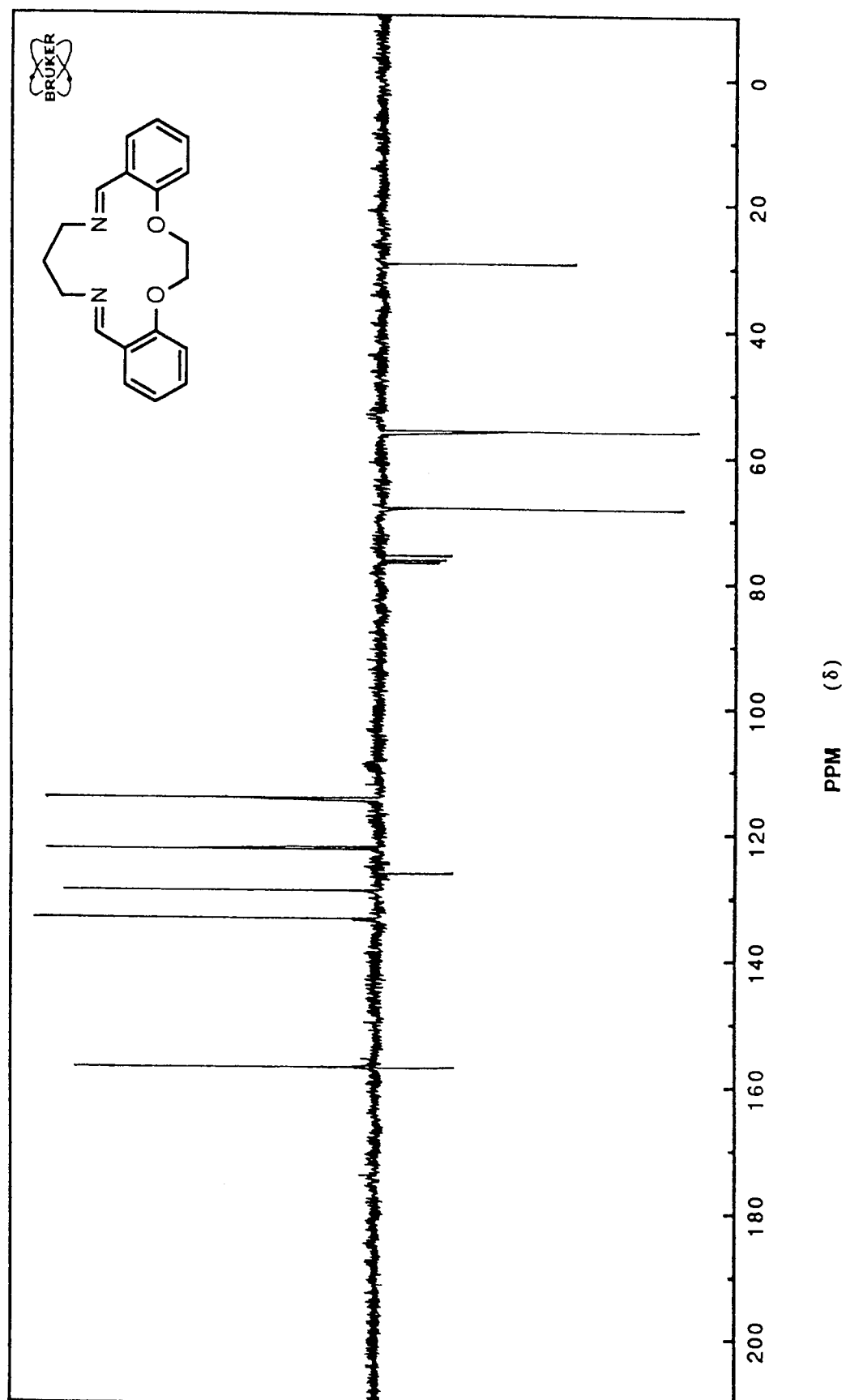
The <sup>1</sup>H nmr spectrum of *O-en-N-tn* in CDCl<sub>3</sub> is shown in Figure 6.10. Again, this is a very clean spectrum indicating no impurities, except for trace water at 4.8δ. The bridging O-CH<sub>2</sub> methylenes appear as a singlet at 4.36δ, with the imine-bridging methylenes occurring as a quintet for the central methylene at 2.28δ and the N-CH<sub>2</sub> groups as a triplet around 3.57δ. The aromatic protons now appear as a distinct doublet-triplet-triplet-doublet formation (though not symmetrical) with resonances at 6.9δ, 7.02δ, 7.37δ & 7.94δ. The imine proton appears as a sharp singlet at 8.9δ.

Figure 6.11 is the <sup>13</sup>C nmr spectrum of *O-en-N-tn* in CDCl<sub>3</sub>. As for the *O-en* precursor, the position of the ring CH's (113.5δ, 121.7δ, 127δ & 131.7δ (+)) and

**Figure 6.10**  $^1\text{H}$  NMR Spectrum of *O-en-N*-tn.



**Figure 6.11**  $^{13}\text{C}$  (*J*-Mod) NMR Spectrum of *O*-en-*N*-tn.



quaternary carbons (124.4 $\delta$ , 158.5 $\delta$  (-)) remains virtually unchanged, but the imine carbon is present at 158.8 $\delta$  (+), the O-CH<sub>2</sub> at 67.9 $\delta$  (-), the N-CH<sub>2</sub> at -57.7 $\delta$  and the central methylene of the imine bridge at 29.4 $\delta$  (-). Correlation with the expected structure is excellent.

#### **6.2.5 Preparation of 6,7,8,9,10,11,17,18-Octahydro-5H-Dibenzo[e,n][1,4] Dioxo[8,12]**

##### **Diazacyclopentadecine, (*O-en-NH-tn*).**

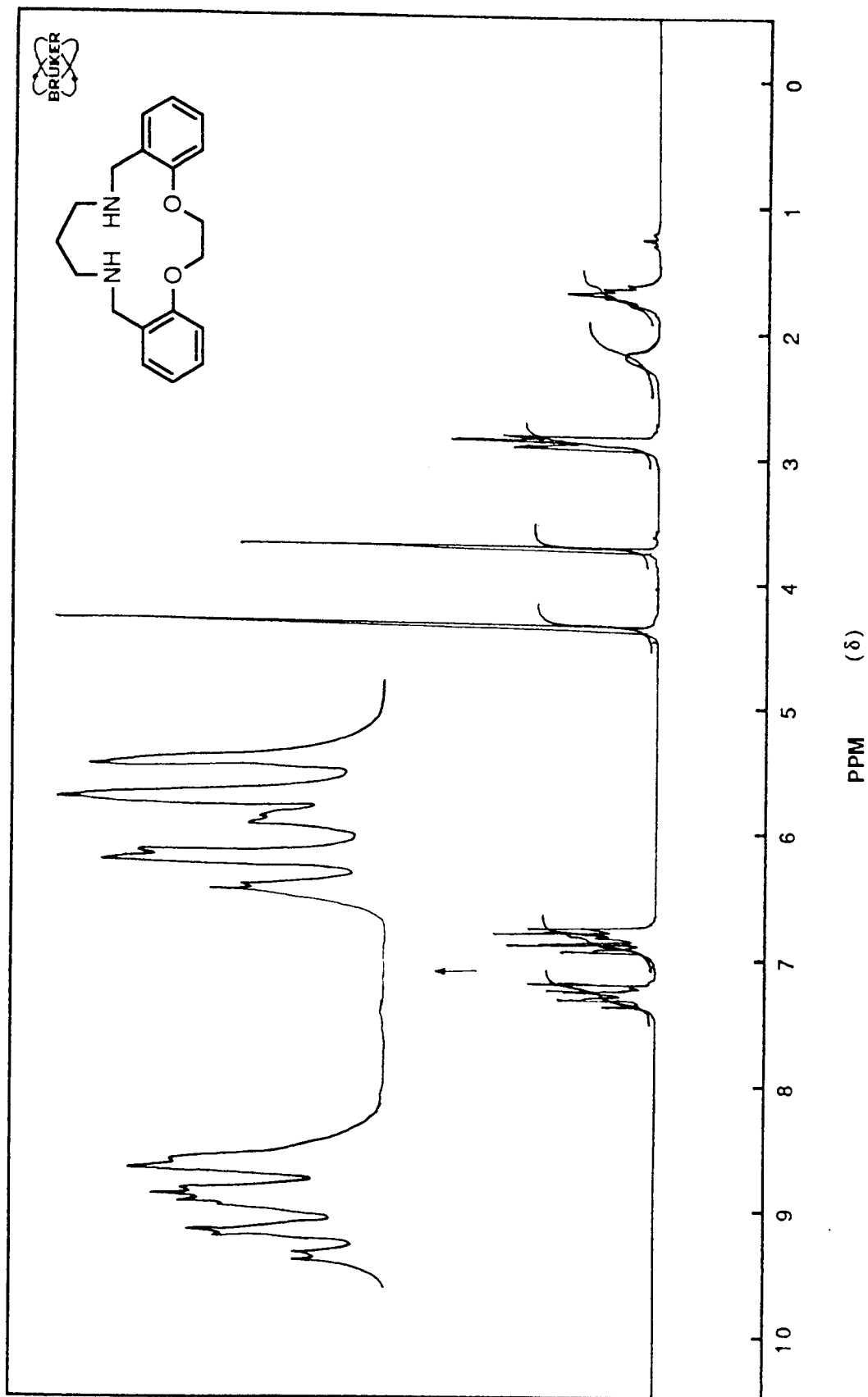
6.2g of *O-en-N-tn* (0.02 mol) was dissolved in 100ml dry methanol, stirred and heated until boiling. To this was slowly added 1.6g borax and 1.86g (0.02 mol) sodium borohydride. The solution was concentrated to 50 ml and cooled. Addition of 200ml of water caused precipitation of a white solid contaminated with a brown material, which was collected and washed in water. Recrystallisation in ether produced 2.5g of a pure white compound (45%) of melting point 144-145°C (literature <sup>186</sup> 80%, m.p. 143°C).

##### **6.2.5.1 Nuclear Magnetic Resonance Spectra of *O-en-NH-tn*.**

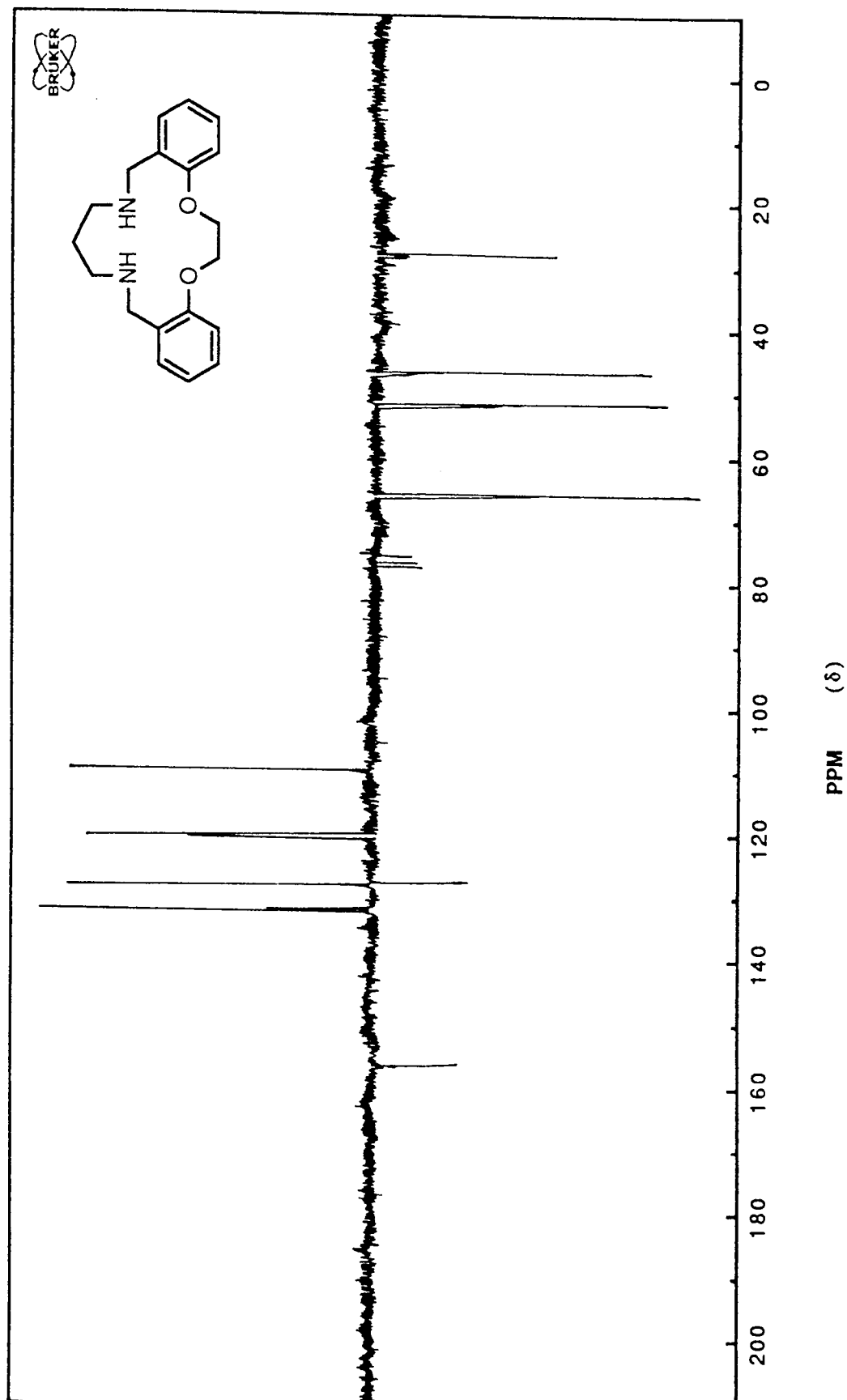
The <sup>1</sup>H spectrum of *O-en-NH-tn* in CDCl<sub>3</sub> is shown in Figure 6.12. The amine N-CH<sub>2</sub> groups occur as a triplet centered around 2.62 $\delta$  and the central methylene of the amine bridge as a quintet around 1.73 $\delta$ . The new features in this spectrum are the broad NH at 2.1 $\delta$ , and the Ar-CH<sub>2</sub>-N singlet at 3.73 $\delta$ . Interestingly, because this methylene has a much less of an inductive effect on the ring compared with the aldehydic and imine carbons of the precursors, the aromatic ring proton resonances has simplified into, what appears to be on a gross scale, a quintet from 6.82-6.92 $\delta$  and a quartet from 7.17-7.28 $\delta$ . Careful analysis of the fine structure suggests that these peak clusters are in fact the expected doublets and triplets observed previously, but overlapping to a greater extent.

Figure 6.13 is the <sup>13</sup>C nmr spectrum for *O-enNH-tn* in CDCl<sub>3</sub>. Aromatic CH's are now

Figure 6.12  $^1\text{H}$  NMR Spectrum of *O*-en-*NH*-tn.



**Figure 6.13**  $^{13}\text{C}$  (*J*-Mod) NMR Spectrum of *O*-en-*NH*-tn.



in slightly shifted positions (110 $\delta$ , 120.5 $\delta$ , 128.4 $\delta$  & 131.1 $\delta$  (+)) with ring quaternary carbons at 129.2 $\delta$  & 156.9 $\delta$  (-). The O-CH<sub>2</sub> groups peak at 65.8 $\delta$  (-), with the Ar-CH<sub>2</sub>-NH and NH-CH<sub>2</sub>- groupings occurring at 51.5 $\delta$  & 47.4 $\delta$  (-) respectively. Finally, the central methylene of the amine bridge peaks at 29.3 $\delta$  (-). Spectroscopy suggests few impurities.

#### **6.2.6 Attempted Preparation of 5,6,7,8,9,10,17,18-Octahydro-16H-Dibenzo[f,n][1,5]Dioxo[9,12] Diazacyclopentadecine, (O-tn-NH-en).**

To 5g of *O*-tn (0.0175 mol) in 150ml of hot methanol was slowly added 1.06g ethane-1,2-diamine (0.0175mol). The yellow solution was stirred for 5 minutes and then 0.25g borax and 1.55g of sodium borohydride (0.04 mol) was slowly added. The solution was concentrated to 30ml and 150ml of water added. At this stage a white product should have separated <sup>186</sup>, but instead, the water became pale yellow in colour. The water was extracted with chloroform and dried over Na<sub>2</sub>SO<sub>4</sub>; evaporation of the solvent left a low yield of a pale yellow oil which had no tendency to crystallise. This preparation was taken no further.

#### **6.2.7 Preparation of 3,4;10,11-Dibenzo-1,12-Diaza-5,8-Dioxacyclopentadecane-1,11-Diene, (O-tn-N-tn).**

*O*-tn-*N*-tn was prepared by a similar procedure to that described for *O*-en-*N*-tn in section 6.2.4, except that to 2.82g of *O*-tn (0.01 mol) in 150ml methanol was added 0.74g (0.01 mol) of 1,3-diaminopropane (Aldrich) in 20ml methanol, and the mixture refluxed for 3 hours. The solution was cooled, 200ml of water added, and the suspension left to settle at 0°C. The resulting white crystals were collected and recrystallised from petroleum ether to yield 1.8g (56%) of melting point 128-129°C (literature <sup>187</sup>, 72%, m.p.129°C).

#### 6.2.7.1 Nuclear Magnetic Resonance Spectra of *O*-tn-*N*-tn.

Figure 6.14 shows the  $^1\text{H}$  nmr spectrum of *O*-tn-*N*-tn in  $\text{CDCl}_3$ . The bridging  $\text{O}-\text{CH}_2$  groups appear as a triplet around  $4.91\delta$ , split by the additional central methylene which itself is a quintet at  $1.7\delta$ . The bridging  $\text{N}-\text{CH}_2$  groups resonate as a triplet at  $3.59$ , split by the central bridge methylene which is another quintet around  $2.29\delta$ . The aromatic protons produce an overlapping doublet-triplet arrangement at  $6.92\delta$ , with a distinct triplet at  $7.36\delta$  and a doublet at  $7.99\delta$ . Finally, the imine proton is present as a singlet at  $8.9\delta$ .

The  $^{13}\text{C}$  nmr spectrum (Figure 6.15) of *O*-tn-*N*-tn in  $\text{CDCl}_3$  shows the ring CH's ( $113.2\delta$ ,  $121.5\delta$ ,  $127.2\delta$  &  $130.9\delta$  (+)) and the ring quaternary carbons ( $124.6\delta$ ,  $158.7\delta$  (-)) at similar positions to those of *O*-en-*N*-tn. The imine carbon is present at  $158.9\delta$ , and the  $\text{O}-\text{CH}_2$  &  $\text{N}-\text{CH}_2$  at  $63.9\delta$  &  $55.4\delta$  (-) respectively. Lastly, the central methylene groups of the two bridges occur at  $28.9\delta$  &  $29.5\delta$  (-) for the oxy and imine links respectively.

#### 6.2.8 Preparation of 6,7,8,9,10,11,18,19-Octahydro-5H,17H-Dibenzof[*o*][1,5]

##### Dioxo[9,13] Diazacyclohexadecine, (*O*-tn-*NH*-tn).

3.22g (0.01 mol) of *O*-tn-*N*-tn was dissolved in 150ml of methanol and brought to reflux with stirring. To this solution was carefully added 3.1g of borax and 0.93g of sodium borohydride (0.03 mol). The clear solution was concentrated to 30ml and cooled. Addition of 200ml of water did not produce a solid product as reported <sup>186</sup>, rather a white emulsion, which was extracted into chloroform and dried over  $\text{Na}_2\text{SO}_4$ . Removal of the solvent left a thick oily residue which slowly solidified over a number of days into a pale yellow solid. The yield of material was 0.9g (28%) with a melting point of  $92-93^\circ\text{C}$  (literature <sup>186</sup>, 40%, m.p.  $91^\circ\text{C}$ ).

**Figure 6.14**  $^1\text{H}$  NMR Spectrum of *O*-tn-*N*-tn.

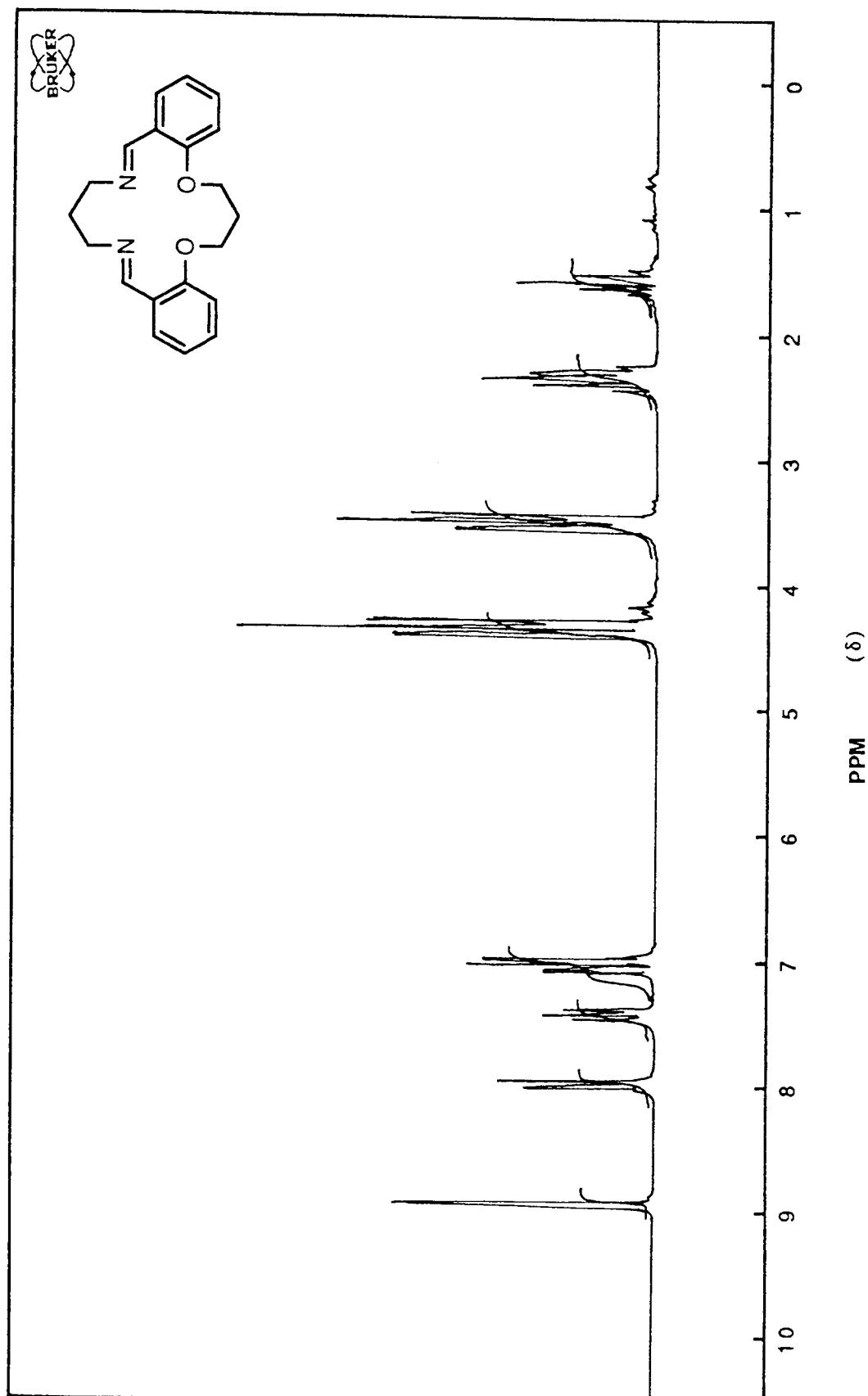
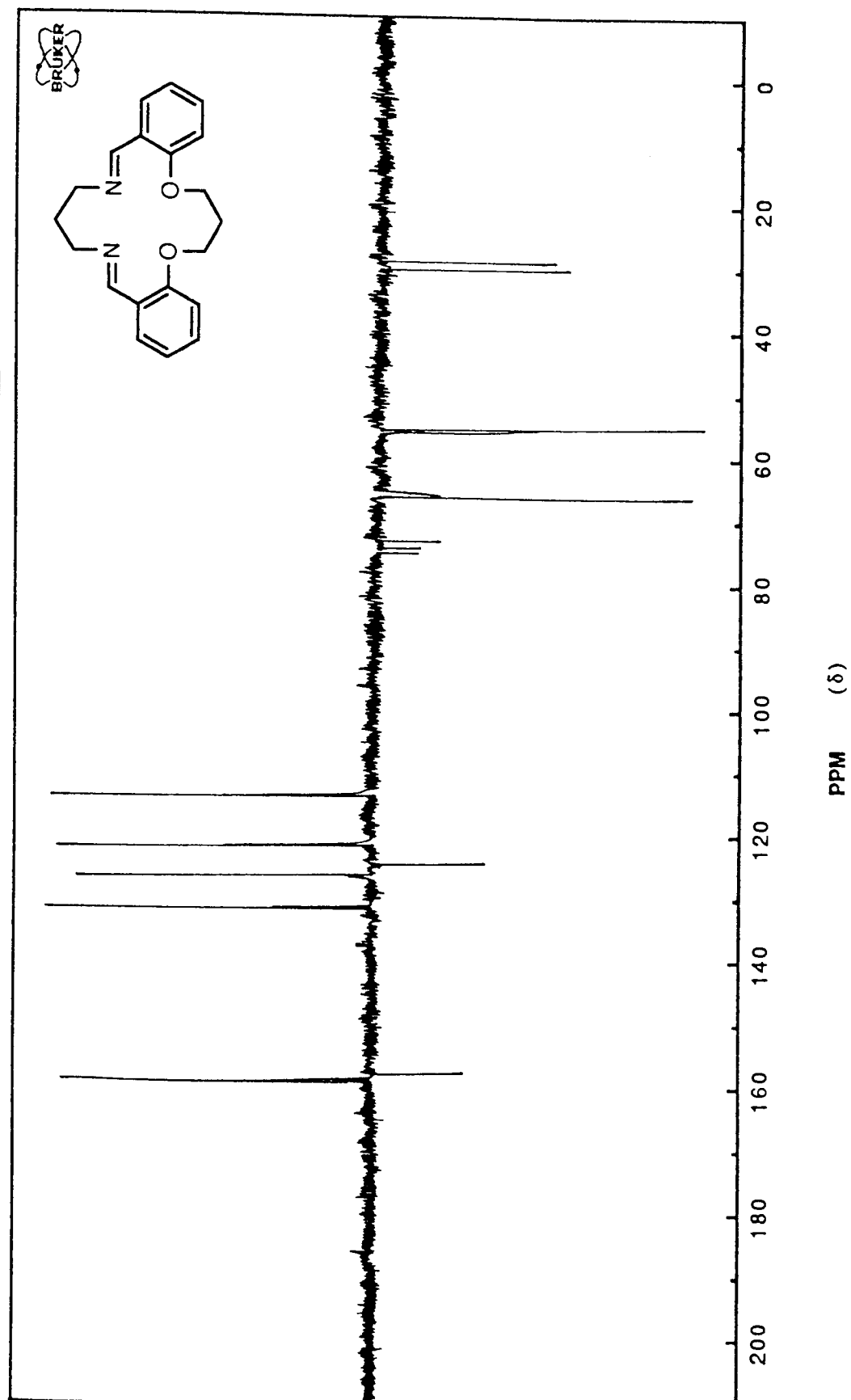


**Figure 6.15**  $^{13}\text{C}$  (*J*-Mod) NMR Spectrum of *O*-tn-*N*-tn.



#### 6.2.8.1 Nuclear Magnetic Resonance Spectra of *O*-tn-NH-tn.

Figure 6.16 is the  $^1\text{H}$  nmr spectrum for *O*-tn-NH-tn in  $\text{CDCl}_3$ . The reduction has obviously proceeded as expected, with the appearance of a broad NH resonance at  $1.79\delta$  and the Ar-CH<sub>2</sub>-N singlet at  $3.72\delta$ . The methylenes of the amine link occur as a triplet at  $2.61\delta$  and the central methylene as a quintet at  $1.59\delta$ . Likewise, the oxy-bridge methylenes appear as a triplet around  $4.28\delta$  and a quintet at  $2.61\delta$ . The aromatic protons are simplified into what appears to be two quartet patterns from  $6.87$ - $6.95\delta$  &  $7.14$ - $7.24\delta$ . Careful analysis this pattern suggests it is a result of the expected doublets and triplets overlapping.

The  $^{13}\text{C}$  nmr spectrum of *O*-tn-NH-tn shown in Figure 6.17 consists of the four ring CH's ( $113.7\delta$ ,  $121.3\delta$ ,  $128.4\delta$  &  $131\delta$  (+)), the quaternary ring carbons ( $129.8\delta$  &  $157.3\delta$  (-)), and the Ar-CH<sub>2</sub>-N and NH-CH<sub>2</sub>- groupings at  $51.7\delta$  &  $47.7\delta$  (-) respectively. The O-CH<sub>2</sub> and central oxy-link methylene occur at  $65.8\delta$  &  $29.3\delta$ , with the central amine-link methylene peaking at  $29.9\delta$  (-). These spectra indicate some minor impurities in this compound, probably unreduced starting material from the position of the peaks.

#### 6.2.9 Attempted Preparation of 1,12,15-Triaza-3,4,9,10-Dibenzo-5,8-

##### Dioxacycloheptadecane, (*O*-en-3NH-dien).

5.15g of Diethylene triamine (Aldrich) in 20ml methanol was slowly added to a stirred boiling solution of *O*-en (13.5g) in 700ml methanol. The solution was refluxed for 15 minutes, then filtered and cooled. 8.0g of Sodium borohydride and 0.5g of borax were slowly added and the volume reduced to 150ml. The solution was cooled to room temperature and 400ml of water added which produced an oily emulsion. The oil was extracted into chloroform, dried over  $\text{Na}_2\text{SO}_4$  and the solvent evaporated to leave a brown

**Figure 6.16**  $^1\text{H}$  NMR Spectrum of *O*-tn-*NH*-tn.

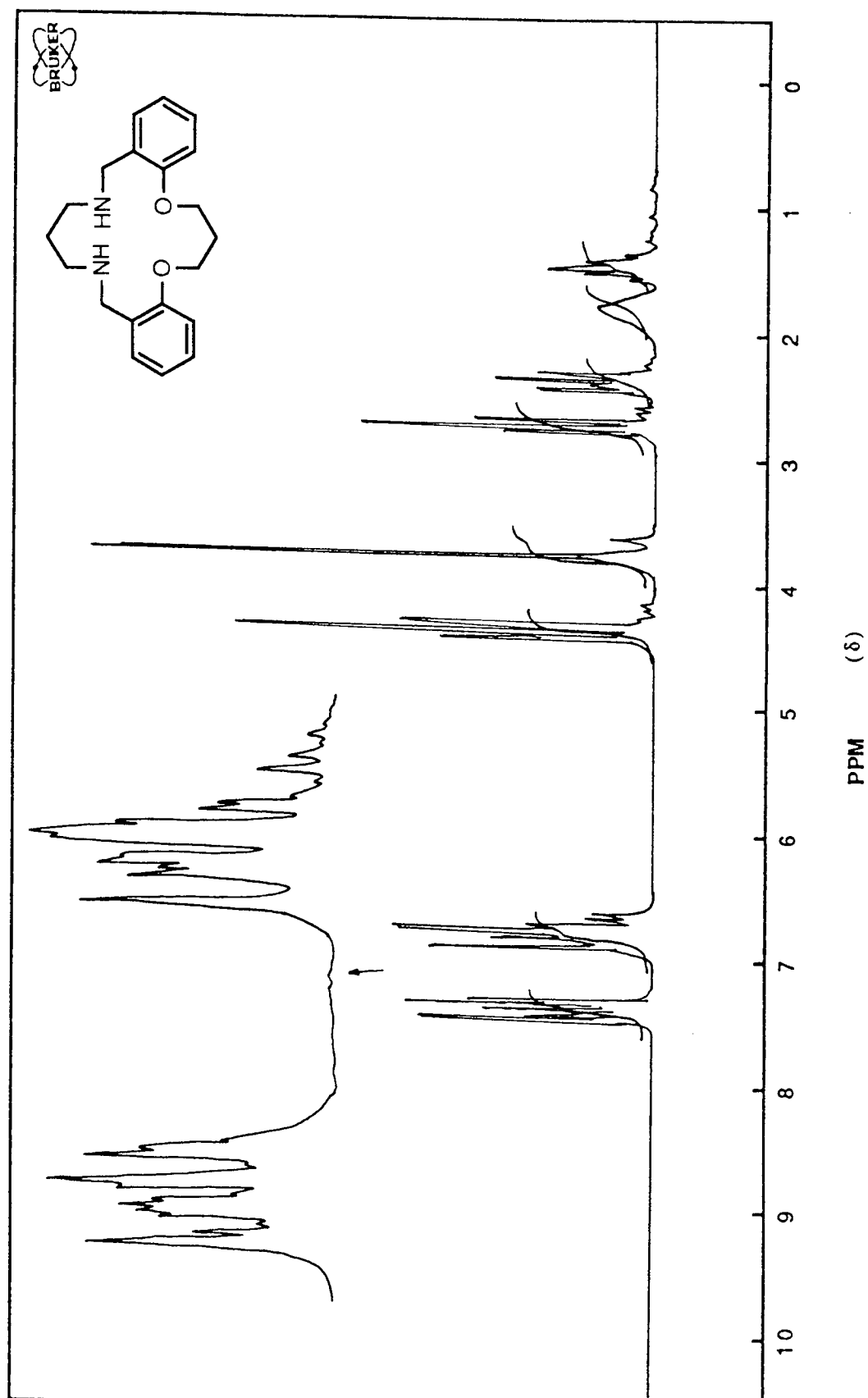
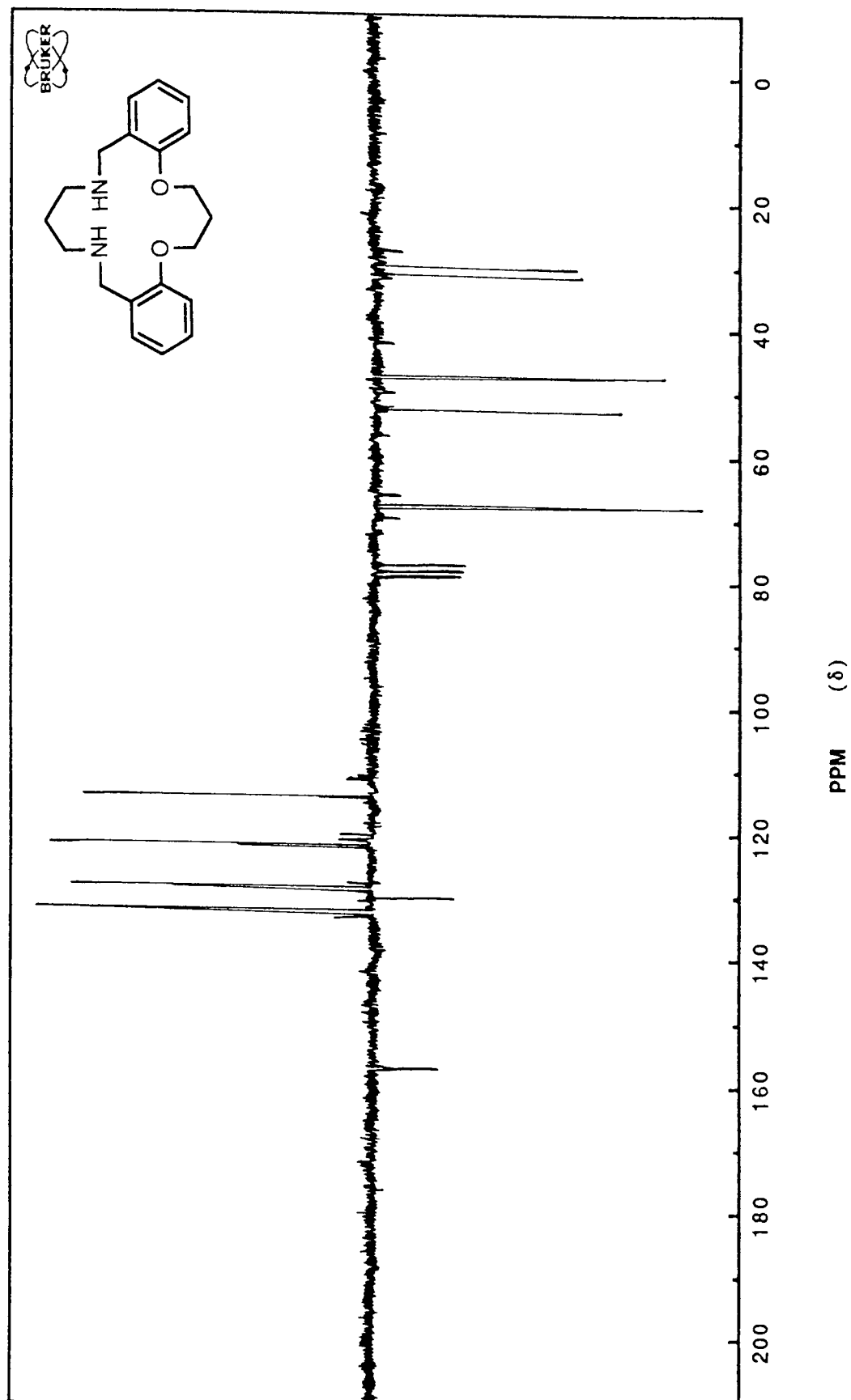


Figure 6.17  $^{13}\text{C}$  (*J*-Mod) NMR Spectrum of *O*-tn-*NH*-tn.



'gum-like' product, rather than the white solid reported in the literature <sup>196</sup>. It had been observed that these gum-type residues often resulted when the product was extracted into chloroform. It was reasonable to assume that the macrocycle was interacting with the solvent to produce a tar. Trituration of the product under ether seemed promising, yielding a white solid. However, brief exposure to the air converted the material back to a brown gum suggesting moisture sensitivity. The preparation of this material was abandoned at this point.

**6.2.10 Attempted Preparation of 5,6:15,16-Dibenzo-1,4-Dioxa-8,13 Diazacyclo-Hexadecine, (*O-en-NH-bn*) & 6,7:16,17-Dibenzo-1,5-Dioxa-9,14-Diazacyclo-Heptadecine, (*O-tn-NH-bn*).**

It was thought that *O-en-NH-bn* might be prepared by the direct one step cyclisation of the alkoxide of N,N'-bis(salicylideneamino)-1,4-butanedi-amine (Lancaster Synthesis) with dibromoethane (as in the production of *O-en*, section 6.2.1), followed by a reduction with sodium borohydride as described previously. This experiment was repeated several times and in each case yielded an unmanageable brown gum, which n.m.r confirmed to be mostly starting material. It was thought that the ethyl linkage may not be long enough to bridge the gap between the benzene rings now that there are four carbon atoms in the amine link. Therefore, the experiment was repeated with dibromopropane in an effort to afford *O-tn-NH-bn*. Unfortunately, this too produced only a brown tar-like material mostly consisting of the starting material. It would be interesting to attempt these reactions with the N,N'-bis(salicylidene) ethylenedi-amine & N,N'-bis(salicylidene) propanedi-amine precursors from Lancaster Synthesis. If a one-step cyclisation and reduction to the produce materials such as *O-en-NH-tn* & *O-tn-NH-tn* was successful with these relatively

inexpensive starting materials, the long time periods necessary to synthesise these materials would be drastically reduced.

### **SECTION (B): Synthesis of the N<sub>4</sub>-Type Macrocyclic Ligands.**

This section is based on work by Lawrance *et al.* 197,198 concerning template synthesis of a series of N<sub>4</sub>-macrocyclic ligands with potential functional groups for polymerisation (Figure 6.4). The three ligands shown were prepared by a novel metal-directed ring-closure, the mechanism for which will be described with reference to Figure 6.18: (A) One of the amine groups from the complex reacts with formaldehyde to produce an alkylated intermediate (B). This tautomerises (C) and dehydrates (E). Similar reaction of another amine group produces the terminal di-imine intermediate (F); one of the imine groups reacts with the nitroethane anion (G) to produce a species that can further attack the imine group on the opposite ligand (H). Thus, the ligands are bridged to produce a nitro-functionalised macrocyclic complex (I).

The reason for interest in these complexes is that it was thought that the nitro group could be reduced to give a pendent amino group, which could be further reacted with acryloyl chloride in an effort to obtain a vinyl functional group for subsequent copolymerisation with HEMA (Figure 6.19). Once immobilised in the polymer, the template metal could be removed by acid leaching or stripping with EDTA. Unfortunately, this could not be proven because of the failure to isolate the reduced complex.

#### **6.2.11 Preparation of (Diethylene Diamine) Copper (II) Perchlorate.**

One of the precursor materials for macrocyclic complex formation was [Cu(II)(en)<sub>2</sub>](ClO<sub>4</sub>)<sub>2</sub>. This was prepared by dissolving 24.2g (0.1 mol) of

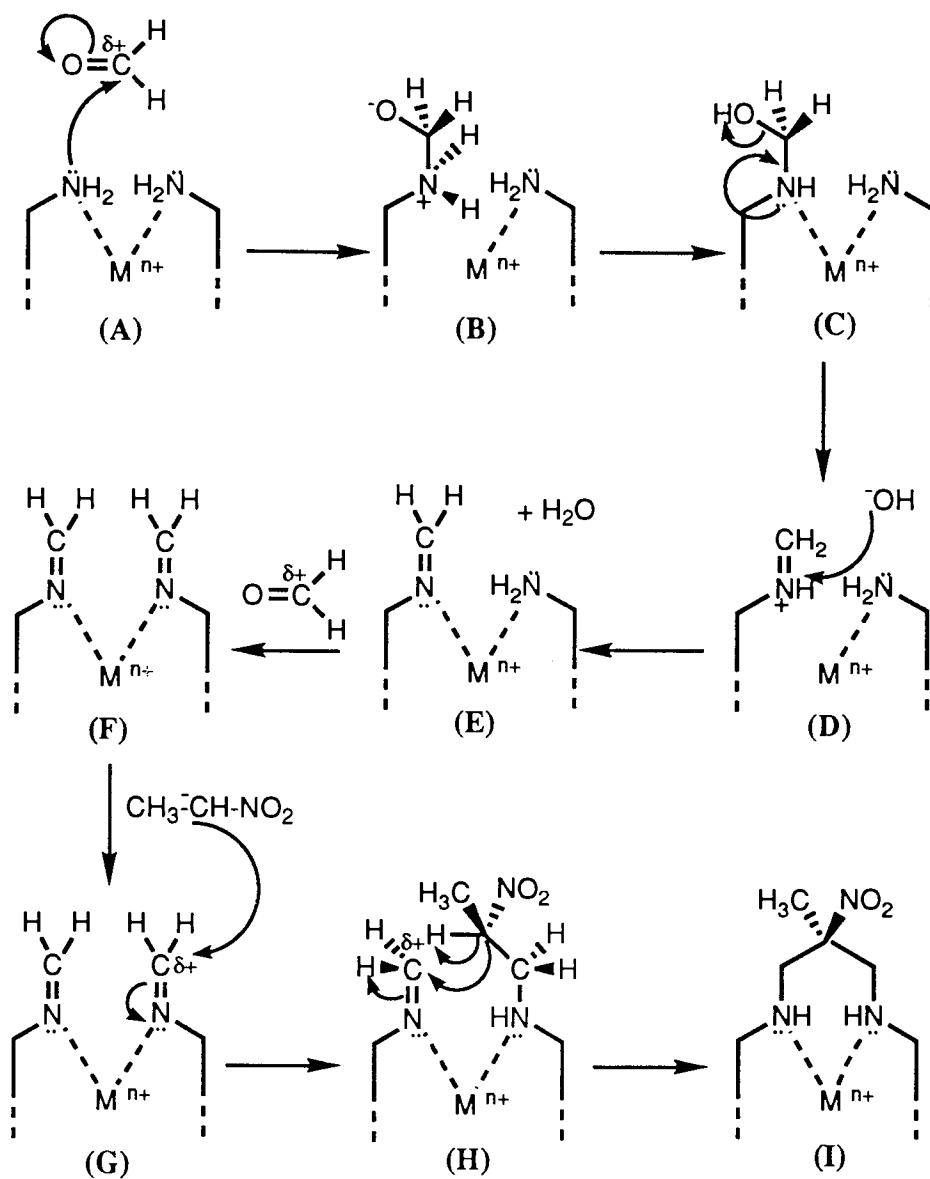


**Figure 6.18** Mechanism for Template Synthesis of Macrocycles.

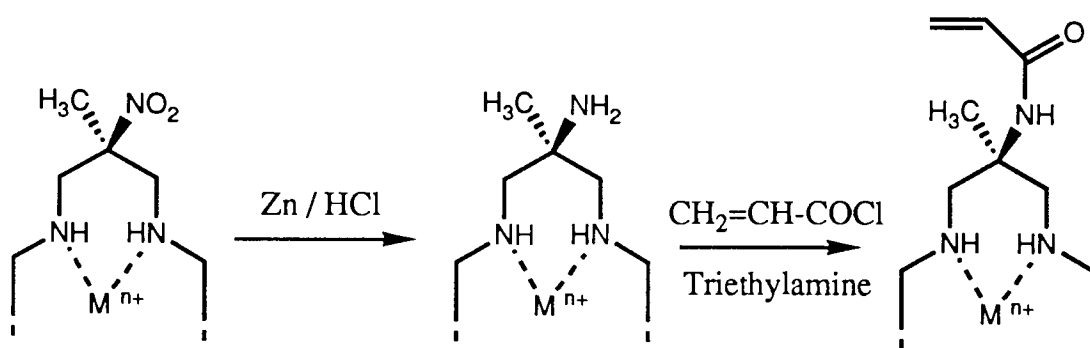


**Figure 6.19** Route for Functionalisation of Macrocycle.

$\text{Cu}(\text{NO}_3)_2 \cdot 3\text{H}_2\text{O}$  (B.D.H.) in 300ml of water, and adding to it in a dropwise fashion, 15.6g (0.2mol) of ethylene diamine (Aldrich). The solution turned from blue to deep purple in colour. 28g (0.2 mol) of sodium perchlorate was added and the solution evaporated down to ~ 200ml in volume. This was then cooled at  $\sim 5^\circ\text{C}$  for a few hours to yield 36g of deep purple crystals of the desired product (94%), which were washed in ethanol and air-dried.

Elemental analysis for  $\text{C}_4\text{H}_{16}\text{N}_4\text{CuCl}_2\text{O}_8$ :

Anal. Calc.: C, 12.53; H, 4.17; N, 14.62.

Found: C, 12.5; H, 4.2; N, 14.5.

#### **6.2.12 Preparation of (3,10-Dimethyl-3,10-Dinitro-1,4,8,11-Tetraazacyclodecane)**

##### **Copper (II) Perchlorate, $(\text{Cu}(\text{Dinamac})(\text{ClO}_4)_2)_n$**

To 11.5g (0.03 mol) of  $[\text{Cu}(\text{II})(\text{en})_2](\text{ClO}_4)_2$  in 200ml of methanol was added 10ml of nitroethane (Aldrich) and 10ml of triethylamine. The mixture was refluxed with stirring and 15ml of 37% formalin (B.D.H.) was added dropwise over a 1 hour period, after which the solution was cooled in an ice bath and the product collected and washed with ethanol. Recrystallisation from acetonitrile/propan-2-ol yielded 9.5g (55%, literature <sup>197</sup> 63%) of purple crystals.

Elemental analysis for  $\text{C}_{12}\text{H}_{26}\text{N}_6\text{CuCl}_2\text{O}_{12}$ :

Anal. Calc.: C, 24.8; H, 4.51; N, 14.47.

Found: C, 24.65; H, 4.7; N, 14.5.

#### **6.2.13 Preparation of the Multidentate Ligand (1,9-Diamino-5-Methyl-5-Nitro-3,7-**

##### **Diazonane) Copper (II) Perchlorate, $(\text{Cu}(\text{Nelin})(\text{ClO}_4)_2)_n$**

This ligand was synthesised by an exactly analogous procedure to that described in 6.2.12

for Cu(Dinemac) perchlorate except that half the quantities of formalin and nitroethane were used in order to bridge just one end of the complex, {It was thought that comparison of the coordination chemistry of this multidentate ligand with the macrocyclic compounds might be of interest}. After washing with ethanol and drying in vacuo, 5.5g (38%, literature <sup>197</sup> 55%) of a powdery product resulted which had an electronic spectrum in water with  $\lambda_{\text{max}} \sim 530\text{nm}$ .

Elemental Analysis for  $\text{C}_8\text{H}_{21}\text{N}_5\text{CuCl}_2\text{O}_{10}$ :

Anal. Calc.: C, 19.95; H, 4.39; N, 14.54.

Found: C, 20.2; H, 4.4; N, 14.6.

#### **6.2.14 Preparation of (10-Methyl-10-Nitro-1,4,8,12-Tetraazacyclopentadecane)**

##### **Copper (II) Nitrate, $(\text{Cu}[\text{Nemac}](\text{ClO}_4)_2$ .**

This macrocyclic complex was prepared by the method of Lawrance & O'Leary <sup>19</sup>. 35g (0.2 mol) of 1,10-diamino-4,7-diazadecane (Aldrich) was added to 48g (0.2 mol) of  $\text{Cu}(\text{NO}_3)_2 \cdot 3\text{H}_2\text{O}$  (B.D.H.) in 1.5l methanol. The dark blue solution was warmed and 22g of triethylamine, 37g of nitroethane and 100ml of 37% formalin were added. After heating at  $\sim 55^\circ\text{C}$  for 30 minutes the solution was left to crystallise the complex as the nitrate overnight. 57g of blue crystals (62%, literature <sup>198</sup> 74%) were collected and which possessed an electronic spectrum in water with  $\lambda_{\text{max}} \sim 570\text{nm}$ .

Elemental analysis for  $\text{C}_{12}\text{H}_{27}\text{N}_7\text{CuO}_8$ :

Anal. Calc.: C, 31.24; H, 5.85; N, 21.25.

Found: C, 31.0; H, 6.0; N, 21.3.

#### **6.2.15 Attempted Reduction of the Nitro-Functions of Cu(Dinemac), Cu(Nemac) & Cu(Nelin).**

All of the  $\text{N}_4$ -type nitro-functionalised complex precursors were subjected to zinc/HCl

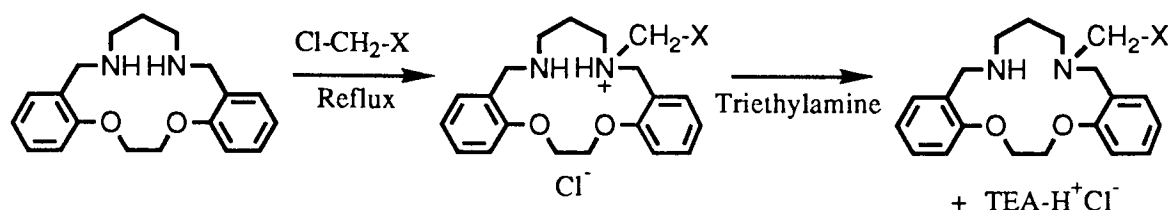
treatment in order to reduce the nitro to an amine group. 6g of the precursor material was added to 250ml of warm 1M HCl. 10g of zinc granules were added and the solution reacted until all colour had disappeared (~2 hours). The solution was filtered and NaOH added to precipitate the zinc as  $\text{Zn(OH)}_2$  (pH ~ 10). The filtrate was adjusted to pH ~9 and excess  $\text{Cu(NO}_3)_2 \cdot 3\text{H}_2\text{O}$  added with stirring. The solution was adjusted to pH~4 and the volume reduced to 100ml. Addition of excess sodium perchlorate did not precipitate the complex. Cooling at 0°C, further reductions in volume and addition of more perchlorate failed to yield the desired product. This occurred with *all* the compounds that required reduction. Attempts at using tin/acid reduction also failed. Therefore, the products Diammach $\text{H}_2$ , AmmachH & AmlinH (Figure 6.14) were never isolated.

### **6.3 ATTEMPTED FUNCTIONALISATION AND IMMOBILISATION OF**

#### ***O-en-NH-tn* & *O-tn-NH-tn* MACROCYCLES.**

In order to obtain a polymer which possesses chemically-linked pendent macrocyclic ligands, two strategies for immobilisation can be applied. The first is the actual functionalisation of the macrocycle with a polymerisable moiety. This approach is synthetically more difficult but is more desirable, as it allows accurate control of the extent of immobilisation. The second approach involves the synthesis of a copolymer which contains a group that is potentially reactive towards the macrocycle. This is the approach used by Lindoy *et al.* in their studies of immobilisation onto polystyrene and silica gel matrices<sup>194,195</sup>. This however, is a rather unpredictable method of anchoring the ligand and the extent of immobilisation is uncontrollable. This section describes attempts at both approaches using the *O-en-NH-tn* & *O-tn-NH-tn* macrocycles synthesised as discussed in the previous section. Both the functionalisation and direct immobilisation procedures are based on the alkylation reaction of secondary amines described by

Hickenbottom <sup>199</sup>. This involves refluxing the amine with the appropriate alkyl halide (usually the chloride) but usually results in a mixture of products because of the HCl released. Use of a HCl-scavenger base such as triethylamine will reduce the tendency for side reactions but necessitates removal of the triethylamine hydrochloride salt [Scheme 6.3(a)]:



## **SECTION (C): Functionalisation of *O-en-NH-tn*.**

### **6.3.1 Reaction with Allyl Chloride.**

The alkyl halide, allyl chloride, was thought to possess the desired characteristics for reaction according to scheme 6.3(a). 4g of *O-en-NH-tn* (0.013 mol) was dissolved in 200ml of chloroform, to which 1.3g of triethylamine was added. 0.98g (1.1ml) of allyl chloride (Aldrich) in 30ml of chloroform was added dropwise to the warm solution. After complete addition the mixture was refluxed for 4 hours. The yellow solution was cooled to room temperature, extracted with 3 x 100ml of water to remove triethylamine hydrochloride and then dried over  $\text{Na}_2\text{SO}_4$ . The volume of solution was reduced to 50ml and 200ml of diethyl ether was added to yield a milky precipitate. When collected, this product proved to be a yellow gum; attempts at trituration failed and a sample of the product was subjected to NMR analysis to see if any functionalisation had occurred.

#### **6.3.1.1 Nuclear Magnetic Resonance Study of Allyl Chloride Product.**

Comparison of the  $^1\text{H}$  &  $^{13}\text{C}$  nmr spectrum for the reaction product (Figures 6.20 &

6.21) with those for pure *O*-en-*NH*-tn (Figures 6.12 & 6.13) suggests that some of this product contains unreacted starting material. However, there are many additional peaks, and the disappearance of the broad NH resonance at  $\delta$  2.18 seems to confirm reaction at one or both secondary amine sites. Certainly the introduction of an allyl-type resonance pattern between 4.77 - 5.88 $\delta$  would indicate that some functionalisation has occurred as predicted, but there are however, a number of extra inexplicable peaks in both the proton and carbon nmr spectra which suggests that a number of side reactions have taken place. This is not surprising, as over-alkylation in this type of reaction is a problem. This can be countered by using excess amine but needs the amine to be freely available, and volatile enough to remove afterwards. This product was not used in any subsequent polymerisation attempts.

### **6.3.2 Reaction with Acryloyl Chloride.**

0.5g of *O*-en-*NH*-tn (0.0016 mol) and 0.16g (0.0016 mol) of triethylamine were added to 40ml of dry tetrahydrofuran (THF), stirred and warmed. 0.145g of acryloyl chloride (0.0016 mol) in 20ml of THF was added dropwise to this solution over a 1 hour period. The clear solution turned cloudy after 30 minutes, probably due to the formation of the triethylamine hydrochloride salt. After the addition period the solution was refluxed for a further 30 minutes, cooled and allowed to stand overnight. The insoluble salt settled out to leave a pale yellow solution; this was subsequently filtered and the solvent evaporated to leave 0.3g of a yellow gum as encountered in section 6.3.1. Crystallisation from THF and diethyl ether failed, as did attempts at trituration. The product was subjected to NMR analysis to check for functionalisation.

#### **6.3.2.1 Nuclear Magnetic Resonance Study of Acryloyl Chloride Product.**

Figures 6.22 & 6.23 are the  $^1\text{H}$  &  $^{13}\text{C}$  nmr spectra for the product in  $\text{CDCl}_3$ . Comparing

**Figure 6.20**  $^1\text{H}$  NMR Spectrum of Reaction Product Between *O*-en-*NH*-tn & Allyl Chloride.

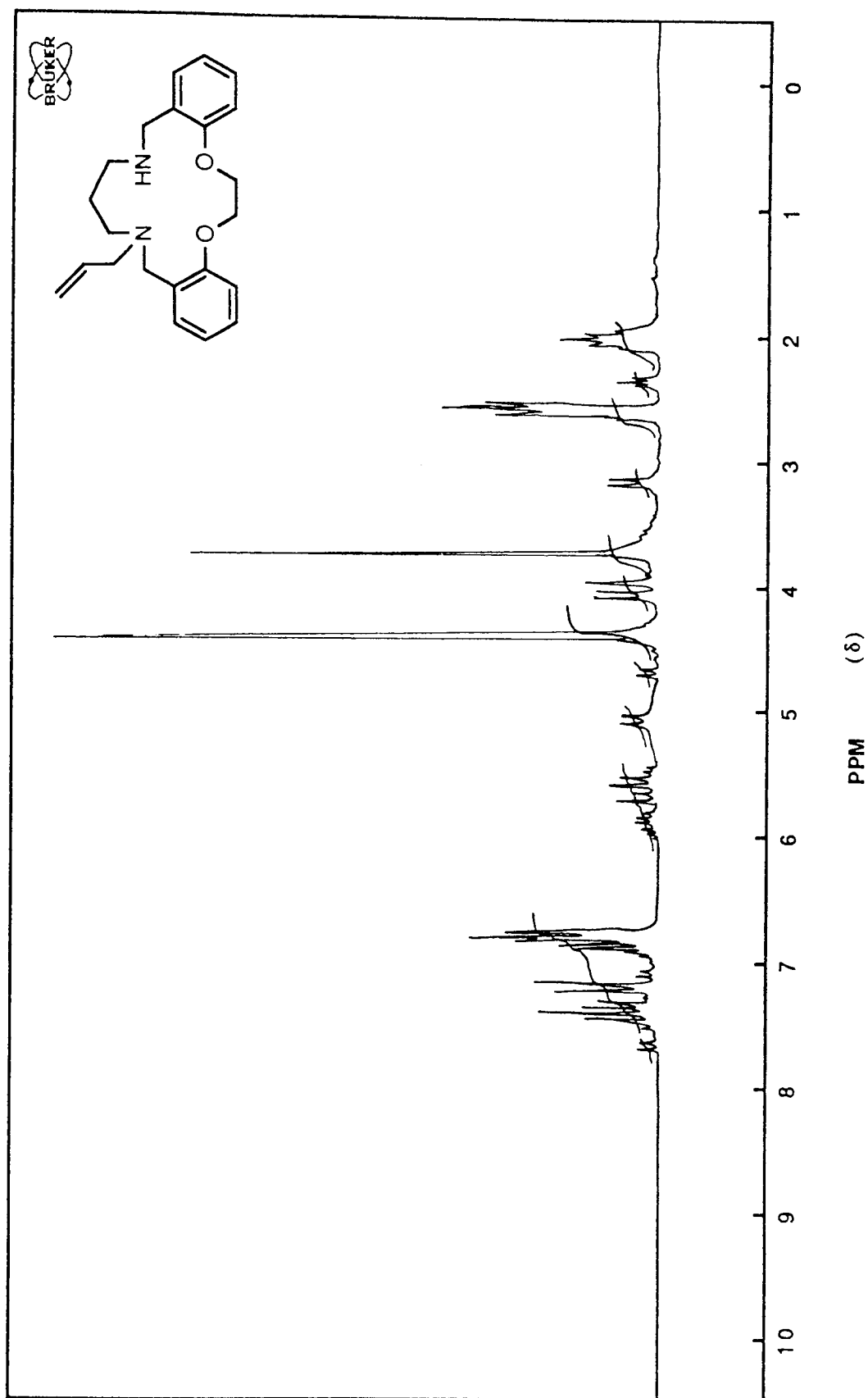
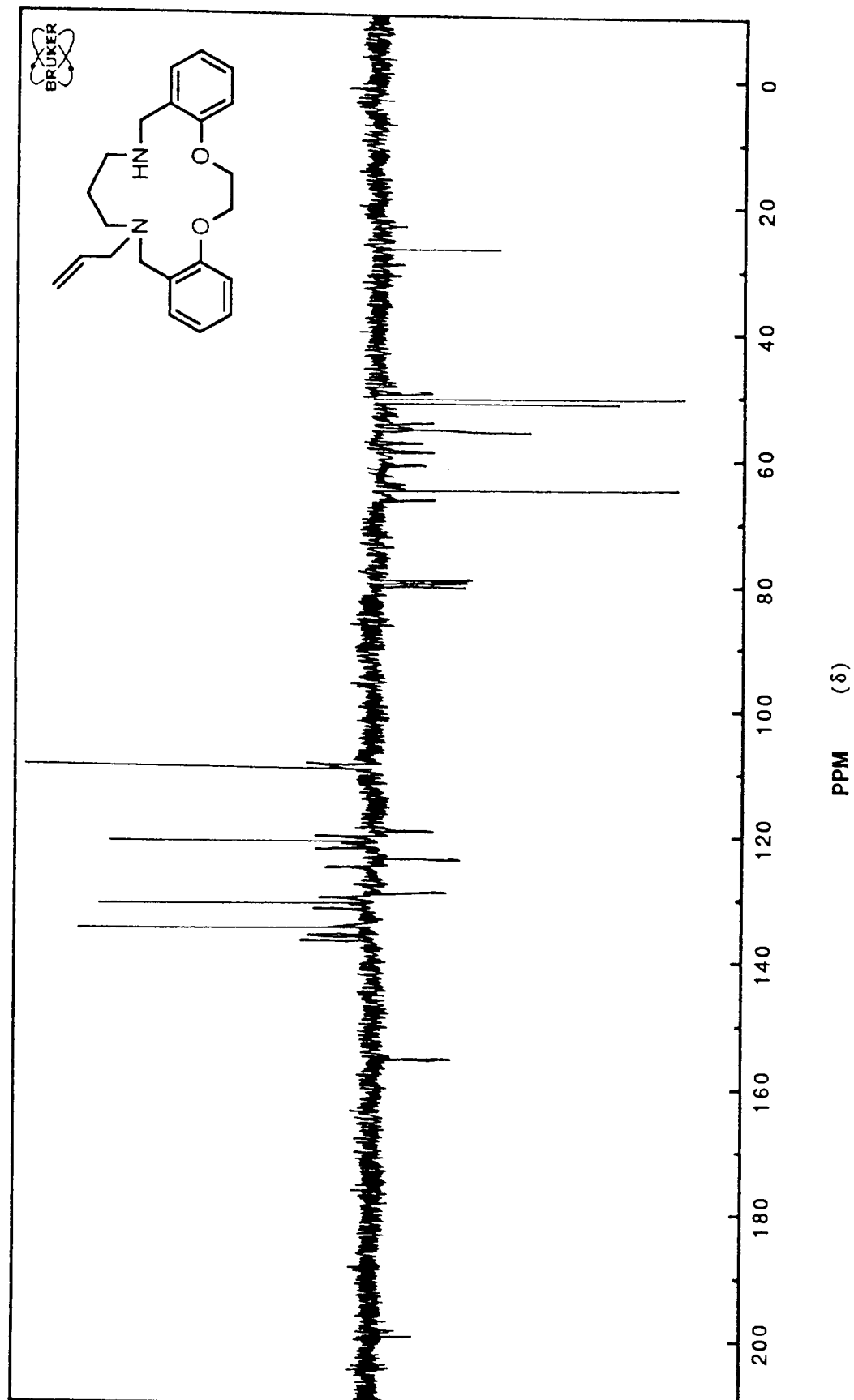


**Figure 6.21**  $^{13}\text{C}$  (*J*-Mod) NMR Spectrum of Reaction Product Between *O*-en-*NH*-tn & Allyl Chloride.



these spectra with Figures 6.12 & 6.13 for the pure compound shows that the product to be a result of a very *unclean* reaction. The proton spectrum possesses the fundamental peaks associated with the starting material but many of the peaks have splitting patterns that would not be predicted. If the product has indeed been functionalised at one amine site only, then the asymmetry of the compound coupled with through-space interactions of the pendent acryolyl group could give rise to a rather complicated spectrum. A vinyl-type pattern between 5.6 - 6.75 $\delta$  and the presence of a carbonyl in the  $^{13}\text{C}$  at 184 $\delta$  suggests that some functionalisation has occurred as predicted. The broad NH resonance has been reduced to a shoulder on the quintet at 1.75 $\delta$ . However, there are once again many additional peaks that confirm the presence of impurities. This product was not used in any subsequent polymerisation studies.

#### **SECTION (D): Direct Immobilisation of *O*-en-NH-tn & *O*-tn-NH-tn.**

The use of a reactive co-monomer to prepare a copolymer that can itself, directly react with the macrocycle, is the approach used by Lindoy *et al.* <sup>194,195</sup> to avoid the synthetic difficulties previously described. They chose to use chloromethylated styrene ( $\text{CH}_2=\text{CH}-\text{C}_6\text{H}_4-\text{CH}_2-\text{Cl}$ ) as described by Melby <sup>200</sup>. This would be totally inappropriate in this study, as the styrene co-monomer would introduce unwanted degrees of hydrophobicity into the membrane; therefore, an alternative was necessary.

#### **6.3.3 Allyl Chloride Copolymer Membranes.**

Attempts to fabricate a copolymer membrane with reactive groupings using allyl chloride as a co-monomer with HEMA produced opaque membranes with large voided areas. It is thought that the polymerisation temperature is too high for the use of allyl chloride as a co-monomer, because it boils at 44-46°C.

**Figure 6.22**  $^1\text{H}$  NMR Spectrum of Reaction Product Between  
*O*-en-*NH*-tn & Acryloyl Chloride.

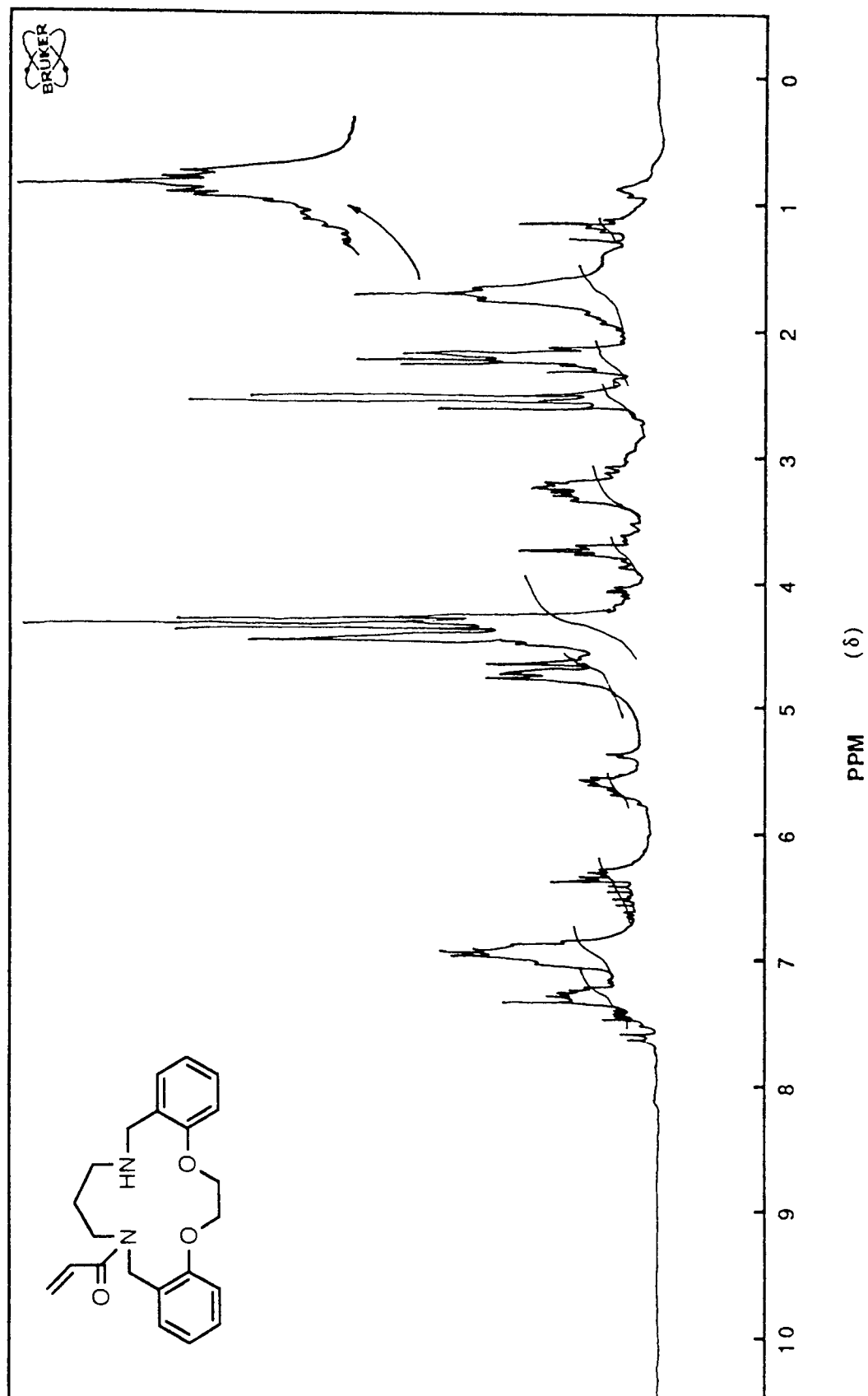
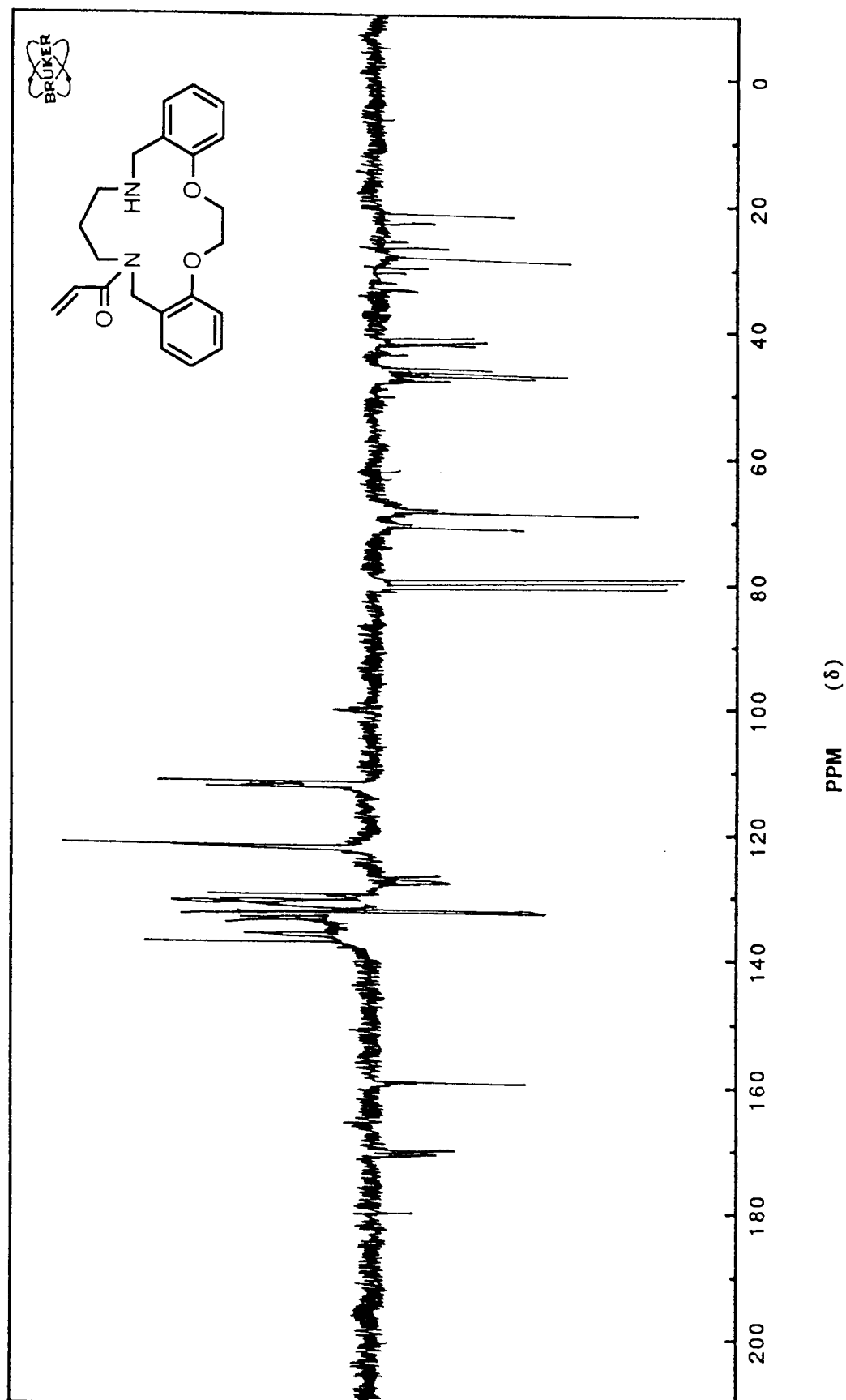


**Figure 6.23**  $^{13}\text{C}$  (*J*-Mod) NMR Spectrum of Reaction Product Between *O*-en-*NH*-tn & Acryloyl Chloride.



#### **6.3.4 Chloro-Ethyl Vinyl Ether Copolymer Membranes.**

Chloro-ethyl vinyl ether ( $\text{Cl-CH}_2\text{-CH}_2\text{-O-CH=CH}_2$ ) was thought to possess an ideal pendent chloro-alkyl group for reaction with the macrocycles. This monomer was successfully copolymerised into a HEMA membrane by the procedure outlined in Chapter Two, section 2.5.2.

#### **6.3.5 2-(Chloro-Ethyl) Methacrylate Membranes.**

2-(Chloro-ethyl) methacrylate ( $\text{CH}_2=\text{C}(\text{CH}_3)\text{-CO-O-CH}_2\text{-CH}_2\text{-Cl}$ ) (Polysciences Ltd.) is the chloro-analogue of HEMA and as such should produce an ideal copolymer membrane as this too has a pendent chloro-alkyl chains for anchoring the macrocycles. This monomer was successfully copolymerised according to the method of section 2.5.2.

#### **6.3.6 Procedure for Immobilisation onto Membranes.**

The procedure for direct macrocycle immobilisation onto membranes involved suspending the membrane in a PTFE frame into 500ml of methanol containing 5g of the desired macrocycle and the appropriate amount of base to remove HCl. The solution was refluxed for 6 hours after which the polymer membrane was removed and desolvated in an oven. Methanol is an excellent swelling agent for this type of membrane which guaranteed total solution penetration, but often weakened the membrane to such an extent that it was torn from the supporting frame. The solution was evaporated to recover unreacted macrocycle and base.

Both types of membrane described in sections 6.3.4 & 6.3.5 were reacted with samples of both *O-en-NH*-tn & *O-tn-NH*-tn. In all four cases, the FT-IR spectrum of the product membrane was identical to the starting membrane and elemental analysis showed no

nitrogen content in the polymer. From this evidence it was simple to deduce that the reaction was not progressing as anticipated. It was thought that the solution in which the membranes were refluxed might be too dilute. Since it was impractical to use higher concentrations of macrocycle, a series of linear copolymers in solution (using the comonomers of sections 6.3.4 & 6.3.5) were made by the method described in section 2.5.3, Chapter Two. 30ml of a 10% (wt/wt) copolymer solution in ethanol, was refluxed for 6 hours with 2g of macrocycle and excess base. Again, for every copolymer/macrocycle combination the product had an identical IR spectrum to the starting material and elemental analysis showed no nitrogen incorporation. It could only be concluded that the chloro-alkyl chain was not sufficiently reactive to anchor the macrocycle. Chemical immobilisation attempts were abandoned at this stage.

#### **6.4 TRANSPORT OF IONS THROUGH MEMBRANES WITH ENTRAPPED MACROCYCLES.**

It was noted that the macrocyclic ligands dissolved within the HEMA monomer to give clear solutions which could then be polymerised into membranes in which the macrocycle was physically entrapped. The presence of the two phenyl rings in the macrocycle structure endows a degree of hydrophobicity. However, on coordination of a metal ion, the complex is rendered water soluble and it was thought that the entrapped compound would simply leach from the membrane. Therefore, attempts were made to cross-link the membrane (using EGDM) to such an extent that the complex was unable to diffuse out of the network. A number of combinations were fabricated into membranes and tested for transport (Table 6.1, overleaf). The combination of cross-linking and the presence of the hydrophobic ligand component reduced the EWC of the membrane below the extent at which transport across the gel was permissible. Only when low levels of both cross-linker

and ligand were used, did any transport phenomena occur.

<u>% Cross-Linker</u>	<u>% Macrocycle</u>	<u>Transport Observed?</u>
10	2.5	No
5	2.5	No
2.5	2.5	No
2.5	5	No
1	5	No- weak colour developed
1	2	Yes

**Table 6.1 Membranes Tested with Entrapped Macrocycles.**

The remainder of this chapter describes a series of transport studies with Cu(II), Co(II) & Ni(II) ions across membranes containing *O-en-NH*-tn, and an analogous set containing *O*-tn-*NH*-tn. No leaching of the complexes was observed.

#### **6.4.1 Transport of Binary Salt Solutions Across Membranes with Entrapped Macrocylic Ligands.**

A series of competitive transport studies were performed, analogous to those described in Chapter Five, section 5.6, using two series of membranes containing 2% (by weight) *O-en-NH*-tn in one set, and a molar equivalent of *O*-tn-*NH*-tn in the other. All studies were performed at 25°C and with 0.25M salt solutions. Figures 6.24 -6.26 are the primary transport curves for the permeation of the binary transition metal chloride solutions. Table 6.2 outlines the important transport data collected from these experiments. As Figure 6.27 highlights, analysis of the permeability coefficients for the metal ions in binary solutions reveals that, as described in Chapter Five, the general trend in the *O-en-NH*-tn system is for both species to permeate through the membrane at similar rates. The pattern for ion-dominance on transport effects cannot be explained fully, but both ligands seem to show  $P_c$ 's in the order Cu/Ni > Cu/Co > Ni/Co, which is the sequence in which the stability constants of these ligands varies (Table 6.3).

Figure 6.24: Permeability of Cu(II)/Ni(II) Binary Salt Solutions through

Membranes Containing Entrapped Macrocycles.

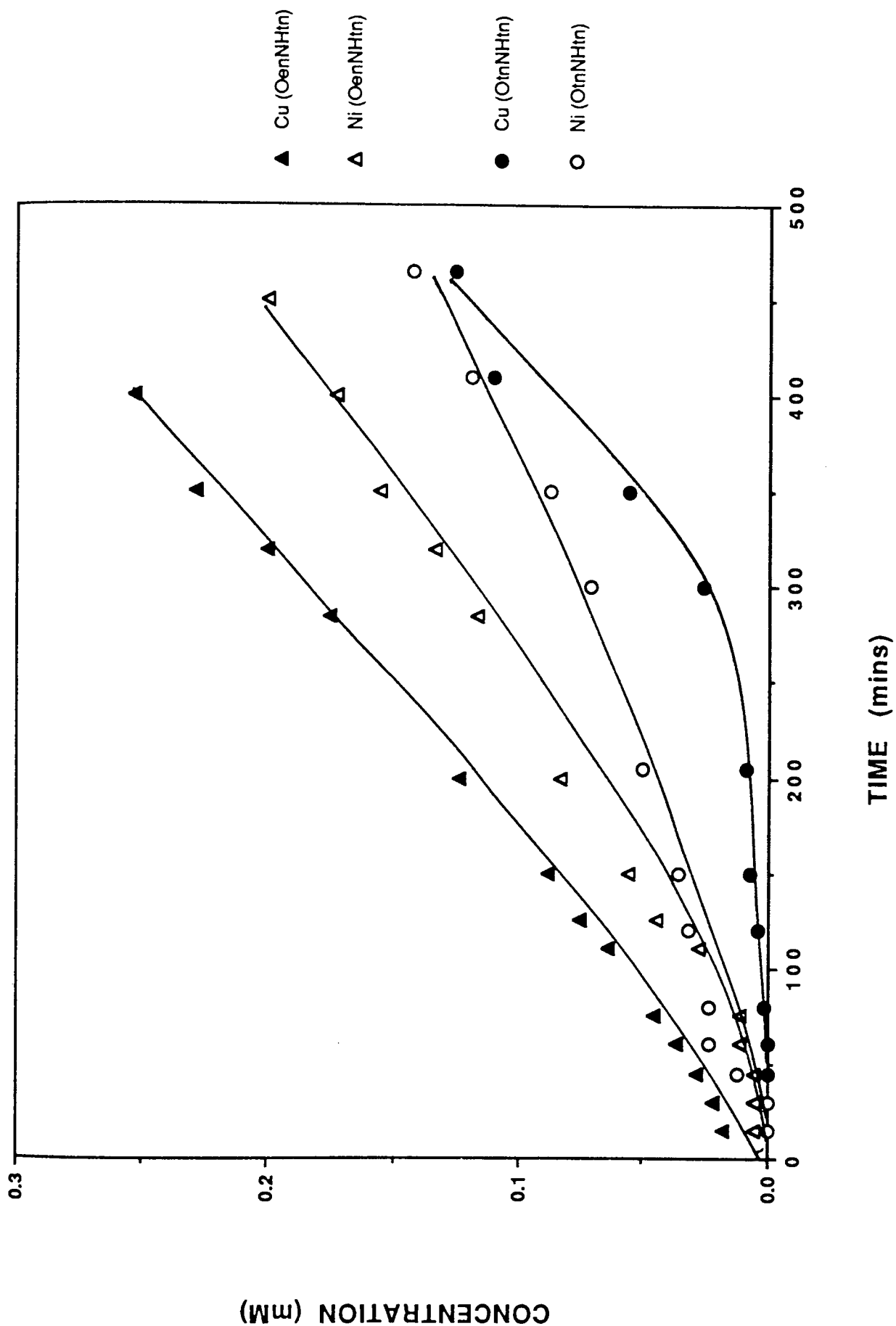


Figure 6.25: Permeability of  $\text{Cu(II)/Co(II)}$  Binary Salt Solutions through

# Membranes Containing Entrapped Macrocycles.

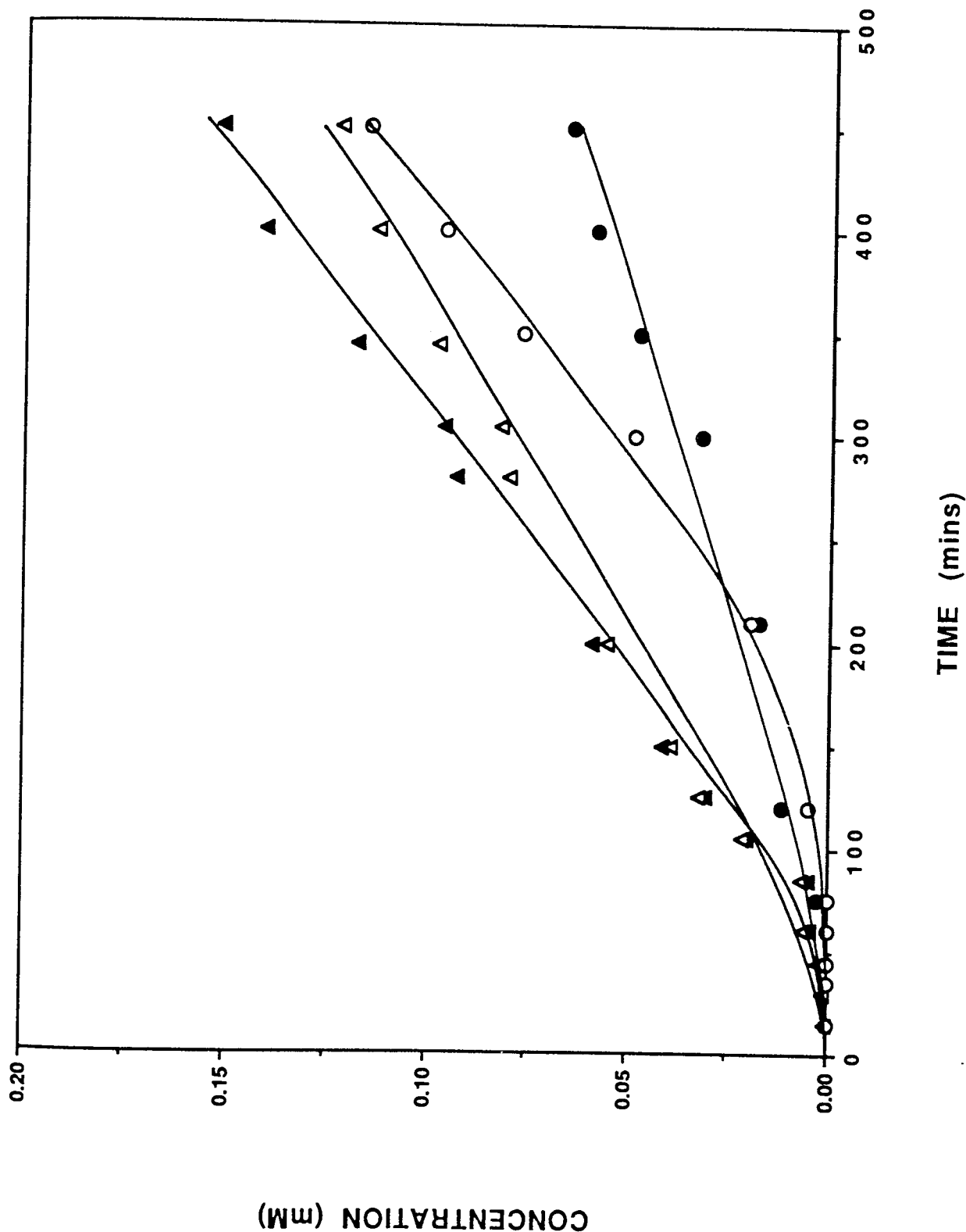
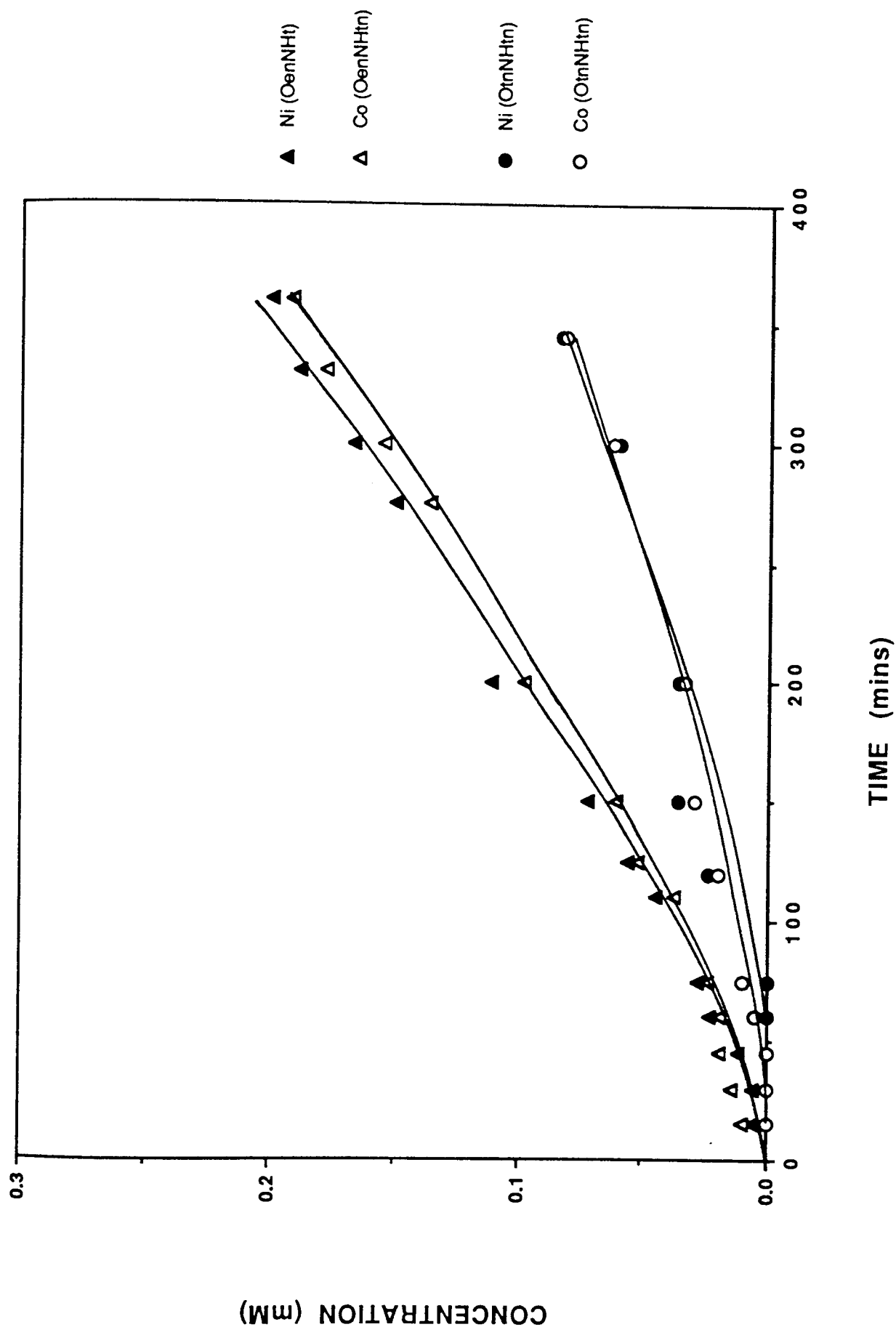


Figure 6.26: Permeability of NiOD/CoOD Binary Salt Solutions through

Membranes Containing Entrapped Macrocycles.



<u>Binary Solution</u>	<u>Ion Monitored</u>	<u>O-en-NH-tn</u>		<u>O-tn-NH-tn</u>	
		<u>P<sub>c</sub></u> (cm <sup>2</sup> min <sup>-1</sup> )	<u>Lag-Time</u> (mins)	<u>P<sub>c</sub></u> (cm <sup>2</sup> min <sup>-1</sup> )	<u>Lag-Time</u> (mins)
Ni/Co	Ni(II)	2.2 x 10 <sup>-7</sup>	20	8.6 x 10 <sup>-7</sup>	75
Ni/Co	Co(II)	2.2 x 10 <sup>-7</sup>	20	8.3 x 10 <sup>-7</sup>	50
Cu/Ni	Cu(II)	2.3 x 10 <sup>-6</sup>	20	2.2 x 10 <sup>-6</sup>	200
Cu/Ni	Ni(II)	1.8 x 10 <sup>-6</sup>	30	1.2 x 10 <sup>-6</sup>	30
Cu/Co	Cu(II)	1.3 x 10 <sup>-6</sup>	50	5.1 x 10 <sup>-7</sup>	70
Cu/Co	Co(II)	1.1 x 10 <sup>-6</sup>	50	1.2 x 10 <sup>-6</sup>	100

**Table 6.2 Competitive Transport Data for Macrocycle-Entrapped Membranes.**

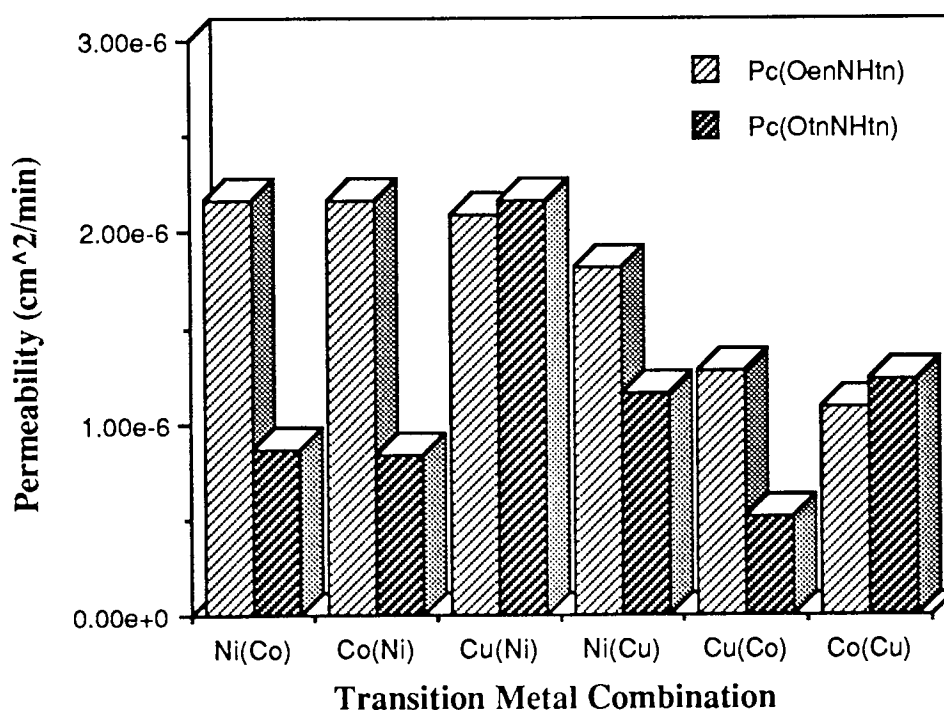


**Figure 6.27 Comparison of Permeabilities for TM ion Combinations through Membranes Containing Entrapped Macrocycles.**

For the *O*-tn-*NH*-tn system, the Cu(II)/Ni(II) & Cu(II)/Co(II) combinations do appear to

permeate at significantly different rates. Why this is so is unclear, but it may be that the 16-membered ring size is beginning to selectively distinguish between particular metal ions.

Examination of the lag-time data reveals a similar story: metal ion combinations transported across *O-en-NH*-tn systems experience similar lag-times, whereas those for the *O-tn-NH*-tn ligand show some differentiation (Figure 6.28). At this point it is useful to consider the stability constants for these ligands in solution <sup>192</sup>:

Macrocycle Type	Ring Size	$\log K$ [ $\log K: M^{2+} + L = ML^{2+}$ ]			
		Co(II)	Ni(II)	Cu(II)	Zn(II)
<i>O-en-NH</i> -tn	15	<4.5	5.4	7.7	4.1
<i>O-tn-NH</i> -tn	16	<4.5	5.8	7.7	4.3

**Table 6.3 Stability Constants for Macrocyclic Ligands in Solution.**

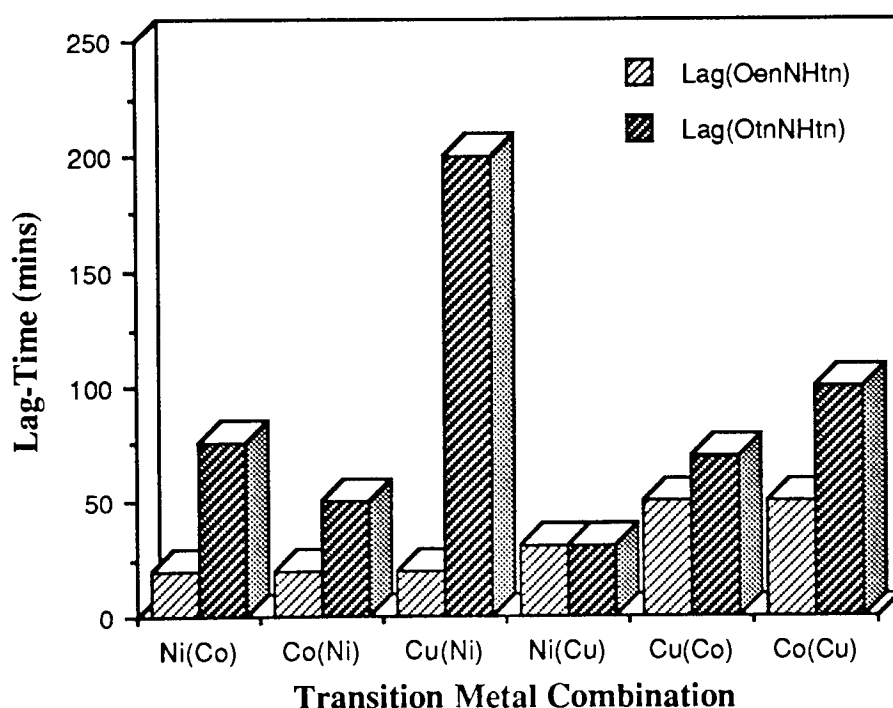


**Figure 6.28 Comparison of Lag-Times for TM ion Combinations through Membranes Containing Entrapped Macrocycles.**

According to the stability constant data in Table 6.3, the *O*-tn-*NH*-tn ligand does generally form a slightly more stable complex in solution compared with *O*-en-*NH*-tn. It seems unlikely that this small difference alone is responsible for the alternative modes of transport observed for the two systems. On the grounds of stability constants alone, one would predict that the order of increasing interaction, and thus length of lag-time experienced by the metal ion, would follow the Irving-Williams series of  $\text{Co} < \text{Ni} < \text{Cu} > \text{Zn}$ . Once again, no simple pattern is evident for this system. When in combination with  $\text{Ni(II)}$ ,  $\text{Cu(II)}$  experiences by far the longest lag-time (~200 minutes); but when combined with  $\text{Co(II)}$ , the lag-time is reduced to ~70 minutes. It might be possible to interpret this observation by considering  $\text{Co(II)}$  as the dominant ion which defines the transport conditions when in combination with  $\text{Cu(II)}$  (which would be opposite to the stability constant prediction). But  $\text{Co(II)}$  is in fact subservient when in a  $\text{Ni(II)}$  mixed solution- and the circle is complete.

### **6.5 CONCLUDING REMARKS.**

What ever the explanation for the observed trends in transport properties for membranes containing macrocyclic ligands, it is clear that there is insufficient evidence from this small amount of data to produce a mechanistic model. There are obviously subtle interactions between the ligands and the polymeric environment within which they are trapped, which result in less than predictable systems that in fact show more promise for transition metal ion separation than the pyridyl- and bipyridyl-based membranes reviewed in Chapter Five. It was stressed at the start of this chapter that the results obtained formed more of a brief feasibility study of macrocyclic ligand incorporation into hydrogel polymers. The rather more complex approach of chemical immobilisation is required in an ideal situation, but the outcome of this work suggests that the effort may be worth-while.

## **CHAPTER SEVEN**

### **DISCUSSION AND CONCLUSIONS.**

## **7.1 SUMMARY OF THE THESIS.**

This thesis is concerned with the investigation of the factors influencing the complexation of a variety of first-row transition metal ions with a series of hydrogel membranes, based on copolymers of vinyl-pyridine and bipyridine with 2-hydroxyethyl methacrylate. It was first necessary to characterise these systems and obtain some foundations of understanding as to how the hydrogel environment affects the coordination process, and indeed the properties of the complex formed. This is the basis of the work described in Chapters Three and Four. However, the main driving force behind the study of membrane-based systems was their potential application to the selective separation of TM ions in solution. It was with this objective in mind, that the work discussed in Chapters Five and Six was carried out.

Visible spectroscopy has proved to be a most useful investigative tool for the characterisation of coloured complexes immobilised in membranes. PolyHEMA, a material commonly used in the manufacture of soft contact lenses, is optically clear in the visible region, which allows thin membranes to be placed directly in a spectro-photometer beam and absorption spectra between 810-350nm, that will be solely due to the immobilised complex, to be obtained.

One of the first observations made during the early stages of this study was that bipyridyl-based membranes turned an intense red colour when left to equilibrate in a ferrous salt solution. What was so striking about this process was that the formation of the  $\text{Fe(II)}$  *tris*(bipyridyl) complex, an "instantaneous" reaction in free solution, was exceedingly slow for the polymer-bound analogue. This led to the detailed series of kinetics experiments that constitute Chapter Four.

In view of the overwhelming evidence in this thesis, and elsewhere, for the dominating influence that anions have on transport properties within hydrogel membranes, it is of little surprise to find that the rate and extent of  $\text{Fe(II)}$  *tris*(bipyridyl) complex formation is affected by the ferrous salt used. The sulphate salt follows what approximates to a first order process, and the chloride and perchlorate salts tend to first order at very low  $\text{Fe(II)}$  concentrations but show second order kinetics at high  $\text{Fe(II)}$  concentrations. These differences are explained in terms of alternative rate-determining steps which require reorganisation of the polymer chains for complexation to occur.

What was initially an unexpected observation was the fact that in terms of the extent of complex formation, the conversion of ligand to *tris*-complex was shown to follow the order  $\text{SO}_4^{2-} > \text{Cl}^- > \text{ClO}_4^-$ . This is opposite to the order in which the salts swell the polymeric matrix. One might have expected the  $\text{ClO}_4^-$ , which produces the greatest swelling effect on the gel, to have made more of the ligand groups available for coordination by opening-up the structure and increasing the mobility of the polymer chains by an enhanced plasticising effect; and *vice versa* for the  $\text{SO}_4^{2-}$ . However, this initially anomalous phenomenon is explained in terms of an  $\text{Fe(II)}$  concentration-dependent equilibrium. It is shown that a very large excess of  $\text{Fe(II)}$  results in the formation of the *mono*-complex, for which there is spectroscopic evidence. The  $\text{ClO}_4^-$  indeed has its predicted effect on the swelling of the membrane, but this simply opens the structure and results in higher concentrations of  $\text{Fe(II)}$  within the gel; thus, an equilibrium between the *tris*- and *mono*-complexes results, controlled by the concentration of  $\text{Fe(II)}$ .

This type of inorganic/coordination chemists' approach to characterisation of the membrane system gives a new insight into the coordination process occurring. Certainly, this type of

detailed study could be applied to the investigation of the parameters surrounding the redox chemistry of the Co(I) *tris*(bipyridyl) complex mentioned briefly in this study.

Armed with a basic understanding surrounding the coordination processes in these systems, Chapter Five discusses the evaluation of complexing hydrogel membranes as a means for selective TM ion separations. Transport studies using polyHEMA only membranes highlights the dominance of the anion on the permeation of a range of TM salts; those classed as water-structuring, such as  $\text{SO}_4^{2-}$ , permeating much slower than the structure-breakers, e.g.  $\text{ClO}_4^-$ . We see that the effect of ligand incorporation into the polymer is twofold: (i) there is a distinct, metal ion-dependent, lag-time period before steady-state permeability is achieved, and (ii) in some cases, the final permeability of the salt is different to that shown in the pure polyHEMA membranes. The lag-time phenomenon is examined in more detail, and comparisons are drawn with the relative lengths of the lag-times and the stability constants for particular metal:ligand combinations. Additional correlation is found between the lag-time and the equilibrium water content imposed on the pyridine-based gels by complexation with the metal. Calculations show that the increase in EWC could be attributable to the extra water associated with the large hydration sphere of the complex. The lag-time is considered to be the time taken for the reorganisation necessary for the polymer chains to accommodate the complex. Analogies can be drawn here with the rate-determining reorganisational step seen for  $\text{Fe(II)}$  salt coordination in these polymers, which together serve to demonstrate the effect of the steric restrictions imposed on the ligands by the macromolecular chains.

A series of competitive studies are described in which the transport properties of the

membranes are evaluated using salt solutions with a combination of two transition metal ion species, the counterion being the same for each. One strongly, and one weakly coordinating metal ion type were chosen in order that any resultant effect would be more noticeable. It was shown that, when in combination as a binary solution they exhibit similar lag-times and permeability coefficients, characteristic of the more strongly coordinating ion. One interpretation of this is that complexation with the strongly coordinating ion 'conditions' the membrane so that the complex essentially defines the path for further transport of both species across the membrane. One conclusion is clear from this work: the 'anti-selective' nature of these systems renders them totally useless as far as selective separation of transition metal ions is concerned. It is quite probable that the anti-selectivity might be useful as a process in its own right, but for what type of applications is unclear at this stage.

The brief study of the macrocyclic-based systems in Chapter Six implies that there may be scope for a tailor-made separation system with these ligands. Entrapped, or even pendently-attached macrocyclic ligands will not incur cross-linking interactions within the polymer, selective uptake being controlled by the ring size of the ligand molecule. The small amount of transport data presented would seem to be consistent with a different type of coordination process within these membranes. Here lies an obvious challenge for future work in the field of metal ion-complexing membranes.

This thesis then, has used a multidisciplinary approach to investigate the factors surrounding metal/ligand, ligand/polymer and metal/polymer interactions in complexing hydrogel membranes. An understanding of these parameters is invaluable in assessing the potential of these systems for selective metal ion separations in aqueous solution.

## **7.2 SUGGESTIONS FOR FURTHER WORK.**

Work presented here has been exclusively restricted to the use of polyHEMA-based hydrogel systems. There are however, a number of alternative vinyl monomers such as N-vinyl pyrrolidone (NVP) and N,N' dimethyl acrylamide (NNDMA) that will form hydrogel membranes with even higher equilibrium water contents than that of polyHEMA. Although NVP was avoided during this work because of its tendency to form block-copolymers, there is still scope for the use of these alternatives monomers for complexing membrane fabrication.

It was mentioned in passing, that techniques are available for the preparation of these copolymers in a bead- ,as opposed to a membrane-form, that are capable of producing a Cu(II) ion-selective resin (Chapter Five, section 5.8). Similar technology could be applied to the formation of water-swellaable beads containing the immobilised Co(II) *tris*(bipyridine) complex, for use in the deoxygenation of solvent samples <sup>145</sup>. Treatment of the beads with a sodium borohydride solution would reduce the Co(II) to Co(I), resulting in the formation of the deep-blue colour of the Co(I) *tris*(bipyridine) complex. The complex can be stabilised by decanting the solution from the beads, dehydrating them in an oven, and storing them in a dry environment. When needed, a column could then be packed with beads and flushed with nitrogen; the solution to be deoxygenated would be added to the top of the column, and collected oxygen-free at the bottom. The colour transition from deep-blue to pale yellow as the Co(I) complex is reoxidised would provide a perfect colorimetric indicator for the degree of oxygen removal from the sample.

Further along the lines of catalytic properties of immobilised complexes within these

materials, unpublished work by the author has shown that the immobilisation of  $\text{Ru(II)}_{\text{bis}}(\text{Bipy})(\text{VBipy})$  &  $\text{Ru(II)}_{\text{tris}}(\text{VBipy})$  is possible, and the visible absorption spectra of the respective membranes have been measured. Although the complex content of these membranes was too high to obtain fluorescent and luminescent spectra, this could easily be rectified. Interest in this complex stems from its use as a 'water-splitting' catalyst, for the production of hydrogen and oxygen by photoreduction of water. In this respect, much work has been done on the use of the  $\text{Ru(II)}$  &  $\text{Co(II)}$ -Bipyridyl systems in combination <sup>143,144</sup>, and the hydrogel-type polymers seem to offer an ideal support on which these two components could be immobilised.

In retrospect, these materials seem ideally suited to analysis by the so-called *Spectro-electrochemical* techniques. This basically involves the utilisation of a spectroscopic technique, (in this case UV/Visible spectroscopy) in combination with an electrochemical study. Thin ligand copolymer films could be formed on conducting glass, and then complexed by contact with a metal ion solution. By connecting electrodes to opposite sides of the plate, and placing the assembly in an appropriately modified spectrophotometer, it would be possible to monitor the absorption spectrum of the complex as a function of the current applied. This might prove extremely interesting given the difference in the absorption spectra of the  $\text{Fe(II)/(III)}$  &  $\text{Co(I)/(II)}$  *tris*(bipyridyl) systems.

Finally, the use of these membranes for separation or pre-concentration of metal ions warrants further work. In addition to the macrocycle approach previously discussed, there might be a possibility of using the current system for Donnan-dialysis <sup>83</sup> (Chapter One, section 1.4.1). This would involve the use of high pH's, which up to now has been avoided in the hydrogel system because of the massive swelling effects obtained. If the swelling

could be curtailed to some extent by increased cross-link density, but without the loss of mechanical integrity or freezing water content, the slow rate of transport of the sulphate ion across these membranes may be sufficient to drive a Donnan Effect if sulphuric acid is used in the receiver solution.

This thesis illustrates that there is indeed great potential for the use of coordinating hydrophilic polymer systems in a variety of areas of chemical research. It outlines some fundamental observations relating to metal ion complexation in these systems, and focuses on one such potential application of the membranes.

## **REFERENCES.**

## REFERENCES.

- [1] Pittman, C.U., Jr., Carraher, C.E. & Reynolds, J.R., "Organometallic Polymers", Enc. Polymer Sci. & Engineering, 10, 541-594, 2<sup>nd</sup> Edition, Edited by Mark, H.F., Bikales, N.M., Overberger, C.G., Menges, G., J.Wiley N.Y. (1987), ISBN 0-471-88789-7.
- [2] Hartley, F.R., "Supported Metal Complexes- A New Generation of Catalysts", D.Reidel Pub. Co. (1985).
- [3] Carraher, C.E., Sheats, J.E. & Pittman, C.U., Jr., "Metal-Containing Polymeric Systems", Plenum Press N.Y. (1985).
- [4] Carraher, C.E., Sheats, J.E. & Pittman, C.U., Jr., "Organometallic Polymers", Academic Press N.Y. (1978).
- [5] Kaneko, M. & Tsuchida, E., Formation, Characterisation & Catalytical Activity of Polymer-Metal Complexes, *J. Polym. Sci., Mac. Rev.*, 16, 397-522, (1981).
- [6] Hodgkin, J.H., "Chleate-Forming Polymers", in reference [1], 3, 363-381, (1987).
- [7] May, P.M. & Bulman, R.A., The Present Status of Chelating Agents in Medicine, *Progr. Medicinal Chem.*, 20, 225-336, (1983).
- [8] Bulman, R.A., The Chemistry of Chelating Agents in Medical Science, *Struct. & Bonding*, 67, 91-141, (1987).
- [9] Myasoedova, G.V. & Savvin, S.B., Chelating Sorbents in Analytical Chemistry, *CRC Critical Rev. in Anal. Chem.*, 17(1), 1-63, (1986).
- [10] Sahni, S.K. & Reedijk, J., Coordination Chemistry of Chelating Resins & Ion Exchangers, *Coord. Chem. Rev.*, 59, 1-139, (1984).
- [11] Schmuckler, G., Chelating Resins- Their Analytical Properties & Applications, *Talanta*, 12, 281-290, (1965).
- [12] Warshawsky, A., Selective Ion-Exchange Polymers, *Die Angew. Makromol. Chemie*, 109/110, 171-196, (1982).
- [13] Hancock, R.D. & Martell, A.E., Ligand Design for Selective Complexation of Metal Ions in Aqueous Solution, *Chem. Rev.*, 89, 1875-1914, (1989).

- [14] Pearson, R.G., Hard and Soft Acids and Bases, *J. Am. Chem. Soc.*, 85 (22), 3533-3539, (1963).
- [15] Lehn, J.M., Supramolecular Chemistry- Scope & Perspective, Molecules, Supramolecules & Molecular Devices (Nobel Lecture), *Angew. Chem., Int. Ed. Engl.*, 27, 89-112, (1988).
- [16] Kálal, J., Kálalová, E., Jándrova, L. & Svec, F., Reactive Polymers, 45; Use of Macroporous Glycidyl Methacrylate-Ethylene Dimethacrylate Copolymer Modified by Diethylamine, for the Separation of Pt(IV), Pd(II) & Rh(II), *Angew. Makromol. Chem.*, 115, 13-22, (1983).
- [17] Janák, K. & Janák, J., Chelating Ion Exchangers with Bonded 8-Quinolinol on a Glycidyl Methacrylate Gel, *Collect. Czech. Chem. Commun.*, 48, 2352-2360, (1983).
- [18] Slovák, Z. & Docekal, B., Sorption of Arsenic, Antimony and Bismuth on Glycomethacrylate Gels with Bound Thiol Groups for Direct Sampling in Electrothermal Atomic Absorption Spectrometry, *Anal. Chim. Acta*, 117, 293-300, (1980).
- [19] Slovák, Z., Smrz, M., Docekal, B. & Slovákova, S., Analytical Behavior of Hydrophilic Glycomethacrylate Gels with Bound Thiol Groups, *Anal. Chim. Acta*, 111, 243-249, (1979).
- [20] Slovák, Z., Slovákova, S. & Smrz, M., Analytische Eigenschaften von Hydrophilen Glykomethacrylate Gelen mit Chemisch Gebundener Salicylsäure, *Anal. Chim. Acta*, 87, 149-155, (1976).
- [21] Slovák, Z. & Slovákova, S., Use of Hydrophilic Glycomethacrylate Gels with Bound 8-Hydroxyquinoline in Trace Analysis, *Z. Anal. Chem.*, 292, 213-215, (1978).
- [22] Slovák, Z. Slovákova, S. & Smrz, M., Analytische Eigenschaften von Hydrophilen Glykomethacrylate Polymeren mit Chemisch Gebundener 8-Oxychinolin, *Anal. Chim. Acta*, 75, 127-138, (1975).
- [23] Slovák, Z. & Toman, J., Use of Hydrophilic Glycomethacrylate Gels with Bound 8-Hydroxyquinoline in Trace Analysis, *Z. Anal. Chem.*, 278, 115-120, (1976).

- [24] Hock, P.J. & Reedijk, J., Coordination of Transition Metals by Chelating Cation-Exchange Resins: Co(II), Ni(II), Zn(II) & Cu(II) Coordinated by the 8-Quinolinoyl Group in Spheron Oxine 1000, *J. Inorg. Nucl. Chem.*, 42, 1759-1765, (1980).
- [25] Baker, G.L., Fritschel, S.J., Stille, J.R. & Stille, J.K., Transition Metal-Catalysed Asymmetric Organic Syntheses *via* Polymer-Attached Optically Active Phosphine Ligands 5: Preparation of Amino Acids in High Optical Yield *via* Catalytic Hydrogenation, *J. Org. Chem.*, 46, 2954-2960, (1981).
- [26] Baker, G.L., Fritschel, S.J. & Stille, J.K., Asymmetric Hydrogenation with a Polymer Catalyst Containing Optically Active Pendant Alcohols, *J. Org. Chem.*, 46, 2960-2965, (1981).
- [27] Pedley, D.G. & Tighe B.J., Water Binding Properties of Hydrogel Polymers for RO and Related Applications, *Br. Polym. J.*, 11, 130-136, (1979).
- [28] Corkhill, P.H., Novel Hydrogel Polymers, PhD Thesis, The University of Aston in Birmingham, (1988).
- [29] Hamilton, C.J., Transport Phenomena in Hydrogel Membranes, PhD Thesis, The University of Aston in Birmingham, (1988).
- [30] Corkhill, P.H., Jolly, A.M., Ng, C.O. & Tighe, B.J., Synthetic Hydrogels: 1. Hydroxyalkyl Acrylate & Methacrylate Copolymers- Water Binding Studies, *Polymer*, 28, 1758-1766, (1987).
- [31] Orlova, N.N., Tolmachev, V.N. & Simonenko, E.A., Investigation of Sorption Kinetics of Metal Ions by Means of Complexing Oxinrescorcinol-Formaldehyde Resin, *Vysokomol. Soed.*, 14B, 335-338, (1972).
- [32] Svec, F., Kálal, J., Kálalová, E. & Marek, M., Reactive Polymers, XXVII: Kinetics of Chemical Reactions of Metal Ions with Functional Groups of Glycidyl Methacrylate-Ethylene Dimethacrylate Copolymers and Ethylenediamine, *Angew. Makromol. Chem.*, 87, 95-117, (1980).
- [33] Kopolow, S., Hogen-Esch, T.E. & Smid, J., Cation Binding Properties of Poly(Vinyl) Macrocyclic Polyethers, *Macromolecules*, 4, 359-360, (1971)
- [34] Smid, J., Solute Binding to Polymers Containing Macroheterocyclic Rings, *Pure Appl. Chem.*, 48, 343-353, (1976).

- [35] Warshawsky, A., Kalir, R., Deshe, A., Berkovitz, H. & Patchornik, A., Polymeric Pseudocrown Ethers. 1: .Synthesis & Complexation with Transition Metal Anions, *J. Am. Chem. Soc.*, 101, 4249-4258, (1979).
- [36] Gramian, P. & Frere, Y., Synthesis and Ion Binding Properties of Epoxy Polymers with Diazacrown Ethers, *Macromolecules*, 12, 1038-1042, (1979).
- [37] Gramian, P. & Frere, Y., Water Soluble Poly(Diazacrown Ethers): Evidence for a Polymer-Sandwich Complex with Barium, *Polymer*, 21, 921-924, (1980).
- [38] Blasius, E., Adrian, W., Janzen, K.P. & Klaute, G., Darstellung und Eigenschaften von Austauschern auf Basis von Kronenverbindungen, *J. Chromatogr.*, 96, 89- 97, (1974).
- [39] Blasius, E., Janzen, K.P., Keller, M., Lander, H., Nguyen, T.T. & Sholten, G., Austauscher mit Cyclischen Polyethern als Ankergruppen 1: Herstellung und Charakterisierung, *Talanta*, 27, 107-126, (1980).
- [40] Gramain, P., Un Nouveau Type de Polymère Complexant: Les Polymacrocycles. Applications Potentielles à la Catalyse et à la Séparation de Cations, *Inf. Chim.*, 226, 231-236, (1982).
- [41] Hodgkin, J.H., Synthesis of Metal Chelating Polymers, *Chem. Ind.*, 3, 153-156, (1979).
- [42] Green, B.P. & Hancock, R.O., Useful Resins for the Selective Extraction of Cu, Ni & Co, *J. South African Inst. Mining & Metallurgy*, 82, 303-307, (1982).
- [43] Agnew, N.H. & Larkworthy, L.F., Cobalt (II) Complexes of 2- & 4-Vinylpyridines, *J. Chem. Soc.*, 4669-4671, (1965).
- [44] Agnew, H.N., Transition Metal Complexes of Poly(Vinylpyridines), *J. Polym. Sci., Polym. Chem. Ed.*, 14, 2819-2830, (1976).
- [45] Tsuchida, E. & Nishide, H., Selective Adsorption of Metal Ions on Resins in which the Coordination Sphere is Controlled by a Template Reaction, *Proc. 2nd Jpn-USSR Polym. Symp., Kyoto Jpn.*, 4650 (432), 219-229, (1976).
- [46] Tsuchida, E. & Nishide, Polymer-Metal Complexes & Their Catalytic Activity, *Adv. Polym., Chem.*, 24, 1-124, (1977).

- [47] Kaneko, M. & Tsuchida, E., Formation, Characterisation & Catalytic Activity of Polymer-Metal Complexes, *J. Polym. Sci., Mac. Rev.*, 16, 397-522, (1981).
- [48] Burchette, I., Coordination Chemistry of Vinylpyridine Polymers, PhD Thesis The University of Aston in Birmingham, (1982).
- [49] Brandt, W.W., Dwyer, F.P. & Gyarfas, E.C., Chelate Complexes of 1,10-Phenanthroline & Related Compounds, *Coord. Chem. Revs.*, 2, 173-193, (1954).
- [50] Irving, H. & Mellor, D.H., The Stability of Metal Complexes of 1,10-Phenanthroline & Its Analogues Pt.1: 1,10-Phenanthroline & 2,2'-Bipyridine, *J. Chem. Soc.*, 5222-5237, (1962).
- [51] Lindoy, L.F. & Livingstone, S.E., Complexes of Fe(II), Co(II) & Ni(II) with Diimine Related Bidentate Ligands, *Coord. Chem. Revs.*, 2, 173-193, (1967).
- [52] Miller, J.D. & McWhinnie, W.R., The Chemistry of Complexes Containing 2,2'-Bipyridine, 1,10-Phenanthroline or 2,2',6,2''-Terpyridine as Ligands, *Adv. Inorg. Chem. Rad. Chem.*, 12, 135-215, (1969).
- [53] Tamagaki, S., Card, R.J. & Neckers, D.C., (Polystyrylbipyridine)(Tetracarbonyl) Tungsten. An Active, Reusable Heterogeneous Catalyst for Metathesis of Internal Olefins, *J. Am. Chem. Soc.*, 100 (21), 6635-6639, (1978).
- [54] Card, R.J. & Neckers, D.C., (Polystyrylbipyridine)Palladium(0)- Catalysed Isomerisation of Quadricyclene, *J. Org. Chem.*, 43 (15), 2958-2960, (1978).
- [55] Card, R.J. & Neckers, D.C., (Polystyrylbipyridine)Palladium(0)- Heterogeneous Catalyst for the Mild Hydrogenation of Dienes to Monoenes, *Isr. J. Chem.*, 17 (4), 269-273, (1979).
- [56] Card, R.J., Liesner, C.E. & Neckers, D.C., (Polystyrylbipyridine)Palladium Complexes as Heterogeneous Catalysts for Hydrogenation of Alkenes and Alkynes, *J. Org. Chem.*, 44 (7), 1095-1098, (1979).
- [57] Card, R.J. & Neckers, D.C., Preparation of Polymer-Bound Bipyridine and some of its Transition Metal Complexes, *J. Am. Chem. Soc.*, 99 (23), 7733-7734, (1977).
- [58] Card, R.J. & Neckers, D.C., (Polystyrylbipyridine): Synthesis and Formation of Transition Metal Complexes and Some of Their Physical, Chemical and Catalytic Properties, *Inorg. Chem.*, 17 (9), 2345-2349, (1978).

- [59] Neckers, D.C., Polymeric Bipyridines as Chelating Agents and Catalysts, in reference [3], pg. 385-403.
- [60] Neckers, D.C., Polymeric Metal Catalysts and Reagents, *J. Macromol. Sci.*, A24 (3-4), 431-448, (1987).
- [61] Zhang, K. & Neckers, D.C., Diaminobipyridine-TDI Polyureas: Synthesis, Metal Complexes, and Catalytic Activity, *J. Polym. Sci., Polym. Chem. Ed.*, 21 (11), 3115-3127, (1983).
- [62] Zhang, K. & Neckers, D.C., Diaminobipyridine-TDI Polyureas: Synthesis, Metal Complexes, and Catalytic Activity, *Polym. Mater. Sci. Eng.*, 49, 207-209, (1983).
- [63] Miller, J.D. & Morton, D.S., Complex Formation Between Polymers Containing the 2,2'-Bipyridine Group & Iron (II), *J. Chem. Soc., Dalton Trans.*, 1511-1514, (1983).
- [64] Calvert, J.M. & Meyer, T.J., Polypyridyl Complexes of Ru (II) Bound to Poly(4-Vinylpyridine). Synthesis, Characterisation & Thin-Film Electrochemistry of a Series of Bis(Bipyridyl) Metallopolymers, *Inorg. Chem.*, 21, 3978-3989, (1982).
- [65] Denisevich, P., Abruna, H.D., Leidner, C.K., Meyer, T.J. & Murray, R.W., Electropolymerisation of Vinylpyridine & Vinylbipyridine Complexes of Iron (II) & Ru (II), *Inorg. Chem.*, 21 (6), 2153-2161, (1982).
- [66] Ellis, C.D., Margerum, L.D., Meyer, T.J. & Murray, R.W., Oxidative Electropolymerisation of Polypyridyl Complexes of Ru (II), *Inorg. Chem.*, 22, 1283-1291, (1983).
- [67] Kelly, J.M., Long, C., O'Connell, C.M., Vos, J.G. & Tinnemans, A.H.A., Preparation, Spectroscopic Characterisation and Photochemical & Electrochemical Properties of Some Bis(2,2'-Bipyridine) Ru (II) & Tetracarbonyl W(0) Complexes of 6-*p*-Tolyl 2,2'-Bipyridine and of 6-*p*-Styryl 2,2'-Bipyridine & its Copolymers, *Inorg. Chem.*, 22, 2818-2824, (1983).
- [68] Calvert, J.M., Schmehl, R.H., Sullivan, B.P., Facci, J.S., Meyer, T.J. & Murray, R.W., Synthetic & Mechanistic Investigation of the Reductive Electrochemical Polymerisation of Vinyl-Containing Compounds of Fe (II), Ru (II) & Os (II), *Inorg. Chem.*, 22 (15), 2154-2161, (1983).

- [69] Potts, K.T., Usifer, D.A., Guadalupe, A. & Abruna, H.D., 4-Vinyl, 6-Vinyl, 4'-Vinyl 2,2',6',2''-Terpyridine Ligands: Their Synthesis & the Electrochemistry of Their Transition Metal Coordination Compounds, *J. Am. Chem. Soc.*, 109, 3961-3967, (1987).
- [70] Leidner, C.R., Sullivan, B.P., Reed, R.A., White, B.A., Crimmins, M.T., Meyer, T.J. & Murray, R.W., Synthesis & Electropolymerisation of Distyryl Bipyridine & Methylstyryl Bipyridine Compounds of Fe, Ru, Os, Re & Co, *Inorg. Chem.*, 26, 882-891, (1987).
- [71] Elliott, C.M., Baldy, C.J., Nuwaysir, L.M. & Wilkins, C.L., Electrochemical Polymerisation of 4-Methyl-4'-Vinyl-2,2'-Bipyridyl-Containing Metal Complexes. Polymer Structure & Mechanism of Formation, *Inorg. Chem.*, 29, 389-392, (1990).
- [72] Woltermann, A., Kauffmann, T. & König, J., Protophane und Polyaromaten XXII: Nucleophile Alkylierung und Arylierung des 2,2'-Bipyridyls, *Chem. Ber.*, 109, 3864-3868, (1976).
- [73] Ghosh, P.K. and Spiro, T.G., Photoelectrochemistry of *tris*(bipyridyl) Ruthenium (II) Covalently Attached to n-Type SnO<sub>2</sub>, *J. Am. Chem. Soc.*, 102, 5543-5549, (1980).
- [74] Newkome, G.R. & Yoneda, A., Synthesis, Characterisation & Complex Formation of Poly(5-Vinyl-6,6'-Dimethyl-2,2'-Bipyridine), *Makromol. Chem., Rapid Commun.*, 4, 575-581, (1983).
- [75] Kashig, J. & Lohmann, D., Vinyl-Substituted 2,2'-Bipyridine Compounds, U.S. Patent 4,424,859, (1985).
- [76] Gupta, S.N. & Neckers, D.C., Template Effects in Chelating Polymers, *J. Polym. Sci., Polym. Chem. Ed.*, 20 (6), 1609-1622, (1982).
- [77] Furue, M., Nozakura, S.I. & Sumi, K., Synthesis & Luminescence Properties of *tris*(Bipyridyl) Ruthenium (II)- Containing Vinyl Polymers, *Chem. Lett.*, 1349-1352, (1981)
- [78] Furue, M., Nozakura, S.I. & Sumi, K., Properties of Poly(Vinyl-2,2'-Bipyridine) & Complex Formation with Various Metal Ions, *J. Polym. Sci., Polym. Lett. Ed.*, 20, 291-295, (1982).

- [79] Furue, M., Nozakara, S.I. & Sumi, K., Preparation & Luminescence Properties of *tris*(Bipyridyl) Ru (II)-Containing Polymers: Ru(Bipy)<sub>2</sub> (Poly-6-Vinyl-2,2'-Bipy)Cl<sub>2</sub> & Ru(Bipy)<sub>2</sub> (Poly-4-Methyl-4'-Vinyl-2,2'-Bipy)Cl<sub>2</sub>, *J. Polym. Sci., Polym. Chem. Ed.*, 22, 3779-3788, (1984).
- [80] Kaschig, J., Finter, J. & Freiburg, D.E., Strahlungsempfindliche, Metallkomplex bildende Polymere, Verfahren zur Polymerisation von Acetylen und beschichtetes Material, Germ. Offen., DE 3510133 A1, (1985).
- [81] Pitt, C.G., Bao, Y. & Seltzman, H.H., The Synthesis of Polymers Containing the 2,2'-Bipyridine Ligand, *J. Polym. Sci., Polym. Lett. Ed.*, 24, 13-16, (1986).
- [82] Isreal, C., "Membranes", in reference [1], 9, 509-578, (1987).
- [83] Based on the 'Osmonics Filtration Spectrum', Osmonics Inc., 5951 Clearwater Drive, Minnetonka, Minnesota, 55343, USA.
- [84] Peppas, N.A., Moynihan, H.J. & Lucht, L.M., The Structure of Highly Cross-Linked PHEMA Hydrogels, *J. Biomed. Mater. Res.*, 19, 397-411, (1985).
- [85] Hwang, S.T. & Kammermeyer, K., Techniques of Chemistry Vol. VII, "Membranes in Separation", John Wiley & Sons, N.Y. (1975).
- [86] Spacek, P. & Kubin, M., Diffusion in Gels, *J. Polym. Sci.*, (Part C) 16, 705-714, (1967).
- [87] Cox, J.A. & Di Nunzio, J.E., Donnan Dialysis Enrichment of Cations, *Anal. Chem.*, 49 (8), 1272-1275, (1977).
- [88] Cox, J.A., Oibrych, E. & Brajter, K., Separation of a Mixture of Cations by Donnan Dialysis, *Anal. Chem.*, 53, 1308-1309, (1981).
- [89] Cox, J.A., Gajek, R., Litiwinski, G.R. & Carnahan, J., Optimisation of Ion-Exchange Membrane Structures for Donnan Dialysis, *Anal. Chem.*, 54, 1153-1157, (1982).
- [90] Cox, J.A., Brajter, K. & Slovawska, K., Separation of Pt-Group Metal ions by Donnan Dialysis, *Anal. Chem.*, 57, 2405-2407, (1985), and references therein.
- [91] Nishiki, T. & Bautista, R.G., Pt(IV) Extraction with Supported Liquid Membranes Containing Trioctylamine Carrier, *A. I. Ch. E. J.*, 31 (12), 2093-2095, (1985).

- [92] Maruyama, K., Tsukube, H. & Araki, T., Highly Selective Membrane Transport of Copper (II) Ions by Synthetic Linear Oligomer Carriers, *J. Chem. Soc., Dalton Trans.*, 7, 1486-1491, (1981).
- [93] Dohno, R. & Hakushi, T., Solvent Extraction and Liquid Membrane Transport of Transition Metals by Non-Cyclic Diamides, *Senryo to Yakuhin*, 34 (12), 336-347, (1989).
- [94] Cho, M.H., Seon-Woo, K.H., Heo, M.Y., Lee, I.C., Yoon, C.J. & Kim, S.J., Studies on Macrocyclic-Mediated Transport in a Bulk Liquid Membrane System of Transition Metal Ions, *Bull. Korean Chem. Soc.*, 9 (5), 292-295, (1988).
- [95] Kobuke, Y., Hanji, K., Horriguchi, K., Asuda, M., Nakayama, Y. & Furikawa, J., Macrocyclic Ligands Composed of THF for the Selective Transport of Monovalent Cations through Liquid Membranes, *J. Am. Chem. Soc.*, 98, 7414-7419, (1976).
- [96] Di Casa, M., Fabbrizzi, L., Perotti, A., Poggi, A. & Riscassi, R., Ligand Field Effects on the Transport of 3d Metal Ions Across a Bulk Liquid Membrane by Lipophilic Tetraamine Carriers, *Inorg. Chem.*, 25 (22), 3984-3987, (1986).
- [97] Hasegawa, M. & Kawakutsu, K., Active Transport & Selective Transport of Alkali Metal Ions through Poly(3-Vinyl-1,4-Butyrolactone-co-Acrylonitrile) Membranes, *Macromol.*, 14, 170-175, (1981).
- [98] Shimidzu, T., Yoshikawa, M. & Ohtani, B., Synthesis of Poly(3-(4-Vinylphenoxy) Phthalide-co-Acrylonitrile) & the Selective Transport Properties of its Membranes, *Macromol.*, 14, 506-509, (1981).
- [99] Uragami, T., Watanabe, S., Nakamura, R., Yoshida, F. & Sugihara, M., Studies on the Synthesis & Permeability of Special Polymer Membranes XLVIII- Active Transport & Selective Transport of Metal Ions through Membranes of Poly(Isobutylene-alternate co-Maleic Anhydride) & PVA, *J. Appl. Polym. Sci.*, 28 (5), 1613-1623, (1983).
- [100] Uragami, T., Watanabe, S., Nakamura, R., Yoshida, F. & Sugihara, M., Studies on the Synthesis & Permeability of Special Polymer Membranes 50- Transport of Metal Ions Against their Concentration Gradient through Water-Insoluble Poly(Styrene-Sulphonic Acid) Membranes, *Polymer*, 24 (5), 559-564, (1983).
- [101] Dohno, R., Takeshita, J., Kinugasa, M. & Hakushi, T., Active Transport of Transition Metal Ions through Poly(Vinyl Alcohol) & Poly(Acrylic Acid) Blend Membranes, *Maku*, 12 (6), 351-356, (1987).

- [102] Hamilton, C.J., Murphy, S.M., Atherton, N.D. & Tighe, B.J., Synthetic Hydrogels:4. The Permeability of Poly(2-Hydroxyethyl Methacrylate) to Cations- An Overview of Solute-Water Interactions and Transport Processes, *Polymer*, 29, 1879-1886, (1988).
- [103] Murphy, S.M., Hamilton, C.J. & Tighe, B.J., Synthetic Hydrogels:5. Transport Processes in 2-Hydroxyethyl Methacrylate Copolymers, *Polymer*, 29, 1887-1894, (1988).
- [104] Oxley, H.R., Crown-Mediated Transport in Hydrogel Membranes, PhD Thesis, The University of Aston in Birmingham, (1991).
- [105] Cox, J.A., Dabek-Zlotorzynska, E. & Brajter, K., Preparation of a Chelating Polymeric Membrane and Application to Uphill Transport, *Anal. Lett.*, 20 (8), 1149-1156, (1987).
- [106] Oyobikawa, E., Separation of Solutes by Complex-Forming Polymer Films, *Kobunshi Kako*, 35 (10), 475-480, (1986).
- [107] Saunders, J. and Hunter, B., "Modern NMR Spectroscopy- A Guide for Chemists" Ch.3: Multi-Pulse Experiments, Oxford University Press (1987), ISBN 0-19-855202-5.
- [108] Abruna, H.D., Denisevich, P., Umana, M., Meyer, T.J. and Murray, R.W., Rectifying Interfaces Using Two-Layer Films of Electrochemically Polymerised Vinylpyridine and Vinylbipyridine Complexes of Ruthenium and Iron on Electrodes, *J. Am. Chem. Soc.*, 103, 1-5, (1981).
- [109] Abruna, H.D., Breikss, A.I. and Collum, D.B., Improved Synthesis of 4-Vinyl 4'-Methyl-2,2'-Bipyridine, *Inorg. Chem.*, 24, 987-988, (1985).
- [110] Guarr, T.F. and Anson, F.C., Electropolymerisation of Ruthenium Bis(1,10-Phenanthroline)(4-Methyl-4'-Vinyl-2,2'-Bipyridine) Complexes through Direct Attack on the Ligand Ring System, *J. Phys. Chem.*, 91, 4037-4043, (1987).
- [111] Terasawa, I. and Kawakatsu, T., Process for the Preparation of High Purity 4-Methyl-4'-Vinyl-2,2'-Bipyridine as a Material for Organic Semiconductors, Japanese Patent, *Jpn. Kokai Tokkyo Koho*, JP 86-295291, 5pp, (1988).

- [112] Sprintschnik, G., Sprintschnik, H.W., Kirsch, P.P. & Whitten, D.G., Preparation and Photochemical Reactivity of Surfactant Ru(II) Complexes in Monolayer Assemblies and at Water-Solid Interfaces, *J. Am. Chem. Soc.*, 99, 4947-4954,(1977).
- [113] Badger, G.M. and Sasse, W.H.F., Synthetic Applications of Activated Metal Catalysts, Part II, *J. Chem. Soc.*, 616-620, (1956).
- [114] Sasse, W.H.F. and Whittle C.P., Synthetic Applications of Activated Metal Catalysts, Part VII, *J. Chem. Soc.*, 3045-3049, (1959).
- [115] Sasse, W.H.F. and Whittle C.P., Synthetic Applications of Activated Metal Catalysts, Part XII, *J. Chem. Soc.*, 1347-1350, (1961).
- [116] Cagle, F.W., Jr. and Smith, G.F., 2,2'-Bipyridine Ferrous Complex Ion as an Indicator in the Determination of Iron, *Anal. Chem.*, 19, 384-385, (1947).
- [117] Atwal, U.S., Hydrogels for Liver Support Systems, PhD Thesis, The University of Aston in Birmingham, (1978).
- [118] Linford, R.G., "Electrochemical Science & Technology of Polymers", Elsevier Applied Science Pub. Ltd., (1987), ISBN 1-85166-031-3.
- [119] Martin, C.R. & Freiser, H., Coated-Wire Ion-Selective Electrodes and Their Application to the Teaching Laboratory, *J. Chem. Education*, 57 (7), 512-514, (1980).
- [120] Cattrall, R.W., Tribuzio, S. & Freiser, H., Potassium Ion Responsive Electrode Based on Valinomycin, *Anal. Chem.*, 46 (14), 2223-2224, (1974).
- [121] Skoog, D.A., "Principles of Instrumental Analysis", Chapter 22, 3<sup>rd</sup> Ed. Holt-Saunders, (1985), ISBN 4-8337-0282-7.
- [122] Heinze, J., Cyclic Voltammetry- 'Electrochemical Spectroscopy', *Angew. Chemie, Int. Ed. Engl.*, 23 (11), 831-918, (1984).
- [123] Sawyer, D.T. & Roberts, J.L., Jr., "Experimental Electrochemistry for Chemists", Chapter 2, J. Wiley & Sons, (1974), ISBN 0-471-75560-5.
- [124] Glidle, A. & Hillman, A.R., Spectroscopy of Electroactive Polymer Films, *Chemistry in Britain*, 26 (3), 255-259, (1990).

- [125] Flynn, G.L. & Smith, E.W., Membrane Diffusion 1: Design & Testing of a New Multifeatured Diffusion Cell, *J. Pharm. Sci.*, 60, 1713-1717, (1971).
- [126] Misra, A.L., Hunger, A. & Keberle, H., A Note on the Diffusion of Drugs through Artificial Phospholipid Membranes, *J. Pharm. Pharmacol.*, 18, 531-535, (1966).
- [127] Atherton, N.D., Drug-Water Interactions in Hydrogel Matrices, PhD Thesis, The University of Aston in Birmingham, (1982).
- [128] Gilman, L.B. & Engelhart, W.G., A.A. Digestions by Microwave, *Spectr. Int.*, 2 (1), 16, (1990).
- [129] Abusaura, A., Recent Advances in Microwave Sample Preparation, *Anal. Chem.*, 47, 1475-1477, (1975).
- [130] Cowie, J.M.G., "Polymers: Chemistry & Physics of Modern Materials", ITC Ltd., (1973), ISBN 0-7002-02226.
- [131] Hathaway, B.J., Stereochemistry & Electronic Properties of the Cu(II) Ion, *Essays in Chemistry*, 2, 61-92, (1971), Academic Press, London.
- [132] Greenwood, N.N. & Earnshaw, A., "Chemistry of the Elements", Chapters 19 & 28, Pergamon Press (1984), ISBN 0-08-022057-6.
- [133] Carlin, R.L., Electronic Structure & Stereochemistry of Co(II), *Transition Metal Chemistry*, 1, 1-33, (1965).
- [134] Reference [132], Chapters 19 & 26.
- [135] Nicholls, D., "Complexes & First Row Transition Elements", Macmillan, (1983), ISBN 0-333-170881.
- [136] Vlcek, A.A., A New Compound of Univalent Cobalt, *Nature*, 180, 753-754, (1957).
- [137] Waind, G.M. & Martin, B., Polarographic Reduction of Co(II), *Coord. Chem. Conference, Rome*, (1957).
- [138] Waind, G.M. & Martin, B., Low Valency Stabilisation. 2,2'-Bipyridyl Complexes of Co, Rh, & Ir, *Proc. Chem. Soc.*, 169, (1958).

- [139] Waind, G.M. & Martin, B., Low Valency Stabilisation. Salts of the *tris*  $\alpha,\alpha'$ -Dipyridyl Cobalt (I) Cation, *J. Inorg. Nuc. Chem.*, 8, 551-556, (1958).
- [140] Waind, G.M., Martin, B. & McWhinnie, W.R., 2,2'-Dipyridyl Complexes of Co(II), Rh(II) & Ir (II), *J. Inorg. Nuc. Chem.*, 23, 207-223, (1961).
- [141] Morgel, S., Smith, W. & Anson, F.C., Electrochemistry of 2,2'-Bipyridyl Complexes of Co in the Presence of Acrylonitrile, *J. Electrochem. Soc.*, 125 (2), 241-246, (1978).
- [142] Kaizu, Y., Torii, Y. & Kobayashi, H., Electronic Absorption Spectra of *tris*(2,2'-Bipyridyl) Co(I) Complex, *Bull. Chem. Soc. Jpn.*, 43, 3296-3297, (1970).
- [143] Krishnan, C.V. & Sutin, N., Homogeneous Catalysis of the Photoreduction of Water by Visible Light 2: Mediation by a *tris*(2,2'-Bipyridyl) Ru(II)-Co(II) Bipyridyl System, *J. Am. Chem. Soc.*, 102, 2141-2142, (1981).
- [144] Krishnan, C.V., Cruetz, C., Mahajan, D., Schwarz, H.A. & Sutin, N., Homogeneous Catalysis of the Photoreduction of Water by Visible Light 3: Mediation by Polypyridyl Complexes of Ru(II) & Co(II), *Isr. J. Chem.*, 22 (2), 98-106, (1982).
- [145] Homer, J., Dudley, A.R. & McWhinnie, W.R., Removal of Oxygen from Samples Used in NMR Studies of Spin-Lattice Relaxation Times, *J. Chem. Soc., Chem. Commun.*, 893-894, (1973).
- [146] Ng, C.O. & Tighe, B.J., Polymers in Contact Lens Applications VI: The Dissolved Oxygen Permeability of Hydrogels & the Design of Materials for Use in Continuous-Wear Lenses, *Br. Polym. J.*, 8, 118-123, (1976).
- [147] Reference [132], Chapters 19 & 25.
- [148] DeYoung, H.G., Biosensors- The Mating of Biology & Electronics, *High Technol.*, 3, 41-49, (1983).
- [149] Czaban, J.P., Electrochemical Sensors in Clinical Chemistry: Yesterday, Today, Tomorrow, *Anal. Chem.*, 57, 345A-356A, (1985).
- [150] Turner, A.P.F., Karabe, I. & Wilson, G.S., "Biosensors- Fundamentals & Applications", Oxford Science Publications, (1987), ISBN 0-19-854724-2.

- [151] Vadgama, P., Membrane-Based Sensors- A Review, *J. Membr. Sci.*, 50, 141-152, (1990).
- [152] Freiser, H. & Fernando, Q., "Ionic Equilibria in Analytical Chemistry", pp. 22-25, John Wiley & Sons Inc., NY (1963).
- [153] Bartlett, P.N., Chung, L-Y., Moore, P., Conducting Polymer Films: Attachment of Pyrrole Groups to Aza-Macrocycles & Attempted Electrochemical Polymerisation of the Resulting Monomers, *Electrochim. Acta.*, 35 (6), 1051-1055, (1990).
- [154] Spritzer, M.S., Costa, J.M. & Elving, P.J., Polarographic Reduction of Pyridinium Ion in Pyridine: Application to the Determination of Bronsted and Lewis Acids, *Anal. Chem.*, 37 (2), 211-217, (1965).
- [155] Mark, J.E., The Use of Model Polymer Networks, *Adv. Polym. Sci.*, 44, 1-26, (1982).
- [156] Kopeikin, V.V., Polymeric 1,3-Dicarbonyl Compounds & Their Derivatives, *Acta Polymerica*, 34 (6), 307-315, (1983).
- [157] Yeh, H.C., Eichinger, B.E. & Andersen, N.H., Metal Ac-Ac Chelate Cross-Linked Gels, *J. Polym. Sci., Polym. Chem. Ed.*, 20, 2575-2602, (1982).
- [158] Ning, Y-P., Mark, J.E., Iwamoto, N. & Eichinger, B.E., Elastomeric Properties of Some Isoprene-Styrene Networks Cross-Linked through Metal-Acetylacetonate Chelation, *Macromolecules*, 18, 55-57, (1985).
- [159] Mark, J.E., Eisenberg, A., Graessley, W.W., Mandelkern, L. & Koenig, J.L., "Physical Properties of Polymers", Chpt. 1, ACS Washington D.C., (1984), ISBN 0-8412-0851-4.
- [160] Labana, S.S., "Cross-Linking", in reference [1]. 4, 350-395, (1987).
- [161] Hadley, D.W. & Ward, I.M., "Mechanical Properties", in reference [1]. 9, 379-466, (1987).
- [162] Erman, B., Wagner, W. & Flory, P.J., Elastic Modulus and Degree of Cross-Linking of Poly(Ethyl Acrylate) Networks, *Macromolecules*, 13, 1554-1558, (1980).
- [163] Rees, R.W., "Cross-Linking, Reversible", in reference [1]. 4, 395-417, (1987).

- [164] Wetton, R.E., James, D.B. & Whiting, W., Modification of Polyethers by Transition Metal Chlorides, *J. Polym. Sci., Polym. Lett. Ed.*, 14, 577-583, (1976).
- [165] Pineri, M., Meyer, C. & Bourret, A., Ion Clustering in Poly(Butadiene-Styrene-4-Vinylpyridine) Cross-Linked by Iron (II) Chloride. Differential Enthalpic Analysis and Electron Microscopy, *J. Polym. Sci., Polym. Phys. Ed.*, 13, 1881-1891, (1975).
- [166] Blau, F., Die Destillation Pyridinmonocarbonsaurer Salze, *Ber.*, 21, 1077-1078, (1888).
- [167] Cagle, F.W.M. & Smith, G.F., Effect of Symmetrical Substitution of Methyl Groups on the Property of Dimethyl-2,2'-Bipyridine to Complex the Ferrous Ion, *J. Chem. Soc.*, 69, 1860-1862, (1947).
- [168] Guggenheim, E.A., On the Determination of the Velocity Constant of a Unimolecular Reaction, *Phil. Mag.*, 2, 538-543, (1926).
- [169] King, E.L., The Spectrophotometric Determination of the Rate Constant of First Order Reactions, *J. Am. Chem. Soc.*, 74, 563, (1952).
- [170] Kezdy, F.J., Kaz, J. & Braylants, A., Cinétique de l'Action de l'Acide Nitreux sur les Amides. 1. Méthode Générale, *Bull. Soc. Chim. Belges*, 67, 687-706, (1958).
- [171] Swinbourne, E.S., Method for Obtaining the Rate Coefficient & Final Concentration of a First Order Reaction, *J. Chem. Soc.*, 2371-2372, (1960).
- [172] Espenson, J.H., A Time Lag Method for Second Order Kinetics, *J. Chem. Educ.*, 57, 160, (1980).
- [173] Krumholz, P., Ferrous Mono- $\alpha, \alpha'$ -Dipyridyl, *J. Am. Chem. Soc.*, 71, 3654-3656, (1949).
- [174] Baxendale, J.H. & George, P., Equilibria in Solutions of Ferrous Ions and  $\alpha, \alpha'$ -Dipyridyl, *Trans. Faraday Soc.*, 46, 55-63, (1950).
- [175] Ghosh, P.K. & Spiro, T.G., Electroactive Coatings of *tris*(Bipyridine) and *tris*(o-Phenanthroline) Ruthenium (II) Attached to Electrodes, *J. Electrochem. Soc.*, 128, 1281-1287, (1981).

- [176] Kojima, Y., Furuhashi, K. & Miyasaka, K., Diffusive Permeabilities of Solutes in Poly(Vinyl Alcohol) Membranes as a Function of the Degree of Hydration, *J. Appl. Polym. Sci.*, 29, 533-546, (1984).
- [177] Kim, S.W., Cardinal, J.R., Wisinowski, S. & Zentner, G.M., Solute Permeation through Hydrogel Membranes, in Water, in Polymer, (Ed. Rowland, S.P.), ACS Symposium Series 127, ACS, Washington D.C. (1980), 347.
- [178] Nightingale, Jr., E.R., Phenomological Theory of Ion Solvation. Effective Radii of Hydrated Ions, *J. Phys. Chem.*, 63, 1381-1387, (1959).
- [179] Sillén, L.G. & Martell, A.E., "Stability Constants of Metal-Ion Complexes", Special Publication No. 17, The Chemical Society, London, (1964).
- [180] Burgess, J., "Metal Ions in Solution", Ellis Horwood Ltd., (1978), ISBN 0-85312-027-7.
- [181] Stryer, L., "Biochemistry", 2<sup>nd</sup> Ed., W.H. Freeman & Co., (1981), ISBN 0-7167-1226-1.
- [182] Izatt, R.M., Clark, G.A., Bradshaw, J.S., Lamb, J.D. & Christensen, J.J., *Sep. Purif. Methods*, 15, 21-72, (1986).
- [183] (i) Pedersen, C.J., Cyclic Polyethers & Their Complexes with Metal Salts, *J. Am. Chem. Soc.*, 89, 2495-2496, (1967); (ii) Pedersen, C.J., Cyclic Polyethers & Their Complexes with Metal Salts, *ibid*, 89, 7017-7036, (1967).
- [184] Harrison, P.M. & Hoare, R.J., "Metals in Biochemistry", Chapman & Hall, (1980), ISBN 0-412-13160-9.
- [185] Lindoy, L.F., Transition Metal Complexes of Synthetic Macrocyclic Ligands, *Chem. Soc. Rev.*, 4 (3), 421-441, (1975).
- [186] Grimsley, P.G., Lindoy, L.F., Lip, H.C., Smith, R.J. & Baker, J.T., Synthesis of New 14, 15 & 16-Membered Crown Compounds Containing O & N Heteroatoms, *Aust. J. Chem.*, 30 (9), 2095-2098, (1977).
- [187] Armstrong, L.G. & Lindoy, L.F., Studies Involving N-O Donor Macrocyclic Ligands I: Ni(II) Complexes of a New Series of Cyclic Ligands Derived from Salicylaldehyde, *Inorg. Chem.*, 14 (6), 1322-1326, (1975).

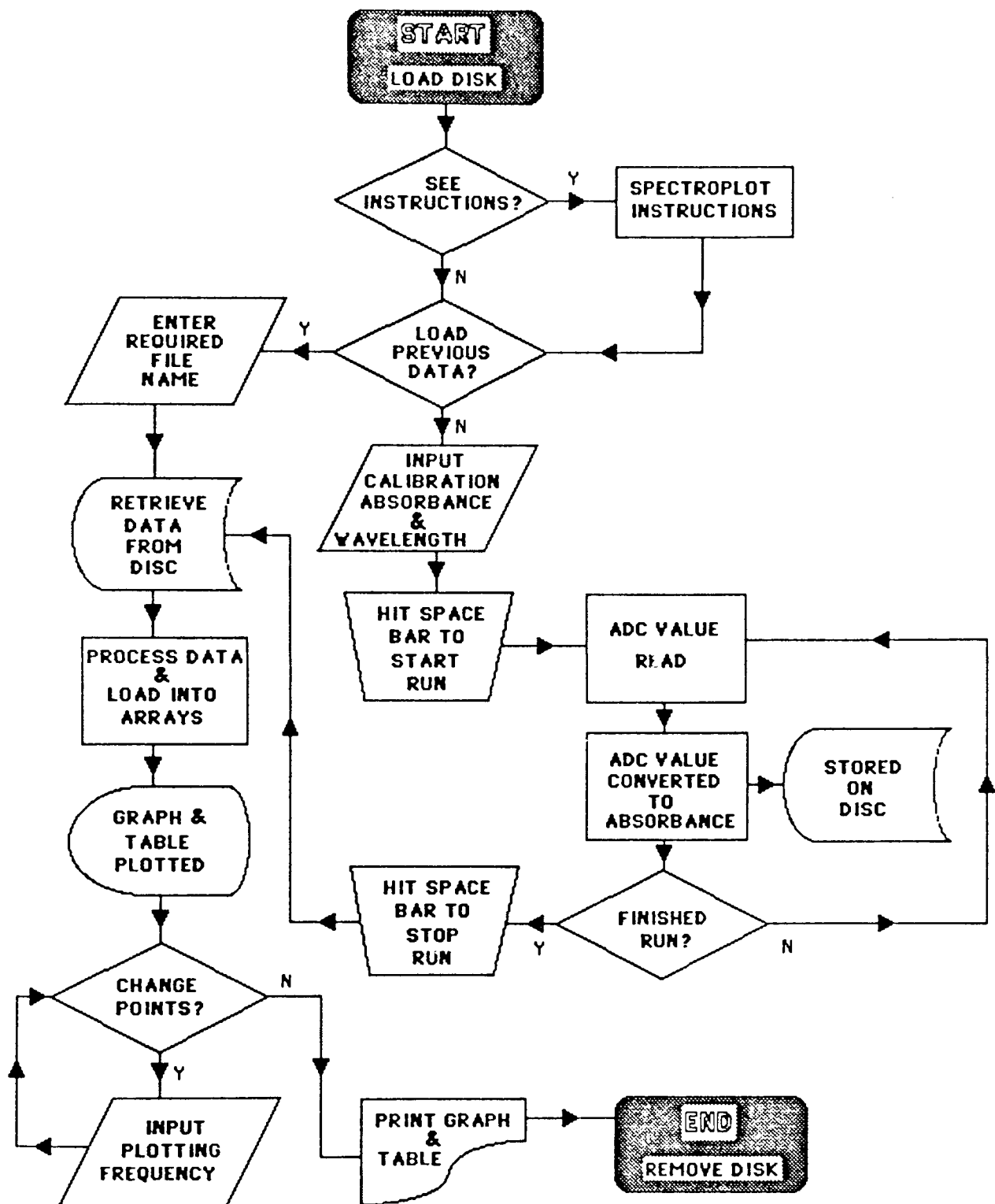
- [188] Adam, K.R., Leong, A.J., Lindoy, L.F., McCool, B.J., Ekstrom, A., Liepa, I., Harding, P.A., Henrick, K., McPartlin, M. & Tasker, P.A., Studies Involving Mixed Donor Macrocyclic Ligands. Comparative X-Ray Diffraction, I.R. & F.A.B.M.S. Studies of the Nickel Thiocyanate Complexes of Three O<sub>2</sub>N<sub>3</sub>-Donor Macrocycles, *J. Chem. Soc., Dalton Trans.*, 2537-2542, (1987).
- [189] Fenton, D.E., Murphy, B.P., Leong, A.J., Lindoy, L.F., Bashall, A. & McPartlin, M., Studies of Metal-Ion Recognition. The Interaction of Co(II), Ni(II) & Cu(II) with New O,N-Donor Macrocycles; X-Ray Structures of Complexes of Cu (II) & Ni(II) with a 15-Membered O<sub>2</sub>N<sub>3</sub> Derivative, *J. Chem. Soc., Dalton Trans.*, 2543-2553, (1987).
- [190] Adam, K.R., Baldwin, D., Duckworth, P.A., Leong, A.J., Lindoy, L.F., McPartlin, M. & Tasker, P.A., A New Series of Quinquedentate Macrocycles Exhibiting Systematic Donor Atom Variation: Equilibrium & X-Ray Structural Data for Their Interaction with Cu(II), *J. Chem. Soc., Chem. Commun.*, 1124-1125, (1987).
- [191] Adam, K.R., Leong, A.J., Lindoy, L.F. & Anderegg, G., Studies Involving Mixed Donor Macrocyclic Ligands: A Comparative Study of the Influence of Media Effects on the Stability of Complexes of Co(II), Ni(II) & Cu(II) with 14 to 16 Membered O<sub>2</sub>N<sub>2</sub> Donor Macrocycles, *J. Chem. Soc., Dalton Trans.*, 1733-1735, (1988).
- [192] Lindoy, L.F., Heavy Metal Chemistry of Mixed Donor Macrocyclic Ligands-Strategies for Obtaining Metal-Ion Recognition, *Prog. Macrocyclic Chem.*, 3 (Synthetic Macrocycles), 53-92, (1987).
- [193] Lindoy, L.F., Baldwin, D.S., Ligand Design for Selective Metal-Ion Transport through Ligand Membranes, *Pure & Appl. Chem.*, 61 (5), 909-914, (1989).
- [194] Parades, R.S., Valera, N.S. & Lindoy, L.F., The Interaction of Co(II), Ni(II), Cu(II) & Zn(II) with O,N-Donor Macrocycles Immobilised on a Polystyrene Matrix, *Aust. J. Chem.*, 39 (7), 1071-1079, (1986).
- [195] Dudler, V., Lindoy, L.F., Sallin, D. & Schlaepfer, C.W., An O,N-Donor Macrocycle Immobilised on Silica Gel. A Reagent Showing High Selectivity for Cu(II) in the Presence of Co(II), Ni(II), Zn(II) & Cd(II), *Aust. J. Chem.*, 40 (9), 1557-1563, (1987).
- [196] Adam, K., Lindoy, L.F., Lip, H.C., Rea, J.H., Skelta, B.W. & White, A.H., Studies Involving N,O-Donor Macrocycles, *J. Chem. Soc., Dalton Trans.*, 74-79, (1981).

- [197] Comba, P., Curtis, N.F., Lawrance, G.A., Sargeson, A.M., Skelton, B.W. & White, A.H., Template Syntheses Involving Carbon Acids, *Inorg. Chem.*, 25, 4260-4263, (1986).
- [198] Lawrance, G.A., & O'Leary, M.A., Macrocyclic Tetramines from Reaction of the (1,10 Diamino-4,7 Diazadecane) Cu(II) Cation with Formaldehyde and the Carbon Acids Nitroethane & Dimethyl Malonate: Variability in Reactivity, *Polyhedron*, 6 (6), 1291-1294, (1987).
- [199] Hickenbottom, W.J., "Reactions of Organic Compounds", 3<sup>rd</sup> Ed., Longmans, (1959).
- [200] Melby, L.R., Polymers for Selective Chelation of Transition Metal Ions, *J. Am. Chem. Soc.*, 97, 4044-4051, (1975).

## **APPENDIX ONE**

### **COMPUTER PROGRAM LISTINGS AND FLOW CHARTS.**

AL1 SPECTROPLOT FLOWCHART.



## A1.2 SPECTROPLOT LISTING.

```
10      REM SPEC
20      REM ***** CREDITS *****
30      CLS
40      PRINT:PRINT:PRINT:PRINT:PRINT:PRINT:PRINT:PRINT:PRINT:PRINT
50      PRINT "                WELCOME TO SPECTROPLOT"
60      FOR Q=1 TO 3000
70      NEXT Q
80      PRINT
90      PRINT "        WRITTEN BY ANDREW L. LEWIS 1989"
100     PRINT
110     PRINT "THE DEPARTMENT OF APPLIED CHEMISTRY AND CHEMICAL ENGINEERING,
        THE UNIVERSITY OF ASTON IN BIRMINGHAM"
120     FOR Q=1 TO 8000
130     NEXT Q
140     CLS
150     PRINT:PRINT:PRINT:PRINT:PRINT:PRINT:PRINT:PRINT:PRINT:PRINT:PRINT
160     PRINT "    DO YOU WISH TO READ THE RELEASE NOTE DOCUMENTATION (Y/N)?"
170     INPUT RL$
180     IF RL$="Y" THEN GOTO 3220
190     CLS
200     PRINT:PRINT:PRINT:PRINT:PRINT:PRINT:PRINT:PRINT:PRINT:PRINT:PRINT
210     PRINT "DO YOU WANT TO PLOT A PREVIOUS RESULTS (Y/N)?"
220     INPUT YES$
230     IF YES$="Y" THEN GOTO 2200
240     REM ***** ARRAY CONSTANTS SET TO ZERO *****
250     C=0
260     V=0
270     CLS
280     REM ***** INPUT SAMPLE DATA *****
290     PRINT:PRINT:PRINT:PRINT:PRINT:PRINT:PRINT:PRINT:PRINT:PRINT:PRINT
300     PRINT "ENTER SAMPLE CODE (NO MORE THAN 6 FIGS). "
310     INPUT OS$
320     CLS
330     PRINT:PRINT:PRINT:PRINT:PRINT:PRINT:PRINT:PRINT:PRINT:PRINT:PRINT
340     PRINT "INPUT THE WAVELENGTH YOU ARE STUDYING."
350     INPUT WL
360     CLS
```

```

370 PRINT:PRINT:PRINT:PRINT:PRINT:PRINT:PRINT:PRINT:PRINT:PRINT
380 PRINT "      WHAT TIME INTERVAL DO YOU REQUIRE BETWEEN READINGS (in
    minutes)?"
390 REM **** SETS REQUIRED TIME INTERVAL ****
400 INPUT INV
410 INH=INV
420 CLS
430 PRINT:PRINT:PRINT:PRINT:PRINT:PRINT:PRINT:PRINT:PRINT:PRINT
440 PRINT "ABSORBANCE SETTING ON SP8-100 SHOULD BE ON ABS 2"
450 PRINT
460 PRINT "      ENTER ABS READING"
470 PRINT " (FOR CALIBRATION PURPOSES)."
480 REM **** SP8 ABS READING ****
490 INPUT A
500 REM **** CONSTANTS FOR AVERAGING ADC VALUE ****
510 R=0
520 H=0
530 CLS
540 REM **** CALCULATION OF CALIBRATION CONSTANTS ****
550 FOR U=1 TO 500
560 X=ADVAL(1)
570 F=X/16000
580 H=H+F
590 NEXT U
600 P=H/500
610 PRINT P
620 G=A/P
630 REM **** OPENS FILE FOR WRITING ****
640 M=OPENOUT O$
650 REM **** RECORDS WAVELENGTH ON FILE ****
660 PRINT#M,WL
670 CLS
680 REM **** START RUN ROUTINE ****
690 PRINT:PRINT:PRINT:PRINT:PRINT:PRINT:PRINT:PRINT:PRINT:PRINT
700 PRINT "      * * * * * "
710 PRINT " * PRESS SPACE TO START RUN. *"
720 PRINT "      * * * * * "
730 VDU 7
740 FOR Y=1 TO 650
750 NEXT Y

```

```

760      CLS
770      PRINT:PRINT:PRINT:PRINT:PRINT:PRINT:PRINT:PRINT:PRINT:PRINT
780      PRINT "          * * * * * * * * * * * * * * * *"
790      PRINT "                PRESS SPACE TO START RUN."
800      PRINT "          * * * * * * * * * * * * * * * *"
810      REM ***** DETECTS SPACE BAR HIT *****
820      X=INKEY(50)
830      IF X=32 THEN GOTO 850
840      GOTO 670
850      CLS
860      REM ***** DEFINES TIME *****
870      TIME=0
880      MIN=(TIME DIV 6000)
890      GOSUB 2960
900      MIN=(TIME DIV 6000)
910      REM ***** DETECTS REQUIRED TIME INTERVAL *****
920      IF MIN=INH THEN GOSUB 2950
930      REM ***** DETECTS SPACE BAR TO STOP RUN *****
940      X=INKEY(50)
950      IF X=32 THEN GOTO 970
960      GOTO 900
970      CLS
980      REM ***** CLOSES FILE AFTER WRITING *****
990      CLOSE#M
1000     GOTO 3170
1010     CLS
1020     GS=0
1030     REM ***** OPENS FILE FOR READING *****
1040     M=OPENIN OS$
1050     REM ***** OVERRIDES PRINTER LINEFEED CHARACTER FILTRATION"
1060     *FX6,0
1070     REM ***** SETS ARRAY FOR DATA STORAGE *****
1080     DIM K(C)
1090     DIM B(C)
1100     REM ***** TURNS PRINTER ON *****
1110     GOSUB 3720
1120     PRINT TAB(7);"SAMPLE CODE= ";OS$
1130     PRINT
1140     INPUT#M,WL

```

```

1150 PRINT TAB(7);"WAVELENGTH= ";WL;" nm"
1160 PRINT
1170 PRINT TAB(7);"ABSORBANCE";TAB(22);"TIME(mins)"
1180 REM **** READS DATA FROM DISK AND LOADS INTO ARRAYS ****
1190 REPEAT
1200 INPUT#M,L,MIN
1210 PRINT TAB(10);L;TAB(24);MIN
1220 K(V)=L
1230 B(V)=MIN
1240 V=V+1
1250 UNTIL EOF#M
1260 PRINT:PRINT
1270 REM **** PRINTER OFF & CLOSE FILE ****
1280 VDU3
1290 CLOSE#M
1300 FOR I=1 TO 4000
1310 NEXT I
1320 CLS
1330 REM **** SET GRAPH CONDITIONS ****
1340 PRINT "YOU MUST NOW PROVIDE THE LIMITS OF THE AXES ON YOUR GRAPH
(WITH REFERENCE TO THE PRINTOUT)"
1350 PRINT
1360 PRINT "INPUT MAX ABS VALUE"
1370 INPUT DC
1380 PRINT DC
1390 PRINT "INPUT MAX TIME"
1400 INPUT TC
1410 PRINT TC
1420 FOR I=1 TO 2000
1430 NEXT I
1440 GOSUB 2710
1450 GOSUB 2480
1460 REM **** SETS GRAPHIC MODE ****
1470 MODE 132
1480 REM **** DRAWS FRAME & LABELS ****
1490 VDU5
1500 XA=60:XB=1260:YB=950:YA=100
1510 DX=10:DY=10:SX=(XB-XA)/DX:SY=(YB-YA)/DY
1520 MOVE XA,YA
1530 DRAW XB,YA:DRAW XB,YB:DRAW XA,YB:DRAW XA,YA

```

```

1540   FOR I=XA TO XB STEP SX:MOVE I,YA:DRAW I,YA+15:MOVE
      I,YB:DRAW I,YB-15:NEXT I
1550   FOR I=YA TO YB STEP SY:MOVE XA,I:DRAW XA+15,I:MOVE
      XB,I:DRAW XB-15,I:NEXT I
1560   MOVE 300,1000
1570   PRINT "SAMPLE ";OS;" AT ";WL;" nm"
1580   GOSUB 1800
1590   REM **** CALCULATES PLOT POINTS AND DETECTS OFF SCALE POINTS ****
1600   FOR U=0 TO V STEP PFQ
1610   IF K(U)=0 THEN GOTO 3120
1620   PL=(850/(DC/K(U)))+100
1630   IF B(U)=0 THEN GOTO 3140
1640   IF B(U)>TC THEN GOTO 1700
1650   OT=(1200/(TC/B(U)))+60
1660   REM **** PLOTS DATA ****
1670   MOVE OT,PL
1680   DRAW OT,PL
1690   NEXT U
1700   VDU4
1710   IF GS=1 THEN GOTO 1740
1720   GOTO 2090
1730   REM **** DUMP GRAPH TO PRINTER ****
1740   VDU2
1750   *GDUMP1
1760   MODE7
1770   VDU3
1780   GOTO 2870
1790   REM **** LABELS AXES ****
1800   MOVE 10,750
1810   PRINT "A"
1820   MOVE 10,710
1830   PRINT "B"
1840   MOVE 10,670
1850   PRINT "S"
1860   MOVE 10,630
1870   PRINT "O"
1880   MOVE 10,590
1890   PRINT "R"
1900   MOVE 10,550

```

```

1910 PRINT "B"
1920 MOVE 10,510
1930 PRINT "A"
1940 MOVE 10,470
1950 PRINT "N"
1960 MOVE 10,430
1970 PRINT "C"
1980 MOVE 10,390
1990 PRINT "E"
2000 MOVE 450,90
2010 PRINT "T I M E (mins)"
2020 MOVE -225,990
2030 PRINT DC
2040 MOVE 10,90
2050 PRINT "0"
2060 MOVE 960,95
2070 PRINT TC
2080 RETURN
2090 FOR I=1 TO 8000
2100 NEXT I
2110 MODE7
2120 CLS
2130 PRINT:PRINT:PRINT:PRINT:PRINT:PRINT:PRINT:PRINT:PRINT:PRINT
2140 PRINT "DO YOU WANT TO CHANGE THE PLOTTING FREQUENCY?"
2150 INPUT CPF$
2160 IF CPF$="Y" THEN GOTO 1440
2170 CLS
2180 GS=1
2190 GOTO 1470
2200 CLS
2210 PRINT "DO YOU WISH TO SEE THE FILE CATALOGUE?"
2220 INPUT CAT$
2230 IF CAT$="Y" THEN GOSUB 2440
2240 PRINT
2250 REM **** ROUTINE TO LOAD EXISTING DATA ****
2260 C=0
2270 V=0
2280 PRINT "ENTER FILE CODE YOU WISH TO PROCESS."
2290 INPUT O$
2300 REM **** OPENS FILE FOR READING ****

```

```

2310 M=OPENIN O$
2320 INPUT#M,WL
2330 CLS
2340 PRINT "FILE ";O$;" AT WAVELENGTH ";WL;" nm"
2350 REM **** COUNTS DATA TO GIVE ARRAY SIZE ****
2360 REPEAT
2370 INPUT#M,L,MIN
2380 PRINT "ABS= ";L;" TIME= ";MIN
2390 C=C+1
2400 UNTIL EOF#M
2410 FOR I=1 TO 4000
2420 NEXT I
2430 GOTO 970
2440 CLS
2450 REM **** SHOWS DISK CATALOGUE ****
2460 *CAT
2470 RETURN
2480 CLS
2490 REM **** PRINTS SPECTRAL PARAMETERS ****
2500 VDU 2
2510 PRINT "      *+*+*+*+*+*+*+*+*+*"
2520 PRINT "      + SPECTRAL PARAMETERS +"
2530 PRINT "      *+*+*+*+*+*+*+*+*+*"
2540 PRINT
2550 PRINT "          SAMPLE ";O$
2560 PRINT
2570 PRINT "          AT WAVELENGTH ";WL;" nm"
2580 PRINT "          ABSORBANCE SCALE IS FROM"
2590 PRINT "          0 TO ";DC; "UNITS"
2600 PRINT
2610 PRINT "          TIME SCALE IS FROM"
2620 PRINT "          0 TO ";TC;" MINUTES"
2630 PRINT
2640 PRINT "          PLOTTING FREQUENCY= ";PFQ
2650 PRINT:PRINT:PRINT:PRINT
2660 VDU 3
2670 FOR I=1 TO 4000
2680 NEXT I
2690 CLS

```

```

2700 RETURN
2710 CLS
2720 REM **** ROUTINE TO CHANGE PLOTTING FREQUENCY ****
2730 PRINT:PRINT:PRINT:PRINT:PRINT:PRINT:PRINT:PRINT:PRINT:PRINT
2740 PRINT " **** GRAPH MANIPULATION ****"
2750 PRINT:PRINT
2760 PRINT "DO YOU WANT TO CHANGE HOW OFTEN THE DATA POINTS ARE PLOTTED?"
2770 INPUT GR$
2780 IF GR$="N" THEN GOTO 2840
2790 PRINT:PRINT
2800 PRINT "WHAT IS THE REQUIRED PLOTTING FREQUENCY"
2810 INPUT PFQ
2820 CLS
2830 RETURN
2840 CLS
2850 PFQ=1
2860 RETURN
2870 CLS
2880 REM **** PROGRAM SHUT DOWN ****
2890 PRINT:PRINT:PRINT:PRINT:PRINT:PRINT:PRINT:PRINT:PRINT:PRINT:PRINT
2900 PRINT "IF YOU WISH TO RUN ANOTHER SAMPLE OR PROCESS ANOTHER FILE, YOU
MUST RERUN THE PROGRAM TO CLEAR THE ARRAY FILES."
2910 PRINT
2920 PRINT TAB(15);"BYE!"
2930 END
2940 REM **** SAVES AND COUNTS DATA ****
2950 INH=INV+INH
2960 FOR W=1 TO 100
2970 X=ADVAL(1)
2980 D=X/16000
2990 T=D*G
3000 R=R+T
3005 FOR DLT=1 TO 50: NEXT DLT
3010 NEXT W
3020 REM **** CONVERTS ADC TO ABS VALUE ****
3030 Y=(R/100)*1000
3040 P=INT(Y)
3050 L=P/1000
3060 PRINT TAB(3);"TIME= ";MIN;TAB(18);" ABS= ";L
3070 PRINT#M,L,MIN

```

```

3080     C=C+1
3090     R=0
3100     RETURN
3110     REM **** NECESSARY TO PREVENT DIVISION BY ZERO ****
3120     PL=100
3130     GOTO 1630
3140     OT=60
3150     GOTO 1670
3160     REM **** PRINTOUT OR END? ****
3170     PRINT:PRINT:PRINT:PRINT:PRINT:PRINT:PRINT:PRINT:PRINT:PRINT
3180     PRINT "DO YOU WISH TO PRINT A HARD COPY OF THE DATA AS A GRAPH?"
3190     INPUT DTA$
3200     IF DTA$="Y" THEN GOTO 1010
3210     GOTO 2870
3220     CLS
3230     REM **** INSTRUCTIONS ****
3240     PRINT "***** SPECTROPLOT RELEASE NOTES *****"
3250     PRINT
3260     PRINT "By Andrew L. Lewis 1989 Version 1.2"
3270     PRINT:PRINT
3280     PRINT "The basis of the whole program is to plot graphically, data taken from the SP8-100
UV/VIS spectrophotometer over an extended time period."
3290     PRINT
3300     PRINT "In order to dump screen graphics in mode(132), the BBC must be fitted with an Epson
PRINTER V1.0 ROM chip. The BBC then has a new set of commands available for printing
graphics e.g. *GDUMP."
3310     PRINT
3320     PRINT "The only documentation on this chip is that held in the ROM, called up by *H.P."
3330     PRINT
3340     GOSUB 3680
3350     PRINT "The ADC on the BBC is only capable of handling 0-1.8V; this is fine on the SP8 if
ABS 2 is used. If the ABS scale is increased, an output of 7V can be reached which will
damage the computer."
3360     PRINT "Therefore, this particular program is to be used only on the ABS 2 scale."
3370     PRINT
3380     PRINT "The program first asks if you want to plot data already stored on disk. All answers to
yes & no questions should be either 'Y'<RET> or 'N'<RET>."
3390     PRINT

```

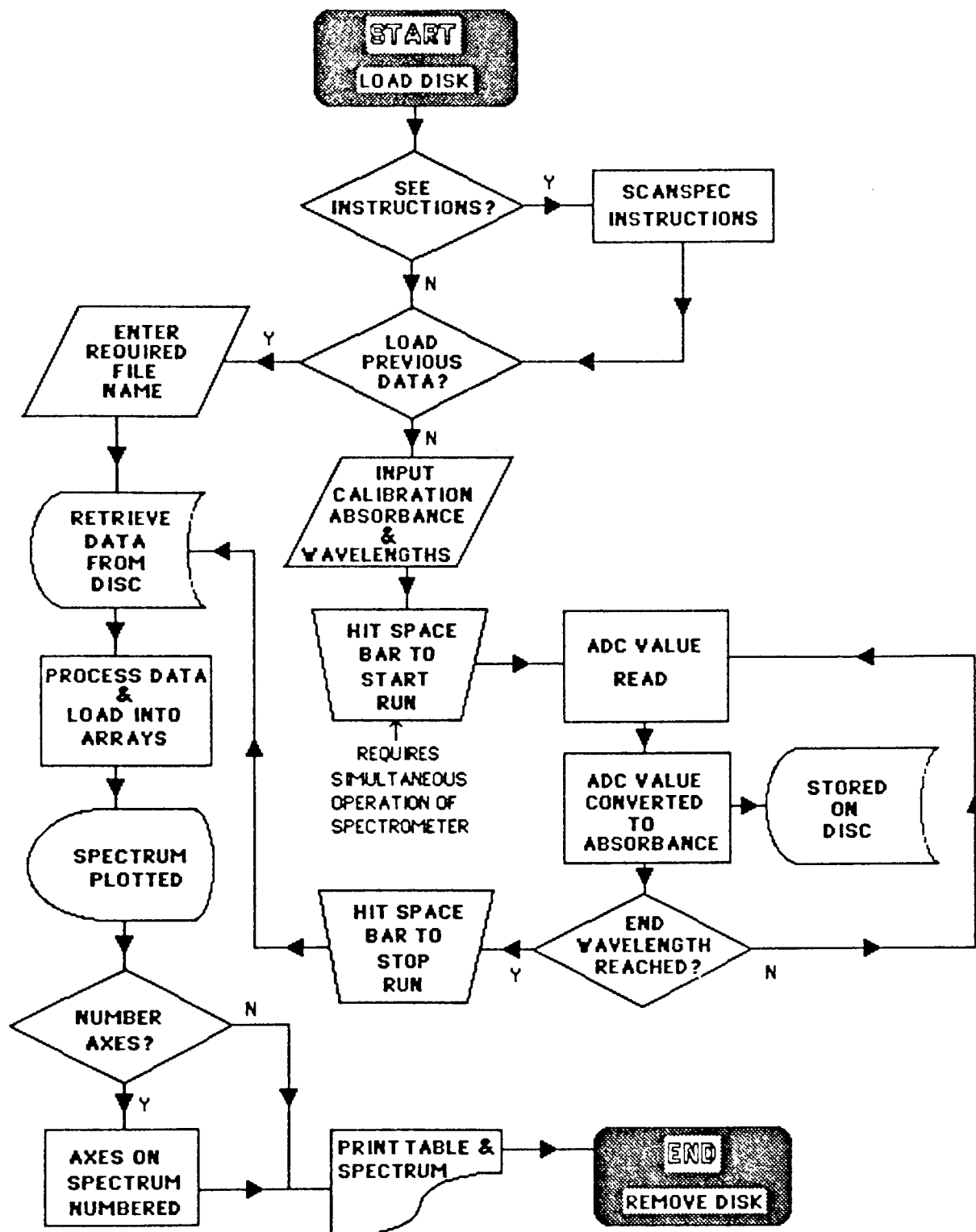
```

3400 PRINT "If you refuse to plot previous results the program assumes you want to start a run.
Enter the necessary variables when prompted."
3410 PRINT
3420 PRINT "When asked to enter ABS for calibration, the spectrophotometer should be reading
between 0.2 & 0.3 (as set by the zero control )."
3430 PRINT
3440 GOSUB 3680
3450 PRINT "The computer uses this value to calibrate the analogue input voltage. Since the ADC
value fluctuates markedly, it is necessary to average 100 readings to produce a reasonable
calibration."
3460 PRINT
3470 PRINT "The program then sets a clock running and takes readings at the frequency you
specify. The screen display serves only to monitor that the readings are being taken and that
they are comparable to the SP8 readout."
3480 PRINT
3490 PRINT "Remember, the chart recorder button must be pushed in on the SP8, otherwise no
input will be received (analogue output taken from across chart recorder)."
3500 GOSUB 3680
3510 PRINT "When printing out data, the tables ate better printed in NLQ, achieved on the Epson
LX80 by pressing the buttons on the front panel in the order listed in the manual."
3520 PRINT
3530 PRINT "The graph dump will be unaffected by NLQ and will be printed out vertically to allow
full A4 size fitting."
3540 PRINT
3550 PRINT "The computer does not transfer data to the disk as it reads each value. The data is
stored in a buffer and transferred when the buffer is full."
3560 PRINT
3570 PRINT "If a run is stopped with the data in the buffer, the data is first saved to disk before the
file is closed."
3580 PRINT
3590 PRINT "The buffer is a safeguard to prevent over-working the drive and the wear
of disks; however, if power is lost, data in the buffer will also be lost."
3600 GOSUB 3680
3610 PRINT "The plotting frequency simply specifies whether to plot every point, every other point,
every 10 points etc.."
3620 PRINT
3630 PRINT "PRESS SPACE BAR TO RETURN TO THE PROGRAM"
3640 REM **** DETECTS SPACE BAR HIT ****
3650 X=INKEY(50)

```

```
3660    IF X=32 THEN GOTO.220
3670    GOTO 3650
3680    PRINT "<space for more>"
3690    X=INKEY(50)
3700    IF X=32 THEN RETURN
3710    GOTO 3690
3720    PRINT:PRINT:PRINT:PRINT:PRINT:PRINT:PRINT:PRINT:PRINT:PRINT
3730    PRINT "DO YOU WANT TO PRINT OUT THE SAVED DATA AS A TABLE IN ADDITION
        TO A GRAPH?"
3740    INPUT SD$
3750    IF SD$="Y" THEN GOSUB 3780
3760    CLS
3770    RETURN
3780    CLS
3790    VDU 2
3800    RETURN
```

# **A1.3 SCANSPEC FLOWCHART.**



#### A1.4 SCANSPEC LISTING.

```
10      REM SCAN
20      REM **** VERSION 1.1 ****
30      REM **** CREDITS ****
40      GK=0
50      CLS
60      PRINT:PRINT:PRINT:PRINT:PRINT:PRINT:PRINT:PRINT:PRINT:PRINT
70      PRINT "          WELCOME TO SCANSPEC"
80      FOR Q=1 TO 3000
90      NEXT Q
100     PRINT
110     PRINT "      WRITTEN BY ANDREW L. LEWIS 1989"
120     PRINT
130     PRINT "THE DEPARTMENT OF APPLIED CHEMISTRY AND CHEMICAL ENGINEERING,
        THE UNIVERSITY OF ASTON IN BIRMINGHAM"
140     FOR Q=1 TO 8000
150     NEXT Q
160     CLS
170     PRINT:PRINT:PRINT:PRINT:PRINT:PRINT:PRINT:PRINT:PRINT:PRINT
180     PRINT "  DO YOU WISH TO READ THE RELEASE NOTE DOCUMENTATION (Y/N)?"
190     INPUT RL$
200     IF RL$="Y" THEN GOTO 2690
210     REM **** V & C ARRAY CONSTANTS SET TO ZERO ****
220     CLS
230     PRINT:PRINT:PRINT:PRINT:PRINT:PRINT:PRINT:PRINT:PRINT:PRINT
240     PRINT "DO YOU WANT TO PLOT A PREVIOUSLY SAVED SPECTRUM(Y/N)?"
250     V=0
260     INPUT PSS
270     IF PSS="Y" THEN GOTO 2390
280     C=0
290     CLS
300     REM **** INPUT SAMPLE DATA ****
310     PRINT:PRINT:PRINT:PRINT:PRINT:PRINT:PRINT:PRINT:PRINT:PRINT
320     PRINT "ENTER SAMPLE CODE (NO MORE THAN 6 FIGS). "
330     INPUT OS$
340     CLS
350     PRINT:PRINT:PRINT:PRINT
360     PRINT "ABSORBANCE SCALE ON SP8-100 SHOULD BE 2."
370     PRINT
```

```

380 PRINT " ENTER ABS READING FOR CALIBRATION."
390 INPUT A
400 PRINT
410 PRINT " ENTER STARTING WAVELENGTH."
420 INPUT WR
430 PRINT
440 PRINT " ENTER FINISHING WAVELENGTH."
450 INPUT WB
460 PRINT
470 PRINT " ENTER THE WAVELENGTH SPEED."
480 INPUT WS
490 REM **** CONSTANTS FOR AVERAGING ADC VALUE ****
500 R=0
510 H=0
520 CLS
530 REM **** CALCULATION OF CALIBRATION CONSTANTS ****
540 FOR U=1 TO 500
550 X=ADVAL(1)
560 F=X/16000
570 H=H+F
580 NEXT U
590 P=H/500
600 G=A/P
610 PRINT G
620 GOTO 810
630 CLS
640 REM **** START RUN ROUTINE ****
650 PRINT:PRINT:PRINT:PRINT:PRINT:PRINT:PRINT:PRINT:PRINT:PRINT
660 PRINT " * * * * * "
670 PRINT " * PRESS SPACE TO START RUN. *"
680 PRINT " * * * * * "
690 VDU 7
700 FOR Y=1 TO 650
710 NEXT Y
720 CLS
730 PRINT:PRINT:PRINT:PRINT:PRINT:PRINT:PRINT:PRINT:PRINT:PRINT
740 PRINT " * * * * * "
750 PRINT " PRESS SPACE TO START RUN."
760 PRINT " * * * * * "

```

```

770 REM **** DETECTS SPACE BAR HIT ****
780 X=INKEY(50)
790 IF X=32 THEN GOTO 870
800 GOTO 630
810 CLS
820 REM **** OPENS FILE FOR WRITING ****
830 M=OPENOUT O$
840 PRINT#M,WR,WB,WS
850 GOTO 640
860 REM **** DEFINES TIME ****
870 TIME=0
880 CLS
890 SEC=(TIME DIV 100)
900 REM **** CALCULATES ADC VALUE ****
910 FOR W=1 TO 50
920 X=ADVAL(1)
930 D=X/16000
940 T=D*G
950 R=R+T
960 NEXT W
970 REM **** DETECTS SPACE BAR HIT ****
980 X=INKEY(50)
990 IF X=32 THEN GOTO 1120
1000 REM **** CONVERTS ADC TO ABS VALUE ****
1010 Y=(R/50)*1000
1020 P=INT(Y)
1030 L=P/1000
1040 WLEN=WR-(WS*SEC)
1050 PRINT "AVERAGE ABS= ";L
1060 PRINT "AT WAVELENGTH ";WLEN
1070 C=C+1
1080 R=0
1090 REM **** WRITES DATA TO DISK ****
1100 PRINT#M,L,WLEN
1110 GOTO 890
1120 CLS
1130 REM **** CLOSSES FILE ****
1140 CLOSE#M
1150 REM **** OPENS FILE FOR READING ****
1160 J=OPENIN O$

```

```

1170 REM **** OVERRIDES PRINTER LINEFEED CHARACTER FILTRATION"
1180 *FX6,0
1190 GOSUB 3170
1200 REM **** SETS ARRAY FOR DATA STORAGE ****
1210 DIM K(C)
1220 DIM B(C)
1230 REM **** READS DATA FROM DISK ****
1240 PRINT "FILE= ";O$
1250 INPUT#M,L,WLEN
1260 PRINT "WLENGTH ";WR;" TO ";WB
1270 REM **** LOADS DATA INTO ARRAYS ****
1280 REPEAT
1290 INPUT#M,L,WLEN
1300 PEINR "ABS= ";L;" WLENGTH ";WLEN
1310 K(V)=L
1320 B(V)=(WR-WLEN)/WS
1330 V=V+1
1340 UNTIL EOF#M
1350 REM **** PRINTER OFF AND CLOSE FILE ****
1360 VDU3
1370 CLOSE#M
1380 REM **** SET SPECTRUM CONDITIONS ****
1390 PRINT:PRINT:PRINT
1400 PRINT "INPUT MAX ABS VALUE"
1410 INPUT DC
1420 PRINT
1430 TC=(WR-WB)/WS
1440 GOSUB 2640
1450 PRINT
1460 PRINT " DO YO WANT THE AXES NUMBERED?"
1470 INPUT NU$
1480 IF NU$="Y" THEN LET GK=1
1490 REM **** SETS GRAPHIC MODE ****
1500 MODE 132
1510 REM **** DRAWS FRAME ****
1520 VDU5
1530 XA=60:XB=1260:YB=950:YA=100
1540 DX=10:DY=10:SX=(XB-XA)/DX:SY=(YB-YA)/DY
1550 MOVE XA,YA

```

```

1560 DRAW XB,YA:DRAW XB,YB:DRAW XA,YB:DRAW XA,YA
1570 FOR I=XA TO XB STEP SX:MOVE I,YA:DRAW I,YA+15:MOVE
I,YB:DRAW I,YB-15:NEXT I
1580 FOR I=YA TO YB STEP SY:MOVE XA,I:DRAW XA+15,I:MOVE
XB,I:DRAW XB-15,I:NEXT I
1590 GOSUB 1910
1600 REM **** DETECTS IF NUMBERING OF AXES REQUIRED ****
1610 IF GK=1 THEN GOSUB 2140
1620 REM **** CALCULATES PLOT POINTS AND DETECTS OFF SCALE
POINTS ****
1630 FOR U=0 TO C
1640 IF K(U)=0 THEN GOTO 1770
1650 PL=(850/(DC/K(U)))+100
1660 IF B(U)=0 THEN GOTO 1790
1670 OT=(1200/(TC/B(U)))+60
1680 REM **** PLOTS DATA ****
1690 MOVE OT,PL
1700 DRAW OT,PL
1710 NEXT U
1720 REM **** DUMP GRAPH TO PRINTER ****
1730 VDU2
1740 *GDUMP1
1750 VDU3
1760 GOTO 1810
1770 PL=100
1780 GOTO 1660
1790 OT=60
1800 GOTO 1690
1810 MODE7
1820 REM **** END PROGRAM ****
1830 CLS
1840 PRINT:PRINT:PRINT:PRINT:PRINT:PRINT:PRINT:PRINT:PRINT:PRINT
1850 PRINT " IF YOU WISH TO PLOT ANOTHER SPECTRUM OR PROCESS ANOTHER
FILE, YOU MUST RERUN THE PROGRAM TO CLEAR THE ARRAY FILES."
1860 PRINT
1870 PRINT TAB(15);"BYE!"
1880 END
1890 REM **** LABELS AXES ****
1900 REM **** NUMBERS ABS AXIS ****

```

```

1910    MOVE 10,750
1920    PRINT "A"
1930    MOVE 10,710
1940    PRINT "B"
1950    MOVE 10,670
1960    PRINT "S"
1970    MOVE 10,630
1980    PRINT "O"
1990    MOVE 10,590
2000    PRINT "R"
2010    MOVE 10,550
2020    PRINT "B"
2030    MOVE 10,510
2040    PRINT "A"
2050    MOVE 10,470
2060    PRINT "N"
2070    MOVE 10,430
2080    PRINT "C"
2090    MOVE 10,390
2100    PRINT "E"
2110    MOVE 400,90
2120    PRINT "WAVELENGTH (nm)"
2130    RETURN
2140    MOVE DEC,282
2150    PRINT DC*.2
2160    MOVE DEC,455
2170    PRINT DC*.4
2180    MOVE DEC,620
2190    PRINT DC*.6
2200    MOVE DEC,792
2210    PRINT DC*.8
2220    MOVE DEC,930
2230    PRINT DC
2240    MOVE 30,147
2250    REM ***** NUMBERS WL AXIS *****
2260    PRINT WR-(2*((WR-WB)/10))
2270    MOVE 272,147
2280    PRINT WR-(4*((WR-WB)/10))
2290    MOVE 510,147
2300    PRINT WR-(6*((WR-WB)/10))

```

```

2310     MOVE 752,147
2320     PRINT WR-(8*((WR-WB)/10))
2330     MOVE -200,95
2340     PRINT WR
2350     MOVE 960,95
2360     PRINT WB
2370     VDU4
2380     RETURN
2390     CLS
2400     REM **** SHOWS DISK CATALOGUE ****
2410     PRINT "DO YOU WISH TO SEE THE FILE CATALOGUE?"
2420     INPUT CAS$
2430     IF CAS$="Y" THEN GOSUB 2670
2440     REM **** SETS ARRAY CONSTANTS TO ZERO ****
2450     C=0
2460     V=0
2470     PRINT:PRINT
2480     PRINT "ENTER SPECTRUM CODE YOU WISH TO PLOT."
2490     INPUT O$
2500     REM **** OPENS FILE FOR READING ****
2510     M=OPENIN O$
2520     INPUT#M,WR,WB,WS
2530     CLS
2540     PRINT "FILE ";O$;" FROM ";WR;" TO ";WB;" nm"
2550     REM **** INPUTS AND COUNTS DATA ****
2560     REPEAT
2570     INPUT#M,L,WLEN
2580     C=C+1
2590     UNTIL EOF#M
2600     REM **** CLOSSES FILE ****
2610     CLOSE#M
2620     GOTO 1160
2630     REM ****.CHANGES PRINT POSITION ACCORDING TO ABS VALUE ****
2640     IF DC>1.99 THEN LET DEC=-145
2650     IF DC<1.99 THEN LET DEC=-115
2660     RETURN
2670     *CAT
2680     RETURN
2690     CLS

```

```

2700 REM **** SCANSPEC INSTRUCTIONS ****
2710 PRINT "***** SCANSPEC RELEASE NOTES *****"
2720 PRINT:PRINT
2730 PRINT "Scanspec is a spin-off utility program that has been developed by simple alterations
to Spectroplot."
2740 PRINT
2750 PRINT "In order to dump the spectrum onto hard copy, the BBC must be fitted with an Epson
PRINTER V1.0 ROM chip. The BBC then has a new set of commands available for printing
graphics e.g. *GDUMP."
2760 PRINT
2770 PRINT "The only documentation on this chip is that held in the ROM, called up by *H.P."
2780 PRINT
2790 GOSUB 3100
2800 PRINT "The ADC on the BBC is only capable of handling 0-1.8V; therefore, for this particular
program, only ABS scale 2 on the SP8-100 can be used. Changing this scale will not only
throw-out the soft-"
2810 PRINT "ware calibration, but could produce output voltages up to 7V, which will damage the
computer."
2820 PRINT
2830 PRINT "The program will ask you if you want to plot a previously saved spectrum. All
answers are 'Y'<RET> or 'N' <RET> unless specified. If you do not want to plot a graph from
disk the program will assume you want to start a run."
2840 PRINT
2850 PRINT "When asked to enter ABS for calibration, the spectrophotometer should be reading
between 0.2 & 0.3 (as set by the zero control ). Make sure the SP8-100 recorder button is on."
2860 GOSUB 3100
2870 PRINT "The computer uses this value to calibrate the analogue input voltage."
2880 PRINT
2890 PRINT "To start a run, push the wavelength drive button in (the recorder should already be on)
and enter the readings as prompted."
2900 PRINT "The program has an intrinsic 2 second delay before data is taken after the run is
started. Therefore, taking into account the wavelength speed, the wavelength dial must be set
the equivalent of 2 seconds ahead."
2910 PRINT
2920 PRINT "EXAMPLE:- Starting at 500nm with a W/L speed of 2nm/sec, set the dial to 504nm.
After the 2 second delay the dial will be at 500nm as data acquisition starts."
2930 GOSUB 3100
2940 PRINT
2950 PRINT "The program samples the ABS once a second and counts the time. Using the W/L
speed the time is converted into a W/L for storage (but converted back into time for graph

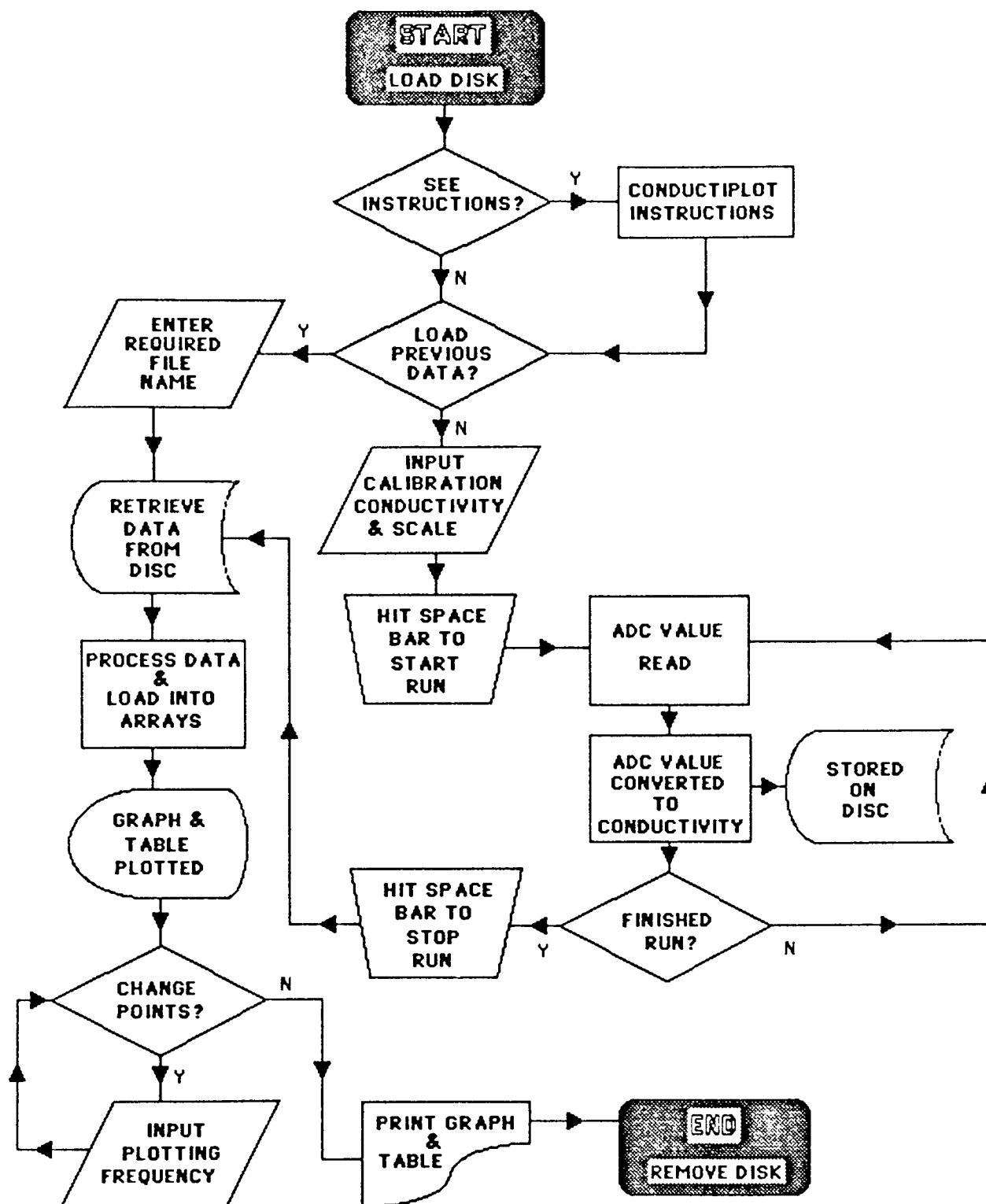
```

```

        plotting purposes)."
2960 PRINT
2970 PRINT "Once you have entered the required data the bell sounds; set the W/L dial and press
        the start on the spectrophotometer. The instant the drive engages press the space bar. Data
        collection begins after 2 seconds."
2980 PRINT
2990 PRINT "Data processing is automatic but you must enter the graph scale maxima. When
        asked for the max ABS look at the data printout and enter a round number greater than the
        max ABS."
3000 GOSUB 3100
3010 PRINT "You can choose whether or not to have the axes numbered, and the \spectrum is
        plotted sideways for neat A4 presentation."
3020 PRINT
3030 PRINT "Remember, when you record a spectrum, it is automatically stored to the disk and
        can be processed immediately, or later from disk."
3040 PRINT
3050 PRINT "PRESS SPACE BAR TO RETURN TO THE PROGRAM"
3060 REM **** DETECTS SPACE BAR HIT ****
3070 X=INKEY(50)
3080 IF X=32 THEN GOTO 220
3090 GOTO 3070
3100 PRINT
3110 PRINT "<space for more>"
3120 PRINT
3130 X=INKEY(50)
3140 IF X=32 THEN RETURN
3150 GOTO 3130
3160 REM **** OPTION TO PRINT OUT DATA TABLE ****
3170 PRINT:PRINT:PRINT:PRINT:PRINT:PRINT:PRINT:PRINT:PRINT:PRINT
3180 PRINT "DO YOU WANT TO PRINT OUT THE SAVED DATA AS A TABLE IN ADDITION
        TO A GRAPH?"
3190 INPUT SD$
3200 IF SD$="Y" THEN GOSUB 3220
3210 RETURN
3220 CLS
3230 REM **** TURNS PRINTER ON ****
3240 VDU2
3250 RETURN

```

# A1.5 CONDUCTIPILOT FLOW CHART



## A1.6 CONDUCTI PLOT LISTING.

```
10      REM COND
20      REM **** CREDITS ****
30      CLS
40      PRINT:PRINT:PRINT:PRINT:PRINT:PRINT:PRINT:PRINT:PRINT:PRINT
50      PRINT "          WELCOME TO CONDUCTI PLOT"
60      FOR Q=1 TO 3000
70      NEXT Q
80      PRINT
90      PRINT "      WRITTEN BY ANDREW L. LEWIS 1989"
100     PRINT
110     PRINT "THE DEPARTMENT OF APPLIED CHEMISTRY AND CHEMICAL ENGINEERING,
        THE UNIVERSITY OF ASTON IN BIRMINGHAM"
120     FOR Q=1 TO 8000
130     NEXT Q
140     CLS
150     PRINT:PRINT:PRINT:PRINT:PRINT:PRINT:PRINT:PRINT:PRINT:PRINT:PRINT
160     PRINT "  DO YOU WISH TO READ THE RELEASE NOTE DOCUMENTATION (Y/N)?"
170     INPUT RLS
180     IF RLS="Y" THEN GOTO 3220
190     CLS
200     PRINT:PRINT:PRINT:PRINT:PRINT:PRINT:PRINT:PRINT:PRINT:PRINT:PRINT
210     PRINT "DO YOU WANT TO PLOT A PREVIOUS RESULTS (Y/N)?"
220     INPUT YES$
230     IF YES$="Y" THEN GOTO 2200
240     REM **** ARRAY CONSTANTS SET TO ZERO ****
250     C=0
260     V=0
270     CLS
280     REM **** INPUT SAMPLE DATA ****
290     PRINT:PRINT:PRINT:PRINT:PRINT:PRINT:PRINT:PRINT:PRINT:PRINT:PRINT
300     PRINT "ENTER SAMPLE CODE (NO MORE THAN 6 FIGS).\"
310     INPUT OS$
320     CLS
330     PRINT:PRINT:PRINT:PRINT:PRINT:PRINT:PRINT:PRINT:PRINT:PRINT:PRINT
340     PRINT "INPUT THE CONDUCTIVITY RANGE YOU ARE USING (in Siemens/cm).\"
350     INPUT SC
360     CLS
```

```

370 PRINT:PRINT:PRINT:PRINT:PRINT:PRINT:PRINT:PRINT:PRINT:PRINT
380 PRINT "      WHAT TIME INTERVAL DO YOU REQUIRE BETWEEN READINGS (in
minutes)?"
390 REM **** SETS REQUIRED TIME INTERVAL ****
400 INPUT INV
410 INH=INV
420 CLS
430 PRINT:PRINT:PRINT:PRINT:PRINT:PRINT:PRINT:PRINT:PRINT:PRINT
440 PRINT "      CONDUCTIVITY METER SHOULD BE SET ON OHM^-1 ATC"
450 PRINT
460 PRINT "SET METER TO HALF SCALE DEFLECTION AND ENTER THE READING FOR
CALIBRATION."
470 INPUT MAG
480 FOR U=1 TO 500
490 X=ADVAL(1)
500 F=X/16000
510 H=H+F
520 NEXT U
530 AV=H/500
540 CC=MAG/AV
550 REM **** OPENS FILE FOR WRITING ****
560 M=OPENOUT O$
570 REM **** RECORDS CONDUCTIVITY RANGE ON FILE ****
580 PRINT#M,SC
590 CLS
600 REM **** START RUN ROUTINE ****
610 PRINT:PRINT:PRINT:PRINT:PRINT:PRINT:PRINT:PRINT:PRINT:PRINT:PRINT
620 PRINT "      * * * * * "
630 PRINT "      * PRESS SPACE TO START RUN. *"
640 PRINT "      * * * * * "
650 VDU 7
660 FOR Y=1 TO 650
670 NEXT Y
680 CLS
690 PRINT:PRINT:PRINT:PRINT:PRINT:PRINT:PRINT:PRINT:PRINT:PRINT:PRINT
700 PRINT "      * * * * * "
710 PRINT "      PRESS SPACE TO START RUN."
720 PRINT "      * * * * * "
730 REM **** DETECTS SPACE BAR HIT ****
740 X=INKEY(50)

```

```

750     IF X=32 THEN GOTO 770
760     GOTO 590
770     CLS
780     REM ***** DEFINES TIME *****
790     TIME=0
800     MIN=(TIME DIV 6000)
810     GOSUB 2920
820     MIN=(TIME DIV 6000)
830     REM ***** DETECTS REQUIRED TIME INTERVAL *****
840     IF MIN=INH THEN GOSUB 2910
850     REM ***** DETECTS SPACE BAR TO STOP RUN *****
860     X=INKEY(50)
870     IF X=32 THEN GOTO 890
880     GOTO 820
890     CLS
900     REM ***** CLOSES FILE AFTER WRITING *****
910     CLOSE#M
920     GOTO 3130
930     CLS
940     GS=0
950     REM ***** OPENS FILE FOR READING *****
960     M=OPENIN O$
970     REM ***** OVERRIDES PRINTER LINEFEED CHARACTER FILTRATION"
980     *FX6,0
990     REM ***** SETS ARRAY FOR DATA STORAGE *****
1000    DIM K(C)
1010    DIM B(C)
1020    REM ***** TURNS PRINTER ON *****
1030    GOSUB 3660
1040    PRINT TAB(7);"SAMPLE CODE= ";O$
1050    PRINT
1060    INPUT#M,SC
1070    PRINT TAB(7);"SCALE= ";SC;" Siemens"
1080    PRINT
1090    PRINT TAB(5);"CONDUCTIVITY";TAB(22);"TIME(mins)"
1100    REM ***** READS DATA FROM DISK AND LOADS INTO ARRAYS *****
1110    REPEAT
1120    INPUT#M,L,MIN
1130    PRINT TAB(10);L;TAB(24);MIN

```

```

1140    K(V)=L
1150    B(V)=MIN
1160    V=V+1
1170    UNTIL EOF#M
1180    PRINT:PRINT
1190    REM **** PRINTER OFF & CLOSE FILE ****
1200    VDU3
1210    CLOSE#M
1220    FOR I=1 TO 4000
1230    NEXT I
1240    CLS
1250    REM **** SET GRAPH CONDITIONS ****
1260    PRINT "YOU MUST NOW PROVIDE THE LIMITS OF THE AXES ON YOUR GRAPH
(WITH REFERENCE TO THE PRINTOUT)"
1270    PRINT
1280    PRINT "INPUT MAX ABS VALUE"
1290    INPUT DC
1300    PRINT DC
1310    PRINT "INPUT MAX TIME"
1320    INPUT TC
1330    PRINT TC
1340    FOR I=1 TO 2000
1350    NEXT I
1360    GOSUB 2670
1370    GOSUB 2440
1380    REM **** SETS GRAPHIC MODE ****
1390    MODE 132
1400    REM **** DRAWS FRAME & LABELS ****
1410    VDU5
1420    XA=60:XB=1260:YB=950:YA=100
1430    DX=10:DY=10:SX=(XB-XA)/DX:SY=(YB-YA)/DY
1440    MOVE XA,YA
1450    DRAW XB,YA:DRAW XB,YB:DRAW XA,YB:DRAW XA,YA
1460    FOR I=XA TO XB STEP SX:MOVE I,YA:DRAW I,YA+15:MOVE
I,YB:DRAW I,YB-15:NEXT I
1470    FOR I=YA TO YB STEP SY:MOVE XA,I:DRAW XA+15,I:MOVE
XB,I:DRAW XB-15,I:NEXT I
1480    MOVE 300,1000
1490    PRINT "SAMPLE ";O$;" AT ";SC;" Siemens"

```

```

1500    GOSUB 1710
1510    REM **** CALCULATES PLOT POINTS AND DETECTS OFF SCALE POINTS ****
1520    FOR U=0 TO V STEP PFQ
1530    IF K(U)=0 THEN GOTO 3080
1540    PL=(850/(DC/K(U)))+100
1550    IF B(U)=0 THEN GOTO 3100
1560    IF B(U)>TC THEN GOTO 1620
1570    OT=(1200/(TC/B(U)))+60
1580    REM **** PLOTS DATA ****
1590    MOVE OT,PL
1600    DRAW OT,PL
1610    NEXT U
1620    VDU4
1630    IF GS=1 THEN GOTO 1660
1640    GOTO 2050
1650    REM **** DUMP GRAPH TO PRINTER ****
1660    VDU2
1670    *GDUMP1
1680    MODE7
1690    VDU3
1700    GOTO 2830
1710    REM **** LABELS AXES ****
1720    MOVE 10,790
1730    PRINT "C"
1740    MOVE 10,750
1750    PRINT "O"
1760    MOVE 10,710
1770    PRINT "N"
1780    MOVE 10,670
1790    PRINT "D"
1800    MOVE 10,630
1810    PRINT "U"
1820    MOVE 10,590
1830    PRINT "C"
1840    MOVE 10,550
1850    PRINT "T"
1860    MOVE 10,510
1870    PRINT "I"
1880    MOVE 10,470
1890    PRINT "V"

```

```

1900    MOVE 10,430
1910    PRINT "I"
1920    MOVE 10,390
1930    PRINT "T"
1940    MOVE 10,350
1950    PRINT "Y"
1960    MOVE 450,90
1970    PRINT "T I M E (mins)"
1980    MOVE -225,990
1990    PRINT DC
2000    MOVE 10,90
2010    PRINT "0"
2020    MOVE 960,95
2030    PRINT TC
2040    RETURN
2050    FOR I=1 TO 8000
2060    NEXT I
2070    MODE7
2080    CLS
2090    PRINT:PRINT:PRINT:PRINT:PRINT:PRINT:PRINT:PRINT:PRINT:PRINT
2100    PRINT "DO YOU WANT TO CHANGE THE PLOTTING FREQUENCY?"
2110    INPUT CPF$
2120    IF CPF$="Y" THEN GOTO 1360
2130    CLS
2140    GS=1
2150    GOTO 1390
2160    CLS
2170    PRINT "DO YOU WISH TO SEE THE FILE CATALOGUE?"
2180    INPUT CAT$
2190    IF CAT$="Y" THEN GOSUB 2400
2200    PRINT
2210    REM **** ROUTINE TO LOAD EXISTING DATA ****
2220    C=0
2230    V=0
2240    PRINT "ENTER FILE CODE YOU WISH TO PROCESS."
2250    INPUT O$
2260    REM **** OPENS FILE FOR READING ****
2270    M=OPENIN O$
2280    INPUT#M,SC

```

```

2290 CLS
2300 PRINT "FILE ";O$;" SCALE= ";SC;" Siemens"
2310 REM **** COUNTS DATA TO GIVE ARRAY SIZE ****
2320 REPEAT
2330 INPUT#M,L,MIN
2340 PRINT "COND= ";L;" TIME= ";MIN
2350 C=C+1
2360 UNTIL EOF#M
2370 FOR I=1 TO 4000
2380 NEXT I
2390 GOTO 890
2400 CLS
2410 REM **** SHOWS DISK CATALOGUE ****
2420 *CAT
2430 RETURN
2440 CLS
2450 REM **** PRINTS SPECTRAL PARAMETERS ****
2460 VDU 2
2470 PRINT "      *+*+*+*+*+*+*+*+*+*+*+*"
2480 PRINT "      + SPECTRAL PARAMETERS +"
2490 PRINT "      *+*+*+*+*+*+*+*+*+*+*+*"
2500 PRINT
2510 PRINT "          SAMPLE ";O$
2520 PRINT
2530 PRINT "          WITH A SCALE OF ";SC;" Siemens"
2540 PRINT "          CONDUCTIVITY SCALE IS FROM"
2550 PRINT "          0 TO ";DC;" UNITS"
2560 PRINT
2570 PRINT "          TIME SCALE IS FROM"
2580 PRINT "          0 TO ";TC;" MINUTES"
2590 PRINT
2600 PRINT "          PLOTTING FREQUENCY= ";PFQ
2610 PRINT:PRINT:PRINT:PRINT
2620 VDU 3
2630 FOR I=1 TO 4000
2640 NEXT I
2650 CLS
2660 RETURN
2670 CLS
2680 REM **** ROUTINE TO CHANGE PLOTTING FREQUENCY ****

```

```

2690 PRINT:PRINT:PRINT:PRINT:PRINT:PRINT:PRINT:PRINT:PRINT:PRINT
2700 PRINT "    **** GRAPH MANIPULATION ****"
2710 PRINT:PRINT
2720 PRINT "DO YOU WANT TO CHANGE HOW OFTEN THE DATA POINTS ARE PLOTTED?"
2730 INPUT GR$
2740 IF GR$="N" THEN GOTO 2800
2750 PRINT:PRINT
2760 PRINT "WHAT IS THE REQUIRED PLOTTING FREQUENCY"
2770 INPUT PFQ
2780 CLS
2790 RETURN
2800 CLS
2810 PFQ=1
2820 RETURN
2830 CLS
2840 REM **** PROGRAM SHUT DOWN ****
2850 PRINT:PRINT:PRINT:PRINT:PRINT:PRINT:PRINT:PRINT:PRINT:PRINT
2860 PRINT "IF YOU WISH TO RUN ANOTHER SAMPLE OR PROCESS ANOTHER FILE, YOU
MUST RERUN THE PROGRAM TO CLEAR THE ARRAY FILES."
2870 PRINT
2880 PRINT TAB(15);"BYE!"
2890 END
2900 REM **** SAVES AND COUNTS DATA ****
2910 INH=INV+INH
2920 FOR W=1 TO 100
2930 X=ADVAL(1)
2940 R=R+X
2950 FOR DLT=1 TO 50: NEXT DLT
2960 NEXT W
2970 REM **** CONVERTS ADC TO CONDUCTIVITY VALUE ****
2980 Y=(R/100)/16
2990 P=(Y*CC)*1000
3000 PAG=INT(P)
3010 L=PAG/1000
3020 PRINT TAB(3);"TIME= ";MIN;TAB(14);" CONDUCT.= ";L
3030 PRINT#M,L,MIN
3040 C=C+1
3050 R=0
3060 RETURN

```

```

3070 REM **** NECESSARY TO PREVENT DIVISION BY ZERO ****
3080 PL=100
3090 GOTO 1550
3100 OT=60
3110 GOTO 1590
3120 REM **** PRINTOUT OR END? ****
3130 PRINT:PRINT:PRINT:PRINT:PRINT:PRINT:PRINT:PRINT:PRINT:PRINT
3140 PRINT "DO YOU WISH TO PRINT A HARD COPY OF THE DATA AS A GRAPH?"
3150 INPUT DTA$
3160 IF DTA$="Y" THEN GOTO 930
3170 GOTO 2830
3180 CLS
3190 REM **** INSTRUCTIONS ****
3200 PRINT "***** CONDUCTILOT RELEASE NOTES *****"
3210 PRINT
3220 PRINT "By Andrew L. Lewis 1989 Version 1.2"
3230 PRINT:PRINT
3240 PRINT "CONDUCTILOT is a modified program that is based on SPECTROLOT."
3250 PRINT "The basis of the whole program is to plot graphically, data taken from a standard
conductivity meter over an extended time period."
3260 PRINT
3270 PRINT "In order to dump screen graphics in mode(132), the BBC must be fitted with an Epson
PRINTER V1.0 ROM chip. The BBC then has a new set of commands available for printing
graphics e.g. *GDUMP."
3280 PRINT
3290 PRINT "The only documentation on this chip is that held in the ROM, called up by *H.P."
3300 PRINT
3310 GOSUB 3620
3320 PRINT
3330 PRINT "The program first asks if you want to plot data already stored on disk. All answers to
yes & no questions should be either 'Y'<RET> or 'N'<RET>."
3340 PRINT
3350 PRINT "If you refuse to plot previous results the program assumes you want to start a run.
Enter the necessary variables when prompted."
3360 PRINT
3370 PRINT "In order to calibrate the micro so that it produces the same output as the meter, it is
necessary to enter a calibration value at about half scale deflection when prompted."
3380 PRINT
3390 GOSUB 3620
3400 PRINT "The computer uses this value to calibrate the analogue input voltage. Since the ADC

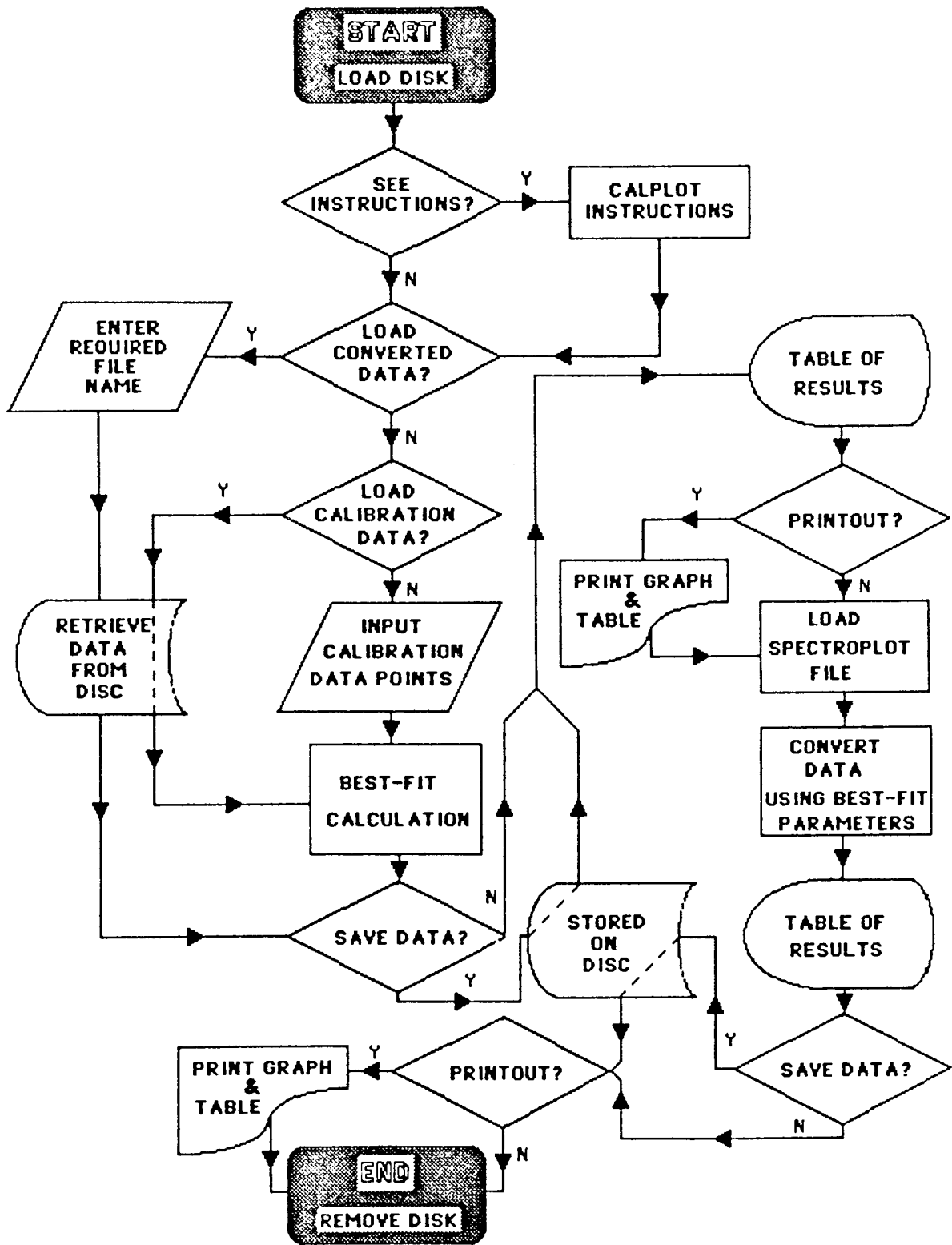
```

value fluctuates markedly, it is necessary to average 500 readings to produce a reasonable calibration."

```
3410 PRINT
3420 PRINT "The program then sets a clock running and takes readings at the frequency you
specify. The screen display serves only to monitor that the readings are being taken and that
they are comparable to the meter readout."
3430 PRINT
3440 GOSUB 3620
3450 PRINT "When printing out data, the tables are better printed in NLQ, achieved on the Epson
LX80 by pressing the buttons on the front panel in the order listed in the manual."
3460 PRINT
3470 PRINT "The graph dump will be unaffected by NLQ and will be printed out vertically to allow
full A4 size fitting."
3480 PRINT
3490 PRINT "The computer does not transfer data to the disk as it reads each value.
The data is stored in a buffer and transferred when the buffer is full."
3500 PRINT
3510 PRINT "If a run is stopped with the data in the buffer, the data is first saved to disk before the
file is closed."
3520 PRINT
3530 PRINT "The buffer is a safeguard to prevent over-working the drive and the wear of disks;
however, if power is lost, data in the buffer will also be lost."
3540 GOSUB 3620
3550 PRINT "The plotting frequency simply specifies whether to plot every point, every other point,
every 10 points etc.."
3560 PRINT
3570 PRINT "PRESS SPACE BAR TO RETURN TO THE PROGRAM"
3580 REM **** DETECTS SPACE BAR HIT ****
3590 X=INKEY(50)
3600 IF X=32 THEN RETURN
3610 GOTO 3590
3620 PRINT "<space for more>"
3630 X=INKEY(50)
3640 IF X=32 THEN RETURN
3650 GOTO 3630
3660 PRINT:PRINT:PRINT:PRINT:PRINT:PRINT:PRINT:PRINT:PRINT:PRINT
3670 PRINT "DO YOU WANT TO PRINT OUT THE SAVED DATA AS A TABLE IN ADDITION
TO A GRAPH?"
3680 INPUT SD$
```

```
3690    IF SD$="Y" THEN GOSUB 3720
3700    CLS
3710    RETURN
3720    CLS
3730    VDU 2
3740    RETURN
```

AL7 CALPLOT FLOWCHART.



## A1.8 CALPLOT LISTING.

```
10      REM CALPLOT
20      REM **** FR & RF OPTION TO PRINT CONSTANTS TO ZERO ****
30      FR=0
40      RF=0
50      REM **** CANCELS LINE FEED CHARACTER FILTER ****
60      *FX6,0
70      REM **** CREDITS ****
80      PRINT:PRINT:PRINT:PRINT:PRINT:PRINT:PRINT:PRINT:PRINT:PRINT
90      PRINT "          WELCOME TO CALPLOT"
100     FOR QP=1 TO 3000
110     NEXT QP
120     PRINT
130     PRINT "      WRITTEN BY ANDREW L. LEWIS 1989"
140     PRINT
150     PRINT "THE DEPARTMENT OF APPLIED CHEMISTRY AND CHEMICAL ENGINEERING,
        THE UNIVERSITY OF ASTON IN BIRMINGHAM."
160     FOR QP=1 TO 8000
170     NEXT QP
180     CLS
190     PRINT:PRINT:PRINT:PRINT:PRINT:PRINT:PRINT:PRINT:PRINT:PRINT
200     PRINT "DO YOU WISH TO READ THE RELEASE NOTE DOCUMENTATION (Y/N)?"
210     INPUT RL$
220     IF RL$="Y" THEN GOSUB 4320
230     CLS
240     PRINT "DO YOU WISH TO PRINT A PREVIOUSLY SAVED FILE?"
250     INPUT PS$
260     IF PS$="Y" THEN GOSUB 3520
270     PRINT "DO YOU WISH TO LOAD EXISTING CALIBRATION DATA?"
280     INPUT XD$
290     IF XD$="Y" THEN GOTO 1830
300     REM **** CALIBRATION DATA ENTERING SEQUENCE ****
310     CLS
320     PRINT "*****"
330     PRINT "*** CALIBRATION DATA ENTERING SEQUENCE ***"
340     PRINT "*****"
350     PRINT:PRINT
360     PRINT "      ENTER THE NUMBER OF X,Y DATA PAIRS"
```

```

370     INPUT N
380     GOTO 580
390     REM **** SPECTRO PLOT FILE LOADING SEQUENCE ****
400     PRINT "DO YOU WISH TO SEE THE FILE CATALOGUE?"
410     INPUT CA$
420     IF CA$="Y" THEN GOSUB 1460
430     REM **** AC & VC COUNTING VARIABLES SET TO ZERO ****
440     AC=0:VC=0
450     PRINT:PRINT
460     PRINT "    ENTER THE FILE CODE YOU WISH TO PROCESS"
470     INPUT O$
480     REM **** OPENS FILE FOR READING & COUNTS DATA ****
490     Z=OPENIN O$
500     INPUT#Z,WL
510     CLS
520     REPEAT
530     INPUT#Z,L,MIN
540     AC=AC+1
550     UNTIL EOF#Z
560     GOTO 1490
570     REM **** ARRAYS FOR DATA STORAGE ****
580     DIM XO(N):DIM YO(N):DIM YC(N)
590     PRINT:PRINT
600     REM **** INPUT OF DATA INTO ARRAYS ****
610     PRINT "    INPUT CALIBRATION DATA"
620     PRINT "(Conc. values first, strating with the smallest- then the corresponding abs. value)"
630     PRINT "-----"
640     PRINT"CONC. VALUES"
650     FOR DP=1 TO N
660     INPUT XO(DP)
670     NEXT DP
680     PRINT "ABS. VALUES"
690     FOR DP=1 TO N
700     INPUT YO(DP)
710     NEXT DP
720     CLS
730     PRINT "-----"
740     PRINT "-  CONCENTRATION      ABSORBANCE  -"
750     PRINT "===== "
760     PRINT

```

```

770     FOR DP=1 TO N
780     PRINT TAB(7);XO(DP);TAB(30);YO(DP)
790     NEXT DP
800     PRINT
810     PRINT "-----"
820     REM **** LEAST SQUARES CALCULATION OF BEST-FIT LINE DATA ****
830     SU=0: SX=0: SY=0: XX=0: XY=0: SR=0
840     FOR I=1 TO N
850     X=XO(I): Y=YO(I)
860     SU=SU+1
870     SX=SX+X
880     SY=SY+Y
890     XY=XY+X*Y
900     XX=XX+X*X
910     YY=YY+Y*Y
920     NEXT I
930     D=SU*XX-SX^2
940     C=(XX*SY-SX*XY)
950     Q=SU*XY-SX*SY
960     M=Q/D
970     J=ABS(D*(SU*YY-SY^2))
980     JJ=SQR(J)
990     RO=Q/JJ
1000    FOR I=1 TO N
1010    YC(I)=M*XO(I)+C
1020    R=YO(I)-YC(I)
1030    SR=SR+R*R
1040    NEXT I
1050    SIGMA=SQR(SR/(N-2))
1060    DM=SIGMA*SQR(SU/D)
1070    DC=SIGMA*SQR(XX/D)
1080    PRINT:PRINT
1090    PRINT "WOULD YOU LIKE A PRINTOUT OF THE DATA AND THE REGRESSION
PARAMETERS?"
1100    REM **** RAP$ OPTION TO PRINT TABLE ****
1110    INPUT RAP$
1120    CLS
1130    IF RAP$="Y" THEN VDU2
1140    REM **** DATA TABLE ****

```

```

1150 PRINT "*****"
1160 PRINT "          CALIBRATION DATA          *"
1170 PRINT "*****"
1180 PRINT
1190 PRINT "-----"
1200 PRINT "CONCENTRATION  ABSORBANCE  Y=M*X+C"
1210 PRINT "===== "
1220 PRINT
1230 FOR DP=1 TO N
1240 PRINT TAB(4);XO(DP);TAB(16);YO(DP);TAB(26);YC(DP)
1250 NEXT DP
1260 PRINT "-----"
1270 PRINT TAB(5);"SLOPE OF LINE= ";M
1280 PRINT TAB(5);"INTERCEPT= ";C
1290 PRINT TAB(5);"CORRELATION COEFFICIENT= ";INT(10000*RO+.5)/10000
1300 PRINT TAB(5);"VARIANCE OF FIT= ";SIGMA
1310 PRINT:PRINT
1320 IF RAP$="Y" THEN VDU3
1330 PRINT "OPTION TO SAVE THE CALIBRATION DATA (Y/N)?"
1340 INPUT CD$
1350 IF CD$="Y" THEN 1710
1360 PRINT:PRINT
1370 REM **** GRAPH CONSTRUCTION & PLOTTING SUBROUTINE ****
1380 PRINT "DO YOU WANT TO PLOT THE DATA AS A GRAPH"
1390 INPUT GR$
1400 IF GR$="Y" THEN GOSUB 4060
1410 IF GR$="Y" THEN GOSUB 2660
1420 IF GR$="Y" THEN GOSUB 3740
1430 IF GR$="Y" THEN GOSUB 2360
1440 IF GR$="Y" THEN GOSUB 3390
1450 GOTO 500
1460 PRINT:PRINT:PRINT
1470 *CAT
1480 RETURN
1490 CLOSE#Z
1500 CLS
1510 REM **** OPENS SPECTRO PLOT FILE & LOADS DATA ****
1520 Z=OPENIN OS
1530 DIM K(AC):DIM B(AC)
1540 PRINT TAB(7);"SAMPLE CODE= "OS

```

```

1550 PRINT
1560 INPUT#Z,WL
1570 PRINT TAB(7);"WAVELENGTH= ";WL;" nm"
1580 PRINT
1590 PRINT TAB(7);"ABSORBANCE";TAB(22);"TIME (mins)"
1600 FOR QJ=1 TO AC
1610 INPUT#Z,L,MIN
1620 PRINT TAB(10);L;TAB(24);MIN
1630 K(VC)=L:B(VC)=MIN
1640 VC=VC+1
1650 NEXT QJ
1660 PRINT:PRINT
1670 CLOSE#Z
1680 FOR II=1 TO 10000
1690 NEXT II
1700 GOTO 2000
1710 CLS
1720 REM **** SAVE CALIBRATION BEST-FIT DATA ****
1730 PRINT "INPUT FILE NAME FOR CALIBRATION DATA"
1740 INPUT T$
1750 Z=OPENOUT T$
1760 PRINT#Z,N
1770 FOR DP=1 TO N
1780 PRINT#Z,XO(DP),YO(DP),YC(DP)
1790 NEXT DP
1800 PRINT#Z,M,C,RO,SIGMA
1810 CLOSE#Z
1820 RETURN
1830 CLS
1840 PRINT "DO YOU WISH TO SEE THE FILE CATALOGUE?"
1850 INPUT CAT$
1860 IF CAT$="Y" THEN *CAT
1870 PRINT:PRINT
1880 REM **** LOADS PREVIOUSLY SAVED CALIBRATION DATA ****
1890 PRINT "    ENTER DATA FILE YOU WISH TO LOAD"
1900 INPUT T$
1910 Z=OPENIN T$
1920 INPUT#Z,N
1930 DIM XO(N):DIM YO(N):DIM YC(N)

```

```

1940   FOR DP=1 TO N
1950   INPUT#Z,XO(DP),YO(DP),YC(DP)
1960   NEXT DP
1970   INPUT#Z,M,C,RO,SIGMA
1980   CLOSE#Z
1990   GOTO 1080
2000   CLS
2010   REM **** CALCULATION FOR CONVERSION OF ABS->CONC ****
2020   DIM BF(VC)
2030   FOR GH=0 TO VC-1
2040   BF=(GH)=INT((K(GH)-C)*10000)/10000
2050   NEXT GH
2060   PRINT "DO YOU WANT A PRINTOUT OF THE CONVERTED DATA?"
2070   INPUT PCD$
2080   REM **** PCD$ OPTION TO PRINT CONC VS TIME DATA ****
2090   IF PCD$="Y" THEN VDU2
2100   PRINT "*****"
2110   PRINT "**   USING CALIBRATION BEST-FIT DATA   *"
2120   PRINT "*****"
2130   PRINT:PRINT
2140   PRINT "-----"
2150   PRINT TAB(5);"CONCENTRATION";TAB(21);"TIME(mins)"
2160   PRINT "===== "
2170   FOR UT=0 TO VC-1
2180   PRINT TAB(10);BF(UY);TAB(24);B(UY)
2190   NEXT UY
2200   PRINT:PRINT
2210   PRINT "-----"
2220   IF PCD$="Y" THEN VDU3
2230   PRINT "DO YOU WISH TO SAVE THE CONVERTED DATA?"
2240   INPUT SV$
2250   IF SV$="Y" THEN GOSUB 4170
2260   REM **** SET GRAPH LIMITS ****
2270   PRINT "ENTER THE MAX. CONC."
2280   INPUT DC
2290   PRINT:PRINT
2300   PRINT "ENTER THE MAX.TIME"
2310   INPUT TC
2320   GOSUB 2660
2330   GOSUB 2780

```

```

2340      GOTO 3160
2350      REM **** ACTUAL CALIBRATION DATA PLOTTING ROUTINE ****
2360      FOR CP=1 TO N
2370      IF YO(CP)=0 THEN GOTO 2620
2380      PL=(850/(DC/YO(CP)))+100
2390      IF XO(CP)=0 THEN GOTO 2640
2400      OT=(1200/(TC/XO(CP)))+60
2410      MOVE OT,PL
2420      DRAW OT,PL
2430      REM **** BOX AROUND POINTS ****
2440      MOVE (OT-5),(PL-5)
2450      DRAW (OT+5),(PL-5)
2460      DRAW (OT+5),(PL+5)
2470      DRAW (OT-5),(PL+5)
2480      DRAW (OT-5),(PL-5)
2490      NEXT CP
2500      REM **** BEST-FIT LINE PLOTTING ROUTINE ****
2510      IF C>0 OR C=0 THEN PL=(850/(DC/C))+100
2520      IF C>0 OR C=0 THEN OT=60
2530      IF C<0 THEN OT=(1200/(TC/(-C/M)))+60
2540      IF C<0 THEN PL=100
2550      MOVE OT,PL
2560      VQ=(1200/(TC/XO(N)))+60
2570      PS=(850/(DC/YC(N)))+100
2580      DRAW VQ,PS
2590      REM **** FR PRINT CONSTANT- FR=0 IGNORE, FR=1 PRINT ****
2600      IF FR=1 GOSUB 4280
2610      RETURN
2620      PL=100
2630      GOTO 2390
2640      OT=60
2650      GOTO 2410
2660      CLS
2670      REM **** DRAWS FRAME ****
2680      MODE 132
2690      VDU5
2700      XA=60:XB=1260:YB=950:YA=100
2710      DX=10:DY=10:SX=(XB-XA)/DX:SY=(YB-YA)/DY
2720      MOVE XA,YA

```

```

2730  DRAW XB,YA:DRAW XB,YB:DRAW XA,YB:DRAW XA,YA
2740  FOR I=XA TO XB STEP SX:MOVE I,YA:DRAW I,YA+15:MOVE I,YB:DRAW I,YB-
      15:NEXT I
2750  FOR I=YA TO YB STEP SY:MOVE XA,I:DRAW XA+15,I:MOVE XB,I:DRAW XB-
      15,I:NEXT I
2760  RETURN
2770  REM **** LABELS AXES ****
2780  MOVE 300,1000
2790  PRINT "SAMPLE ";O$;" AT ";WL;" nm"
2800  MOVE 10,750
2810  PRINT "C"
2820  MOVE 10,710
2830  PRINT "O"
2840  MOVE 10,670
2850  PRINT "N"
2860  MOVE 10,630
2870  PRINT "C"
2880  MOVE 10,590
2890  PRINT "E"
2900  MOVE 10,550
2910  PRINT "N"
2920  MOVE 10,510
2930  PRINT "T"
2940  MOVE 10,470
2950  PRINT "R"
2960  MOVE 10,430
2970  PRINT "A"
2980  MOVE 10,390
2990  PRINT "T"
3000  MOVE 10,350
3010  PRINT "I"
3020  MOVE 10,310
3030  PRINT "O"
3040  MOVE 10,270
3050  PRINT "N"
3060  MOVE 450,90
3070  PRINT "T I M E (mins)"
3080  REM **** NUMBERS AXES ****
3090  MOVE -225,990

```

```

3100 PRINT DC
3110 MOVE 10,90
3120 PRINT "0"
3130 MOVE 960,95
3140 PRINT TC
3150 REM **** CONC. VS TIME PLOTTING ROUTINE ****
3160 FOR U=0 TO VC-1
3170 IF BF(U)=0 THEN GOTO 3480
3180 PL=(850/(DC/BF(U)))+100
3190 IF B(U)=0 THEN GOTO 3500
3200 OT=(1200/(TC/B(U)))+60
3210 MOVE OT,PL
3220 DRAW OT,PL
3230 NEXT U
3240 IF RF=1 THEN GOSUB 4280
3250 FOR PU=1 TO 8000
3260 NEXT PU
3270 CLS
3280 MODE7
3290 VDU4
3300 PRINT "IS THE GRAPH SUITABLE?- DO YOU WANT TO PRINT A HARD COPY (Y/N)?"
3310 INPUT RF$
3320 IF RF$="Y" THEN RF=1
3330 PRINT:PRINT
3340 PRINT "IF YOU WISH TO PROCESS ANOTHER FILE, RE-RUN THE PROGRAM TO
CLEAR THE ARRAY FILES"
3350 PRINT:PRINT
3360 PRINT TAB(15);"BYE"
3370 REM **** PROGRAM TERMINATION ****
3380 END
3390 FOR PU=1 TO 8000
3400 NEXT PU
3410 CLS
3420 VDU4
3430 MODE7
3440 PRINT "IS THE GRAPH SUITABLE?- DO YOU WANT TO PRINT A HARD COPY (Y/N)?"
3450 INPUT HC$
3460 IF HC$="Y" THEN FR=1
3470 GOTO 1360
3480 PL=100

```

```

3490    GOTO 3190
3500    OT=60
3510    GOTO 3210
3520    PRINT:PRINT
3530    REM **** LOADS PREVIOUSLY SAVED CONVERTED FILE ****
3540    PRINT "DO YOU WISH TO SEE THE FILE CATALOGUE?"
3550    INPUT CAT$
3560    IF CAT$="Y" THEN *CAT
3570    PRINT:PRINT
3580    PRINT "ENTER FILE CODE YOU WISH TO PRINT"
3590    INPUT O$
3600    Z=OPENIN O$
3610    INPUT#Z,WL
3620    CLS
3630    PRINT "FILE ";O$;" AT WAVELENGTH ";WL;" nm"
3640    INPUT#Z,VC
3650    DIM BF(VC):DIM B(VC)
3660    FOR TQ=1 TO VC-1
3670    INPUT#Z,BF(TQ),B(TQ)
3680    PRINT "CONC.= ";BF(TQ);" TIME= ";B(TQ)
3690    NEXT TQ
3700    CLOSE#Z
3710    PRINT:PRINT
3720    GOTO 2270
3730    REM **** LABELS CALIBRATION GRAPH AXES ****
3740    MOVE 300,1000
3750    PRINT "CALIBRATION- ";T$
3760    MOVE 10,750
3770    PRINT "A"
3780    MOVE 10,710
3790    PRINT "B"
3800    MOVE 10,670
3810    PRINT "S"
3820    MOVE 10,630
3830    PRINT "O"
3840    MOVE 10,590
3850    PRINT "R"
3860    MOVE 10,550
3870    PRINT "B"

```

```

3880     MOVE 10,510
3890     PRINT "A"
3900     MOVE 10,470
3910     PRINT "N"
3920     MOVE 10,430
3930     PRINT "C"
3940     MOVE 10,390
3950     PRINT "E"
3960     MOVE 450,90
3970     PRINT "CONCENTRATION"
3980     REM ***** NUMBERS AXES *****
3990     MOVE-270,990
4000     PRINT DC
4010     MOVE 10,90
4020     PRINT "0"
4030     MOVE 960,90
4040     PRINT TC
4050     RETURN
4060     PRINT:PRINT
4070     PRINT "INPUT GRAPH TITLE CODE (6 CHARACTERS)"
4080     INPUT T$
4090     PRINT:PRINT
4100     REM ***** SET GRAPH LIMITS *****
4110     PRINT "INPUT LIMITS FOR THE GRAPH- MAX ABS=?"
4120     INPUT DC
4130     PRINT "MAX CONC=?"
4140     INPUT TC
4150     RETURN
4160     REM ***** SAVE CONVERTED DATA *****
4170     PRINT "ENTER CONVERTED DATA FILE CODE"
4180     INPUT O$
4190     Z=OPENOUT O$
4200     PRINT#Z,WL
4210     PRINT#Z,VC
4220     FOR WT=0 TO VC
4230     PRINT#Z,BF(WT),B(WT)
4240     NEXT WT
4250     CLOSE#Z
4260     RETURN
4270     REM ***** GRAPHICS DUMP COMMAND *****

```

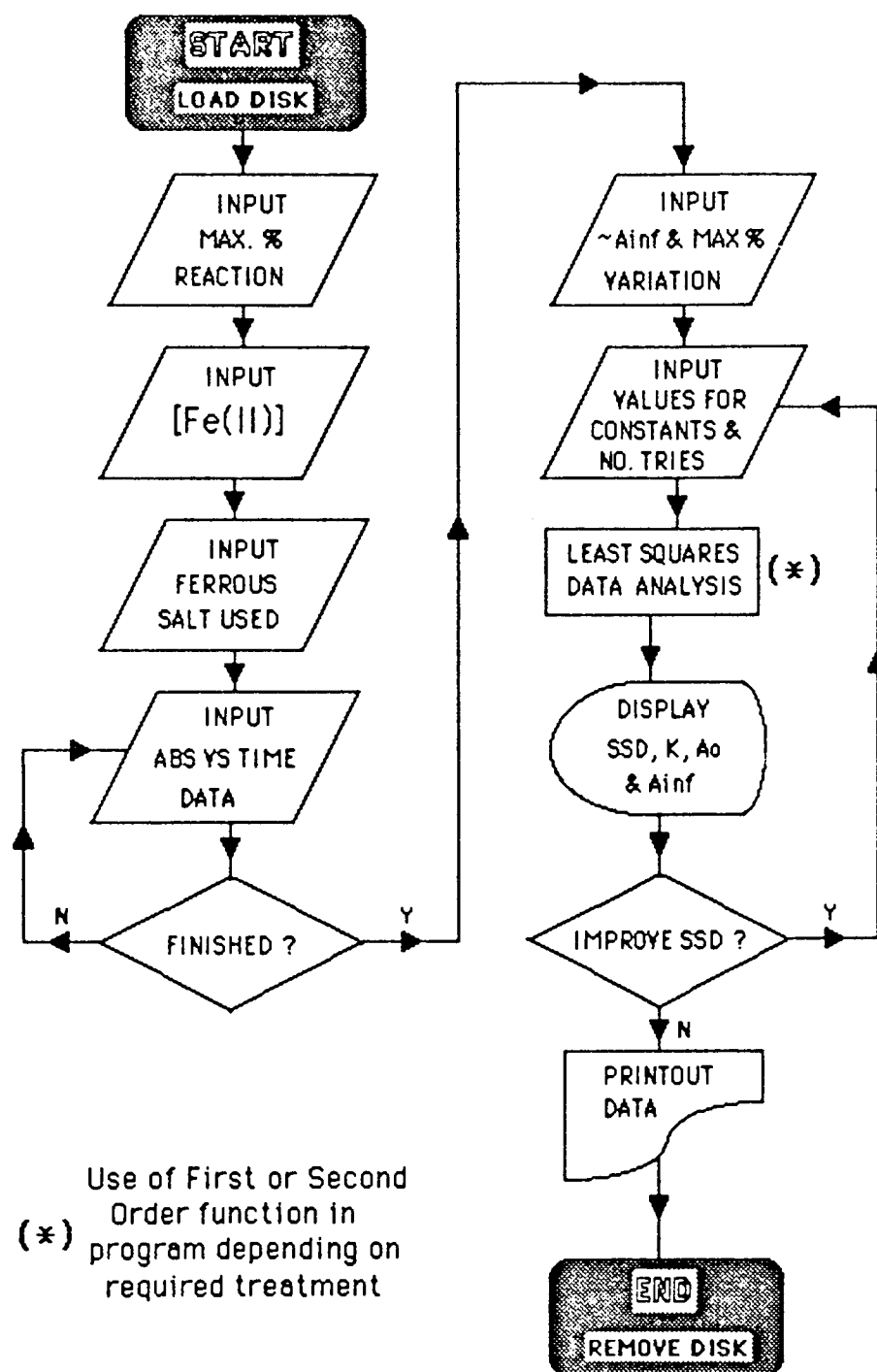
```

4280   VDU2
4290   *GDUMP1
4300   VDU3
4310   RETURN
4320   CLS
4330   PRINT "***** CALPLOT RELEASE NOTES *****"
4340   PRINT
4350   REM **** RELEASE NOTES ****
4360   PRINT "V1.3 by Andrew L. Lewis 1989"
4370   PRINT
4380   PRINT "CALPLOT is a utility designed to be used in conjunction with SPECTROPLOT. The
latter measures the absorbance at set time intervals & the final form of the data is represented
as ABS vs TIME."
4390   PRINT
4400   PRINT "However, a more useful form would be CONC (of species responsible for the
absorbance) vs TIME. If the species under study obey Beers law, CALPLOT can be used to
convert the SPECTROPLOT files into the CONC/TIME form."
4410   PRINT
4420   GOSUB 4620
4430   PRINT "A range of calibration solutions of the compounds under study should be made and the
data input into CALPLOT. The program then calculates the best-fit line for the data and gives
the option of table & graph printouts."
4440   PRINT
4450   PRINT "The program then asks for the SPECTROPLOT file to be converted, and using the
calculated calibration data it converts the ABS into CONC values."
4460   PRINT
4470   PRINT "*NOTE ON CALCULATION*"
4480   PRINT "The best-fit data is calculated by a least squares method where X=CONC & Y=ABS;
CALPLOT reads the SPECTROPLOT file, substitutes ABS into  $Y=M*X+C$  (or
 $ABS=slope*CONC+intercept$ )"
4490   PRINT "and produces the corresponding CONC values. Converted data can be saved and/or
printed as table & graph forms."
4500   PRINT
4510   GOSUB 4620
4520   PRINT "This program uses the Epson PRINTER V1.0 ROM chip and the *GDUMP1 command
for graphics."
4530   PRINT "It utilises a large number of arrays to store all the data, and a memory expansion
maybe necessary to process large data files."
4540   PRINT

```

```
4550 PRINT "CALPLOT may be used simply as a calibration line plotting program, and can be
      easily altered to allow use with parameters other than ABS & CONC."
4560 PRINT
4570 REM **** DETECTS SPACE BAR HIT ****
4580 PRINT "<space for return>"
4590 X=INKEY(50)
4600 IF X=32 THEN RETURN
4610 GOTO 4590
4620 PRINT "<space for more>"
4630 X=INKEY(50)
4640 IF X=32 THEN RETURN
4650 GOTO 4630
```

# A1.9 FIRST & SECOND ORDER "BEST-FIT" KINETICS LISTINGS.



## AL10 PROGRAM FOR LEAST SQUARES FIT OF FIRST AND SECOND

### ORDER DATA WHERE THE END-POINT READING IS UNRELIABLE.

#### FIRST ORDER.

```
10  TEXT: HOME: PR£1 :PRINT "LEAST SQUARES FIT TO REVERSIBLE FORMATION WITH
    ONLY AN APPROXIMATE INFINITY READING"
20  PRINT "PROGRAM CAN BE CHANGED TO ANY FUNCTION MERELY BY ALTERING
    LINES 10, 410, 460 & 500"
30  PRINT: PRINT "ALLOWS Rinf TO VARY BY SPECIFIED %"
40  PR£0
50  INPUT "MAX % REACTION ALLOWED =";MR
60  DIM A(30), T(30), L(30), SA(30), C(30)
70  HOME: INPUT "[Fe] =";FE
80  INPUT "SALT USED IS ";TS
90  SS = 1E10
100 PRINT "INPUT t,R; USE -1,-1 AS TERMINATOR"
110 INPUT TT,RR
120 N = 0
130 INPUT "T,R ";T,R: IF T = -1 THEN 160
140 N = N+1: T(N) = T-TT
150 A(N) = R-RR: GOTO 130
160 NN = N
170 INPUT "APPROX Rinf ";RI
180 RI = RI-RR: SI = RI
190 X = 0: FOR I = 1 TO N: X = X+T(I)*T(I): NEXT I
200 INPUT "MAX % VARIATION =";MV: U = MV/100
210 PRINT "INPUT VALUES FOR CONSTANT AS UPPER AND LOWER LIMITS AND
    NUMBER OF TRIES"
220 PRINT "TO FIX VALUE AT Z TYPE <Z,-1,1>"
230 INPUT "VALUES = ?"; CL,CU,CN
240 FOR P = 0 TO CN: IF CU = -1 THEN P = CN
250 CC = CU-P*(CU-CL)/CN
260 FOR I = 1 TO 3: IF U = 0 THEN I = 3
270 U = 0.544*U: LI = SI*(1-U): UI = SI*(1+U)
280 FOR Q = 1 TO 3: IF U = 0 THEN Q = 3
290 AI = UI+Q*(LI-UI)/3
300 AI = INT(AI)
310 ET = AI+SQR(AI*CC): EA = ET+CC/2
```

```

320 EB = SQR(EA*EA-ET*ET)
330 QA = EA-EB
340 QB = EA+EB
350 QQ = QB/QA: IF QQ > 0 THEN 370
360 PRINT "NEGATIVE LOG": GOTO 230
370 LL = LOG(QB/QA)
380 S = 0: Y = 0
390 FOR J = 1 TO N: IF A(J) < MR*AI/100 THEN 410
400 NN = NN-1: GOT 430
410 L(J) = LOG ((AJ)-QB)/(A(J)-QA))-LL
420 YY = L(J)*T(J)
430 Y = Y+YY
440 NEXT J
450 K = -Y/X
460 FOR J = 1 TO N: EE = EXP(LL-K*T(J)): C(J) = INT((QB-QA*EE)/(1-EE))
470 E = C(J)-A(J): S = S+E*E: IF S > SS THEN 540
480 NEXT J
490 SS = S: EE = EXP(LL+K*TT): SK = -K/(2*EB)
500 SC = INT((QB-EE*QA)/(1-EE))
510 CS = CC: SI = AI
520 FOR J = 1 TO N: SA(J) = -RR: NEXT J
530 FOR J = 1 TO NN: SA(J) = C(J): NEXT J
540 NN = N: NEXT Q
550 NEXT I
560 NEXT P
570 PRINT " CONSTANT = "CS
580 PRINT "SSD = "SS"    K= "SK
590 PRINT "ZERO = "SC"  INF = "SI+RR
600 INPUT "IMPROVE THE FIT?";A$
610 IF A$ = "N" THEN 640
620 IF A$ = "Y" THEN 200
630 GOTO 600
640 PR£1: PRINT: PRINT: PRINT
650 PRINT "LEAST SQUARES FIT FOR "FE"M "T$: PRINT
660 PRINT "SUM OF SQUARED DIFFERENCES = "SS"    K = "SK
670 PRINT "ZERO AND INFINITY READINGS ARE "SC+RR" AND " SI+RR: PRINT
680 PRINT "CONSTANT = "CS
690 PRINT "TIME, OBSERVED AND CALCULATED READINGS ARE": PRINT
700 PRINT TT"    "RR"    "RR

```

```

710  FOR I = 1 TO N
720  PRINT TT+T(I) "      "A(I)+RR"      "SA(I)+RR
730  NEXT I
740  PR£0: GOTO 70
750  END

```

## SECOND ORDER.

10 TEXT: HOME: PR£1 :PRINT "LEAST SQUARES VARIENT FOR SECOND ORDER WITH ONLY AN APPROXIMATE INFINITY READING"

20 - 300 AS WITH FIRST ORDER PROGRAM

```

310  AK = AI*CC: AA = AI*AK
320  S = 0: Y = 0
330  FOR J = 1 TO N: C(J) = AA*T(J)/(1+AK*T(J))
340  E = C(J)-A(J): S = S+E*E: IF S > SS THEN
350  NEXT J
360  SS = S

```

370 - 500 NOT NECESSARY

510 ONWARDS AS WITH FIRST ORDER PROGRAM EXCEPT LINES:

```

660  PRINT "SUM OF SQUARED DIFFERENCES = "SS"      K = "CS
670  PRINT "INFINITY READING IS "SI+RR: PRINT

```

## **APPENDIX TWO**

### **SELECTED ABSORBANCE & WAVELENGTH DATA FROM CHAPTER THREE.**

## **A2.1 SELECTED ABSORBANCE & WAVELENGTH DATA FROM**

### **CHAPTER THREE.**

**Figure 3.7: Visible Absorption Spectra of Cu(II) Complexes of Pyridine.**

<u>Complex</u>	<u><math>\lambda_{\max}(\text{nm})</math></u>	<u>Absorbance</u>
Cu(H <sub>2</sub> O) <sub>6</sub>	810	0.281
Cu(Py) <sub>1</sub>	715	0.353
Cu(Py) <sub>2</sub>	670	0.436
Cu(Py) <sub>3</sub>	640	0.620
Cu(Py) <sub>4</sub>	620	0.921

**Figure 3.8(a): Effect of [Ligand] on Cu(II) Visible Absorption Spectra of Pyridyl Copolymers.**

<u>%[Ligand]</u>	<u><math>\lambda_{\max}(\text{nm})</math></u>	<u>Absorbance</u>
0.5	810	0.202
1	805	0.250
2	793	0.324
4	776	0.571
8	747	0.840

**Figure 3.8(b): Effect of Leaching Cu(II) from Pyridyl Copolymers.**

<u>%[Ligand]</u>	<u><math>\lambda_{\max}(\text{nm})</math></u>	<u>Absorbance</u>
0.5	619	0.082
1	620	0.101
2	622	0.124
4	626	0.324
8	630	0.435

**Figure 3.10: Effect of [Cu(II)] on Visible Absorption Spectra of Pyridyl Copolymer Membrane.**

<u>[Cu(II)](mmol)</u>	<u><math>\lambda_{\max}(\text{nm})</math></u>	<u>Absorbance</u>
0.05	643	0.201
0.1	644	0.324
0.25	647	0.349
0.5	650	0.537
1	680	0.949
1.5	684	1.053
2	695	0.862
4	742	0.944

**Figure 3.11(a): Effect of Dehydrating CuCl<sub>2</sub>-Soaked Pyridyl Copolymers Membranes on Vis. Absn. Spectra.**

<u>%[Ligand]</u>	<u><math>\lambda_{\max}(\text{nm})</math></u>	<u>Absorbance</u>
0.5	808	0.195
1	807	0.396
2	805	0.610
4	803	1.103
8	792	1.964

**Figure 3.13(a): Effect of [Ligand] on Cu(II) Visible Absorption Spectra of Bipyridyl Copolymers.**

<u>%[Ligand]</u>	<u><math>\lambda_{\max}(\text{nm})</math></u>	<u>Absorbance</u>
0.5	800	0.110
1	795	0.122
2	788	0.203
4	750	0.365
8	743	0.581

{ Intense band <400nm, off scale }

**Figure 3.13(b): Effect of Leaching Cu(II) from Bipyridyl Copolymers.**

<u>%[Ligand]</u>	<u><math>\lambda_{\text{max}}(\text{nm})</math></u>	<u>Absorbance</u>
0.5	726	0.082
1	727	0.124
2	729	0.180
4	731	0.381
8	735	0.753

**Figure 3.15(a): Effect of [Ligand] on Co(II) Spectra of pyridyl Membranes.**

<u>%[Ligand]</u>	<u><math>\lambda_{\text{max}}(\text{nm})</math></u>	<u>Absorbance</u>
0.5	515	0.025
1	512	0.061
2	510	0.110
4	510	0.225
8	505	0.413

**Figure 3.15(b): Absorption Spectrum of Co(SCN)<sub>2</sub> in Pyridyl Copolymers.**

<u>%[Ligand]</u>	<u><math>\lambda_{\text{oct}}</math></u>	<u><math>\lambda_{\text{tet}}</math></u>	<u>Abs.</u>
0	622	510	0.521
0.25	" "	" "	0.563
0.5	" "	" "	0.622
1	" "	" "	0.720
2	" "	" "	0.849
4	" "	" "	1.223
8	" "	" "	1.924

**Figure 3.17: Effect of Dehydration on the Visible Absorption Spectrum Pyridyl Copolmyer Membranes.**

<u>%[Ligand]</u>	<u><math>\lambda_{\text{max}}(\text{nm})</math></u>	<u>Absorbance</u>
0	660	0.712
0.25	662	0.973
0.5	657	1.105
1	616	0.953
2	619	1.730
4	off scale	-
8	off scale	-

**Figure 3.18: Visible Absorption Spectra of Bipyridyl Copolymer Membranes Soaked in CoCl<sub>2</sub>.**

**As Soaked in 0.25M CoCl<sub>2</sub>:**

<u>%[Ligand]</u>	<u><math>\lambda_{\text{max}}(\text{nm})</math></u>	<u>Absorbance</u>
0.5	495	0.075
1	480	0.105
2	475	0.123
4	462	0.152
8	452	0.364

**After Leaching in Water:**

<u>%[Ligand]</u>	<u><math>\lambda_{\text{max}}(\text{nm})</math></u>	<u>Absorbance</u>
0.5	452	0.035
1	" "	0.042
2	" "	0.111
4	" "	0.245
8	" "	0.649

**Figure 3.20: Visible Absorption Spectra of Co(I)tris(VBipy) in Membranes of Various Ligand Loadings.**

<u>%[Ligand]</u>	<u><math>\lambda_{\text{max}}(\text{nm})</math></u>	<u>Absorbance</u>
0.5	570	0.281
1	580	0.573
2	590	0.879
4	610	1.832
8	off scale	off scale

**Figure 3.27: Effect of [Ligand] on Fe(II) Spectra of Bipyridyl Copolymer Membranes.**

<u>%[Ligand]</u>	<u><math>\lambda_{\text{max}}(\text{nm})</math></u>	<u>Absorbance</u>
0.05	534	0.151
0.1	" "	0.382
0.25	" "	0.922
0.5	" "	1.924
1	off scale	off scale
2	off scale	off scale

**Figure 3.21: Reoxidation of Co(I) to Co(II) in a Co(I)-Coordinated Bipyridyl Copolymer Membrane.**

<u>Time(mins)</u>	<u><math>\lambda_{\text{max}}(\text{nm})</math></u>	<u>Absorbance</u>
0	610	1.604
15	602	1.169
30	598	0.953
45	595	0.803
75	590	0.601
105	560	0.352
135	~550	0.071

**Figure 3.28: Effect of Anion on Abs<sub>∞</sub> of Fe(II) tris(Bipyridyl) Complex.**

<u>Anion</u>	<u><math>\lambda_{\text{max}}(\text{nm})</math></u>	<u>Absorbance</u>
SO <sub>4</sub> <sup>2-</sup>	534	1.853
Cl <sup>-</sup>	" "	1.542
ClO <sub>4</sub> <sup>-</sup>	" "	0.907

## **APPENDIX THREE**

### **SPREAD-SHEET TABLES FOR THE CALCULATION OF STRESS-STRAIN DATA.**

### A3.1 TENSILE DATA FOR VBIPY COPOLYMER MEMBRANES.

1% VBipy:					
Force	Nominal Force	Extension	Strain function	Reduced Force	$1/\alpha$
f (N)	f* (F/A)	L/Li	$L/Li-(1/L/Li)^2$	[f*]	Li/L
0.1	0.125	1.09	0.248	0.453	0.917
0.2	0.25	1.2	0.506	0.445	0.833
0.3	0.375	1.35	0.801	0.421	0.741
0.4	0.5	1.5	1.056	0.426	0.667
0.5	0.625	1.68	1.326	0.424	0.595
0.6	0.75	1.87	1.584	0.426	0.535
0.7	0.875	2.05	1.812	0.435	0.488
0.8	1	2.2	1.993	0.451	0.455
0.9	1.125	2.36	2.180	0.464	0.424
4% VBipy:					
Force	Nominal Force	Extension	Strain function	Reduced Force	$1/\alpha$
f (N)	f* (F/A)	L/Li	$L/Li-(1/L/Li)^2$	[f*]	Li/L
0.1	0.125	1.18	0.462	0.244	0.847
0.2	0.25	1.25	0.610	0.369	0.800
0.3	0.375	1.4	0.890	0.379	0.714
0.4	0.5	1.6	1.209	0.372	0.625
0.5	0.625	1.75	1.423	0.395	0.571
0.6	0.75	1.9	1.623	0.416	0.526
0.7	0.875	2.1	1.873	0.420	0.476
0.8	1	2.25	2.052	0.438	0.444
0.9	1.125	2.4	2.226	0.455	0.417
1	1.25	2.6	2.452	0.459	0.385
1.1	1.375	2.76	2.629	0.471	0.362
8% VBipy:					
Force	Nominal Force	Extension	Strain function	Reduced Force	$1/\alpha$
f (N)	f* (F/A)	L/Li	$L/Li-(1/L/Li)^2$	[f*]	Li/L
0.1	0.125	1.17	0.439	0.256	0.855
0.2	0.25	1.25	0.610	0.369	0.800
0.3	0.375	1.375	0.846	0.399	0.727
0.4	0.5	1.59	1.194	0.377	0.629
0.5	0.625	1.75	1.423	0.395	0.571
0.6	0.75	1.97	1.712	0.394	0.508
0.7	0.875	2.15	1.934	0.407	0.465
0.8	1	2.32	2.134	0.422	0.431
0.9	1.125	2.495	2.334	0.434	0.401
1	1.25	2.7	2.563	0.439	0.370
1.1	1.375	2.825	2.700	0.458	0.354

### A3.2 TENSILE DATA FOR VBIPY:[Fe(II)]-COORDINATED COPOLYMER MEMBRANES.

1% VBipy:[Fe]					
Force	Nominal Force	Extension	Strain function	Reduced Force	$1/\alpha$
f (N)	f* (F/A)	L/Li	$L/Li-(1/L/Li)^2$	[f*]	Li/L
0.1	0.125	1.095	0.261	0.431	0.913
0.2	0.25	1.18	0.462	0.487	0.847
0.3	0.375	1.28	0.670	0.504	0.781
0.4	0.5	1.395	0.881	0.511	0.717
0.5	0.625	1.49	1.040	0.541	0.671
0.6	0.75	1.62	1.239	0.545	0.617
0.7	0.875	1.75	1.423	0.553	0.571
0.8	1	1.875	1.591	0.566	0.533
4% VBipy:[Fe]					
Force	Nominal Force	Extension	Strain function	Reduced Force	$1/\alpha$
f (N)	f* (F/A)	L/Li	$L/Li-(1/L/Li)^2$	[f*]	Li/L
0.25	0.3125	1.135	0.359	0.784	0.881
0.5	0.625	1.25	0.610	0.922	0.800
0.75	0.9375	1.375	0.846	0.997	0.727
1	1.25	1.505	1.064	1.058	0.664
1.25	1.5625	1.62	1.239	1.135	0.617
1.5	1.875	1.75	1.423	1.185	0.571
1.75	2.1875	1.8	1.491	1.320	0.556
2	2.5	1.88	1.597	1.409	0.532
2.25	2.8125	2	1.750	1.446	0.500
2.5	3.125	2.07	1.837	1.531	0.483
8% VBipy:[Fe]					
Force	Nominal Force	Extension	Strain function	Reduced Force	$1/\alpha$
f (N)	f* (F/A)	L/Li	$L/Li-(1/L/Li)^2$	[f*]	Li/L
0.5	0.625	1.12	0.323	1.743	0.893
1	1.25	1.265	0.640	1.758	0.791
1.5	1.875	1.4	0.890	1.897	0.714
2	2.5	1.515	1.079	2.085	0.660
2.5	3.125	1.61	1.224	2.297	0.621
3	3.75	1.7	1.354	2.493	0.588
3.2	4	1.735	1.403	2.566	0.576

### A3.3 TENSILE DATA FOR VPy COPOLYMER MEMBRANES.

2% VPy:					
Force	Nominal Force	Extension	Strain function	Reduced Force	$1/\alpha$
f (N)	f* (F/A)	L/Li	$L/Li-(1/L/Li)^2$	[f*]	Li/L
0.1	0.125	1.25	0.610	0.184	0.800
0.2	0.25	1.5	1.056	0.213	0.667
0.3	0.375	1.95	1.687	0.200	0.513
0.4	0.5	2.6	2.452	0.184	0.385
0.5	0.625	3.35	3.261	0.172	0.299
0.6	0.75	3.85	3.783	0.178	0.260
0.7	0.875	4.4	4.348	0.181	0.227
0.8	1	5	4.960	0.181	0.200
0.9	1.125	5.5	5.467	0.185	0.182
1	1.25	5.85	5.821	0.193	0.171
1.1	1.375	6.07	6.043	0.205	0.165
8% VPy:					
Force	Nominal Force	Extension	Strain function	Reduced Force	$1/\alpha$
f (N)	f* (F/A)	L/Li	$L/Li-(1/L/Li)^2$	[f*]	Li/L
0.1	0.125	1.23	0.569	0.198	0.813
0.2	0.25	1.35	0.801	0.281	0.741
0.3	0.375	1.5	1.056	0.320	0.667
0.4	0.5	1.7	1.354	0.332	0.588
0.5	0.625	1.9	1.623	0.347	0.526
0.6	0.75	2.17	1.958	0.345	0.461
0.7	0.875	2.37	2.192	0.359	0.422
0.8	1	2.68	2.541	0.354	0.373
0.9	1.125	2.83	2.705	0.374	0.353
1	1.25	3.1	2.996	0.376	0.323
1.1	1.375	3.22	3.124	0.396	0.311
1.2	1.5	3.37	3.282	0.411	0.297
1.25	1.5625	3.45	3.366	0.418	0.290
16% VPy:					
Force	Nominal Force	Extension	Strain function	Reduced Force	$1/\alpha$
f (N)	f* (F/A)	L/Li	$L/Li-(1/L/Li)^2$	[f*]	Li/L
0.25	0.3125	1.075	0.210	1.341	0.930
0.5	0.625	1.4	0.890	0.632	0.714
1	1.25	2.3	2.111	0.533	0.435
1.5	1.875	3.1	2.996	0.563	0.323
2	2.5	3.7	3.627	0.620	0.270
2.5	3.125	4.1	4.041	0.696	0.244
3	3.75	4.38	4.328	0.780	0.228
3.3	4.125	4.57	4.522	0.821	0.219

### A3.4 TENSILE DATA FOR VPy:[Cu(II)]-COORDINATED COPOLYMER MEMBRANES.

2% VPy:[Cu]					
Force	Nominal Force	Extension	Strain function	Reduced Force	$1/\alpha$
f (N)	f* (F/A)	L/Li	$L/Li-(1/L/Li)^2$	[f*]	Li/L
0.1	0.125	1.25	0.610	0.184	0.800
0.2	0.25	1.5	1.056	0.213	0.667
0.3	0.375	2.2	1.993	0.169	0.455
0.4	0.5	2.8	2.672	0.168	0.357
0.5	0.625	3.5	3.418	0.165	0.286
0.6	0.75	4.3	4.246	0.159	0.233
0.7	0.875	4.9	4.858	0.162	0.204
8% VPy:[Cu]					
Force	Nominal Force	Extension	Strain function	Reduced Force	$1/\alpha$
f (N)	f* (F/A)	L/Li	$L/Li-(1/L/Li)^2$	[f*]	Li/L
0.5	0.625	1.12	0.323	1.743	0.893
1	1.25	1.22	0.548	2.052	0.820
1.5	1.875	1.45	0.974	1.732	0.690
2	2.5	1.95	1.687	1.334	0.513
2.5	3.125	2.42	2.249	1.250	0.413
3	3.75	2.98	2.867	1.177	0.336
4	5	3.61	3.533	1.274	0.277
4.5	5.625	3.89	3.824	1.324	0.257
16% VPy:[Cu]					
Force	Nominal Force	Extension	Strain function	Reduced Force	$1/\alpha$
f (N)	f* (F/A)	L/Li	$L/Li-(1/L/Li)^2$	[f*]	Li/L
2.6	3.25	1.05	0.143	20.459	0.952
5.4	6.75	1.1	0.274	22.208	0.909
5.6	7	1.2	0.506	12.462	0.833
5.3	6.625	1.3	0.708	8.418	0.769
5.2	6.5	1.4	0.890	6.575	0.714
5.15	6.4375	1.5	1.056	5.489	0.667
5.15	6.4375	1.6	1.209	4.791	0.625
5.2	6.5	1.7	1.354	4.321	0.588
5.4	6.75	1.8	1.491	4.073	0.556
5.5	6.875	1.9	1.623	3.812	0.526
5	6.25	2	1.750	3.214	0.500